UNIVERSITÀ
DEGLI STUDI
FIRENZE

DOTTORATO DI RICERCA IN SCIENZE DELLA TERRA

CICLO XXIX

COORDINATORE Prof. Lorenzo Rook

A Mediterranean perspective on the Early-Middle Pleistocene transition with emphasis on marine isotope stage 19

Settori Scientifici Disciplinari GEO/01-02

Dottorando
Dott. Toti Francesco

Tutore
Prof. Bertini Adele

Co-Tutore
Dr. Combourieu Nebout Nathalie

Coordinatore
Prof. Rook Lorenzo

Anni 2013/2017

Acknowledgements

This work of thesis was carried out during the years 2013-2017 at the Department of Earth Sciences of the University of **FLORENCE** and at the Muséum national d'Histoire naturelle of **PARIS**, two places to which I am particularly attached.

This thesis is the outcome of years of research, discovery and personal commitment. But it would not have been possible unless the support of my Ph.D. Tutor Prof. **Adele BERTINI**, who guided me through the doctoral journey providing unwavering support and mentoring.

I also express my gratitude to my co-Tutor Dr. **Nathalie COMBOURIEU NEBOUT** (Muséum national d'Histoire naturelle, Paris), who shared intellectual support, suggestions and recommendations that contributed to the making of this thesis.

Warmest gratitude goes to **Maria MARINO**, **Patrizia MAIORANO**, **Angela GIRONE** and **Neri CIARANFI** (University of Bari 'Aldo Moro') for sharing valuable stratigraphical and micropalaeontological skills and for giving me the opportunity to explore the enchanted Montalbano Jonico badlands, definitely the best stratigraphical section in the world.

Special mention goes to **Sébastien NOMADE** and **Franck BASSINOT** (Laboratoire des Sciences du Climat et de l'Environnement, Gif-sur-Yvette),

for the cooperation which we have enjoyed in the frame of the surveys carried out at Montalbano Jonico and ODP Site 976.

I want to express my gratitude to the reviewers of the manuscript **Odile PEYRON** (Institut des Sciences de l'Evolution de Montpellier) and **Elda RUSSO ERMOLLI** (University of Naples Federico II).

I would also like to extend my thanks to the technicians of the laboratories of Montpellier (**SANDRINE**) and Paris (**MEHDI**) for their help in preparing palynological samples from ODP core 976 (one-hundred and four samples) and Montalbano Jonico (eleven samples).

I am also very thankful to **Antonella BUCCIANTI** (University of Florence), for providing me with assistance in order to compute statistical analysis on palynological datasets. She helped me a lot to finalize the paper (Toti, 2015) which earned me a travel grant to attend the amazing XIX INQUA Congress at Nagoya, Japan.

Finally, my deepest thanks go to my **MOM**, **DAD** and **SISTER**, for almost unbelievable support, and to **LORENA**, for her encouragement, patience and for keeping me sane towards the end. They are the most important people in my life and I dedicate this thesis to them.

I am also indebted to one and all who, directly and indirectly, have lent their helping hand in this venture.

Contents

Synopsis

Over the last 2.6 million years (Ma), North Hemisphere ice-sheets fluctuations, which we refer to as Glacials and Interglacials, started to exert a major influence on Earth's climate. According with the 'astronomical theory of climate', which gained strength with the implications proposed by M. Milankovitch before the World-War II, the periodicity of such changes is function of cyclical variations of the Earth's orbital parameters - including the tilt of rotation axis (obliquity), the precession of the equinoxes and the orbital eccentricity. To date, however, this theory appears unable to give comprehensive explanation of many aspects related to the Glacial-Interglacial (G-IG) rhythm. Few is known, for example, on the factors that caused the G-IG cycles to change, during the so-called Early-Middle Pleistocene Transition (EMPT, 1.4-0.4 Ma), from a 41,000-years (41-kyr: obliquity-driven) to a quasi-periodical 100-kyr dominant periodicity (eccentricity-driven), in absence of significant changes in the astronomical forcing. The 41-kyr signal, which dominated the G-IG cyclicity during most of the Early Pleistocene, was thus overshadowed by a low-frequency, higher amplitude one, which governs the climate cycles since the mid-late Pleistocene.

To trace a detailed image of the Mediterranean terrestrial and marine ecosystems during the EMPT, two marine sedimentary successions were analyzed by means of palynology. The successions, respectively located in the western and the central Mediterranean, are: i) core 976, a deep-sea section sampled in the Alboran Sea in the frame of the Ocean Drilling Program (ODP) and covering Marine Isotopic Stages (MISs) 20 and 19), and ii) Montalbano

Jonico, cropping out in Basilicata Region (Italy) and covering a longer time-interval between MIS 22-MIS 17. Palynology has proven to be a valuable tool for palaeovegetation and palaeoclimatic reconstructions in this time-span, through the identification and counting of terrestrial vegetal micro-remains, such as pollen and spores, and of organic cysts of marine dinoflagellates (dinocysts). The simultaneous analysis of terrestrial and marine palynomorphs resulted in direct land-sea correlations which were also improved by the parallel multiproxy analyses carried out in the frame of national and international collaborations (Department of Earth and Geoenvironmental Science, Università di Bari 'Aldo Moro', Italy; Laboratoire des Sciences du Climat et de L'Environnement, Gif-Sur-Yvette, France).

The interval MIS 20-MIS 19, captured in both sedimentary successions, was investigated in high detail, representing one of the main topics of this thesis. This interval is, in fact, a key to successfully understanding the climate dynamics governing the present epoch (best analogue of the Holocene, e.g. Tzedakis et al., 2010; Yin and Berger, 2012, 2015) and to achieve the chronostratigraphic purpose of defining the GSSP of the Middle Pleistocene.

Structure of the thesis

Besides this **Synopsis**, the thesis includes an introductive chapter and three main sections (A-C), of which A and B are preceded by a general thematic summary.

- **Introduction** focuses on the main Quaternary climate issues especially including those covered in this thesis.

- **Section A** concerns palynological datasets and results from the spectacular on-land marine succession of Montalbano Jonico ('Interval B': MIS 22-17), in Southern Italy.

  The **Montalbano Jonico summary** integrates data and results developed in six contributions including five articles (A1-A5) and one report (A6).

  In **Contribution A1** (**Toti, 2015**), the history of consecutive 'warm' climate oscillations from 860 to 655 ka was examined. A multivariate statistical approach was used to check for the presence of peculiar

vegetation dynamics across different warm periods. Results showed that the selected intervals could be distinguished on the base of the proportions of fast-spreading taxa (e.g. deciduous *Quercus* and herbs) and taxa with slower migration rates (*Cedrus*, evergreen *Quercus* …). In particular, only during the warmest, more forested periods (corresponding to the 'truly' interglacials, i.e. MIS 21, 19 and 17) all the conditions are met for the temperate vegetation alliances to include slow-spreading populations.

In **Contributions A2** and **A3** (**Marino et al., 2015; Bertini et al., 2015**), pollen data were used to reconstruct the vegetation and climate changes in the central Mediterranean between 860-745 ka (MIS 21-MIS 19). During interglacials MIS 21 and 19, the expansion of temperate mesophilous forest describes enhanced precipitation and temperatures, whereas during glacial phases MIS 20 and 18, the spread of steppe and semi-desert communities suggests a dryer climate. The occurrence of short-term, dry events in both glacial and interglacial phases was linked to global-scale pattern recognized in other successions, thus highlighting the high potential of correlation of the Montalbano Jonico section. Such an improvement of the bio- and climatostratigraphy across the Montalbano Jonico sedimentary succession represented a milestone to illustrate (**Contribution A4: Marino et al., 2016**) the good potential of this section to host the 'Global Boundary Stratotype Section and Point' (GSSP) for the Middle Pleistocene.

In **Contribution A5** (**Maiorano et al., 2016),** climate changes in the interval MIS 20-19 were analyzed at a higher time resolution with respect to the previous Contributions, integrating palynological (pollen and dinocysts), marine biostratigraphical (coccoliths and foraminifera) and mineralogical-granulometric proxies. The reconstruction displays that during phases characterized by aridity and lower arboreal cover, lower sea-surface temperatures (SST) and higher terrigenous discharge determined enhanced erosional processes; phases with moister conditions and increased temperate forest were conversely associated to higher SST and pronounced chemical weathering. During the latest part of MIS 20, we recognized two distinct cold-dry phases that were tentatively correlated with 'H 1' and 'Younger Dryas' events of the last

deglaciation according to their peculiar signature (strong aridity and polar water influx in the Mediterranean) and timing. During the first sub-stage of MIS 19 (19c), an event of SST maximum concurs with ocean stratification, reduced surface water salinity and, on land, increased runoff and maximum precipitations. We therein recognized most of the conditions that generally lead to the formation of organic enriched layers (sapropels), potentially useful as astrochronological control-points. During late MIS 19 (substages 19b-a) the high-frequency climate variability expressed by both marine and continental proxies strikingly mirrors coeval oscillations in North Atlantic records, thus validating the excellent correlation potential of the Montalbano Jonico section.

- **Section B**. To better characterize MIS 19, new high-resolution palynological investigations were carried out along a portion of the deep-sea core ODP 976, recovered in the Alboran Sea, western Mediterranean, in the frame of the Ocean Drilling Program (ODP). Results from parallel micropalaeontological analyses (coccoliths and foraminifera) as well as foraminiferal $\delta^{18}O$ measurements integrated the palynological investigations along an interval encompassing MIS 19 and the transitions with the adjacent glacial stages MIS 20 and 18 (these results are reported in the manuscript by **Toti et al., in preparation**).

  The reconstruction revealed terrestrial vegetation and sea surface waters changes linked to both internal and external (orbital) climate forcing. The glacial termination was marked by an episode of extreme cooling and aridification, correlated with massive iceberg discharges and ice-rafted debris deposition in the subpolar North Atlantic. The onset of MIS 19 was expressed by the temperate deciduous and evergreen forest expansion as well as by a discrete ocean surface warming. The full interglacial phase (MIS 19c) was punctuated by a quasi-periodic climate instability with contrasting land-sea responses, superimposed on a long-term change of seasonality driven by insolation-precessional forcing. The late MIS 19 exhibits a climate variability characterized by repeated stadial (interstadial) oscillations, documented by temperate forest contractions (expansions) and relative cooling (warming) of the ocean. These phases are unambiguously

correlated with equivalent features of the North-Atlantic and Mediterranean climate variability.

- **Section C.** The distinct climate variability recognized along the MIS 20-19 interval encourages a comparison (W-E transect) between the Montalbano Jonico and ODP Site 976 successions. Such an approach is enhanced by the use of a common protocol of analysis.

  For the purpose of this section, we dealt with a systematic evaluation of the differential climate impact in both terrestrial and marine environments, using an improved pollen and dinocysts dataset. During the main cold-dry phases of MIS 20 and late MIS 19, Site 976 was especially prone to recording episodes of forest depletion and ocean surface cooling, probably because of the more efficient teleconnections with the North Atlantic basin. Moreover, the palynological comparison illustrates an enhanced Mediterranean-type seasonality in the western part of the basin, suggesting an atmosphere circulation pattern similar to modern one. On the contrary, the magnitude of seasonal variations and of rapid climate changes at Montalbano Jonico was apparently lower with respect to Site 976, providing a key to interpret the diversity of plant communities between the two areas.

Introduction

1. Linking past and future Earth's climate

Over the last decades, major efforts have been undertaken to advance the understanding of the Earth's climate change and its causes. Research activity in this field is stimulated by the alarms linked to the global warming and the consequent risks for the stability of the natural ecosystems and human cultures, as well as by the increase of extreme weather events (IPCC, 2013).

The primary tools for making projections of the future climate are global climate models, which basically are numerical simulations performed on super-computers, set up to monitor the dynamics of the ocean-atmosphere system (output) in response to multiple physical and geochemical variables (input), such as insolation (of the incoming solar radiation), land-sea distribution, ice-sheets and vegetation distribution, etc. (Karl and Trenberth, 2003). The outcomes of these experiments combined with palaeoclimate data have contributed to create a public awareness of the role played by greenhouses gasses in the global warming scenario within the industrial-era (e.g. Abram et al., 2016). Although the robustness of these models and predictions has been convincingly confirmed by several surveys of the refereed literature (e.g. Knutti and Jan Sedláček, 2013; Marcott et al., 2013; Cowtan et al., 2015), the presence of people disillusioned with science and of politicians who brand scientific evidences as 'inconvenient'[1] remains a major

[1] e.g. U.S. President Donald Trump's nominee for Secretary of State R. Tillerson said in 2017 "our ability to predict the effect of the increase in greenhouse-gas concentrations in the atmosphere is very limited" (Tollefsone, 2017)

obstacle to the proposal of a more urgent measures of mitigation for the climate warming.

Another indispensable tool to gain an accurate and deep understanding on the present and future climate is the study of past climate changes through palaeoclimatology and stratigraphy. The rich geochemical and palaeontological documentation preserved in sedimentary strata has revealed that Earth's climate has a complex history of repeated variations. The Quaternary Period – the interval spanning the last ~2.6 million years (Ma) – is the most accessible time interval with a very prominent climate variability.

2. Short narrative of Quaternary climate

Quaternary Period (International Commission of Stratigraphy - ICS, http://www.stratigraphy.org/index.php/ics-chart-timescale), including Pleistocene (2.588-0.0117 Ma) and Holocene (0.0117 Ma-recent) Epochs, is what we informally refer to as 'ice-ages'. This interval was indeed characterized by repeated expansions and contractions of large Northern Hemisphere ice-sheets (e.g. Berger et al., 1984; Hodell and Channell, 2016) (Fig. 1). The terms 'glacial' and 'interglacial' emphasize the ice-volume changes and the consequent variations of sea-levels linked to the sequestration and release of water from large continental ice-sheets (Lang and Wolff, 2011).

More than fifty Glacial-Interglacial (G-IG) cycles punctuate the history of Quaternary looking like a wavy signal superimposed on progressively cooling temperatures (e.g. Zachos et al., 2001) (Fig. 1).

During the Early Pleistocene (2.58-0.78 Ma) the G-IG cyclicity was paced by the change of the Earth's axial tilt (obliquity), at a rhythm of 40,000 years ('41-ky world': Ruddiman et al., 1989; Imbrie et al., 1992; Tiedemann et al., 1994; Clark et al., 2006; Elderfield et al., 2012). Conversely, the dominant G-IG period in the Middle and Late Pleistocene was of ~100,000 years ('100-ky world': Ruddiman et al., 1986; Zachos et al., 2001). The change from the 41-ky to the 100-ky world occurred progressively between 1.4 and 0.4 Ma and has been called by the earlier authors 'Mid-Pleistocene Revolution' (e.g. Berger and Jansen 1994; Maslin and Ridgwell, 2005) or 'Mid-Pleistocene Transition'

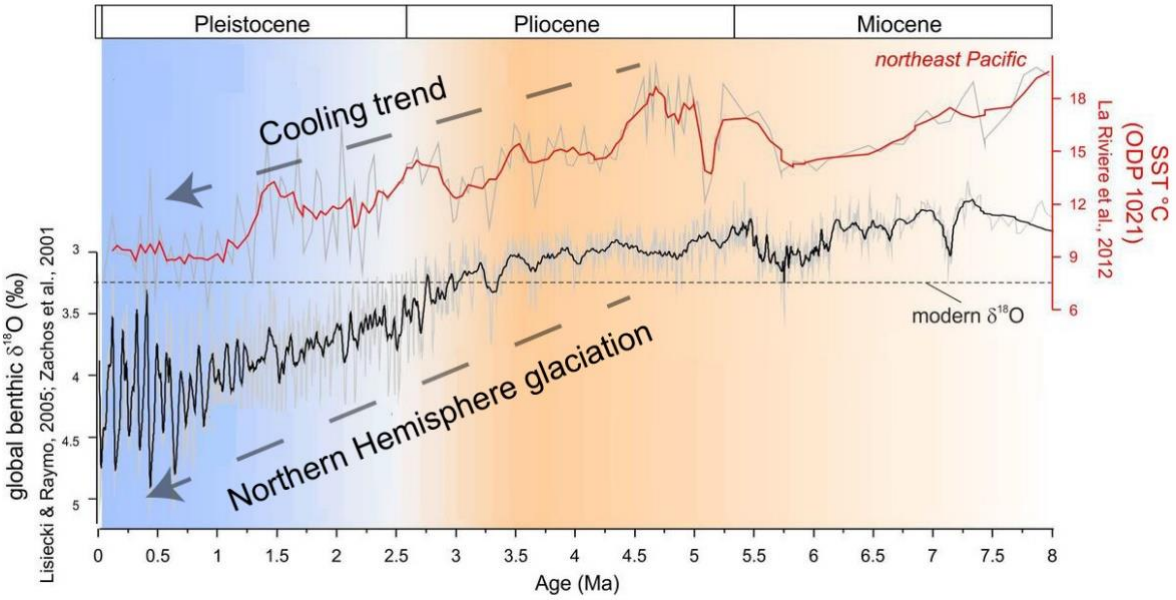

Fig. 1 – Sea-surface temperatures record from ODP Site 1021 in northeast Pacific and global benthic $\delta^{18}O$ record (modified after Zachos et al., 2001; Lisiecki and Raymo 2005; La Riviere et al., 2012) for the last 8 Ma. Note that $\delta^{18}O$ can be regarded as an indicator of the global ice volume for the Quaternary.

(e.g. Mudelsee and Schulz, 1997; Raymo et al., 1997; Clark et al., 2006; McClymont et al., 2013) (Fig. 2). Today, however, we more appropriately refer to it as 'Early-Middle Pleistocene Transition' (EMPT), because since the base of the Pleistocene was lowered from 1.8 to 2.58 Ma (Gibbard and Head, 2010; Gibbard et al., 2010) the midpoint of this transition does not longer fall in the middle part of the Pleistocene (Head and Gibbard, 2015a).

The causes of the EMPT are still debated by scientists (Pena et al., 2014). What is certain, however, is that the 100-ky problem cannot be solved in terms of changes of the Earth's orbital parameters, i.e. the so-called Milankovitch forcing. This raises a need to have a much clearer picture of the past climate changes, which can certainly be reached by studying high resolution stratigraphic records.

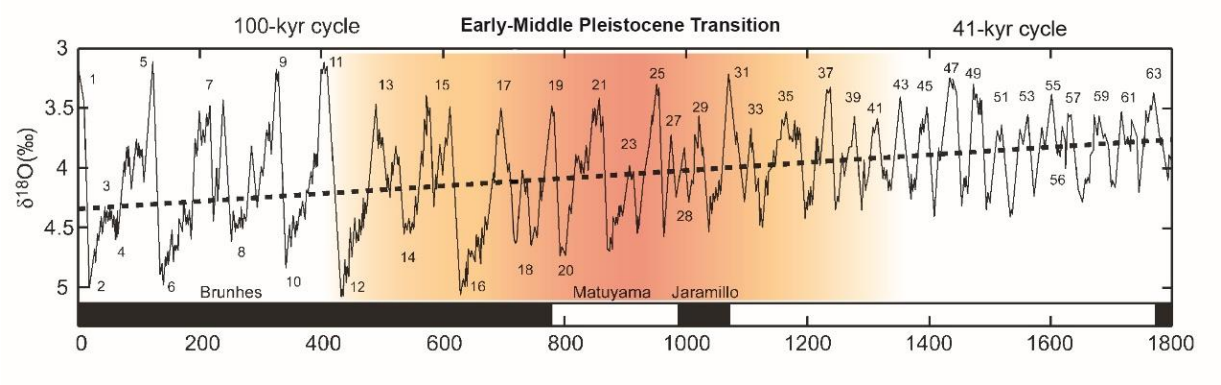

Fig. 2 – Global reference oxygen isotope record for the last 1.8 Ma, obtained combining 57 globally distributed benthic marine $\delta^{18}O$ records (after Lisiecki and Raymo 2005) and palaeomagnetic time scale. Note the long-term cooling (dotted line) and the timing of the Early-Middle Pleistocene Transition (colored bar). Modified after Walker and Lowe (2007).

3. Is there an equivalent of the current climate in the Quaternary?

Quaternary palaeoclimatology, in addition to refining the prediction of the past climate cycles, also deals with an issue of finding the best analogue of the present warm period. The interglacial we are currently experiencing is called Holocene and started about 11,700 years before present (Walker et al., 2009).

The Last Interglacial (LIG), dating back to 130-115 ka (NEEM community members, 2013), has long been considered a benchmark period for the Holocene, because it is the most accessible interglacial period prior to the present one. It includes the 'Eemian' in northwest Europe pollen records, and marine isotope stage (MIS[2]) 5e in the marine isotope stratigraphy (Shackleton et al. 2003). Being the LIG characterized by a pronounced summer warming of the Arctic and reduction in ice sheets with consequent

[2] 'Marine isotope stages' are used to characterize the global climate history and are defined on the base of the $^{18}O/^{16}O$ isotopic ratio measured in marine carbonates. According to this subdivision, interglacials are designed with odd-numbered isotope stages while glacials are designed with even-numbered isotope stages; the numbering scheme starts from the Holocene which is MIS 1 (Bassinot, 2007 and references therein).

sea-level rise, it has been considered crucial to understanding the climate response to the strong greenhouse gasses emissions during the present industrial-era (e.g. Kukla et al., 1997; Bintanja et al., 2005; McKay et al., 2011).

Loutre and Berger (2000, 2003) listed numerous arguments against this analogy, stressing that the LIG has an enormously bigger amplitude of insolation change compared to the Holocene. These authors stated that a better analogue should be found in the interval between 405–340 ka, including interglacial MIS 11, as it shows an insolation change pattern very similar to that predicted for the recent past and the near future of the Earth. However, the alignment Holocene-MIS 11 reveals some ambiguities especially in the trajectory of deglaciations (Ruddiman et al., 2007; Rohling et al., 2010, Tzedakis, 2010).

Using computer simulations, Yin and Berger (2012, 2015) drew an analogy between the Holocene and MIS 19, an interglacial between 790 and 760 ka. The two intervals, in fact, share a very similar insolation distribution pattern and climate response. Such a suggested similarity is currently seeking attention, as showed by the numerous scientific papers – published or in preparation – on this matter. If confirmed by further investigations, such a discovery could have major implications upon predictability of the Earth's climate for the next centuries. An essential tool to investigate MIS 19 is an in-depth study of the past sedimentary successions.

4. The Mediterranean perspective: a key to solve complex climate issues

Southern Europe – and in particularly the Mediterranean – is affected by major center of actions of the global atmosphere and ocean circulation, e.g. the Azores High, the South Asian Monsoon and the Siberian high-pressure system (Lionello et al., 2006). At the geological time-scale, this region has been proved to be very sensible to short-term climate changes produced in relatively remote areas, ranging from the polar North Atlantic to the sub-tropics. Especially during glacial periods, southern Europe experienced abrupt cool and dry phases associated to both polar and equatorial perturbations,

such as disruptions of the Atlantic Meridional Overturning Circulation (AMOC) and southward displacements of the Intertropical Convergence Zone (ITCZ) (e.g. Cacho et al., 1999; Sánchez Goñi et al., 2000; Combourieu-Nebout et al., 2002; Chiang and Bitz, 2005; Tzedakis et al., 2009).

The Mediterranean is also a privileged area for the study of long-term climate changes, especially across the EMPT. In this interval, in fact, floral and faunal records show significant responses to climate-driven environmental changes (Head and Gibbard, 2015b). Southern Europe sites distributed in Spain, France and Italy show significant regional reorganization in the small and large mammal communities (Magri and Palombo, 2013). A major faunal turnover occurred between the 'late-Villafranchian' and the 'Galerian' mammal ages, marked by the arrival of faunas from Asia and Africa (e.g. Azzaroli et al., 1988). This faunal renewal was, however, progressive as the Villafranchian assemblages were not completely replaced by 'modern' taxa until ~0.5 Ma (Palombo et al., 2005; Marra et al., 2014). In the plant communities, the interval of the EMPT was characterized by the progressive disappearance of many warm temperate taxa, leading to an overall loss of floristic diversity (Magri and Palombo, 2013). *Liquidambar*, *Carya* and *Pterocarya*, for example, diminished their abundance from the Early to the Middle Pleistocene, (Suc et al., 1995; Bertini, 2003, 2010; Magri and Palombo, 2013). Other trees which were dominant in the late Early Pleistocene, such as *Tsuga* and *Cedrus*, disappeared or diminished entering the Middle Pleistocene. For some of them (e.g. *Tsuga* according to Bertini, 2003; 2010) an increased summer aridity would have been fatal. Some of these taxa now live in regions relatively in eastern Europe, such as *Liquidambar* (Turkey) and *Pterocarya* (Causacus), while others are currently distributed in more distant regions, as for example *Tsuga*, *Carya* (north America and southwest Asia), *Cathaya* and *Engelhardia* (southwest Asia). The enhanced severity of glacial phases across the EMPT seems to have also determined the change in the composition of the *Artemisia*-steppes. Between 2.6 and 1 Ma, indeed, such steppes included thermophilous elements (like Cistaceae and *Phlomis fruticosa*), while after 1 Ma they contained more cool-tolerant taxa, such as Cupressaceae and *Hippophae rhamnoides*, thus indicating a lowering in temperature (Suc et al., 1995; Bertini, 2003, 2010; Suc and Popescu, 2005).

4.1. A palynological guidance to explore the EMPT history

Since vegetal micro-remains and algal organisms are generally conspicuous and well preserved in most marine and continental deposits, their relative abundances values can be used as palaeovegetation proxies[3], useful to obtain high-resolution climate and oceanographic records across subsequent G-IG phases. Over the last 10 years, more and more Mediterranean successions have been targets of palynological and micropaleontological surveys aimed to delve deeply into the mechanisms of biological response to the Quaternary climate changes, including the EMPT (e.g. Bertini, 2000; Okuda et al., 2002; Rossi, 2003; Capraro et al., 2005, 2017; Tzedakis et al., 2006; Joannin, 2008, 2011; Girone et al., 2013; Marino et al., 2015; Bertini et al., 2015, Toti, 2015; Sánchez Goñi et al., 2016; Oliveira et al., 2016).

In the present thesis, we present the results of palynological (pollen and dinocysts) analyses performed in two Mediterranean sedimentary successions encompassing the EMPT (Fig. 3). Such a documentation integrates already existing palynological datasets with the aim to reconstruct the vegetation and oceanographic variability over this crucial interval as well as to illustrate a very detailed climate, ecological and environmental history. Palynological analyses were performed on the interval MIS 22-MIS 17, which ranges approximately between 890 and 650 thousand years ago (ka).

We devoted a special attention to MIS 19, captured in both the successions. This interval was first analyzed along the exposed marine succession of Montalbano Jonico (MJ), South Italy. Italian Peninsula only offers two other palynological sites with detailed registrations of MIS 19, i.e. the relatively close Valle di Manche (VdM, South Italy: Capraro et al., 2005, 2017) and Pianico-Sellere (North Italy: Rossi, 2003). A parallel record of MIS 19 was also obtained from the succession of core 976, recovered in the Alboran Sea (Western Mediterranean) in the leg 161 of the Ocean Drilling Program (ODP). Interestingly, this site is not far from the Integrated Ocean Drilling

[3] So-called proxies are variables used to reconstruct the past climate history. The term proxy refers to measurable descriptors which stands for desired variables that are not directly observable (Fischer and Wefer, 1999). All the climate quantifications for periods prior to the advent of meteorological instruments are made by proxies.

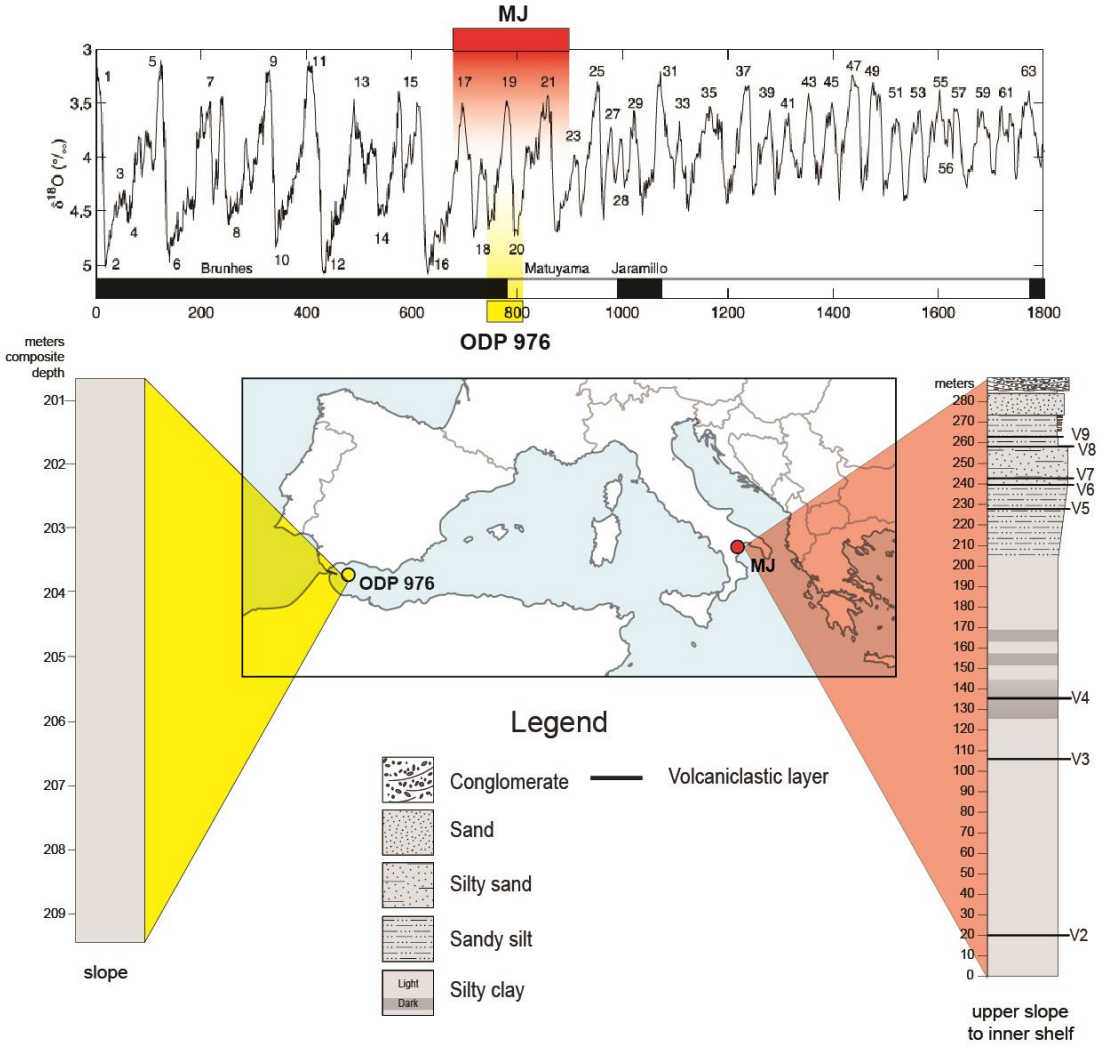

Fig. 3 - Location and lithological logs of the sites investigated in the thesis. The stratigraphical interval covered by each succession is also displayed as colour bands positioned on the global benthic $\delta^{18}O$ record (Lisiecki and Raymo, 2005)

Programm (IODP) Site U1385, in the Iberian Margin, where Sánchez-Goñi (2016) carried out significant investigations on a coeval interval. The new palynological data collected from MJ and ODP Site 976 are thus fundamental to illustrate the climate response of the Mediterranean ecosystems during MIS 19.

4.2. Tracking Mediterranean scenarios across the Early-Middle Pleistocene

The palynological record from MJ and ODP Site 976 spans at least three climate cycles from MIS 22 to MIS 17. This new dataset enables us to give a complement to the rather incomplete mosaic of the Italian and Iberian floral distribution in the Pleistocene.

The new palynological records, assisted by their respective oxygen isotope data, provide an opportunity to reconstruct the mode and tempo of vegetation (pollen) and surface marine environments (dinocysts) response to changes associated with the onset of the 100-ky G/I cyclicity. Moreover, past ecological signals are the base to accomplish a more ambitious objective: the identification of the most favorable times and conditions for the migration and subsequent colonization of the genus *Homo*, from Africa to Eurasia, a process that took place within EMPT

The land/sea registrations are also considerably meaningful in the analysis of the causes of short-lived and abrupt events embedded in periods of (apparent) glacial and interglacial stability. The duration and amplitude of rapid climate oscillations are crucial matters of debate, especially in the context of present global warming. The high-resolution analyses carried out at the two Mediterranean sites accordingly meet this need, as such high-frequency climate fluctuations pose a real risk to the future climate contexts.

This work finally approaches an issue of an accurate biostratigraphical monitoring, that will indubitably contribute to the enhancement of the stratigraphical research in the Mediterranean. This region is, in fact, the cradle of a large number of Global Boundary Stratotype Section and Point (GSSP) of the Neogene and Quaternary Stages/Ages (Fig. 4), including Eraclea Minoa Section, Sicily, Italy (Zanclean Stage), Punta Piccola Section, Sicily, Italy (Piacenzian Stage), Monte San Nicola Section, Sicily, Italy (Gelasian Stage), Vrica Section, Italy (Calabrian Stage) (https://engineering.purdue.edu/Stratigraphy/gssp/).

A very active area of research is currently focused on the definition of the GSSP of the Middle Pleistocene subSeries/subEpoch, corresponding to the "Ionian" Stage/Age. The assignation of this GSSP will be disputed among three candidates, including the MJ section (Head and Gibbard, 2015a). The new

palynological data will improve the correlation potential at the MJ section by means of an accurate selection of climatostratigraphic constrains.

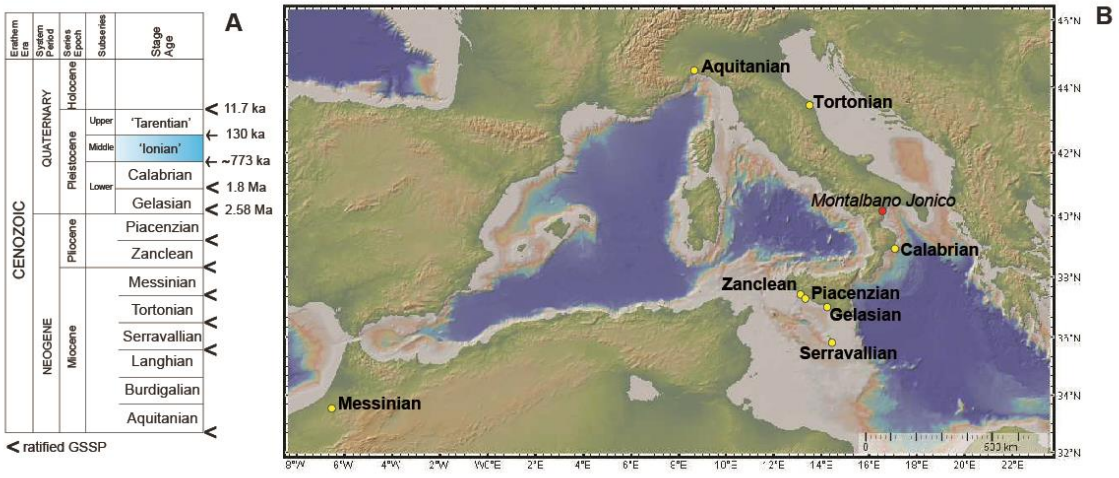

Fig. 4 - A: Chronostratigraphy of Quaternary and Neogene System/Period; B: Map of the Mediterranean showing the location of the Montalbano Jonico section (red) and ratified Neogene and Pleistocene GSSPs (yellow) (Modified after Marino et al., 2017)

References

Abram, N.J., McGregor, H.V., Tierney, J.E., Evans, M.N., McKay, N.P., Kaufman, D.S., The PAGES 2k Consortium, 2016. Early onset of industrial-era warming across the oceans and continents. Nature 536, 411-418.

Azzaroli, A., De Giuli, C., Ficcarelli, G., Torre, D., 1988. Late Pliocene to Early Mid-Pleistocene mammals in Eurasia: Faunal succession and dispersal events. Palaeogeography Palaeoclimatology Palaeoecology 66, 77-100.

Bassinot, F.C. 2007. Oxygen isotope stratigraphy of the oceans. In: Elias, A.S., editor. Encyclopedia of Quaternary Science. Elsevier Ltd., Vol. 18. pp. 1740–1748.

Berger, A., Imbrie, J., Hays, J., Kukla, G., Saltzman, B., (Eds.) 1984. Milankovitch and climate. Understanding the response to orbital forcing, vol 126, NATO ASI series C. Reidel, Dordrecht, 895 pp.

Berger, W.H., Jansen, E., 1994. Mid-Pleistocene climate shift: The Nansen connection. In: Johannessen, O.M., Muench R.D., Overland, J.E. (Eds.). The Polar Oceans and Their Role in Shaping the Global Environment, AGU, Washington, D.C., pp. 295-311

Bertini, A., 2000. Pollen record from Colle Curti and Cesi: Early and Middle Pleistocene mammal sites in the Umbro-Marchean Apennine mountains (central Italy). Journal of Quaternary Science 15(8), 825-840.

Bertini, A., 2003. Early to Middle Pleistocene changes of the Italian flora and vegetation in the light of a chronostratigraphic framework. Il Quaternario (Italian Journal of Quaternary Sciences) 16(1bis), 19-36.

Bertini, A., 2010. Pliocene to Pleistocene palynoflora and vegetation in Italy: state of the art. Quaternary International 225(1), 5-24.

Bertini, A., Toti, F., Marino, M., Ciaranfi, N., 2015. Vegetation and climate across the Early-Middle Pleistocene transition at the Montalbano Jonico section (southern Italy). Quaternary International, 383, 74-88.

Bintanja, R., van deWal, R.S.W., Oerlemans, J., 2005. Modelled atmospheric temperatures and global sea levels over the past million years. Nature 437, 125-128.

Cacho, I., Grimalt, J.O., Pelejero, C., Canals, M., Sierro, F.J., Flores, J.A., Shackleton, N.J., 1999. Dansgaard–Oeschger and Heinrich event imprints in the Alboran Sea paleotemperatures. Paleoceanography 14, 698–705.

Capraro, L., Asioli, A., Backman, J., Bertoldi, R., Channell, J.E.T., Massari, F., Rio., D., 2005. Climatic patterns revealed by pollen and oxygen isotope records across the Matuyama-Brunhes Boundary in the central Mediterranean (southern Italy). In: Head, M.J., Gibbard, P.L. (Eds.), Early-Middle Pleistocene Transitions: The Land-Ocean Evidence. Geological Society London, Special Publications 247, pp. 159-182.

Capraro, L., Ferretti, P., Macrì, P., Scarponi, D., Tateo, F., Fornaciari, E., Bellini, G., Dalan, G., 2017. The Valle di Manche section (Calabria, Southern Italy): A high resolution record of the Early-Middle

Pleistocene transition (MIS 21-MIS 19) in the Central Mediterranean. Quaternary Science Reviews, 165, 31-48.

Chiang, J.C.H., Bitz, C.M., 2005. Influence of high latitude ice cover on the marine Intertropical Convergence Zone. Climate Dynamics 25, 477–496.

Clark, P.U., Archer, D., Pollard, D., Blum, J.D., Rial, J.A., Brovkin, V., Mix, A.C., Pisias, N.G., Roy, M., 2006. The middle Pleistocene transition: characteristics, mechanisms, and implication for long-term changes in atmospheric pCO_2. Quaternary Science Reviews 25, 3150-3184.

Combourieu Nebout, N., Turon, J.-L., Zahn, R., Capotondi, L., Londeix, L., Pahnke, K., 2002. Enhanced aridity and atmospheric high-pressure stability over the western Mediterranean during the North Atlantic cold events of the past 50 k.y. Geology 30, 863–866.

Cowtan, K., Hausfather, Z., Hawkins, E., Jacobs, P., Mann, M.E., Miller, S.K., Steinman, B.A., Stolpe, M.B., Way, R.G., 2015. Robust comparison of climate models with observations using blended land air and ocean sea surface temperatures. Geophysical Research Letters 42 (15) 6526-6534.

Elderfield, H., Ferretti, P., Greaves, M., Crowhurst, S., McCave, I.N., Hodell, D., Piotrowski, A.M., 2012. Evolution of ocean temperature and ice volume through the mid-Pleistocene climate transition. Science 337, 704-709.

Fischer, G., Wefer, G., (Eds.) 1999. Use of Proxies in Paleoceanography: Examples from the South Atlantic. Springer-Verlag Berlin Heidelberg, 735 pp.

Gibbard, P.L., Head, M.J., 2010. The newly-ratified definition of the Quaternary System/Period and redefinition of the Pleistocene Series/Epoch, and comparison of proposals advanced prior to formal ratification. Episodes 33, 152-158.

Gibbard, P.L., Head, M.J., Walker, M.J.C., The Subcommission on Quaternary Stratigraphy, 2010. Formal ratification of the Quaternary System/Period and the Pleistocene Series/Epoch with a base at 2.58 Ma. Journal of Quaternary Science 25(2), 96-102.

Girone, A., Maiorano, P., Marino, M., Kucera, M., 2013. Calcareous plankton response to orbital and millennial-scale climate changes across the Middle Pleistocene in the western Mediterranean. Palaeogeography, Palaeoclimatology, Palaeoecology 392, 105-116.

Head, M.J., Gibbard, P.L., 2015a. Formal subdivision of the Quaternary System/Period: Past, present, and future. Quaternary International 383.

Head, M.J., Gibbard, P.J., 2015b. Early-Middle Pleistocene transitions: linking terrestrial and marine realms. Quaternary International 389, 7-46.

Hodell, D. A., Channell, J., 2016. Mode transitions in Northern Hemisphere glaciation: co-evolution of millennial and orbital variability in Quaternary climate. Climate of the Past 12,1805-1828.

Imbrie, J., Boyle, E.A., Clemens, S., Duffy, A., Howard, W., Kukla, G., Kutzbach, J., Martinson, D.G., McIntyre, A., Mix, A.C., Molfino, B., Morley, J.J., Peterson, L.C., Pisias, N.G., Prell, W.L., Raymo, M.E., Shackleton, N.J., Toggweiler, J.R., 1992. On the structure and origin of major glaciation cycles 1. Linear responses to Milankovitch forcing. Paleoceanography 7, 701-738.

IPCC, 2013. Climate Change 2013: The Physical Science Basis. Contribution of Working Group I to the Fifth Assessment Report of the Intergovernmental Panel on Climate Change. In: Stocker, T.F., Qin, D., Plattner, G.-K., et al. Cambridge and New York: Cambridge University Press, 1535 pp.

Joannin S., Bassinot F., Combourieu Nebout N., Peyron O., Beaudouin C., 2011. Vegetation response to obliquity and precession forcing during the Mid-Pleistocene Transition in Western Mediterranean region (ODP site 976). Quaternary Science Reviews 30, 280-297.

Joannin, S., Ciaranfi, N., Stefanelli, S., 2008. Vegetation changes during the late Early Pleistocene at Montalbano Jonico (Province of Matera, Southern Italy) based on pollen analysis. Palaeogeography, Palaeoclimatology, Palaeoecology 270, 92-101.

Karl, T.R., Trenberth, K.E. 2003. Modern global climate change. Science 302, 1719-1723.

Knutti, R., and Sedláček, J., 2013. Robustness and uncertainties in the new CMIP5 climate model projections. Nature Climate Change 3, 369-373.

Kukla, G., McManus, J.F., Rousseau, D.D., Chuine, I., 1997. How long and how stable was the last interglacial? Quaternary Science Reviews 16, 605-612.

La Riviere, J.P., Ravelo, A.C., Crimmins, A., Dekens, P.S., Ford, H.L., Lyle, M., Wara, M.W., 2012. Late Miocene decoupling of oceanic warmth and atmospheric carbon dioxide forcing. Nature 486, 97-100.

Lang, N., Wolff, E.W., 2011. Interglacial and glacial variability from the last 800 ka in marine, ice and terrestrial archives. Climate of the Past 7, 361-380.

Lionello, P., Malanotte-Rizzoli, P., Boscolo, R. (Eds.) 2006. Mediterranean Climate Variability. Elsevier, 438 pp.

Lisiecki, L.E., Raymo, M.E., 2005. A Pliocene-Pleistocene stack of 57 globally distributed benthic $\delta^{18}O$ records. Paleoceanography 20, 1003.

Loutre, M. F., Berger, A., 2000. Future climatic changes: Are we entering an exceptionally long interglacial?. Climate Change 46(1-2), 61-90.

Loutre, M.F., Berger, A., 2003. Marine Isotope Stage 11 as an analogue for the present interglacial. Global and Planetary Change 36, 209-217.

Magri, D., Palombo, M.R., 2013. Early to Middle Pleistocene dynamics of plant and mammal communities in South West Europe. Quaternary International 288, 63-72.

Maiorano, P., Bertini, A., Capolongo, D., Eramo, G., Gallicchio, S., Girone, A., Pinto, D., Toti, F., Ventruti, G., Marino, M., 2016. Climate signatures through the Marine Isotope Stage 19 in the Montalbano Jonico section (Southern Italy): a land-sea perspective. Palaeogeography, Palaeoclimatology, Palaeoecology, 461, 341–361.

Marcott, S.A., Shakun, J.D., Clark, P.U., Mix, A.C., 2013. A reconstruction of regional and global temperature for the past 11,300 years. Science 339,1198-1201.

Marino M., Ciaranfi N., Girone A., Maiorano P., Gallicchio S., Bassinot F., Nomade S., Simon Q., Bourlès D.L., Dewilde F., Blamart D., Scao V., Bertini A., Toti F., Petrosino P., Isguder G., Pereira A., 2017. Formal proposal for the Global Boundary Stratotype Section and Point (GSSP) of the Middle Pleistocene SubSeries/SubEpoch and Ionian Stage/Age in the Montalbano Jonico section.18pp.

Marino, M., Aiello, G., Barra, D., Bertini, A., Gallicchio, S., Girone, A., La Perna, R., Lirer, F., Maiorano, P., Petrosino, P., Quivelli, O., Toti, F., Ciaranfi, N., 2016. The Montalbano Jonico section (South Italy) as a reference for the Early/Middle Pleistocene boundary. Alpine and Mediterranean Quaternary 29 (1), 45–57.

Marino, M., Bertini, A., Ciaranfi, N., Aiello, G., Barra, D., Gallicchio, S., Girone, A., La Perna, R., Lirer, F., Maiorano, P., Petrosino, P., Toti, F., 2015. Paleoenvironmental and climatostratigraphic insights for Marine

Isotope Stage 19 (Pleistocene) at the Montalbano Jonico section, South Italy. Quaternary International, 383, 104-115.

Marra, F., Pandolfi, L., Petronio, C., Di Stefano, G., Gaeta, M., Salari, L., 2014. Reassessing the sedimentary deposits and vertebrate assemblages from Ponte Galeria area (Rome, central Italy): an archive for the Middle Pleistocene faunas of Europe. Earth-Science Reviews 139, 104-122.

Maslin, M.A., Ridgewell, A., 2005. Mid-Pleistocene Revolution and the Eccentricity Myth. Special Publication of the Geological Society of London 247, 19-34.

McClymont, E., Sodian, S., Rosell-Mele, A., Rosenthal, Y., 2013. Pleistocene sea-surface temperature evolution: early cooling, delayed glacial intensification, and implications for the mid-Pleistocene climate transition. Earth-Science Reviews 123, 173-193.

McKay, N.P., Overpeck, J.T., Otto-Bliesner, B.L., 2011. The role of ocean thermal expansion in Last Interglacial sea level rise. Geophysical Research Letters 38, L14605.

Mudelsee, M., Schulz, M., 1997. The Mid-Pleistocene climate transition: onset of 100 ka cycle lags ice volume build-up by 280 ka. Earth and Planetary Science Letters 151, 117-123.

NEEM community members, 2013. Eemian interglacial reconstructed from a Greenland folded ice core. Nature 493, 489-494.

Okuda, M., Van Vugt, N., Nakagawa, T., Ikeya, M., Hayashida, A., Yasuda, Y. and Setoguchi, T., 2002. Palynological evidence for the astronomical origin of lignite-detritus sequence in the Middle Pleistocene Marathousa Member, Megalopolis, SW Greece. Earth and Planetary Science Letters, 201, 143-157.

Oliveira, D., Desprat, S., Rodrigues, T., Naughton, F., Hodell, D., Trigo, R., Rufino, M., Lopes, C., Abrantes, F., Sánchez-Goñi, M.F., 2016. The complexity of millennialscale variability in southwestern Europe during MIS 11. Quaternary Research 86, 373-387.

Palombo, M.R., Raia, P., Giovinazzo, C., 2005. Early-Middle Pleistocene structural changes in mammalian communities from the Italian peninsula. In: Head, M.J., Gibbard, P.L. (Eds.), Early-Middle Pleistocene Transitions: The Land-Ocean Evidence, Special Publications, 247. Geological Society, London, pp. 251-262.

Pena, L.D., Goldstein, S.L., 2014. Thermohaline circulation crisis and impacts during the mid-Pleistocene transition. Science, 345, 318-322.

Raymo, M.E., Oppo, D.W., Curry, W., 1997. The mid-Pleistocene climate transition: a deep sea carbon isotopic perspective. Paleoceanography 12, 546-559.

Rohling, E.J., Braun, K., Grant, K., Kucera, M., Roberts, A.P., Siddall, M., Trommer, G., 2010. Comparison between Holocene and marine isotope stage-11 sea-level histories. Earth and Planetary Science Letters 291, 97-105.

Rossi, S., 2003. Etude pollinique de la sequence lacustre Pleistocene de Piànico-Sèllere (Italie). Ph.D. thesis, Université de Droit, d'Economie et des Sciences d'Aix Marseille III, France.

Ruddiman, W. F., Raymo, M., McIntyre, A., 1986. Matuyama 41,000-year cycles: North Atlantic Ocean and northern hemisphere ice sheets. Earth and Planetary Science Letters 80, 117-129.

Ruddiman, W.F., 2007. The early anthropogenic hypothesis: Challenges and responses. Reviews Geophysics 45(4), RG4001.

Ruddiman, W.F., Raymo, M.E., Martinson, D.G., Clement, B.M., Backman, J., 1989. Pleistocene evolution: Northern hemisphere ice sheets and north Atlantic ocean. Paleoceanography 4(4), 353-412.

Sánchez Goñi, M.F., Turon, J.L., Eynaud, F., Gendreau, S., 2000. European climatic response to millennial-scale changes in the atmosphere-ocean system during the Last Glacial Period, Quaternary Research 54, 394–403.

Sánchez-Goñi, M.F., Rodrigues, T., Hodell, D.A., Polanco-Martínez, J.M., Alonso-García, M., Hernández-Almeida, I., Desprat, S., Ferretti, P., 2016. Tropically-driven climate shifts in southwestern Europe during MIS 19, a low eccentricity interglacial. Earth Planetary Science Letters 448, 81-93

Shackleton, N.J., Sánchez Goñi, M.F., Pailler, D., Lancelot, Y., 2003. Marine Isotope substage 5e and the Eemian Interglacial. Global and Planetary Change 757, 1-5.

Suc, J.-P., Bertini, A., Combourieu Nebout, N., Diniz, F., Leroy, S., Russo-Ermolli, E., Zheng, Z., Bessais, E., Ferrier, J., 1995. Structure of West Mediterranean vegetation and climate since 5.3 Ma. Acta Zoological

Cracoviense, 38(1), 3-16.
Suc, J.-P., Popescu S.-M., 2005. Pollen records and climate cycles in the North Mediterranean region since 2.7 Ma. Geological Society of London, Special Publications 247, 147–158.
Tiedemann, R., Sarnthein, M., Shackleton, N.J. 1994. Astronomic timescale for the Pliocene Atlantic ~180 and dust flux records of Ocean Drilling Program Site 659. Paleoceanography 9, 619-638.
Tollefson, J., 2017. Trump nominee backs Paris climate agreement and questions Iran nuclear deal. Nature News. doi:10.1038/nature.2017.21291
Toti, F., 2015. Interglacial vegetation patterns at the Early-Middle Pleistocene transition: a point of view from Montalbano Jonico section (southern Italy). Alpine and Mediterranean Quaternary, 28(2), 131-143.
Tzedakis, P.C., 2010. The MIS 11-MIS 1 analogy, southern European vegetation, atmospheric methane and the "early anthropogenic hypothesis". Climate of the Past 6, 131-144.
Tzedakis, P.C., Hooghiemstra, H., Pälike, H., 2006. The last 1.35 million years at Tenaghi Philippon: revised chronostratigraphy and long-term vegetation trends. Quaternary Science Reviews 25, 3416-3430.
Tzedakis, P.C., Pälike, H., Roucoux, K.H., de Abreu, L., 2009. Atmospheric methane, southern European vegetation and low–mid latitude links on orbital and millennial timescales. Earth and Planetary Science Letters 277, 307–317.
Walker, M., Johnsen, S., Rasmussen, S.O., Steffensen, J.P., Popp, T., Gibbard, P., Hoek, W., Lowe, J., Bjorck, S., Cwynar, L., Hughen, K., Kershaw, P., Kromer, B., Litt, T., Lowe, D.J., Nakagawa, T., Newnham, R., Schwander, J., 2009. Formal definition and dating of the GSSP (Global Stratotype Section and Point) for the base of the Holocene using the Greenland NGRIP ice core and selected auxiliary records. Journal of Quaternary Science 24, 3-17.
Walker, M., Lowe, J., 2007. Quaternary science 2007: a 50-year retrospective. Journal of the Geological Society 164, 1073-1092.
Yin Q.Z., Berger, A., 2015. Interglacial analogues of the Holocene and its natural near future. Quaternary Science Reviews 120, 28-46.

Yin, Q.Z., Berger, A., 2012. Individual contribution of insolation and CO_2 to the interglacial climates of the past 800,000 years. Climate Dynamics 38, 709-724.

Zachos, J., Pagani, M., Sloan, L., Thomas, E., Billups, K., 2001. Trends, rhythms, and aberrations in global climate 65 Ma to present. Science 292, 686-693.

SECTION A

Palynological contribution to the study of the Early–Middle Pleistocene transition in the central Mediterranean: the Montalbano Jonico section (Southern Italy) between MIS 22 and MIS 17

1. Introduction

Southern Italy is an area of great relevance to the study of the Early and Middle Pleistocene climate, due to the presence of numerous stratigraphic archives containing terrestrial and marine proxies, such as pollen, vertebrate remains, mollusks, foraminifera, nannoplankton and stable isotopes (e.g. Bertini et al., 2010 and references therein). 'Crotone Series', including the Vrica section in Calabria Region (Fig. A1), is to date the most investigated Early Pleistocene succession after the numerous studies used to draw up the formal proposal to establish the GSSP of the Calabrian Stage (Cita et al., 2012). In the recent years, other two South Italian sections have been intensively studied for their adequacy to represent the basal boundary of the Middle Pleistocene (or "Ionian" Stage): the Montalbano Jonico (MJs) and the Valle di Manche section (VdMs) (Ciaranfi and D'Alessandro, 2005; Capraro et al., 2005, 2015, 2017; Marino et al., 2015). The MJs is especially relevant for its ~600-kyr long (1240-645 ka), virtually continuous isotope and marine biostratigraphic documentation (Ciaranfi et al., 2010) which is source of valuable palaeoclimate information during the entire EMPT. At this site, until the last few years, palynological investigations documenting terrestrial palaeovegetation and palaeoclimate only involved the 1,250-900 ka interval (MIS 37-23; Joannin et al., 2008).

2. General setting and chronostratigraphy of the Montalbano Jonico section

The succession of Montalbano Jonico crops out in Basilicata (Southern Italy) at 40°17'N 16°34'E (292 m above the sea level) and is composed of a 450 m-thick muddy clayey to muddy sandy deposits of upper slope to inner shelf

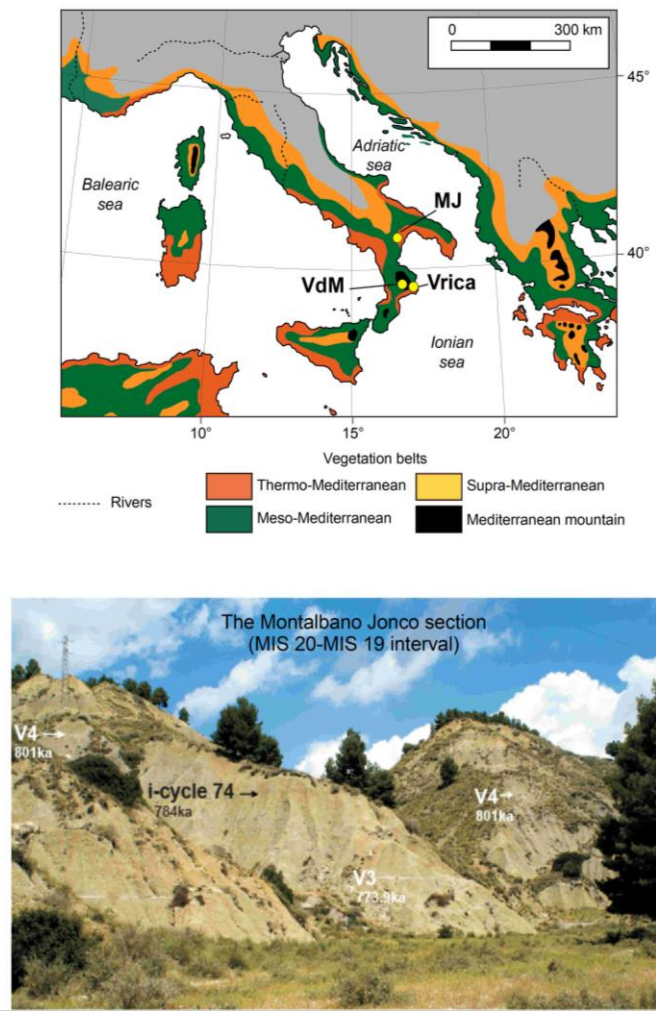

Fig. A1 - Upper panel: location of the cited pollen sites and distribution of Mediterranean-climate zones (modified after Quézel & Médail, 2003). Lower panel: Picture of the Montalbano Jonico 'Intervallo B' sub-section and main chronostratigraphic constrains through MIS 20 and MIS 19 (modified after Marino et al., 2015, 2016).

setting (D'Alessandro et al., 2003; Stefanelli, 2003). Such deposits are interbedded to nine volcaniclastic layers (V1-V9) and several dark horizons (including sapropels) which constrain the chronostratigraphic setting of the section (Ciaranfi et al., 2010; Marino et al., 2015; Simon et al., 2017) (Fig. A1). The MJs represents the Early-Middle Pleistocene filling of the southern

Apennine foredeep (Ciaranfi et al., 1996, 2005, 2010; D'Alessandro et al., 2003; Maiorano et al., 2004, 2010) and encompasses the MIS 37 to 17 interval (Maiorano et al., 2010). The succession can be seen as the missing (upper) interval needed by the nearby Vrica/Crotone section to cover the entire Calabrian Stage (Maiorano et al., 2010). To date, the MJs is under consideration for the Middle Pleistocene GSSP together with the VdMs and the Ciba Section in Japan (Head & Gibbard, 2015).

3. Aims

In order to document the history of vegetation and climate change in southern Italy during the upper part of the EMPT, in this thesis:

1. We carried out analyses on pollen and spores to extend the MJ record up to cover the interval from 900 to 650 ka (MIS 22-17);
2. We focused on the sedimentary portion crucial for the definition of the Early-Middle Pleistocene boundary, which is recommended to be 'close' to the Mathuyama-Brunhes polarity reversal (Head et al., 2008), at the beginning of MIS 19;
3. For the latter interval, dinocysts analyses were also performed to envisage the palaeoceanographic context, revealed by the calcareous plankton, ostracods, otholiths, benthic micro- and macro-invertebrates records as well (Girone & Varola, 2001; Stefanelli, 2003, 2004; D'Alessandro et al., 2003; Aiello et al., 2015; Marino et al., 2015, 2016; Maiorano et al., 2016).

4. Materials and methods

Quantitative pollen analyses were carried out on a total of 141 samples between 0 and 257.5 m of the 'Intervallo B' sub-section (Fig. A2). The author of this thesis carried out quantitative pollen analyses on most of the samples between 67.7 m and the top of the succession, in addition to quantitative dinocysts analyses in the interval between 116.9 and 176.13 m; below 67.7 m, thirty-two samples were analyzed by M. Vannacci (2016).

Pollen and dinocysts relative abundances were plotted in diagrams to describe the main vegetation and oceanographic changes attendant on the glacial-interglacial pattern, in turn expressed by the oxygen isotope record. The main vegetation patterns are displayed by the variation of selected taxa or taxa groups.

5. Results

More than 130 pollen taxa were identified, revealing a diversified arboreal and non-arboreal flora in the region surrounding MJ. The mesothermic arboreal taxa are mainly represented by deciduous *Quercus*, *Fagus* and Betulaceae (*Corylus*, *Carpinus* spp. and *Ostrya*). Abundant microthermic conifers like *Cedrus*, *Tsuga*, *Abies*, *Picea* suggest the development of high-altitude forests. Significant amounts of *Pinus* were always detected. The analyses also revealed a low but significant presence of taxa currently disappeared from the Italian Peninsula, such as *Carya*, *Pterocarya* and *Tsuga*, in addition to *Zelkova* which survives in a relict population in Sicily. Mediterranean elements include evergreen *Quercus*, *Olea* and *Pistacia*. Herbs and grasses represent a large portion of the assemblage; they are dominated by Poaceae, Asteraceae (mainly Cichorioideae), Polygonaceae, Cyperaceae as well as indicators of steppic and salty environments including *Artemisia*, *Ephedra* and Amaranthaceae. Percentages of the main pollen taxa are plotted against stratigraphic height in Fig. A2.

The increase of mesophilous arboreal and Mediterranean taxa depicts phases of relative climate amelioration (higher precipitation and temperatures), appearing with the names of local rivers and highlighted by colour bands (Fig. A3). Maximum afforestation phases correspond to the climatic optima of the interglacial complexes MIS 21, 19 and 17 (dark-red bands). The pattern of the non-arboreal pollen (NAP), especially of steppic and semi-desert elements (e.g. *Artemisia*, *Ephedra*, Amaranthaceae, …), varies in opposition with the previous taxa and depicts increases of continental aridity. Maximum peaks of these taxa are recorded during MIS 22, latest MIS 20 and latest MIS 18. The major vegetation changes are significantly in phase with the main variations of the $\delta^{18}O$ curve. The evidence of distinct rapid

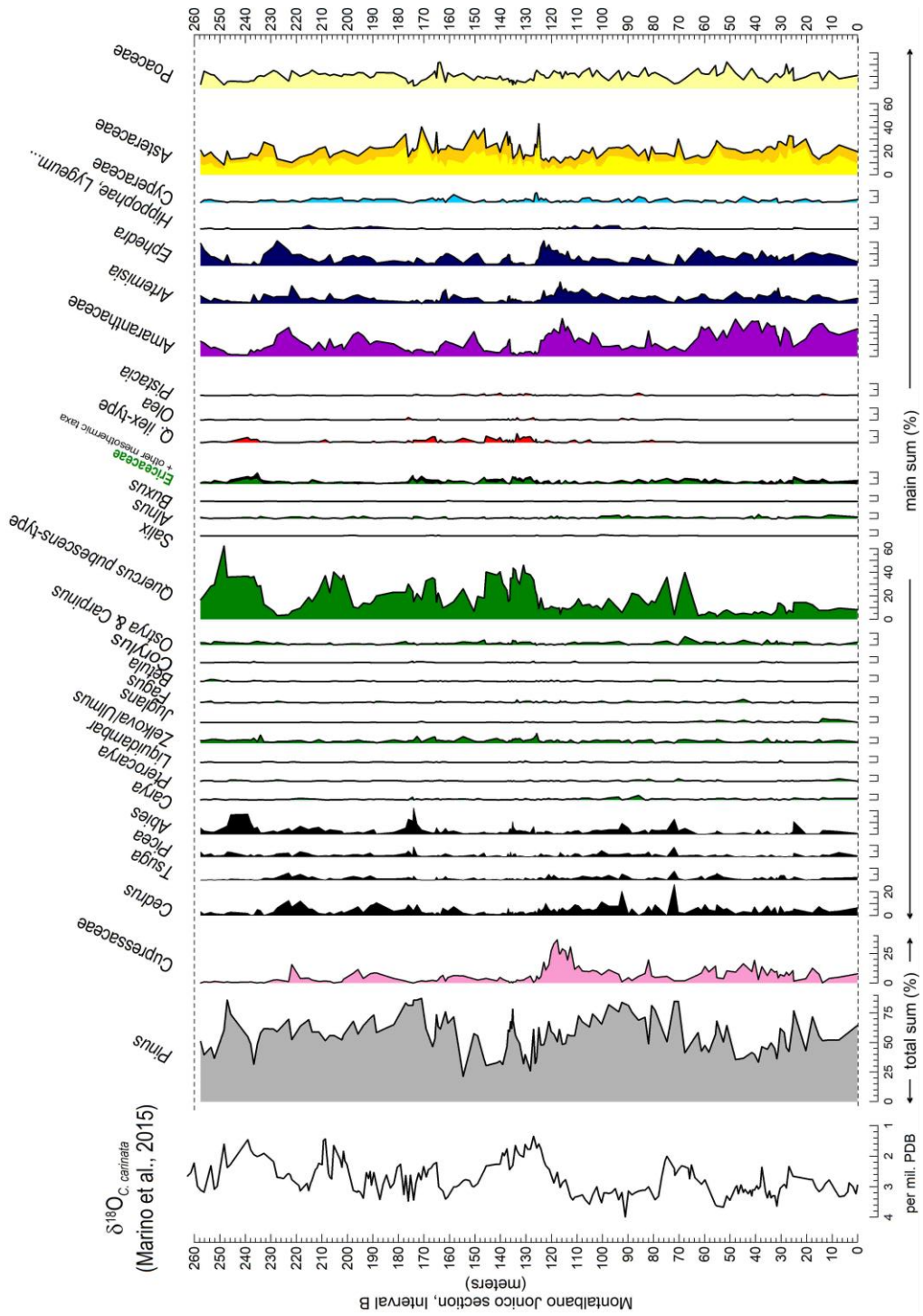

Fig. A2 - Main taxa percentage along stratigraphic height of the Montalbano Jonico section, 'Interval B'. Data collected by F. Toti, A. Bertini and M. Vannacci (after Marino et al., 2015, Bertini et al., 2015, Toti, 2015; Vannacci, 2016).

events in both glacials and interglacials attests the sensitivity of the pollen site to the millennial-scale climate variability. Finally, pollen-inferred climate phases are consistent with the sea-surface changes described by the marine proxies, showing the impact of climate change in the air-sea system.

6. Main advances in the knowledge of the EMPT

The palynological study of the MJs allowed the following goals to be accomplished:

- A description of the palaeoflora in the area of Montalbano Jonico during the EMPT. The woodland appears already depleted of several mega-mesothermic and thermophilous elements commonly detected in Southern Italy during the Pliocene and Early Pleistocene. Nonetheless, a consistent number of taxa today disappeared from Italy are still present, including *Tsuga*, *Cedrus* and *Carya*.
- A description of the tempo and amplitude of the main phases of forest expansion, favored by the global interglacial conditions within MIS 21, 19 and 17. The study of the phase relationships between pollen and benthic $\delta^{18}O$ record is a critical information for the understanding of the timing between the onset of the deglaciation and the establishment of truly interglacial climate in Southern Europe.
- A description of the flora during the (cold-) arid periods, associated to glacial stages 22, 20 and 18. The structure of these phases appears particularly complex when considering the occurrence of short-lived episodes marked by relatively humid conditions. The most emblematic ones are those occurring during MIS 18 ('Cavone' and 'Sinni') which suggest the temporary re-establishment of 'interglacial' climate conditions before the onset of MIS 17.
- The response of regional vegetation to rapid cold-dry phases during MIS 20 and MIS 19b-a, correlated to coeval episodes of cooling and iceberg discharge in the North Atlantic.

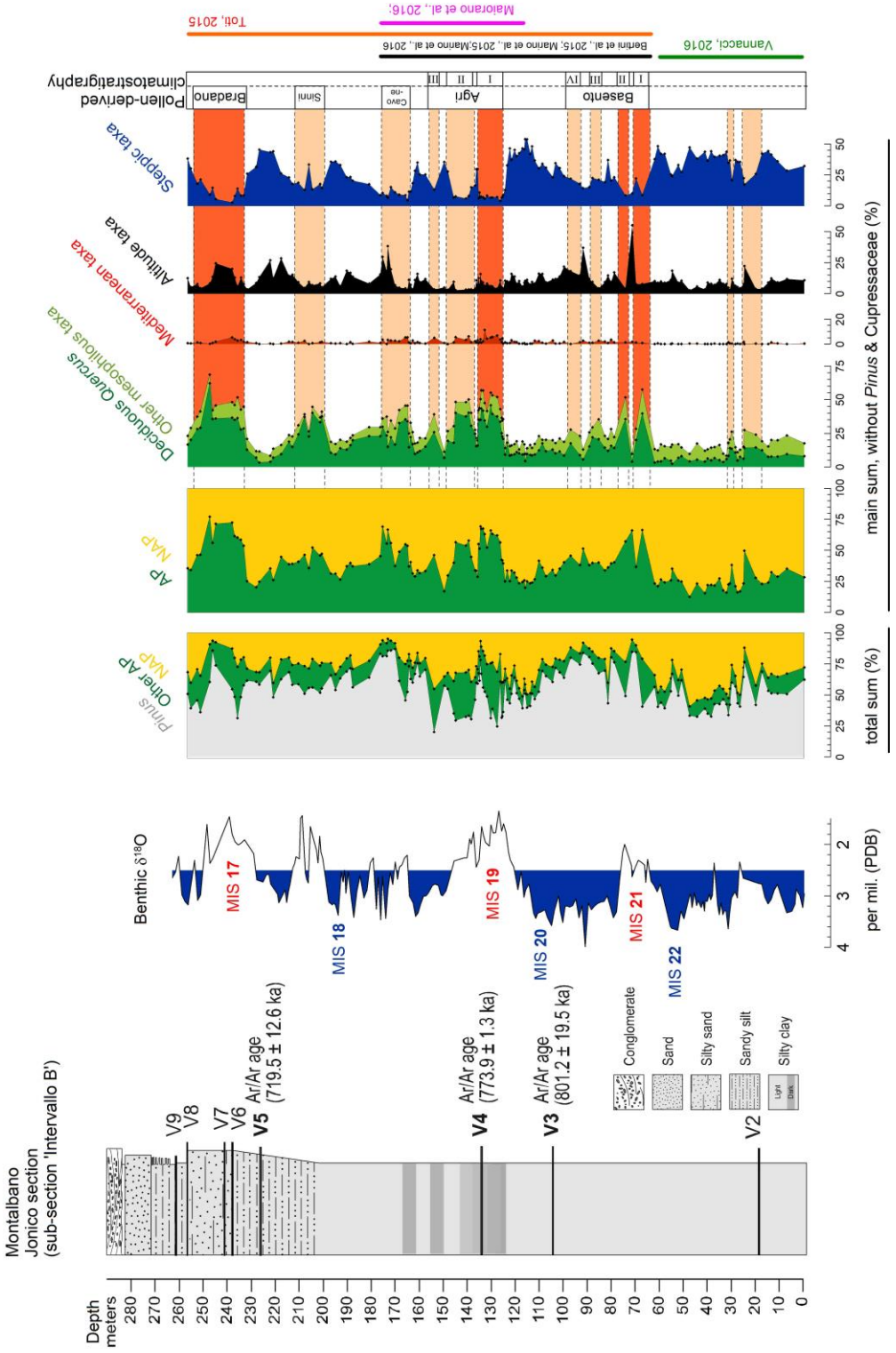

Fig. A3 – Lithology, stratigraphical features and summary pollen diagrams in the Montalbano Jonico 'Intervallo B' sub-section. AP: Arboreal pollen; NAP: Non-Arboreal pollen.

7. Implications for the Early-Middle Pleistocene GSSP

The pollen and dinocysts registration across latest MIS 20 and MIS 19 contributed to defining a solid stratigraphic framework for the proposal of the Early-Middle Pleistocene boundary. The identified pollen events served indeed as stratigraphic markers for the correlation of the succession worldwide. One event deserves to be singled out and corresponds to substage 19b. It is marked by an abrupt cooling after the full-interglacial of MIS 19 and approximates the position of the tephra V4. This layer was proposed to host the 'golden spike' of the Early-Middle Pleistocene (Marino et al., 2017) due to the vicinity to the Matuyama-Brunhes boundary inferred on the base of the 10Be record (Simon et al., 2017).

The inferred vegetation and climate reconstructions summarized above are illustrated in detail in the published papers by Bertini et al. (2015), Marino et al. (2015, 2016, 2017), Toti (2015), Maiorano et al. (2016) and contained in this Section:

- **Toti, F.**, 2015. Interglacial vegetation patterns at the Early-Middle Pleistocene transition: a point of view from Montalbano Jonico section (southern Italy). Alpine and Mediterranean Quaternary, 28(2), 131-143.

- Bertini, A., **Toti, F.**, Marino, M., Ciaranfi, N., 2015. Vegetation and climate across the Early-Middle Pleistocene transition at the Montalbano Jonico section (southern Italy). Quaternary International, 383, 74-88.

- Marino, M., Bertini, A., Ciaranfi, N., Aiello, G., Barra, D., Gallicchio, S., Girone, A., La Perna, R., Lirer, F., Maiorano, P., Petrosino, P., **Toti, F.**, 2015. Paleoenvironmental and climatostratigraphic insights for Marine Isotope Stage 19 (Pleistocene) at the Montalbano Jonico section, South Italy. Quaternary International, 383, 104-115.

- Maiorano, P., Bertini, A., Capolongo, D., Eramo, G., Gallicchio, S., Girone, A., Pinto, D., **Toti, F.**, Ventruti, G., Marino, M., 2016. Climate

signatures through the Marine Isotope Stage 19 in the Montalbano Jonico section (Southern Italy): a land-sea perspective. Palaeogeography, Palaeoclimatology, Palaeoecology, 461, 341–361.

- Marino, M., Aiello, G., Barra, D., Bertini, A., Gallicchio, S., Girone, A., La Perna, R., Lirer, F., Maiorano, P., Petrosino, P., Quivelli, O., **Toti, F.**, Ciaranfi, N., 2016. The Montalbano Jonico section (South Italy) as a reference for the Early/Middle Pleistocene boundary. Alpine and Mediterranean Quaternary 29 (1), 45–57.

- Marino, M., Ciaranfi, N., Girone, A., Maiorano, P., Gallicchio, S., Bassinot, F., Nomade, S., Simon, Q., Bourlès, D.L., Dewilde, F., Blamart, D., Scao, V., Bertini, A., **Toti, F.**, Petrosino, P., Isguder, G., Pereira, A., 2017. Formal proposal for the Global Boundary Stratotype Section and Point (GSSP) of the Middle Pleistocene SubSeries/SubEpoch and Ionian Stage/Age in the Montalbano Jonico section. 18 pp.

Contribution A1

Interglacial vegetation patterns at the Early-Middle Pleistocene transition: a point of view from the Montalbano Jonico section (southern Italy)*

*Published in Alpine and Mediterranean Quaternary 28(2), 131-143 (**F. Toti**, 2015)

Abstract

The Montalbano Jonico succession (southern Italy) represents a rich stratigraphic archive of the Early to Middle Pleistocene environmental and climatic changes in the central Mediterranean. Pollen analyses associated to multivariate statistical methods (principal component and cluster analyses) have been carried out in the sedimentary portion including Marine Isotope Stages (MIS) 21 to 17 (~200 kyrs and ~190 m). The pollen ratio between mesotherm and steppic taxa (Pollen Temperature Index), used as a proxy of temperature, permits to precise consecutive warmer and cooler phases associated, respectively, to interglacials/interstadials and glacials/stadials (sub-stages 21.3 to 18.3 plus stage 17). Pollen data suggest major expansions of mixed oak forests during warm phases, whereas open vegetation typically marks cool to cold phases. The statistical processing puts in evidence both analogies and differences among the successive interglacials/interstadials. Mid- to high-altitude trees and Mediterranean taxa appear to expand slower than hydrophytes plus deciduous oaks and other herbs, which conversely act like pioneers. Moreover *Tsuga*, *Cedrus* plus steppic plants and Poaceae are inversely related to Mediterranean xerophytes and mesotherm deciduous taxa, possibly due to the different tolerance to temperature decreases. On this basis, three main vegetation patterns seem to occur during warm periods. The 1st pattern (including MIS 21.3, 19.3 and 17) shows a tripartite structure with a middle warm phase including higher abundances of slow-spreading taxa, sandwiched between cooler intervals (at the beginning and the end of the sub-stage) with the increase of faster-expanding taxa. The 2nd pattern (in MIS 21.1 and 19.1) shows a complex structure characterized by rapid changes in proportions between fast- and slow-spreading taxa as well as among plants with different tolerance to temperature decrease. The 3rd pattern (in two interstadials within MIS 18), is characterized by relatively high abundances of fast-spreading taxa and low abundances of warmth-demanding taxa. This

work represents a first attempt for a better understanding of interglacial vegetation dynamics during the Early-Middle Pleistocene Transition; deeper investigations are in progress with the specific aim to better characterize the observed multiple patterns and possibly to define their causes.

Keywords: Early-Middle Pleistocene Transition, interglacials, MIS 19, Montalbano Jonico, southern Italy, principal component analysis, pollen analysis.

1. Introduction

During the transition between Early and Middle Pleistocene (EMPT, 1.2-0.5 ka; e.g. Head & Gibbard, 2005; Maslin & Ridgwell, 2005), Earth's climate experienced a gradual change in the Glacial-Interglacial (G-I) oscillations mode. The orbital obliquity-driven 41 kyrs cyclicity, which had dominated the earlier part of the Pleistocene, was overshadowed by a high-amplitude, lower-frequency 100 kyrs-rhythm. A profound impact on terrestrial and marine biota is recorded across the EMPT as a result of changes in the intensity and duration of both glacials and interglacials (e.g. Head et al., 2008). In the Italian pollen and calcareous nannoplankton records a major shift seems to coincide with the Marine Isotope Stages (MIS) 25 to 20, at the end of the Jaramillo sub-chron, where several turnovers in the nannofossil communities and the progressive disappearance of the most thermophilous pollen taxa occurred (Bertini et al., 2010 and references therein). On the other hand, no remarkable events have been recorded at the Calabrian-Ionian transition (e.g. Head & Gibbard, 2005; Bertini et al., 2015). Quaternary European and Mediterranean pollen records display recurrent patterns of vegetation succession paralleling G-I cyclicity. In Italy, four main patterns have been summarized on the basis of latitudinal, geomorphological and local factors by Bertini (2010). Pattern 1, is expressed by open vegetation-thermophilous forest alternations especially in Mediterranean littoral zones (e.g. Suc et al., 1995). Pattern 2, which is typical of several Northern Apennines sites, exhibits prevalent alternations between altitudinal coniferous and thermophilous forests (e.g. Bertini 2001 and references therein). Patterns 3 and 4 show the

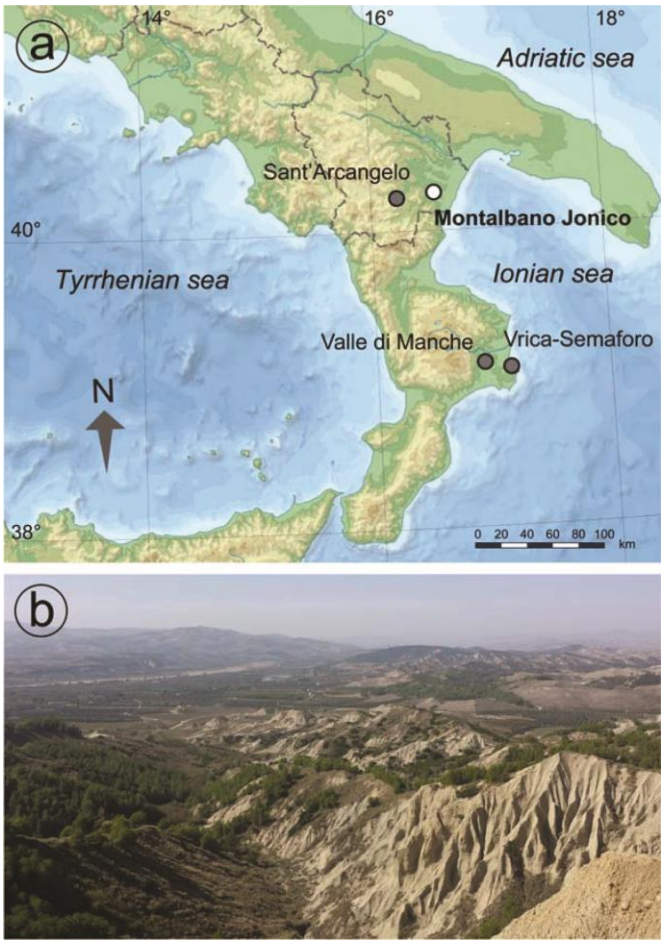

Fig. 1 - (a) Location of Montalbano Jonico and the main sites of southern Italy cited in the text. (b) View of the Montalbano Jonico succession in the "Calanchi" badlands area, with the Agri Valley in the background.

presence of thermophilous and coniferous forest, respectively, during glacials, and open vegetation and steppe, respectively, during interglacials (e.g. Bertoldi et al., 1989; Capraro et al., 2005). The interglacial structure, its duration and intensity, as well the seasonality, strongly depend on the Earth orbital geometry, which is a major factor of climate forcing (e.g. Hays et al., 1976; Berger, 1981; 1988). According to many authors, the vegetation succession of each interglacial is "unique" because of the peculiar combination of its astro-climatic variables (e.g. Watts, 1988; Bartlein & Prentice, 1989;

Huntley & Webb, 1989). Moreover, even where some interglacials exhibit virtually identical orbital configurations, the occurrence of stochastic factors (e.g. relationships among taxa and/or between taxa and climate) can make the system unpredictable (e.g. Bennett et al., 1991; Tzedakis et al., 2012a). At the same time, the existence of interglacials characterized by very different climate conditions but showing similar vegetation patterns cannot be excluded (Tzedakis & Bennett, 1995); in this case, internal biotic forcings should be invoked.

One of the longest composite Quaternary pollen record, including subsequent interglacials since the base of the Gelasian, has been reconstructed by the study of both marine and continental successions of southern Italy (Fig. 1) (e.g. Combourieu-Nebout et al., 1990; Combourieu Nebout and Vergnaud Grazzini, 1991; Combourieu-Nebout, 1993; Capraro et al., 2005; Klotz et al., 2006; Joannin et al., 2008; Russo Ermolli et al., 2010a, b, 2014; Suc et al., 2010; Amato et al., 2014; Petrosino et al., 2014; Robustelli et al., 2014; Bertini et al., 2015; Marino et al., 2015). The knowledge of past interglacials is particularly significant not only because it allows the documentation of ancient paleoenvironments but also for its key role in modeling the natural course of the present interglacial (Holocene), permitting predictions about the future climate changes. For this study a selected portion of the Montalbano Jonico (MJ) section, spanning the MIS 21-16, has been submitted to detailed palynological analyses which have strongly improved those recently produced in Bertini et al. (2015), and extend the previous pollen documentation concerning MIS 37-23 (Joannin et al., 2008).

The main purpose of this paper is to recognize similarities and differences in the vegetation dynamics between subsequent warm periods (either interstadials or interglacials), assuming that each one is marked by a peculiar astronomical and vegetation signature. To achieve this aim, warmer phases have been singled out and compared using a multivariate statistical approach. The significance of the MJ pollen record is enhanced by the possibility to exclude the presence of consistent stratigraphic gaps thanks to the strong stratigraphical frame established for this marine section (e.g. Marino et al., 2015 and references therein).

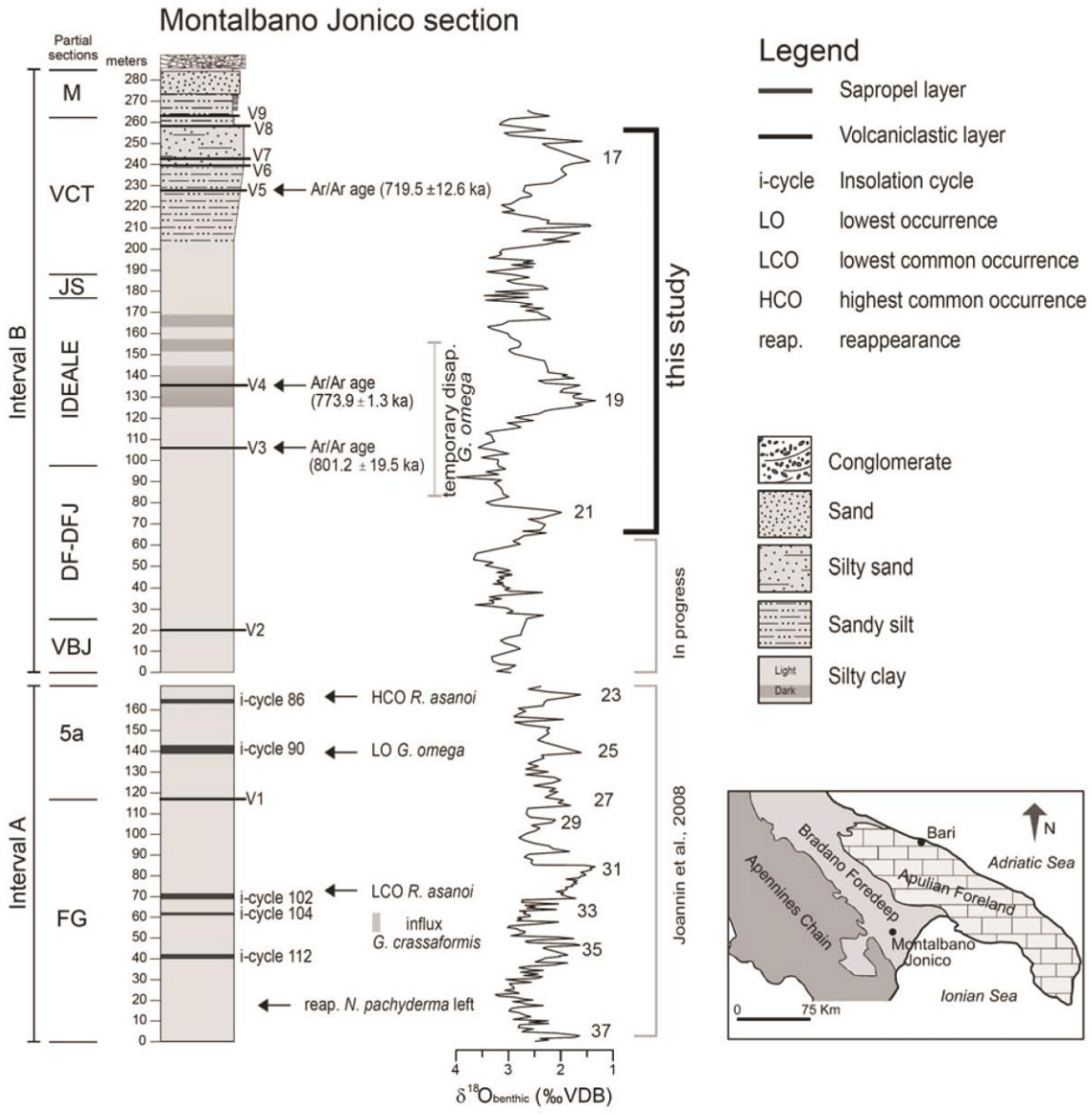

Fig. 2 – Lithostratigraphy and benthic $\delta^{18}O$ record of the Montalbano Jonico composite section (Brilli et al., 2000; Ciaranfi et al., 2010; Maiorano et al., 2010; Marino et al., 2015); the age of volcaniclastic layer V4 is after Petrosino et al. (2015); the studied portion is indicated on the right. (Modified from Bertini et al., 2015).

2. Case study: the Montalbano Jonico section

2.1. Geological and stratigraphical setting

MJ composite succession is located in the Basilicata region (southern Italy), near the eponymous village, at 40°17'N 16°34'E (292 m above the sea level). Its deposition occurred within the Bradanic foredeep, a perisutural basin bounded westward by the Apennine orogenic front and eastward by the Murge highlands. The MJ succession covers more than 630 kyrs (Lower to Middle Pleistocene; Ciaranfi et al., 2010) and has been reconstructed sewing up 10 sub-sections (Ciaranfi et al., 1997; 2001). The succession is divided in two distinct portions by a stratigraphic gap (Fig. 2). The lower portion ("Interval A") consists of ~180 m thick muddy turbidites including a volcaniclastic layer (V1). Benthic paleocommunities assign "Interval A" to an upper-slope environment involved in a prevalent shallowing upward trend (D'Alessandro et al., 2003; Stefanelli, 2004). The upper portion ("Interval B") is more than 300 m thick and includes silty sands and silty clays in which eight volcaniclastic layers (V2-V9) are embedded; repeated deepening-shallowing cycles, from outer to inner shelf environment, have been recognised (D'Alessandro et al., 2003; Stefanelli, 2004) (Fig. 2). Bathymetric changes have been firstly related to the north-eastward thrusting of the southern Apennines units (Ciaranfi et al., 1996; D'Alessandro et al., 2003), and secondly to the orbital-scale G-I ciclicity and climate-driven eustatic variations, in the frame of the progressive Plio-Pleistocene cooling (e.g. Joannin et al., 2008; Ciaranfi et al., 2010).

Based on the most recent radiometric datings ($^{39}Ar/^{40}Ar$) on V1-V5 tephra layers (Petrosino et al., 2015) and the constrains provided by the calcareous plankton (Maiorano et al., 2004), sapropel (Stefanelli et al., 2005) and isotopic (Brilli et al., 2000) stratigraphy, Marino et al. (2015) have proposed the age-model shown in Fig. 2, closely related to the astronomical tuning of the section by Ciaranfi et al. (2010). Correlations with LR04 benthic stack (Lisiecki and Raymo, 2005), Pacific (Mix et al., 1995a,b; Shackleton et al., 1995) and Atlantic (Bickert et al., 1997) $\delta^{18}O$ benthic records allow the isotopic shifts related to MIS 22-16 to be outlined (Ciaranfi et al., 2010; Marino et al., 2015).

According to the calcareous plankton-inferred relative chronology (Maiorano et al., 2004), "Interval B" extends from the top of *Pseudoemiliania lacunosa* Zone to the base of *Emiliania huxleyi* Zone of Rio et al. (1990) (Fig. 2). Two nannofossil events are recorded: the beginning (826.89 ka) and the end (771.04 ka) of the second temporary disappearance of *Gephyrocapsa omega* (Maiorano et al., 2004). Although no sapropels occur within the "Interval B" (Stefanelli et al., 2005), three bands with higher organic carbon content are visible (Fig. 2): the oldest one encloses V4 tephra (773.9 ± 1.3 ka, Petrosino et al., 2015), the second and last one are located below and above the end of the second temporary disappearance of *Gephyrocapsa omega*.

The present work is based on the study of eighty-three palynological samples from the 67.7 m (858 ka, MIS 21)-257.5 m (656.05 ka, MIS 16) portion of "Interval B" (Fig. 2), this generating a mean time resolution of ~2463 years. However this result is based on highly uneven values throughout the succession, ranging from 60 years to more than 14 kyrs.

2.2. Present climate and vegetation

The MJ section lies between the Metapontine Jonian coast, to the south-east, and the Agri valley, to the north-west. The latter is part of a wider hydrographic basin including all the Apennines rivers with drainage towards the Taranto gulf (Fig. 1). The Agri valley is bordered northward by reliefs ranging from ~1700 to ~2000 m. 50 km southwest of MJ, the Pollino massif, with several peaks over 2000 m, separates Basilicata from Calabria region. The Agri valley approximates the intersection between three climatic zones: the coastal Metapontine area, characterized by a meso-Mediterranean regime, the eastern hinterlands, with semi-continental climatic features, and the western mountain area, with rainfalls well distributed throughout the year and strong thermal and humidity gradients depending on orography.

The MJ section is embedded in the evocative badlands landscape, molded by the erosion of Plio-Pleistocene marine clays. The vegetation cover is firstly influenced by edaphic factors, being the substrate the result of sediment weathering (Di Pietro et al., 2004). Halo-xerophytic components, such as *Camphorosma monspeliaca*, *Lygeum spartum* and *Mantisalca duriaei*, colonize

the steepest slopes, enriched by *Sulla coronata* when slopes are weaker. Terophytes grow in more sandy and detritic soils (Fascetti et al., 2001). Amaranthaceae (i.e. *Camphorosma*, *Atriplex*, *Suaeda*) occupy flat and more humid zones at the base of the slopes. In weakly steep areas, poorly affected by erosion processes, terophytic Fabaceae (including *Hedysarium* and *Scorpiurus*) dominate the floristic assemblage, with sporadic ingressions of *Plantago afra*. On flat to sub-flat surfaces, some patchy Mediterranean maquis occurs; here *Pistacia lentiscus* dominates in association with *Rubia peregrina*, *Phillyrea latifolia*, *Juniperus oxycedrus*, *Asparagus acutifolius* and *Helictotrichon convolutum* (Biondi et al., 1992; Fascetti et al., 2001). The basal horizon of the surrounding relief, which extends from a few meters to 300-400 m, belongs to the olive tree-carob tree alliance (Mediterranean climax), also including holm oak; it is worth noting that the latter is an important component of higher (submontane) belts, forming mid-altitude (up to 800-1000 m) woodlands (Corbetta, 1974). Cypresses and Aleppo pines occur as reforestation elements. SubMediterranean to submontane horizons are marked by the presence of *Quercus pubescens*, commonly with *Fraxinus ornus* (plus *Ostrya carpinifolia*, *Carpinus betulus* and *C. orientalis* in moisture-rich stations), *Pyrus communis*, *Sorbus domestica*, *Crataegus oxyacantha*, *Ligustrum vulgare*, *Spartium junceum*, *Osyris alba*, and sclerophyll taxa such as *Asparagus acutifolius* and *Pistacia terebinthus*. At higher elevations *Quercus pubescens* tends to be replaced by *Q. cerris*, which, together with chestnut woods, characterizes the submontane horizon. Beechwoods and *Abies alba* relict formations punctuate mountain belts, together with *Pteridium aquilinum* brackens. The undergrowth composition varies with the altitude and includes noteworthy taxa such as *Ilex aquifolium*, *Geranium striatum*, and *Stellaria nemonum* (Corbetta, 1974).

3. Methods

3.1. Palynological analyses

Palynological analyses have been performed on samples from the MJ section's "Interval B" ("Ideale", "JS" and "VCT" sub-sections: see Fig. 2) during the first

year of PhD of the author; the pollen study is still in progress in order to increase the resolution in selected intervals. At present, eighty-three sediment samples have been processed using a standard palynological technique, at the Laboratory of Palynology of the Department of Earth Science of the Florence University. Samples have been first weighted before starting the physical-chemical treatment. *Lycopodium* tablets have been added to each sample to estimate palynomorph concentrations. Attacks with acid (HCl and HF), KOH and hexametaphosphate solutions have been followed by enrichments procedures ($ZnCl_2$ and 10μm sieving in ultrasonic bath). Residues have been mounted in slides using glycerol and finally analyzed by optical microscope (using x750 and 1250 magnifications) for quantitative pollen analyses. A mean of 284 pollen grains per sample have been counted, *Pinus* and Cupressaceae excluded. *Pinus*, which is generally over-represented in the marine sediments (Heusser, 1988; Beaudouin et al., 2005), at MJ reaches very high percentage values and for this reason has been excluded from the total pollen sum (see pollen diagram in Fig. 3); for the taphonomic and palaeo-environmental significance of *Pinus* pollen grain, see Bertini et al. (2015) and Marino et al. (2015). Cupressaceae pollen grains have been also removed from the total pollen sum as they exhibit in some levels both very high frequencies and morphologic features which do not support their unequivocal determination.

Pollen data are expressed as percentages normalized to the total pollen sum, excluding *Pinus*, Cupressaceae, indeterminate and indeterminable grains; the summary pollen diagram (Fig. 3) shows eleven selected informal pollen groups established on the basis of climate and ecological requirements of correlative modern taxa, which are: (1) *Cedrus* and *Tsuga*; (2) High-altitude taxa (*Abies* and *Picea* plus *Betula* and *Fagus*); (3) deciduous *Quercus*; (4) Broad-leaved deciduous taxa minus *Quercus*, e.g. *Carpinus*, *Ostrya*, *Alnus*, *Ulmus*, *Zelkova*, *Alnus*, *Carya*, *Pterocarya*, Ericaceae and *Hedera*; (5) Mediterranean sclerophyll taxa, e.g. *Quercus ilex* type, *Olea*, *Pistacia* and Cistaceae; (6) Asteraceae except *Artemisia*; (7) Poaceae; (8) Hydrophytes, principally Cyperaceae and *Sparganium*/*Typha angustifolia* type;(9) Halophytes, e.g. Amaranthaceae, Caryophyllaceae and Plumbaginaceae; (10) Steppic taxa, e.g. *Artemisia* and *Ephedra*; (11) Other non-arboreal plants, e.g. Brassicaceae, Dipsacaceae, *Plantago*, Rosaceae and Saxifragaceae.

Arboreal Pollen (AP) relative abundances have also been plotted (Fig. 3) as

they are expected to reflect the spreading/shrinkage of the woodland in response, respectively, to the increase/decline of the atmospheric humidity. In order to discriminate warm (temperate) from cooler to cold phases, a pollen-derived palaeo-temperature index (Pollen Temperature Index: PTI, Fig. 3; e.g. Joannin et al., 2008, 2011; Bertini et al., 2015) has been used. PTI, which is given by the ratio between mesothermic and steppic taxa, puts in evidence the glacial/stadial (lower values)-interglacial/interstadial (higher values) alternation in the pollen record. We have included deciduous *Quercus*, *Corylus*, *Carpinus*, *Ostrya*, *Alnus*, *Ulmus*, *Zelkova*, *Carya*, *Pterocarya*, *Tilia*, *Hedera* and Ericaceae (just to mention the most abundant) among mesothermic taxa and *Artemiasia*, *Ephedra*, *Lygeum* and *Hippophae* among steppic taxa. A threshold-value of the PTI has been proposed at ~2 to divide warmer by cooler phases, so that they have distinct separations (Fig. 3). The so defined glacial/stadial (PTI < ~2) and interglacial/interstadial (PTI > ~2) phases are in good agreement - in terms of both chronologic position and time extension - with the major shifts in the ä^{18}O curve (e.g. sub-stages 21.3, 21.1, 19.3 and 19.1 after: Marino et al.; 2015) of the same succession.

3.2. Multivariate statistical analyses

Pollen data relative to the samples with a PTI > ~2 (assumed to belong to interglacials/interstadials, as described in Methods), in which the variables are represented by the eleven (1-11) selected informal groups, have been examined through Principal Component Analysis (PCA) using variance-covariance matrix as data input. PCA has been adopted as a tool for transposing the original dataset variability in a lower dimension representation. In this simplified panorama, few principal components are assumed to summarize the associations among correlated variables. Centered log-ratio transformation as proposed by Aitchison (1982) have been carried out to avoid biases deriving from the compositional (constrained) nature of the data. Variability similarities between selected pollen groups have been also evaluated through hierarchical cluster analysis, that has been applied on log-centered variables by using the Euclidean distance as similarity measure and Ward's method as the subsequent linkage algorithm.

4. Results

Palynological analyses point out a rich flora consisting of more than 120 taxa. They are largely herbaceous; among them Asteraceae, Poaceae, Amaranthaceae and *Ephedra* are dominant. *Artemisia* and *Ephedra* show subsequent phases of significant increase, reasonably linked to steppe expansion during (cold/dry) glacial periods at the expenses of forest taxa, Amaranthaceae usually paralleling the steppe taxa trends (Fig. 3).

Among arboreal taxa, *Pinus* pollen grains reach the highest percentage values. *Quercus* is also well represented and its increase has been associated to the expansion of the forest during warm-temperate conditions. Among the other deciduous broad-leaved taxa, *Carpinus betulus*, *C. orientalis*/*Ostrya* type, *Ulmus*, *Zelkova,* etc. follow. Along with *Zelkova,* other taxa which progressively disappears in the course of the Pleistocene, such as *Carya*, *Pterocarya* and *Liquidambar*, are still found in this portion of the MJ section, where *Taxodium* type shows scattered occurrences. *Cedrus* and *Abies* are the most abundant taxa among mid- and high-altitude conifers, respectively.

As a whole the floristic composition at MJ is quite uniform as pointed out and discussed for the MIS 21 to MIS 18 interval by Bertini et al. (2015); in fact neither disappearance nor appearance events have been recorded.

4.1. Vegetation and climatic signature of interglacials and interstadials

The subsequent changes in the arboreal and non-arboreal pollen taxa throughout the MJ succession (858 to 656.05 ka) permit to recognize a clear alternation between forest and open landscapes. They are well expressed especially by the contraposition between steppe plus other non-arboreal taxa and *Quercus* plus other mesophilous taxa (Fig. 3). Based on these vegetation data, it is possible to discriminate between warmer and cooler phases. It is further possible to determine the extension of such zones through the PTI. In fact, as specified in Methods, PTI values higher than ~2 have been assumed to depict warm-temperate conditions associated to interglacials/interstadials

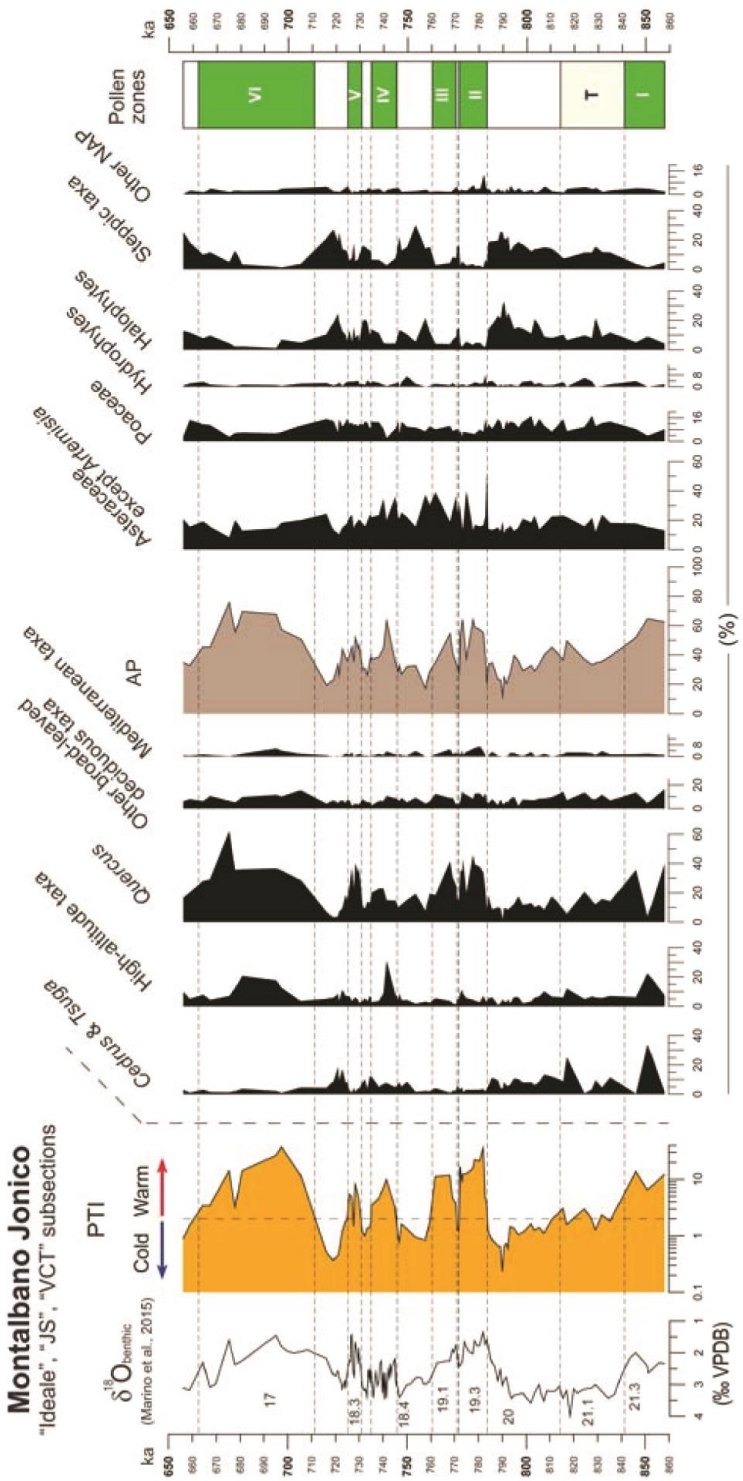

Fig. 3 - Pollen Temperature Index (PTI) and percentage values of selected pollen groups in the MIS 21-17 interval of the Montalbano Jonico section. On the left, the age-model (Marino et al., 2015) and the benthic $\delta^{18}O$ curve (Brilli et al., 2000; Ciaranfi et al., 2010). The horizontal dashed lines define informal pollen zones corresponding to the successive warm periods (i.e. Zones I-VI plus T), as specified in the column on the right. AP: Arboreal Plants.

whereas values lower than ~2 approximate glacials/stadials (Fig. 3). Forty-three samples have been thus included into seven informal "warm" zones: those labeled with roman numbers (I-VI) include samples with PTI stably above 2, whereas that labeled with T (=Transition) includes samples with PTI quickly oscillating between 1.3 and 3 (Fig. 3 and Tab. I). Each zone can be generally correlated with a stage or sub-stage of the marine isotope stratigraphy by considering the astronomical tuning after Marino et al. (2015) and the oxygen isotope stack after Bassinot et al. (1994) (Fig. 3). A short description of the informal zones is provided below.

Zone I - It is described by three pollen samples covering ~12 kyrs. AP percentages are constantly high, even if changes in proportions between mid- to high-altitude trees and mesophilous taxa pollen are recorded. Zone I is consistent with MIS 21.3.

Zone T - AP are in low percentages, with a main fall at 827.5 ka. Both steppic and halophytic taxa reach a peak at 824.5 ka. Short-term variations of *Cedrus* and *Tsuga* diffusely occur. This zone correlates with sub-stage 21.1.

Zone II - Mesophilous arboreal taxa show quite high percentages, decreasing only in correspondence with two short-term events (at 783.5 and 774.8 ka, Bertini et al., 2015) marked by the expansion of Asteraceae due to humidity drops. Mediterranean taxa show a significant abundance at 780.56 ka, predating the acme of *Quercus* and a subsequent increase of high-altitude taxa. This zone correlates with isotopic sub-stage 19.3.

Zone III - The first portion of the interval is marked by a positive excursion of oak and Mediterranean taxa. Afterwards, the other mesophilous taxa plus the mid- to high-elevations trees slightly increase. A correlation of this zone with MIS 19.1 is consistent.

Zone IV - As a whole AP percentage values are similar to those of the previous Zone III (Tab. I). The AP curve shows a peak centered at 741.41 ka. Such an event coincides with an increase in mid- to high-altitude taxa and predates the start of *Quercus* increase at 740.12 ka. The zone extension ranges between 18.4 and 18.3 isotope sub-stages.

Zone V - AP percentages stay quite similar to those of the previous zones. *Quercus* relative abundances rapidly increase between 728.28 and 726.9 ka, with secondary superimposed oscillations well appreciable due to the high time-resolution. A correlation with the 18.3 isotope sub-stage can be

proposed.
Zone VI - It corresponds to MIS 17 and represents the longest interglacial. It is also marked by the highest AP values (a huge shift is located at 675.42 ka). Between 697.31 and 677.96 ka, high-altitude taxa are considerably abundant, whereas *Cedrus* and *Tsuga* show sparse occurrences. Mediterranean taxa peak at 695 ka, while deciduous *Quercus* is involved in a gradual increase up to 680.69 ka, followed by a dramatic rise 5 kyrs after, when high-altitude elements collapse.

4.2. Principal component analysis

Statistical calculations on selected pollen data allow three principal components to be extracted. They are able to take into account for about 69% of the total variance, thus providing a reasonable summary of the information contained in the dataset (Tab. II). The first principal component (PC 1) encloses 30.62% of the total variance and expresses a balance in which hydrophytes, *Quercus*, Poaceae and steppic taxa (with positive loadings) are opposed to *Tsuga* and *Cedrus*, high-altitude taxa and Mediterranean taxa (with negative loadings). PC 1 could reflect the different timing of expansion

Pollen Zone	Age (ka)	Mean PTI	Mean AP %	Marine oxygen isotopic stratigraphy
VI	705.31 - 664.47	14.36	58.44	MIS 17
V	729.91 - 725.81	4.94	43.88	MIS 18.3
IV	745.13 - 734.95	5.65	43.77	MIS 18.4 - MIS 18.3
III	770.74 - 761.82	7.86	41.14	MIS 19.1
II	783.53 - 772.19	15.49	51.22	MIS 19.3
T	835.24 - 815.41	2.15	37.89	MIS 21.1
I	858 - 846	10.86	59.73	MIS 21.3

Tab. I - Montalbano Jonico section: pollen-based zonation for the studied interval, associated with summary vegetation indexes. Correlation with isotopic stages is also shown.

Pollen groups	PC 1	PC 2	PC 3
Tsuga & Cedrus	-0.63	0.506	0.04
High-altitude taxa	-0.407	-0.14	0.45
Quercus	0.29	-0.34	0.1
Deciduous broad-leaved taxa	-0.072	-0.3	0.16
Mediterranean taxa	-0.358	-0.66	-0.45
Poaceae	0.24	0.19	-0.11
Asteraceae except *Artemisia*	-0.02	0.09	-0.023
Hydrophytes	0.76	-0.09	0.13
Halophytes	0.043	0.44	-0.21
Steppic taxa	0.24	0.41	-0.11
Other NAP	-0.094	-0.1	0.03

Tab. II – Montalbano Jonico section: principal component loadings for the first three axes.

exhibited by taxa with positive loadings (faster-expanding taxa) versus negative loadings (slower-expanding taxa). The analysis of vegetation successions in many sites of southern Europe with sufficient moisture availability confirms that non-synchronous taxa expansions occur at the onset of warm-humid periods. Deciduous *Quercus* often expands early, followed by other mesophilous trees, such as *Carpinus* and *Ostrya*, and then by *Abies*, *Fagus* and sometimes *Picea* (Tzedakis, 2007; Brauer et al., 2007). In fact, some water-demanding arboreal taxa can show delays in migration because they require well developed soils, which do not form until several millennia from the beginning of an interglacial; conversely, deciduous oaks can grow on less organic soils (Sadori et al., 2011). Further, we may expect that hydrophytes and other herbaceous taxa react more rapidly to an increase of humidity with respect to arboreal taxa. The second principal component (PC 2) accounts for

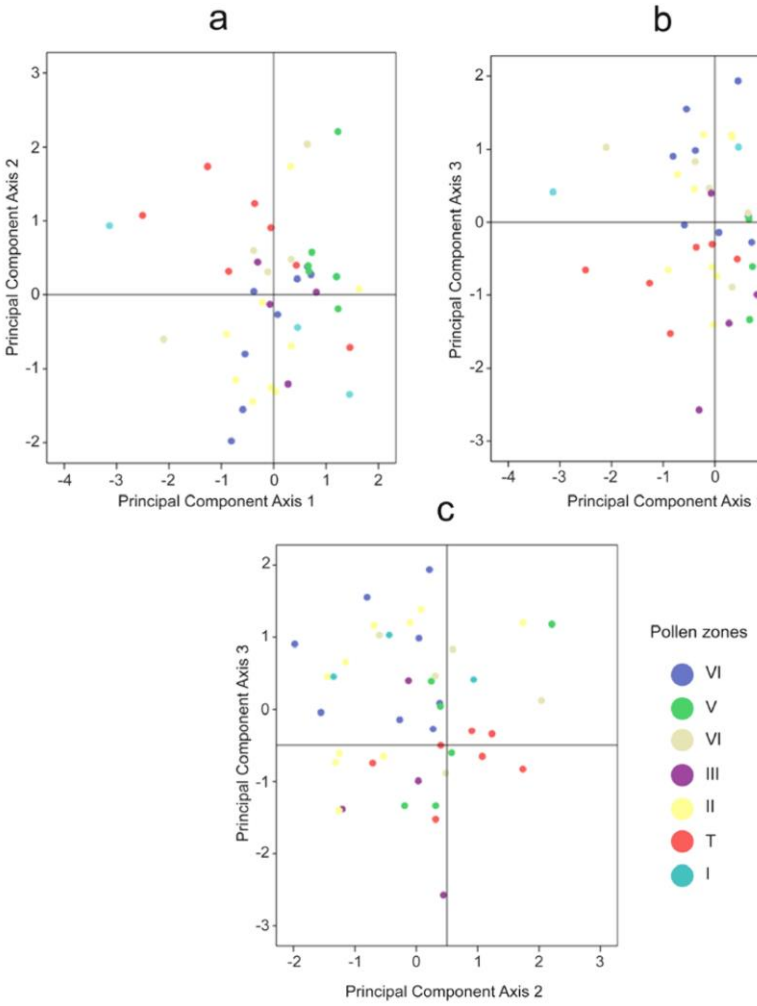

Fig. 4 - Montalbano Jonico section: plot of sample scores. (a) First vs second principal component, (b) first vs third principal component and (c) second vs third principal component. Samples colours indicate the correspondent pollen zone.

the 27.73% of the total variance, and expresses a balance between mid-altitude taxa, halophytes, steppic taxa (with positive loadings) and Mediterranean elements, *Quercus*, plus other broad-leaved thermophilous trees (with negative loadings) (Tab. II). Conceivably, this balance can be considered expression of the differential vegetation's response to cooler (with mid-

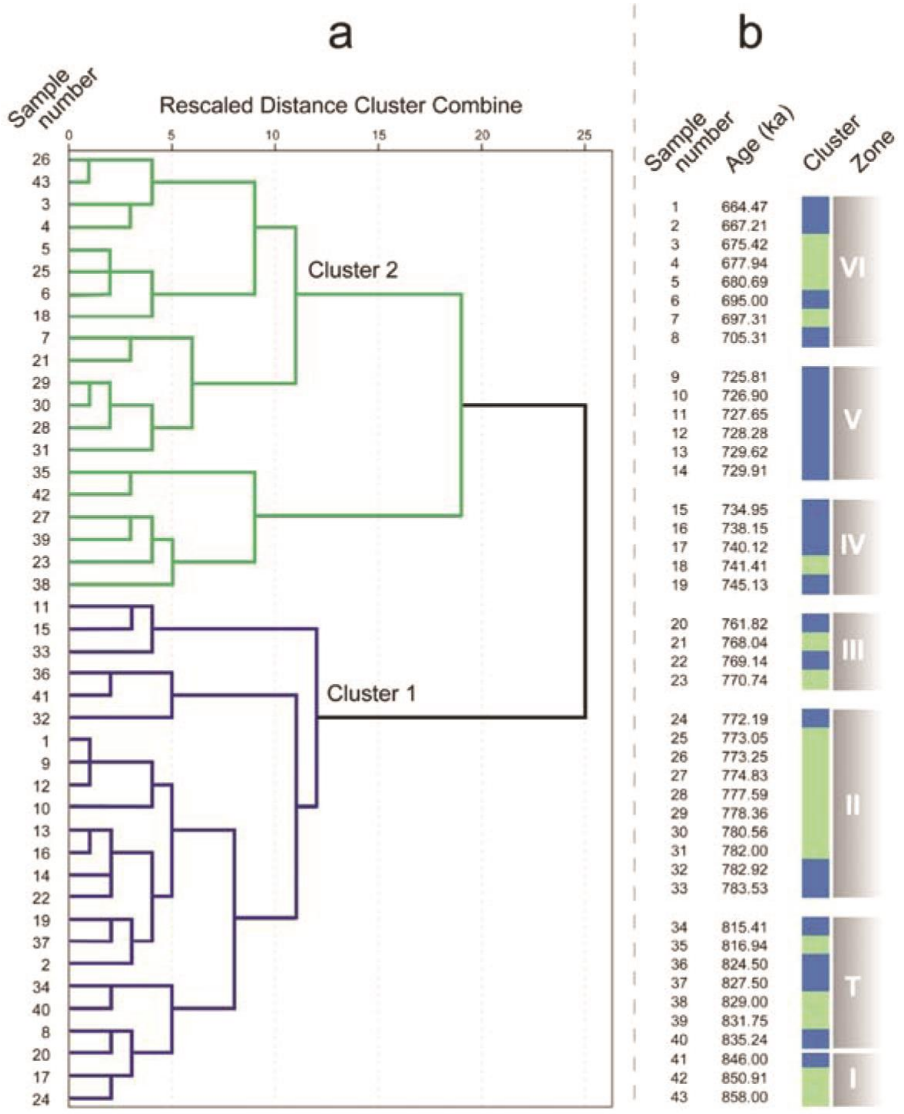

Fig. 5 – (a) Cluster analysis on the selected warm periods from the Montalbano Jonico record; dendrogram has been obtained using Ward method. (b) Clustered samples are sorted in function of the age.

altitude taxa and herbs increase) and warmer (with broad-leaved deciduous taxa and Mediterranean xerophytes increase) climate contexts. The third principal component (PC 3), contributing for the 10.89% to the total data variability, appears to be almost exclusively controlled by high-altitude taxa

(with positive loadings) and Mediterranean taxa (with negative loadings). This component can reflect the different moisture requirements of Mediterranean sclerophylls (adapted to seasonal draught) and high-altitude trees (demanding more constant humidity).

Samples from the seven statistical units associated with Zones I-VI and T, plotted as scores (the coordinates of the samples in the space of the components) on the three main components (Fig. 4) show scattered distributions and overlapping domain areas. In other words, "warm" zones, regarded as groups of samples defined *a priori*, cannot be discriminated if the variance-covariance structure of taxa groups is applied.

4.3. Cluster analysis

Cluster analysis on the centered-log data has therefore been run in order to discover the presence of natural associations in the dataset. The obtained dendrogram (Fig. 5a) permits to point out the presence of two well distinct groups of samples, marked with different colors (blue cluster vs green cluster)

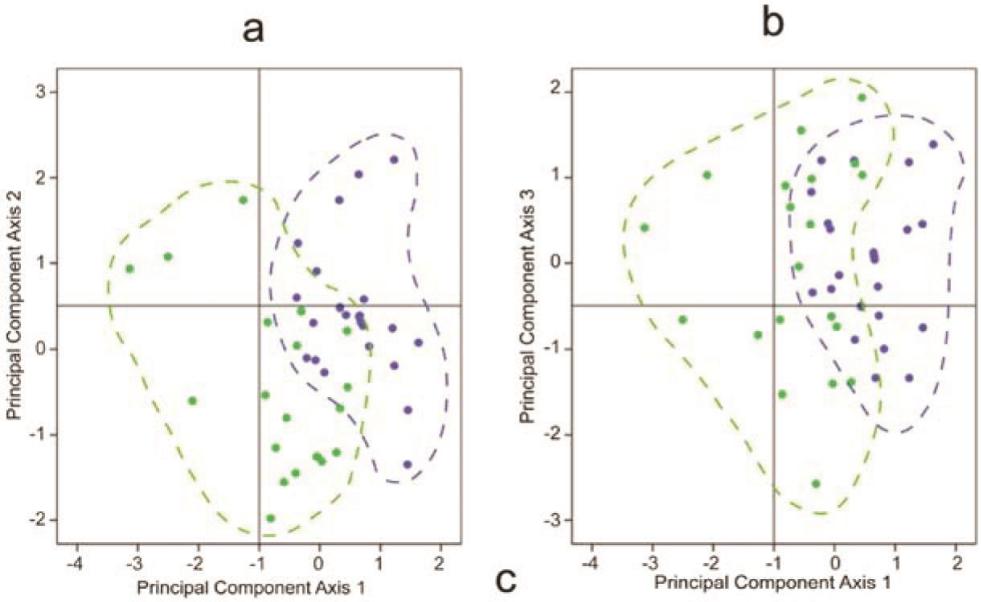

Fig. 6 - Montalbano Jonico section: plot of sample scores on the component axes already used in Fig. 4. Samples are marked with colours of natural associations revealed by the cluster analysis.

which further help us to sight them across the seven "warm" zones (Fig. 5b). The main clusters obtained have been separated by considering that theiroccurred only for a high rescaled distance representing anof high dissimilarity. The two clusters have been then plotted as scores on the three main components revealed by multivariate analysis (Fig. 6). In Fig. 6a we can see that PC 1 and PC 2 are both involved in marking the separation between the two clusters. The blue cluster shows higher values for both axes with respect to the green cluster. In Fig. 6b the two clusters are plotted in a PC 1 vs PC 3 diagram, and discrimination is operated by the former. Again, the blue cluster assumes higher values than green cluster. No significant discrimination is obtained by plotting the samples in a PC 2 vs PC 3 diagram.

5. Discussion

Palynological analyses point out, in agreement with the isotopic record (Marino et al., 2015), the succession of climatic oscillations between MIS 21 and MIS 16. In particular interglacials and interstadials are well expressed by major increases in deciduous *Quercus* and other mesophilous taxa and by PTI values higher than ~2. On the other hand, glacials and stadials are characterized by the large expansion of steppe and halophytic taxa as well as by PTI values lower than ~2.

Cluster analysis on the pollen samples from the "warm" zones (I-VI plus T) indicates that the variability in taxa percentages is expressed by two main associations of samples (i.e. blue and green clusters), showing well sorted distributions on the PCA plots (Fig. 6a and b). Each studied interval (Zones I-VI and T) includes samples associated to both blue and green cluster, except for the Zone V, wich is exclusively represented by blue cluster's samples (Fig. 7). A first observation is that a similar "blue-green-blue" arrangement unites Zone II and Zone VI (MIS 19.3 and 17, respectively) (Fig. 7). (Zone I represents the last ~12 kyrs of MIS 21.3 and shows a pattern very close to those better expressed in both Zone II and Zone VI). Analogies can also be recognised between Zone IV and Zone V (MIS 18.3-18.4 interval and MIS 18.3, respectively), since they both show the predominance (up to totality) of "blue" samples (Fig. 7). Instead Zone T and Zone III (MIS 21.1 and 19.1, respectively)

show a thickly alternate blue-green pattern.

Key remarks arise when samples are plotted into the PC 1 vs PC 2 diagram (Fig. 6a). Increasing values of the PC 1 highlight major differences on the rapidity of plant community changes: hydrophytes and deciduous *Quercus* as well as other herbaceous taxa (with positive loadings), are expected to react more quickly to palaenvironmental changes than mid- to high-altitude forest taxa and Mediterranean sclerophylls (with negative loadings) (Tab. II). On the other hand, the PC 2 can be thought to reflect the duality among plants with different tolerance to cold: *Tsuga*, *Cedrus*, halophytes and steppic taxa - with positive loadings -, though diffused in very different environments, can tolerate decrease in temperature; conversely, Mediterranean taxa and deciduous broad-leaved elements - with negative loadings - have a lower tolerance to temperature decreases. Blue cluster's samples are marked by higher values for both principal component axes than green cluster's samples (Fig. 6a). Hence, the former reflects periods marked by (a) not very high temperatures (higher values on PC 2) and (b) the increase of fast-spreading taxa (higher values on PC 1); vice versa, the latter suggest contexts with (c) higher temperatures (lower values on PC 2) and (d) lower abundances of pioneer taxa (lower values on PC 1).

This allow some considerations to be made, in the light of the three patterns previously described:

- Vegetation succession during MIS 19.3 and 17 (and possibly 21.3) is characterized by a warm mid-phase with a relatively high percentage of slow-spreading taxa, rimmed by cooler intervals with higher abundance of fast-expanding plants (*sandwich* pattern).
- The vegetation landscape within MIS 21.1 and 19.1 constantly changes from warmer states, with the increase of slow-spreading taxa, to cooler states, in which higher frequencies of fast-spreading taxa are recorded.
- Interstadial between MIS 18.4 and MIS 18.3, as well as MIS 18.3, show a rather monotonous vegetation pattern, marked by the constant relatively low presence of both slow-spreading and warmth-demanding taxa. This is probably due to the shortness of the warm phase that prevent those plants to settle.

Selected warm periods at MJ section, "Interval B" are different under many points of view, being their duration, time-scale position, intensity and orbital

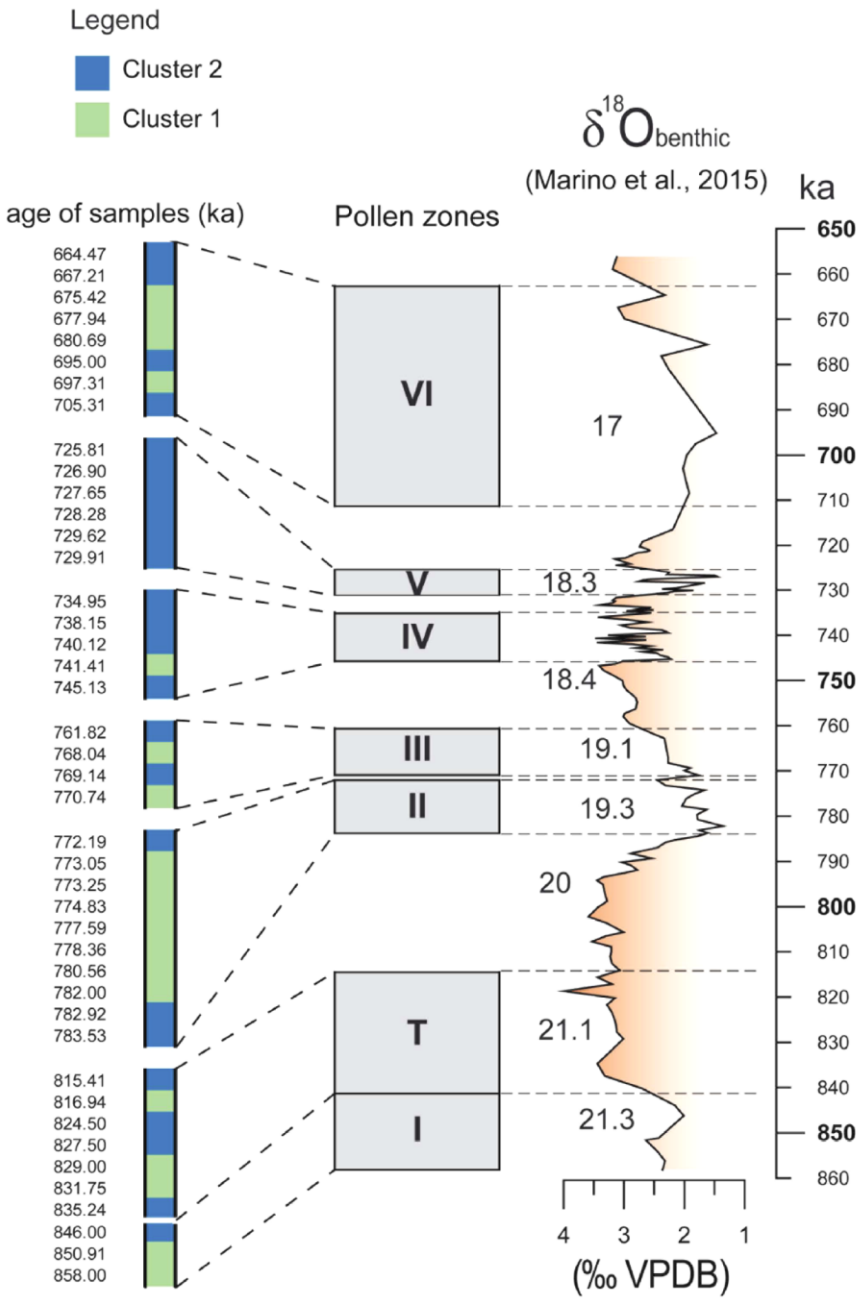

Fig. 7 – Selected samples of the warm periods of the Montalbano Jonico pollen record – marked with colours from the cluster analysis –, "warm" pollen zones and oxygen isotopic curve (Brilli et al., 2000; Ciaranfi et al., 2010; Marino et al., 2015).

configurations widely varying. Nevertheless, cluster analysis shows that most of the variability is described by only two main classes of samples, which generally coexist within each interval. At one level, warm periods globally show more similarities than initially predicted. As hinted by Tzedakis & Bennet (1995), internal biotic factor such as inter- and intra-specific competition can be invoked to justify these analogies. At the same time, it is worth nothing that each period is characterized by a specific vegetation dynamics (see the presence of three patterns), which induce to stress the role of the forcing by external factors.

6. Conclusions and perspectives

MJ section represents an important stratigraphic archive for the reconstruction of the Early-Middle Pleistocene G-I cycles in the central Mediterranean basin. In-depth studies on flora and vegetation changes have been previously carried out by Joannin et al. (2008) and Bertini et al. (2015), for the MIS 37-23 and MIS 21-18 intervals, respectively.

Here, high resolution palynological analyses and statistical processing of pollen data have been performed for the interval MIS 21 to 16. Such an approach has permitted to characterize and compare successive warm periods in terms of duration, intensity and vegetation dynamics. The PCA carried out on PTI-based statistical groups has not permitted to discriminate the different warm periods. On the other hand, cluster analyses underline the presence of two natural association of samples, which bear vegetational signatures when they are plotted on principal component axes. Such a double type of samples is not randomly arranged across the succession and points out three main patterns in the warm periods.

Since the age-model of the MJ section allows correlations with the orbital geometry predicted for each period (e.g. after Laskar et al., 2004), it would be possible to verify if astronomical forcing can be (at least partially) responsible for the different structure of warm periods. The chronologic model suggests a major role especially of the 100 kyrs-period oscillations. In particular, (absolute or relative) eccentricity maxima correlate well with the first (*sandwich*) structure. An in-depth statistical approach would permit to test

relationships between orbital and vegetation phenomena but also to better understand how astronomical factors modulate vegetation changes during interglacials and warm phases (Tzedakis, 2012a, b).

The present study also fits the issue concerning the extent of the impact of the EMPT on terrestrial ecosystems. Finally, the high-resolution record of one of the investigated interglacials, i.e. MIS 19, represents a particularly appreciable datum as it is now considered one of the "best analogues" of the present interglacial (Berger et al., 2012; Tzedakis at al., 2012a).

Contribution A2

Vegetation and climate across the Early-Middle Pleistocene transition at Montalbano Jonico, southern Italy*

*Published in Quaternary International 383, 74-88
(A. Bertini, **F. Toti**, M. Marino, N. Ciaranfi, 2015)

Abstract

Pollen analysis of the Montalbano Jonico marine succession (MJS), southern Italy, provides a continuous vegetational record between 858 ka and 745.13 ka which includes Marine Isotope Stage (MIS) 19, now considered the closest orbital analogue to the Holocene. A comparison between paleoclimate proxies and global signals of past climate change allows the pollen record to be interpreted in terms of major environmental and climate modifications through MIS 21–18 at the orbital- and sub-orbital-scale. This is also central to understanding migration patterns of the genus *Homo*. Interglacials are expressed by the dominance of a mesophilic vegetation typical of a (warm) temperate and relatively humid climate. Deciduous *Quercus* dominated fully temperate arboreal forest already devoid of subtropical taxa. Wooded steppes to steppes expanded during glacials when cold and dry conditions prevailed. At MJS the main expansion of temperate forest, dominated by broad-leaved trees, correlates to MIS 19.3, whereas the expansion of steppe vegetation, during drier conditions, marks MIS 19.2 directly above the volcaniclastic layer V4, dated at 773.9 ± 1.3 ka. More intensively arid conditions developed during MIS 20 and MIS 18; the Pollen Temperature Index reaches its minimum in uppermost MIS 20 in agreement with a significant cold and arid climate phase of wide significance in the North Hemisphere, as documented by prominent peaks in North Atlantic ice rafted debris (IRD) and Mediterranean aeolian dust records. On the other hand, *Artemisia*, a significant component of steppes, shows its maximum expansion during earlier phases of MIS 18. Millennial to sub-millenial-scale climate variability is evidenced by two abrupt short-term pollen events within MIS 19.3, which show a dominant increase of the cosmopolitan herbaceous component at around 783.54 ka and 774.84 ka, respectively. The vegetational and inferred climate changes for MIS 19 offer two possibilities: (1) to investigate the interglacial climate variability and discuss the linkage between climate and changes in geomagnetic field

intensity close to the Matuyama–Brunhes paleomagnetic boundary (MBB), and (2) to help evaluate the role of the MBB in defining the Middle Pleistocene global boundary stratotype section and point (GSSP). With respect to point 2, a comparison of data at MJS with the pollen record at the nearby and coeval Valle di Manche section is relevant and evidences the complex response of vegetation to climate events possibly under the effects of both astronomical and local factors.

Keywords: MIS 19, Early–Middle Pleistocene transition, Pollen, Vegetation and climate, Montalbano Jonico succession, Southern Italy

1. Introduction

Southern Italy, located in the central Mediterranean region, is a key area for studying past and present climate changes, including those associated with future scenarios under the effects of global warming and aridification (e.g. Lionello et al., 2012). Quantitative fossil records today are of major importance for numerically modelling past climates. In particular, the documentation of past interglacials is key for understanding the present interglacial, especially regarding its duration, trends, and intensity, and for anticipating the future effects of global climate change. Studies of the mid-Piacenzian warm period, between 3.264 and 3.025 Ma (e.g. Haywood et al., 2009; Dowsett et al., 2010), have contributed significantly to these issues. This time interval, preceding the onset of Northern Hemisphere glaciation when global mean temperatures were warmer than at present, was considered a useful analogue for a modern greenhouse world (e.g. Raymo et al., 1996). However, interglacials during the past 2.6 Ma have also received much attention (e.g. Kukla et al., 1997; Droxler et al., 2003; Tzedakis et al., 2009; Tzedakis, 2010), with some now considered potentially the best analogues for our current warm interval. Their study provides an opportunity to verify interglacial history in the absence of anthropogenic inferences, and to observe the impact of abrupt climatic events on terrestrial and marine ecosystems during homogenous climate conditions. High-resolution studies have concentrated especially on MIS 5e (the last interglacial, ca. 125 ka; e.g. Kukla et al., 1997; Rioual et al., 2001; Kukla et al.,

2002), MIS 11 (ca. 410 ka; e.g. Berger and Loutre, 2002; Tzedakis, 2010; Candy et al., 2014 and references therein), and now especially on MIS 19 which shows orbital configuration, greenhouse gases concentration, and temperature features comparable to the present (e.g. Tzedakis et al., 2012). Climatic

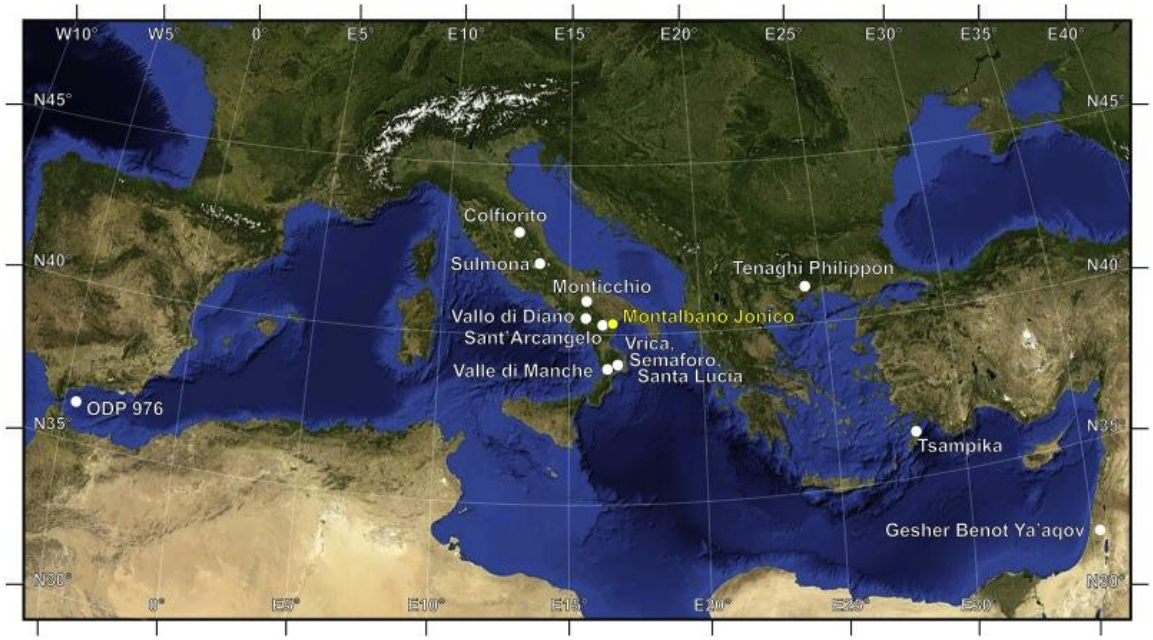

Fig. 1. Location of Montalbano Jonico and the main Mediterranean sites (between ca. 43° and 33° N) cited in the text.

vicissitudes across the Early–Middle Pleistocene transition, sometimes preserving a continuous record of MIS 19, have been documented by the study of many Mediterranean (Fig. 1) and extra-Mediterranean sites (e.g. Lake Baikal, southeast Siberia, Prokopenko et al., 2006; Colfiorito, central Italy, Bertini, 2000; Sant'Arcangelo, south Italy, Sabato et al., 2005; Valle di Manche, south Italy, Capraro et al., 2005; Tenaghi Philippon, Greece, Tzedakis et al., 2006; Tsampika, Greece, Joannin et al., 2007; Gesher Benot Ya'aqov, Israel, Van Zeist and Bottema, 2009) as well as of the EPICA Dome C (EDC) ice core (e.g. Pol et al., 2010).

The present palynological study of the Montalbano Jonico succession (MJS) describes the sequence of floristic and vegetational changes from MIS 21

to the beginning of the glacial MIS 18, ranging between 858 ka and 745 ka. Vegetation reconstructions and climate inferences from this central Mediterranean record may provide a useful contribution for the knowledge of MIS 19, and allow the comparison of the new pollen record with the key climatic characteristics from the pollen archives available for this time interval. Further, the mode and timing of climate evolution as revealed by pollen records during the Early–Middle Pleistocene transition may improve the understanding of climatically-induced vegetation changes throughout the whole Pleistocene in the Mediterranean area.

2. The Montalbano Jonico section

The Lower–Middle Pleistocene MJS, about 450 m thick, crops out along the internal border of the southern Apennines foredeep, and ranges from marly clays to silty sands, including nine volcaniclastic layers (V1–V9), and five dark horizons referred to sapropel layers (e.g. Maiorano et al., 2008; Ciaranfi et al., 2010 and references therein) (Fig. 2). Based on calcareous nannofossils, the section belongs to the small *Gephyrocapsa* and *Pseudoemiliania lacunosa* zones of Rio et al. (1990). Many calcareous plankton bioevents have been recorded throughout the section (Fig. 2, Marino, 1996; Maiorano et al., 2004, 2010; Girone et al., 2013). No paleomagnetic record is available for the Montalbano sediments because of remagnetization phenomena (Sagnotti et al., 2010). However the oxygen isotopic signal is excellent and the glacial–interglacial (G/I) pattern compares well with both the oceanic and stacked Mediterranean $\delta^{18}O$ records (Ciaranfi et al., 2010). Stable oxygen isotope analyses on planktonic and benthic foraminifera together with biostratigraphy, radiometric data ($^{40}Ar/^{39}Ar$), and sapropel stratigraphy have allowed recognition of the MIS 37 to MIS 17/16 time interval and permit astronomical calibration of the MJS, which covers an interval from 1240 ka to 645 ka (D'Alessandro et al., 2003; Stefanelli, 2004; Stefanelli et al., 2005; Maiorano et al., 2008, 2010; Ciaranfi et al., 2010).

The MJS includes the regressive part of a third-order cycle with superimposed Milankovitch scale climate cyclicity (Ciaranfi et al., 1997). It is part of the “Special Nature Reserve of the Montalbano Jonico Badlands”, and

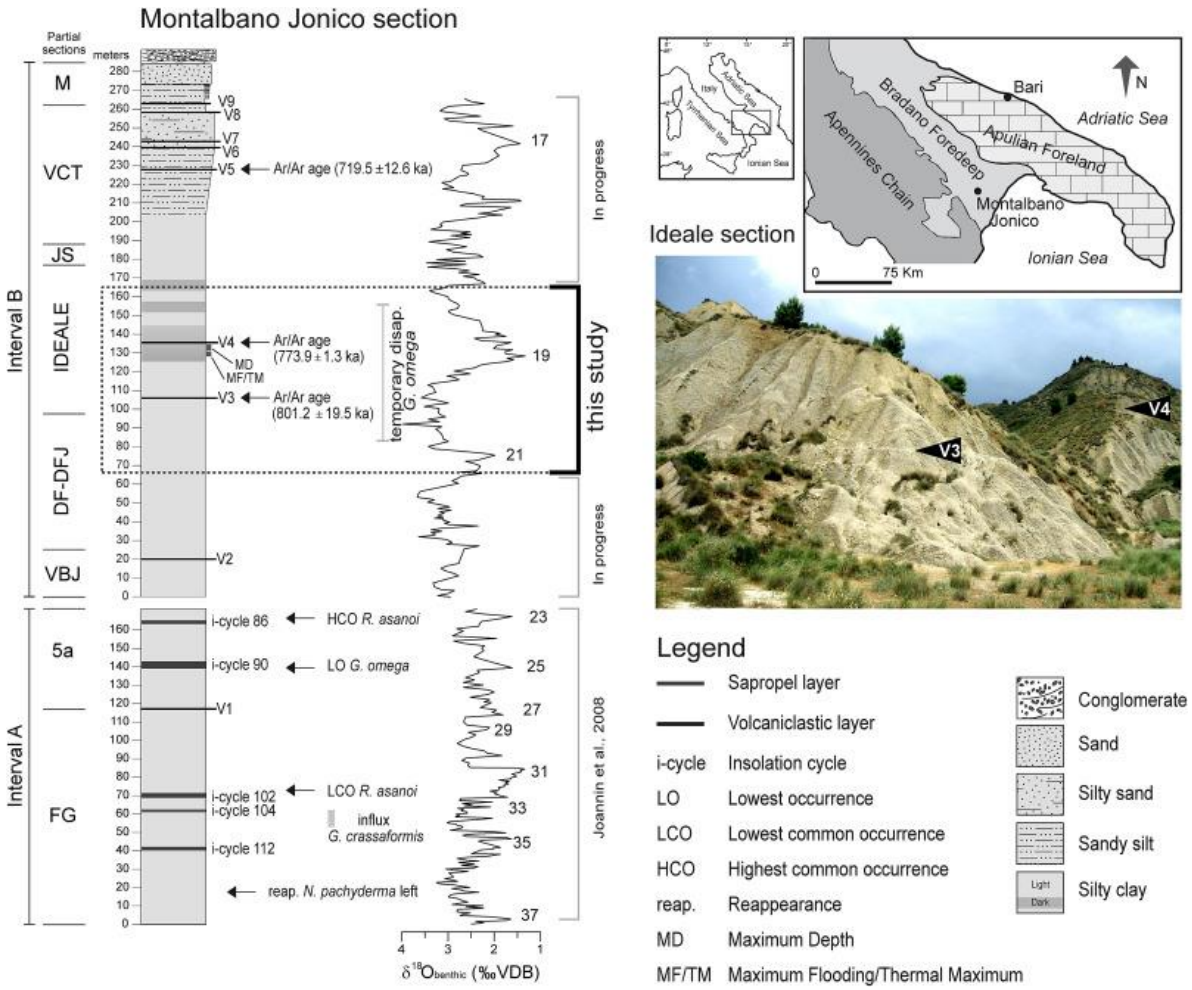

Fig. 2. Lithostratigraphy, benthic $\delta^{18}O$ record, and location of the Montalbano Jonico composite section (Brilli et al., 2000; Ciaranfi et al., 2010; Maiorano et al., 2010). Marine isotope stages are from Ciaranfi et al. (2010). The age of volcaniclastic layer V4 is from Petrosino et al. (2015). MD and MF according to D'Alessandro et al. (2003), TM according to Girone and Varola (2001). The image of the badlands including V3 and V4 volcaniclastic layers, in the Ideale partial section, is also visible on the right.

The lower one ("Interval A") is 168 m thick, and accumulated in an upper slope/outer shelf setting (Ciaranfi et al., 1997, 2001, 2010). In this portion, previous pollen analyses between 1240 and 900 ka (MIS 37 to 23) revealed cyclic changes associated with climate and eustasy (Joannin et al., 2008). The upper portion ("Interval B") is 280 m thick, and accumulated in a shelf setting with alternating fluctuations towards a slope environment (e.g. Ciaranfi et al., 2010). It encompasses MIS 19, which closely approximates the MBB (Lisiecki and Raymo, 2005) and falls within the second temporary disappearance interval of the nannofossil *Gephyrocapsa omega* (Maiorano and Marino, 2004; Maiorano et al., 2004).

Detailed studies carried out on the Ideale (marine) partial section including MIS 19 (Fig. 2) revealed the co-occurrence of a maximum flooding (MF) and thermal maximum (TM) in the interval from 128 to 131 m based on the *Neopycnodonte* mollusk paleocommunity (D'Alessandro et al., 2003) and mesopelagic tropical–subtropical Atlantic teleostean *Bonapartia pedaliota* (Girone and Varola, 2001), followed by a maximum water depth (MD) up to about 135.2 m (D'Alessandro et al., 2003; Stefanelli, 2003).

The new $^{40}Ar/^{39}Ar$ age of 773.9 ± 1.3 ka for the volcaniclastic layer V4 (Petrosino et al., 2015), combined with the $^{40}Ar/^{39}Ar$ age of V3 (801.2 ± 19.5 ka, Maiorano et al., 2010), have allowed the age–model to be refined through the studied interval (Marino et al., 2015).

3. Present climate and vegetation in the Montalbano area

The Montalbano Jonico succession is exposed near the eponymous village located at about 40°17′00″N, 16°34′00″E (292 m above sea level) in the Basilicata region of southern Italy (Figs. 1 and 2). It lies between the Metapontine Ionian coast, to the east, and the Agri valley, to the north north-west. The surrounding relief ranges between 1200 and 1500 m whereas higher mountains (up to 2250 m) are more distantly located to the south-west in the Lucano Apennines (Lagronese and Pollino areas; Fig. 2). The Basilicata is a region characterized by strong gradients from the interior mountains to

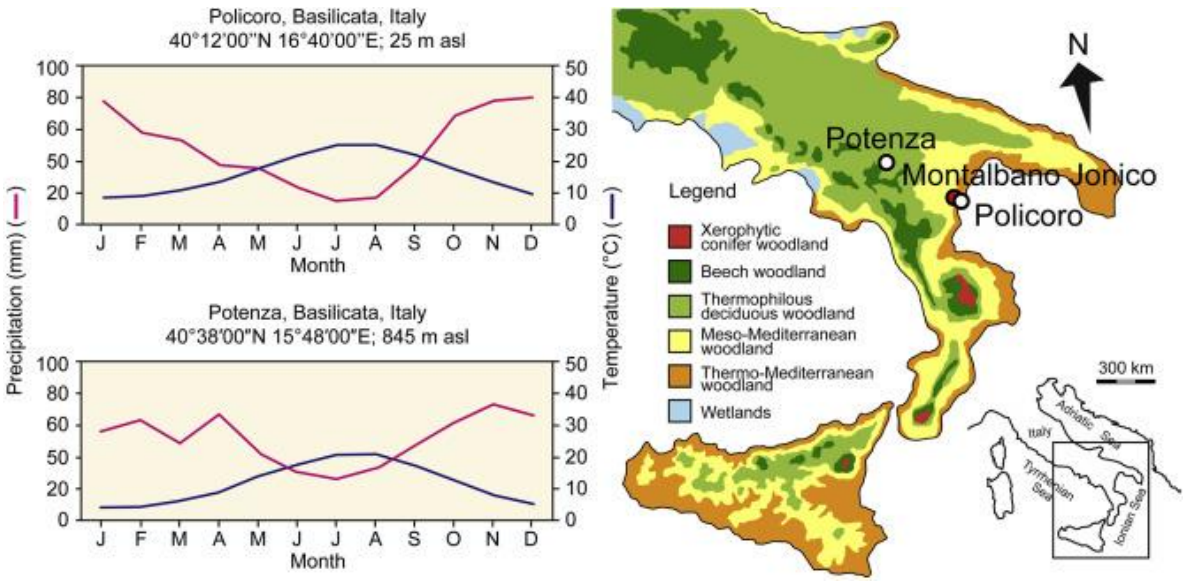

Fig. 3. Ombrothermic diagrams of the Policoro and Potenza stations (Basilicata), on the left (for climate data see on http://en.climate-data.org/location/13970/). Map of the potential vegetation in southern Italy (modified from Pignatti, 2011), on the right.

coastline, with dominant (cool) temperate to Mediterranean climates (Cantore et al., 1987). This is evident from the analysis of ombrothermic diagrams of two sites in Fig. 3 (see for climate data on http://en.climate-data.org/location/13970/), representative of the Ionian coast (Policoro) and middle-altitude interior (Potenza) areas, respectively.

Along the coast, rainfall is lower than 100 mm during June–September, giving rise to summer drought. Above 1600 m, rainfall exceeds 150 mm during the critical summer months. The mean monthly temperature of the warmest months reaches values greater than 23 °C along the coast, whereas at higher altitudes (800–1000 m) the climate is cooler (20–23 °C) without significant increase of summer rainfall values. Across most of the nearby Agri basin, included between the 8 °C and 16 °C isotherms (for mean annual temperatures), the average annual temperature ranges from 12 °C to 15 °C. At MJS the mean annual precipitation, over 50 years between 1921 and 1970, has been 676 mm; similar conditions are present in the adjacent Policoro (Fig. 3). Intense rainfall events are frequent and produce severe damage to prevalently

unstable settings. For instance, a cloudburst occurred in the Basilicata and Ionian coast of Calabria on 24 and 25 November 1959, and resulted in intense precipitation at MJS (322.4 mm during these two days) and consequent widespread flooding (Basso et al., 2002).

According to Corbetta (1974), the vegetation from the coastal portions of the basal belt (e.g. in the Ionian littoral zone) includes psammophyle and halophyte taxa. Inland, hygrophilous riparian woods can be present such as at Policoro (Fig. 3). The basal belt also includes the Oleo-Ceratonion climax (Mediterranean horizon), which is especially well expressed in Plio-Pleistocene marine clays of the "Calanchi" area. The peculiar geographical position of the Basilicata, with its valleys running into both the Tyrrhenian and Ionian seas, favored the spreading of numerous taxa typical of the thermo-Mediterranean horizon (Corbetta et al., 1991). Incursions from the eastern (Ionian–Adriatic) side include *Lygeum spartum* prairies. The Camphorosmo-Lygeetum (Lygeo-Stipetalia, Thero-Brachypodietea) association is known in the low Basento valley especially on the Plio-Pleistocene clays where remnants of *Pistacia lentiscus* macchia (Oleo-Ceratonion) and *Quercus pubescens* woods are also present. In the Ionic valleys, *Cistus* garrigues are common. Within the subMediterranean and submontane horizons, the main arboreal taxa are *Quercus ilex* and *Q. pubescens* together with *Fraxinus ornus*, *Ostrya carpinifolia* and scarce *Carpinus betulus* and *C. orientalis*, *Pyrus communis*, *Sorbus domestica* etc. At higher elevations, large *Quercus cerris* formations increase in importance at the expense of *Q. pubescens*, and together with chestnut woods they characterize the submontane horizon. In the higher altitudinal mountain belts (e.g. at Mount Volturino), beechwoods are present with relict nuclei of *Abies alba*. High altitude prairies and *Pinus leucodermis* are present in the cacuminal belt (Corbetta et al., 1991).

4. Methods

Forty-nine pollen samples were collected from the interval 67.70–165.10 m which includes the partial sections DF-DFJ and Ideale of Interval B at the MJS (Fig. 2). The sampling interval is about 0.5–1.7 m, and rarely 2.8–6.0 m in the

basal and upper parts of the studied record. This represents a temporal resolution often of 0.4–1 ka, with values of 4–7 ka in a few intervals within MIS 21 and MIS 18, according to the age model established by Marino et al. (2015).

Samples were processed using standard chemical–physical procedures at the Department of Earth Science, University of Florence. Dry samples were first weighed (19.3–28.5 g with the exception of one sample of 7.4 g), and *Lycopodium* tablets were added to each sample to provide palynomorph concentrations. The procedure included treatments with HCl (10%), HF (48%), sodium hexametaphosphate, KOH (10%) and $ZnCl_2$ separation (solution density ca. 2.0). Residues were sieved at 10 μm and mounted using glycerol. Transmitted light microscopy, using ×750 and ×1250 (oil immersion) magnifications, was used for identification and counting of pollen. More than 34,836 pollen grains were counted (excluding Cupressaceae), corresponding to a mean value of about 265 grains per sample excluding *Pinus* and Cupressaceae.

A detailed pollen diagram was then plotted, with pollen expressed as a percentage of the total pollen grains excluding *Pinus* and Cupressaceae. *Pinus*, as frequently observed in marine depositional settings, is in fact consistently and largely over-represented (e.g. Beaudouin et al., 2007). Its abundance was normalized to the total pollen sum (excluding Cupressaceae) and represented as an individual curve. The Cupressaceae pollen may be present in high amounts but sometimes exhibit an unusually thick exine: we have therefore removed them from the pollen sum pending their detailed study by electron microscopy. However their highest occurrences are marked on the right of the detailed palynological diagram (Fig. 4).

In a summary pollen diagram (Fig. 5), selected taxa were plotted with respect to a pollen sum including all taxa except *Pinus*, Cupressaceae, and indeterminate and indeterminable grains. Moreover, an additional summary diagram (Fig. 6) includes five main groups informally established on the basis of the ecological and climatic requirements of their present correlatives. In the first group, within the non-arboreal pollen taxa (NAP), three subgroups have been described in succession: steppe taxa including *Artemisa*, *Ephedra* and *Hippophaë*; other halophytes including Caryophyllaceae and Amaranthaceae; and other non-arboreal taxa. The second group includes meso- to microthermic conifers such as *Tsuga*, *Cedrus*, *Abies* and *Picea* (plus

Fagus and *Betula*). The third group principally includes broad-leaved deciduous forest taxa characteristic of warm-temperate and temperate climates (*Quercus* is the most abundant taxon followed by *Ulmus*, *Zelkova*, *Acer* and *Juglans* etc.) as well as the Ericaceae and sclerophyll forest taxa (such as *Q. ilex* type, *Pistacia*, *Olea*) typical of regions with Mediterranean climate having wet winters and dry summers.

Two ratios have been calculated following Joannin et al. (2008) and Suc et al. (2010). The first is mesothermic arboreal taxa (e.g., *Quercus*, *Carpinus* and *Carya*) vs. steppe taxa (*Artemisia* and *Ephedra*), to discriminate warm-temperate from cold phases (Pollen Temperature Index, PTI). High values of aeolian dust from records of the east Mediterranean Sea (Larrasoaňa et al., 2003) have been also taken into account as a proxy for continental cold and arid conditions, whereas ice-rafted debris (IRD) peaks from Ocean Drilling Program (ODP) Site 980 in the North Atlantic (Wright and Flower, 2002) provide indications of extreme cold phases. The second ratio is *Pinus* vs. halophytes (e.g. Caryophyllaceae, Amaranthaceae, *Ephedra*), used as an indirect proxy of sea-level fluctuations to indicate changes in distality (e.g. Cambon et al., 1997; Beaudouin et al., 2005).

Botryococcus, *Pediastrum*, *Pseudoschizaea* and *Classopollis* abundances (for each taxon normalized to the sum of AP and NAP) have been reported on the right of the detailed pollen diagram (Fig. 4).

5. Results

The pollen record from the 98-m thick portion of the MJS (Fig. 2) is represented by 49 samples in which 109 pollen taxa were identified (Fig. 4). The mean pollen concentration is 1675 pollen grains per gram (Fig. 5). The rich and diverse pollen flora is characterised by the dominance of herbaceous taxa, particularly the Asteraceae, Amaranthaceae and Poaceae (Fig. 4). Among the Asteraceae, *Artemisia* is sometimes abundant. *Ephedra*, another steppe element, is also well represented by several species (*E.* cf. *distachia*, *E. fragilis* and *E. altissima*). The Ericaceae, Cyperaceae, Caryophyllaceae, Brassicaceae and Rosaceae (including *Poterium* and *Neurada*), *Plantago*, Cannabaceae, and Urticaceae follow in abundance. Low numbers of Apiaceae, Liliaceae,

Polygonaceae (represented by a range of taxa including *Rumex* and *Polygonum*), Cistaceae (including *Cistus* and *Helianthemum*), Dipsacaceae (including *Scabiosa* and *Knautia*), Lamiaceae, and *Sparganium* grains are also present. The Gentianaceae, Geraniaceae (including *Erodium*), Ranunculaceae, *Phlomis*, Fabaceae, *Linum*, Plumbaginaceae (including *Armeria*), Resedaceae, *Galium*, Convolvulaceae (including *Convolvulus*), *Myriophyllum*, *Potamogeton*, and *Typha latifolia* show scattered occurrences. Pollen grains of *Tricolporopollenites sibiricum* (Lubomirova) Nagy have been sporadically recorded in the lower portion of the section. Trees are mainly represented by *Pinus* whose pollen attains very high proportions (Fig. 4): 21,841 pollen grains of *Pinus* have been counted throughout the section. Among other Pinaceae, *Abies* and *Picea* are present throughout, as well as *Cedrus* and *Tsuga*. Deciduous broad-leaved trees are mainly represented by *Quercus*. *Carpinus*, *Ulmus*, *Carya*, *Zelkova*, *Acer*, *Tilia*, and *Juglans* pollen follow. *Liquidambar* is represented by sporadic grains. *Taxodium* type is also present, as well as other Cupressaceae (Fig. 4). Mediterranean xerophytes include *Q. ilex* type with smaller quantities of *Pistacia*, *Phillyrea* and *Cistus*.

Pollen transport as well as post-depositional processes linked to diagenesis and weathering seem to have contributed to the degradation (e.g. mechanical damage and oxidation) of palynomorphs. Bisaccate pollen are mostly broken and fragmented. Reworked palynomorphs, especially of *Classopollis*, are present (Fig. 4). Reworked specimens were often recognized by poor preservation and stratigraphic range, although such recognition is problematic when specimens are not obviously older than the enclosing sediments (e.g. *Taxodium* type and other Cupressaceae).

Among other palynomorphs, the Pteridophyta as well as cysts of dinoflagellates (Dinophyceae) are common. Other algae, such as *Botryococcus* (Botryococcaceae), *Pediastrum* (Hydrodictyaceae), and other aquatic microplankton including *Pseudoschizaea* (Incertae sedis) show scattered occurrences (Fig. 4).

The pollen record shows a peak in abundance of pollen of deciduous *Quercus* (up to ca. 40%) at 858 ka (Figs. 4 and 5) in the DF-DFJ partial section (Fig. 2). However, at ca. 851 ka, deciduous *Quercus* markedly decreases in abundance whereas mid- (especially *Cedrus*) to high-altitude (*Abies* and *Picea*) conifers increase to ~34% and 22%, respectively. *Pinus* also shows a

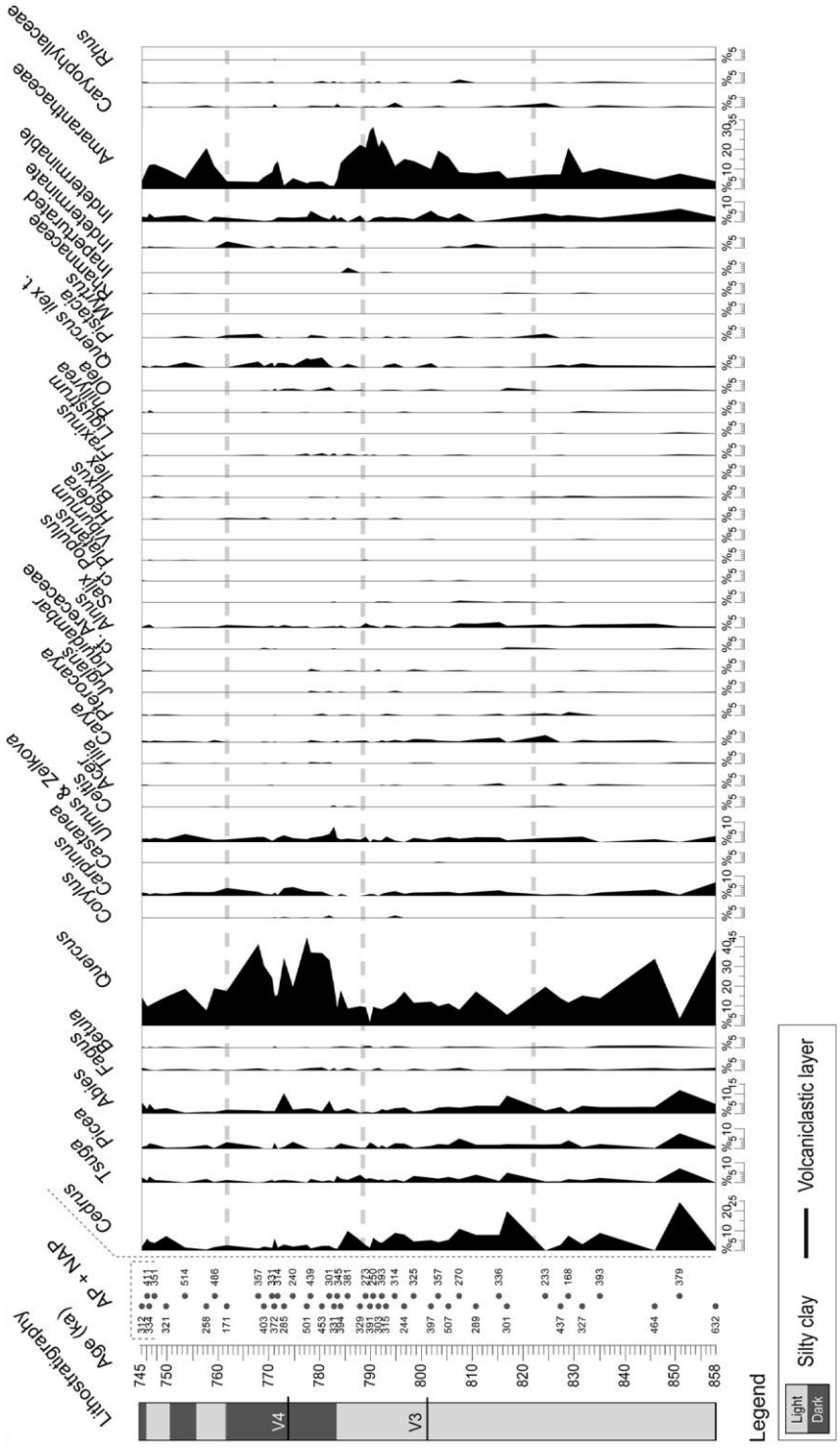

Fig. 4. Detailed pollen diagram of the Montalbano Jonico section (DF-DFJ and Ideale partial sections: Fig. 2) versus age (according to the age model of Marino et al., 2015). All percentages of pollen taxa (except Pinus *and Cupressaceae) are calculated using the total sum of pollen without* Pinus *and Cupressaceae. Pinus abundance is normalized to the total pollen sum (excluding Cupressaceae). Cupressaceae abundance is normalized to the total pollen sum (excluding* Pinus*). AP: arboreal pollen; NAP: non-arboreal pollen. On the right,* Pseudoschizaea*, Pediastrum,* Botryococcus *and* Classopollis *abundances. Dashed gray lines indicate the main phases described in the text.*

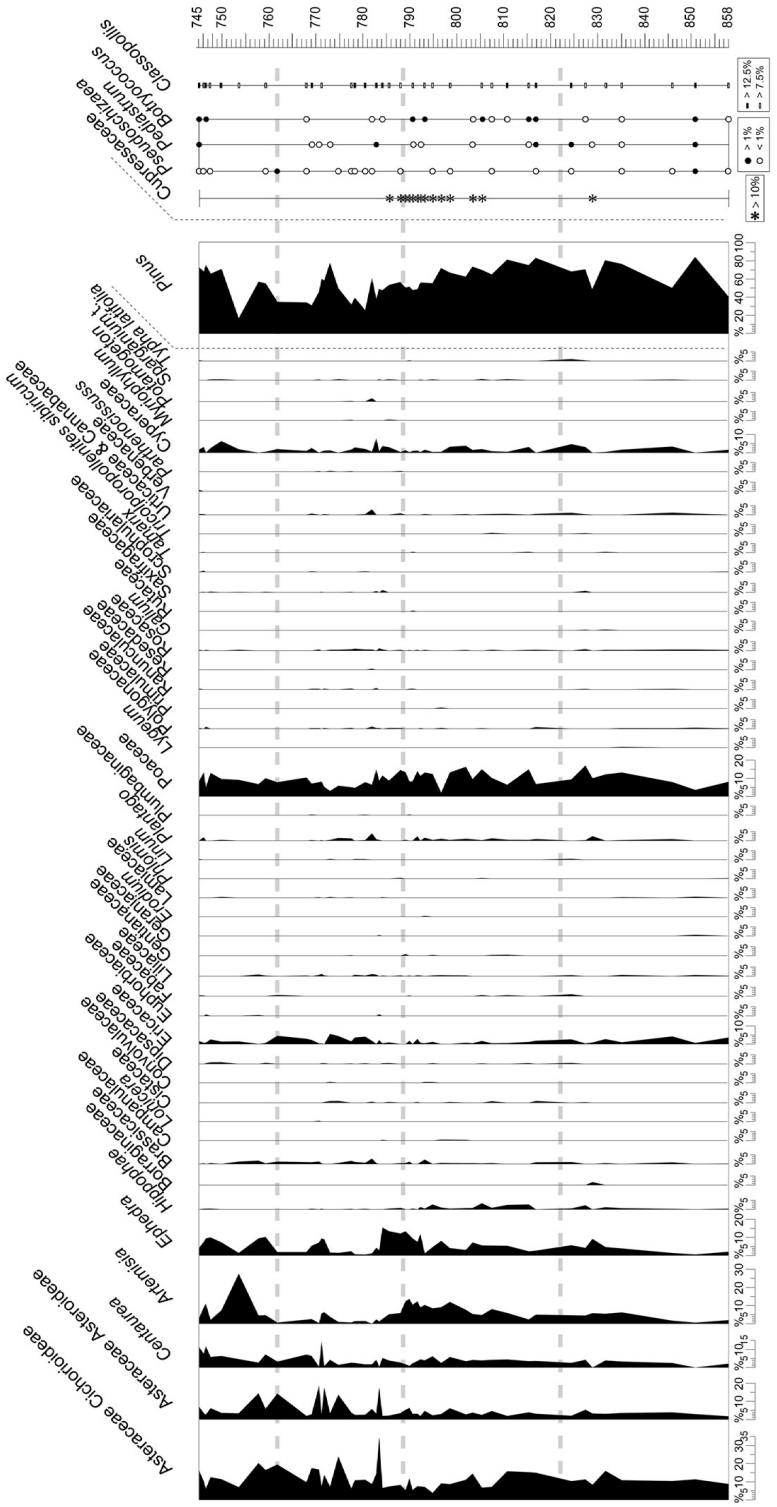

Fig. 4 Continued.

marked percentage increase (Fig. 4). Non-arboreal taxa do not show a significant rise, with the exception of a slight increase in Amaranthaceae and Cichorioideae (Asteraceae). Reworking is evidenced by a peak occurrence of *Classopollis* (Fig. 4). A new recovery of broad-leaved deciduous taxa, with deciduous oaks again abundant (35%; Fig. 4), is documented at 846 ka. Thereafter, the predominant vegetation characterized by temperate broad-leaved forest taxa is interrupted by successive increases of both meso-to microthermic conifers (especially *Cedrus* and *Picea*) and, among herbaceous plants (Fig. 4), of Amaranthaceae (up to 21%), *Ephedra* (up to 9%) and *Artemisia* (up to 6%) at 829–830 ka. At 816.9 ka, *Pinus* reaches its maximum value (84%); moreover, the percentage increase of meso- (especially *Cedrus*) and microthermic (especially *Picea*) conifers again parallels a quite significant reduction of the deciduous forest taxa, which remains always below 30% and more often close to 20% up to 793.2 ka. Soon after, however, deciduous forest taxa decline, their main phase of decrease centered at 790 ka when values fall below 5% (Figs. 4–6). At the same time, herbs with steppe and halophyte taxa as the main components exceed 90%. Among the pollen assemblages, a notable concurrent increase of Cupressaceae is recorded. Starting at 789.15 ka, mesophilous arboreal taxa increase with *Quercus* values rising to 18% at 784.23 ka, whereas steppe and halophyte taxa progressively decrease until a sudden and significant increase of Asteraceae (53%) and other cosmopolitan herbaceous taxa, at 783.54 ka. Between 783.54 ka and 782.92 ka, mesothermic forest taxa suddenly increase from ca. 13% to ca. 34%. Subsequently they increase steadily up to a maximum of ca. 53% at 779.59 ka. Although deciduous *Quercus* accounts for most of this increase, reaching its abundance peak of ca. 46% at 779.59 ka, a diverse range of other taxa including warm-temperate summergreen species is also present (Fig. 4). Pollen of evergreen sclerophyllous forests, especially *Q. ilex*-type and *Pistacia*, today characteristic of the Mediterranean region, increases in abundance between 780.56 ka and 777.59 ka (Figs. 4 and 5). Successive increases in the abundance of pollen of herbaceous taxa have been observed throughout, even when broad-leaved deciduous taxa, after each short decline, show rapid increases to reach high values until 768 ka. The low sample resolution limits detail in the pollen data after 774.83 ka. Herbaceous taxa strongly increase at this time, especially cosmopolitan herbs (principally Asteraceae), but with *Ephedra* and *Artemisia*

being extremely reduced. A second and indeed main intense decline in broad-leaved deciduous taxa is centered at 771.84 ka. It parallels a significant increase of herbs, especially Amaranthaceae (ca. 14%), followed by *Ephedra* (ca. 9%) and *Artemisia* (ca. 6%); and mid-to high-altitude conifers show a slight increase (Figs. 4–6). At 768 ka, deciduous *Quercus* shows a rapid increase up to ca. 41%. Among the warm-temperate sclerophyllous taxa, pollen of *Q. ilex*-type and of *Pistacia* is more abundant than previously recorded in older intervals of the MJS. Broad-leaved deciduous taxa decrease (up to 18%) at least from 761.8 ka, and then further decline to ca. 8% at 757.82 ka. Mediterranean xerophytes disappear whereas successive increases of herbaceous taxa, i.e. *Ephedra* (up to 10%), Amaranthaceae (up to 20%), and then *Artemisia* (28%), are present between 759.32 ka and 753.61 ka. *Artemisia* peaks at 753.61 ka with its highest values throughout the section. Correspondingly, *Pinus*shows a decline in relative abundance (17%). Towards the top of the investigated interval, meso-to microthermic conifers show successive increases, as do herbaceous taxa (Figs. 4–6).

6. Discussion

The present palynological study of the MJS provides evidence for the main climate-related floristic and vegetational changes between 858 ka and 745 ka. It accordingly contributes to the documentation of nearly two millions years of climate variability, including 39 G/I cycles, from MIS 97 to MIS 18 (i.e. between 2470 ka and 745 ka) in southern Italy, in the area between 39 and 40°N and 16–17°E, which includes the Crotone and the Bradano Foredeep areas (Figs. 1 and 2; e.g. Bertini, 2010 and references therein). This composite climatic record is one of the longest obtained from Quaternary sediments of the Mediterranean area, and it may be extended upwards by climate data from such geographically close sites as Acerno, Mercure, and Vallo di Diano (MIS 16–12, ca. 650–450 ka; e.g. Petrosino et al., 2014a,b; Russo Ermolli et al., in press; Fig. 1) as well as Monticchio (from the top of MIS 6, ca. the last 130 ka; e.g. Brauer et al., 2007).

6.1. Floristic changes through the Early-Middle Pleistocene transition in southern Italy

The MJS pollen record highlights a progressive impoverishment of the flora, and documents reciprocal changes in taxa abundances at the beginning of the Middle Pleistocene. This was a time characterized by changes in the flora and vegetation in response to major expansions of the Arctic ice-sheet, as the Crotone record shows, starting from 2470 ka (Fig. 1; Semaforo and Vrica: 2470–1360 ka, MIS 97–37; e.g. Combourieu Nebout et al., 1990, 1995; Combourieu Nebout and Vergnaud Grazzini, 1991; Klotz et al., 2006; Suc et al., 2010. Santa Lucia: 1356–1240 ka, MIS 43–40; Joannin et al., 2007. Valle di Manche: 870–730 ka, MIS 22–18.3; Capraro et al., 2005).

In southern Italy, the disappearance of subtropical ecosystems and the subsequent increase of deciduous broad-leaved temperate forests and Mediterranean xerophytes occurred about 1200–1300 ka (e.g. Combourieu Nebout and Vergnaud Grazzini, 1991; Bertini et al., 2010). Mega-to mesothermic taxa (e.g. *Myrica*, *Nyssa*, *Distylium*, *Symplocos*, Sapotaceae, *Magnolia*), living under a humid subtropical climate characterized by a regime with a small range of temperature and abundant and well distributed rainfall throughout the year, are absent from our pollen record. However, *Engelhardia* and *Taxodium*-type are still present, though with scattered occurrences.

Engelhardia is absent (to virtually absent) from late Calabrian Italian sites, including the nearby continental succession of Sant'Arcangelo (San Lorenzo cycle: ca. 1100–800 ka; Sabato et al., 2005) (Fig. 1); hence, the few pollen grains of this taxon in our record are considered reworked.

Concerning the sparse occurrence of *Taxodium*-type pollen grains, we observe that, at Vrica, "Taxodiaceae" (principally *Sequoia* type) undergo their major decline close to 1200 ka, which follows the first significant demise at ca. 2380 ka. "Taxodiaceae" are recorded in low abundances at Santa Lucia (as well as *Cathaya*), in the lower portion of Sant'Arcangelo, and at Valle di Manche. At the MJS, they already have scattered occurrences between 1240 ka and 900 ka (Joannin et al., 2008). On the basis of both the local stratigraphical distribution of *Taxodium*-type and the fact that it increases frequently with glacial phases, i.e. during climate conditions incompatible with its ecological

preference and concurrent with intense erosional phases, it seems reasonable to interpret such occurrence as primarily due to reworking, although the possibility of minor sparse in-situ occurrences cannot be denied. *Taxodium*-type, as well as others that disappeared from Italy in the Early Pleistocene (e.g. Bertini, 2010and references therein), probably persisted in refuge areas as relicts (see below for *Carya*).

Among the other conifers, *Cathaya*, already sporadic between MIS 37 and MIS 23 (Joannin et al., 2008), is virtually absent from our record. This mid-altitude plant, today restricted to China, at Vrica expanded particularly from ca. 1920 ka to 1740 ka, after the first decline of the "Taxodiaceae" forest (e.g. Combourieu Nebout and Vergnaud Grazzini, 1991).

Cathaya was in turn replaced by *Tsuga*, as observed at Vrica, at ca. 1470 ka (i.e. above laminite q), when high-altitude trees also reached their highest percentages (e.g. Klotz et al., 2006). *Tsuga* was an important element during transitional phases of the G/I cycles at Santa Lucia (Joannin et al., 2007). Nowadays it grows in temperate zones of the Northern Hemisphere (North America, China, Japan and the Himalayas), both as a dominant taxon and in association with deciduous taxa where its distribution is dependent especially on precipitation (at least 1000 mm during the year). In the Sant'Arcangelo continental site, *Tsuga* progressively disappears and is absent from the upper portion (latest Early Pleistocene). In contrast, our record of *Tsuga* reaches decisively higher percentages (up to 3%), and it is even more abundant at Valle di Manche. The Lucania drainage basin was probably wide enough at the location of the MJS to allow a larger pollen input from more distal areas where this taxon likely persisted in refugia. The eastern Mediterranean region is often considered a refugium during this period, but as attested by the Tenaghi Philippon pollen record (Tzedakis et al., 2006), *Tsuga* already had sporadic appearances in the latest Early Pleistocene. In fact, *Tsuga* shows earlier shifts to lower abundances around MIS 26, well before *Cedrus* whose main decrease has been observed around MIS 16.

At the MJS, *Cedrus* reaches high percentage values during the transition between MIS 21 and MIS 20 as it does at Valle di Manche, whereas from MIS 19 to the beginning of MIS 18 its abundance never exceeds 7%. *Liquidambar*, almost continuously present up to MIS 40 (at Santa Lucia; Joannin et al., 2007) and recorded discontinuously starting at MIS 37 at MJS Interval A

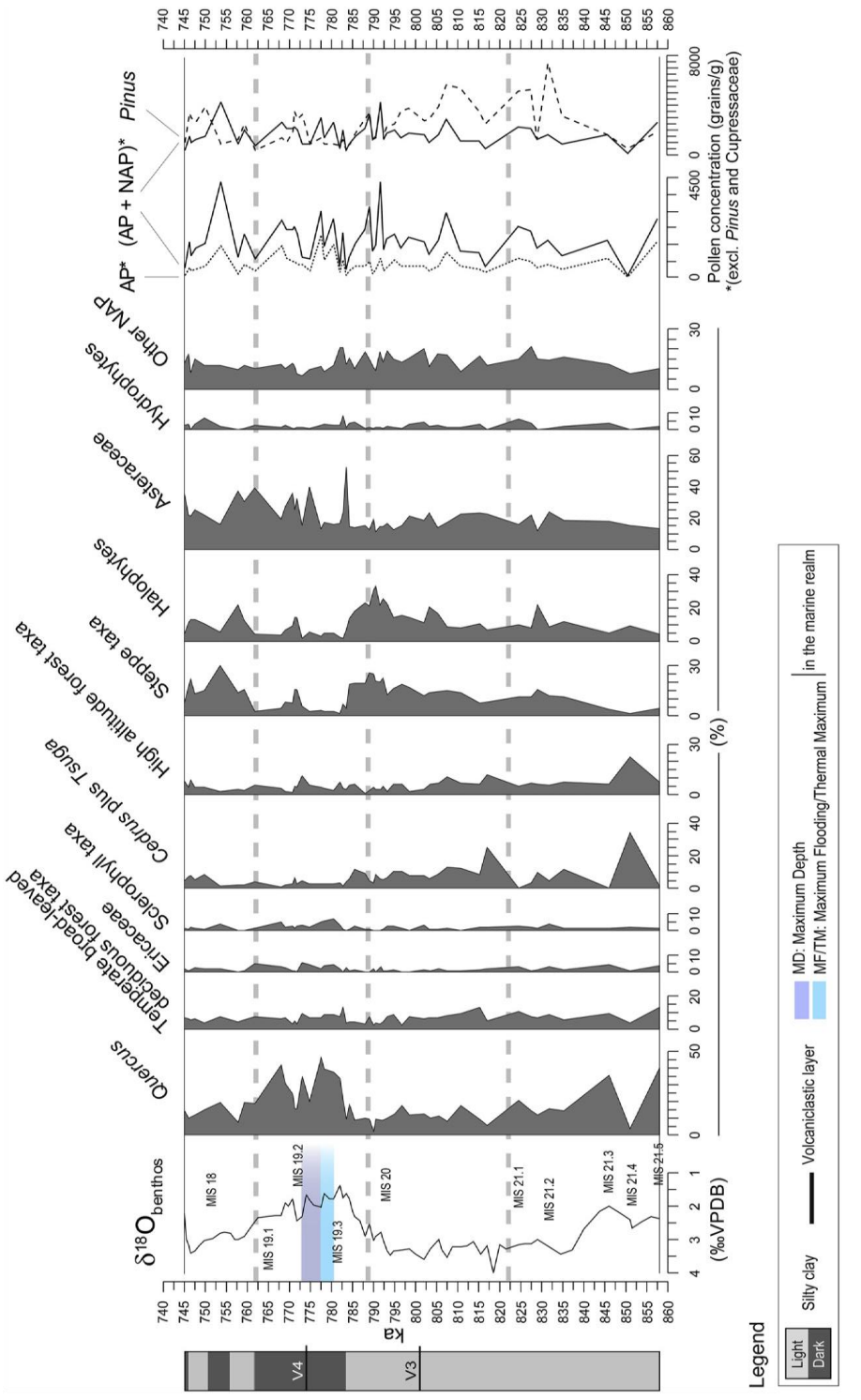

Fig. 5. Quantitative abundance of selected pollen taxa versus age (using the age model of Marino et al., 2015). On the left, lithostratigraphy (see Fig. 2 for legend; Ciaranfi et al., 2010) and benthic $\delta^{18}O$ record from the Montalbano Jonico section (Brilli et al., 2000; Ciaranfi et al., 2010). The age of volcaniclastic layer V4 is from Petrosino et al. (2015). Dashed gray lines indicate the main phases described in the text. MD, MF and TM are marked according to Marino et al. (2015, and references therein).

(Joannin et al., 2008), is represented by few and sparse pollen grains in both the MJS and Valle di Manche records.

Carya, *Pterocarya* and *Zelkova*, although never recorded in high abundances, are still present at the MJS as well as at Valle di Manche. *Carya* was an important element of interglacials in the Santa Lucia section until 1300 ka. Despite being more abundant in the basal portion of the MJS, it is strongly reduced, rarely exceeding 1%, during MIS 19. Previously assumed to have disappeared before MIS 15 (Russo Ermolli et al., 2010a, 2010b), *Carya* has recently been recovered from the Boiano basin (Molise region, southern Italy) in a stratigraphical interval attributed to MIS 9 (Orain et al., 2012, 2013). Its persistence appears to have been favoured by the occurrence of an ecological refuge connected to high edaphic humidity (Orain et al., 2013). Throughout the Lower Pleistocene pollen record, the decline of *Carya* parallels the expansion of deciduous *Quercus*. As recorded at the MJS Interval A, deciduous *Quercus* and *Cedrus* replaced *Carya* and *Tsuga* from 1250 ka onwards (Joannin et al., 2008). In our record, *Quercus* is the main component during interglacials reaching abundances up to 45% during MIS 19.

Along with the progressive changes in tree populations, herbaceous plants, including steppe taxa, show significant expansions. In our record, *Artemisia*, an important component of steppe vegetation along with *Ephedra* and subordinately *Hippophaë*, shows successive increases with a peak (27%) in the basal portion of MIS 18, at 753.61 ka. In the Crotone basin, the first main spread of *Artemisia* was observed at Vrica from ca. 1870 ka (Combourieu Nebout and Vergnaud Grazzini, 1991; Combourieu Nebout, 1993; Klotz et al., 2006). Such changes in vegetational composition indicate a progressive temperature drop during steppe (and forest) phases through the successive G/I cycles of the Middle Pleistocene. In particular, the diffusion of *Hippophaë rhamnoides* has been associated with the expansion of "cold steppes" at the expense of "warm steppes", including such thermophilous taxa as *Cistus* and *Phlomis fruticosa* (Suc et al., 1995), during the Middle Pleistocene. In our record, a single pollen grain of *Phlomis* has been detected, and *Cistus* is uncommon.

6.2. Vegetation and climate inferences between MIS 20 and MIS 18

The analysis of pollen assemblages throughout the DF-DFJ and Ideale partial sections (Figs. 2, 4–6) enables the succession of vegetation and climatic conditions of the MJS to be investigated, thereby improving the framework of paleoenvironmental changes during the MIS 20–18 interval.

6.2.1. MIS 21

During MIS 21, sedimentation occurred in a lower circalittoral environment until 820 ka, according to evidence from ostracod assemblages (Aiello et al., 2015) and in agreement with circalittoral micro- and macrobenthic paleocommunities (D'Alessandro et al., 2003; Stefanelli, 2003). In detail, the slight shallowing based on ostracods and centered at ca. 835 ka (Aiello et al., 2015) parallels a significant decrease of the *Pinus*vs. halophytes ratio as well as a major expansion of both halophyte and steppe taxa, centered at 829 ka (Fig. 6), supporting an extension of coastal areas. Moreover, the slight deepening at about 820–824 ka (Aiello et al., 2015) matches the successive increase of the *Pinus* vs. halophytes ratio. In terrestrial settings, the dominance of temperate forest taxa, mostly deciduous *Quercus*, supports the interpretation of climate conditions similar to the present day, with warm temperatures and a seasonal precipitation regime, between 858 ka and 824.5 ka. Pollen-inferred warmer phases, including three peaks in the PTI and high percentage values of temperate AP, are centered at 858 ka, 846 ka, and 824.5 ka, approximating oxygen isotopic fluctuations close to MIS 21.5 (upper part), 21.3 and 21.1, respectively. Percentage values of *Quercus* and other temperate forest taxa are higher in correspondence with the event close to MIS 21.5 and progressively decrease up to MIS 21.1. However, when comparing the PTI values (Fig. 6) for the last three substages of MIS 21, the highest values (i.e. warmer conditions) correspond to MIS 21.3. This principally reflects the lower expansion of steppe vegetation at that time than in MIS 21.5 and especially MIS 21.1. In the nearby Valle di Manche, a mesic forest dominated by oaks was also identified from the pollen record and correlated to an undifferentiated MIS 21 (Capraro et al., 2005). Two successive episodes of decline in temperate forest taxa punctuated

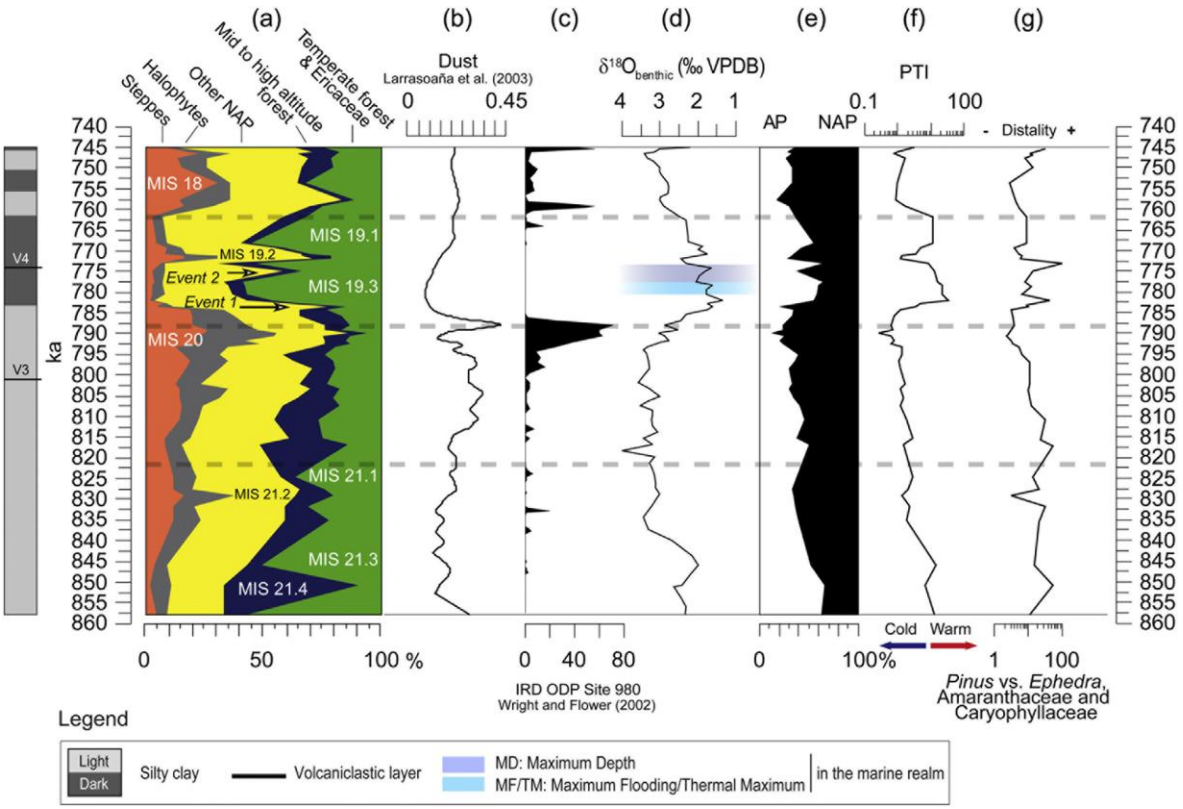

Fig. 6. Comparison of selected pollen records (a, e-g) with the East Mediterranean dust record (b) based on hematite content derived from magnetic properties of sediments from ODP Site 967 (Larrasoa_na et al., 2003), Ice Rafted Debris (IRD) curve (c) from North Atlantic ODP Site 980 (Wright and Flower, 2002), and benthic $\delta^{18}O$ record from the Montalbano Jonico section (d) (Brilli et al., 2000; Ciaranfi et al., 2010). On the left, lithostratigraphy (see Fig. 2 for legend; Ciaranfi et al., 2010) versus age, according to Marino et al. (2015). Pollen records: (a) summary pollen diagram, (e) cumulative frequencies of AP (arboreal pollen) and NAP (non-arboreal pollen), (f) Pollen Temperature Index (PTI, in logarithmic scale), (g) Pinus *vs. Caryophyllaceae, Amaranthaceae,* Ephedra *(in logarithmic scale). Dashed gray lines indicate the main phases described in the text. MD, MF and TM are marked according to Marino et al. (2015, and references therein).*

the entire MIS 21 interval. The first, at ca. 851 ka (close to MIS 21.4), corresponds to the increase of mid-to high-altitude conifer taxa (Fig. 6), probably in response to a temperature drop without a concurrent humidity decline; in fact only a subordinate slight increase of Amaranthaceae and Cichorioideae (Asteraceae) among the non-arboreal taxa is observed (Fig. 4). The second decline in temperate forest taxa takes place close to MIS 21.2 when the significant expansion of open-vegetation taxa including *Ephedra*, Amaranthaceae and *Artemisia* occurs, and it approximates an IRD peak at ODP Site 980 (Wright and Flower, 2002) (Fig. 6), during cooler and drier conditions. Analyses at higher temporal resolution in this stratigraphical portion of the MJS and also at Valle di Manche are necessary to improve the record of the vegetation and climatic events.

6.2.2. MIS 20

Values of the *Pinus* vs. halophytes ratio decline progressively to the top of MIS 20, with a significant minimum centered at 790 ka (Fig. 6), in accord with the distinctive shallowing trend suggested by the ostracod assemblages (Aiello et al., 2015) and previous data based on micro- and macro-benthic invertebrates (D'Alessandro et al., 2003; Stefanelli, 2003).

The progressive inception of glacial MIS 20 at the MJS caused an expansion of the mid-to high-altitudinal coniferous forest (especially *Cedrus*, followed by *Abies*, *Picea* and *Tsuga*) at 816.94 ka; this change in the pollen assemblages seems to reflect principally a decrease in temperatures but not of precipitation. At the Valle di Manche, such a climate event is expressed by a larger expansion of high altitudinal conifers, especially *Abies* followed by *Picea*, and is associated with a cool to cold climate with abundant precipitation throughout the year (low seasonality) (Capraro et al., 2005). In the Crotone basin, the expansion of high altitudinal conifers precedes the re-establishment of an environment dominated by a (wooded) steppe-like vegetation during the MIS 20–19 transitional phase. The expansion of a wooded steppe is evident also at the MJS where mesophilous arboreal taxa together with steppe taxa are the main components of the pollen assemblages up to 793.2 ka (Figs. 5 and 6). However, from 815.41 ka upwards, herbaceous taxa show a persistently increasing presence with a maximum centered at

790.64 ka. The strong increase of Amaranthaceae, *Artemisia* and *Ephedra* indicates a phase of expansion of the open landscape, supporting the interpretation of a prevalent dry steppe (Figs. 5 and 6) during the interval of time including Termination IX (e.g. Lisiecki and Raymo, 2005; Channell et al., 2010). Minimum values recorded by the PTI (Fig. 6) correlate approximately to a sharp peak both in dust (Larrasoaňa et al., 2003) and IRD records (Wright and Flower, 2002; Kleiven et al., 2011), documenting a distinct cold and arid climate event at a wide North Hemisphere scale across the MIS 20–19 shift. A drier phase dominated by open-vegetation taxa possibly corresponds to the pollen assemblage zone CR-4 of Capraro et al. (2005) which is characterized by the establishment of a non-forested environment (with AP at very low values) dominated by steppes, under a very dry to arid climate with precipitation irregularly scattered throughout the year.

6.2.3. MIS 19

Deep-water marine conditions are documented for MIS 19 at the MJS (D'Alessandro et al., 2003; Stefanelli, 2003), starting from 783.54 ka (Aiello et al., 2015). On land, MIS 19 corresponds to the spread of a temperate forest characteristic of relatively warm and moist conditions. Such climate might have favored water-column stratification in the basin due to the enhanced freshwater input (increased runoff and river supply) that can be expected during an intense interglacial phase. This could indeed have caused the darker sediment colour in the Ideale partial section (Figs. 2, 4–6), possibly linked to low-oxygen bottom conditions and high organic matter preservation.

From 789.15 ka, the progressive increase in thermophilous arboreal taxa (wooded steppe) is soon interrupted twice. The first time is by the successive expansion of mid- and then high-altitude forest taxa up to 785.61 ka, implying a slight decrease in temperature. Then, at 783.54 ka, thermophilous arboreal taxa are replaced by a predominance of cosmopolitan herbaceous taxa, especially Asteraceae and Poaceae, indicating an enlargement of the open landscape (event 1, Figs. 5 and 6; see also in Marino et al., 2015) but not associated with the expansion of steppe or halophyte vegetation. From 782.9 ka, the increase in thermophilous arboreal taxa is more pronounced; it precedes by about 2 ka the onset of maximum flooding (MF, Fig. 6) at 780.56

ka (Marino et al., 2015). The MF phase, between about 780.56 ka and 777.31 ka, coincides with a marine thermal maximum (TM, Fig. 6; Marino et al., 2015), elevated values of the PTI curve at 782 ka (Figs. 4–6), and the low $\delta^{18}O$ values in MIS 19.3. On the other hand, the major percentage increase of deciduous *Quercus* at 777.59 ka approximates the onset of the interval of MD (D'Alessandro et al., 2003) between 777.31 ka and 773.25 ka (Marino et al., 2015).

As a whole, the consistent occurrence of warm-temperate woody taxa together with the moderate abundance of herbaceous taxa (including *Artemisia* and *Ephedra*) indicate either some relatively open forests or perhaps the persistence of some open areas in drier areas of the landscape. The first thermophilous forest-dominated phase, correlated with substage MIS 19.3, possibly developed under conditions similar to present day. However it is punctuated by at least two abrupt increases of herbaceous taxa, the low pollen record resolution between 768.04 ka and 761.83 ka preventing us from verifying the potential occurrence of successive additional short-term events. At 774.84 ka, just below the V4 layer recently dated at 773.9 ± 1.3 ka (Petrosino et al., 2015), the earliest expansion of open vegetation (event 2, Fig. 6; see also in Marino et al., 2015) is mainly characterized by the Asteraceae (up to 40%) and not *Artemisia*. On the other hand, steppe and halophyte taxa (such as *Artemisia*, *Ephedra*and Amaranthaceae) strongly increase together with other herbaceous taxa later, around 772 ka, in coincidence with an increase of $\delta^{18}O$ values (MIS 19.2). At the same time, arboreal taxa show a strong decrease. Such changes in vegetation and the lowering of both PTI and AP% values point to a significant decrease in both temperature and precipitation values. The following significant increase of arboreal mesothermic taxa centered at 768.04 ka, again prevalently marked by the spread of deciduous *Quercus* (up to ca. 41%), probably correlates with substage MIS 19.1 (Figs. 4–6).

At Valle di Manche, the development of mesic assemblages in the phase named CR-5 in Capraro et al. (2005) was correlated with MIS 19. The two successive phases (i.e. CR-6a and -6b) have been interpreted to postdate the interglacial MIS 19, although no more precise correlations were attempted with the oxygen isotope stratigraphy (Capraro et al., 2005). The first phase (CR-6a in Capraro et al., 2005) is characterized by an evident preeminence of altitudinal coniferous forest taxa with a low abundance of NAP, associated

with a cool to cold climate with abundant precipitation throughout the year (low seasonality). The second phase (CR-6b in Capraro et al., 2005), however, documents the new recovery of a forested environment dominated by broad-leaved trees, thus supporting a new climate amelioration. In our opinion, it cannot be excluded that these two successive events could be correlated with MIS 19.2 and MIS 19.1, respectively. However, a difference is evident when comparing the MJS and Valle di Manche pollen records for the phase correlated to MIS 19.2. The high altitude conifer forest-dominated phase (at Valle di Manche) vs. a steppe phase (at MJS) possibly reflects the different paleogeographical contexts of the two sites, as summarized below (6.3).

6.2.4. MIS 18

A circalittoral environment is documented during MIS 18 (D'Alessandro et al., 2003; Stefanelli, 2003) including short-term slight deepenings (Aiello et al., 2015).

The pollen record reveals a significant change in the ratio between AP and NAP (Fig. 6), although the low temporal resolution between ca. 768 ka and ca. 761 ka hinders a better understanding of the mode of transition between MIS 19 and MIS 18. It is worth noting the coincident increase in steppe and halophyte taxa during the episode marked by lighter-coloured sediments between ca. 761 ka and 755 ka (Figs. 5 and 6). This attests to new environmental conditions within the marine setting, possibly reflecting different climate conditions from those described for the darker sediments in MIS 19. In fact, from 761.83 ka to the end of the pollen record at 745.14 ka, AP values remain below 35% (Fig. 6). The decreasing trend of mesothermic arboreal taxa parallels the increase of open vegetation taxa, concomitant with heavier $\delta^{18}O$ values (Figs. 5 and 6). The succesive acme phases of *Ephedra*, the Amaranthaceae, and *Artemisia* mark together with heavy $\delta^{18}O$ values the glacial inception of MIS 18.

For Valle di Manche, Capraro et al. (2005) described an initial forested environment dominated by mountain conifers, followed by a decline in oak forest and low NAP percentages during MIS 18.4, and subsequent increase in NAP associated with a very dry to arid climate.

6.3. Glacial-interglacial pollen pattern

The MJS pollen record documents the main changes in vegetational assemblages and patterns associated with G/I cycles. The spread of temperate forest taxa correlates with MIS substages 21.5 (upper portion), 21.3, 21.1, 19.3, and 19.1 of the oxygen isotope record (Figs. 5 and 6). In contrast, the expansion of open vegetation including steppe development, often preceded by an increase in mid-to high-altitudinal forest taxa, corresponds to glacials MIS 20 and MIS 18 (lower portion). According to Combourieu Nebout and Vergnaud Grazzini (1991), in the Mediterranean littoral zone each G/I cycle, as defined in the Vrica section, includes, when complete, four main subzones: (a) deciduous forest (transitional phase following a glacial, with increasing temperatures but still dry conditions), (b) sub-tropical humid forest (interglacial with maximal temperatures and precipitation), (c) high-altitude coniferous forest (transitional phase with cooler but still humid conditions), and finally (d) expansion of open vegetation, including steppe taxa (full glacial phase with cooler and dry conditions). This pattern is close to that observed at the MJS, the only difference being the absence of subtropical humid taxa within the arboreal assemblages (subzone b) because of the progressive demise of such taxa throughout the Calabrian (e.g. Combourieu Nebout and Vergnaud Grazzini, 1991; Combourieu Nebout et al., submitted for publication).

At Valle di Manche, however, according to Capraro et al. (2005), the glacial MIS 20 (as well MIS 18) was instead characterized by an alpine-type forest (*Picea*, *Abies*, *Fagus*), a wooded steppe landscape becoming established only later at the beginning of the deglaciation from MIS 20 to MIS 19. Such a pattern provides an unusual vegetation record in southern Italy, i.e. G/I cycles associated with alternations in coniferous forest/wooded steppes. As a consequence, as remarked by Capraro et al. (2005), steppe (i.e. arid conditions) should not be equated with glacial maxima without independent supporting evidence.

The presence of several distinct patterns of G/I has been well known for the Italian peninsula since the first palynological investigations on the earlier G/I cycles from the Northern Apennines. Here, glacials are mainly represented by altitudinal conifer taxa, with steppe expansions often

subordinate in time and space (Lona and Bertoldi, 1972; Bertini, 2010 and references therein). Local and/or astronomical factors can be invoked to explain such peculiar patterns. More specifically, the effects of the precession-related warm/dry–cold/humid cycles superimposed upon obliquity-related warm/humid–cold/dry interglacial–glacial cycles have been noted and extensively discussed by many authors, with special focus on the Mediterranean area (Klotz et al., 2006; Tzedakis et al., 2006; Joannin et al., 2007; Tzedakis, 2007).

The MJS and Valle di Manche pollen records, together with their respective oxygen isotope data, provide a unique opportunity to document the tempo (especially at MJS) and modality of vegetation response to changes associated with G/I cycles, including the interaction among obliquity and precession cycles, as these sites cover the same interval of time and are not far from one another (Fig. 1). Accordingly, the observed differences in patterns during the G/I transition probably relate to substantially different local terrestrial paleogeographical contexts (and associated taphonomy) rather than to the superposition of precession on obliquity cycles and its associated effects. At Valle di Manche, the pollen input in the depositional basin possibly included a large component from the high altitudinal belts in the closest high relief (probably the Sila Mountains in Calabria), where high-altitudinal coniferous taxa (the so-called "alpine vegetation" in Capraro et al., 2005) thrived and expanded during glacials when temperature decreased but humidity remained at high values at those altitudes. In contrast, at the MJS, the subordinate role of less prominent and more distant high reliefs (Apennines Chain) could explains the sometimes significant expansion of *Cedrus* from the nearest middle altitude areas, during the phase of decrease of temperature but with still sufficient humidity, whereas steppes expanded in the drier and larger coastal plains.

6.3.1. Landscape changes and human migration at the Early-Middle Pleistocene transition

The detailed formulation of paleoenvironmental scenarios during successive Pleistocene G/I cycles is central to understanding the role of climate in the migration and subsequent colonization of the genus *Homo*, including the

identification of the most favorable times and conditions for their accomplishment (e.g. Dennell et al., 2011; Manzi et al., 2011; Messager et al., 2011 and references therein). Chronologically well-framed pollen records offer a solid database for both climate quantification and the compilation of regional to continental-scale paleogeographic maps, which are extremely helpful in identifying the most likely migration routes of hominin expansion and settlement. Such a complex topic is beyond the scope of the present research, although the Pleistocene successions of the Crotone basin and Bradano Foredeep (MJS, Sant'Arcangelo) fully meet the aforementioned requirements, and crucially complement the often discontinuous and short pollen records from hominin sites. More specifically, the importance of our record lies in its stratigraphical coverage centered on the first undisputed and well-dated phases of human colonization in Europe at the beginning of the mid-Pleistocene Transition (e.g. Head and Gibbard, 2005; Head et al., 2008; Muttoni et al., 2010; O'Regan et al., 2011; Abbate and Sagri, 2012). This period includes the last of the 40-ka climate cycles, when hominins expanded from Africa to the Eurasian continent, predating the colonization and withdrawal between 600 and 400 ka that was driven by stable 100-ka cyclicity at latitudes between 40 and 50°N (e.g. Dennell et al., 2011 and references therein). According to Leroy et al. (2011), the Early Pleistocene interval potentially fits the latest best narrow windows of opportunity for hominins to disperse into Europe during the transition from glacial to interglacial periods, the full glacials being too cold for them and the interglacial to glacial transition too forested. Faunal immigrants including hominins found a composite landscape in the area between 39 and 40°N and 16–17°E where wooded-steppe to steppe were widely distributed. Tree taxa typical of subtropical systems were no longer part of the vegetation, whereas temperate arboreal taxa especially *Quercus* and herbaceous vegetation had significantly increased. The more open and fragmented settings might have represented an advantage for archaic hominins and other mammals, promoting a larger spectrum of possibilities and ecological behaviors.

6.4. Synthesis of regional expressions of climate changes at MJS and their global correlation

Climate quantifications are not yet available between MIS 21 and MIS 18 at the MJS, although they are planned using high-resolution analyses of key intervals between MIS 22 and MIS 16. Meanwhile, data from the earliest G/I cycles recorded at Semaforo (ca. 2460 to ca. 2110 ka; Klotz et al., 2006) evidence a trend towards both a reduction in annual and winter temperatures by more than 2.3 °C, and higher seasonality along consecutive interglacials; a trend toward a strong reduction in all temperature parameters of at least 1.6 °C was also found along consecutive glacials. A decline in winter temperature and annual precipitation in interglacial maxima and glacial minima during 1300–1400 ka and at 500 ka has been confirmed through recent climate reconstructions using selected pollen records from southern Italy (Combourieu Nebout et al., submitted for publication). Such progressive changes explain, in our record, both the absence of the subtropical contingent and the increasing abundance of tree populations, already locally present (e.g. deciduous *Quercus*). No complete disappearances are documented between 858 ka and 745.13 ka due to the absence of major drastic climate events; indeed a number of tree genera are shown to be relicts, and testify to the local long-term persistence of some tree populations (see 6.1.).

Such floristic and vegetational evidence, through integration with marine records (Marino et al., 2015), significantly contributes to the understanding of responses and interactions of global to regional events at the middle latitudes of the central Mediterranean. In this respect, environmental and climatic changes, especially documented for MIS 19, show a remarkable correspondence between marine and terrestrial realms. The climatic inferences from the MJS pollen data are in agreement with those from Tenaghi Philippon (Tzedakis et al., 2006) in the eastern Mediterranean area, whereas they show some differences with vegetational and climatic reconstructions for MIS 19 based on records from Osaka Bay, Japan (e.g. Kitaba et al., 2009, 2012, 2013; Hyodo and Kitaba, 2013). At Osaka Bay, the progressive warming during MIS 19, according to pollen data (e.g. an increase of *Cyclobalanopsis*), was reversed at ca. 784 ka by a cool phase lasting 5 kyr (ca. 783–778 ka) that coincided with a sea level highstand (Kitaba et al., 2012,

2013). The chronology of the Osaka Bay site is based on Hyodo et al. (2006). At MJS, cooling event 1 effectively interrupts a warming phase, at 783.54 ka; but for a very short time interval (Fig. 6). Another element of difference is that at Osaka Bay, a successive rapid warming (after 778 ka) and the following pollen-derived thermal maximum at ca. 776 ka, developed well after the highest sea level. At the MJS, in contrast, the thermal maximum for the terrestrial realm parallels the MD, MF, and TM of the marine realm, within 780 and 777.31 ka, with peaks in both PTI (at 778.36 ka) and *Quercus* (at 777.59 ka), as previously reported in detail. At Osaka Bay, based on high resolution paleomagnetic data (Hyodo et al., 2006), the cooling event, between ca. 783 and 778 ka, falls in the interval of extremely weak magnetic field intensity (ca. 785–776 ka) during the MB transition estimated to occur at ca. 777 ka (Hyodo et al., 2006). Moreover, as it slightly postdates the Northern Hemisphere July insolation peak at 787 ka (Laskar et al., 2004) and largely predates the minimum at 776 ka, it was connected with the effects of cloud formation induced by galactic cosmic rays as a consequence of the geomagnetic field minimum during polarity reversal (Kitaba et al., 2009, 2012, 2013). At the MJS, the occurrence of the anomalous cooling events 1 and 2 within the warm phase associated with MIS 19.3, invites comparison with the Osaka Bay record, even though caution is necessary because the established age model for Osaka Bay is indirectly inferred (Hyodo et al., 2006). But the comparison is interesting because it could also provide evidence for an indirect correlation with the MBB (i.e. a virtual location). In fact, the two paleointensity lows would be located, according to Hyodo et al. (2006), respectively ca. 6 kyr before and 1 kyr after the MBB (Hyodo et al., 2006; Hyodo and Kitaba, 2013). In this perspective cooling event 1, could represent the response to the lowest values of paleointensity before the MBB whereas cooling event 2 (at 774.84 ka according to the model age established at the MJS) approximate the younger lowest paleointensity values after MBB.

Whatever the cause of the short-term cooling events, they express quite rapid climate variability during MIS 19.3, in good agreement with similar abrupt events in both Atlantic and Mediterranean areas during the late Quaternary (e.g. Bond et al., 1993, 1997; Rohling et al., 1998; Cacho et al., 2001; Combourieu Nebout et al., 2009; Sanchez Goni and Harrison, 2010; Wolff et al., 2010; Candy et al., 2014). Hence, the MJS as well as other Mediterranean records attest, once more, that the climate of this region oscillated rapidly not

solely during glacials, as already largely documented, but also during warm periods. The duration and amplitude of rapid climate oscillations are crucial matters of debate, especially in the context of present global warming. However, to evaluate whether they represent a reliable analogue for understanding future climate scenarios, a more complete identification and description of such high-frequency climate fluctuations, as well as their comparison with similar events within MIS 11, MIS 5 and the Holocene (e.g. events at 9.2 and 8.2 ka), are essential. The higher resolution analyses in progress at MJS accordingly meet this need.

7. Conclusions and perspectives

The present pollen analysis from the marine Montalbano Jonico sequence contributes to the reconstruction of both the long-term behaviour of individual taxa and vegetation trends within the context of global Quaternary climate changes on land, in the interval 858–745 ka, in the central Mediterranean.

i. Pollen assemblages, not yet possessing "modern" characters, are dominated by temperate taxa and exhibit reduced diversity associated with the disappearance of subtropical ecosystems from the southern Italian area around 1200 ka. However, a number of relict tree genera are still present, and there is no evidence of clear patterns of extinction. Some tree populations already present in the area, notably deciduous oaks, show progressively increasing importance.
ii. Comparison of pollen and marine isotope records from the same sediments reveals a remarkable correspondence. The arboreal (AP) and non-arboreal pollen (NAP) signal along with the Pollen Temperature Index (PTI) show the same orbital to sub-orbital variability as the benthic $\delta^{18}O$ record. The recurrent pattern of vegetation change (wooded steppe to steppe/thermophilous forest), during G/I cycles between MIS 21 and MIS 18, associated with specific climate conditions is in good agreement with orbital signatures. Intervals of heavy benthic $\delta^{18}O$ values, concomitant with glacials (i.e. MIS 20 and MIS 18),

correspond to equally significant drops in AP and PTI values. The predominance of NAP, especially *Artemisia*, *Ephedra* and Amaranthaceae, indicates steppe vegetation and a climate with severe seasonal moisture deficiency and marked temperature seasonality. In contrast, light benthic $\delta^{18}O$ values (MIS 21 and MIS 19) correspond to synchronous expansions of thermophilous arboreal populations, mainly deciduous *Quercus*, suggesting a period of mild winters and warm summers, with reduced seasonal moisture deficiency. The persistent presence of arboreal pollen and the relative rapidity of its increases at the end of cold episodes indicate that temperate tree populations were present in areas not far away even during the coolest episodes. The apparent discrepancy in the G/I pattern as reconstructed from pollen analysis in the nearby Valle di Manche site seems prevalently related to the effects of local factors.

iii. The *Pinus* vs. Caryophyllaceae, Amaranthaceae and *Ephedra* ratio as an expression of distality shows fairly good correspondence with sea level fluctuations related to G/I cycles by the study of the marine fauna, and provides additional lines of evidence for paleoenvironmental reconstructions.

iv. Millennial scale climate variability occurs during MIS 19, as evidenced by two abrupt short-term events (events 1 and 2), both characterized by an expansion of cosmopolitan herbs. Event 1, at 783.54 ka, marks the MIS 20–19 transition, interrupting the earlier progressive increase of thermophilous forest taxa after the steppe-dominant episode centered at 790 ka. Event 2, at 774.84 ka, is stratigraphically located just below the volcaniclastic layer V4 which is radiometrically dated at 773.9 ± 1.3 ka. This short-term expansion of herbaceous vegetation postdates the MF, and interrupts the TM in the marine realm which is expressed on land by the major expansion of deciduous *Quercus,* at 777.59 ka. Moreover, it precedes the major expansion of steppe vegetation correlated to MIS 19.2, at 771.85 ka. The evaluation of causes and mechanisms for events 1 and 2 recalls the suggested connection between Earth's magnetic field and climate, an issue already addressed for the Early–Middle Pleistocene transition. Our contribution to the topic seems promising due to the environmental and stratigraphic

context of the MJS. The pollen record from marine sediments at the MJS facilitates direct land–sea comparisons, which allow reliable stratigraphic reconstructions and the chronologic definition of marine and terrestrial events.

v. The new paleoclimatic and stratigraphic dataset for the MJS, especially across MIS 19, is of utmost significance in improving chronostratigraphic constraints for the Early–Middle Pleistocene transition close to the MBB. In particular, the development of a detailed correlation between the Valle di Manche and the MJS should add new information and stratigraphic resolution to the climate context across the MBB. The critical comparison between Mediterranean and Japanese mid-latitude records has climatic and stratigraphical implications for the global expression of MIS 19, as well as the selection of the Middle Pleistocene GSSP.

vi. The chronologically well constrained floristic, vegetational and climate database for the MJS contributes significantly to our understanding of Mediterranean climate and landscape development, of relevance to human migration and colonization during the Early–Middle Pleistocene transition. Once quantifications have been implemented, it will allow key physical (temperature, precipitation etc.), vegetational (biomes, diversity etc.) and geographical (topography etc.) parameters to be precisely reconstructed. All these data are indispensable for mapping the spatial and temporal characteristics of potential migration routes, and to understand in detail the influence of environmental factors on bio-cultural adaptation of hominins affecting the timing and mode of expansion into Europe.

Finally, the MJS record, in revealing a more general view of the climate issue, contributes also to the debate on present climate change, especially by the documentation of MIS 19 which is now considered a close analogue for the present interglacial. Such evidence meets an essential requirement for scientists studying climate today, whose objective analyses require quantitative knowledge of the extent of the forcing introduced by human activity, the sensitivity of the climate system to these pressures, and the time required for climate to respond. Understanding climate change in the

geological past, and especially the potential for rapid changes in the near future, poses questions about the real human capacity for adaptation as well as the possible need for society to adopt drastic and onerous measures. The strategies of economists, influenced by ethical principles, should take into account paleodata that help to describe precisely the causes and effects of climate changes.

Contribution A3

Paleoenvironmental and climatostratigraphic insights for Marine Isotope Stage 19 (Pleistocene) at the Montalbano Jonico succession, South Italy*

*Published in Quaternary International 383, 104-115
(M. Marino, A. Bertini, N. Ciaranfi, G. Aiello, D. Barra, S. Gallicchio, A. Girone, R. La Perna, F. Lirer, P. Maiorano, P. Petrosino, **F. Toti**, 2015)

Abstract

Quantitative analyses on pollen and ostracods were performed on the Montalbano Jonico succession (MJS) through Marine Isotope Stages (MIS) 18–21 in order to acquire details of paleoenvironmental changes and climate pattern during MIS 19, which includes the Matuyama–Brunhes paleomagnetic boundary (MBB). While the MJS does not record the MBB, which is the main criterion for defining the Early–Middle Pleistocene boundary, it is a candidate Global Boundary Stratotype Section and Point (GSSP) for the Ionian Stage and Middle Pleistocene Subseries because of its excellent exposure, continuous deposition, and astronomically tuned record between MIS 37 and MIS 16. The new $^{40}Ar/^{39}Ar$ age of 773.9 ± 1.3 ka for volcaniclastic layer V4 allows the age-model for the succession to be refined. Ostracod assemblages show significant paleodepth fluctuations at the glacial–interglacial scale, in agreement with the pollen distality index (*Pinus* vs. Caryophyllaceae, Amaranthaceae and *Ephedra*) which also suggests higher values during MIS 19. Pollen analysis provides supplementary paleoclimate data that are valuable to reconstruct temperature variation during the identified phases. A major expansion of steppic vegetation at 790 ka in the uppermost MIS 20 correlates with a significant cold and arid Northern Hemisphere climate phase, as documented by a concurrent peak both in North Atlantic ice rafted debris and Mediterranean dust records. Climate conditions recorded in MIS 19.3 were similar to those of the present interglacial, whereas a dry climate phase marks MIS 19.2 at 771.84 ka, slightly above the V4 layer. Millennial scale climate variability occurred during MIS 19 as evidenced by two abrupt short-term moderately dry pollen events at 783.5 ka and 774.8 ka that could be related to a period of reduced geomagnetic field intensity through the MBB transition. Additional environmental/chronological events accompanied this stratigraphic interval: i) the volcaniclastic layers V3 and V4, radiometrically dated at 801.2 ± 19.5 ka and 773.9 ± 1.3 ka, respectively; ii) the co-occurrence of

maximum flooding and thermal maximum in agreement with the previously recorded co-occurrence of the *Neopycnodonte* community and tropical–subtropical mesopelagic teleostean *Bonapartia pedaliota*, close to the increase of *Quercus*; and iii) the maximum depth (MD) between 777.3 and 773.25 ka as recorded by outer shelf/upper slope macroinvertebrate fauna, close to the highest value of pollen distality index in MIS 19. Results enhance the understanding of orbital-suborbital paleoenvironmental change during the mid-Pleistocene, and particularly of the climate pattern during MIS 19 and across the MBB.

Keywords: Montalbano Jonico succession; MIS 19; Early–Middle Pleistocene transition; Climatostratigraphy; Pollen; Ostracods

1. Introduction

Marine Isotope Stage (MIS) 19 is the mid-Pleistocene interglacial that includes the Matuyama–Brunhes (MB) magnetic reversal (Shackleton et al., 1990), indicated as the primary criterion for defining the Lower–Middle Pleistocene boundary (Richmond, 1996; Pillans, 2003; Head and Gibbard, 2005; Cita et al., 2006; Head et al., 2008). This geomagnetic polarity boundary has an age assignment slightly but significantly variable depending on the nature of the record (rock, ice core), rock type and quality of sedimentary records (volcanic, marine, continental), sedimentation rate estimate, and method of age-model construction (e.g. radiometric dating, orbital tuning by correlation to stable oxygen isotope stage and GRAPE density/magnetic susceptibility stratigraphies, ^{10}Be peak in ice core, and correlation to ice volume model of Imbrie and Imbrie (1980) (Channell and Raymo, 2003; Channell et al., 2004, 2010). Therefore, the MB boundary has been referred to 730 ka (Mankinen and Dalrymple, 1979; Imbrie et al., 1984; Ruddiman et al., 1989), 766.4 ka (Raisbeck et al., 2006), 770 ka (Dreyfus et al., 2008), 773–774 ka (Channell et al., 2004, 2010), 776 ka (Coe et al., 2004; Singer et al., 2008), 775.5 ka (Bassinot et al., 1994), 780 ka (Shackleton et al., 1990; Lourens et al., 2004), 786.1 ka (Sagnotti et al., 2014), and to older ages down to 790 ka (Kuiper et al., 2008; Renne et al., 2010). Age assignments ranging from 766 ka to 820 ka are indicated in

Chinese loess deposits, implying a correlation of the MB boundary to MIS 19–21 (Dodonov, 2005; Yang et al., 2007, and reference therein).

Furthermore, the MB reversal is characterised by a transition in polarity lasting 5–8 kyrs (Channell and Kleiven, 2000; Channell et al., 2004; Leonhardt and Fabian, 2007) that is site location dependent (Clement, 2004; Leonhardt and Fabian, 2007), and by the occurrence of at least one (Sagnotti et al., 2014) or even four (Hyodo et al., 2006, 2011; Wang et al., 2006; Yang et al., 2008; Channell et al., 2010) short-lived reversal episodes. The latter have been associated with millennial scale pollen-derived climate variations possibly induced by changes in the geomagnetic field intensity and cosmic ray flux (Kitaba et al., 2009, 2013). Low paleointensity minima before the Matuyama–Brunhes boundary (MBB) are a common feature in several globally-distributed records (Dinarès-Turell et al., 2002) and might have driven climate variability on the Earth (Kitaba et al., 2012, 2013). Such a detailed climatostratigraphy through MIS 19 and the MB transition may represent additional constraints for a potential wide-scale stratigraphical correlation and for the best selection of the Middle Pleistocene global boundary stratotype section and point (GSSP). Taking in mind that "the MBB is only one of multiple criteria that will be used for local, global and regional correlation of the boundary" (Head et al., 2008), several recommendations are given for the establishment of a GSSP (Remane et al., 1996) such as: exposure on land and over an adequate thickness in a marine succession, continuous sedimentation and high sedimentation rate, absence of synsedimentary and tectonic disturbances, absence of metamorphism and strong diagenetic alteration, abundance and diversity of well preserved fossils, absence of vertical facies changes, favourable facies for wide-scale biostratigraphic correlations, radioisotopic dating, chemostratigraphy, accessibility, free access, and permanent protection of the site. Furthermore, MIS 19 is of interest to the scientific community since it has been suggested as being the closest analogue of the present interglacial in terms of its astronomical signature and similarity of paleoclimate signal (Tzedakis, 2010; Tzedakis et al., 2012). Hence, the present study aims to acquire new paleoenvironmental data across MIS 19 at the Montalbano Jonico succession (MJS), a potential GSSP for the Middle Pleistocene Subseries (Ciaranfi and D'Alessandro, 2005; Ciaranfi et al., 2010; Maiorano et al., 2010), even though the paleomagnetic signal does

not allow the recognition of the MBB due to secondary normal magnetization (Sagnotti et al., 2010). The MJS adequately satisfies most of the recommendations indicated for a global boundary stratotype because it is a continuous and expanded fossil-bearing sedimentary record, spanning MIS 37–16 (Fig. 1), that preserves multiple astronomically-tuned chronological constraints (Brilli et al., 2000; Ciaranfi et al., 2001, 2010; Girone and Varola, 2001; D'Alessandro et al., 2003; Stefanelli, 2003, 2004; Maiorano et al., 2004, 2010; Stefanelli et al., 2005; Joannin et al., 2008; Girone et al., 2013a), additionally supported by $^{40}Ar/^{39}Ar$ ages of volcaniclastic layers V3 and V5 (Ciaranfi et al., 2010; Maiorano et al., 2010). The MJS is also included in the "Special Nature Reserve of the Montalbano Jonico Badlands" owing to a ratified law of the Basilicata Region (Regional Law, January 27th, 2011, n. 3) guaranteeing its protection. The MJS, together with the Vrica section which contains the GSSP of the Calabrian Stage (Cita et al., 2008, 2012), cover the entire Calabrian time, from MIS 65 to MIS 37 (in the Vrica section) to MIS 37 to 19 (in MJS), thus representing a potential unit-stratotype for the Calabrian Stage (Maiorano et al., 2010). Both the sections are astronomically-tuned and are not too far from each other in South Italy (Fig. 1), a reference region for Quaternary chronostratigraphy, and also not far from the Il Fronte section (Taranto, Fig. 1) that is a potential candidate for the GSSP of the Tarentian Stage (Upper Pleistocene Subseries) (Amorosi et al., 2014).

The sedimentary interval spanning MIS 19 in the MJS was deposited in an open marine environment from an inner–outer shelf to transition to slope setting (D'Alessandro et al., 2003), and is characterised by high sedimentation rates helpful for high resolution studies and long distance stratigraphical correlations. The available stable oxygen-isotope stratigraphy across MIS 20–18 is at high temporal resolution mainly ranging from 0.5 ka to 1.8 ka. It records the main Pleistocene wide-scale glacio-eustatic fluctuations (Ciaranfi et al., 2010), and so provides useful support for detailed paleoenvironmental reconstruction. Accordingly, analyses of pollen assemblages have been carried out at high temporal resolution in the MIS 18–21 portion of the MJS, with the aim to improve the paleoclimate reconstruction through the selected interval and attempt a correlation with other coeval sedimentary records in which climate phases and/or the MBB are observed. The new pollen data will extend the floristic and vegetational data set for the Mediterranean (Tzedakis et al.,

2006; Joannin et al., 2007) and extra-Mediterranean (Prokopenko et al., 2006; Kitaba et al., 2013) areas, and in particular in the Italian peninsula which is characterized by a complex mosaic of climate and topographic gradients influencing both stand structures and species composition (e.g. Capraro et al.,

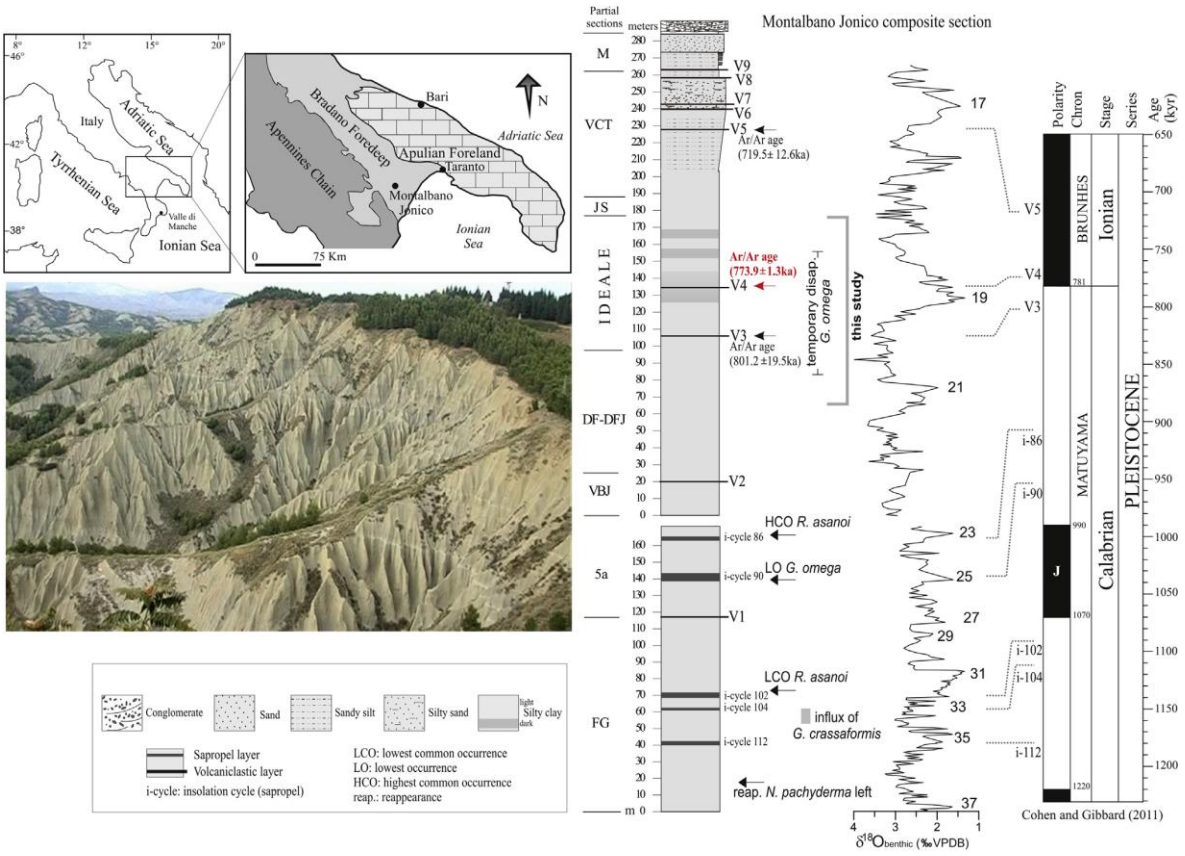

Fig. 1. Location of the Montalbano Jonico succession (MJS). Main lithological features of the composite section, obtained by correlating several partial sections (FG-M). Chrono-biostratigraphic constraints are shown on the right together with benthic $\delta^{18}O$ (Brilli et al., 2000; Ciaranfi et al., 2010; Maiorano et al., 2010). Marine Isotope Stages are according to Ciaranfi et al. (2010). In red, the age of volcaniclastic layer V4 (Petrosino et al., 2015). Correlation of selected chronostratigraphic constraints at the MJS with the standard chronostratigraphy (Cohen and Gibbard, 2011) is drawn on the right. The image of the badlands including V5 to V7 volcaniclastic layers is also visible on the left. (For interpretation of the references to colour in this figure legend, the reader is referred to the web version of this article.)

2005; Sabato et al., 2005; Suc and Popescu, 2005; Bertini, 2010; Bertini et al., 2010; Suc et al., 2010; Magri and Palombo, 2013).

The new studies on benthic ostracod assemblages mainly focus on paleodepth changes through the interval MIS 18–21 in order to improve documentation of the glacio-eustatic rise correlated with MIS 19 and the MBB, which possibly corresponds to the major Pleistocene sequence boundary "I01" ('Ionian', 0.78 Ma) of Snedden and Liu (2010). Data are compared with regional to global-scale climate signals in order to support paleoenvironmental reconstruction at the MJS. Specifically, high values of aeolian dust from the eastern Mediterranean Sea record (Larrasoaña et al., 2003) are taken into account as a proxy of continental cold and arid conditions, while peaks of ice rafted detritus (IRD) from North Atlantic Ocean Drilling Program (ODP) Site 980 (Wright and Flower, 2002) provide an indication of extreme cold phases. Data on micro- and macrobenthic invertebrate fauna available at the MJS (Stefanelli, 2003; D'Alessandro et al., 2003) are also considered in our discussion to outline a more complete paleoenvironmental framework through the investigated interval.

Finally, the $^{40}Ar/^{39}Ar$ age of the volcaniclastic layer V4 is given, which improves the age-model of the MJS and enhances its chronological constraints.

2. The Montalbano Jonico succession

The MJS was deposited during the Early and Middle Pleistocene (Ciaranfi et al., 1996, 1997, 2005; 2010; Marino, 1996; D'Alessandro et al., 2003; Maiorano et al., 2004, 2010) in an upper slope to inner shelf setting along the southern part of the Apennines Foredeep Basin (Fig. 1). The Lower–Middle Pleistocene composite section, based on the study of several partial sections (Fig. 1), crops out in the Lucania Basin (Balduzzi et al., 1982). This is a minor basin of the foredeep (Bradano Trough, in Casnedi, 1988) between the Apennines Chain and the Apulia Foreland (Fig. 1). The Bradano Trough was formed in the Early Pliocene and underwent significant modifications during the Late Pliocene and Early Pleistocene. Its inner border, which was deformed by polyphasic

active thrusts, moved north-eastward; its outer margin spread gradually over the Apulia Foreland units (Casnedi et al., 1982).

The MJS is well exposed in the badlands along the east bank of Agri River, and with a thickness of about 450 m consists of coarsening upward deposits formed by hemipelagic silty clays and, in its upper part, by sandy clays (Fig. 1). It includes nine volcaniclastic layers (V1–V9). Restricted to its lower part are five dark horizons (Fig. 1) that evidence depleted oxygen conditions at the sea bottom and have been referred to sapropel layers owing to their micro- and macro-invertebrate benthic assemblages (D'Alessandro et al., 2003; Stefanelli, 2004; Stefanelli et al., 2005; Maiorano et al., 2008) and planktonic foraminiferal $\delta^{18}O$ signatures (Maiorano et al., 2008; Ciaranfi et al., 2010). These layers have been correlated, from oldest to youngest, to insolation cycles i-112, i-104, i-102, i-90, and i-86, using the Mediterranean sapropel stratigraphy of Lourens (2004) and Lourens et al. (2004). A short stratigraphical gap divides the Montalbano Jonico succession into two portions: the lower one, 168 m thick, was accumulated in an upper slope/outer shelf setting; the upper one, 280 m thick, suggests deposition in a shelf setting with intermittent transition to slope environment (D'Alessandro et al., 2003; Stefanelli, 2003; Ciaranfi and D'Alessandro, 2005; Girone, 2005; Ciaranfi et al., 2010). The whole section represents the regressive part of a third-order cycle with several fourth and fifth-order cycles mainly induced by climate change (Ciaranfi et al., 1997, 2001). The calcareous nannofossil biostratigraphy (Marino, 1996; Ciaranfi et al., 1997; Maiorano et al., 2004) suggests that the succession belongs to the small *Gephyrocapsa* and *Pseudoemiliania lacunosa* zones, based on the biostratigraphic scheme of Rio et al. (1990). Stable oxygen isotope analyses performed throughout the entire succession on planktonic (*Globigerina bulloides*) and benthic (*Cassidulina carinata*) foraminifer tests, combined with calcareous plankton biostratigraphy, radiometric data ($^{39}Ar/^{40}Ar$) on V3 and V5 volcaniclastic layers, and sapropel stratigraphy, have allowed the astronomical calibration of the MJS that covers the time interval MIS 37–16, i.e., 1.24–0.645 Ma (Ciaranfi et al., 2010; Maiorano et al., 2010). Several worldwide calcareous plankton bioevents were recognized in the MJS (Fig. 1), and the updated biochronology is reported in Maiorano et al. (2010) and Girone et al. (2013a).

The MJS clearly encompasses the timing of the MBB, which should be located in the Ideale partial section within the MIS 19 time interval (Fig. 1). The beginning and end of the second temporary disappearance (td2 *sensu*Maiorano and Marino, 2004) of *Gephyrocapsa omega* are the calcareous nannofossil bioevents recorded across the upper DF–DFJ and Ideale partial sections (Fig. 1). In this portion of the succession, the sedimentation rate ranges between 0.5 and 2 m/kyr.

3. Methods

The new ostracod analyses are from the upper part of the partial section DF–DFJ to the top of Ideale section in Fig. 1. Ostracod assemblages were analyzed in forty samples at the same levels used for $\delta^{18}O$ analysis, between 65.1 and 176.1 m (Fig. 1), usually with a spacing of 1–4 m, rarely up to 6 m, which corresponds to a time resolution mainly ranging from 0.5 kyrs to 2.5 kyrs, and seldom 3–6 kyrs. Sediment samples with a dried weight of 300 g were disaggregated and washed through 230 and 120 mesh sieves (63 μm and 125 μm, respectively). The two fractions were analyzed and all the ostracod shells were picked from the coarsest fraction (>125 μm). Assemblages were quantitatively analyzed and taxa identified according to the Neogene–modern taxonomic literature, with special regard to the Mediterranean area (i.e. Müller, 1894; Sissingh, 1972; Bonaduce et al., 1976; Colalongo and Pasini, 1980; Aiello et al., 2000; Aiello and Szczechura, 2004; Aiello et al., 2015, for extensive references). Paleoecological reconstructions are based on autochthonous taxa only and on available data for both living and extinct species.

Palynological analyses are still in progress throughout the interval between MIS 22 and MIS 16, and were performed on 49 samples from the interval 74.70–165.1 m (Fig. 1), mainly taken at the same stratigraphic levels from which stable oxygen isotope analyses had been obtained. The sampling interval was about 0.5–1.7 m and rarely up to 6 m at the basal and upper parts of the section. According to our age model, the temporal resolution is 0.4–1 kyrs, with values of 4–7 kyrs for a few intervals within the lower portion of the section (MIS 21) and in MIS 18. Samples were subjected to standard chemical–physical procedures at the Department of Earth Science, Florence University.

An exotic marker (*Lycopodium* spores) was added at the beginning of the preparation to estimate pollen concentration. The procedure includes treatments with HCl (10%), HF (48%), sodium hexametaphosphate, KOH (10%), $ZnCl_2$ separation (solution density ca. 2.0), and sieving at 10 µm. Transmitted light microscopy, at ×750 and ×1250 (oil immersion) magnifications, was used for identification and counting of palynomorphs (pollen and dinoflagellate cysts). More than 34,836 pollen grains were counted, which corresponds to a mean value of about 265 grains (excluding *Pinus* and Cupressaceae) per sample. Pollen percentages have been calculated on the total of pollen grains excluding *Pinus* and Cupressaceae. *Pinus* while frequently observed in marine depositional settings is in fact constantly and largely over-represented (e.g. Beaudouin et al., 2007). Cupressaceae pollen was also exceptionally abundant in some levels. *Pinus* abundance was normalized to the total pollen sum (excluding Cupressaceae) whereas Cupressaceae were normalized to the total pollen sum (excluding Pinaceae). Two ratios were calculated based on Joannin et al. (2008) and Suc et al. (2010): 1, mesothermic arboreal taxa (e.g., *Quercus*, *Carpinus* and *Carya*) vs. steppe taxa (*Artemisia* and *Ephedra*) to discriminate warm-temperate from cold phases (pollen temperature index, PTI); and 2, *Pinus* vs. halophytes (e.g. Caryophyllaceae, Amaranthaceae, *Ephedra*), used as an indirect proxy of sea-level fluctuations to indicate changes in distality, i.e. distance from the shore (e.g. Cambon et al., 1997; Beaudouin et al., 2005). The curve of the total percentage of arboreal (AP) and non-arboreal (NAP) pollen grains (without *Pinus*) was also traced; the NAP, as a record of all the herbaceous community (including cosmopolitan herbaceous elements), is a signal of paleoenvironmental and paleoclimatic changes at local to global scales. The curve of the total percentage of arboreal pollen (AP), calculated from the sum of arboreal plus non-arboreal (NAP) pollen excluding *Pinus*, was also traced.

4. Results

The new $^{40}Ar/^{39}Ar$ age assignment of the volcaniclastic layer V4 is 773.9 ± 1.3 ka (Petrosino et al., 2015) when combined with the $^{40}Ar/^{39}Ar$ age of 801.2 ± 19.5 ka of V3 layer it allows a stringent chronological constraint of the studied

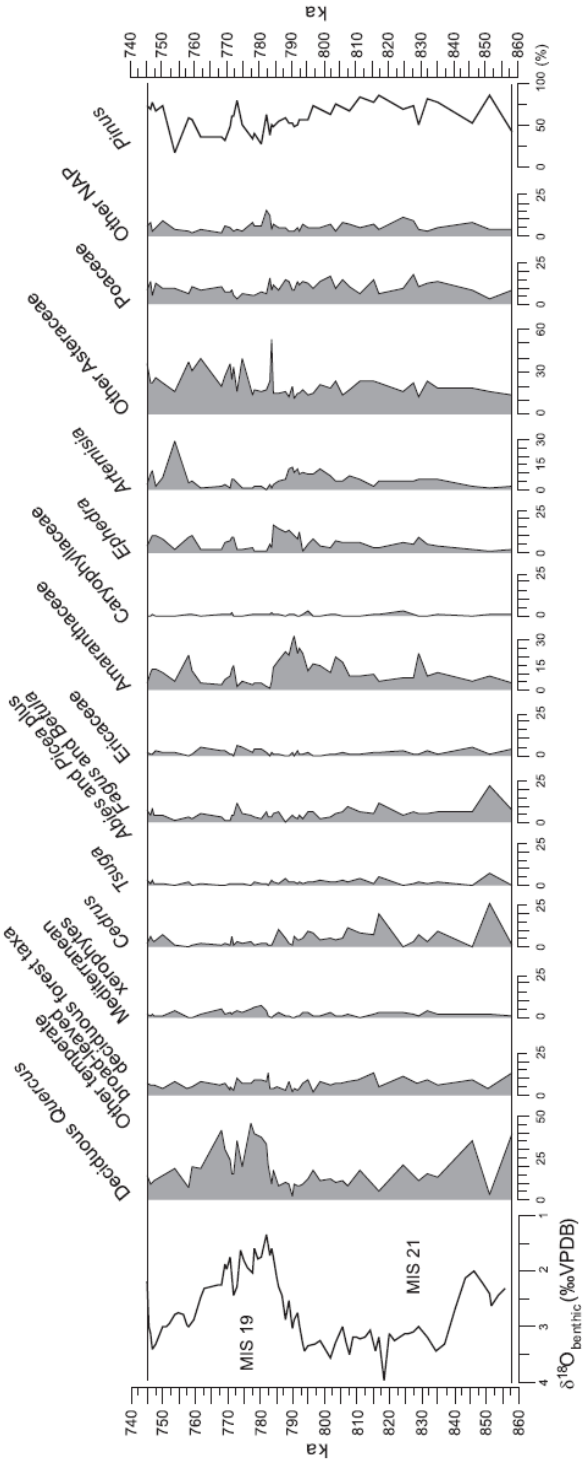

Fig. 2. Percentage abundance of selected pollen taxa calculated without Pinus *and Cupressaceae at the Montalbano Jonico succession. On the right the Pinus percentage abundance is normalized to the total pollen sum excluding Cupressaceae. Age model is from Maiorano et al. (2010) slightly updated (this study).*

section between MIS 20 and MIS 19. Therefore, a small adjustment of the previous age model (Ciaranfi et al., 2010; Maiorano et al., 2010) is here provided, based on the new radiometric age of V4 and on a refined tuning of the MJS benthic $\delta^{18}O$ record with the benthic stack of Lisieki and Raymo (2005). The temporal resolution of the benthic $\delta^{18}O$ record at the MJS through the section studied here is 0.3–1.5 kyrs in the interval MIS 18–upper MIS 21, and 2.0–2.5 kyrs in a few portions of lower MIS 21.

The ostracod assemblages include 138 species in 54 genera (see details in Aiello et al., 2015). None of the samples was barren of ostracods. The analysis of the ostracofaunas showed both autochthonous and mixed (*sensu* Fagerstrom, 1964) assemblages. Some samples (at the levels 76.8 m, 130.3 m, 138.5 m, 146.4 m, and 154.6 m) yielded only autochthonous specimens, while the remaining assemblages are mixed, i.e. formed by both autochthonous and allochthonous specimens, the latter being displaced from shallower marine environments or even from continental water bodies. Two groups of shallow marine taxa were recognized, the first including 15 consistently displaced species pertaining to the genera *Carinocythereis*, *Caudites*, *Cistacythereis*, *Costa*, *Loxoconcha*, *Paradoxostoma*, *Pontocythere*, *Procytherideis*, *Urocythereis* and *Xestoleberis*; and the second formed by six species assigned to *Aurila*, *Paracytheridea* and *Pterygocythereis* that show either allochthonous or autochthonous characters. Numerous species (115) are autochthonous in all samples. The distributions of taxa through the studied section, and the known depth preferences of the most important taxa (see figure 5 in Aiello et al., 2015), have allowed bathymetric variations to be reconstructed using assemblage compositions supported by cluster analysis (see Aiello et al., 2015). Assemblages are indicative of paleodepth variations within the Lower Circalittoral Subzone (LCS, *sensu* Sgarrella and Moncharmont-Zei, 1993). The paleobathymetry ranges from a minimum paleodepth of about 100 m to a maximum paleodepth of about 200 m (Aiello et al., 2015). The shallowest assemblages include taxa well represented in circalittoral as well as infralittoral zones (e.g. *Aurila bradleyana*, *Leptocythere bacescoi*), whereas assemblages indicating the deepest paleoenvironments are characterized by lower circalittoral/bathyal taxa (e.g. *Henryhowella sarsii*, *Bairdoppilata conformis*, *Bosquetina dentata*) and such species as *Krithe compressa* presently living deeper than 150 m below sea level. There is no evidence of an

infralittoral environment because autochthonous specimens belonging to such typical shallow-marine genera as *Carinocythereis*, *Pontocythere*, *Urocythereis*, widespread in Neogene–recent Mediterranean waters, are represented only by scattered, mainly juvenile, displaced valves.

The pollen record is from 49 samples in which 109 pollen taxa were identified. The most significant taxa are shown in a summary pollen diagram (Fig. 2), with other palynological diagrams, as well as floristic and vegetational evidence, being discussed in detail in Bertini et al. (2015). Among arboreal plants, mesothermic taxa especially deciduous *Quercus* dominate, followed by *Carpinus betulus* and *C. orientalis*/*Ostrya*-type; and present but disappearing progressively from the Italian peninsula are such taxa as *Carya*, *Zelkova*, *Liquidambar*, *Pterocarya* and *Taxodium*/*Glyptostrobus* type. Mediterranean xerophytes (e.g. *Olea*, *Quercus ilex* type and *Cistus*), although present throughout the record, generally occur in very low values. Altitudinal coniferous taxa (microthermic) such as *Abies* and *Picea* are consistently present although never in high amounts; and among the meso-microthermic coniferous taxa, *Tsuga* is still present as well as *Cedrus*, with their highest values at 816.94 ka. Among the non-arboreal plants, Amaranthaceae, Asteraceae and Poaceae dominate, principally followed by Ericaceae, Rosaceae, Apiaceae, Cyperaceae, Cistaceae and Caryophyllaceae. Over-representation is evident for *Pinus* pollen ("Neves effect"; Traverse, 1988). Moreover, reworking is not negligible, and is attested by the presence of *Classopollis* as well as taxa not exclusively from Mesozoic strata, including saccate pollen of the Pinaceae. In this regard, the presence of *Engelhardia*, *Taxodium*/*Glyptostrobus* type and other Cupressaceae pollen is problematic when they are not corroded, abraded and degraded, features characteristics of reworking. The overall high abundance of NAP not only during glacials but also interglacials is frequent for Pliocene–Pleistocene southern Italian sections, as recorded by numerous palynological studies (e.g., Capraro et al., 2005; Suc et al., 2010 and references therein) including one from Montalbano (Joannin et al., 2008). As a whole, pollen assemblages reveal repeated vegetational changes. They are expressed during interglacials by the dominance of a mesophilic vegetation typical of warm and relatively humid climate, and during glacials by wooded steppes to steppes when cold and dry

conditions prevailed. No notable expansions of microthermic conifers have yet been recorded.

5. Discussion

5.1. Paleodepth fluctuation

Previous studies have revealed that significant and repeated variations in paleobathymetry are represented in the MJS based on benthic foraminifera (Stefanelli, 2003) and macroinvertebrate fauna (D'Alessandro et al., 2003). Such variations are mainly related to eustatic changes, although possible local (tectonic) influences have not been excluded for certain intervals (D'Alessandro et al., 2003).

With special regard to MIS 19, the data available from D'Alessandro et al. (2003) and Stefanelli (2003) depict a detailed pattern of deepening and evolving environmental conditions at the sea-bottom through the interglacial, and these data are here evaluated using the new age model proposed in this study. The first sign of deepening after MIS 20 is at about 784.8 ka based on benthic foraminiferal assemblages (Stefanelli, 2003) (Fig. 3). At about 782 ka, deepening evidence is also provided by the occurrence of *Funiculina quadrangularis* (D'Alessandro, unpublished), a pennatulacean octocoral mainly living at bathyal depths and requiring soft muddy bottoms with a particularly fluid surface (Pérès and Picard, 1964; Porporato et al., 2009; Greathead et al., 2014). The occurrence of *F. quadrangularis* then suggests a phase of high muddy sedimentation rate. Maximum flooding (MF) has been documented by D'Alessandro et al. (2003) between about 780.56 ka and 777.31 ka (Fig. 3) based on the occurrence of a mollusk community characterized by the deep-water oyster *Neopycnodonte cochlear* (in scattered clusters), a species that thrives during low sedimentation rates and low turbidity conditions on the bottom (Massari et al., 2002; Ceregato et al., 2007; Wisshak et al., 2009). An interval of maximum depth (MD) (from 777.31 ka to 773.25 ka), following MF (Fig. 3), is characterized by dispersed macrobenthic content, possibly in relation to higher sedimentation rates and deeper waters

(D'Alessandro et al., 2003) that prevented the *Neopycnodonte* community from developing, and the occurrence, even as rare specimens, of such bathyal species as the foraminifer *Discospirina italica*, and the mollusks *Dentalium agile*, *Cadulus ovulum*, *Neilonella pusio* and *Delectopecten vitreus*, all typical of

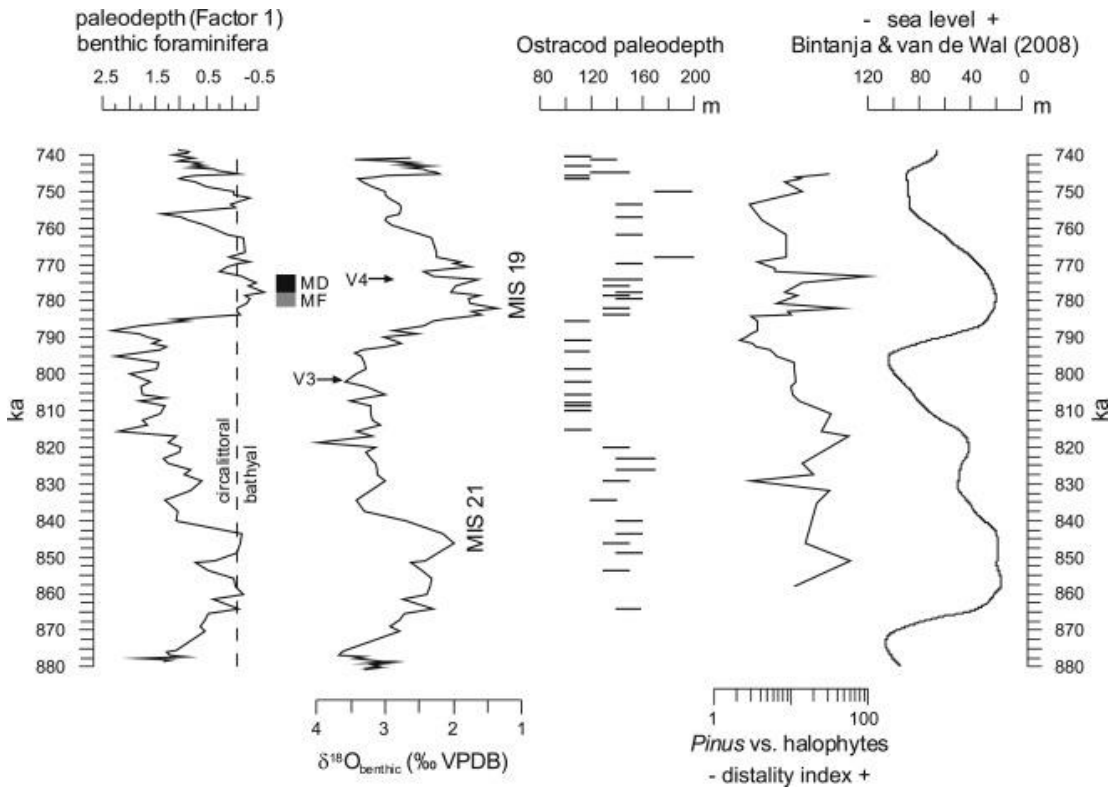

Fig. 3. Comparison of the ostracod paleodepth curve and the Pinus *vs. halophyte ratio (on a logarithmic scale) with benthic* $\delta^{18}O$ *at the Montalbano Jonico succession. On the left, Factor 1 (Principal Component Analysis on benthic foraminiferal assemblages, Stefanelli, 2003) shows negative values for higher paleodepth, having negative loading for deep-water taxa* Sphaeroidina bulloides, Gyroidina *spp.*, Cibicidoides ungerianus, C. pachyderma, Planulina *spp.; Factor 1 positively loads* Ammonia beccari, Bulimina elegans, Elphidium crispum, E. advenum, Quinqueloculina seminula, Cribroelphidium decipiens, Protelphidium granosus, Valvulineria *spp. MF and MD are maximum flooding and maximum depth, respectively (D'Alessandro et al., 2003). Marine Isotope Stages are from Ciaranfi et al. (2010); age model is from Maiorano et al. (2010)slightly updated (this study). The record of sea level changes on the right is from Bintanja and van de Wal (2008). Position of volcaniclastic layers V3 and V4 is also shown.*

Pleistocene bathyal mollusk assemblages (Di Geronimo and La Perna, 1997; Di Geronimo et al., 1997). This paleocommunity suggests a transition to a slope setting ("*Discospirina*, *Nassarius*" communities in D'Alessandro et al., 2003), in good agreement with the major deepening reconstructed during MIS 19 using benthic foraminiferal assemblages (Stefanelli, 2003) from ca. 779 ka to 773 ka (Fig. 3).

Ostracod assemblages also provide a paleodepth reconstruction (Fig. 3) that in general follows the patterns of global sea-level change described by Bintanja and van de Wal (2008) and $\delta^{18}O$ records. The *Pinus* vs. halophyte pollen ratio gives additional evidence of sea-level fluctuations, in terms of changes in distality (Fig. 3).

In detail, the lower portion of the investigated interval, from 864 ka (65.1 m) to 820 ka (89.8 m), was deposited during MIS 21 in the lower part of the LCS based on the high relative abundance of the ostracods *Krithe* spp., *Cytheropteron* spp., *Henryhowella sarsii sarsii*, and *Sagmatocythere concentrica*; the genus *Aurila*, typical of infralittoral/upper circalittoral waters, not being present. This portion of the section correlates with a high sea level according to Bintanja and van de Wal (2008). It is, however, interrupted by a slight shallowing centered at about 835 ka, inferred by the relatively low percent values of circalittoral/bathyal taxa, the presence of the infralittoral/circalittoral species *Leptocythere bacescoi*, and dominance of *Palmoconcha subrugosa*. This datum finds broad correlation with the shallowing in the benthic foraminiferal paleodepth curve, the short interval of minor sea level fall within MIS 21 in the Bintanja and van de Wal (2008) curve, and with heavier values in the $\delta^{18}O$ record (Fig. 3). The pollen record further supports this paleodepth reconstruction since the *Pinus* vs. halophyte ratio shows a significant decrease at about 829 ka implying the proximity of the coastal area where halophytes and other open-vegetation taxa are common. The successive increase of this ratio matches the slight rise in the sea-level curve at about 815–824 ka. On the other hand, a distinctive shallowing trend is evidenced towards the onset of MIS 20 by both ostracod and pollen assemblages, in agreement with the lower sea-level trend recorded in the curve of Bintanja and van de Wal (2008) (Fig. 3). An upper LCS ostracod association is in fact recorded during the interval from 815.42 ka (93.37 m) to 785.62 ka (122.3 m), owing to the high relative abundance of *Leptocythere* spp.,

Aurila spp., *Sagmatocythere versicolor* and *Semicytherura ruggierii*. The genera *Cytheropteron*and *Krithe* are mainly represented by a single species (*Cytheropteron ruggierii* and *Krithe praetexta* respectively). The species *B. conformis* and *B. dentata* are lacking, *H. s. sarsii* is rare, and *E. mistrettai* is very rare. The pollen record confirms a progressive decrease in distality, with low values centered at 790 ka (Fig. 3).

A pronounced lightening of benthic $\delta^{18}O$ values in the MJS record (Fig. 3) is visible from about 3.5‰ (at about 794 ka) to 1.4‰ (at 782 ka) when a pronounced shift in the benthic foraminiferal paleodepth curve is visible (Fig. 3), and it may correspond to the significant sea level rise at the major sequence boundary "Io1" (base of Ionian Stage, 0.78 ka; Snedden and Liu, 2010). The onset of MIS 19 records the replacing of the upper LCS assemblages with lower LCS ostracofaunas (Fig. 3). Specifically, between 783.54 ka (125 m) and 749.91 ka (158.3 m), ostracod assemblages are characterized by *B. conformis*, *B. dentata*, *H. s. sarsii*, *Cytheropteron* spp., *E. mistrettai*, and *S. concentrica*. The paleodepth increase during MIS 19 at the MJS correlates with the rising sea-level record of Bintanja and van de Wal (2008) (Fig. 3). The *Pinus* vs. halophyte ratio records the major sea level rises at 782 ka and 773.05 ka and a distinct fall from 771.84 ka to 769 ka, almost synchronous with the shallowing indicated by benthic foraminifera (Fig. 3).

Based on the ostracod assemblages, the general paleodepth increase during MIS 19 is comparable to the pattern observed during MIS 21 and follows the global sea level curve of Bintanja and van de Wal (2008) (Fig. 3). However, at ca. 768 ka (within MIS 19) and 749.91 ka (in MIS 18), the ostracod assemblages show a clear dominance of such species as *B. conformis*, *B. dentata*, *K. compressa* and *S. concentrica*, typical of the lower LCS/upper bathyal environment. The percent values of these "deep" taxa range from 73.4 % to 95.15 % (details in Aiello et al., 2015) indicating that sedimentation occurred in proximity to the LCS lower limit. On the other hand, the *Pinus* vs. halophyte ratio (Fig. 3) distinctly records the more prominent peak within the interval of MD in MIS 19 (Fig. 3), in agreement with the major deepening phase evidenced by benthic foraminiferal curve (Fig. 3).

The upper part of the studied section (MIS 18) ends with a new shallowing trend between 746.6 ka (161.6 m) and 740.54 ka (176.1 m), with the ostracod taxa *L. bacescoi*, *S. ruggierii*, *S. versicolor*, and *Aurila* spp. being the main

components of the assemblages. This part of the section also includes two short-term deepening phases at 745.14 (165.1 m) and 741.42 ka (174 m). The older deepening is reflected by high relative abundances of *B. conformis*, *H. sarsii*, *E. mistrettai*, and *S. concentrica*; at this time the *Pinus* vs. halophyte ratio and benthic foraminiferal paleodepth curve both show higher values. The younger ostracod-derived deepening is characterized by the temporary disappearance of the genus *Aurila* and relatively high abundances of lower LCS taxa (*B. dentata*, *E. mistrettai*, *Krithe marialuisae*) contemporaneous with a slight sea-level rise in the curve of Bintanja and van de Wal (2008) (Fig. 3).

5.2. Paleoclimate phases

A comparison between paleoclimate proxies at the MJS and global signals of past climate change allows us to interpret our results in terms of major paleoenvironmental modifications that occurred through MIS 21–18 at the orbital and suborbital scale, which is also in agreement with previous pollen records (Capraro et al., 2005; Prokopenko et al., 2006; Tzedakis et al., 2006; Joannin et al., 2007, 2008). The MJS palynological record, summarized in Fig. 4 (f and g), documents the main climate-related vegetational changes that may be associated with fluctuations in the MJS $\delta^{18}O$ curve (Fig. 4e); the latter apparently shows three and two precession-related oscillations in MIS 21 and MIS 19, respectively, in agreement with $\delta^{18}O$ stack of Bassinot et al. (1994) (Fig. 4h). Some pollen climate changes may be correlated with selected peaks in the eastern Mediterranean aeolian dust record (Larrasoaña et al., 2003) (Fig. 4b) and in the Northern Atlantic IRD patterns (Wright and Flower, 2002) (Fig. 4c). A comparison is also attempted with the palynological record from the Valle di Manche section (VMS) in the nearby Calabria region (Fig. 1) (Capraro et al., 2005).

The PTI and AP% (Fig. 4), in agreement with evidence from the detailed and summary palynological diagrams as reported in Bertini et al. (2015) and in Fig. 2, document successive changes in temperature and precipitation. These consist of major warm and humid phases characterized by the expansion of mesothermic forest taxa, mostly deciduous *Quercus* (orange bars A, C, G, I, in Fig. 4f), separated by relatively drier, cool to cold phases characterized by the

expansion of open vegetation (B, D, E, F, H, J, Fig. 4f). This dominant pattern, related to glacial/interglacial (G/I) and substage fluctuations, is punctuated by shorter-term fluctuations (events 1 and 2, Fig. 4g). The high abundance of mesothermic forest taxa, mostly deciduous *Quercus*, supports warm-humid conditions between 846 and 824.5 ka (phases A and C in Fig. 4f), with the exception of the cooler and drier episode centered at 829 ka (phase B, Fig. 4f) as expressed by the significant occurrence of open vegetation taxa including *Ephedra*, Amaranthaceae and *Artemisia*. Despite the low resolution of the pollen record from this basal portion of the studied interval, it is worth noting the correlation between the pollen-derived phases A and C and substages MIS 21.3 and 21.1, respectively (Fig. 4f). Furthermore, the pollen-derived episode (phase B, Fig. 4f) at about 827–831 ka appears quite correlatable with substage MIS 21.2 and an IRD peak (ca. 832.5 ka) at North Atlantic ODP Site 980 (Fig. 4c), possibly recording a wide-scale cooler climate event. In the nearby VMS, a mesic forest dominated by oaks is associated with MIS 21 without appreciable interruption by open vegetation. At the MJS, the progressive inception of the glacial MIS 20 is expressed, at 816.94 ka (in both PTI and AP%), by a slight expansion of altitudinal coniferous forest (i.e. *Cedrus*, *Abies*, *Picea* and *Tsuga*) attesting to a decrease in temperature. In contrast, at the VMS a sharp and more significant expansion of altitudinal coniferous taxa was recorded (Capraro et al., 2005); it precedes the re-establishment of an environment dominated by a (wooded) steppe-like vegetation during the MIS 20–19 transitional phase. The same occurred at the MJS where, during this latter interval, a wooded steppe developed as documented by the presence of both arboreal mesothermic and steppe taxa (phase D in PTI curve, Fig. 4f). Interestingly, the pollen-derived phase D falls within the interval of fairly high values in the dust record. However, starting from about 798.61 ka upwards, the Amaranthaceae, *Artemisia*, and *Ephedra* became even more important elements, as reflected in the pattern of the PTI curve (Fig. 4f), which supports a main dry acme phase centered at 790 ka (phase E, Fig. 4f). This episode interestingly correlates, within the limits of individual age models, with a sharp peak both in dust and IRD records (Fig. 4b, c), supporting the existence in the North Hemisphere of a distinct, widespread cold and arid climate event across the MIS 20–19 shift, at the end of a long-term glacial cooling trend. This deglacial interval (Termination IX) is marked by the first decrease of benthic

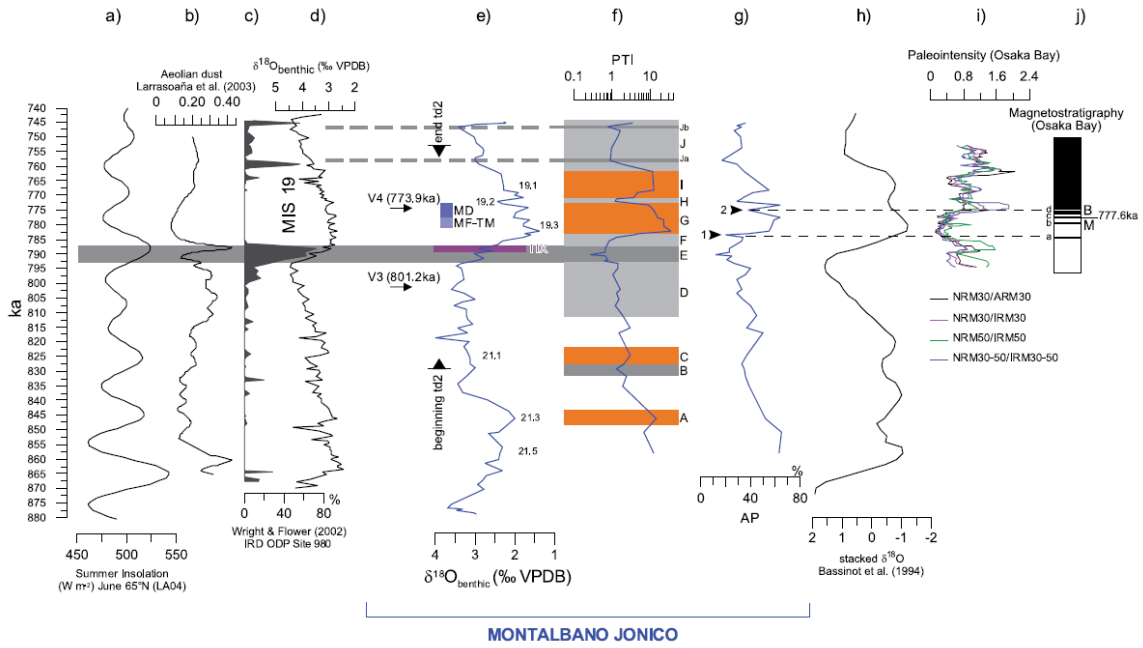

Fig. 4. Comparison between the Montalbano Jonico succession and other reference Lower-Middle Pleistocene records. a) Insolation (Laskar et al., 2004); b) East Mediterranean dust record based on hematite content derived from magnetic properties of sediments from ODP Site 967 (Larrasoaña et al., 2003); c) ice rafted detritus (IRD) curve from North Atlantic ODP Site 980 (Wright and Flower, 2002) versus age according to Lisiecki and Raymo (2005); d) benthic δ18O curve from Site 980 (Wright and Flower, 2002); e) benthic δ18O at the Montalbano Jonico succession (MJS); f) pollen temperature index, PTI, in logarithmic scale at the MJS (see text for details); g) arboreal pollen, AP% (see text for details); h) stacked δ18O record (Bassinot et al., 1994); i) paleointensity curves at core from Osaka Bay (Hyodo et al., 2006; Hyodo and Kitaba, 2015); j) paleomagnetic stratigraphy at Osaka Bay (Hyodo et al., 2006; Hyodo and Kitaba, 2015) with the Matuyama-Brunhes boundary (M-B) on the right and short-term paleomagnetic events (a-d) on the left. Age model of the MJS records (e-g) is from Maiorano et al. (2010) slightly updated (this study). Substage nomenclature is according to Bassinot et al. (1994) (h). Light-dark grey bars and orange bars on the PTI curve are the main climate phases (A-J); minor short-term climate events are indicated as 1 and 2 on the AP% curve, and as Ja and Jb on the PTI record (see text for details). V3 and V4: volcaniclastic layers; TM: Thermal Maximum (Girone and Varola, 2001); MF: Maximum Flooding (D'Alessandro et al., 2003); MD: Maximum Depth (D'Alessandro et al., 2003); td2: second temporary disappearance of G. omega *(sensu Maiorano and Marino, 2004); TIX: Termination IX; dotted lines correlate events 1 and 2 at MJS with paleointensity low at Osaka Bay.*

$\delta^{18}O$ and the final disappearance of IRD at Site 980 (Fig. 4c,d), between 795 ka and 788 ka (Wright and Flower, 2002). An insolation maximum occurs at this time (Fig. 4a) and it could have caused a degree of North Atlantic ice-sheet instability and promoted the IRD deposition at the latitude of Site 980. The above-mentioned age of glacial termination at the MIS 20/MIS 19 transition is close to the time interval spanning the lowering of $\delta^{18}O$ from 3.5‰ (at about 794 ka) to 1.4‰ (at 782 ka) at MJS (Fig. 4) and to the age (787 ka) for glacial termination given in Bassinot et al. (1994). Such a pattern in the $\delta^{18}O$ curve and pollen data, combined with the sharp change in benthic foraminiferal paleodepth reconstruction (see Fig. 3), allow the recognition of Termination IX at MJS (TIX in Fig. 4e). A prominent IRD peak has also been recorded at North Atlantic ODP Site 983 (Kleiven et al., 2011), coincident with the first signal of lowering in $\delta^{18}O_{planktonic}$ values at the MIS 20–19 transition. Therefore, the Mediterranean signals of millennial-scale climate change related to the high- to low-latitude North Atlantic occurrence of sharp deglaciations (Oppo et al., 1998; Hodell et al., 2008; Stein et al., 2009; Marino et al., 2014) may be extended down to the studied interval, since the Mediterranean response to abrupt global climate signals had until now been documented at the terminations IV and V (Girone et al., 2013b). After an initial recovery of thermophilous arboreal taxa (wooded steppe), starting at 789.15 ka, a secondary peak of open vegetation is recorded at 783.53 ka (Fig. 2), as shown in the AP% curve (event 1 in Fig. 4g). This phase, dominated by cosmopolitan herbaceous taxa (especially Asteraceae and Poaceae; Fig. 2; see also Bertini et al., 2015), pre-dates the rather sharp increase in thermophilous arboreal vegetation culminating at 782 ka and reflected in the higher values of the PTI curve (Fig. 4f). The forest expansion associated with the prevalent warm and humid conditions of MIS 19 extended as a whole between 782 and 759.32 ka (see PTI and AP% patterns during phase G, Fig. 4f, g). The beginning of this event is concurrent with the lowest $\delta^{18}O$ values in MIS 19.3 (phase G, Fig. 4e), and occurs slightly (about 1.4 kyr) before the maximum flooding (MF in Fig. 4). A thermal maximum (TM in Fig. 4e) has also been documented by Girone and Varola (2001) at the same level as the occurrence of *Neopycnodonte* based on the tropical–subtropical mesopelagic teleostean fish *Bonapartia pedaliota*.

Within the temperate phase associated with substage MIS 19.3, an abrupt increase in herbaceous taxa (Fig. 2) is visible at 774.83 ka (event 2 in Fig. 4g),

just below the V4 layer. Moreover, at 771.84 ka, coincident with an increase of $\delta^{18}O$ values (MIS 19.2), the lowering of both PTI and AP% values suggests a successive and even more significant decrease in humidity and possibly temperature (phase H, Fig. 4f). A significant increase in arboreal mesothermic taxa (Fig. 2) extending to ca. 759 ka, with a maximum at 768.04 ka, is associated with substage MIS 19.1 (phase I, Fig. 4f). The subsequent decreasing trend in mesothermic arboreal taxa parallels the increase of open vegetation taxa concomitant with heavier $\delta^{18}O$ values (Fig. 4).

An acme phase with *Ephedra*, Amaranthaceae and *Artemisia* marks the onset of MIS 18 (Fig. 2), with two distinct drier subphases "Ja" and "Jb" developed during this glacial stage (phase J, Fig. 4f). These short-term pollen climate subphases again approximate the IRD peaks in the North Atlantic Site 980 (Fig. 4c). This co-occurrence reinforces Mediterranean–North Atlantic climate interconnections, since the coincidence between cold and dry climate phases in the Mediterranean area and IRD peaks in North Atlantic region has already been noted from the pollen records of ODP Site 976 (Alboran Sea) during the interval 1.09–0.9 Ma (Joannin et al., 2011) and of Tenaghi Philippon (Tzedakis et al., 2003) during selected cold and dry glacial intervals of the last 450 kyrs. The same global climate changes recorded at the MJS during the beginning of MIS 18 favored different vegetational scenarios at the VMS, expressed by the evident preeminence of altitudinal coniferous forest taxa and low abundance of NAP during the phase correlated with MIS 18.4 (Capraro et al., 2005). The VMS and MJS are not far from each other (Fig. 1) but are characterized by different local terrestrial paleogeographical contexts. In particular, at the VMS the dominant pollen input is evidently from the high altitudinal belts of the closest high relief (possibly the Sila Mountains in Calabria). Here, high altitudinal coniferous taxa (see the so called "alpine vegetation" in Capraro et al., 2005) thrived and expanded during glacials when temperature decreased, but humidity remained at high values. In contrast, at the MJS the subordinate role of less prominent relief (Apennines Chain) can explain the greater expansion of steppe taxa associated with decreases in both temperature and precipitation.

5.3. Climatostratigraphy and the Matuyama-Brunhes boundary

The V4 volcaniclastic layer is located in the uppermost MIS 19.3, and has a $^{40}Ar/^{39}Ar$ dated age of 773.9 ka ± 1.3 ka (Petrosino et al., 2015), which is very close to the age-assignment of 773 ka for the MBB in several marine records (Channell et al., 2010). At the regional scale, V4 can potentially be correlated with other tephra cropping out in sections where the MBB is recognized. The age of V4 seems comparable with the chronology of tephra SUL2-16 ($^{40}Ar/^{39}Ar$ 781.3 ± 2.3 ka, Sagnotti et al., 2014) in the lacustrine Sulmona Basin (Central Italy) when calculated relative to the Alder Creek standard age of 1.186 Ma (rather than 1.194 Ma), which then provides an age of 776.7 ± 2.3 ka (Petrosino et al., 2015); however a strict comparison is hindered because data on glass chemistry or mineral assemblages for SUL2-16 are lacking (Petrosino et al., 2015). This tephra layer occurs slightly above the MBB at 786.1 ka, an interpolated age estimated on the basis of $^{40}Ar/^{39}Ar$ dating of tephra layers bracketing the MB transition (Sagnotti et al., 2014). Based on published data, the position, within MIS 19, of the undated Pitagora ash recorded in the VMS (very close to MIS 19.2, Fig. 7 in Capraro et al., 2005) appears somewhat similar to the record of V4 in the MJS (Fig. 4). However, no more stringent stratigraphical correlation between the two tephra layers is attempted since the study of the VMS is currently under review (Capraro, pers. comm.).

Nevertheless, the new pollen results combined with previous data at the MJS provide additional detailed climatostratigraphic insights for MIS 19. The pollen record has identified several vegetational and climate fluctuations that are not exclusively associated with marine isotope stages and substages. Specifically, the abrupt short-term dry climate events 1 and 2 in substage MIS 19.3, while needing to be interpreted more clearly in terms of regional or global environmental changes, are evidence of abrupt millennial-scale climate shifts during warm climate phases, in agreement with records from the North Atlantic where such variability has been documented (e.g. Kleiven et al., 2011). Interestingly, the chronology of events 1 and 2 (at 783.5 ka and 774.8 ka, respectively) implies that they should be evaluated also with respect to the hypothesis of Kitaba et al. (2009, 2012) that climate during the MB magnetic polarity transition was influenced by a reduction in the geomagnetic field and

hence increase in the galactic cosmic ray flux and climate cooling. According to Kitaba et al. (2012)the postglacial warming after MIS 20 was interrupted by a cooling phase, as identified by the pollen record, that coincides with the middle of the paleointensity low during the MB transition. This cooling began just before the sea-level highstand correlated with MIS 19.3 and persisted until about the mid-point between substages 19.3 and 19.2, followed by a rapid warming and concurrent paleointensity recovery. The thermal maximum inferred by these authors during MIS 19.3 at Osaka Bay clearly postdates the highest sea-level highstand by 4 kyr (according to the age model of Hyodo and Kitaba, 2015), when the connection between orbital forcing and climate was disrupted. In contrast, data from the marine fauna and pollen at the MJS do record a co-occurrence of the maximum flooding and thermal maximum (Fig. 4e) (occurrences of the *Neopycnodonte* community, the tropical–subtropical mesopelagic teleostean *B. pedaliota*), together with the increase of *Quercus* and PTI values at about the same level (Fig. 4). These observations are recorded just below the higher sea level (MD, Fig. 4e), contemporary with highest value of pollen distality index. The exceptional agreement among data from both marine and continental realms suggests that the paleoenvironmental framework at MJS through the investigated interval is reliable. The slight differences in the sequence of paleoenvironmental changes occurring at the MJS and Osaka Bay (Japan) may depend on the complex sedimentary setting at Osaka Bay where sea level changes, estimated on the basis of fluctuations in marine to freshwater and brackish diatom assemblages (Hyodo et al., 2006), strictly controlled the alternating marine to lacustrine/fluviatile environments (Kitaba et al., 2009). On the other hand, the terrestrial documentation from the pollen record suggests more complex climatic and vegetational changes (see Bertini et al., 2015) that possibly relate events 1 and 2 at the MJS with the interval of low paleointensity at Osaka Bay (Fig. 4i) (Hyodo et al., 2006; Kitaba et al., 2012) before the main MBB (777.6 ka, Hyodo and Kitaba, 2015). Although having slightly different ages, paleointensity minima through the MB transition are documented widely (e.g. Dinarès-Turell et al., 2002). This encourages the collecting of more extensive and high temporal resolution data-sets on continental and marine biological climate proxies, to clarify the relationship between climate and geomagnetic

field intensity and to establish supplementary tools to better characterize the MB transition.

In fact, the transitional mode of the MBB, as mentioned in the Introduction, emphasizes that the MBB cannot be the exclusive tool for establishing the Lower–Middle Pleistocene GSSP, but should be supported by additional classical and non-conventional climatostratigraphic, ecostratigraphic, and chronostratigraphic constraints.

6. Conclusions

New evidence from pollen and ostracod analyses has improved our understanding of paleoenvironmental changes at the MJS in both terrestrial and marine realms during the MIS 21–18 interval. The record is constrained by a detailed chronological framework further supported by two radiometrically-dated volcaniclastic layers, V3 and V4. Our data also provide new information on climatostratigraphy, this being valuable for the wide-scale correlation of the MBB within MIS 19. The latter is very well depicted through the section and the substages 19.1, 19.2 and 19.3 are undoubtedly recognized in the $\delta^{18}O$ record, and supported by patterns of pollen and marine proxies. Changes in ostracod assemblages show a clear primary link with paleodepth variations, and document deepening and shallowing phases during interglacials and glacials, respectively, in agreement with the pattern of the global sea-level curve of Bintanja and van de Wal (2008). Such fluctuations, including the highest sea level during MIS 19, are clearly evident also in the pattern of the pollen distality index. The main vegetational changes associated with global climate fluctuations match the $\delta^{18}O$ record, improving the recognition of stages and substages within MIS 21 to MIS 18, including the warmer phase during MIS 19.3. The major arid phase centered at 790 ka correlates with the uppermost MIS 20 and to the prominent peak in the North Atlantic IRD and Mediterranean aeolian dust records, documenting an almost synchronous Mediterranean response to the North Hemisphere climate pattern. This prominent cold and arid phase, combined with the significant lowering of $\delta^{18}O$ values by about 2‰ between ca. 794 ka and 782 ka and a high-amplitude change in benthic foraminifera-derived paleodepth, help to locate

Termination IX which is considered the prominent marker in the $\delta^{18}O$ record just before the MBB in MIS 19 (Channell et al., 2010). The co-occurrence of dry and probably relatively cold climate conditions at the MJS with IRD at Site 980 during selected intervals in glacial MIS 18 is additional evidence of the climate teleconnection between the Mediterranean area and North Atlantic region. The relatively dry pollen phase at 771.84 ka is associated with substage MIS 19.2. The two additional minor abrupt short-term dry events at 783.5 ka (pollen event 1) and 774.8 ka (pollen event 2) possibly relate to the climate variability already described during Middle Pleistocene interglacials in the North Atlantic. However, the stratigraphic position of these events with respect to the oxygen isotope stratigraphy (MIS 19.3) could imply that they represent those climate fluctuations induced by geomagnetic field minima observed during the MB transition, in agreement with Kitaba et al. (2012).

The new data collected at the MJS and their regional to global correlation, furnish valuable climatostratigraphic constraints for understanding the behavior of MIS 19 and to appreciate the MJS as a potential candidate for the Middle Pleistocene GSSP. It is worth noting that the excellent oxygen isotope record at the MJS, in particular the onset of MIS 19, was indicated as valuable for the definition of the Middle Pleistocene GSSP (Maiorano et al., 2010), in agreement with suggestions of Remane et al. (1996), who considered acceptable the isotopic signal for the definition of boundary stratotypes, as has been adopted for the GSSP of the Serravallian Stage (Hilgen et al., 2009).

Additionally, numerous events are recorded that significantly enhance the stratigraphic/paleoenvironmental framework of MIS 19 at the MJS. Any of the following might be suitable element for the Middle Pleistocene GSSP:

- the $^{40}Ar/^{39}Ar$ ages of volcaniclastic layers V3 (801.2 ± 19.5 ka) and V4 (773.9 ± 1.3 ka), the latter being very close to the age of MBB (773 ka, Channell et al., 2010);
- the coldest and arid pollen event at 790 ka coincident with a prominent peak of ice rafted debris in the North Atlantic Ocean and aeolian dust in eastern Mediterranean;
- Termination IX representing the rapid, high-amplitude shift to lighter $\delta^{18}O$ values at the MIS 20/19 deglaciation;

- the short-term arid pollen events 1 and 2, characterized by the expansion of herbs, at 783.5 ka and 774.8 ka, respectively;
- the increase of steppe and halophyte elements associated with MIS 19.2 at 771.84 ka, just above the V4 layer;
- the co-occurrence of the maximum flooding (*Neopycnodonte* mollusk community, high pollen distality index) and thermal maximum (tropical–subtropical mesopelagic teleostean *B. pedaliota*, highest percentage values of *Quercus* and PTI) during the 780.56–777.31 kyr interval within MIS 19.3, slightly above the lowest value in the $\delta^{18}O$ record at 782 ka and just below the V4 layer at 773.9 ka;
- the maximum depth from 777.31 ka to 773.25 ka based on macrobenthic invertebrate communities, concurrent with the highest value in the pollen distality index and increased deepening recorded from benthic foraminiferal assemblages;
- the second temporary disappearance of the calcareous nannofossil *Gephyrocapsa omega*, between 829 ka and 752.76 ka, a valuable bioevent for long distance correlation.

The fine-scale dataset, detailing events and phases in the MJS, represents a useful tool to improve understanding of how the climate developed during MIS 19 at orbital–suborbital and millennial scale, and to constrain the chronostratigraphy of the Lower–Middle Pleistocene transition close to the MBB.

Contribution A4

Climate signatures through Marine Isotope Stage 19 in the Montalbano Jonico section (Southern Italy): A land-sea perspective*

*Published in Palaeogeography, Palaeoclimatology, Palaeoecology 461, 341-361 (P. Maiorano, A. Bertini, D. Capolongo, G. Eramo, S. Gallicchio, A. Girone, D. Pinto, **F. Toti**, G. Ventruti, M. Marino, 2015)

Abstract

A multi-proxy record based on calcareous plankton, dinocysts, pollen, mineralogy and grain size has been acquired from the "Ideale" section, the portion of Montalbano Jonico succession (Southern Italy) that could host the GSSP for the Middle Pleistocene. The direct correlation between marine and terrestrial proxies provides a valuable indication of atmospheric and oceanic connections. The record shows a distinct climate variability well expressed by the vegetational changes, sediment input into the basin and sea surface–water modifications. Biotic proxies indicate that, during the study interval, periods of prevailing subpolar/transitional surface–water conditions were concurrent with steppe and halophytic vegetation. Erosional processes on the hillslopes and terrigenous supply, during these periods, were likely favored due to reduced arboreal vegetation, as attested to by sediment composition and pollen assemblages. Temperate/subtropical surface water conditions were concomitant with prevalent expansions of thermophilous arboreal plants and moister conditions on land, which likely promoted chemical weathering leading to an enhanced supply of kaolinite and smectite in the basin. A relationship between mineral content and the nature of the outcropping units in the source area, as well as sea-level fluctuations, has also been considered. A well-defined period of polar–subpolar water incursion, ranging from 793.2 ka to 788.1 ka, matches the major expansion of steppic vegetation on land and the increase of terrigenous supply into the basin. It likely represents the local response to North Atlantic ice-rafted debris deposition. Short-lived warming/cooling episodes punctuate the latest part of MIS 20 and are tentatively correlated with analogue climate phases predating MIS 1 inception. Full interglacial conditions of MIS 19c, lasting 10.6 kyr, started at 784.3 ka and were characterized by warm, oligotrophic and stratified surface–waters coupled with forest expansion, suggesting prevalent warm and humid conditions on land. A potential sapropel-like interval is identified within MIS

19c and correlated to i-cycle 74. The MIS 19c/19b transition is marked, at 773.2 ka, by the reestablishment of millennial-scale variability, similarly to North Atlantic marine and ice-core records. The results improve the paleoclimate framework of a Middle Pleistocene reference section and add further insight regarding climate development across MIS 19 and on potential similarities with its closest Holocene analogue.

Keywords: MIS 19, Montalbano Jonico section, Terrestrial and marine proxies, Orbital and millennial-scale climate variability

1. Introduction

Paleoenvironmental and paleoclimatic reconstructions are key tools for modeling and understanding future climatic changes. Interglacial Marine Isotope Stage (MIS) 19 is considered a potential analogue of the present interglacial (Tzedakis et al., 2012a; Ferretti et al., 2015). Similarities between MIS 1 and MIS 19 are essentially driven by the astronomical analogies of radiative forcing of the corresponding orbital configurations (Tzedakis et al., 2009, 2012a; Tzedakis, 2010; Yin and Berger, 2012, 2015). Evidence of the response of the climate system to orbital forcing essentially relies on isotope records and atmospheric gas concentration measurements (Tzedakis et al., 2012a). Only recently, the deglaciation history associated with the beginning of MIS 19 has been suggested to be interrupted, in analogy with the last deglaciation, by a Younger Dryas-like cold event recorded in lacustrine deposits in central Italy (Giaccio et al., 2015). However, the subject is still not extensively explored and deserves further consideration. Special attention has been given to the duration of the early half of MIS 19 that is MIS 19c, which could provide an indication of the next glacial inception and therefore of when the hypothetical end of the current interglacial might be expected (Tzedakis et al., 2012a). Recent high resolution results from the North Atlantic indicate relatively stable conditions during the peak warmth of MIS 19, based on benthic and planktonic foraminiferal $\delta^{18}O$ values (Ferretti et al., 2015). Evidence from surface water proxies has revealed that MIS 19c was characterized by stable warm and oligotrophic surface–water conditions

(Emanuele et al., 2015), while a major expansion of Mediterranean forest cover has been documented to occur on land (Sánchez-Goñi et al., 2016). The occurrence of rapid cooling/drying episodes indicates that millennial/submillennial-scale climate variability punctuated MIS 19 (e.g., Tzedakis et al., 2012a; Giaccio et al., 2015; Marino et al., 2015; Sánchez-Goñi et al., 2016), with substantial SST decreases and fresh water pulses related to ice-sheet instability from MIS 19c/19b transition up to MIS 18. In the sedimentary records, the identification of millennial-scale oscillations related to North Hemisphere iceberg discharges is relevant in this temporal framework, since it may provide indirect proxies for defining glacial/interglacial boundaries (Tzedakis et al., 2012b). Millennial variability during the glacial inception from MIS 19 to MIS 18 has been derived from the measurement of δD (Jouzel et al., 2007; Pol et al., 2010), CH_4(Loulergue et al., 2008), and CO_2 (Lüthi et al., 2008), as well as N_2O concentrations (Schilt et al., 2010) in ice cores. The onset of such a climate variability at the end of MIS 19c is well expressed in marine North Atlantic deep-sea sequences based on oxygen isotope pattern (Channell and Kleiven, 2000; Kleiven et al., 2011; Tzedakis et al., 2012a) and on the evidence of polar melt water arrival (Naafs et al., 2011, 2013; Ferretti et al., 2015; Sánchez-Goñi et al., 2016). An asynchronous interhemispheric phasing in the millennial scale climate variability is found between North Atlantic and Antarctic records within MIS 19 and post-dates the minimum in boreal summer insolation by 2.5–4.5 kyr (Tzedakis et al., 2012a). This mechanism, known as the onset of thermal bipolar-seesaw variability (Broecker, 1998; Stocker and Johnsen, 2003), is a response to changes in interhemispheric heat transport. North Atlantic iceberg discharges is in fact believed to have shut down the density-driven meridional overturning circulation, with consequent rapid cooling of the North Atlantic and gradual warming of South Atlantic Basin and Antarctica.

In this paleoclimate framework, we have investigated a portion of the lower-middle Pleistocene on land Montalbano Jonico succession, in the "Ideale" section, which is a candidate for the definition of the Global Boundary Stratotype Section and Point (GSSP) of the Middle Pleistocene (Head and Gibbard, 2015a and references therein). The aim is to unravel, in such a reference record, high frequency climate variability in the interval straddling the late MIS 20 and the MIS 18 glacial inception. Supra-regional/global

climate variations are clearly expressed in the Montalbano Jonico section (e.g., Ciaranfi et al., 2010; Marino et al., 2015); here, high sedimentation rates offer the opportunity to investigate an expanded stratigraphic succession valuable for obtaining a high-resolution dataset. The previously acquired paleonvironmental signals in the same section have essentially focused on specific proxies, such as ostracod and pollen content (Aiello et al., 2015; Bertini et al., 2015; Marino et al., 2015), combined with a benthic oxygen isotope record. In the present study we have been adopting a multidisciplinary approach at higher temporal resolution, based on both biotic (calcareous plankton, dinocysts and pollen) and abiotic (grain size and mineralogy) proxies, correlated with benthic and planktonic oxygen isotope records. In the past studies, a comparable multiproxy approach was successfully applied for the paleoenvironmental investigation of older portions of the Montalbano Jonico section (Maiorano et al., 2008; Girone et al., 2013a) in order to build confidence in inferences about past climate changes. Such an approach is particularly valuable in rather proximal setting such as the shelf–upper slope environment of the investigated section. Here, climate signatures are captured not only by typical marine proxies, but also through multiple variables, which provide valuable information to unravel climate-induced modifications acting in the borderland area, such as vegetation changes, river runoff, erosional and depositional processes. Recent studies have shed lights on the interplay between tectonics, climate and erosion/deposition during the Middle Pleistocene–Holocene in the Basilicata region (Boenzi et al., 2008; Piccarreta et al., 2011). They show that the riverine system draining the region, in which the Montalbano Jonico section is located, is sensitive to hydrological and vegetational changes, causing flooding/erosional processes which are primarily driven by climate changes. The combined occurrence of both continental and marine proxies within a single succession, as is the case for the “Ideale” section, gives an intrinsic advantage towards the correlation between land–sea processes and a more comprehensive climate reconstruction.

The overall paleoclimate signals, identified in the “Ideale” section, are compared with global paleoclimate indicators from North Atlantic deep-sea sediments and ice-core records, in order to frame the investigated interval within a global paleoclimate context. A comparison with the succession of

climate phases occurring during the Late Glacial-Holocene transition has also been attempted, to obtain further insights on the analogy between MIS 19 and the current interglacial.

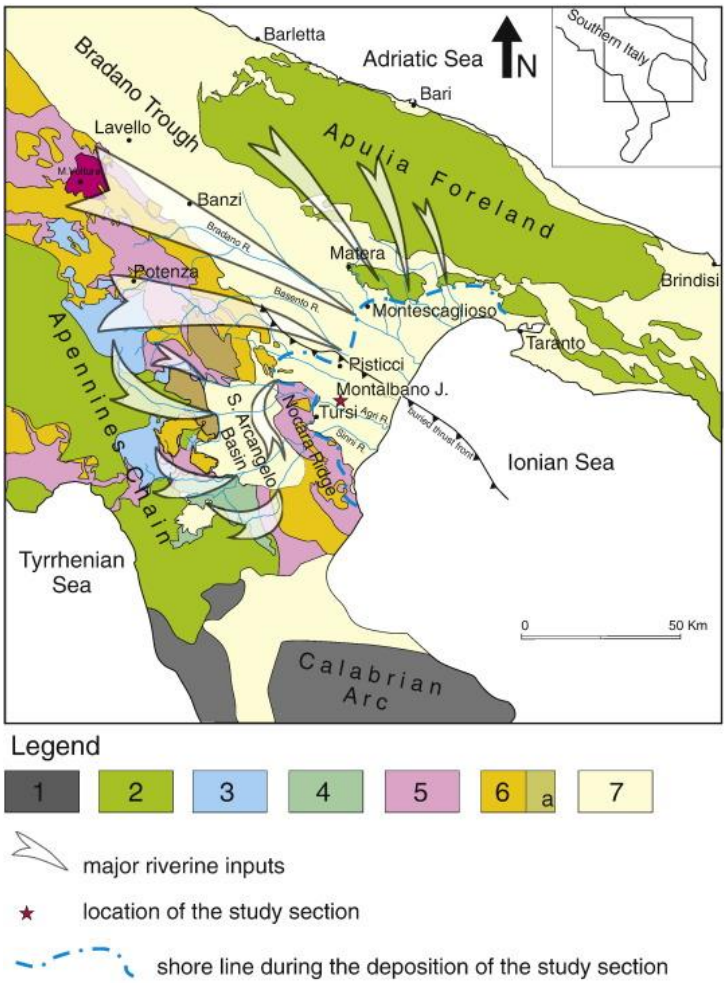

Fig. 1. Simplified geological sketch map of the Southern Apennines and location of the study area.
Legend: 1) Paleozoic igneous and metamorphic basement and Cenozoic siliciclastic sedimentary covers; 2) Mesozoic-Cenozoic calcareous/dolomitic units; 3) Mesozoic calcareo-silico-marnoso succession of the Lagonegro Basin; 4) Mesozoic serpentinites, ophiolitic metabasalts, phillytes, and low-grade metamorphic carbonates (Liguride Units); 5) Cretaceous to Paleogene shaley units of the Argille Variegate and Flysch Rosso formations ("argille varicolori" auctt.); 6) Neogene arenaceous/pelitic successions of the Southern Apenninic foredeep; Quaternary siliciclastic units of the Southern Apennine foredeep; a) "Flysch di Gorgoglione" formation; 7) Messinian to Holocene siliciclastic deposits. Modified from Bonardi et al. (1988).

2. The investigated area

2.1. Geological and paleogeographical setting

The Montalbano Jonico succession represents the middle-upper portion of the "argille subappennine" formation (e.g., Azzaroli et al., 1968; Pieri et al., 2011; Carbone, 2013), which crops out in the Lucania Basin (Balduzzi et al., 1982). The latter is part of the Bradano Trough (Casnedi, 1988), located between the Apennines Chain to the west and the Apulia foreland eastward (Fig. 1).

The Bradano Trough is considered the post-Messinian Apennines foredeep and is controlled by the eastward roll-back of the subduction hinge of the Apulia platform (e.g., Patacca and Scandone, 2007 and references therein). This basin was characterized by high rates of subsidence until the Calabrian, then it underwent a diachronous uplift, starting from the central area of the basin (the Genzano–Banzi area) in the late Calabrian and proceeding south-eastward to the actual Ionian coast until the Holocene. In the late Calabrian, the central sector of the Bradano Trough emerged while the southern sector, where the study section is located (Fig. 1), was still subsiding. Simultaneously, on the western side of the trough the uplift of Nocara ridge was taking place, isolating a western piggy-back depocenter, known as the Sant'Arcangelo Basin (e.g., Pieri et al., 1996a; Patacca and Scandone, 2007 and references therein). In particular, the study section belongs to a sedimentary succession that deposited unconformably on the external allochthonous sheets of the Apennine thrust front (falda di Metaponto, Mostardini and Pieri, 1967) and reached its maximum deepening in the Early–Middle Pleistocene (e.g., Ciaranfi et al., 1996). From the Middle Pleistocene, the study deposits underwent a shoaling-upward trend due to the uplift of the area (uplift rate of 0.1–0.5 mm/years, Doglioni et al., 1994, 1996) that proceeded until the Holocene (e.g., Pieri et al., 1996b; Patacca and Scandone, 2001). In the Early–Middle Pleistocene, the shoreline of the foredeep was about 15 km landward of its present day position (Fig. 1) and hosted deltas of the five major rivers (Sinni, Agri, Cavone, Basento and Bradano) occurring today on the Metaponto Coastal Plain (Tropeano et al., 2013). The catchment basins of these rivers, which represented the major tributary for the study succession depocenter,

mainly eroded Apenninic terrains referable to the following units (Fig. 1): calcareous/dolomitic units of the Apenninic Platform (e.g., Patacca and Scandone, 2007), the calcareo-silico-marnoso succession of the Lagonegro Basin (Scandone, 1972), the Cretaceous to Paleogene shaley units of the Argille Variegate and the Flysch Rosso formations (e.g., Apat, 2007) and the Neogene arenaceous/pelitic successions of the Southern Apenninic foredeep (e.g., Pescatore, 1988). Source sediments from the calcareous Mesozoic Apulian foreland can be considered negligible due to the reduced drainage area of the catchment basins and poor drainage density, which is related to the high permeability of the bedrock. During the Early–Middle Pleistocene, the mountain front was already well developed, with a topographic gradient similar to the modern relief. It was bordered by a wide, low-gradient, fluvial plain that extended eastward from the foot of the chain to the coastline (Tropeano et al., 2002; Boenzi et al., 2014). Based on morphology, lithology and relief we can now broadly identify two different drainage areas that developed on the mountain chain–emerged foredeep system: an innermost part characterized by higher relief and an outermost part characterized by lower relief. In particular, several thrust sheets, that were active during the Early–Middle Pleistocene, characterize the inner part of the chain. Differential erosion processes, acting on these thrusts, resulted in a series of linear ridges consisting mainly of sandstone turbidite successions and clayey flysch units. The Bradano Trough represents the outermost part and is morphologically characterized by several tabular reliefs. They represent relicts of the former alluvial plain that was extended eastward from the foot of the chain and then uplifted starting in the Early–Middle Pleistocene. The resulting base level change and river incision have been unsteady due to climate changes; therefore, river valleys are punctuated by a series of strath and thread terraces along river valleys developed during the Middle–Late Pleistocene (Boenzi et al., 2014).

2.2. The "Ideale" section

The study focuses on the "Ideale" section, a partial interval of the Lower–Middle Pleistocene Montalbano Jonico composite succession (Fig. 2). Several

papers have focused on the reconstruction of the whole composite section (e.g., Ciaranfi et al., 1996; Marino, 1996) as well as on its stratigraphical and paleonvironmental features (e.g., Maiorano et al., 2004; Ciaranfi and D'Alessandro, 2005; Ciaranfi et al., 2010). Recent studies (Bertini et al., 2015;

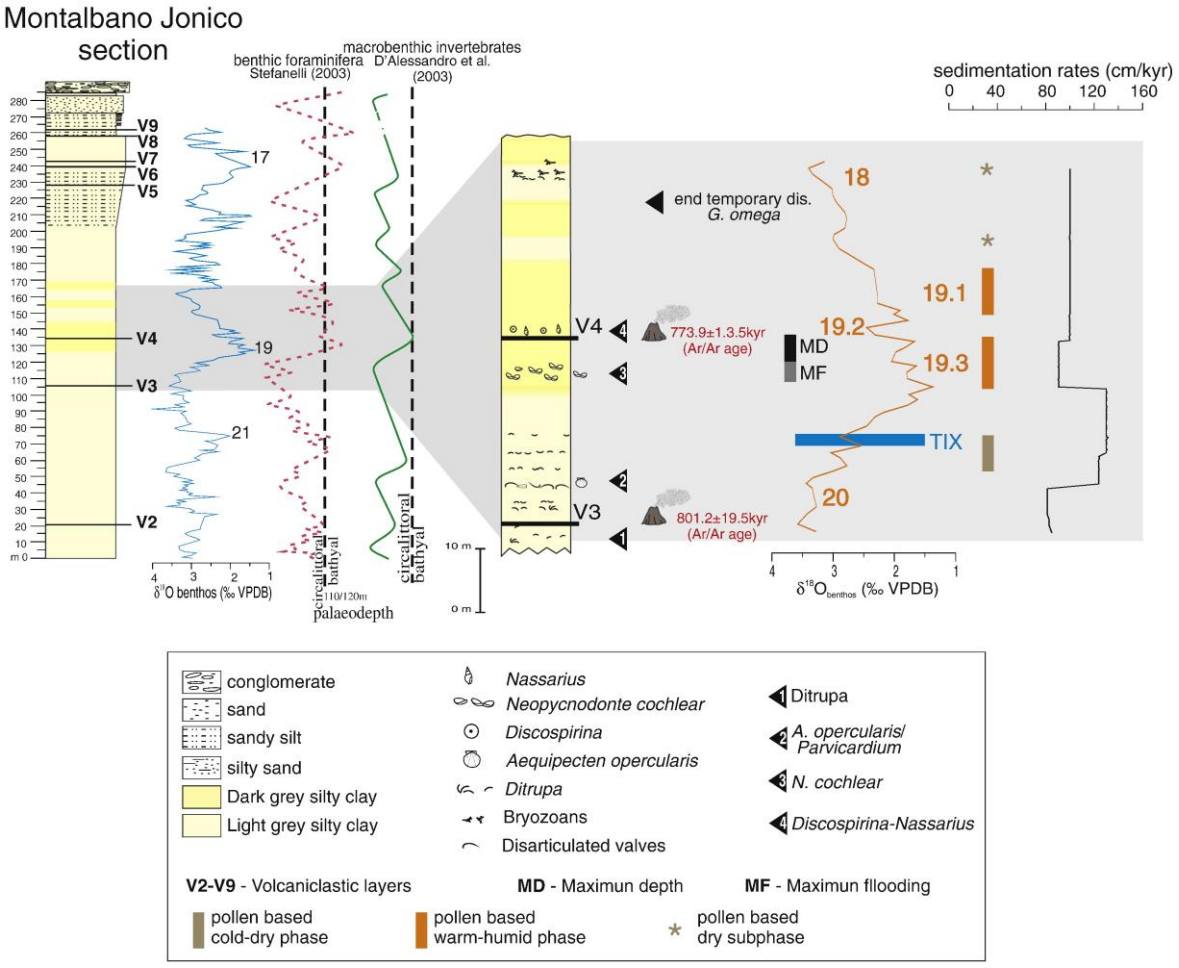

Fig. 2. Lithological and stratigraphical features of the composite Montalbano Jonico section (Interval B) and of the "Ideale" section. Chronological, stratigraphical and paleonvironmental details have been traced according to Marino et al. (2015 and references therein). $\delta^{18}O$ from Brilli (1998), Brilli et al. (2000) and Ciaranfi et al. (2010). MIS 19.3, 19.2 and 19.1 are the numbered counterparts of the lettered substages MIS 19c, 19b, and 19a adopted in the present study.

Marino et al., 2015; Toti, 2015; Marino et al., 2016and references therein) addressed specifically the "Ideale" section, which contains MIS 19 and the potential GSSP of the Lower-Middle Pleistocene (Head and Gibbard, 2015a). The section investigated in the present study is about 60 m thick (Fig. 2), and mainly represented by dark-light grey silty clays. Two volcaniclastic layers (V3 and V4) are interbedded in the lower and middle parts of the section. Previous paleoenvironmental investigations, based on macroinvertebrate paleocommunities (D'Alessandro et al., 2003) and benthonic foraminifera (Stefanelli, 2003), indicated that the sediments were mainly deposited in inner to outer shelf environments (Fig. 2), with sporadic transition to upper slope. Relative paleodepth ranges from a minimum of about 100 m to a maximum of about 200 m (Aiello et al., 2015). The available oxygen isotope record through the section was widely discussed in several previous papers (Brilli, 1998; Brilli et al., 2000; Ciaranfi et al., 2010) and clearly displays the onset of the interglacial MIS 19, which also correlates with a general deepening of the basin and a peculiar paleontological content (Fig. 2). Specifically, a maximum flooding interval has been identified based on the *Neopycnodonte* paleocommunity (D'Alessandro et al., 2003), that is also concurrent with warmer conditions deeper in the water column (Girone and Varola, 2001; Marino et al., 2015). The deep-water oyster *Neopycnodonte cochlear* thrives during low sedimentation rates and low turbidity conditions on the sea floor (Massari et al., 2002; Ceregato et al., 2007; Wisshak et al., 2009). A lowered sedimentation rate is indeed recorded during this interval (Fig. 2). Maximum depth is then reached slightly above (Fig. 2), as indicated by macro- and microbenthic invertebrate communities (D'Alessandro et al., 2003; Stefanelli, 2003). In addition, the main vegetational changes have been recently identified through the "Ideale" section (Bertini et al., 2015; Marino et al., 2015; Toti, 2015; Marino et al., 2016), suggesting the occurrence of succeeding cold-dry and warm-humid phases/subphases (Fig. 2) associated with global climate fluctuations. A differentiation in numbered isotopic events 19.3, 19.2 and 19.1 (Fig. 2) has been used in Marino et al. (2015), in agreement with nomenclature of Bassinot et al. (1994). They represent the counterparts of the lettered MIS 19c, 19b, and 19a (Head and Gibbard, 2015b; Railsback et al., 2015) that we have been adopting in the present paper according to Railsback et al. (2015). Finally, the Ar/Ar age of volcaniclastic layers V3 (Maiorano et al., 2010) and V4

(Petrosino et al., 2015), together with the tuning of the oxygen isotope pattern to the reference isotope records (Ciaranfi et al., 2010; Marino et al., 2015) and the occurrence of the worldwide calcareous nannofossil bioevent (end temporary disappearance of *Gephyrocapsa omega*) (Fig. 2), provide a robust chronological framework for further improvement of paleoclimate reconstruction throughout the section.

3. Methods

The sample resolution adopted generally varies from 0.6 to 2 kyr through 760–790 ka, just across the interval from late MIS 20 to late MIS 19. In the lower and upper portions of the investigated interval, the analyses were performed at lower sampling resolution, generally ranging between 2 and 3 kyr. Occasionally, the temporal resolution reaches 2–5 kyr due to poor outcrop exposure.

3.1. Micropaleontology

3.1.1. Calcareous plankton

Calcareous plankton investigations were performed on 57 samples. For planktonic foraminifera analyses the samples were dried and washed on a 63 μm sieve, and the residue > 150 μm was used to obtain the quantitative abundances of taxa. The residues were split until a representative aliquot, containing about 300 specimens, has been obtained. The species abundances were quantified as percentages on the total number of planktonic foraminifers. Sixteen species or species groups were distinguished: *Globigerinoides ruber* group (gr.) includes morphotype *Globigerinoides ruber* white, and *Globigerinoides elongatus* (sensu Aurahs et al., 2011); *Trilobatus sacculifer* includes *Trilobatus trilobus*, *Trilobatus sacculifer* and *Trilobatus quadrilobatus* (sensu Hemleben et al., 1989; André et al., 2013; Spezzaferri et al., 2015). For the taxonomy of *Neogloboquadrina* spp. the criteria from Darling et al. (2006) have been adopted: *Neogloboquadrina incompta*

corresponds to what has been previously referred to *N. pachyderma* (dextral) and includes intergrades between *N. pachyderma* (dextral) and *N. dutertrei*; *N. pachyderma* only includes the left coiling specimens. The SPRUDTS group (sensu Rohling et al., 1993) groups *Trilobatus sacculifer*, *Hastigerina pelagica*, *Globoturborotalita rubescens*, *Orbulina universa*, *Beella digitata*, *Globoturborotalita tenella* and *Globigerinella siphonifera*.

Slides for coccolithophore analysis were prepared according to the method of Flores and Sierro (1997) to estimate absolute coccolith abundances. Quantitative analyses were performed using a polarized light microscope at 1000 × magnification and abundances were determined by counting at least 300 coccoliths of all sizes, in a varying number of fields of view. Reworked calcareous nannofossils were estimated separately during this counting. Additional areas of slides were analyzed up to total 100 fields of view, in order to improve the counting of taxa that were determined as uncommon and rare in the 300-count. The abundances of *Umbilicosphaera sibogae*s.l., *Calciosolenia* spp., *Oolithotus* spp. are grouped as warm-water taxa, according to ecological preferences of these taxa (McIntyre and Bé, 1967; Winter et al., 1994; Ziveri et al., 2004; Baumann et al., 2004; Boeckel and Baumann, 2004; Saavedra-Pellitero et al., 2010; Palumbo et al., 2013; Maiorano et al., 2015). Taxonomy of gephyrocapsids follows the criteria synthetized in Maiorano et al. (2013).

3.1.2. Palynology

Forty-eight palynological samples contributed to reconstruction of the paleovegetation and paleoclimate changes in both terrestrial and marine realms. Fifteen new pollen samples have been added to those already acquired in the frame of previous works (Bertini et al., 2015; Marino et al., 2015; Toti, 2015). Twelve samples have also been analyzed for their dinocyst content. Samples, each weighing 20 to 25 g, were processed using standard chemical-physical procedures at the Department of Earth Science, University of Florence. Following the addition of one *Lycopodium* tablet to determine palynomorph concentrations, samples were treated with HCl (10%), HF (48%), sodium hexametaphosphate, KOH (10%) and $ZnCl_2$ separation (solution density approximately 2.0). Residues were sieved at 10 μm and

mounted using glycerol. Transmitted light microscopy, using × 750 and × 1250 (oil immersion) magnifications, was used for identification and counting of pollen. > 250 grains per sample were counted, excluding *Pinus*. Curves of both selected taxa and groups of taxa were plotted. Cupressaceae percentages were calculated on the total pollen sum, including all arboreal (AP) and non-arboreal (NAP) pollen taxa plus their individual count. On the other hand, all other pollen taxa refer to a pollen sum, including all pollen taxa except *Pinus* and Cupressaceae.

The groups of pollen taxa informally established on the basis of the ecological and climatic requirements of their present correlatives include: high-altitude forest taxa (*Abies* and *Picea* plus *Fagus* and *Betula*); mid-altitude forest taxa (*Tsuga* and *Cedrus*); broad-leaved deciduous forest taxa characteristic of warm-temperate and temperate climates (*Quercus* followed by *Ulmus*, *Zelkova*, *Acer*, *Juglans*, etc.) plus Ericaceae; sclerophyll forest taxa (such as *Q. ilex* type, *Pistacia*, *Olea*), typical of regions with a Mediterranean climate having wet winters and dry summers. Asteraceae (*Artemisia*except); halophyte taxa (Caryophyllaceae and Amaranthaceae); steppe taxa (*Artemisa*, *Ephedra* and *Hippophae*); hydrophytes (especially represented by Cyperaceae). The Pollen Temperature Index (PTI), expressed by the ratio between mesothermic arboreal taxa (e.g., *Quercus*, *Carpinus* and *Carya*) and steppe taxa, has been calculated to discriminate, according to Suc et al. (2010), warm-temperate from cold phases.

The dinoflagellate cysts (plus the scanty acritarchs) have been illustrated both as individual curves and as groups of taxa according to their concentrations and percentages.

3.2. Inorganic proxies

3.2.1. Grain size and mineralogical analyses

Forty-nine samples were analyzed for grain size and mineralogical investigations. Samples were initially homogenized and disaggregated by water immersion and then wet sieved at 63 μm to estimate the sand portion of the sediment. A Coulter Multisizer was used to determine the inorganic grain

size distribution in the interval of ϕ from + 4.0 (0.063 mm) to + 9 (0.002 mm), with steps of 1/2 ϕ, where ϕ = colog_2d (d = diameter of particle). An Isoton II electrolytic solution was used for the Coulter analyses and diluted samples were ultrasonicated for 1 min before the measurement in order to avoid particle aggregation effects. Results were processed by a custom software (Multisizer 4), which shows volume percentages of grain size distributions in intervals of 1/2 ϕ. Coulter data were then converted into weight percentages and normalized to the total weight by including also the values of wet-sieved fractions > 63 μm.

Mineralogical investigations were performed by the X-ray powder diffraction (XRD) technique, using a PANalytical Empyrean diffractometer equipped with a real-time multiple strip (RTMS) PIXcel3D detector (CuKα radiation). Initial qualitative analyses of the clay minerals (fraction < 2 μm) were performed on air-dried, ethylene glycol-saturated and heated (550 °C) oriented samples. XRD mineralogical data were collected on bulk samples in the angular range 3–70° (2θ) using a virtual step scan of 0.026° and a counting time of 360.0 s/step. The X-ray tube operated at 40 kV and 40 mA. A 0.125° divergence slit, a 0.25° anti-scattering slit and a soller slit (0.02 rad) were mounted in the incident beam pathway, whereas the diffracted beam pathway included a Ni filter, a soller slit (0.02 rad) and an antiscatter blade (7.5 mm). The data were collected from carefully ground powders, using side-loaded sample holders. Quantitative mineralogical data were obtained from Rietveld analysis, by means of the fundamental parameters based on the Rietveld program BGMN, Version 1.8.6b (Bergmann et al., 1998). The following generalized refinement strategy was applied for the analyzed samples: background was modeled by a 5-parameter polynomial; zero point (limits ± 0.02°) and sample displacement (± 0.03 mm) were always refined; lattice parameters were refined for all phases with 'reasonable' interval restraints and spherical harmonic models were used to correct preferred orientation, which was observed especially for layer silicates. All the structures used for the Rietveld refinements were taken from the BGMN database; kaolinite and smectite were refined according to a disordered kaolinite and a Na-smectite-structure model, respectively.

3.3. Data processing

Multivariate statistical analysis was applied to mineralogical and micropaleontological data for a better understanding of the existing correlations among variables of each dataset. Principal component analysis (PCA) was carried out by means of SPSS 9.0 software, using relative abundances of three different datasets: planktonic foraminifera, calcareous nannoplankton and mineralogy. Only variables with none or few missing values and highest variance were considered. Loading values are reported in Tables 1–3. For microfossils, null values were set to 0.01 to allow the data processing. Standardization was necessary to ensure the normal distribution and the same variance ($\mu = 0$; $\sigma = 1$) for all the processed variables (e.g., Davis, 2002, p. 517).

4. Results

4.1. Paleontological proxies

4.1.1. Calcareous plankton

The planktonic foraminifera are well preserved and diversified at the "Ideale" section. In several samples collected within MIS 19c, pyrite is rarely identified under the microscope as infill in foraminifera tests, steinkerns of other small components or framboidal particles. However, it was not detected by XRD. The planktonic foraminiferal assemblages are dominated by *Globigerina bulloides* and the *G. ruber*group which may reach about 50% and 60% of the assemblages respectively (Fig. 3a). The *G. ruber* group and SPRUDTS group are the main components of the total assemblages during MIS 19 and particularly during the phase of highest depletion of the $\delta^{18}O_{benthic}$ record. During the glacial phase the assemblages are mainly composed by *Globigerinita glutinata*, *Globorotalia scitula* and *Neogloboquadrina* spp. (mainly *N. incompta*), with the exception of the late phase of MIS 20, when the assemblages mainly consist of *Globorotalia inflata*. *Turborotalita*

quinqueloba occurs throughout the entire studied interval, during glacial and interglacial phases, although never representing the most abundant taxon.

Calcareous nannofossils are common to rare throughout the whole investigated section and display a moderate to good state of preservation. Fig. 3 shows the distribution of the most significant taxa as percentages (Fig. 3b) and total concentrations (Fig. 3c). The dominant component of the assemblage is represented by small *Gephyrocapsa* (< 3 μm) and gephyrocapsids > 3 μm (*Gephyrocapsa caribbeanica* and *G. oceanica*) (Fig. 3b) which may reach about 80% and 60% of the total assemblage respectively. The total coccolith abundance varies significantly from about 90 × 10^6 to about 1000 × 10^6 coccolith/g sediment (Fig. 3c) showing the most remarkable increase across MIS 19c, concurrent with the abundance increase of *Gephyrocapsa* > 3 μm (Fig. 3c). Minor variations are observed in the lower and upper parts of the studied interval. In general terms, the increase of coccolith abundance essentially follows the lighter values of the oxygen isotope record. Subordinate components of the assemblages (Fig. 3b) are represented by *Coccolithus pelagicus* s.l. (mainly *C. pelagicus* spp. *pelagicus*), and reticulofenestrids (> 3 μm) showing higher abundance in the lower part of the

	PC1
Globigerina bulloides	– 0.433
Globigerina falconensis	– 0.082
Globigerinita glutinata	**0.807**
***Globigerinoides ruber* group**	**– 0.803**
Trilobatus sacculifer	– 0.409
Globoturborotalita tenella	– 0.382
Globoturborotalita rubescens	– 0.623
Globigerinella calida	– 0.634
Orbulina universa	0.138
Turborotalita quinqueloba	0.571
Neogloboquadrina pachyderma	**0.751**
Neogloboquadrina dutertrei	– 0.067
Neogloboquadrina incompta	0.534
Globorotalia inflata	**0.762**
Globorotalia scitula	– 0.049

Table 1. Loadings of planktonic foraminifera taxa on the first principal component of the "Ideale" section. The most relevant component loadings are indicated in bold.

section (late phase of MIS 20), as well as in the uppermost portion (MIS 18).

Rare taxa in the assemblages are *Florisphaera profunda*, *Helicosphaera* spp. (mainly *H. carteri* and subordinately *H. pavimentum*), *Syracosphaera* spp. (mainly *S. pulchra* and *S. histricha*) and *Calcidiscus leptoporus* s.l. (Fig. 3b). Despite *F. profunda* and the warm-water taxa representing a minor component of the whole assemblage (Fig. 3b), they show distinct abundance fluctuations throughout the section and increased values essentially during MIS 19c (Fig. 3c). Very rare taxa are represented by *Braarudosphaera bigelowi*, *Rhabdosphaera clavigera* var. *stylifera*, *Pontosphaera* spp. and are grouped as "others" in Fig. 3b. Reworking is not insignificant in the analyzed samples and consists of Cretaceous to Miocene coccolith taxa.

	PC1
Gephyrocapsa oceanica	**0.910**
small *Gephyrocapsa*	**0.723**
Reticulofenestra spp.	– 0.154
Florisphaera profunda	**0.774**
Helicosphaera carteri	0.036
Helicosphaera pavimentum	0.685
Syracosphaera spp.	0.507
Rhabdosphaera clavigera var. *stylifera*	0.559
Oolithotus spp.	0.488
***Umbilcosphaera sibogae* s.l.**	**0.787**
Calcidiscus leptoporus s.l.	0.087
Calciosolenia spp.	0.355
Coccolithus pelagicus* spp. *pelagicus	**– 0.423**
Gephyrocapsa caribbeanica	**0.807**

Table 1. Loadings of planktonic foraminifera taxa on the first principal component of the "Ideale" section. The most relevant component loadings are indicated in bold.

4.1.2. Palynology

4.1.2.1. Pollen

The detailed distribution of palynomorphs (relative abundances and total concentrations) has been demonstrated in previous studies (Bertini et al.,

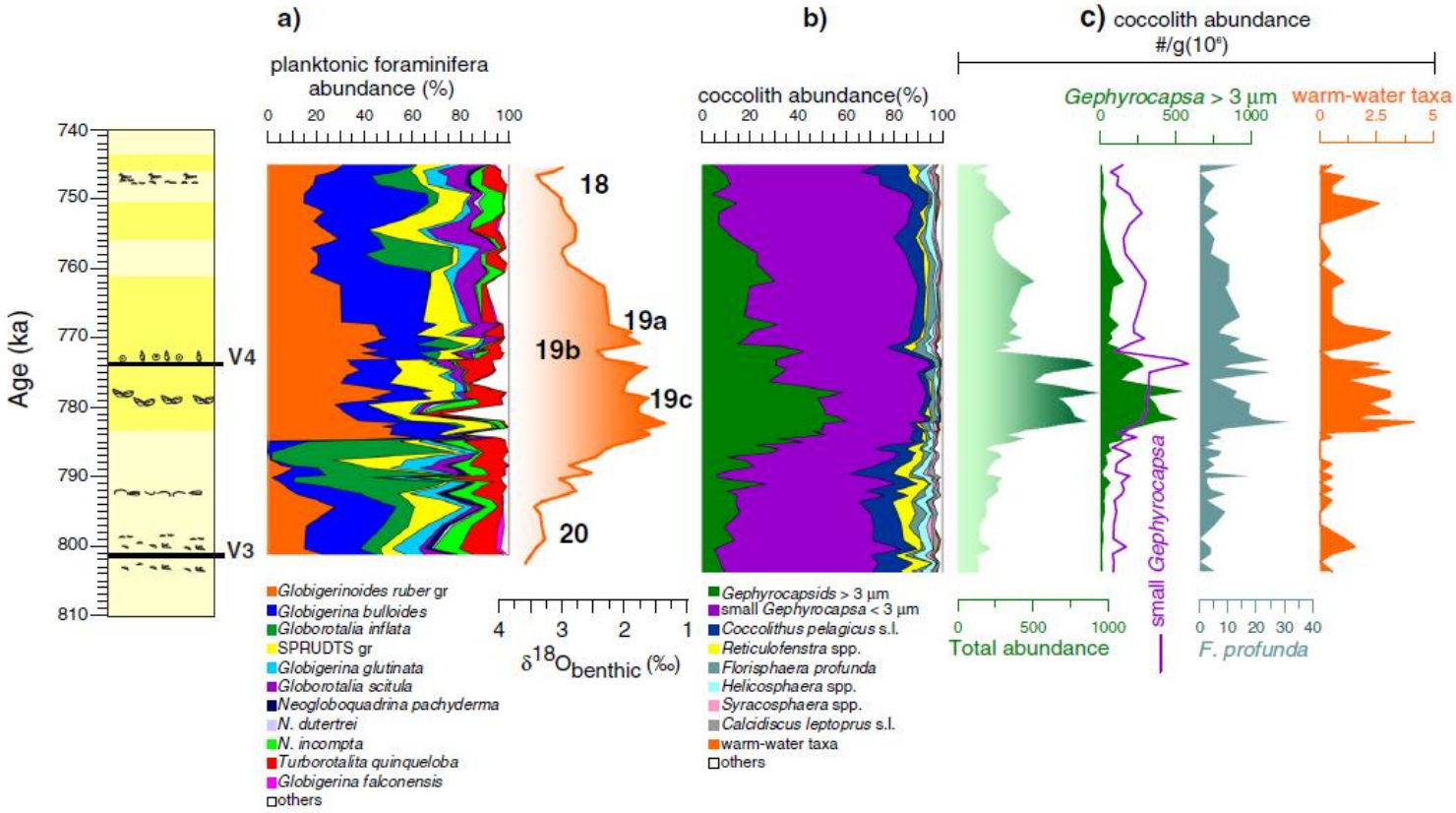

Fig. 3. Abundance variations through time of a) planktonic foraminifera and b-c) calcareous nannofossil assemblages at the "Ideale" section. For lithological legend refer to Fig. 2.

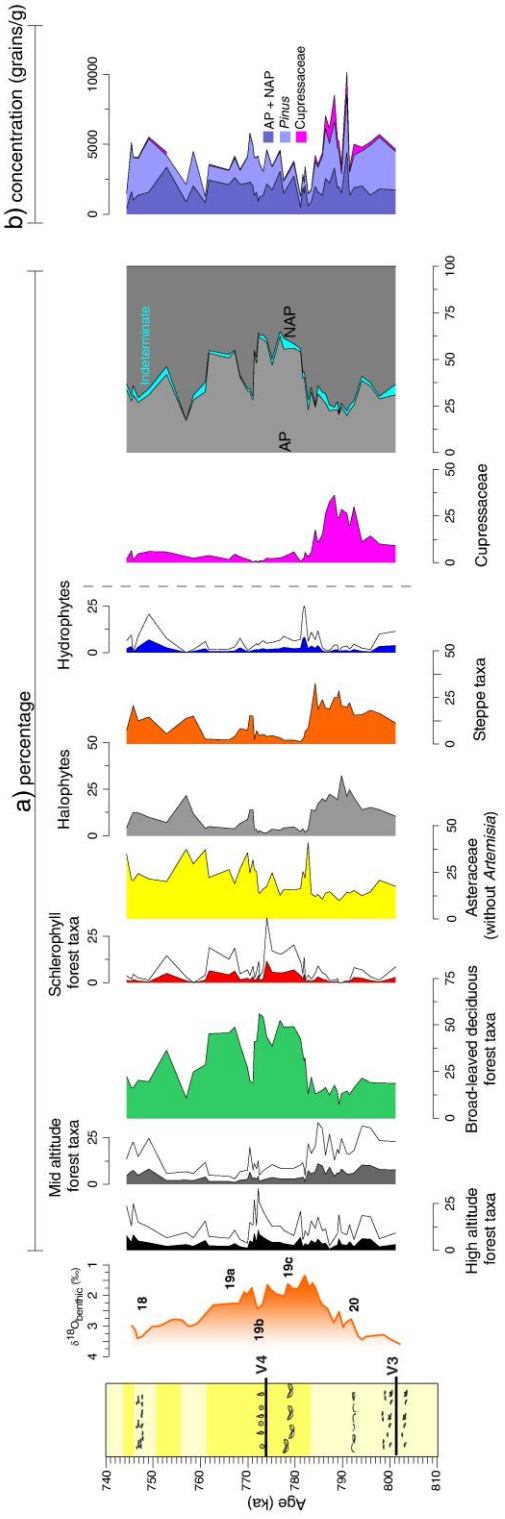

Fig. 4. a) Percentage of selected pollen taxa at the "Ideale" section. All the curves, except Cupressaceae, are calculated on the total pollen sum without Pinus *and Cupressaceae. The latter taxon is normalized to the sum of total pollen without* Pinus*. b) Cumulative concentration (grains/g) of total pollen (AP + NAP without* Pinus*), Pinus and Cupressaceae. Exaggerated curves have been drawn with 3 x exaggeration. For lithological legend refer to Fig. 2.*

2015; Marino et al., 2015; Toti, 2015). Here, the main floristic and vegetational evidence is summarized, with the integration of the new data (Fig. 4a, b). The pollen record includes > 120 pollen taxa. Pollen concentration ranges from 1449 to 10151 pollen grains per gram. Over-representation is evident for *Pinus* and Cupressaceae pollen. Moreover, reworking is not negligible and is attested by the presence of *Classopollis*, as well as taxa not exclusively of Mesozoic strata, including saccate pollen of Pinaceae.

Throughout the MIS 20 to MIS 19 transitional phase (Fig. 4), steppe taxa, after the first significant increase of halophytes and Cupressaceae, exhibited a persistently increasing presence, as well as two main acme phases. At the beginning of MIS 19 (base of 19c), the first notable expansion of the mesothermic taxa (from 13.2 to 21.9%), including especially broad-leaved forest taxa, is soon interrupted by an herb-dominated event. The latter, with NAP at 79%, is marked by the sudden, short-time expansion of Asteraceae (41%); Poaceae keeps staying well represented, whereas steppe and halophyte taxa are subordinate. Successively, mesothermic forest taxa show a new stronger increase, which shortly anticipates the minimum reached by steppe taxa (1.2%). After that, deciduous *Quercus*, plus other broad-leaved forest taxa, exhibit their major percentage increase. The consistent occurrence of woody taxa, together with the moderate abundance of herbaceous taxa is, as a whole, clearly evident during MIS 19c. However, in the upper part of this interval, the increase in mesothermic broad-leaved taxa is interrupted by an herb-dominated event, which involves Asteraceae, but neither *Artemisia* nor halophytes. Just few thousand years later, broad-leaved forest taxa decrease again in favor of Asteraceae (showing two close abundance peaks), halophyte and steppe taxa, contributing to the characterization of MIS 19b. The subsequent significant increase of arboreal taxa is again prevalently marked by the spread of deciduous *Quercus* (up to approximately 40%), during MIS 19a. Among the NAP, we observe a succession of peaks which mark the late part of MIS 19 and MIS 18 glacial inception. Specifically, Asteraceae show two successive remarkable increases, the younger one concomitant with a peak of halophytes. At the same time, a good increase in steppe taxa is also evident. It predates the most important expansion of steppes. AP, as a whole, keeps staying below 34% (Fig. 4), with the exception of a remarkable increase (up to 42%) at the onset of MIS 18.

4.1.2.2. Dinoflagellate cysts

At least 30 marine dinoflagellate cyst taxa were recorded, with estimated concentrations ranging from 188 to 618 cysts per gram. Their overall very low concentration did not allow an ideal number of cysts to be counted in all the samples. In Fig. 5 only those samples containing at least 50 cysts have been plotted. Assemblages are dominated by the following autotrophic cysts: *Lingulodinium machaerophorum* including forms with reduced processes, *Operculodinium centrocarpum* (identified as *O. centrocarpum* sensu Wall and Dale, 1966), *O. israelianum*, *Spiniferites mirabilis*, *S. hyperacanthus*, *S. ramosus*, *S. membranaceous*, *S. elongatus*, *Achomosphaera* spp., *Impagidinium patulum*, *I. aculeatum*, *I. pallidum*, *I. sphaericum*, cysts of *Pentapharsodinium dalei*, *Polysphaeridium zoharyi*, *Tuberculodinium vancampoe*, *Bitectatodinium tepikiense*, *Tectatodinium pellitum*, and *Nematosphaeropsis labyrinthus*. The acritarch genus *Nannobarbophora* was also present. Heterotrophic cysts, including *Brigantedinium* spp. and *Selenophenphix* spp., were sporadically recorded. Reworked dinoflagellate cysts were recognized by differential preservation and discordant stratigraphic presence; they are present

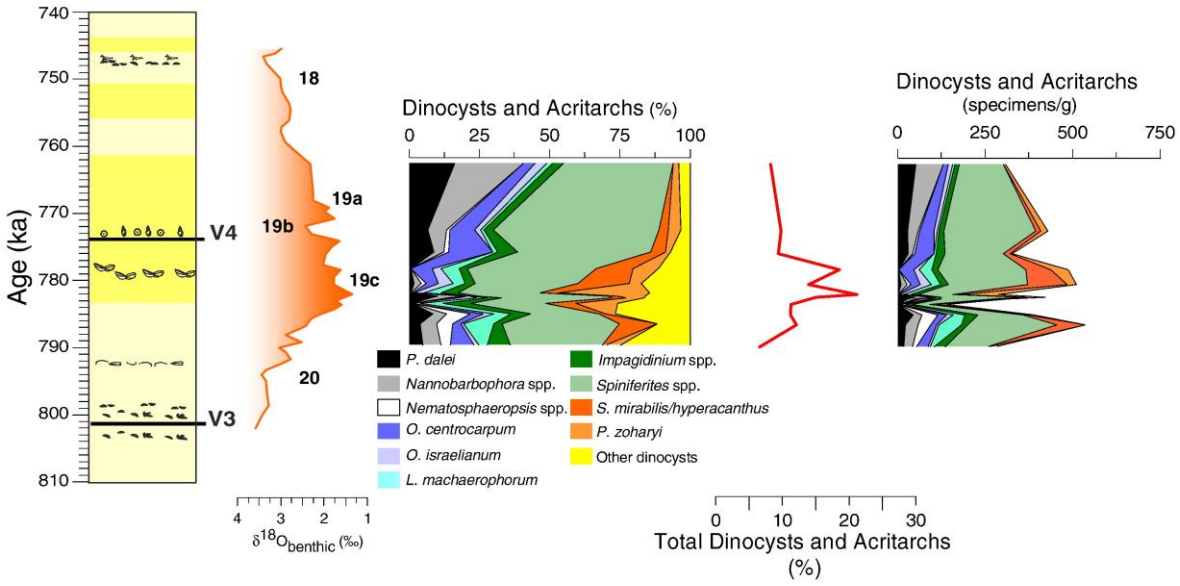

Fig. 5. Dinocyst and acritarch frequencies and concentration at the "Ideale" section. Total Dinocyst and acritarch percentage was calculated on the total pollen sum plus their individual count. For lithological legend refer to Fig. 2.

throughout with concentrations up to 236 cysts per gram. The previous evidence supports the occurrence of relevant taphonomic biases affecting the dinocyst assemblages. The almost total absence of heterotrophic taxa, as well as the composition of the autothrophic assemblages, suggest a major role of aerobic degradation phenomena (e.g., Zonneveld et al., 2001, 2008 and references therein). The latter are especially well expressed by the paucity of sensitive cyst species (s-cyst), with respect to the resistant (r-cyst) taxa. Such a selective preservation of the organic-walled dinoflagellate cysts clearly prevents to achieve a comprehensive reconstruction of the original dinoflagellate communities. Nonetheless, the major changes can be pointed out in the fossil assemblage (Fig. 5). In the lower part of the dinocyst record, including the end of MIS 20, assemblages include both warm- to temperate-water dinocyst genera, such as *Spiniferites*, *Impagidinium* and *Operculodinium* and the cool-water taxa *N. labyrinthus* and *P. dalei* followed by *B. tepikiense* (included in the curve of other dinocysts). An increase in the percentage values of *S. mirabilis*/*hyperacanthus* marks the late glacial record, before the onset of MIS 19. During MIS 19c an increase in taxa richness is attested by *Spiniferites*, *Impagidinium* (including *I. aculeatum*) and *Operculodinium*. *S. mirabilis*/*hyperacanthus*along with *P. zoharyi* show successive phases of increase.

4.2. Inorganic variables

4.2.1. Grain size

The main mode varies from 5.6 to 22 μm, indicating a detrital fraction varying from fine to coarse silt. The percentage of clay (< 4 μm), fine, medium and coarse silt (4–8 μm, 8–16 μm, 16–63 μm) and sand (> 63 μm) are plotted through time in Fig. 6a. It is shown that the clay fraction is generally less abundant during MIS 20 (15–24%, average 19%), whereas it increases significantly (20–31%, average 24%) from the onset of MIS 19 onwards, although several fluctuations have been observed through this interval. This trend is further emphasized in the cumulative curve of fine-silt, whereas

general opposite trends have been detected for both sand and coarse silt fractions (Fig. 6a).

4.2.2. Mineralogy

All the investigated samples consisted of phyllosilicate minerals, carbonates (calcite and dolomite), quartz and feldspars, with traces of accessory minerals (Fe-oxides, halite and gypsum) occurring sporadically in some samples and therefore not further considered in the discussion. Table 1 (Supplementary data) shows the mineral composition obtained from the Rietveld method, while Fig. 6b displays changes in the mineral composition through the investigated section. Phyllosilicates (Phyl) are the most abundant component in the examined samples and are predominantly composed of illite/muscovite (21–33%, average 26%), an intermediate percentage of smectite (7–17%, average 13%) and relatively low percentages of kaolinite (5–9%, average 6%) and chlorite (3–5%, average 4%). Carbonates range from 16 to 24% (average 21%) of the total sediment, whereas quartz and feldspar range from 17 to 24% (average 20%) and from 7 to 14% (average 9%), respectively (Fig. 6b). The

	PC1
Calcite	0.460
Quartz	**0.809**
Illite/muscovite	**– 0.546**
K feldspar	0.422
Dolomite	**0.727**
Chlorite	– 0.240
Smectite	**– 0.689**
Kaolinite	**– 0.840**
Plagioclase	0.455

Table 3. Loadings of mineral phases on the first principal component of the "Ideale" section. The most relevant component loadings are indicated in bold.

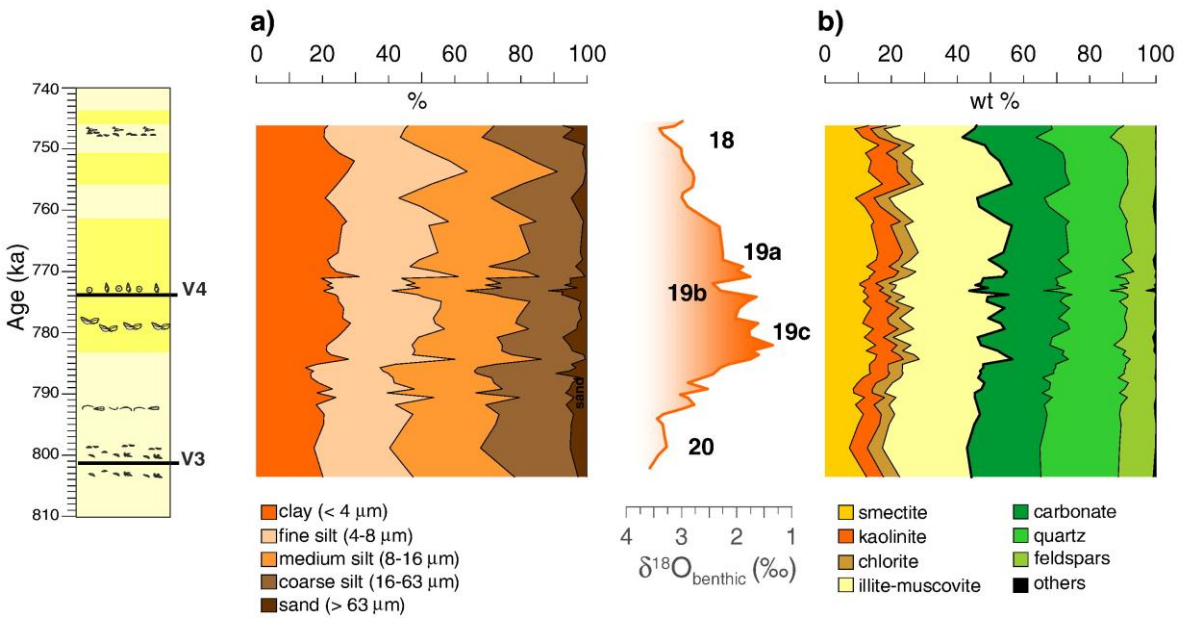

Fig. 6. Cumulative plots of grain size variation distribution (a) and mineralogical content (b) through time at the "Ideale" section. Bold line (b) highlights cumulative phyllosilicate contents. For lithological legend refer to Fig. 2.

relative abundance of phyllosilicate minerals (bold-line in Fig. 6b) through time shows a prominent increase at the MIS 20–MIS 19 transition, with respect to non-phyllosilicates. Kaolinite and smectite contents display rather similar trends and more dispersed data compared to illite/muscovite and chlorite contents. Among the non-phyllosilicate minerals, a distinct increase in quartz was observed during the MIS 20 and stadial phases.

5. Discussion

Both biotic and abiotic proxies clearly display comparable variations between surface water and terrestrial environments throughout the "Ideale" section, which suggests climate-induced sea surface temperature variations, terrestrial vegetational changes and sediment-supply modifications. In the text below, we discuss the general pattern of the overall paleoclimate framework and then

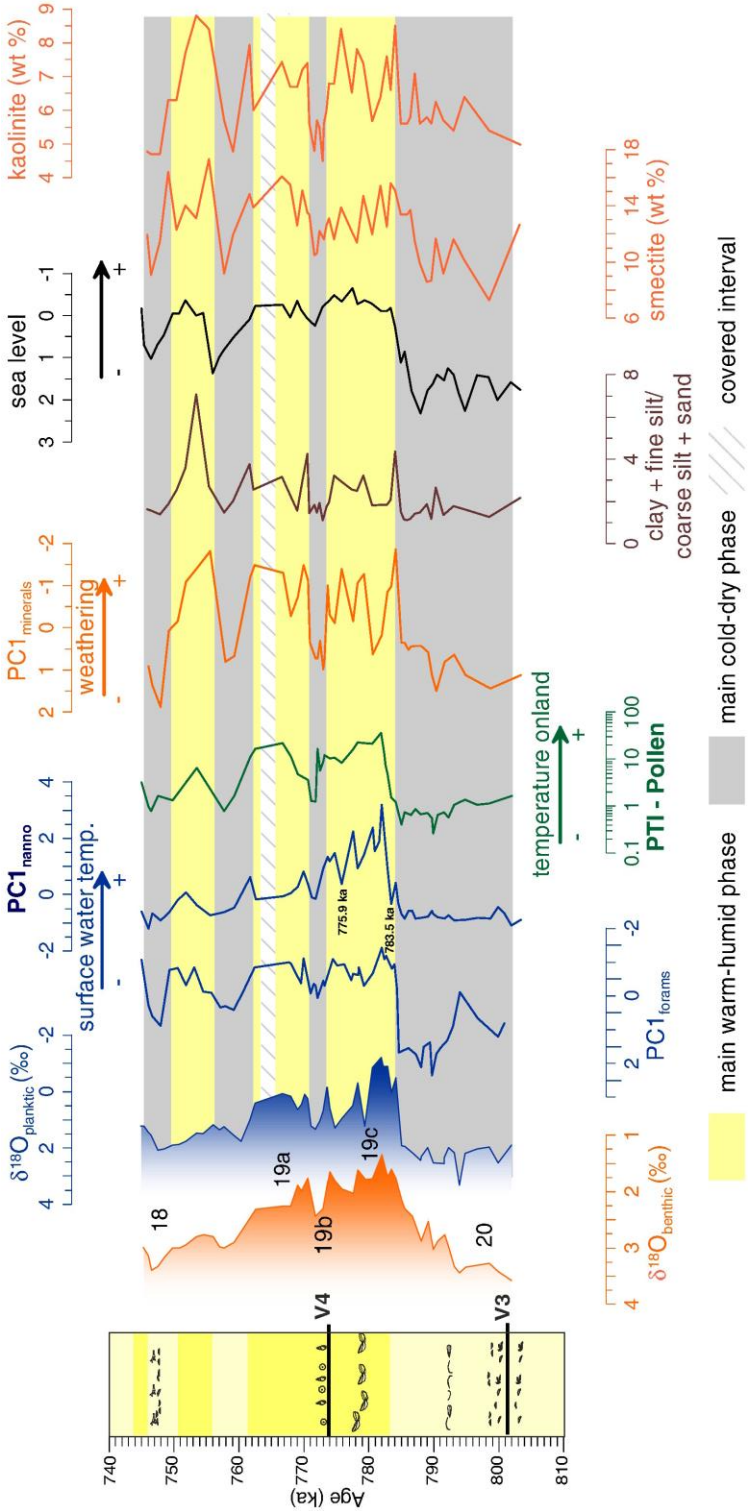

Fig. 7. Paleonvironmental variations observed through time at the "Ideale" section as deriving from principal component analysis of calcareous plankton and mineral phases (PC1foram, PC1nanno, PC1minerals) and from Pollen Temperature Index (PTI), correlated with grain size distribution and sea level variation. The latter is based on benthic foraminifera assemblages from Stefanelli (2003). Selected mineral phases are also shown. Grey/yellow bands highlight main cold-dry/warm-humid phase respectively. For lithological legend refer to Fig. 2.

focus on the stadial/interstadial and millennial-scale variations with particular attention to the late MIS 20, MIS 19c and late MIS 19/18.

5.1. Marine realm: sea surface temperature changes

Results from principal component analysis on the calcareous plankton assemblage (Tables 1–2 and Fig. 7) revealed that surface water temperature primarily affected calcareous plankton across the record. In fact, both $PC1_{forams}$ and $PC1_{nanno}$ relate essentially to the thermal preferences of the taxa. $PC1_{forams}$ (Fig. 7) explains 29% of the variance and gives the highest negative component loadings (Table 1) for the oligotrophic and tropical-subtropical warm-water *G. ruber* group (Bé and Hamlin, 1967; Bé, 1971; Bé and Tolderlund, 1971; Hemleben et al., 1989; Pujol and Vergnaud-Grazzini, 1995), while it positively loads *G. glutinata*, *G. inflata* and *N. pachyderma*. It is known that *G. glutinata* is a high productivity-related taxon, both at low and high latitudes (Bé and Tolderlund, 1971; Thunell and Reynolds, 1984; Hemleben et al., 1989), while the transitional water taxon *G. inflata* prefers mixed and cool environments (Tolderlund and Bé, 1971; Fairbanks et al., 1982; Pujol and Vergnaud-Grazzini, 1995). The polar – subpolar *N. pachyderma* is considered a reliable signal of cold-water conditions in the Mediterranean waters during the Pleistocene (Huber et al., 2000; Kucera and Kennett, 2002; Yamasaki et al., 2008; Incarbona et al., 2013; Girone et al., 2013a; Capotondi et al., 2016). Based on the mentioned paleoecological requirements it is possible to infer that negative scores in $PC1_{forams}$ (Fig. 7) highlight the occurrence of temperate-subtropical water conditions into the basin, while positive values record intervals with subpolar-transitional surface water conditions.

With regard to the calcareous nannofossil assemblage, $PC1_{nanno}$ (34% variance) (Table 2; Fig. 7) groups together *G. oceanica*, *G. caribbeanica*, small gephyrocapsids, *F. profunda* and *U. sibogae* s.l., with high positive component loadings, while negative values are related to *C. pelagicus* spp. *pelagicus*. *C. pelagicus* is a subarctic species and a traditional cold water indicator (Baumann et al., 2000; Geisen et al., 2002); the subspecies *C. pelagicus* spp. *pelagicus* has higher abundances in the northern Atlantic, in areas with SST < 10 °C (Ziveri et al., 2004). On the other hand, *G. oceanica* is considered a

warm-water species with a preference for marginal seas (McIntyre and Bé, 1967; Okada and Honjo, 1975; Jordan et al., 1996). *G. caribbeanica* thrives in oligotrophic-subtropical water mass conditions (Bollmann, 1997), although the ecology of the taxon is actually not well established (López-Otálvaro et al., 2008; Maiorano et al., 2013). Small *Gephyrocapsa* are likewise indicative of higher temperature surface waters (Colmenero-Hidalgo et al., 2004) and abundant during interglacial stages (Flores et al., 1999; Henriksson, 2000). A warm surface water temperature preference is also known for *F. profunda*, since its distribution is limited to waters warmer than 10–12 °C (Okada and Honjo, 1973). However, due to the relatively proximal setting of the studied section, a relationship between species abundance and variation in climate-induced basin depth, observed throughout the section, cannot be excluded. *F. profunda* is in fact a major deep dwelling species (Okada and Honjo, 1973; Molfino and McIntyre, 1990a, 1990b) and its clear relationship to bathymetry has been identified (Incarbona et al., 2008). Based on the above mentioned ecological preferences, we suggest that positive scores of $PC1_{nanno}$ (Fig. 7) may indicate the arrival of warmer (subtropical) waters into the basin, while negative values indicate polar/subpolar water influx.

5.2. Climate on land: vegetational and sediment supply changes

On land, the curve of the PTI index, an indicator of vegetation sensitivity to climate changes, depicts relatively warmer vs. colder phases (Fig. 7). During colder sea surface water intervals, the predominance of non-arboreal pollen plants (Figs. 4, 7), especially *Artemisia*, *Ephedra* and Amaranthaceae, supports the expansion of steppe and halophytic vegetation, under a climate with severe seasonal moisture deficiency and marked temperature seasonality. However, repeated expansions of cosmopolitan herbaceous taxa, principally expressed by acme phases at Asteraceae, are also present. On the other hand, during warmer surface water conditions, we observe on land the prevalent expansions of thermophilous arboreal plants (Figs. 4a, 7), mainly deciduous *Quercus*, suggesting a period of mild winters and warm summers, with reduced seasonal moisture deficiency.

With regard to inorganic variables, bulk XRD analyses show that the studied sediments are mainly composed of phyllosilicates (mostly clay minerals), quartz, calcite, dolomite and feldspars. Such mineralogical composition is a result of both terrigenous supply from land and biogenic content. The nature of lithological units outcropping in the source area, mainly represented by Cretaceous-Neogene shaley units (Patacca and Scandone, 2007) and characterized by high content of smectite, illite, quartz and carbonates (Cavalcante et al., 2003; Perri et al., 2012), have influenced significantly the high detrital component of the sediments. The prevalent detrital character of the phases within the clay fraction of "argille subappennine" formation has been previously documented, as based on the morphology and chemical nature of minerals (Dell'Anna and Laviano, 1986) and supposed to be mainly inherited from the outcropping units, such as the Cretaceous "argille varicolori" auctt., and the Miocene "Flysch di Gorgoglione" formation (Selli, 1962). In our dataset, the ternary diagram Qz–Fsp–Dol (Fig. 8) shows poor dispersion of such non-clay terrigenous minerals, suggesting a common sediment provenance for the coarser detrital fraction. On the other hand, looking at the phyllosilicates ternary diagrams (Fig. 8), we observe that illite/muscovite and chlorite amounts are rather higher than those of smectite and kaolinite, as expected from the fine to medium-fine eroded lithologies and from the limited degree of soil leaching in middle latitude areas. Conversely, the relative higher variability of smectite and illite/muscovite + chlorite among the phyllosilicates (Fig. 8) could be related to a differential erosion in the source area, mainly represented by the smectite-rich Cretaceous "argille varicolori" formation (Pescatore et al., 1980; Cavalcante et al., 2003) and the illite/muscovite-rich Miocene siliciclastic units (Abbaticchio et al., 1981; Perri et al., 2012; Cavalcante et al., 2015). Notwithstanding the substantial homogeneity in the bulk mineral assemblage of samples and the observed signature inherited from the source area, some significant changes have been detected in mineral relative abundances and grain size distribution through all the investigated section, which can be likely interpreted in term of climate changes. Looking at $PC1_{mineralogy}$ (Fig. 7; Table 3), which explains 36.8% of the variance, the highest positive factor scores are found for quartz and dolomite; negative loadings are relative to kaolinite, smectite and to a lesser extent to illite/muscovite (Table 3). The positive scores of $PC1_{mineralogy}$, also

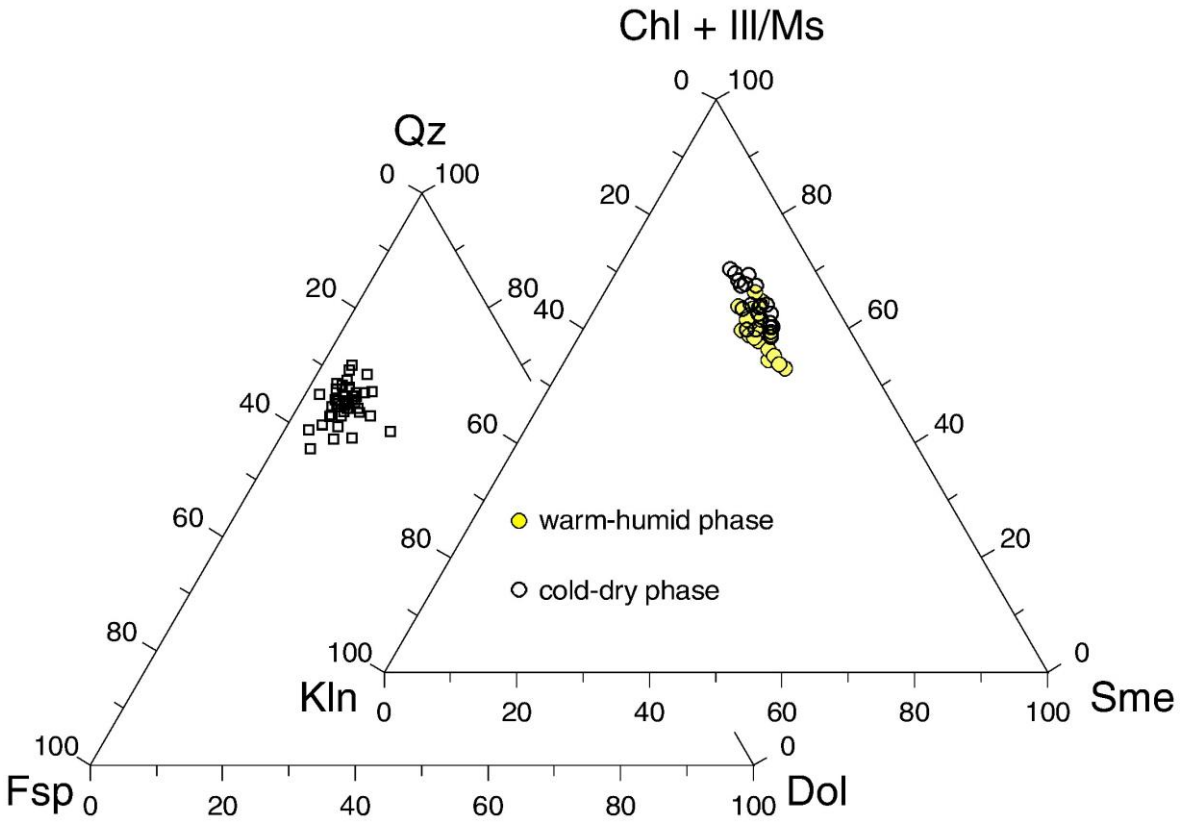

Fig. 8. Ternary diagram of non-clay terrigenous minerals (Qz-Fsp-Dol) and phyllosilicates (Chl + Ill/Ms.-Kln-Sme) at the "Ideale" section. Cold-dry and warm-humid phases are differentiated according to Fig. 7. Mineral abbreviations after Whitney and Evans (2010): feldspar (Fsp), dolomite (Dol), quartz (Qz), chlorite (Chl), illite (Ill), muscovite (Ms), kaolinite (Kln), smectite (Sme).

correlated with enhanced coarser grain size fraction supply (Fig. 7), reflect an increase of the coarser detrital mineral components into the basin, whereas the negative values, mainly loaded by kaolinite and smectite, are most likely linked to the occurrence of warmer and wetter climate, favoring chemical weathering (Berner, 1971; Singer, 1984; Chamley, 1989). The $PC1_{mineralogy}$ increases/decreases match well with the cold–dry/warm–humid phases, respectively (Fig. 7). It is reasonable to assume that increased aridity on land

and related reduced arboreal vegetation during colder phases have promoted erosional processes on the hillslopes and specifically on the higher relief of the chain, represented principally by the western Mesozoic calcareous and dolomitic units of the Apennines platform and by the arenitic units of the Miocene foredeep l.s. (Fig. 1). The positive correlation of Cretaceous-Neogene coccolith reworked taxa, a proxy of higher continental input (Flores et al., 1997; Colmenero-Hidalgo et al., 2004), with both quartz (r = 0.73) and dolomite (r = 0.68), supports the relation of higher abundances of these minerals with increased erosional processes on land. The increase of sediment input in the river systems, during cold phases, is consistent with the evidence of a general aggradation of the rivers and consequent formation of alluvial terraces (Pazzaglia, 2013; Wegmann and Pazzaglia, 2009; Boenzi et al., 2014). On the other hand, warmer and more humid conditions on land are concurrent with enhanced clay mineral content ($PC1_{mineralogy}$ decrease), particularly kaolinite and smectite, with increased supply of finer grain size fraction (mainly clay < 4 μm and fine silt at the expense of coarser silt and sand) into the basin, and with sea level rise, as documented from previous results based on benthic foraminifera (Stefanelli, 2003) (Fig. 7). This is likely the result of enhanced chemical weathering of the hillslopes, due to the changed hydrological/vegetational conditions on land, as well as by more distal depositional environment (Fig. 7). However, looking at the kaolinite and smectite variations through time, we observe that, although very similar, the trends of these two minerals do not match completely. In particular, the close similarity between the smectite and the sea level variations (Fig. 7), suggests a relation with climate-induced sea level variations. In contrast, kaolinite maxima, correlating very well with warm phases (Fig. 7), suggest an increase of this mineral in the detrital supply because of the increase in the hydrolyzing capacity of the weathering environment during warmer and wetter climates that favored the kaolinite formation (Berner, 1971; Singer, 1984; Chamley, 1989). The poor or almost absent correlation of illite/muscovite and chlorite with warm/cold phases may indicate their continuous and almost constant supply as finer detrital material during both cold and warm periods.

5.3. Higher frequency climate variability

5.3.1. Late MIS 20 and Heinrich-like event

This interval extends from 803.4 ka to 784.6 ka and predates the onset of MIS 19c (Figs. 7, 9). It contains a distinct deglacial phase as indicated by the $\delta^{18}O_{benthic}$profile (Fig. 9.1), showing a major depletion from 3.5‰ (at about 794 ka) to 2.15‰ (at 784.6 ka) and including Termination IX (Marino et al., 2015) (Fig. 2), dated at 790 ka, according to Lisiecki and Raymo (2005). Within this interval, the reduced amount of the finer grain size fraction (Fig. 7) is compatible with the shallower depth of the basin recorded in this part of the section with respect to younger portions, as inferred by benthic foraminiferal assemblage variations (Fig. 7). Looking at shorter-term fluctuations, it is noteworthy that previous examination of the vegetational changes (Bertini et al., 2015; Marino et al., 2015) allowed identification of a main dry acme phase, centered at 790 ka. The same authors suggested a possible correlation of the event with North Atlantic ice-rafted detritus (IRD) peak and with the eastern Mediterranean aeolian dust record. It is documented that the western Mediterranean surface waters respond with simultaneous abrupt SST decreases to the massive release of icebergs in the North Atlantic (Cacho et al., 1999, 2000; Sierro et al., 2005; Girone et al., 2013b). At the "Ideale" section calcareous plankton assemblages indicate that, superimposed upon the prevalence of transitional-subpolar assemblages, compatible with MIS 20 glacial conditions (Fig. 7), higher abundance peaks of *T. quinqueloba*, *N. pachyderma*, and *C. pelagicus* spp. *pelagicus*, occurring between 793.2 ka and 788.1 ka (Fig. 9.2, 9.4, 9.6), are an indication of remarkable sea surface water temperature decrease, likely related to the intensification of cold and arid conditions and/or to polar-subpolar water incursion into the Mediterranean (Cacho et al., 1999; Pérez-Folgado et al., 2003; Sierro et al., 2005; Marino et al., 2011; Girone et al., 2013b; Capotondi et al., 2016) and at the site location. Concurrent peaks of *N. pachyderma* sin. (*N. pachyderma* sensu Darling et al., 2006 in the present paper), and *C. pelagicus* spp. *pelagicus* have been successfully used as tracers of Heinrich-like (H-like) events in surface waters off western Iberia (Parente et al., 2004; Marino et al., 2014). A more prominent arrival of colder and fresher Atlantic surface water likely occurred at 789.8 ka,

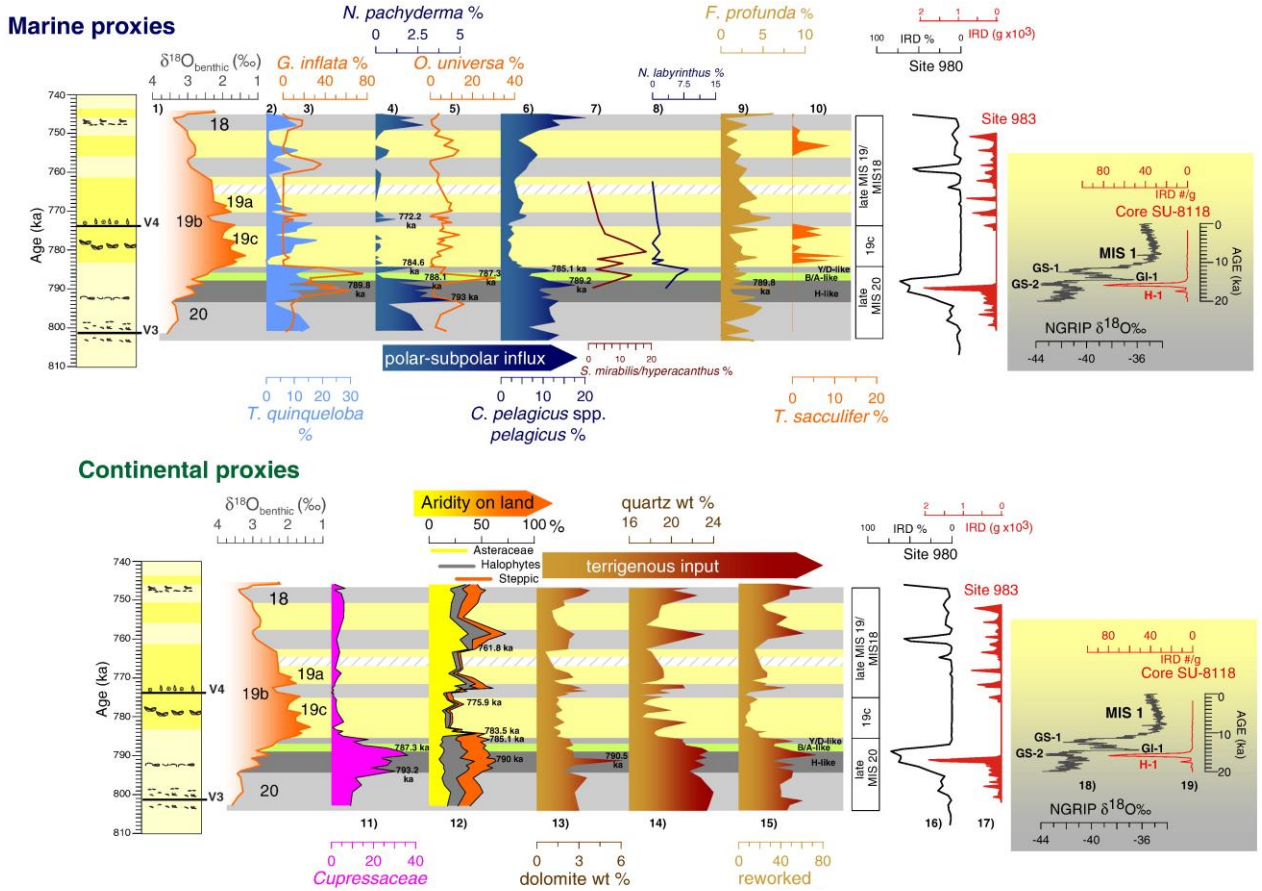

Fig. 9. Benthic oxygen isotope (1) compared with selected paleonvironmental marine (3-10) and terrestrial (11-15) indicators at the "Ideale" section. Oceanic and ice-core records are shown for comparison: ice rafted detritus (IRD) curves from North Atlantic ODP Site 980 (Wright and Flower, 2002) (16) and Site 983 (Kleiven et al., 2011) (17) through the interval between MIS 20 and MIS 18; NGRIP δ18O ‰ (NGRIP members, 2004) (18) and IRD in core SU-8118 off Portugal (Bard et al., 2000) (19) for the last 20 ka. GS: Greenland Stadial; GI: Greenland Interstadial. Heinrich-like (H-like) and Bølling-Allerød (B/A)/Younger Dryas (YD) - like events have been indicated in the "Ideale" section as inferred from the present study. Cold-dry (grey bands) and warm-humid (yellow bands) phases have been differentiated according to Fig. 7. For lithological legend refer to Fig. 2.

where a marked increase of *T. quinqueloba* (Fig. 9.2) and *F. profunda* (Fig. 9.9), has been observed. It is reasonable to assume that fresher surface water conditions may have promoted the abundance of *T. quinqueloba*(Rohling et al., 1997; Retailleau et al., 2012), while enhanced water stratification and warmer subsurface waters at the thermocline/nutricline depth (Colmenero-Hidalgo et al., 2004; Marino et al., 2014; Maiorano et al., 2015) has favored the development of the deep dwelling *F. profunda*. Relative freshening of surface waters during Heinrich events, well known in the western Mediterranean (Cacho et al., 1999, 2000; Sierro et al., 2005), have also been documented in the central/eastern Mediterranean for the last 70 kyr (Sprovieri et al., 2012).

Despite the scanty dinocyst documentation in this interval, the late MIS 20 is marked by the occurrence of several cool-water species such as *N. labyrinthus, P. dalei*, *B. tepikiense* and *S. elongatus* (Fig. 5). Many of them were significant components of the cold Mediterranean assemblages during the so-called H-like events of the late Quaternary (e.g., Rouis-Zargouni et al., 2010), in agreement with calcareous plankton indications. On land, the inception of progressively harsher conditions in the latest part of MIS 20 is indicated by both the lowest value of the PTI, which is centered at 790 ka (Fig. 7), and by the larger occurrence of Cupressaceae up to approximately 788 ka (Fig. 9.11). At a higher level of detail, the interval between 793.2 ka and 787.3 ka, that is coeval with the higher values of *N. pachyderma* and *C. pelagicus* spp. *pelagicus*, records the main phase of deterioration as attested by the strong increase of halophytes and then steppe pollen taxa (Figs. 4, 9.12), indicating a significant phase of enlargement of the open landscape, and supporting the expansion of a prevalent dry steppe vegetation.

Through the same interval, mineralogical data indicate an increase of quartz, suggesting an increase of terrigenous supply into the basin, which is in good agreement with higher percentages of reworked coccoliths (Fig. 9.15). In addition, a marked peak of dolomite is recorded at 790.5 ka (Fig. 9.13), indicating a modification in the sediment supply related to a relative increase of coarse and carbonate-rich alluvial materials. The dolomite increase could be related to peculiar erosion on the carbonate bedrock during cold periods (Giraudi and Giaccio, 2015). The latter authors have suggested that during cold phases of the Middle Pleistocene in the Apennines, the glacier meltwater could not penetrate the limestone because of the reduced permeability related

to a bedrock, mainly covered by ice or fractures obstructed by frozen ground. Consequently, the rivers supply a larger volume of eroded sediments with relative dolomites enrichment produced in glacial environment. A similar increase in carbonate sediments during glacial periods was documented in Greece (Woodward et al., 1992). Furthermore, several authors documented the increase of alluvial phases during cold periods in the Mediterranean and the Italian peninsula (e.g., Macklin and Lewin, 2008; Giraudi, 2014).

The distinct cold and dry phase correlates with the chronology of IRD from North Atlantic Ocean Drilling Program (ODP) Site 980 (Wright and Flower, 2002) and Site 983 (Kleiven et al., 2011) (Fig. 9.16–17). Hence, the interval across 793.2 ka and 788.1 ka could be the regional equivalent of IRD discharge event (Heinrich-like event) related to millennial-scale Northern Hemisphere ice-sheet collapse. Numerous authors infer the chronological correlations between IRD and climatic events in the Italian peninsula during the Holocene (Giraudi, 2014), the Upper Pleistocene (Magny et al., 2006; Giraudi, 2015) and the Middle Pleistocene within MIS 12 (Regattieri et al., 2016), based on continental records. Our data suggest a similar correlation during MIS 19, supporting an increase of alluvial frequency, due to the high sensitivity of river response to short-term climate change during IRD events. The simultaneous response of both marine environment and atmospheric conditions to record the effect related to massive IRD discharge, is documented in the Late Pleistocene (Combourieu-Nebout et al., 1998, 2009; Cacho et al., 1999, 2000; Tzedakis, 1999; Sánchez-Goñi et al., 2002; Moreno et al., 2002; Colmenero-Hidalgo et al., 2004; Sierro et al., 2005). Our data, based on a direct correlation between terrestrial and marine proxies strengthen an atmospheric/oceanic connection in the Middle Pleistocene to millennial-scale Northern Hemisphere ice-sheet instability.

5.3.2. Towards the MIS 19c inception

Slightly above the H-like interval, before the onset of MIS 19c, a reduction in the abundance of *N. pachyderma* and of *C. pelagicus* spp. *pelagicus* (Fig. 9.4, 9.6) as well as a concurrent abrupt increase in *G. inflata* and *O. universa* (Fig. 9.3, 9.5) was observed from 787.3 ka to 786.2 ka. *G. inflata* and *O. universa*, that together form > 80% of the entire assemblage in this interval, point to a

slight warming in the surface waters and reduced seasonal upwelling conditions. The coeval drastic drop of *G. bulloides* abundances (Fig. 3a), an opportunistic species thriving in eutrophic setting related to upwelling, strong seasonal mixing or river input (Tolderlund and Bé, 1971; Pujol and Vergnaud-Grazzini, 1995; Rohling et al., 1997; Bárcena et al., 2004; Geraga et al., 2005, 2008), confirms these findings. The warm episode is apparently supported by the significant increase of *S. mirabilis*/*hyperacanthus*, which is known to prefer sea-surface temperature between 10 and 15 °C during winter and between 15 and 22 °C during summer (e.g., Rochon et al., 1999). On the other hand, both pollen assemblages (except the slight decrease of Cupressaceae) and PTI values do not show evidence for such a climatic amelioration.

This phase was interrupted by a secondary abrupt and brief polar-subpolar surface water influx centered at 784.6 ka, as deduced mainly by a secondary peak of *T. quinqueloba*, *N. pachyderma* and *C. pelagicus* spp. *pelagicus* at 785.1 ka (Fig. 9.2, 9.4, 9.6). Among dinocyst assemblages, colder conditions are expressed at 785.1 ka by the increase especially of *N. labyrinthus* (Fig. 9.8).The latter, already interpreted as an ecostratigraphical tracer of the Younger Dryas in the western Mediterranean sea (e.g., Rouis-Zargouni et al., 2012), reaches its higher percentage values during such cold short-event. At the same time, a climatic deterioration on land is especially well expressed by an impressive expansion of steppes, reaching up to 32.5% (Figs. 4, 11.12), supporting the instauration of dry conditions.

We do not provide a synchronized record between MIS 19 in the “Ideale” section and MIS 1, which will be the focus of a future work (Simon et al., in prep.) based on a centennial temporal resolution dataset; however, it is noteworthy that the succession of the identified phases appears quite comparable with the timing of climate phases characterizing deglaciation associated with the beginning of MIS 1 in the central and eastern Mediterranean basin (Capotondi et al., 1999; Sbaffi et al., 2001; Asioli et al., 2001; Sprovieri et al., 2003; Di Stefano and Incarbona, 2004; Geraga et al., 2010; Rouis-Zargouni et al., 2010; Kontakiotis, in press). These phases have been interpreted as the response of the Mediterranean system to the short-term North Atlantic climate variability. The good match between the identified phases and variable ice core and oceanic records (Fig. 9.18–19) supports and encourages this comparison, which may sustain a similar deglacial pattern

predating the onset of both MIS 19 and MIS 1. Indeed, the H-like event identified in the "Ideale" section could be considered as analogous to H1 event as identified from North Atlantic records and its Greenland Stadial (GS-2) counterpart (Fig. 9.18–19). The occurrence of the following short-lived warming/cooling episodes appears consistent with the development of Bølling–Allerød (B/A)/Younger Dryas (YD) (Mangerud et al., 1974)-like events equating to Greenland Interstadial (GI)-1 and GS-1 (Björck et al., 1998) respectively (Fig. 9.18), predating the onset of MIS 19c, in analogy with the climate framework evolving just before the Holocene inception.

With regard to the plankton assemblages, it is interesting to observe that, similar to what recorded at the "Ideale" section during late MIS 20, a sudden increase in *G. inflata* is widely documented in the Mediterranean Sea during the B/A transition (Asioli et al., 2001; Sbaffi et al., 2001; Melki et al., 2009; Kontakiotis, in press). Together with *O. universa* and other warm taxa, this characterizes the B/A event in the central Mediterranean (Rouis-Zargouni et al., 2010). In the "Ideale" section, the absence of warmer and oligotrophic taxa could indicate that the surface waters were insufficiently warm to allow the development of seasonal well stratified and oligotrophic sea surface waters, in agreement with the occurrence of *O. universa* in the relatively vertically mixed and nutrient-rich waters within the Mediterranean (de Vargas et al., 1999; Morard et al., 2009). Such conditions could have also prevented the proliferation of warm-water and oligotrophic taxa in the nannofossil assemblages. The durations of B/A and Y/D-like events identified in the "Ideale" section are approximately 1.8 and 1.4 kyr, respectively, which is in line with values recorded during B/A and Y/D of the last deglacial phase in the central Mediterranean (e.g., Combourieu-Nebout et al., 1998; Rouis-Zargouni et al., 2010). Nonetheless, further higher resolution investigations are essential to reinforce this hypothesis. Evidence of B/A and YD analogues during Termination IX has not been documented in the marine sedimentary record so far. The occurrence of a YD cooling event has been presented from the continental record of the Sulmona basin (Giaccio et al., 2015) and also suggested in the "Ideale" section, based on preliminary higher resolution oxygen isotope analyses (Nomade et al., 2015; Simon et al., in prep). Higher resolution investigations at the "Ideale" section in the near future may provide additional information concerning vegetational modifications not recorded in

the present study during the B/A–like event, although clearly expressed, during the B/A event in the Mediterranean by expansion of forest taxa and concomitant contraction of steppe vegetation (e.g., Combourieu-Nebout et al., 1998; Fletcher and Sánchez-Goñi, 2008; Fletcher et al., 2009; Giunta et al., 2003).

5.3.3. Onset of MIS 19c

We traced the onset of this phase based on the first persistent indication of climate amelioration from both marine and terrestrial proxies, starting from the end of the YD-like event. From 784.3 ka a marked surface water warming is inferred on the basis of $PC1_{nanno}$ and $PC1_{forams}$ (Fig. 7), and points to the development of interglacial conditions (MIS 19c) extending up to approximately 773 ka. This phase contains a more prominent increase of total coccolith abundance (Fig. 3c), with respect to younger and older warm phases, which is in agreement with a marked shift toward warm and oligotrophic conditions in surface waters during this interval, which favored the whole coccolithophore assemblage. MIS 19c also displays a distinct occurrence of the tropical *T. sacculifer* (Fig. 9.10) and the highest abundance of *G. ruber* gr. (Fig. 3a), in accordance with more persistent warmer and oligotrophic surface water conditions (Bé, 1977; Vincent and Berger, 1981; Kucera et al., 2005; Munz et al., 2015; Maiorano et al., 2016). The sea surface warming characterizing MIS 19c is also well expressed by the increase of both *S. mirabilis*/*hyperacanthus* and *P. zoharyi*among dinocyst assemblages (Fig. 5). During MIS 19c, the pattern of PTI (Fig. 7) supports a concurrent climatic amelioration on land, with a period of prevalent warm and humid conditions expressed by the increase of arboreal taxa (Figs. 4, 7).

Changes in composition and grain size of sediment supply appear to respond in phase with climate and vegetational changes during this interglacial phase (Fig. 7). According to our age model, and based on the available higher resolution sampling with respect to Marino et al. (2015), the duration of MIS 19c in the “Ideale” section is of about 10.6 ky (784.3–773.7 ka), which compares well with the extent (10.8 ky) of the same interval in the lacustrine Sulmona section (Giaccio et al., 2015), while slightly differs from the

estimation of about 12.5 ky from North Atlantic records (Tzedakis et al., 2012a).

Two abrupt, short-term, moderately dry, pollen events have been confirmed to have occurred during MIS 19c (Events 1 and 2 in Bertini et al., 2015 and Marino et al., 2015), as suggested by two peaks of open vegetation at 783.5 ka and approximately 776 ka, the second one having a slightly different timing compared with previous palynological works, according to subsequent analyses (Fig. 9.12). The mentioned authors have considered the hypothesis that these climate fluctuations were a possible consequence of the geomagnetic field minima observed during the Matuyama/Brunhes transition, in agreement with Kitaba et al. (2012). The concurrent PC1 nanno decrease (Fig. 7) implies that sea surface waters as well, were affected by moderate cooling episodes as recorded on land. Whatever the cause of the previous short-term cooling events, they express quite rapid climate variability during MIS 19c, in good agreement with similar intra-interglacial abrupt events in both Atlantic and Mediterranean areas during the Middle-Late Quaternary (e.g., Bond et al., 1997; Alley and Agustsdottir, 2005; Martrat et al., 2007; Candy et al., 2014).

5.3.4. Sapropel-like interval during MIS 19c

At 782 ka, enhanced stratification in the upper photic zone could be inferred based on the highest abundance of *F. profunda* (Fig. 10) (Molfino and McIntyre, 1990a, 1990b). The concurrent maximum abundance of *G. ruber* white and *G. rubescens* (Fig. 10) points to warmer and stratified surface water conditions as well (Bé and Tolderlund, 1971; Fairbanks et al., 1982; Hemleben et al., 1989; Triantaphyllou et al., 2010). At this time, among dinoflagellate cysts, we record the increase of *P. zoharyi* (Fig. 10) and of several warm species of *Impagidium* and *Spiniferites* especially *S. mirabilis*/*hyperacanthus*, *I. aculeatum* and *I. patulum* (Fig. 5). *P. zoharyi* shows a bloom at 782 ka (Figs. 5, 10), which suggests enhanced stratification phenomena, in agreement with calcareous plankton results. This autotrophic species is the cyst of the potentially toxic and red tide forming dinoflagellate *Pyrodinium bahamense*, a typical lagoonal species hypothesized to have been abundant in the open ocean setting of the Arabian Sea, during the beginning of Late Pleistocene

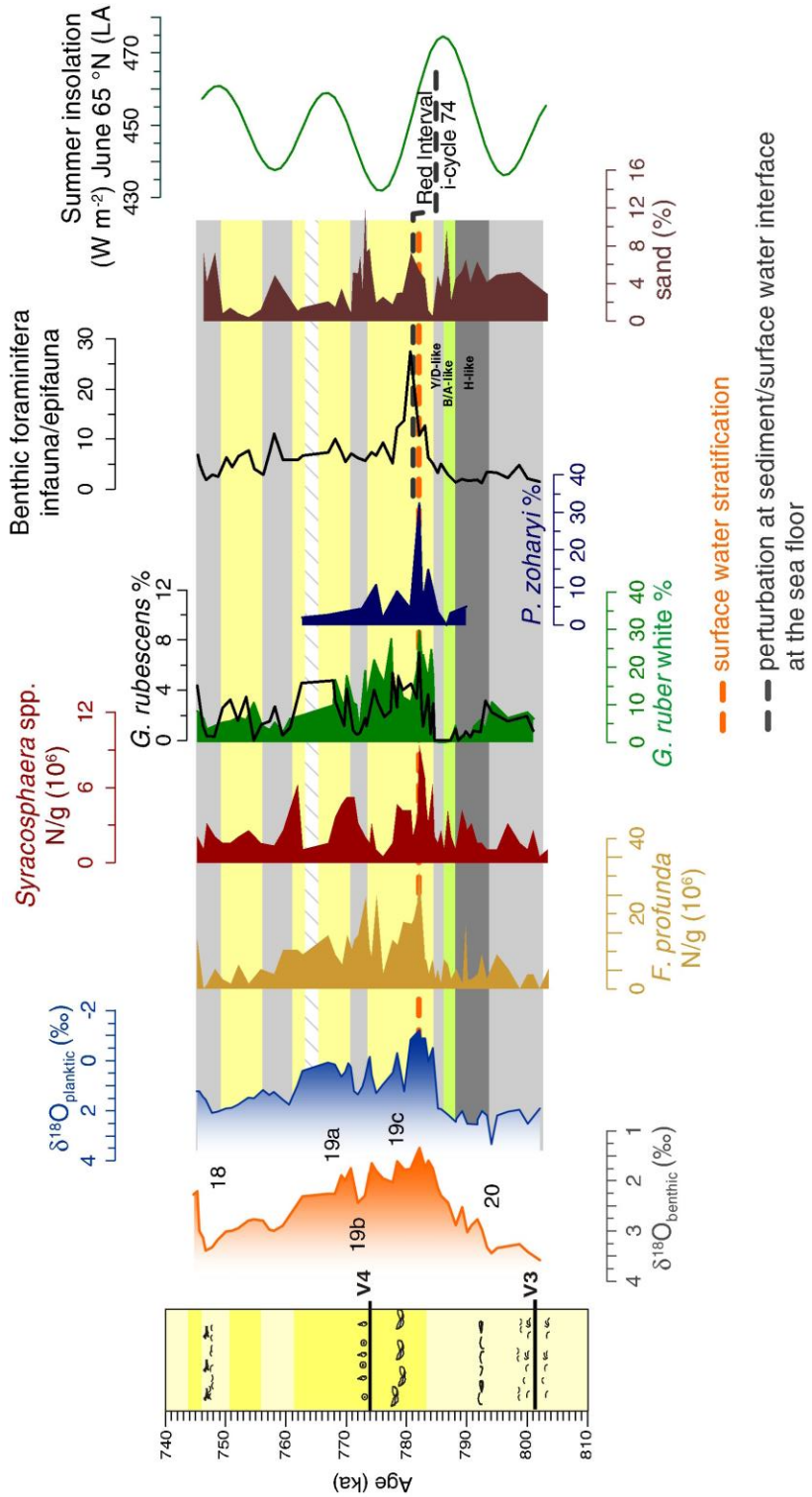

Fig. 10. Calcareous plankton and dinocyst indicators of marked surface water stratification within MIS 19c. Benthic foraminifera infauna/epifauna ratio from Stefanelli (2004) is shown. Insolation is from Laskar et al. (2004). Cold-dry (grey bands) and warm-humid (yellow bands) phases are differentiated as in Fig. 7. For lithological legend refer to Fig. 2.

interstadials, when strong density gradients in the upper water column simulated a shallower seafloor (Reichart et al., 2004). In the terrestrial setting, more humid conditions possibly enhanced fluvial transport and the development of local wetlands, where hydrophilous vegetation expanded (Fig. 4), as attested by the notable increase of Cyperaceae. Wetter climate conditions on land and increased precipitation during warm climate could have been responsible for enhanced detrital input and decreased salinity in surface water, as suggested by concurrent prominent increase of *Syracosphaera* spp. (Fig. 10) (Weaver and Pujol, 1988; Colmenero-Hidalgo et al., 2004; Maiorano et al., 2013). The marked depletion of $\delta^{18}O_{planktic}$ observed at 782 ka (Fig. 10) supports the occurrence of decreased surface water salinity and fresh water input into the basin at this time. The relative enrichment in the sand fraction, usually occurring in colder/cooler phases of the studied record (Fig. 10), could also reflect more efficient fluvial erosion induced by specific rainfall conditions during wetter and warmer climate (Giraudi, 2014). Modified climate conditions in surface waters and in the sediment input into the basin likely affected sea bottom environment as well. In fact, looking at the benthic foraminifera distribution across the interval (Stefanelli, 2004), a prominent increase has been recorded in the infauna/epifauna ratio at 780.6 ka (Fig. 10), suggesting that a perturbation at the sediment-bottom water interface did occur. It is known that epifaunal habitats benefit from food-limited environment with high oxygen levels (Corliss and Chen, 1988; Corliss, 1991; Jorissen et al., 1995). It is likely that enhanced surface water stratification, coupled with increased sediment supply and organic matter at the sea bottom, may have inhibited the proliferation of epifaunal taxa. Despite the absence of clear evidence for oxygen deficiency at the sea bottom, the paleoclimate condition and the surface water features are rather comparable to those occurring during sapropel formation in the Mediterranean deep-sea records (Olausson, 1961; Thunell, 1979; Rossignol-Strick, 1983; Vergnaud-Grazzini, 1985; Rohling and Hilgen, 1991). Such a hypothesis is also supported by the ecological and climate requirements of *P. zoharyi*, as well as by its stratigraphical distribution and abundance in the Quaternary deposits of the Mediterranean. In fact, such dinoflagellate cyst shows peculiar abundance phases up to exceptional blooms during the deposition of sapropels as

attested, for example, during MIS 5e in both eastern (Giunta et al., 2006; Sangiorgi et al., 2006) and central (Negri et al., 2015) Mediterranean sites.

Despite Mediterranean records lack of sapropel layers in the investigated interval (Konijnendijk et al., 2014), the occurrence of "red intervals" is known as an indicator for missing or ghost sapropels and used for tuning sedimentary record to insolation (Emeis et al., 2000). These are actually oxidized sapropels, characterized by a diagenetic stamp. They have been visually identified in several records due to lamination (ghost sapropels) or reddish color ("red intervals"), as a consequence of intense post-depositional flushing (Emeis et al., 2000). Within the chronological interval investigated in the present study, only one red interval was known to occur. It was recorded in the Ionian Sea in core KC01b (Langereis et al., 1997), tuned to i-cycle 74 and dated at 784 ka (Lourens, 2004; Konijnendijk et al., 2014), which compares quite well to the age of the identified level in our record (Fig. 10). It was also recorded in the western Mediterranean (Murat, 1999), within MIS 19.3 (De Kaenel et al., 1999). Therefore, thanks to the multiple paleonvironmental proxies and the good chronological match, we cannot totally exclude that the interval from 782 to 780.6 ka may represent a shallow-water analogue of the isochronous red interval correlated with i-cycle 74. The absence of clear oxygen depletion signature into the sediment could reflect the shallow water environment of the investigated interval.

5.3.5. Late MIS 19 and MIS 18 inception

Distinct signals of climate instability have been recorded in the middle-upper part of the investigated interval, starting from 773.2 ka (Fig. 7), slightly above volcaniclastic layer V4. This part of the section displays a succession of shorter-term climate phases, well attested in both marine and continental proxies (Fig. 7), including MIS 19b, 19a and the early MIS 18. Superimposed upon the observed general pattern of succeeding cold-dry/warm-humid phases, our proxies record signals of climate deterioration in the uppermost part of the section, consistent with the MIS 18 glacial inception, in agreement with benthic and planktonic oxygen isotope curves. In detail, starting from 761.8 ka arboreal formations suffer an overall reduction (Fig. 7). A succession of NAP peaks (Fig. 9.12), involving earlier the cosmopolitan Asteraceae and

then halophyte and steppe taxa, indicates a gradual increase in dryness. Enhanced aridity on land promoted more efficient erosion as attested by more prominent increase in terrigenous input (both mineral content and reworked coccolith taxa, Fig. 9.13–15) into the basin, concomitant with NAP peaks (Fig. 9.12). During the same intervals, more severe conditions in surface waters were supported by enhanced abundances of *G. glutinata* (Fig. 3a), *C. pelagicus* spp. *pelagicus* (Fig. 9.6) and, in the uppermost part of the section, by *N. pachyderma* (Fig. 9.4).

The chronology of the identified colder intervals during the middle and upper portions of the section, which include the late MIS 19 and MIS 18 inception, is in good agreement with the IRD North Atlantic pattern (Fig. 9.16–17), as suggested for the uppermost part of the section by Marino et al. (2015). In particular, the first cold/dry phase correlates with the first more significant IRD signal in North Atlantic. Therefore, it can be considered as representing the reestablishment of the millennial-scale variability, at the beginning of the glacial inception occurring (Tzedakis et al., 2012a). The onset of this climate variability develops at 773–772.6 ka, in good agreement with the age of the beginning of the same climate pattern recorded at 774.5 ka in the North Atlantic ODP 983 record (Tzedakis et al., 2012a), close to the position of the Matuyama/Brunhes paleomagnetic boundary in the same core (Channell et al., 2010). It is noteworthy that a good chronological control is available in our record in this part of the section, due to the Ar/Ar age of the volcaniclastic layer V4 dated at 773.9 ± 1.3 ka (Petrosino et al., 2015).

The comparison of our data with the synthetic records on Greenland climate (Fig. 11) (Barker et al., 2011) indicates a rather good correlation between the succession of climate phases through the late MIS 19 and Greenland seesaw behavior. However, the occurrence of a covered interval prevents a whole correlation (Fig. 11). The overall data suggests that the investigated record preserves a climate variability and a temporal development of the events strictly comparable to those ones recorded in global climate oscillations and specifically with the multiple events of both ice sheet growth and subsequent instability, as identified in both Greenland and Antarctic records (Fig. 11).

This is a relevant climatostratigraphic signature in the investigated section, since the onset of the bipolar-seesaw climate variability may provide a

minimum age for glacial inception (Tzedakis et al., 2012a) and has not been recorded before in Mediterranean marine sections.

6. Conclusion

The cross-examination of marine and continental proxies, throughout the interval containing the interglacial MIS 19, adds further details to the previously achieved paleoclimate reconstruction of this reference Middle

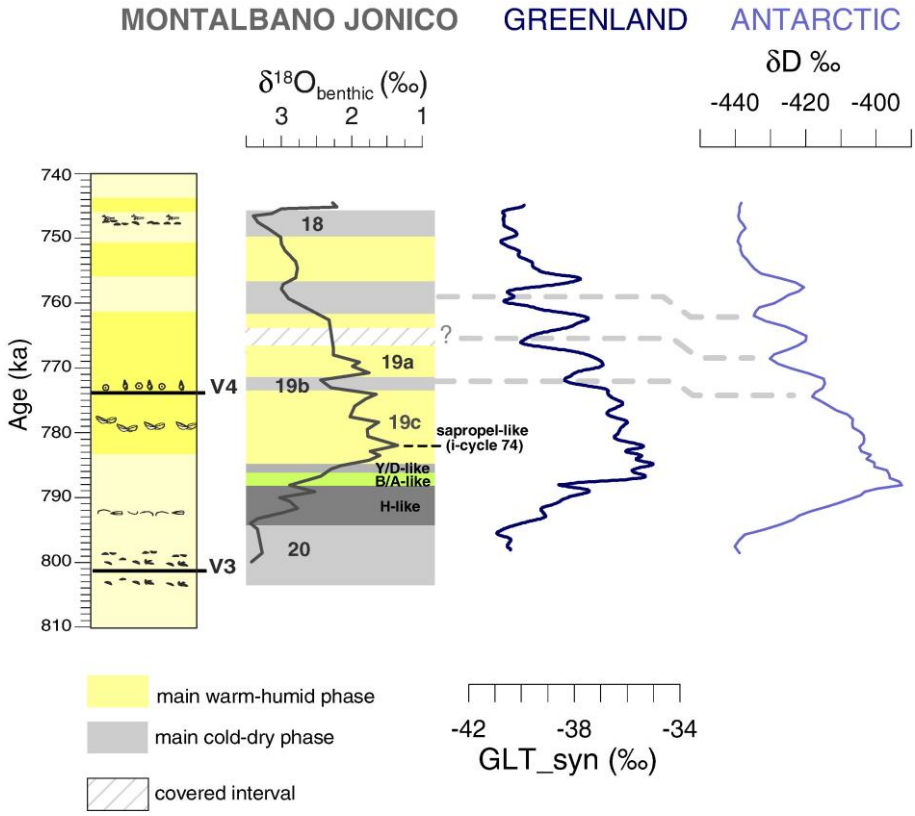

Fig. 11. Comparison of climate phases identified in the "Ideale" section and the synthetic reconstruction of Greenland temperature variability (GLT_syn) (Barker et al. (2011) and δD ‰ from Antarctica (EPICA Dome C, Jouzel et al., 2007) on the age model of Bazin et al. (2013). Climate phases (main warm/humid, cold/dry, H-like, B/A, Y/D-like events and sapropel-like interval) are traced as inferred from the present study and discussed in the text. For lithological legend refer to Fig. 2.

Pleistocene record. The multi-proxy approach is essential in identifying the local vs. global climate signatures and in providing a direct land–sea correlation. Our results indicate that relevant changes occurred over time in the vegetation cover of neighboring continental areas, in the nature of sediment supply into the basin and in sea surface–water features. Although "source-to-sink" patterns are usually complex and controlled by several factors and feedbacks, we have identified some general trends and correlations among climate changes, biological response, sediment production, river transport and marine deposition, which suggests that the main modifications observed within the "Ideale" section are the results of the interplay between climate and landscape changes. Calcareous plankton are primarily affected by modifications in sea-surface temperature, although water stratification, salinity, turbidity and nutrient content have also influenced the distribution of selected taxa. Subpolar/transitional to temperate/subtropical surface water conditions alternate throughout the record and reveal a remarkable correspondence with recurrent changes in steppe and halophytic vegetation as well as prevalent expansions of thermophilous arboreal populations on land. Both proxies clearly track the glacial/interglacial and stadial/interstadial fluctuations. Changes in the mineral composition of sediments, although clearly reflecting the features of the outcropping units in the source area, appear also in relation with vegetation, hydrological and climate changes. Specifically, aridity on land and related reduced arboreal vegetation during colder phases with consequent restraints on soil formation likely promoted erosional processes on the hillslopes and terrigenous supply, as testified to by the increase in coarser detrital mineral components, mainly quartz and dolomite, as well as reworked coccoliths. This is in line with a general aggradation of the rivers and consequent formation of alluvial terraces, which developed during cold periods. Conversely, climate phases characterized by mild winters and warm summers, with reduced seasonal moisture deficiency, promoted chemical weathering on land, as specifically proven by increases in kaolinite. Grain-size changes match climate phases throughout the section, clearly reflecting the existence of climate-induced transgressive/regressive phases and the consequently more distal/proximal environment/setting of the study section.

Millennial-scale variations have also been documented throughout the "Ideale" section, providing further valuable insights regarding climate development across MIS 19 as well as potential similarities with its closest Holocene analogue:

- During the late MIS 20, from 793.2 ka to 788.1 ka, a period of polar-subpolar water incursion, correlated to marked aridity on land, is interpreted as the regional equivalent of the ice-rafted debris event, occurring close to Termination IX in the North Atlantic.
- Throughout the latest MIS 20, shorter warming/cooling surface water episodes seem to develop, as proven by distinct changes in calcareous plankton and dinocyst assemblages. These phases appear analogous to the Bølling–Allerød warm period and to the abrupt cooling of the Younger Dryas, likely suggesting a similar climate evolution in the marine environment at the onset of MIS 19 and MIS 1. Higher resolution investigations are needed in both the "Ideale" section and in additional records to reinforce the occurrence of these abrupt climate phases, which have not previously been identified in other Middle Pleistocene records.
- The onset of MIS 19c at 784.3 ka is marked by the concurrent and distinct climate warming in both continental and marine proxies. The duration of the full interglacial was 10.6 ky.
- Evidence of a wetter climate and more efficient fluvial erosion on land, enhanced stratification and detrital supply, lower surface water salinity in the marine environment, and perturbation/stressed conditions at the sea bottom across 782 and 780.6 ka has been identified. This can be interpreted as a signal of a potential shallow-water analogue of the isochronous red interval, correlated to i-cycle 74, which may provide an additional constraint for a refining of the chronological tuning of the "Ideale" section.
- From 773.2 ka, slightly above volcaniclastic layer V4, the succeeding occurrence of cold/dry–warm/humid phases is related to the reestablishment of millennial-scale variability. This occurs at the MIS 19c/b transition towards the glacial MIS 18 inception and is also identified in North Atlantic marine archives, close to the

Matuyama/Brunhes paleomagnetic boundary, as well as in both Greenland and Antarctic ice-core records.

The high-resolution dataset acquired in the “Ideale” section emphasizes that the observed environmental modifications are strongly influenced by global climatic drivers, improving the prospective correlation of the section at a global scale. The simultaneous agreement between marine and terrestrial signals supports the hypothesis of teleconnection among atmospheric/sea surface-water conditions in the Mediterranean, North Atlantic oceanic events and Northern Hemisphere ice sheet dynamics.

Contribution A5

The Montalbano Jonico section (south Italy) as a reference for the Early/Middle Pleistocene boundary*

*Published in Alpine and Mediterranean Quaternary 29(2), 123-135
(M. Marino, G. Aiello, D. Barra, A. Bertini, S. Gallicchio, A. Girone, R. La Perna, F. Lirer, P. Maiorano, P. Petrosino, O. Quivelli, **F. Toti**, N. Ciaranfi, 2016)

Abstract

The most recent data obtained at the Montalbano Jonico succession (MJS), in the interval including the Marine Isotope Stage (MIS) 19, document the occurrence of numerous chronostratigraphic constraints and paleoenvironmental events contributing to the knowledge of a crucial time through the Lower-Middle Pleistocene transition, characterised by major modifications of the Earth's climate system. Marine and terrestrial biologic data-sets (pollen, ostracods, benthic and planktonic foraminifera, coccolithophores, teleostean fishes, mollusks) are compared with the high resolution astronomically-tuned benthic oxygen isotope curve in order to provide accurate paleonvironmental reconstruction and acquire additional climatostratigraphic and biostratigraphic constraints within a chronostratigraphic framework which also includes the $^{40}Ar/^{39}Ar$ ages of three volcaniclastic layers. Environmental and climatic events (e.g. Termination IX, substages 19.3, 19.2, and 19.1, maximum flooding and climate optimum, maximum depth) highlight a succession of clear paleoenvironmental changes close to MIS 19, showing a remarkable correspondence between the response of marine and terrestrial proxies. Such changes have stratigraphic implication and high potential of correlation as they evidence wide scale climate changes, stressing the tight interconnection between the Mediterranean region and North Atlantic Ocean. Based on these results the MJS reveals to be an excellent candidate for the Lower-Middle Pleistocene Subseries boundary. In fact, at present the MJS fully meets the requirements indicated by Remane et al. (1996) for a GSSP selection with the sole exception that a paleomagnetic signal is missing. ^{10}Be analyses are in progress and should enhance the already rich documentation of several independent age-significant elements, contributing to the recent critical discussion on the significance of the magnetic signal at the Matuyama-Brunhes boundary as well as its role as a primary marker for the Middle Pleistocene GSSP definition.

Keywords: Montalbano Jonico section (South Italy), Early-Middle Pleistocene boundary, chronological and climatostratigraphical constraints

1. Introduction

The Montalbano Jonico section (MJS) is a candidate for the global boundary stratotype section and point (GSSP) of the Middle Pleistocene Subseries (Ciaranfi et al., 1997) due to the detailed biostratigraphic, climatostratigraphic and chronological constraints arising from multidisciplinary studies conducted over the past twenty years (Ciaranfi et al., 1994; 1996; 1997; 2001; 2010; Marino, 1996; Girone & Varola, 2001; D'Alessandro et al., 2003; Stefanelli, 2003; 2004; Maiorano et al., 2004; 2008; 2010; Stefanelli et al., 2005; Girone et al., 2013a; Sagnotti et al., 2014; Aiello et al., 2015; Bertini et al., 2015; Marino et al., 2015; Petrosino et al., 2015) and meets most of the requirements mentioned in Remane et al. (1996) for the selection of a GSSP. The primary criterion for defining the Lower-Middle Pleistocene boundary was indicated as a point to be selected in a marine succession close to the Matuyama-Brunhes boundary (MBB) (Richmond, 1996; Pillans, 2003; Head & Gibbard, 2005; Cita et al., 2006; Head et al., 2008; Head & Gibbard, 2015a). The MBB is a geomagnetic polarity reversal characterised by different age assignments (see syntheses in Channell et al., 2010; Head & Gibbard, 2015b), polarity transition lasting up to 8 kyr (Channell & Kleiven, 2000; Channell et al., 2004; Leonhardt & Fabian, 2007), associated short-lived precursor (s) (Hyodo et al., 2006, 2011; Wang et al., 2006; Yang et al., 2010; Channell et al., 2010; Sagnotti et al., 2014), and by a slightly diachronous character also depending on latitudinal and longitudinal places (Clement, 2004; Leonhardt & Fabian, 2007). Change in sedimentation rate (and related age-depth model), and the influence of burrowing may produce differences in magnetic recording efficiency and timing (magnetic lock-in depth) of remanence acquisition, possibly introducing uncertainties in the natural magnetization process in marine and continental sediments and age-assignment of the MBB (deMenocal et al., 1990; Channell et al., 2010; Suganuma et al., 2010; Roberts et al., 2013; Snowball et al., 2013; Head & Gibbard, 2015b). When correlated to marine oxygen isotope stratigraphy (MIS 19, Shackleton et al., 1990), in sedimentary successions the MBB may fall at

the base, in the middle, or in the upper part of stage 19. On the other hand, climatostratigraphy during MIS 19 is revealed to be a critical means to improve knowledge on climate evolution during this stage and to enhance correlation between marine and terrestrial realms at the global scale. Moreover, according to some authors, paleointensity minima during MBB seem to have affected change in cosmogenic ray flux and Earth's climate (Kitaba et al., 2012; Hyodo & Kitaba, 2015). This aspect strengthens the widely accepted importance of climate in Quaternary stratigraphy, the stage boundaries being characterised by biological/physical/geochemical documentation of profound changes in the global climate. Multiple chrono/climatostratigraphic constraints are then necessary in the interval including MIS 19 and the Matuyama-Brunhes transition in order to have helpful and constructive tools aiding local/regional/global (possibly land–marine) correlation, which is a crucial feature for the selection of GSSP (Remane et al., 1996; Gradstein et al., 2003).

The aim of this paper is to provide a synthesis of recent data sets collected throughout MIS 19 at Montalbano Jonico and supply preliminary new results which improve the reliability of the numerous chronostratigraphic and climatostratigraphic markers recognized in the section close to the Early-Middle Pleistocene boundary. A synthesis of these results was presented at the "Scientific Days" (Florence, June 18-19, 2015) organized by AIQUA (Italian Association for Quaternary Study).

2. The Montalbano Jonico section

The Lower-Middle Pleistocene composite section of Montalbano Jonico crops out in the Lucania Basin (Balduzzi et al., 1982), a minor basin of the foredeep (Bradano Trough, in Casnedi, 1988) between the Apennines Chain and the Apulia Foreland (Fig. 1). The MJS is about 450 m thick and consists of a coarsening upward succession formed by hemipelagic silty clays and, in its upper part, by sandy clays (Ciaranfi et al., 2010) (Fig. 1). The whole section represents the regressive part of a third-order cycle with several fourth and fifth-order cycles mainly induced by climate changes (Ciaranfi et al., 1997; 2001).

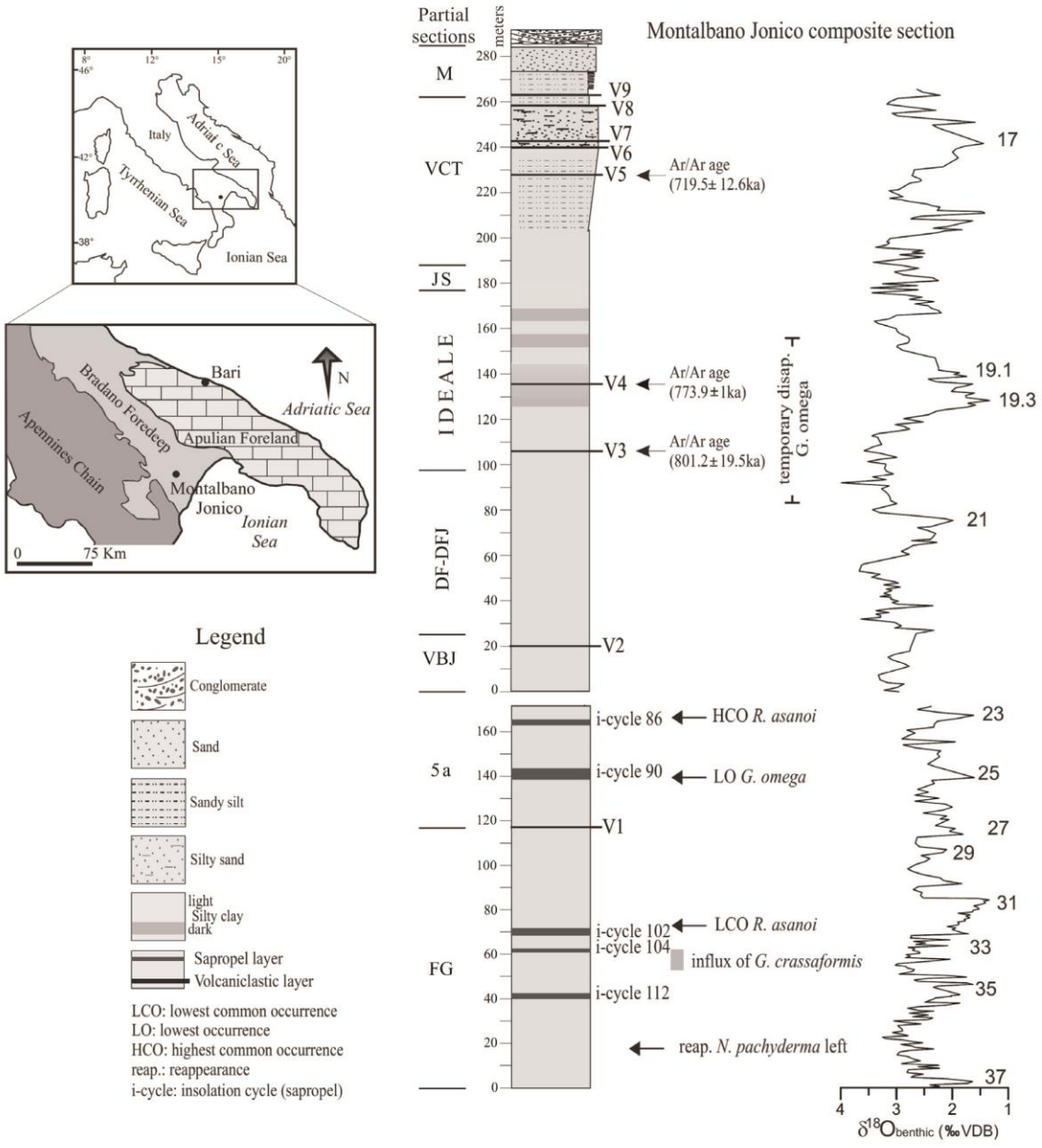

Fig. 1 - Location and stratigraphy of the Montalbano Jonico section. Main lithological features of the composite section obtained by correlating several partial sections (FG-M). Chrono-biostratigraphic constraints are shown together with benthic δ18O (Brilli et al., 2000; Ciaranfi et al., 2010; Maiorano et al., 2010). Marine Isotope Stages are according to Ciaranfi et al. (2010). Ages of volcaniclastic layers are according to Ciaranfi et al. (2010), Maiorano et al. (2010), Petrosino et al. (2015).

Stable oxygen isotope analyses performed throughout the entire succession on planktonic (*Globigerina bulloides*) and benthic (*Cassidulina carinata*) foraminifer tests (Brilli et al., 2000; Ciaranfi et al., 2010), combined with high resolution quantitative calcareous plankton biostratigraphy (Marino, 1996; Maiorano et al., 2004; Ciaranfi et al., 2010; Maiorano et al., 2010; Girone et al., 2013a), $^{40}Ar/^{39}Ar$ data on volcaniclastic layers V3, V4 and V5 (Ciaranfi et al., 2010; Maiorano et al., 2010; Petrosino et al., 2015), pollen data (Joannin et al., 2008), and sapropel stratigraphy (D'Alessandro et al., 2003; Stefanelli, 2004; Stefanelli et al., 2005; Maiorano et al., 2008), have provided the astronomical calibration of the MJS that covers the time interval MIS 37–16, i.e., 1.24–0.645 Ma (Ciaranfi et al., 2010; Maiorano et al., 2010). The calcareous plankton biochronology at Montalbano (Maiorano et al., 2010; Girone et al., 2013a) compares well with that in the Mediterranean Sea and Atlantic and Pacific oceans, suggesting that the section is valuable for long distance biostratigraphic correlation.

The MJS represents a unique on-land continuous succession spanning this long time interval and, together with the astronomically-tuned Vrica section, covers the entire Calabrian Stage (Maiorano et al., 2010). Furthermore, it encompasses the timing of the Matuyama-Brunhes transition. The Ideale section, is one of several comprising the Montalbano Jonico composite section, and is the key stratigraphic succession deposited continuously during MIS 20-18 (Fig. 1).

3. Stratigraphic and paleoenvironmental constraints through MIS 21-MIS 18

Recent multidisciplinary studies improved knowledge across the interval from MIS 21 to MIS 18 time (Aiello et al., 2015; Bertini et al., 2015; Marino et al., 2015; Petrosino et al., 2015), based on orbital to millennial scale marine and terrestrial biological data set (pollen, ostracod, benthic micro- and macroinvertebrates), mainly obtained by the analysis of the same samples studied for oxygen isotope stratigraphy (Fig. 2). Some of the taxa recorded from the rich and diverse micro- and macrofossil assemblages at MJS are

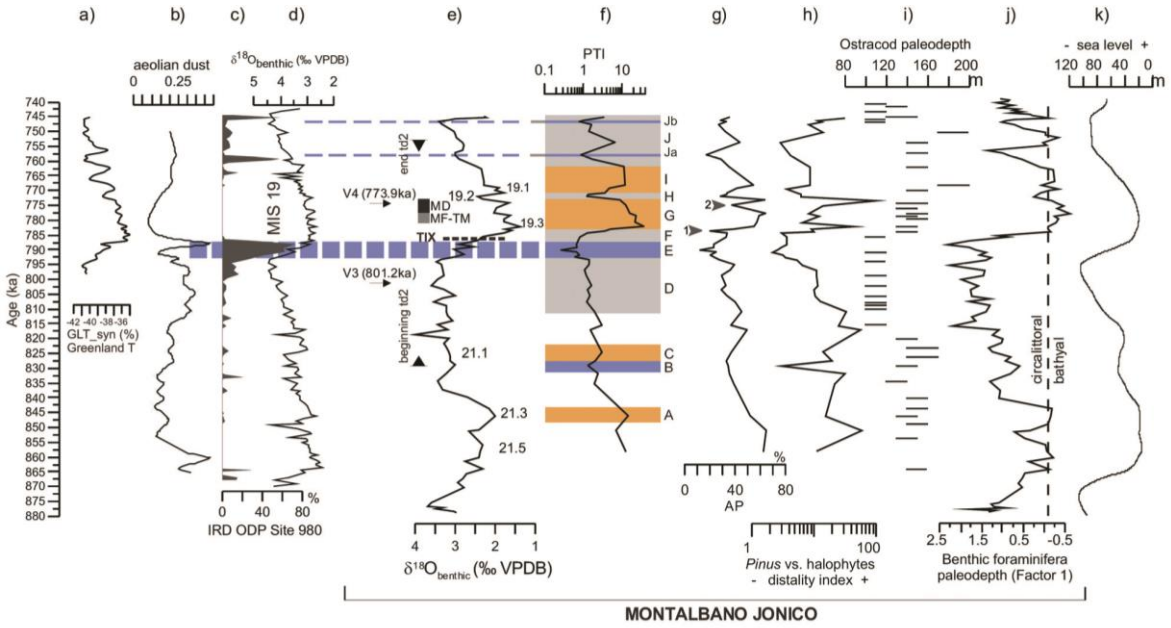

*Fig. 2 - Comparison between the Montalbano Jonico succession and other reference Lower-Middle Pleistocene records (modified from Marino et al., 2015, and this work). a) Synthetic reconstruction of Greenland temperature variability (GLT_syn, Barker et al., 2011); b) East Mediterranean dust record based on hematite content derived from magnetic properties of sediments from ODP Site 967 (Larrasoaña et al., 2003); c) ice rafted detritus (IRD) curve from North Atlantic ODP Site 980 (Wright & Flower, 2002) versus age according to Lisiecki & Raymo (2005); d) benthic δ18O curve from Site 980 (Wright & Flower, 2002); e) benthic δ18O at the Montalbano Jonico section (MJS); f) pollen temperature index in logarithmic scale (PTI, i.e. the ratio between mesothermic arboreal taxa and steppe taxa to discriminate warm-temperate from cold phases, according to Joannin et al. (2008) and Suc et al. (2010); g) arboreal pollen, AP%; h) pollen distality index (*Pinus *vs. halophytes), in logarithmic scale; i) ostracod paleodepth curve; j) benthic foraminifera paleodepth curve (Stefanelli, 2003); k) global sea level curve (Bintanja & van de Wal, 2008). Age model of the MJS records is from Maiorano et al. (2010) slightly updated in Marino et al. (2015). Substage nomenclature is according to Bassinot et al. (1994). Bars on the PTI curve represent climate phases: warm and humid phase A, C, G, I (orange); cool phase D, F, H, J (grey); cold and arid phases B, E, Ja and Jb (blue); minor short-term climate events are indicated as 1 and 2 (cool phases) on the AP% curve. V3 and V4: volcaniclastic layers TM: Thermal Maximum (Girone & Varola, 2001); MF (Maximum Flooding) and MD (Maximum Depth) from D'Alessandro et al. (2003); td2: second temporary disappearance of* G. omega *(sensu Maiorano & Marino, 2004); TIX: Termination IX.*

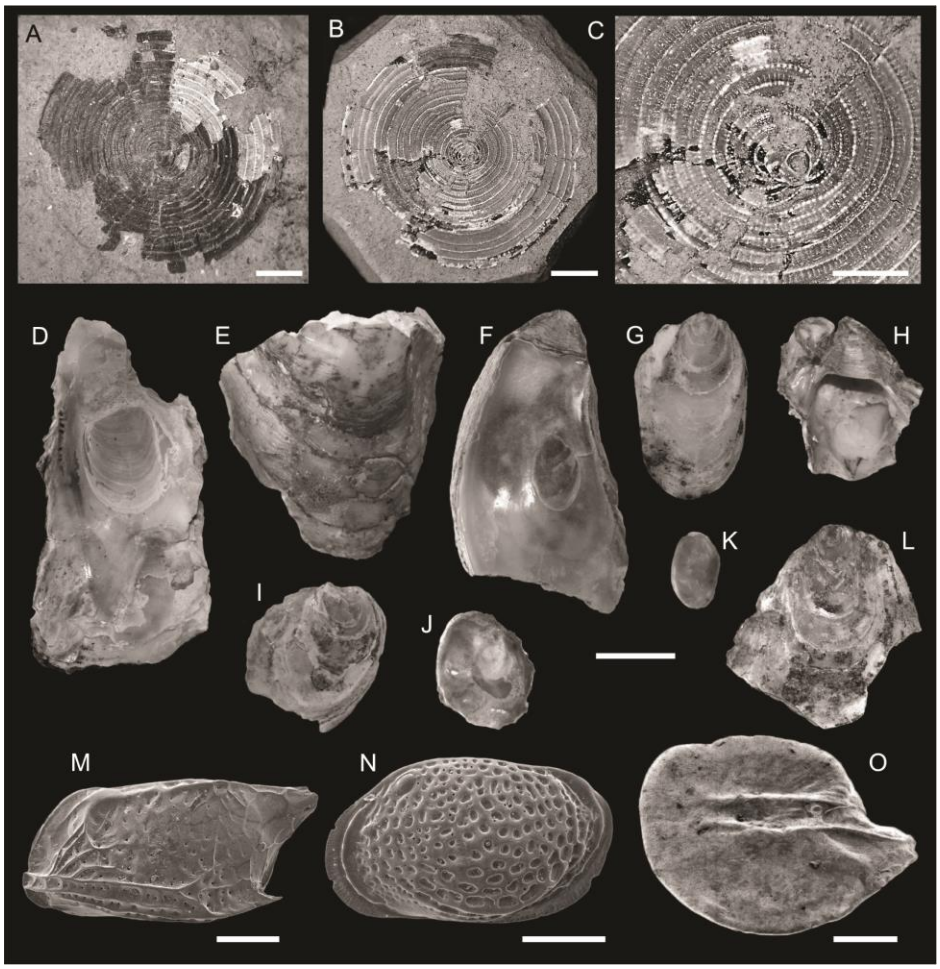

Plate 1 - A-C. benthic foraminifer Discopirina italica (Costa, 1856) with pyrite infilling, scale bar = 2 mm (A, B), 1 mm (C).
D-L. Neopycnodonte cochlear *(Poli, 1795), scale bar = 10 mm. Valves and valve fragments from the Maximum Flooding level in MIS 19. Note the bioeroded and bioencrusted surface of the large fragment E, suggesting exposure on the sea bottom due to low sedimentation rate.*
M, N. Ostracod species commonly recorded in the Montalbano Jonico Section, typical of the circalittoral zone in the Mediterranean. M. Semicytherura ruggieri *Pucci, 1955, left valve, scale bar = 100 μm. N.* Sagmatocythere concentrica *(Bonaduce, Ciampo & Masoli, 1976), left valve, scale bar = 100 μm.*

illustrated in Plates 1 and 2. Chemical studies on juvenile vitric fragments and mineral phases from the volcaniclastic layers allowed these marker levels to be more exhaustively described in terms of their potential source and correlation to other tephra layers in both south-central Italy lacustrine

successions and in marine onland and deep-sea cores within a Lower-Middle Pleistocene Mediterranean tephrostratigraphic framework.

The fine chronostratigraphic and paleoenvironmental outline obtained at the MJS makes the section an excellent candidate for the Lower-Middle Pleistocene GSSP in spite of an absent paleomagnetic signal (including the MBB) throughout the section because of remagnetization (Sagnotti et al., 2014). The several events recorded in the Ideale section have high potential for wide-scale correlation and therefore may provide multiple constraints suitable for the selection of the GSSP.

Focusing on the MIS19, it is clearly depicted between MIS 20 and MIS18 at the MJS by the planktonic and benthic $\delta^{18}O$ records (Ciaranfi et al., 2010; Maiorano et al., 2010). The interval straddling MIS 19 is very well chronologically constrained, bracketed by the $^{40}Ar/^{39}Ar$ ages of two volcaniclastic layers: V3 (801.2±19.5 ka) in MIS 20, and V4 (773.9±1.3 ka) in MIS 19. The age of V4 is very close to the age of the MBB, referred to 773 ka according to Channell et al. (2010). The beginning and end of the second temporary disappearance of the coccolithophore *Gephyrocapsa omega*, at 829 ka and 752.76 ka respectively (Fig. 2e), provide valuable bioevents for long distance correlation as they always enclose MIS 19 in Mediterranean Sea and Atlantic Ocean records (Maiorano & Marino, 2004; Maiorano et al., 2004). Additional higher resolution oxygen isotope studies across MIS 19 are in progress at the MJS and support the excellent climate signal in the section (Nomade et al., 2015).

The main climatostratigraphical constraints are shown in Figures 2 and 3 and discussed below.

3.1. The cold climate phase in the uppermost MIS 20 and Termination IX

The inception of MIS 19 is preceded by a high-amplitude shift to lighter $\delta^{18}O$ values at the MIS 20/19 deglaciation of about 2‰, between ca. 794 ka and 782 ka, marked by a change in sediment color from light gray (MIS 20) to dark gray (MIS 19) (Figs. 1, 3). Pollen data provide evidence of a strong increase of herbs (exceeding 90%) with steppe and halophyte taxa as the main

components, centered at about 790 ka (Bertini et al., 2015; Marino et al., 2015). This event correlates with prominent peaks in the records of North Atlantic ice rafted debris (IRD, at the Ocean Drilling Program Site 980, Wright & Flower, 2002) and Mediterranean aeolian dust (Larrasoaña et al., 2003) (Fig. 2b-d), suggesting a phase of arid and cold climate (see lowest values in the percentage of Arboreal Plant-AP curve and in the Pollen Temperature Index-PTI at MJS) which marks the collapse of North Hemisphere ice-sheet and the end of glacial MIS 20. Calcareous plankton data (Maiorano et al., 2016) support the prominent cold climate phase recording the higher abundance of arctic-subarctic *Coccolitus pelagicus* ssp. *pelagicus* and *Neogloboquadrina pachyderma* left-coiling, and the lowest values of the planktonic foraminifera derived Sea Surface Temperature-SST curve (M. Kucera, work in progress) in the uppermost glacial MIS 20. Similar patterns in key calcareous plankton taxa are documented in the Mediterranean Sea at the glacial-interglacial transition during the mid-Brunhes interval (Girone et al., 2013b; Maiorano et al., 2013; Capotondi et al., 2016), demonstrating that the Mediterranean signal of short-lived global climate change may be extended down to MIS 20/MIS 19 deglaciation. Such result, in agreement with the $\delta^{18}O$ pattern at the transition MIS 20/MIS 19 (Fig. 2e), could represent the Younger Dryas-like cold and dry event (Giaccio et al., 2015); however the ongoing higher resolution oxygen isotope study (Nomade et al., 2015) and calcareous plankton and pollen analyses (Maiorano et al., 2016) may give more conclusive detail on climate evolution at this time. A minimum in the benthic foraminifera paleodepth pattern (Stefanelli, 2003, 2004) is also recorded very close to the cold and arid event highlighting a prominent sea level fall (Fig. 2j). The event, combined with the high-amplitude change in benthic foraminifera and ostracod-derived paleodepth curves recorded just above, enables the identification of Termination IX (Figs. 2, 3) which is considered the most prominent marker in the $\delta^{18}O$ record before the MBB in MIS 19 (Channell et al., 2010). These results together provide the first documentation in Mediterranean onland marine sediments of Termination IX, a characteristic climate signal in global ocean records (i.e. Lisiecki & Raymo, 2005). The prominent sea level change associated with Termination IX is correlatable with the boundary between the third order cycles TB3.8-TB3.9 (Haq et al., 1987) at the major sequence boundary "I01" (ca 0.8 Ma, Hardenbol et al., 1998; ca. 0.78 Ma, Snedden & Liu,

2010) and is recorded in the curve of global sea level of Bintanja & van de Wal (2008) (Fig. 2k). Termination IX may be also recognizable in terrestrial sediments (i.e. Florindo et al., 2007) supporting its value in climatostratigraphy.

3.2. MIS 19.3, Maximum Flooding, Climate Optimum, and Maximum Depth

The $\delta^{18}O$ pattern and all biological proxies clearly record the onset of MIS 19 (Fig. 2) which is also visible in the color sediment change at Termination IX in the Ideale section (Figs 1, 3). The deposition of darker sediments characterizes the MIS 19 interval as may be expected during an interglacial phase and high sea level, when water column stratification could have reduced oxygen levels and thereby increased organic matter preservation on the sea floor. Moreover, the $\delta^{18}O$ pattern distinctively describes substages 19.3, 19.2, and 19.1 (Figs. 1, 3). All biological data from both marine (i.e. Marino et al., 2015) and terrestrial (Bertini et al., 2015; Toti, 2015) realms support the substage subdivision indicating 19.3 as the warmest, based on the elevated values in PTI and AP curves. Increases in the warm-water calcareous plankton taxa confirm the peculiar climate behavior of substage 19.3. In detail, calcareous plankton records the highest abundance of warm water taxa in the lower portion of substage 19.3 (Maiorano et al., 2016) in correspondence with the lowest $\delta^{18}O$ value (ca. 782 ka), suggesting a climate optimum in the sea surface waters. During the 780.56-777.31 kyr interval, the presence of tropical-subtropical mesopelagic teleostean fish *Bonapartia pedaliota* (Girone & Varola, 2001) (Plate 1, O) suggests warmer conditions deeper in the water column; the highest percentages of *Quercus* (here included among the AP, see Bertini et al., 2015 for detail) and PTI, are recorded contemporaneously (Fig. 2f). Concomitantly, the maximum flooding is indicated by the occurrence of a *Neopycnodonte cochlear* community (D'Alessandro et al., 2003) (Figs. 2e, 3, Plate 1, D-L). It is a deep-water oyster forming encrusting clusters, most probably thriving under conditions of low sedimentation rate, as suggested by the ecological data on a congener species (Wisshak et al., 2009; Gofas et al., 2010). Such environmental conditions are possibly related to the rapid sea

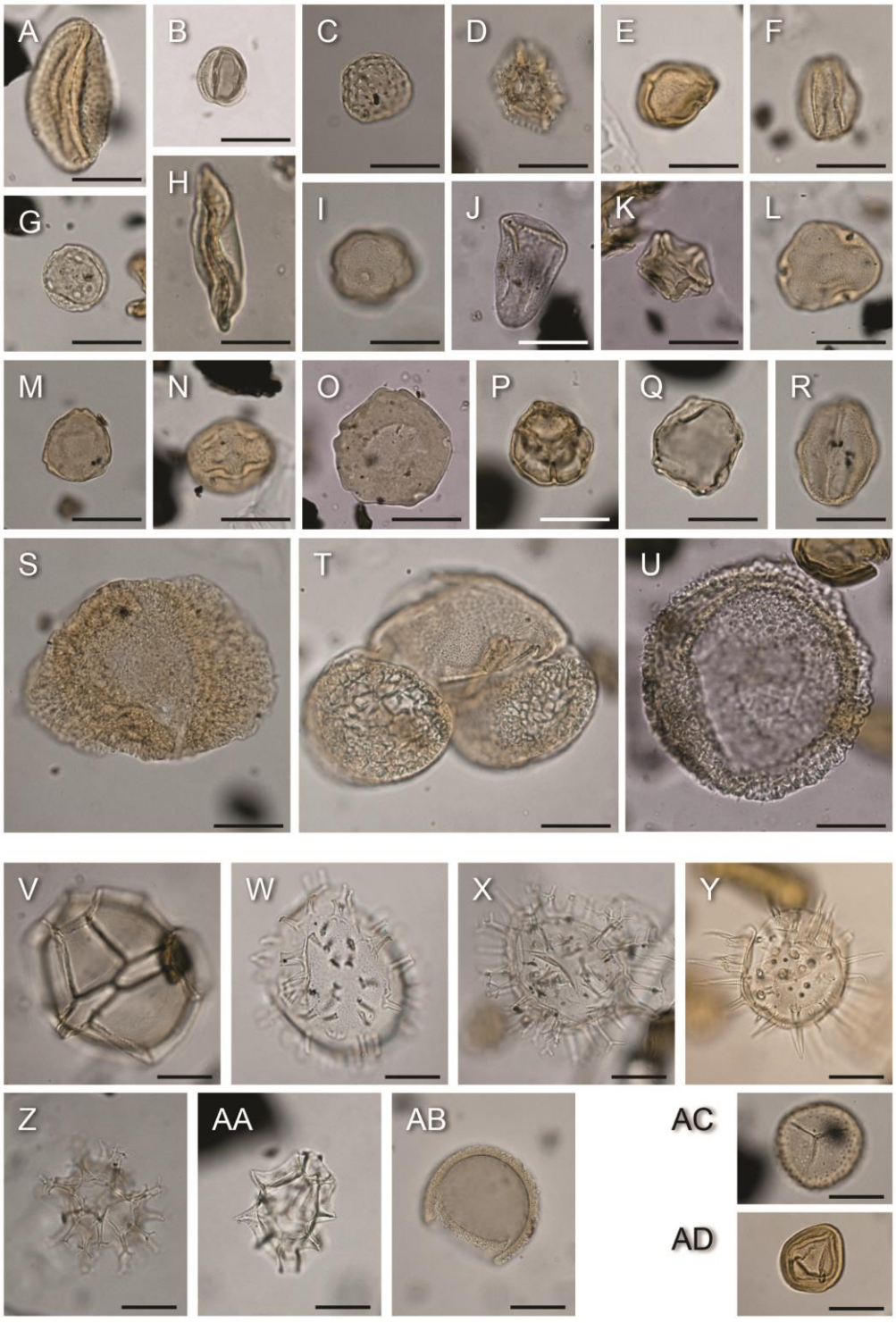
A
B
C
D
E
F
G
H
I
J
K
L
M
N
O
P
Q
R
S
T
U
V
W
X
Y
Z
AA
AB
AC
AD

Plate 2 - Micrographs of representative pollen grains (A-U), organic-walled dinocysts (V-AB) and other palynomorphs (AB, AC) from the MIS 20-18 interval of the MJS. A. Centaurea *(equatorial view). B.* Artemisia *(equatorial view). C. Amaranthaceae. D. Asteraceae, Cichorioideae. E.* Hippophaë *(equatorial view). F. Deciduous* Quercus *(equatorial view). G.* Plantago lanceolata *type. H.* Ephedra distachia *type (equatorial view). I. Poaceae (distal view). J. Cyperaceae (equatorial view). K.* Alnus *(polar view). L.* Tilia *(polar view). M.* Corylus *(polar view). N. Fabaceae (equatorial view). O.* Pterocarya *(polar view). P. Ericaceae (tetrad in polar view). Q.* Carpinus betulus *(polar view). R.* Calligonum *(equatorial view). S.* Cedrus *(proximal view). T.* Pinus *(equatorial view). U.* Tsuga diversifolia *type (proximal view). V.* Impagidinium patulum *(lateral view). W.* Polysphaeridium zoharyi *(apical view). X.* Spiniferites hyperacanthus *type (ventral view). Y.* Lingulodinium machaerophorum *(lateral view). Z.* Spiniferites ramosus *(lateral view). AA.* Impagidinium aculeatum *(cross section). AB.* Tectatodinium pellitum *(cross section). AC.* Ophioglossum *type (proximal view). AD.* Classopollis *(polar view, reworked). All scale bars are 20 μm.*

level rise after deglaciation.

The maximum depth follows the maximum flooding (ca. 777.3 ka-ca. 773.2 ka), and it is highlighted by the benthic invertebrate communities (D'Alessandro et al., 2003) which record dispersed macrobenthic fauna and the occurrence of bathyal taxa such as *Discospirina italica* (Plate 1, A-C), a large miliolid foraminifer from deep waters (Gooday et al., 2013), the mollusks *Dentalium agile, Cadulus ovulum, Neilonella pusio* and *Delectopecten vitreus,* typical of Pleistocene bathyal assemblages (Di Geronimo and La Perna, 1997); this phase probably reflects higher sedimentation rate and deeper waters which prevented the development of the *Neopycnodonte* (*N. cochlear*) community. T*he* occurrence of the bathyal ostracod *Krithe compressa* is consistent with deeper environment. Therefore, this paleocommunity indicates a transition to a slope setting ("*Discospirina*, *Nassarius*" communities in D'Alessandro et al., 2003) during a sea-level high stand, in good agreement with the major deepening during MIS 19 suggested by benthic foraminifera (Stefanelli, 2003) and ostracod assemblages (Aiello et al., 2015) from ca. 779 ka to 773 ka (Marino et al., 2015), close to the increase in the values of pollen distality index (Bertini et al., 2015) (Fig. 2h).

3.3. End of full interglacial, MIS 19.2-19.1 towards MIS 18

The end of substage 19.3 is marked by the increase of steppe and halophyte elements associated with the slightly higher values in the $\delta^{18}O$ record, during substage 19.2, at about 771.8 ka, just above the V4 layer (Fig. 2e-g). The signal of a decrease in sea-surface temperature is also recorded in the calcareous plankton assemblage (Maiorano et al., 2016), since a distinct drop occurs in the abundance of the warm water taxa. A contemporaneous decrease in the pattern of a synthetic (modeled) reconstruction of Greenland temperature (Barker et al., 2011) is evident (Fig. 2a). Upwards, in MIS 19.1, again warm and

Fig. 3 - Main chronological and paleoenvironmental constraints drawn on the outcrop of the Ideale section.

humid conditions are inferred by pollen data (increase in arboreal mesothermic taxa, Fig. 2g) (Bertini et al., 2015), according to lighter values in $\delta^{18}O$ (Fig. 2e). An upward decreasing trend in mesothermic arboreal taxa parallels the increase of open vegetation taxa concomitant with heavier $\delta^{18}O$ values, thus marking the beginning of the climate deterioration associated with MIS 18. Distinct fluctuations in isotope curve and biological proxies, and in sediment color as well (Figs. 1-3), are also recorded in MJS during this glacial inception. They are in good agreement with the IRD and oxygen patterns at the North Atlantic Site 980 (Fig. 2c-d), and with the synthetic reconstruction of Greenland temperature variability (Fig. 2a), evidencing global features of suborbital climate variation widely documented in oceanic and lacustrine (i.e. Wright & Flower, 2002; Kleiven et al., 2011; Giaccio et al., 2015), and ice core (i.e. Jouzel et al., 2007; Pol et al., 2010; Barker et al., 2011) records. A better understanding of climate evolution at the end of the full interglacial MIS 19, considered the best analogous of the Holocene (Tzedakis et al., 2012; Yin & Berger, 2012), is crucial for evaluating the temporal extent of the current interglacial and for future climate prediction.

4. Conclusions

The MJS sedimentary succession provides an exceptional data-set to trace the main palaeoenvironmental and climatic changes through MIS 37-MIS 16 in the central Mediterranean, a historical key area for the study of Quaternary stratigraphy and climate. The timing and mode of such changes are examined closely in the interval MIS 20-MIS 18, and correlated with climate fluctuation from globally-distributed records. The integrations of continental (pollen) and marine (ostracods, benthic and planktonic foraminifera, coccolithophores, teleostean fishes, mollusks) proxies allows us to document, up to millennial scale, the nearly contemporaneous response to paleoenvironmental events in the two biological domains, providing an invaluable tool for marine-terrestrial correlation. Multiple chrono- and climatostratigraphic constraints are recorded and the most important are synthesised in Fig. 3:

a) coldest phase in the uppermost MIS 20;

b) Termination IX;
c) substages 19.3, 19.2, 19.1;
d) events of maximum flooding, climate optimum, and maximum depth;
e) end of the second temporary disappearance of *Gephyrocapsa omega*;
f) radiometric age of volcaniclastic layers V3 and V4 bracketing MIS 19.

The plethora of data for the MIS 20 to MIS 18 interval collected in the continuous succession (Ideale section) makes it possible to consider the MJS highly suitable for hosting the GSSP of the Middle Pleistocene Subseries and its associated stage. In fact, it meets most of the requirements cited in Remane et al. (1996) for a GSSP:

i) geological, i.e. *exposure over an adequate thickness, continuous sedimentation, high sedimentation rate, absence of synsedimentary and tectonic disturbances, absence of metamorphism and strong diagenetic alteration* (see Ciaranfi et al., 2010; Maiorano et al., 2010);
ii) biostratigraphic, i.e. *abundance and diversity of well preserved fossils, absence of vertical facies changes, favourable facies and numerous biovents for long-range biostratigraphic correlations* (see Marino, 1996; Girone & Varola, 2001; D'Alessandro et al., 2003; Stefanelli, 2003, 2004; Maiorano & Marino, 2004; Maiorano et al., 2004; Joannin et al., 2008; Maiorano et al., 2008; Girone et al., 2013a; Aiello et al., 2015; Bertini et al., 2015; Marino et al., 2015);
iii) chemostratigraphic and astrochronology (see Brilli et al., 2000; Ciaranfi et al., 2010; Maiorano et al., 2010);
iv) radioisotopic dating (see Ciaranfi et al., 2010; Maiorano et al., 2010; Petrosino et al., 2015);
v) sapropel stratigraphy (see D'Alessandro et al., 2003; Stefanelli, 2003; Stefanelli et al., 2005; Maiorano et al., 2008).

Finally, accessibility, free access, permanent protection of the MJS site are guaranteed by a regional law (L.R. January 27-2011, n.3) by the Basilicata regional administration that established the ***Special Nature Reserve of the Montalbano Jonico badlands.***

Panoramic views of the badlands and some details of the Ideale section are

visible at the link:
https://youtu.be/PD8AEisZI4M

The section has been visited by people from many countries during several scientific fieldtrips, the most recent held in Bari (Italy, *Field-workshop on the Lower-Middle Pleistocene transition in Italy*, October 11-13, 2014) (Fig. 4) organised by the Dipartimento di Scienze della Terra e Geoambientali (University of Bari), and supported by the Italian Association for Quaternary Study (AIQUA) and International Commission on Stratigraphy (ICS) (Ciaranfi et al., 2015).

The MJS is the focus of new investigations even now; supplementary higher temporal resolution analyses on calcareous plankton and pollen, and on mineralogic features of sediments across MIS 19 have been recently performed (Maiorano et al., 2016). Planktonic and benthic oxygen isotope stratigraphy up to the centennial scale is advancing close to MIS 19 in the Ideale section (Nomade et al., 2015) and will provide the best $\delta^{18}O$ record from an onland marine succession known so far. Analyses on the cosmogenic radionuclide ^{10}Be are in progress; the latter has a distinctive pattern (^{10}Be flux anomaly) during the MB transition as documented in the sediments (e.g., Frank et al., 1997; Christl et al., 2003; Suganuma et al., 2010) and ice cores (e.g., Wagner et al., 2000; Raisbeck et al., 2006; Dreyfus et al., 2008). Results of these analyses are promising and will likely be compared with other worldwide records, with the aim to provide reliable information on the timing of the paleomagnetic reversal, avoiding the possible effect of post-depositional remanent magnetization lock-in of the geomagnetic signal (Suganuma et al., 2011; Roberts et al., 2013).

Fig. 4 - Participants at the Field Workshop on the Lower-Middle Pleistocene transition in Italy (Bari 11-13 October, 2014; Ciaranfi et al., 2015). The Ideale section is visible in the background. 1 P. Lombardi; 2 G. Miraglia; 3 M. Tropeano; 4 F. Toti; 5 P. Maiorano; 6 C. Lin; 7 P. Ferretti; 8 H. Nirei; 9 A. Negri; 10 R. La Perna; 11 A. Fusco; 12 N. Ciaranfi; 13 D. Scarponi; 14 V. De Vincenzis (Mayor of Montalbano Jonico, 2014); 15 L. Capraro; 16 S. Gallicchio; 17 O. Kazaoka; 18 Y. Suganuma; 19 C. Turner; 20 M. Marino; 21 S. Nomade; 22 L. Sabato; 23 N. Combourieu Nebout; 24 A. Girone; 25 F. Lirer; 26 M. Okada; 27 A. Sposato; 28 A. Bertini; 29 P. Petrosino; 30 M. Head; 31 M. Coltorti; 32 V. Rosito. Photo by G. Vai.


V3

Contribution A6

Formal proposal for the Global Boundary Stratotype Section and Point (GSSP) of the Middle Pleistocene subSeries/subEpoch and Ionian Stage/Age, in the Montalbano Jonico section*

*Submitted to the Subcommission on Quaternary Stratigraphy, SQS, part of the International Commission on Stratigraphy, ICS
(M. Marino, N. Ciaranfi, A. Girone, P. Maiorano, S. Gallicchio, F. Bassinot, S. Nomade, Q. Simon, D.L. Bourlès, F. Dewilde, D. Blamart, V. Scao, A. Bertini, **F. Toti,** P. Petrosino, G. Isguder, A. Pereira, 2017)

Summary

The Ideale section (IS) is part of the 450 m thick Montalbano Jonico composite section (MJS). The MJS covers the MIS37-MIS16 interval and, together with Vrica-Crotone section, forms the potential unit stratotype for the Calabrian Stage.

The IS holds all the requirements for the selection of the GSSP of the Middle Pleistocene Subseries/Subepoch and Ionian Stage/Age thanks to multiple stratigraphic, chronological and paleoenvironmental constraints (Figure). The IS deposited in an outer shelf to upper slope environment, and is framed in the accurate regional and local geological settings. It has an excellent exposure (74.19 m thick) and shows sedimentary continuity from MIS 20 to MIS 18. The $^{40}Ar/^{39}Ar$ dated tephra V3 and V4 bracket MIS 19. The IS benefits from a very high resolution (90-200 ky) stable oxygen and carbon isotope data-set, never recorded in other on land marine successions, and thus relies upon a robust astronomical tuning and an accurate age-model. Stages and substages (MIS 20, MIS19c, MIS 19a, MIS 19b, MIS18), Termination IX, and millennial scale oscillations of global-scale significance are recorded through the section as displayed from oxygen stratigraphy and paleontological proxies from both marine and terrestrial realms (pollen, dinocysts, calcareous plankton, benthic foraminifera, macro-benthic invertebrates, ostracods). The "ghost sapropel" (icycle 74, 784ka), identified within MIS 19c based on the minima in $\delta^{13}C$ and $\delta^{18}O$ records as well as additional marine proxies, represents a clear signature of the well dated Mediterranean-scale oceanographic and climate event driven by orbital forcing. It furnishes an additional chronostratigraphic constraint that sustains the age-model and strengthens correlation potential of the IS. The high temporal resolution (up to 180-230 years) record of the distinct $^{10}Be/^{9}Be$ peak during MIS 19c/19b transition, provides the precise recognition of the geomagnetic dipole

moment associated to MBB. The tephra V4 occurs within the $^{10}Be/^{9}Be$ peak, and makes it possible to assess the chronology of ^{10}Be-production and the MBB geomagnetic variations, with an unprecedented accuracy for a marine archive. The stratigraphic occurrence, signature and (sub)millennial chronology of the $^{10}Be/^{9}Be$ peak are similar to those described in several marine and ice core records making the section a global-scale reference for the Lower-Middle Pleistocene boundary.

GSSP definition, stratigraphic position and global significance of the boundary: the golden spike is proposed at the base of tephra V4. This choice respects the most widespread practice to locate the GSSP exactly in a well visible lithologic marker where precise and globally correlatable events occur, specifically: MIS 19c-19b transition, and MBB. The selected point is accurately dated since the $^{40}Ar/^{39}Ar$ age of V4 is the most precise within the MIS 19 archives. The age of MBB, based on the peak of $^{10}Be/^{9}Be$ ratio, is estimated between 771.9 ka and 776.4 ka (duration 4.5 ka), synchronous with the large ^{10}Be-flux peak recorded in the EPICA DOME C ice core, and the age of MBB recorded in most marine sequences.

Additional stratigraphical/paleoenvironmental constraints close to V4 are listed below:

1) the “ghost” sapropel (i-cycle 74, 784 ka)
2) the end of the temporary disappearance of nannofossil Gephyrocapsa omega (760 ka)
3) Termination IX (789.5 ka)
4) the onset of MIS 19c (785.4 ka)
5) the short-term cold/dry phase (YD-like event, 785.8 ka) interpreted as a global signature of the end of terminal bipolar seesaw oscillation
6) the maximum flooding (MF, 777-780 ka)
7) the maximum depth (MD, 777-773 ka)

The IS, with its detailed data-set, the synchronous signals of chronostratigraphical and paleoenvironmental events in geochemical, mineralogical, and marine and terrestrial fossil proxies is a unique and valuable archive for worldwide Quaternary scientists working with both

continental and marine records and therefore for the Middle Pleistocene GSSP selection.

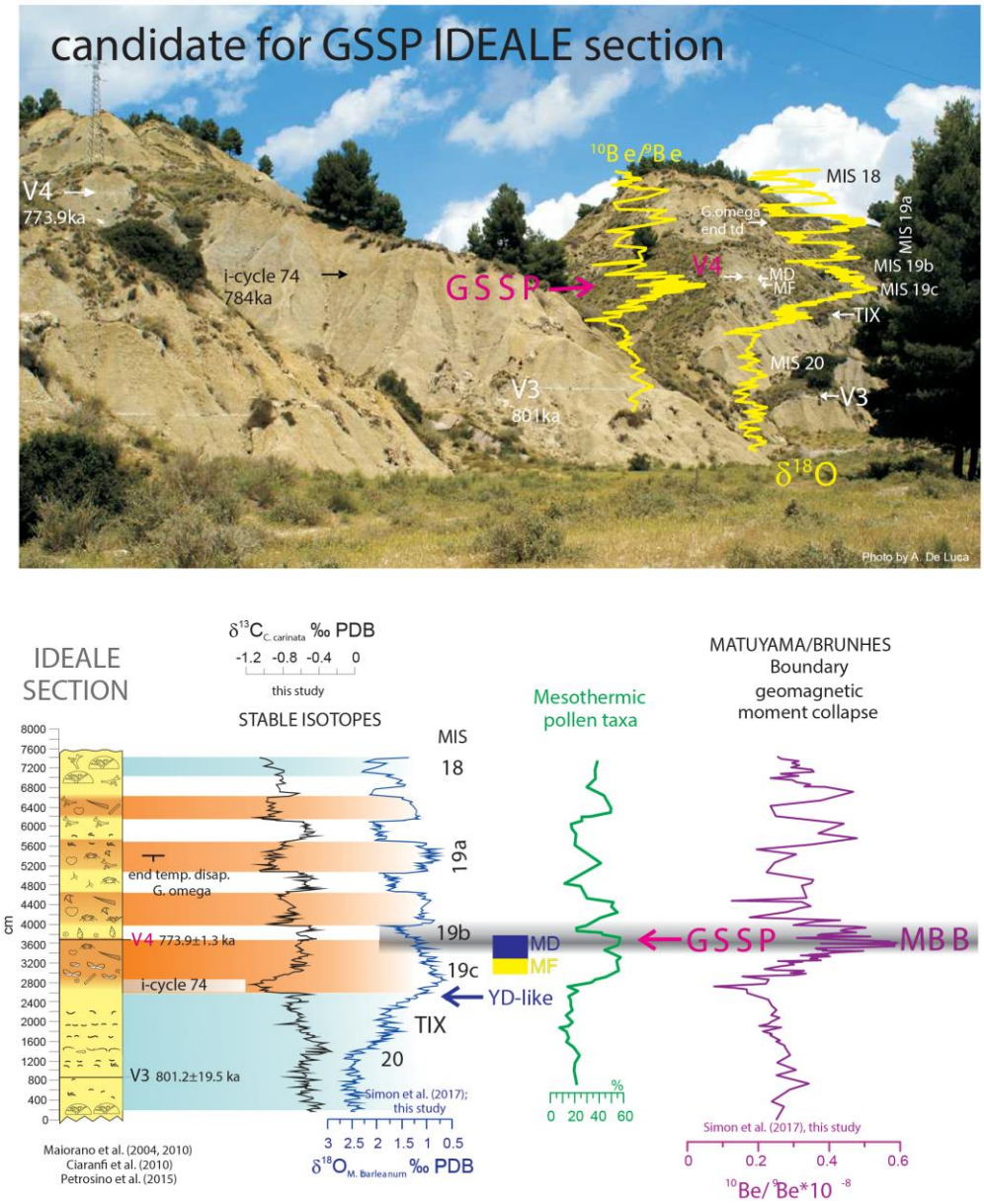

Figure summary

FORMAL PROPOSAL FOR THE GLOBAL BOUNDARY STRATOTYPE SECTION AND POINT (GSSP) OF THE MIDDLE PLEISTOCENE SUBSERIES/SUBEPOCH AND IONIAN STAGE/AGE IN THE MONTALBANO JONICO SECTION

Marino M.[1], Ciaranfi N.[1], Girone A.[1], Maiorano P.[1], Gallicchio S.[1], Bassinot F.[2], Nomade S.[2], Simon Q.[3], Bourlès D.L.[3], Dewilde F. [2], Blamart D.[2], Scao V. [2], Bertini A.[4], Toti F.[4], Petrosino P.[5], Isguder G.[2], Pereira A.[2,6,7,8],

1: Dipartimento di Scienze della Terra e Geoambientali, Università di Bari Aldo Moro, E. Orabona 4, 70125 Bari, Italy
2: Laboratoire des Sciences du Climat et de L'Environnement, UMR8212, LSCE/IPSL, CEA-CNRS-UVSQ and Université Paris-Saclay, Gif-Sur-Yvette, France
3: CEREGE UM34, Aix Marseille Univ, CNRS, IRD, Coll France, Aix en Provence, France
4: Dipartimento di Scienze della Terra, Università di Firenze, via La Pira 4, 50100 Firenze, Italy
5: Dipartimento di Scienze della Terra dell'Ambiente e delle Risorse, Università di Napoli Federico II, Largo San Marcellino 10, 80138, Napoli, Italy
6: Département de Préhistoire du Muséum national d'Histoire naturelle, UMR 7194 du CNRS, 1 rue René Panhard, 75013 Paris, France.
7: Sezione di Scienze Preistoriche e Antropologiche, Dipartimento di Studi Umanistici, Università degli Studi di Ferrara, C.so Ercole d'Este I, 32, Ferrara, Italy
8: Ecole française de Rome, Piazza Farnese, IT-00186, Roma, Italy

Abstract

The numerous stratigraphic, chronological, and paleoenvironmental constraints at the Ideale section from the Montalbano Jonico succession are discussed and resumed. They proved that the Ideale section holds all the requirements indicated by Remane et al. (1996) for the selection of the GSSP of the Middle Pleistocene Subseries/Subepoch and Ionian Stage/Age. The marine section, 74.19 m thick, is easily accessible, has an exceptional exposure, shows sedimentary continuity from MIS 20 to MIS 18, and is astronomically tuned. The stable oxygen and carbon isotope data-set, acquired at a very high resolution (90-200 ky), never recorded in other on land marine successions reveal an excellent climate signature, in agreement with terrestrial and marine paleontological tracers. Stages and substages (MIS 20, MIS 19c, 19b, 19a, MIS 18), Termination IX (TIX), short-term climate oscillations of global-scale significance, and the "ghost sapropel" i-cycle 74 (784 ka) have been identified based on oxygen and carbon isotope stratigraphy, and paleontological proxies from both marine and terrestrial realms. The $^{40}Ar/^{39}Ar$ dated tephra layer V4 (773.9 ± 1.3 ka) provides a robust tie-point that complements and strengthens the astronomically-tuned age-model. The twofold increase of $^{10}Be/^{9}Be$ peak occurs during late MIS 19c/early MIS 19b, and allows the precise stratigraphic determination of the geomagnetic dipole collapse associated with the Matuyama-Brunhes polarity reversal. The V4 tephra falls in the middle of the $^{10}Be/^{9}Be$ peak, making it possible to evaluate the chronology of ^{10}Be-production changes and the MBB geomagnetic variations, with

an unprecedented accuracy for a marine archive. The MBB is precisely dated between 771.9 ka and 776.4 ka, with a duration of 4.5 ka. It is synchronous with the large ^{10}Be-flux peak recorded in the EPICA DOME C ice core, and coeval to the Matuyama-Brunhes polarity reversal recorded in most marine sequences. The GSSP of the Middle Pleistocene Subseries and Stage is proposed at the base of the V4 tephra, a lithological marker well recognizable in the Ideale section, coincident with two globally correlatable events: the MBB and the distinct geochemical/climate change at the MIS 19c/19b transition. Numerous additional events contribute to the long-distance correlation of the section.

1. Introduction

The Pleistocene is subdivided into Lower/Early, Middle and Upper/Late subseries/subepochs. The global boundary stratotype section and point (GSSP) of the Lower Pleistocene Stage/Age is the Gelasian, defined at the Monte San Nicola section (Sicily) (Rio et al., 1998), and coincides with the GSSP of Quaternary System/Period and Pleistocene Series/Epoch at 2.588 Ma (Gibbard et al., 2009; Gibbard and Head, 2010; Gibbard et al., 2010; Fig. 1A). The GSSP of the second Lower Pleistocene Stage, the Calabrian, is defined at the Vrica section (Cita et al., 2012). The Middle and Upper subseries are not yet officially recognized.

All the Quaternary series/epoch GSSPs defined up to now are based on criteria which also include major climate changes as key time points of Earth climate history and recognizable at global scale in marine and terrestrial records of the last 2.588 Ma. The conventional Quaternary stratigraphical subdivision is strongly based on climate evolution which, when characterized with high detail, makes it possible to improve the recognition of individual stratigraphical/geological/climate units. Recently, Miller and Wrigth (2017) have clearly stated that the global (climatic) geochemical (isotopic) changes improve the correlation of GSSPs. Based on such a strategy, which puts emphasis on climato-stratigraphic criteria, the GSSP of Quaternary System/Period and Pleistocene Series/Epoch was lowered from the Calabrian to the Gelasian Stage, the latter recording a major cooling event. This cooling event, which has a clear imprint in the oxygen isotope stratigraphy, coincides (i) with the first major influx of ice-rafted debris into the middle latitude of the North Atlantic and (ii) with major climate changes in many terrestrial records (Shackleton et al., 1984; Shackleton, 1987; Partridge, 1997; Rook and Martinez-Navarro, 2010). Similarly, the Holocene GSSP also rests strongly on climate evolution. It is defined at the warming phase, which follows the Younger Dryas cold event in the NGRIP Greenland ice core (Walker et al., 2009). A similar climato-stratigraphic approach would set the GSSP of Upper Pleistocene Subseries at the base of

last interglacial (coincident with the Eemian Stage) or at the Termination II (see discussion in Head and Gibbard, 2015a, cum references).

For the stratigraphic definition of the Middle Pleistocene GSSP, the Matuyama/Brunhes magnetic polarity boundary (MBB) was chosen as the primary criterion (SQS working group, 32nd International Geological Congress, Florence 2004). Specifically, the Early-Middle Pleistocene boundary should be defined in an on land marine succession at a point "close" to the MBB. Yet, several high-resolution multidisciplinary studies of the Pleistocene showed that a pre-selected primary criterion might be misleading sometimes, since it may not be unambiguously recognizable and could not be suitable for wide scale correlations (Vai, 2001; Walsh et al., 2004). Specifically, the MBB might appear diachronous in distinctive records due to recording artefacts such as poorly constrained (post-) detrital remanent magnetization (pDRM) processes (Roberts et al., 2013; Valet and Fournier, 2016). Thus, the MBB alone does not offer the maximum correlation potential for deciphering the exact position of Middle Pleistocene GSSP worldwide while it is of primary importance to satisfy multiple chronostratigraphic criteria. A synthesis of the recommendations made by Remane et al. (1996) to insure the optimal selection of criteria for GSSP definition can be found in Table 1 of Head and Gibbard (2015a). Those criteria also include the recent approach which uses cosmogenic radionuclide ^{10}Be in marine sediments and ice records for determining changes in the intensity of Earth magnetic field, and in particular the major drops associated with reversal events. Regarding the Middle Pleistocene determination, one of the most promising progresses in Quaternary research, is the fact that the geomagnetic dipole collapse associated with the last geomagnetic polarity reversal triggered an episode of ^{10}Be overproduction. This peak in ^{10}Be has been observed in Antarctic ice-core EPICA Dome C (EDC, Raisbeck et al., 2006) and in marine sediments (Suganuma et al., 2010; Valet et al., 2014; Simon et al., 2016, 2017).

Historically, since the works of Cita and Castradori (1994, 1995) and Van Couvering (1995), the non-official 'Ionian' name has been widely used in the literature for the Middle Pleistocene Stage (more than 400,000 results in google when searching for 'Ionian Stage') including the International Chronostratigraphic Chart (www.stratigraphy.org). The 'Ionian' term was proposed following the workshop-fieldtrip on the sections representing the Early, Middle and Late Pleistocene time intervals (Crotone Basin-Vrica, Apennine Foredeep-Montalbano Jonico, Taranto and Gallipoli area) cropping out in southern Italy. In these areas, the GSSPs of Gelasian and Calabrian have been ratified (Fig. 1B), and the Il Fronte section (Taranto area), represents a potential candidate for the GSSP ('Tarantian' Stage sensu Cita and Castradori, 1995) of the Upper Pleistocene Subseries (Amorosi et al., 2014; Negri et al., 2015).

104 Since the contribution of Ciaranfi et al. (in Cita and Castradori, 1994) , the Montalbano Jonico
105 succession (MJS) has been extensively studied based on numerous investigation methods. The
106 results have been published in international literature and constitute the largest available dataset for
107 reconstructing continuous climatic variations of the Lower-Middle Pleistocene transition
108 (http://www.geo.uniba.it/mjs.html). In the present proposal, we describe in details the MJS and in
109 particular the sedimentary portion (Ideale section) spanning the MIS 20-18 interval, with the aim to
110 document the multiplicity of chronological and bio-chemo-stratigraphic constraints that make the
111 section a global-scale reference for the Lower-Middle Pleistocene boundary and the strongest
112 candidate to host the Middle Pleistocene GSSP.
113
114 **2. Geological setting**
115 The Montalbano Jonico succession crops out in the south-western margin of the Bradanic Trough at
116 about 16 km inland from the Ionian Coast (Figs. 2-3A). The Bradanic Trough (e.g. Casnedi, 1988),
117 located between the Apennines Chain to the west and the Apulian foreland eastward (Fig. 2), is
118 considered the post-Messinian Apennines foredeep basin. Its origin and evolution were due to the
119 eastward roll-back of the subduction hinge of the Apulia platform and the evolution of the external
120 Apennines thrust front during the Plio-Pleistocene (e.g., Patacca and Scandone, 2007 and references
121 therein). The foredeep was characterized by high rates of subsidence until the Calabrian, then it
122 underwent a diachronous uplift starting from the Genzano-Banzi area during late Calabrian and
123 proceeding south-eastward to the actual Ionian coast until the Holocene. In the late Calabrian, the
124 central sector of the Bradanic Trough emerged while the southern sector, where the study section is
125 located, was still subsiding. Simultaneously, on the western side of the trough, the uplift of Nocara
126 ridge was taking place, isolating from the open basin a western piggy-back depocenter, the
127 Sant'Arcangelo Basin (e.g. Patacca and Scandone, 2007 and references therein). The central
128 foredeep sector reached its maximum deepening in the Early-Middle Pleistocene (e.g., Maiorano et
129 al., 2016). From the Middle Pleistocene, the sedimentation underwent a shoaling-upward trend due
130 to the uplift of the area (uplift rate of 0.1–0.5 mm/years, Doglioni et al., 1996) that led to the
131 emersion of the area.
132 The Montalbano Jonico clayey succession belongs to the argille subapennine informal unit
133 (Azzaroli, 1968), representing its middle-upper portion, Early to Middle Pleistocene in age
134 (Ciaranfi et al., 2010). It lies stratigraphically on the allochthonous units of the chain and locally on
135 Pliocene sandy units of coastal environment (sabbie e conglomerati di Serra del Cavallo, Mostardini

and Pieri, 1967), and unconformably passes upward to middle-upper Pleistocene terraced sands and conglomerates of transitional and continental environment (e.g. Pieri et al., 1996).

Figure 3B shows a detailed geological map of the western side of the hillslope of Montalbano Jonico village, that is in the Special Natural Reserve of Montalbano Jonico badlands, quite close to the Ionian coast (Fig. 3A). The argille subappennine unit outcrops widely in this area showing a broad monocline gently dipping toward the eastern quadrants. The monocline is highlighted by the presence of several tephra layers and appears slightly displaced by few normal faults. The sandy and conglomerate marine terraced deposits outcrop at the top of the hill at about 291 m. Upper Pleistocene–Holocene alluvial deposits locally overlay the argille subappennine (Fig. 3B-C).

3. The Montalbano Jonico succession

The Ideale section (Fig. 4A), which is the candidate for the GSSP of the Middle Pleistocene, is part of the MJS, about 450 m thick. The MJS consists of coarsening-upwards deposits ranging from silty clays to silty sands and includes nine tephra layers (V1–V9) (Fig. 4A, B). The tephra layers were chemically and mineralogically characterized and correlated to analogous layers from south-central Italy lacustrine and marine successions, within a Lower-Middle Pleistocene Mediterranean tephrostratigraphic frame (Petrosino et al., 2015). The V3, V4 and V5 layers were radiometrically dated and their $^{40}Ar/^{39}Ar$ ages are 801.2 ± 19.5 ka (Maiorano et al., 2010), 773.9 ± 1.3 ka (Petrosino et al., 2015), 719.5 ± 12.6 ka (Ciaranfi et al., 2010), respectively. New $^{40}Ar/^{39}Ar$ dating in various laboratories (Univ. Wisconsin, Berkeley Geochronology Center - USA and at the LSCE geochronological facility (France) in the frame of an international intercalibration effort have started in 2017 with the goal of providing more robust radio-isotopic age control for the tephra layers of this succession.

The MJS, in its lower part, includes five dark horizons (Fig. 4) interpreted as sapropel layers (D'Alessandro et al., 2003; Stefanelli, 2004; Stefanelli et al., 2005; Maiorano et al., 2008) and correlated, from oldest to youngest, to insolation cycles i-112, i-104, i-102, i-90, and i-86, based on the Mediterranean sapropel stratigraphy of Lourens (2004) and Lourens et al. (2004). In addition, the Ideale section also contains the analogue of the "red interval" ("ghost sapropel", Emeis et al., 2000) correlated to i-cycle 74, as highlighted by micropaleontological indications (Maiorano et al., 2016) and strongly supported by the $\delta^{13}C$ record (this study).

The calcareous nannofossil biostratigraphy indicates that the succession belongs to the small *Gephyrocapsa* and *Pseudoemiliania lacunosa* zones, based on the biostratigraphic scheme of Rio et al. (1990) (Fig. 4A). This is equivalent to the CNPL9 and CNPL10 biozones of Backmann et al.

(2012) and Raffi et al. (2016), that rely on worldwide biohorizons. High-resolution quantitative analyses of calcareous plankton assemblages reveal numerous additional bioevents throughout the section (Fig. 5) never acquired in an on land Lower-Middle Pleistocene succession (Marino, 1996; Ciaranfi et al., 1997; Maiorano et al., 2004, 2010; Joannin et al., 2008; Girone et al., 2013). Several deepening-shallowing cycles, from bathyal to circalittoral environments, have been recognized based on micro- and macro-invertebrate benthic assemblages (Fig. 4A) (D'Alessandro et al., 2003; Stefanelli, 2003; Ciaranfi and D'Alessandro, 2005; Girone, 2005; Aiello et al., 2015). Specifically, benthic paleocommunities from the lower part of succession (Interval A) are indicative of upper slope environments, with a maximum depth of ca. 500 m, while paleocommunities of upper portion (Interval B) indicate outer to inner shelf settings with short-term deepening towards upper slope (Fig. 4A). Stable oxygen isotope analyses performed throughout the entire succession on planktonic (*Globigerina bulloides*) and benthic (*Cassidulina carinata*) foraminifer tests (Fig. 4A), combined with calcareous plankton biostratigraphy, showed that the section encompasses from Marine Isotope Stage (MIS) 37 to 16 (Brilli, 1998; Brilli et al., 2000; Ciaranfi et al., 2010; Maiorano et al., 2004; 2010).

The whole section represents the regressive part of a third-order cycle with several fourth and fifth-order cycles mainly driven by climate changes (Ciaranfi et al., 1997, 2010). The onland climate imprint at the glacial-interglacial timescale is clearly evidenced by the pollen PTI curve (Pollen Temperature Index, sensu Joannin et al., 2008 and Suc et al., 2010) (Joannin et al., 2008; Bertini et al., 2015; Toti, 2015; Vannacci, 2016), which co-varies with $\delta^{18}O$ oscillations and paleodepth variations.

The $\delta^{18}O$ records combined with biostratigraphy, radiometric data, and sapropel stratigraphy, allowed the astronomical calibration of the MJS (Ciaranfi et al., 2010; Maiorano et al., 2010, 2016; Marino et al., 2015, 2016, Fig. 6). The calcareous plankton bioevents have high correlation potential being recognized at global scale (Maiorano and Marino, 2004; Maiorano et al., 2010; Backman et al 2012; Raffi et al., 2006, 2016) (Fig. 6). A detailed biochronology is provided in Table I.

The MJS together with the Vrica-Crotone section (both astronomically-tuned, Lourens et al., 2004 and reference therein; Ciaranfi et al., 2010) cover the entire Calabrian time thus representing a potential unit-stratotype for the Calabrian Stage (Maiorano et al., 2010) (Fig. 6). The two on-land marine records, have been compared with Mediterranean and extra-Mediterranean deep-sea records, supporting the consistency and reliability of the cyclostratigraphic and biostratigraphic constraints (Maiorano et al., 2010). Both the sections are located in South Italy, a reference region for

Quaternary chronostratigraphy, within the Mediterranean area, which is the cradle of most Neogene GSSP (Fig. 1B).

4. The Ideale partial section and the GSSP of Middle Pleistocene

The Ideale section is here proposed to host the GSSP of Middle Pleistocene Subseries. Its stratigraphical relevance has been widely outlined in several papers (e.g. Ciaranfi et al., 2010; Bertini et al., 2015; Marino et al., 2015; Maiorano et al., 2016, Simon et al., 2017). The section contains many stratigraphical and chronological constraints, together with a rich data set of paleoenvironmental/paleoclimate information (synthesis in Fig. **7**). Amongst others, the most important constraint for the GSSP selection, the identification of the MBB, is evidenced at high-resolution within MIS 19c/19b by a ^{10}Be-overproduction episode induced by the Earth magnetic field intensity collapse during the Matuyama-Brunhes reversal (Simon et al., 2017). The Ideale section bears an abundant, diverse and well preserved fossil content essentially consisting of macroinvertebrate, ostracods, foraminifera, calcareous nannofossils, dinocysts and pollen (Plate 1) (see also Marino et al., 2016). The Ideale section has a thickness of 74.19 m and records the MIS 20 to MIS 18 time interval (Fig. 7). The present description of the section rests upon previously published stratigraphic results and new higher resolution δ^{18}O data (Bassinot et al., in prep.), covering a new 14 m thick interval in the uppermost portion of the Ideale outcrop. A slight thickness updating of a 4 meters badly exposed interval above V4 is included thanks to the new measurement of the nearby coeval section named CMs (Ciaranfi Master section). As the Ideale section, the CMs is spectacularly exposed and located slightly to the north (Figs. 3B, 8). The V3 and V4 tephra layers (see cross-section in Fig. 3C) and the dark/light sediment bands are clearly visible in the Ideale and CM sections; the perfect matching of the high resolution oxygen data between both sections confirms the strong (lateral) continuity of the studied stratigraphic interval (Fig. 8).

4.1 Lithostratigraphy

4.1.1 Grain size and mineral content

The Ideale section consists of dark-light grey silty clays (Fig. 7). The main mode of grain size (Maiorano et al., 2016, for details) varies from 5.6 to 22 μm, indicating a detrital fraction varying from fine to coarse silt. The clay fraction is generally less abundant during MIS 20 (15–24%, average 19%), whereas it increases significantly (20–31%, average 24%) from the onset of MIS 19 onwards, although several fluctuations have been observed through this interval. From a

234 mineralogical point of view, sediments mainly consist of phyllosilicate minerals, carbonates (calcite
235 and dolomite), quartz and feldspars (see Maiorano et al., 2016 for details). The mineralogical
236 composition and changes, and the grain size variation through the section are clearly related to the
237 lithological units of source area and to climate changes. The main increases of quartz and dolomite
238 combined with enhanced supplies of coarser grain size fraction, reflect an increase of the coarser
239 detrital mineral components into the basin during cold phases. On the other hand, higher kaolinite
240 and smectite contents occur during warm phases, when chemical weathering increased, in good
241 agreement with pollen-derived climate data (Bertini et al., 2015; Maiorano et al., 2016). Such
242 variations match the light and dark grey bands, visible on the Ideale and CM sections (Fig. 8)
243 starting from the onset of MIS 19 up to the MIS 18 inception, with darker grey sediments
244 corresponding to wetter and warmer periods.
245
246 4.1.2 Tephra layers
247 The V3 tephra layer falls within the MIS 20 interval (at 820 cm) and V4 at the transition from MIS
248 19c and MIS 19b (at 3660 cm). The Vulture stratovolcano is likely the source of V3 and V4, which
249 would represent its oldest products (Petrosino et al., 2015).
250 V3 is less than 5 cm thick and is a silty-sand sized grey layer with clayey matrix. The type of
251 juvenile clasts (2-3Φ) is represented by badly preserved, vesicular whitish pumice fragments. The
252 percentage of crystal grains with respect to glass fragments (2-3Φ) is 70%. The types and percentage
253 of crystal grain are feldspar (60%), greenish to brown clinopyroxene (20%), mica (10%), hauyne
254 (5%), garnet (5%), and non volcanic gypsum. The fraction finer than 250 μm is mainly made up of
255 crystals and very minor glass fragments that are trachyphonolitic in composition. Crystal fragments
256 are often coated with glass. Feldspar is the best-represented crystal phase both as Na-rich Kfeldspar
257 (Or60) and plagioclase (An44), but the layer also contains salitic to Fe-salitic clinopyroxene
258 (Wo59-46, En30-18, Fs25-13) that typically engulfs hauyne microcrysts. Clinopyroxenes are
259 characterized by Mg# ranging from 33 to 55, a CaO content higher than 20 wt.%, and by low values
260 of TiO_2 and Na_2O (ca. 1.5 wt.% and ca. 1 wt.% respectively). This is reflected in large amounts of
261 CaTi-Tschermak (10-17 mol.%) and Esseneite (16-23 mol.%) molecules. Loose hauyne and
262 melanite are also present. Among the components of the non-volcanic fraction, V3 contains a large
263 number of gypsum crystals, as V4 (Petrosino et al., 2015).
264 V4 layer is 10 cm thick and is a silty-sized yellowish grey layer with clayey matrix. The type of
265 juvenile clasts (2-3Φ) is represented by very rare, badly preserved pumice fragments with elongated

vesicles. Crystal grains are coated with glass. A percentage of 80% represents the crystal grains with respect to glass fragments (2-3ϕ). The types and percentage of crystal grain are feldspar (75%), greenish to brown clinopyroxene (15%), amphibole (5%), garnet (5%), and gypsum. The residual fraction is finer than 250 μm and mainly comprises Na-rich K-feldspar (Or60-59) and salitic clinopyroxene (Wo59-55, En36-30, Fs11-9). Very few glass fragments could be analyzed and these yielded a phonolitic composition resembling the chemistry of glasses extracted from the V3 layer.

4.2. Biostratigraphy

No biostratigraphic zonal events occur in the MIS 20-MIS 18 time interval according to biostratigraphic schemes (e.g. Rio et al., 1990; Backman et al., 2012). However, the temporary disappearance of nannofossil *Gephyrocapsa omega* (td2 in Maiorano and Marino, 2004) is well documented as an additional biohorizon at a wide scale in the Mediterranean area and in North Atlantic Ocean (see Fig. 10 in Maiorano et al., 2010). The end of temporary disappearance is the only calcareous plankton event near the MBB. In detail, the beginning and the end of td2 are always recorded in MIS 20/21 and MIS 18/19, respectively; the minor diachronous character of these bioevents (Table I) could be related to environmental features, although the possibility that this apparent diachronism could be associated to inconsistencies in age-models cannot be excluded. At the MJS section the age-assignments of beginning and end of td2 are 0.83 Ma and 0.76 Ma (at 5354 cm in the Ideale section), respectively (Table I).

4.3 Chemostratigraphy

4.3.1 Oxygen isotope record

Low-resolution *C. carinata* and *G. bulloides* $\delta^{18}O$ records spanning the entire Montalbano Jonico series have been published by Brilli et al. (2000) and Ciaranfi et al. (2010; cum reference therein). Recently, the Ideale section was re-sampled at a high-resolution (1 sample every 20 cm, ~90-200 years) and a new $\delta^{18}O_{M.\ barleanum}$ record, that covered from MIS 20 to within MIS 19, was published in Simon et al. (2017). Since this publication, the $\delta^{18}O_{M.\ barleanum}$ has been extended upward to cover a thicker stratigraphic interval up to the top of Ideale section, within MIS 18 (Figs 7-9). A high-resolution $\delta^{18}O_{C.carinata}$ record (not shown here) at the Ideale section is now also available at the same resolution and will be submitted within the next few weeks (Bassinot et al., in prep.). A short $\delta^{18}O_{M.\ barleanum}$ record (14 m thick) at the CMs, has been also performed starting from V4 tephra (Fig. 8).

298 In this document, only the $\delta^{18}O_{\textit{M. barleanum}}$ and $\delta^{13}C_{\textit{C.carinata}}$ records are shown (Fig. 9). As in Simon
299 et al. (2107), the analyses were performed on a GV-Isoprime dual-inlet gas mass spectrometer at
300 LSCE lab-oratory. All results are expressed as $\delta^{18}O$ and $\delta^{13}C$ vs VPDB (in ‰) with respect to NBS
301 19 standard. The internal analytical reproducibility determined from replicate measurements of a
302 carbonate standard is ±0.05%(1σ).
303 Values of $\delta^{18}O_{\textit{M. barleanum}}$ vary between ~0.6 and 2.6‰. This record shows that the Ideale section
304 provides a very detailed marine isotopic record of the Termination IX (TIX), and extends upward
305 into MIS 18. The deglaciation is 16 m-thick, taking place between 1240 and 2860 cm. It
306 corresponds to a decrease of nearly 2‰ of the $\delta^{18}O$ values, which range from ~2.6‰, at the glacial
307 maximum, to ~0.6‰ at the peak of MIS 19c (Fig. 9). From the peak value of MIS 19c, at
308 ~2860cm, the benthic $\delta^{18}O$ record shows a rather progressive increase upward with minor scale
309 oscillations until about 3960 cm, where it reaches ~1.8‰ (Fig. 9). Then, the $\delta^{18}O$ record shows an
310 extremely abrupt decrease, with values dropping by more than 0.7 ‰ (from 1.83 to 1.10‰) in only
311 40 cm, and by ~1‰ in one meter (Fig. 9). This abrupt shift marks the upper portion of the study
312 record, which is characterized by relatively stable intervals with low $\delta^{18}O$ values (suggesting a
313 return to warm/wet conditions), limited by extremely abrupt $\delta^{18}O$ changes at their onsets and
314 terminations (Fig. 9). Three such episodes (interstadials I-IIIi) are clearly visible in the $\delta^{18}O$ record
315 (over the intervals 3994–4640 cm, 5068–5680 cm, and 6119-6596 cm respectively) (Fig. 9).
316 Between 6639 cm and 6769 cm values are of 2.3-2.14‰. The interval from 6800 cm to 7072 cm
317 shows again light $\delta^{18}O$ values ranging between 1.45 and 1.7‰. Upward, above the three oscillation
318 episodes, the isotopic record reveals heavier $\delta^{18}O$ values (2.3‰) that we interpret as belonging to
319 MIS 18 (Fig. 9).
320 The very high-resolution $\delta^{18}O$ curve at the Ideale section provides one of the most detailed record
321 of the MIS 20-MIS 18 interval and of termination IX worldwide. Rapid oscillations are observed
322 above MIS 19c and they resemble the ones recorded in the isotopic record of the Sulmona paleolake
323 (Central Italy, Giaccio et al., 2015), or in the $\delta^{18}O$ record from the North Atlantic (Channell et al.,
324 2010; Ferretti et al., 2015; Sánchez Goñi et al., 2016), in the δD pattern from EPICA Dome C (Pol
325 et al., 2010), and in the synthetic climatic record from Greenland (GL_T-syn), based on the thermal
326 bipolar seesaw model (Barker et al., 2011) (Fig. 9).
327 The $\delta^{13}C_{\textit{C.carinata}}$ record (Fig. 9) shows low values over a short interval located at the onset of MIS
328 19 (~2620 cm – 2840 cm). The drop in $\delta^{13}C$ is coeval with a final, rapid decrease in $\delta^{18}O$, which
329 ends up the deglaciation interval. We interpret this low-$\delta^{13}C$ interval as associated to a sapropel
330 layer, confirming micropaleontological evidences presented in Maiorano et al. (2016). As illustrated

below, this sapropel provides a very useful constrain to help building-up the age model of the Ideale section based on orbital tuning considerations. In addition, the rapid oscillations observed in the $\delta^{18}O$ record of MIS 19 (Fig. 8) are associated to clear variations in $\delta^{13}C$, which suggest a direct response of productivity/ventilation to rapid climatic changes (Bassinot et al., in prep.).

4.3.2 The MBB and authigenic $^{10}Be/^{9}Be$ ratio

Since magnetostratigraphic analyses were not helpful at MJS, due to complete remagnetization resulting from late-diagenetic greigite growth (Sagnotti et al., 2010), authigenic $^{10}Be/^{9}Be$ ratios were analyzed at high resolution at the Ideale section (Fig. 10) by Simon et al. (2017), to which we refer for details. Additional $^{10}Be/^{9}Be$ ratio results are presented in this proposal for the first time, according to method indicated in Simon et al. (2017), which further improve the previous resolution in the MIS 19c and 19b interval (up to 20-30 cm sample spacing, 180-230 years), and cover the uppermost portion up to MIS 18. Along with paleomagnetic measurements, cosmogenic radionuclide beryllium-10 (^{10}Be) in natural archives provides robust information on past variations of the geomagnetic field intensity. This method helps improving understanding of the geodynamo fluctuations. Indeed, and despite the fact that the MBB is among the most studied geomagnetic reversals (Valet and Fournier, 2016), its accurate age is largely debated because i) calibration of lava flow $^{40}Ar/^{39}Ar$ ages is still evolving, ii) there can be problems associated to multicomponent magnetization in paleomagnetic records, iii) many sedimentary records have a poor signal resolution, iv) there are uncertainties of several thousand years associated with the development of astronomical age models, and v) the stratigraphic position of the reversal can be biased by(post-) detrital remanent magnetization (pDRM) effects resulting in delayed magnetization locking-in (Simon et al., submitted). This last point often leads to an “aging” of paleomagnetic signatures versus their input geomagnetic signals (well illustrated at site MD97-2143; Fig 10; Suganuma et al., 2010). All these factors likely explain the existence of two distinct age groups for the MBB: ~770-776 ka (Bassinot et al., 1994; Tauxe et al. 1996; Dreyfus et al., 2008; Channel et al., 2010; Suganuma et al., 2010, 2015; Singer, 2014; Valet et al., 2014; Simon et al., 2016, 2017, submitted; Channell, 2017; Okada et al., 2017), and ~780-786 ka (Lourens et al., 2004; Sagnotti et al., 2014, 2015; Mark et al., 2017; Capraro et al., 2017).

The authigenic $^{10}Be/^{9}Be$ ratio curve shows a peculiar pattern through the Ideale section yielding a subdivision in 5 phases (Fig. 10). Within phase 1, with the exception of V3 level, the $^{10}Be/^{9}Be$ ratio has a mean value of $0.24 \pm 0.05 \times 10^{-8}$ and smoothly decrease to 0.08×10^{-8}. This period is followed by a rather constant increase of the $^{10}Be/^{9}Be$ ratio (phase 2) that stabilized to a plateau at 0.37 ±

364 0.02 $\times 10^{-8}$ within the 3255–3411 cm interval. The highest $^{10}Be/^{9}Be$ ratios corresponding to
365 maximal values of the Ideale section peak at 0.55 ± 0.06 $\times 10^{-8}$ within the 3541–3645 cm interval
366 (Fig. 10). This represents a near doubling of the $^{10}Be/^{9}Be$ ratio compared to the preceding interval
367 (0.27 $\times 10^{-8}$ from 0 to 3411 cm). That sequence is followed by a sharp drop of the $^{10}Be/^{9}Be$ ratios
368 (0.20 ±0.16 $\times 10^{-8}$) associated with sediments deposited during and immediately after the V4 event
369 (Fig. 10), like at the V3 level. The authigenic ^{9}Be inputs associated with tephra layers V3 and V4
370 are related to direct mantle inputs and/or very dense particle environments following the fallout of
371 pyroclastic flow, contributing to modify drastically the concentrations, scavenging rates and/or
372 mixing of dissolved Be in the water column. Thus, we excluded the tephra layers from the
373 geomagnetic $^{10}Be/^{9}Be$ ratio interpretation given the peculiar geochemical behavior of dissolved Be
374 isotopes within these specific intervals. The interval from 3715 to 4075 cm comprises high $^{10}Be/^{9}Be$
375 ratios with mean value of 0.41 ±0.07 $\times 10^{-8}$. Altogether, when removing the layer disturbed by the
376 tephra signal, the highest $^{10}Be/^{9}Be$ ratio values from the Ideale section, i.e. 0.46 ±0.09 $\times 10^{-8}$, are
377 found in two distinct stages between 3430 and 4075 cm (phase 3). From 4075 to 5624 cm (phase 4),
378 the authigenic $^{10}Be/^{9}Be$ ratios return to average mean of 0.28 ±0.08 $\times 10^{-8}$, coherent with values
379 recorded before the major enhancement of phase 3. The $^{10}Be/^{9}Be$ ratios experienced some
380 fluctuation and two sharp lows at 4135 and 4474 cm depth. Phase 5, starting at 5624 cm, is
381 characterized by two $^{10}Be/^{9}Be$ ratio increases (Fig. 10) associated with period of enhanced erosional
382 processes on carbonate (dolomitic) and arenitic bedrock units, coarser grain size fraction supply and
383 coccolith reworking during cold periods (Maiorano et al., 2016; Fig. 2 in Simon et al., 2017).
384 Except for this specific interval, the absence of correlation with environmental proxies or sea level
385 changes (Fig. 2 and Table S2 in Simon et al., 2017) supports geomagnetic interpretation of the
386 authigenic $^{10}Be/^{9}Be$ ratio fluctuations in the Ideale section.
387 The high $^{10}Be/^{9}Be$ ratio values (^{10}Be overproduction episode, Simon et al., 2017) from phase 3
388 result from low geomagnetic dipole moments at the MBB interval, while (sub)millennial ^{10}Be
389 production variations are associated with high frequency geodynamo fluctuations only observed in
390 the best palaeomagnetic records available from globally distributed lava flows (Valet et al., 2012).
391 This ^{10}Be overproduction episode begins during late MIS 19c and extends over the MIS 19b period
392 according to our high-resolution benthic oxygen isotope record (Fig. 10). As discussed in Simon et
393 al. (2017), when the authigenic $^{10}Be/^{9}Be$ ratio from the Ideale section is compared to
394 climatostratigraphic and paleomagnetic proxies of global marine and ice-core records, its increase
395 interval is contemporaneous with the RPI drop at the late MIS 19c-early MIS 19b interval (Fig. 10).
396 This is the clearest evidence of magnetic reversal since the observed slight chronostratigraphic

offsets of directional change (often chosen to pinpoint reversals) among cores might result from not globally synchronous directional reversal features associated with non-dipolar transitional field component, or by unreliable records of transitional directions in low sedimentation rate sequences (Valet et al., 2016).

4. 4. Age model and Chronology of MBB

An astronomical calibration of the lower-middle Pleistocene section at Montalbano Jonico was presented in Ciaranfi et al. (2010). This chronology of the entire MJS rests upon (i) the tuning of 5 sapropels to insolation cycles i-112, i-104, i-102, i-90 and i-86, and (ii) the correlation of MJS low-resolution planktonic $\delta^{18}O$ record to astronomically-tuned ODP Site 975 isotopic stratigraphy (Lourens et al., 2004). In addition, a $^{40}Ar/^{39}Ar$ age of 719.5 ± 12.6 ka was taken into account for tephra V5. Later, the chronological framework of the Ideale section alone was revised by using recently acquired $^{40}Ar/^{39}Ar$ ages for V3 and V4 tephras (Maiorano et al., 2010; Petrosino et al., 2015) and by tuning the benthic $\delta^{18}O$ record to the LR04 benthic stack of Lisiecki and Raymo (2005) (Marino et al., 2015). However, recent works suggest that tuning benthic $\delta^{18}O$ records to a unique global reference curve such as the LR04 stack neglects regional diachronisms (Lisiecki and Stern, 2016). In the Mediterranean basin, those potential diachronisms can result in 2-3 ka offsets between age assignment of major isotopic features at glacial terminations (max. bias ~9 ka for termination TVII, Konijnendijk et al., 2015), and their counterparts in the LR04 stratigraphy.

To circumvent that issue, Simon et al. (2017) set up a regional strategy for developing a more accurate astronomically-derived age model for MIS 20 - MIS 19 in the Ideale section. This strategy rests upon the fact that insolation forcing across termination TIX had been similar to insolation forcing which prevailed across TI (Tzedakis et al., 2012a; Giaccio et al., 2015; Yin and Berger, 2015). Simon et al. (2017) made the assumption that climate changes across TIX may have been similar (major features, phase) to those recorded across TI. They used well-dated (AMS ^{14}C) $\delta^{18}O$ isotopic records covering the last deglaciation in the vicinity of the Ionian Sea (cores MD90-917, MD90-918, Siani et al., 2004; Caron et al., 2012) in order to decipher precisely the phase relationship between climatic changes and insolation and they applied it to phase-lock TIX relative to insolation. The age-model was settled by linear interpolation adding the age of V4 at 773.9 ka (Petrosino et al., 2015) as additional tie-point.

Since the publication by Simon et al. (2017), the high-resolution $\delta^{18}O$ record was extended upward to the top of the Ideale section. This extended record, which reaches MIS 18, reveals two additional rapid climatic oscillations compared to what was available on the slightly shorter record published

430 in Simon et al. (2017). The updated age-model (Bassinot et al., in prep.) takes advantage of this new
431 dataset to improve the strategy presented in Simon et al. (2017). The detailed observation of ^{14}C-
432 dated isotopic records from Ionian cores covering the last deglaciation, reveals that the last, sharp
433 decrease in $\delta^{18}O$ at the end of TI is synchronous with the peak in northern Hemisphere mean
434 summer insolation (65°N, July-August September) (Fig. 11). It is also coeval with the beginning of
435 sapropel S1, clearly marked by a drop in benthic $\delta^{13}C$ in the records (Fig. 11). In the Ideale section,
436 those features (i.e. rapid final decrease in $\delta^{18}O$ coeval with a drop in benthic $\delta^{13}C$) are also found in
437 TIX, and were thus correlated to the peak of northern insolation (i.e. 785.4 ka), equivalent to the
438 peak at 9.0 ka for TI (Fig. 11). The chronology furthermore suggests as slightly younger age for V3
439 (i.e. 796.8 ka) but in agreement with the 801.2 ± 19.5 ka $^{40}Ar/^{39}Ar$ age obtained in Maiorano et al.
440 (2010). Finally, our model is further constrained by the very accurate age-assignment of V4 (i.e.
441 773.9 ±1.3 ka for V4; Petrosino et al., 2015). In this revised tuning solution for the Ideale section,
442 the recognition of the MIS 18 maximum provides an additional robust tie-point (not available in
443 Simon et al., 2017), that we correlated to the minimum of the mean summer insolation at 757 ka
444 (Bassinot et al., in prep.). This chronological framework places the mid-point of the "ghost
445 sapropel" in the Ideale section (Maiorano et al., 2016) at 784 ka, synchronous with the i-cycle 74
446 (784 ka, Langereis et al., 1997; Lourens, 2004). It also yields a MIS 19c duration of ~11.3 ka , in
447 agreement with the duration of MIS 19c recorded in the lacustrine Sulmona succession (i.e. 10.8 ka;
448 Giaccio et al., 2015) or implied by North Atlantic records (i.e. 12.5 ka; Tzedakis et al., 2012b).
449 Interestingly, with this tuning solution, the three rapid oscillations observed above MIS 19c are all
450 contained in one single precession cycle (Fig. 11).
451 The ^{10}Be overproduction episode associated with the MBB is dated between 776.35–771.87 ka at
452 the Ideale section. This geomagnetic intensity collapse episode spans a 4.5 ka duration and is
453 consistent with paleomagnetic measurements from marine and lava flow records globally
454 distributed, with 10Be-proxies from all existing marine records, as well as with the 10Be-flux peak
455 observed in the EPICA Dome C records (Fig. 12).
456
457 4. 5. Paleoenvironmental reconstruction
458 In the Ideale section, multiple paleontological proxies from both marine and terrestrial realms as
459 well as geochemical signals provide a clear frame of paleoenvironmental evolution and a series of
460 changes related to global climate modifications (Figs. 7, 13-14).
461
462 4.5.1. Paleodepth reconstruction

463 The section records a detailed pattern of shallowing-deepening cycles and changeable
464 environmental conditions at the sea-bottom through MIS 20-19 and towards MIS 18 as highlighted
465 by data from marine micro- and macrobenthic assemblages (D'Alessandro et al., 2003; Stefanelli,
466 2003; Aiello et al., 2015; Bertini et al., 2015; Marino et al., 2015, 2016; Maiorano et al., 2016), and
467 terrestrial pollen distality index (Bertini et al., 2015, this study) (Fig. 7).
468 The relative paleodepth throughout the Ideale section varies from about 100 m to 180-200 m section
469 based on ostracod assemblages (Aiello et al., 2015); an upper Lower Circalittoral Subzone (LCS,
470 sensu Sgarrella and Moncharmont-Zei, 1993) ostracod association is recorded in the upper MIS 20
471 (Fig. 7). The paleodepth increase begins from 2700 cm (ostracofauna), nearly concurrent with the
472 increase of distality (decrease of halophyte plants - e.g. Amaranthaceae, Caryophyllaceae, *Ephedra*
473 - used in this context as an indirect proxy of sea-level fluctuations and distality changes) (Fig. 7).
474 Such pattern is in line with a trend of deepening corresponding to deglaciation recorded by decrease
475 in $\delta^{18}O$ that can be partly attributed to the waxing of continental ice caps (Fig. 7). Benthic
476 foraminifera indicate two low sea-level minima at 1370 cm and 2150 cm, and a prominent
477 deepening trend toward 2700 cm, matching the $\delta^{18}O$ pattern (Fig. 7).
478 At about 3000 cm, deepening evidence is also provided by the occurrence of *Funiculina*
479 *quadrangularis* (Marino et al., 2015, cum reference therein). A maximum flooding (MF) is
480 documented by D'Alessandro et al. (2003) between about 3070 cm and 3370 cm (Fig. 7) based on
481 the occurrence of scattered clusters of the deep-water oyster *Neopycnodonte cochlear*, a species that
482 thrives during low sedimentation rates and low turbidity conditions on the sea bottom (Massari et
483 al., 2002; Ceregato et al., 2007; Wisshak et al., 2009) related to rapid sea level rise after
484 deglaciation. The onset of MIS 19c is recorded by the replacing of the upper LCS assemblages with
485 lower LCS ostracofauna (Fig. 7). The maximum depth interval (MD, from 3370 cm to 3770 cm), is
486 characterized by dispersed macrobenthic content and the occurrence of bathyal taxa among
487 foraminifera and ostracods, and, even as rare specimens, in mollusk assemblage (D'Alessandro et
488 al., 2003). Benthic foraminifera and halophyte patterns from 3850 cm to 3980 cm evidence
489 decreased paleodepth, and it is coeval with heavier $\delta^{18}O$ values in MIS 19b. Similarly, the
490 shallowing and deepening phases recorded upwards in the $\delta^{18}O$ pattern, are also documented by
491 changes in pollen, benthic foraminifera and ostracod assemblages, attesting a mostly genuine signal
492 of sea level fluctuations towards MIS 18 onset (Fig. 7).
493
494 4.5.2 Climatostratigraphy

The signature of orbital-suborbital climate variability is clearly imprinted in the Ideale section (Fig. 7A) as recorded by multiproxy investigations (Bertini et al., 2015; Marino et al., 2015, 2016; Maiorano et al., 2016; this study). Climate changes can be also traced on the outcrop as highlighted by the dark-grey (warm phases) and light-grey (cold phases) bands evident in the Ideale and CM sections (Figs. 7B, 8). Cyclic variations in the grain size and mineral content are also a clear marking of climate changes into the sediments all through the section and specifically of succeeding warmer-wetter/colder-arid phases on land (Maiorano et al., 2016).

During the late MIS 20, from ca. 792 ka to 788 ka, the higher abundance of artic-subartic *Coccolithus pelagicus* spp. *pelagicus* and *Neogloboquadrina pachyderma* sinistral, and low abundance of calcareous plankton warm water taxa, suggest low sea surface water temperatures linked to polar-subpolar water incursion into the Montalbano Jonico basin (Fig. 13). On land intensive arid conditions developed, as attested by the PTI curve reaching its minimum in the uppermost MIS 20 (Fig. 7) (Bertini et al., 2015, this study). A nearly concomitant Ice Rafted Detritus peak at the Ocean Drilling Program (ODP) Site 980 (Wright and Flower, 2002) (Fig. 13) might suggest that calcareous plankton pattern at the Ideale section is a local response to Atlantic Heinrich-like event (Maiorano et al., 2016). Upwards, distinct changes in calcareous plankton assemblages highlight shorter warming/cooling surface water episodes throughout the latest MIS 20 (Fig. 13). The decrease of the cold water calcareous plankton taxa (*Coccolithus pelagicus* spp. *pelagicus* and *Neogloboquadrina pachyderma* sinistral) together with a short-term peak of *Florisphaera profunda*, point to a slight warming in the surface waters (from 787.6 ka to 786 ka) and reduced seasonal upwelling conditions (increase of *Globorotalia inflata*), interrupted by a short cool period (centered at 785.8 ka) just before the MIS 19c inception. These warm and cold phases were related to the warm Bølling–Allerød and the cooling episode of Younger Dryas (Mangerud et al., 1974) respectively (see Fig. 9 in Maiorano et al., 2016). The recognition of Younger Dryas-like cold and dry event at the Ideale section, like at the Sulmona record (Giaccio et al., 2015), represents an additional and invaluable means to detect the end of glacial phase and interglacial onset, at the end of terminal bipolar seesaw oscillation (Broecker, 1998; Tzedakis et al., 2012a; Past Interglacials Working Group of PAGES 2016).

The onset of MIS 19c at 785.4 ka is marked by a distinct climate warming in both continental and marine proxies (Fig. 13), suggesting higher temperature of sea surface waters and on land climate amelioration (Maiorano et al., 2016). Higher abundances of calcareous plankton warm-water taxa are recorded during MIS 19c (Fig. 13); the sharp increase of mesothermic arboreal pollen taxa describes a rapid enhance of annual precipitation that persisted through MIS 19c, although pollen

record recognized two short-term relatively dry phases within this sub-stage (events 1 and 2, Fig. 13), marked by an unusual expansion of cosmopolitan herbaceous taxa. The event 2 at 775.9 ka is very close to the beginning of the higher $^{10}Be/^{9}Be$ ratio (771.9-776.4 ka), possibly in relation with the low paleointensity during MBB (see discussion in Bertini e al., 2015).

The end of full interglacial (MIS 19c) at 774.1 ka is marked by $\delta^{18}O$ record and concurrent decrease of mesothermic arboreal pollen taxa, as well as by the patterns of calcareous plankton taxa. The warmer climate conditions during MIS 19c persisted for ~11.3 ka. This extent is in agreement with the duration of MIS 19c recorded in the lacustrine Sulmona section (i.e. 10.8 ka; Giaccio et al., 2015) or implied by North Atlantic records (i.e. 12.5-10.5 ka; Tzedakis et al., 2012b). The warm climate phase of MIS19c, relatively more stable than the following ones, is in agreement with lower sedimentation rate (Fig. 11), which is consistent with lower sediment input into the basin during a high sea-level (higher depth and distality extending slightly above V4 deposition, Fig. 7).

Within MIS 19c, the shallow-water analogue of the "red interval" ("ghost sapropel", Emeis et al., 2000), i-cycle 74 (Lourens, 2004), was inferred by Maiorano et al. (2016) based on continental and marine proxies, here well documented by the very low values in $\delta^{13}C_{C.carinata}$ curve from 785.0 ka to 782.6 ka, concurrent with lower $\delta^{18}O$ values and peculiar patterns of selected taxa (Fig. 14). The lowest benthic $\delta^{13}C$ values suggest higher surface water primary productivity and higher organic matter flux to the sea floor, as expected during a sapropelic event. It is worth noting the distinct co-occurrence of lower oxygen content at the sea-bottom as attested by the increase of benthic foraminifera infauna/epifauna ratio and of the peak of *Polysphaeridium zoharyi* (Maiorano et al. 2016), both consistent with the oceanographic condition during sapropel formation, within the $\delta^{13}C$ minimum. The "red interval"- i-cycle 74 represents a key level of chronological importance at the scale of Mediterranean Basin improving the strong correlation of the section. Furthermore, the Ideale section offers the first estimation for the duration (i.e. 2.5 ka) of this event in an on land marine succession.

Following interglacial MIS 19c, from 774.1 ka to 772.3 ka, the $\delta^{18}O$ depicts the pattern of MIS 19b and upward the pattern of MIS 19a, towards the glacial MIS 18 inception at 757 ka (Fig. 13), that are related to the reestablishment of millennial-scale variability and bipolar seesaw (Fig. 9). The patterns of calcareous plankton and mesothermic arboreal pollen taxa parallel the $\delta^{18}O$ stadials-interstadial oscillations. This climate trend at the Ideale section is more detailed than at any other known marine record, and extremely coherent with patterns in North and Central Atlantic marine archives starting from the end of MIS 19c (Channell et al., 2010; Tzedakis et al., 2012a, b;

560 Emanuele et al., 2015; Ferretti et al., 2015; Sánchez-Goñi et al., 2016), Antarctic EDC ice core
561 record (Jouzel et al., 2007; Pol et al., 2010), Greenland GLT _syn (Barker et al., 2011), and in
562 lacustrine sediments from central Italy (Giaccio et al., 2015) (Fig. 9). In all these records, the most
563 relevant evidence is that the MIS 19c is the true interglacial warm phase; after that the 'MIS 19
564 glacial' (sensu Giaccio et al., 2015) begins with multiple minor cold-warm climate phases (Fig. 9),
565 near the mean insolation minimum and the onset of bipolar-seesaw climate variability, when North
566 Atlantic IRD occurs (Tzedakis et al., 2012a), close to the MBB (Channel et al., 2010). Interestingly,
567 the high-resolution of the Montalbano Jonico succession makes it possible, for the first time, to
568 address properly the duration of such rapid oscillations that are very rapid (i.e. <200 years), and
569 seem to be observed in all paleoceanographic proxies but are especially clear in the $\delta^{18}O$ and $\delta^{13}C$
570 records at the Ideale section (Fig. 9). Similar observations were made by Giaccio et al., (2015) in
571 the continental record of Sulmona. The origin (s) and mechanism(s) behind such fast changes in
572 both oceanic conditions as well as hydrological patterns on land are still under investigation
573 (Bassinot et al., in prep). They could be due to several competing factors such as the arrival of
574 freshwater pulse from the Atlantic ocean linked to the ice shelf destabilizations (Sanchez Goni et
575 al., 2016) combined with rapid and repeated intensification of the tropical moisture transport related
576 to the migration of the InterTropical Convergence Zone front during precession minima (Bassinot et
577 al., in prep). New investigations are in progress including Mg/Ca and Δ47 measurements on
578 planktonic and benthic foraminifera, respectively, that will allow reconstructing the temperature
579 variations in the water column associated to such rapid changes.
580
581 **5. Proposed GSSP for the Middle Pleistocene Subseries/Subepoch and Stage/Age**
582 Name of the boundary: the name proposed for the base of the Middle Pleistocene Stage/Age is
583 Ionian, in accordance with the first name proposed by Cita and Castradori (1994;1995) and widely
584 used in literature.
585 GSSP definition: the golden spike is proposed at the base of tephra V4, a lithologic marker well
586 visible in the Ideale section (Fig. 15A), in the auxiliary twin CM section (Fig. 15B), and identified
587 in many other outcrops in the Montalbano Jonico badlands (Fig. 3). It falls at the MIS19c/19b
588 transition and within the $^{10}Be/^{9}Be$ peak.
589 Stratigraphic position and global significance of the boundary: V4 is at 3660 cm in the Ideale
590 section (15.5528, 40.2928, WGS 84/UTM zone 33N), at the MIS19c/19b transition. It marks the
591 Matuyama-Brunhes boundary since it occurs in the middle of the atmospheric ^{10}Be overproduction
592 linked to the Earth magnetic dipole low which accompanies the last polarity reversal. The $^{10}Be/^{9}Be$

593 ratio shows a characteristic twofold increase from 3430 cm to 4075 cm, at the end of MIS 19c-early
594 MIS 19b, in good agreement with the timing of the large ^{10}Be-flux peak recorded in the EDC ice
595 core and in many marine records (Fig. 12). Therefore, the selection of V4, as the level designed to
596 represent the GSSP, respects the most widespread practice to locate it exactly in a lithologic level
597 where precise and globally correlatable events occur.
598 The best age estimation of V4 and MBB: The ^{40}Ar/^{39}Ar age of V4 is 773.9 ± 1.3 ka; V4 is the most
599 precisely dated tephra within the MIS 19 archives and is furthermore coeval with the global scale
600 MIS 19c-19b transition and with the MBB. The age of concurrent peak of ^{10}Be/^{9}Be ratio is
601 estimated between 771.9 ka and 776.4 ka, based on our robust age-model obtained by orbital
602 tuning, in good agreement with the age of Matuyama-Brunhes polarity reversal recorded in most
603 marine sequences (Fig. 12).
604 Additional stratigraphical/paleoenvironmental constraints close to V4 (Figs. 7-15) are:
605 1) The occurrence of "red interval" (ghost sapropel) in MIS 19c, associated to i-cycle 74, from
606 2620 cm to 2840 cm (mid-point age at 784 ka) as evidenced by the minimum values in
607 $\delta^{13}C_{C.carinata}$ and $\delta^{18}O_{M.barleanum}$ records and by the pattern of selected taxa of calcareous
608 plankton, dinocysts and benthic foraminifera. The sapropel falls at the beginning of the lowest
609 dark-grey band well visible in the field (Figs. 7-8, 14-15).
610 2) The end of the temporary disappearance of nannofossil *Gephyrocapsa omega* at 5354 cm (760
611 ka), the unique biostratigraphic event which approximates the MBB, and is useful for long-
612 distance correlation.
613 3) Termination IX, at 1950 cm (789.5 ka), which corresponds to a phase of expansion of the open
614 landscape (dry steppe), and of polar-subpolar taxa increase in calcareous plankton assemblages.
615 4) The short-term cold/dry phase (YD-like event) centered at ca. 785.8 ka just before the MIS 19c
616 onset, and interpreted as the global-scale signature of the end of terminal bipolar seesaw
617 oscillation.
618 5) The onset of MIS 19c at 2580cm (785.4 ka), marked by a shift to lighter values of oxygen
619 isotope record and by a distinct climate amelioration recorded by several marine proxies and, on
620 land, by temperate forest pollen taxa spread pointing out to warm and moist atmospheric
621 conditions.
622 6) The maximum flooding (MF in Figs. 7, 15) recorded by the occurrence of the *Neopycnodonte*
623 *cochlear* clusters between 3070 cm and 3370 cm (777-780 ka), easy to be found in the field
624 below V4. It is nearly concurrent with the increase of thermophilous arboreal taxa, after a short-
625 term expansion of cosmopolitan herbaceous (Fig. 13).

7) The maximum depth (MD, Figs. 7, 15) from 3370 cm to 3770 cm (777-773 ka), based on macrobenthic invertebrate communities and increased deepening recorded by benthic foraminifera assemblages in marine record, concurrent with the higher pollen distality index and a major expansion of mesothermic arboreal taxa on land.

The stratigraphic, chronological, and paleoenvironmental constraints at the Ideale section (Fig. 15A) prove that it holds all the requirements indicated by Remane et al. (1996) for the selection of the GSSP of the Middle Pleistocene Subseries/Subepoch and Ionian Stage/Age (Table II), as documented by multiple high resolution proxies. The CMs (Fig. 15B) represents a valuable auxiliary reference for the GSSP interval.

Acknowledgments

The engineers (Georges Aumaître and Karim Keddadouche) and the technicians (Sandrine Choy and Laetitia Gacem) from ASTER laboratory are acknowledged for their essential contribution in producing ^{10}Be data. A particular acknowledgement is addressed to A. D'Alessandro who improved the quality of the research at the Montalbano Jonico section as well as many other investigators that in the years have been involved in the study of the Montalbano Jonico sections. Many thanks to L. Sagnotti for his determination in understanding the greigite behavior at the Montalbano clay.

References

Aiello, G., Barra, D., Parisi, R., 2015.Lower-Middle Pleistocene ostracod assemblages from the Montalbano Jonico section (Basilicata, southern Italy). Quaternary International, 383, 47-73. http://dx.doi.org/10.1016/j.quaint.2014.11.010

Amorosi, A., Antonioli, F., Bertini, A., Marabini, S., Mastronuzzi, G., Montagna, P., Negri, A., Rossi, V., Scarponi, D., Taviani, M., Angeletti, L., Piva, A., Vai, G.B., 2014. The Middle-Upper Pleistocene Fronte section (Taranto, Italy): an exceptionally preserved marine record of the last interglacial. Global and Planetary Change 119, 23-38.

Azzaroli, A., Perno, U., Radina, B., 1968. Note illustrative della Carta Geologica d'Italia alla scala 1:100.000, Foglio 188 Gravina di Puglia. Serv. Geol. Ital. 57 pp

Backman, J., Raffi, I., Rio, D., Fornaciari, E., Pälike, H., 2012. Biozonation and biochronology of Miocene through Pleistocene calcareous nannofossils from low and middle latitudes. Newsletters on Stratigraphy, 45(3):221–244. http://dx.doi.org/10.1127/0078-0421/2012/0022

Balduzzi, A., Casnedi, R., Crescenti, U., Mostardini, F., Tonna M., 1982,. Il Plio-Pleistocene del sottosuolo del bacino lucano (Avanfossa appenninica). Geologica Romana, 21, 89-111.

Barker, S., Knorr, G., Edwards, R.L., Rarrenin, F., Putnam, A.E., Skinner, L.C., Wolff, E., Ziegler, M. (2011) - 800,000 years of abrupt climate variability. Science, 334, 347–351.

Bassinot, F., Labeyrie, L., Vincent, E., Quidelleur, X., Shackleton, N. and Lancelot, Y., 1994. The astronomical theory of climate and the age of the Brunhes-Matuyama magnetic reversal. Earth Planet. Sci. Lett., 126 (1-3), 91-108. Doi:10.1016/012-821X(94)90244-5.

665 Bassinot, F., Nomade, S., Marino, M., Maiorano, P., Dewild,e F., Esguder, G., Pereira, A.,
666 Blamart, D., Girone, A., Scao, V., Toti, F., Bertini, A., Simon, Q., Combourieu-NeboutN.,
667 Bourles, D., Ciaranfi, N. High-resolution foraminifer stable isotope record of MIS 19 at
668 Montalbano Jonico, southern Italy: a window into Mediterranean climatic variability during a
669 low-excentricity interglacial and the Early –Middle Pleistocene transition. In prep. Quaternary
670 Science Reviews.
671 Bertini, A., Toti, F., Marino, M., Ciaranfi, N., 2015.Vegetation and climate across the Early-Middle
672 Pleistocene transition at the Montalbano Jonico section (southern Italy). Quaternary International,
673 383, 74-88. http://dx.doi.org/10.1016/j.quaint.2015.01.003
674 Bonardi, G., D'Argenio, B., Di Nocera, S., Marsella, E., Pappone, G., Pescatore, T.S.S., Senatore,
675 M.R., Sgrosso, I., Ciaranfi, N., Pieri, P., Ricchetti, G., 1988. Carta geologica dell'Appennino
676 meridionale. 74° Cong. Soc. Geol. It., Carta geologica in scala 1: 250.000.
677 Brilli, M., 1998. Stratigrafia isotopica del carbonio e dell'ossigeno della successione infra e
678 mesopliocenica di Montalbano Jonico (Basilicata, Italia meridionale). Tesi di Dottorato di
679 Ricerca in Scienze della Terra XI ciclo. Università degli Studi di Roma "La Sapienza", 112 pp.
680 Brilli, M., Lerche, J., Ciaranfi, N., Turi, B., 2000. Evidence of precession and obliquity orbital
681 forcing in Oxygen 18 isotope composition of Montalbano Jonico section (Basilicata, southern
682 Italy). Applied Radiation and Isotope, 52, 957-964.
683 Broecker, W.S., 1998. Paleocean circulation during the last deglaciation: a bipolar seesaw?
684 Paleoceanography 13 (2), 119–121.
685 Brown, L.L., Pickens, J.C., Singer, B.S., Jicha, B.R., 2004. Paleomagnetic directions and
686 40Ar/39Ar ages from the Tatara–San Pedro volcanic complex, Chilean Andes: lava record of a
687 Matuyama–Brunhes precursor? J. Geophys. Res. 109, B12101.
688 http://dx.doi.org/10.1029/2004JB003007..
689 Capraro, L., Ferretti, P., Macrì, P., Scarponi, D., Tateo, F., Fornaciari, E., Bellini, G., Dalan, G.,
690 2017. The Valle di Manche section (Calabria, Southern Italy): A high resolution record of the
691 Early-Middle Pleistocene transition (MIS 21-MIS 19) in the Central Mediterranean. Quaternary
692 Science Reviews, 165, 31-48.
693 Carcaillet, J.T., Thouveny, N., Bourlès, D.L., 2003. Geomagnetic moment instability between 0.6
694 and 1.3Ma from cosmonuclide evidence. Geophys. Res. Lett.30 (15), 1792.
695 http://dx.doi.org/10.1029/2003GL017550.
696 Caron, B., Siani, G., Sulpizio, R., Zanchetta, G., Paterne, M., Santacroce, R., Terna, E., Zanella, E.,
697 2012. Late Pleistocene to Holocene tephrostratigraphic record from the Northern Ionian Sea. Mar.
698 Geol. 311, 41–51.
699 Casnedi R., 1988. La Fossa bradanica: origine, sedimentazione e migrazione. Memorie Società
700 Geologica Italiana, 41, 439-448.
701 Ceregato, A., Raffi, S., Scarponi, D., 2007. The circalittoral/bathyal in the Middle Pliocene of
702 Northern Italy: the case of the Korobkovia oblonga–Jupiteria concave paleocommunity type.
703 Geobios 40, 555–572.
704 Channell, J.E.T, 2017. Complexity in Matuyama–Brunhes polarity transitions from North Atlantic
705 IODP/ODP deep-sea sites. Earth and Planetary Science Letters 467 , 43-56
706 Channell, J.E.T., Curtis, J.F., Flower, B.P., 2004. The Matuyama-Bruhnes interval (500-900 ka) in
707 North Atlantic drift sediments. Geophysical Journal International, 158, 489-505.
708 Channell, J.E.T., Hodell, D.A., Xuan, C., Mazaud, A., Stoner, J.S., 2008. Age calibrated relative
709 paleointensity for the last 1.5Myr at IODP Site U1308 (North Atlantic). Earth Planet. Sci.
710 Lett.274, 59–71.
711 Channell, J.E.T., Hodell, D.A., Singer, B.S., Xuan, C., 2010. Reconciling astrochronological and
712 40Ar/39Ar ages for the Matuyama-Brunhes boundary in the late Matuyama Chron.
713 Geochemistry, Geophysics, Geosystems 11, Q0AA12. http://dx.doi.org/10.1029/2010GC003203.

714 Channell, J.E.T., Xuan, C., Hodell, D.A., 2009. Stacking paleointensity and oxygen iso-tope data
715 for the last 1.5 Myr (PISO-1500). Earth Planet. Sci. Lett.283 (1–4), 14–23.
716 http://dx.doi.org/10.1016/j.epsl.2009.03.012.
717 Ciaranfi, N., D'Alessandro, A., 2005. Overview of the Montalbano Jonico area and section: a
718 proposal for a boundary stratotype for the lower-middle Pleistocene, southern Italy Foredeep.
719 Quaternary International 131, 5-10.
720 Ciaranfi, N., D'Alessandro, A., Girone, A., Maiorano, P., Marino, M., Soldani, D., Stefanelli, S.,
721 2001. Pleistocene sections in the Montalbano Jonico area and the potential GSSP for Early-
722 Middle Pleistocene in the Lucania Basin (southern Italy). Memorie di Scienze Geologiche, 53,
723 67-83.
724 Ciaranfi N., D'Alessandro A., Marino M., 1997. A candidate section for the lower-middle
725 Pleistocene boundary (Apennine foredeep, South Italy). In: Naiwen W., Remane J. (Eds.),
726 Proceedings 30th International Geological Congress. Vol. 11, pp. 201-211.
727 Ciaranfi, N., D'Alessandro, A., Marino, M., Sabato, L., 1994. The Montalbano Jonico Section in
728 the Bradanic Foredeep (southern Italy): a potential early-middle Pleistocene Boundary Stratotype.
729 Contribution in Cita, M.B. and Castradori, D. (1994) "Workshop on marine sections from the
730 Gulf of Taranto (Southern Italy) usable as potential stratotypes for the GSSP of the Lower,
731 Middle and Upper Pleistocene (Bari, Italy, sept. 29- oct. 4, 1994). Il Quaternario, 7, pp. 677-692.
732 Ciaranfi, N., Lirer, F., Lirer, L., Lourens, L.J., Maiorano, P., Marino, M., Petrosino, P., Sprovieri,
733 M., Stefanelli, S., Brilli, M., Girone, A., Joannin, S., Pelosi, N., Vallefuoco, M., 2010. Integrated
734 stratigraphy and astronomical tuning of the Lower-Middle Pleistocene Montalbano Jonico land
735 section (southern Italy). Quaternary International, 210, 109-120.
736 Cita, M.B, Castradori, D., 1994. "Workshop on marine sections from the Gulf of Taranto (Southern
737 Italy) usable as potential stratotypes for the GSSP of the Lower, Middle and Upper Pleistocene
738 (Bari, Italy, sept. 29-oct. 4, 1994). Il Quaternario, 7, 677-692.
739 Cita, M.B., Castradori, D., 1995, Rapporto sul Workshop "Marine sections from the Gulf of
740 Taranto (Southern Italy) usable as potential stratotypes for GSSP of the Lower, Middle and Upper
741 Pleistocene". Boll. Soc. Geol. It., v.114, pp. 319-336
742 Cita, M.B., Gibbard, P.L., Head, M.J., and The Subcommission on Quaternary Stratigraphy, 2012.
743 Formal ratification of the GSSP for the base of the Calabrian Stage (second stage of the
744 Pleistocene Series, Quaternary System). Episodes 35(3): 388–397.
745 Coe, R.S., Singer, B.S., Pringle, M.S., Zhao, X.X., 2004, Matuyama–Brunhes reversal and
746 Kamikatsura event on Maui: Paleomagnetic directions, 40Ar/39Ar ages and implications: Earth
747 and Planetary Science Letters, v. 222, p. 667–684, doi: 10.1016/j.epsl.2004.03.003
748 Cohen, K.M., Gibbard, P. 2011. Global chronostratigraphical correlation table for the last 2.7
749 million years. Subcommission on Quaternary Stratigraphy (International Commission on
750 Stratigraphy), Cambridge, England.
751 D'Alessandro, A., La Perna, R., Ciaranfi, N., 2003 - Response of macrobenthos to changes in
752 paleoenvironment in the Lower-Middle Pleistocene (Lucania Basin, southern Italy). Il
753 Quaternario, 16, 167-182.
754 Doglioni, C., Tropeano, M., Mongelli, F., Pieri, P., 1996. Middle-Late Pleistocene uplift of Puglia:
755 an "anomaly" in the Apenninic foreland. Mem. Soc. Geol. Ital. 51, 101–117.
756 Dreyfus, G.B., Raisbeck ,G.M., Parrenin, F., Jouzel, J., Guyodo, Y., Nomade, S., Mazaud A., 2008.
757 An ice core perspective on the age of the Matuyama-Brunhes boundary. Earth and Planetary
758 Science Letters, 274, 151-156.
759 Emanuele, D., Ferretti, P., Palumbo, E., Amore, F.O., 2015. Sea-surface dynamics and
760 palaeoenvironmental changes in the North Atlantic Ocean (IODP Site U1313) during Marine
761 Isotope Stage 19 inferred from coccolithophore assemblages. Palaeogeogr. Palaeoclimatol.
762 Palaeoecol. 430, 104–117.

763 Emeis, K., Sakamoto, T., Wehausen, R., Brumsack, H.J., 2000. The sapropel record of the eastern
764 Mediterranean Sea - results of Ocean Drilling Program Leg 160. Palaeogeogr. Palaeoclimatol.
765 Palaeoecol. 158, 371–395.
766 Ferretti, P., Crowhurst, S.J., Naafs, B.D.A., Barbante, C., 2015. TheMarine Isotope Stage 19 in the
767 mid-latitude North Atlantic Ocean: astronomical signature and intra-interglacial variability. Quat.
768 Sci. Rev. 108, 95–110.
769 Giaccio, B., Regattieri, E., Zanchetta, G., Nomade, S., Renne, P.R., Sprain, C.J, Drysdale, R.N.,
770 Tzedakis, P.C., Messina, P., Scardia, G., Sposato, A., Bassinot, F., 2015. Duration and dynamics
771 of the best orbital analogue to the present interglacial. Geology. doi:10.1130/G36677.1
772 Gibbard, P. Head, M.J., Walker, M.J.C. & The Subcommission on Quaternary Stratigraphy, 2009.
773 Formal ratification of the Quaternary System/Period and the Pleistocene Series/Epoch with a base
774 at 2.58 Ma. Journal of Quaternary Science 25, 96–102.
775 Gibbard, P.L., Head, M.J., 2010. The newly-ratified definition of the Quaternary System/Period and
776 redefinition of the Pleistocene Series/Epoch, and comparison of proposals advanced prior to
777 formal ratification. Episodes 33, 152-158.
778 Gibbard, P.L., Head, M.J., Walker, M.J.C., The Subcommission on Quaternary Stratigraphy, 2010.
779 Formal ratification of the Quaternary System/Period and the Pleistocene Series/Epoch with a base
780 at 2.58 Ma. Journal of Quaternary Science 25 (2), 96-102.
781 Girone, A., 2005. Response of otolith assemblages to sea-level fluctuations at the Lower
782 Pleistocene Montalbano Jonico section (southern Italy). Bollettino della Società Paleontologica
783 Italiana, 44 (1): 35-45
784 Girone, A., Capotondi, L., Ciaranfi, N., Di Leo, P., Lirer, F., Maiorano, P., Marino, M., Pelosi, N.,
785 Pulice, I., 2013. Paleoenvironmental change at the lower Pleistocene Montalbano Jonico section
786 (southern Italy): global versus regional signals. Palaeogeogr. Palaeoclimat. Palaeoec., 371, 62-79.
787 Gradstein, F.M., Ogg, J.G., Schmitz, M.D., and Ogg, G.M., eds, 2012, The Geological Time Scale
788 2012, Amsterdam, Elsevier, 2 vols., 1144 pp.
789 Head, M.J., Gibbard, P.L., 2015a. Formal subdivision of the Quaternary System/Period: Past,
790 present, and future. Quaternary International, 383, 4–35.
791 Head, M.J., Gibbard, P.L, 2015b. Early-Middle Pleistocene transitions: linking terrestrial and
792 marine realms. Quaternary International, 389, 7-46.
793 Horng, C.S., Lee, M.Y., Palike, H., Wei, K.Y., Liang, W.T., Iizuka, Y., Torii, M., 2002.
794 Astronomically calibrated ages for geomagnetic reversals within the Matuyama chron. Earth
795 Planets Space54, 679–690.
796 Joannin, S., Ciaranfi N., Stefanelli, S., 2008. Vegetation changes during the late Early Pleistocene at
797 Montalbano Jonico (Province of Matera, southern Italy) based on pollen analysis.
798 Palaeogeography, Palaeoclimatology, Palaeoecology, 270, 92–101.
799 Jouzel, J., Masson-Delmotte, V., Cattani, O., Dreyfus, G., Falourd, S., Hoffmann, G., Minster, B.,
800 Nouet, J., Barnola, J.M., Chappellaz, J., Fischer, H., Gallet, J.C., Johnsen, S., Leuenberger, M.,
801 Loulergue, L., Luethi, D., Oerter, H., Parrenin, F., Raisbeck, G., Raynaud, D., Schilt, A.,
802 Schwander, J., Selmo, E., Souchez, R., Spahni, R., Stauffer, B., Steffensen, J.P., Stenni, B.,
803 Stocker, T.F., Tison, J.L., Werner, M., Wolff, E.W., 2007. Orbital and millennial Antarctic
804 climate variability over the past 800,000 years. Science, 317, 793-796.
805 Kleiven, H., Hall, I.R., McCave, I.N., Knorr, G., Jansen, E., 2011. North Atlantic coupled deep-
806 water flow and climate variability in the middle Pleistocene. Geology, 39 (4), 343-346.
807 Konijnendijk, T.Y.M., Ziegler, M., Lourens, L.J., 2014. Chronological constraints on Pleistocene
808 sapropel depositions from high-resolution geochemical records of ODP Sites 967 and 968.
809 Newsl. Stratigr. 47 (3), 263–282.

Konijnendijk, T.Y.M., Ziegler, M., Lourens, L.J., 2015. On the timing and forcing mechanisms of late Pleistocene glacial terminations: Insights from a new high-resolution benthic stable oxygen isotope record of the eastern Mediterranean. Quaternary Science Reviews 129, 308-320.
Langereis, C.G., Dekkers, M.J., de Lange., G.J., Paterne, M., van Santvoort, P.J.M., 1997. Magnetostratigraphy and astronomical calibration of the last 1.1 Myr from an eastern Mediterranean piston core and dating of short events in the Brunhes. Geophys. J. Int. 129, 75–94.
Laskar, J., Robutel, P., Joutel, F., Gastineau, M., Correia, A.C.M., Levrard, B., 2004. A long termnumerical solution for the insolation quantities of the Earth. Astron. Astrophys.428, 261–285. http://dx.doi.org/10.1051/0004-6361:20041335.
Lisiecki, L.E., Raymo, M.E., 2005. A Pliocene-Pleistocene stack of 57 globally distributed benthic δ18O records. Paleoceanography, 20, PA1003.
Lisiecki, L. E., Stern, J. V., 2016. Regional and global benthic $\delta^{18}O$ stacks for the last glacial cycle, Paleoceanography, 31, 1-27, doi:10.1002/2016PA003002.
Lourens, L.J., 2004. Revised tuning of Ocean Drilling Program Site 964 and KC01B (Mediterranean) and implications for the δ18O, tephra, calcareous nannofossil, and geomagnetic reversal chronologies of the past 1.1 Myr. Paleoceanography 19, PA3010.
Lourens, L.J., Hilgen, F.J., Raffi, I., 1998. Base of large Gephyrocapsa and astronomical calibration of early Pleistocene sapropels in Site 967 and Hole 969D: solving the chronology of the Vrica section (Calabria, Italy). in Robertson, H.F., Emeis, K., Richter, C., et al., eds., Proceedings of the Ocean Drilling Program: Scientific Results, v. 160, pp. 191–198. College Station, TX.
Lourens, L., Hilgen, F., Shackleton, N.J., Laskar, J., Wilson, D., 2004. The Neogene period. In: Gradstein, F.M., Ogg, J.G., Smith, A.G. (Eds.), A Geological Time Scale. Cambridge University Press, pp. 409-440.
Maiorano, P., Aiello, G., Barra, D., Di Leo, P., Joannin, S., Lirer, F., Marino, M., Pappalardo, A., Capotondi, L., Ciaranfi, N., Stefanelli, S., 2008. Paleoenvironmental changes during sapropel 19 (i-cycle 90) deposition: evidences from geochemical, mineralogical and microplaoentological proxies in the mid Pleistocene Montalbano Jonico land section (southern Italy). Palaeogeography, Palaeoclimatology, Palaeoecology, 257, 308-334.
Maiorano, P., Bertini, A., Capolongo, D., Eramo, G., Gallicchio, S., Girone, A., Pinto, D., Toti, F., Ventruti, G., Marino, M., 2016. Climate signatures through the Marine Isotope Stage 19 in the Montalbano Jonico section (Southern Italy): a land-sea perspective. Palaeogeography, Palaeoclimatology, Palaeoecology, 461, 341–361.
Maiorano, P., Capotondi, L., Ciaranfi, N., Girone, A., Lirer, F., Marino, M., Pelosi, N., Petrosino, P., Piscitelli, A., 2010. Vrica-Crotone and Montalbano Jonico sections: a potential unit-stratotype of the Calabrian Stage. Episodes, 33, 218-233.
Maiorano, P., Marino, M., 2004. Calcareous nannofossil bioevents and environmental control on temporal and spatial pattern at the early-middle Pleistocene. Marine Micropaleontology, 53, 405-422.
Maiorano, P., Marino, M., Di Stefano, E., Ciaranfi, N., 2004. Calcareous nannofossil events in the lower-middle Pleistocene transition at the Montalbano Jonico section and ODP Site 964: calibration with isotope and sapropel stratigraphy. Rivista Italiana di Paleontologia e Stratigrafia, 110, 547-557.
Mangerud, J., Andersen, S.T., Berglund, B.E., Donner, J.J., 1974. Quaternary Stratigraphy of Norden, a Proposal for Terminology and Classification. Boreas 4, 109–128.
Marino, M., 1996. Quantitative nannofossil biostratigraphy of the lower-middle Pleistocene Montalbano Jonico section, southern Italy. Paleopelagos, 6, 347-360.
Marino, M., Aiello, G., Barra, D., Bertini, A., Gallicchio, S., Girone, A., La Perna, R., Lirer, F., Maiorano, P., Petrosino, P., Quivelli, O., Toti, F., Ciaranfi, N., 2016. The Montalbano Jonico

858 section (South Italy) as a reference for the Early/Middle Pleistocene boundary. Alp.
859 Mediterranean Quat. 29 (1), 45–57.
860 Marino, M., Bertini, A., Ciaranfi, N., Aiello, G., Barra, D., Gallicchio, S., Girone, A., La Perna, R.,
861 Lirer, F., Maiorano, P., Petrosino, P., Toti, F., 2015. Paleoenvironmental and climatostratigraphic
862 insights for Marine Isotope Stage 19 (Pleistocene) at the Montalbano Jonico section, South Italy.
863 Quaternary International, 383, 104-115. http://dx.doi.org/10.1016/j.quaint.2015.01.043
864 Mark, D.F., Renne, P.R., Dymock, R.C., Smith, V.C., Simon, J.I., Morgan, L.E., Staff, R.A., Ellis,
865 B.S., Pearce, N.J., 2017. High-precision 40Ar/39Ar dating of Pleistocene tuffs and temporal
866 anchoring of the Matuyama-Brunhes boundary . Quaternary Geochronology 39, 1-23.
867 http://dx.doi.org/10.1016/j.quageo.2017.01.002.
868 Massari, F., Rio, D., Sgavetti, M., Prosser, G., D'Alessandro, A., Asioli, A., Capraro, L., Fornaciari,
869 E., Tateo, F., 2002. Interplay between tectonics and glacioeustasy, Pleistocene of the Crotone
870 Basin, Calabria (southern Italy). Geol. Soc. Am. Bull. 114, 1183–1209
871 Ménabréaz, L., Thouveny, N., Bourlès, D.L., Vidal, L., 2014. The geomagnetic dipole moment
872 variation between 250 and 800 ka BP reconstructed from the authi-genic 10Be/9Be signature in
873 West Equatorial Pacific sediments. Earth Planet. Sci. Lett.385, 190–205.
874 http://dx.doi.org/10.1016/j.epsl.2013.10.037.
875 Miller, K.G., Wright, J.D., 2017. Success and failure in Cenozoic global correlations using golden
876 spikes: A geochemical and magnetostratigraphic perspective. Episodes, 40 (1), 1-22.
877 Mostardini, F., Pieri, P., 1967. Note illustrative della Carta Geologica d'Italia alla scala 1:100.000,
878 Foglio 212 Montalbano Ionico. La Litograf, Roma.
879 Negri, A., Amorosi, A., Antonioli, F., Bertini, A., Florindo, F., Lurcock, P.C., Marabini, S.,
880 Mastronuzzi, G., Regattieri, E., Rossi, V., Scarponi, D., Taviani, M., Zanchetta, G., Vai, G.B.,
881 2015. A potential global boundary stratotype section and point (GSSP) for the Tarentian Stage,
882 Upper Pleistocene, from the Taranto area (Italy): results and future perspectives. Quaternary
883 International, 383, 145-157. doi: 10.1016/j.quaint.2014.08.057
884 North Greenland Ice Core Project Members (NGRIP), 2004. High-resolution record of Northern
885 Hemisphere climate extending into the last interglacial period. Nature 431, 147–151.
886 Okada, M., Suganuma, Y., Haneda, Y., Kazaoka, O., 2017. Paleomagnetic direction and
887 paleointensity variations during the Matuyama-Brunhes polarity transition from a marine
888 succession in the Chiba composite section of the Boso Peninsula, central Japan. Earth, Planets,
889 and Space, 69, 45, DOI 10.1186/s40623-017-0627-1
890 Partridge, T. C. 1997: Reassessment of the position of the Plio-Pleistocene boundary: is there a case
891 for lowering it to the Gauss–Matuyama Palaeomagnetic reversal? Quaternary International 40, 5–
892 10.
893 Past Interglacials Working Group of PAGES (2016), Interglacials of the last 800,000 years, Rev.
894 Geophys., 54, 162–219, doi:10.1002/2015RG000482
895 Patacca, E., Scandone, P., 2007. Geology of the Southern Apennines. Boll. Soc. Geol. Ital., Spec.
896 Issue 7, 75–119.
897 Petrosino P., Jicha B.R., Mazzeo F.C., Ciaranfi N., Girone A., Maiorano P., Marino M., 2015. The
898 Montalbano Jonico marine succession: An archive for distal tephra layers at the Early-Middle
899 Pleistocene boundary in southern Italy. Quaternary International, 383, 89-103.
900 http://dx.doi.org/10.1016/j.quaint.2014.10.049
901 Pieri, P., Sabato, L., Tropeano, M., 1996. Significato geodinamico dei caratteri deposizionali e
902 strutturali della Fossa bradanica nel Pleistocene. Mem. Soc. Geol. Ital. 51, 501–515.
903 Pol K., Masson-Delmotte V., Johnsen S., Bigler M., Cattani O., Durand G., Falourd S., Jouzel J.,
904 Minster B., Parrenin F., Ritz C., Steen-Larsen H. C., Stenni B., 2010. New MIS 19 EPICA Dome
905 C high resolution deuterium data: hints for a problematic preservation of climate variability in the
906 “oldest ice”. Earth and Planetary Science Letters. doi:10.1016/j.epsl.2010.07.030, 2010.

907 Raffi, I., Agnini, C., Backman, J., Catanzariti, R., 2016. A Cenozoic calcareous nannofossil
908 biozonation from low and middle latitudes: A synthesis. J. Nannoplankton Res. 36 (2), 121–132.
909 Raffi, I., Backman, J., Fornaciari, E., Pälike, H., Rio, D., Lourens, L., and Hilgen, F., 2006. A
910 review of calcareous nannofossil astrobiochronology encompassing the past 25 million years:
911 Quaternary Science Reviews, v. 25, pp. 3113–3137.
912 Raisbeck G.M., Yiou F., Cattani O., Jouzel J., 2006. 10Be evidence for the Matuyama-Brunhes
913 geomagnetic reversal in the EPICA Dome C ice core. Nature, 444, 82–84.
914 Remane J., Basset M.G., Cowie J.F., Gohrbandt K.H., Lane H.R., Michelsen O., Naiwen W. (1996)
915 - Revised guidelines for the establishment of global chronostratigraphic standards by the
916 International Commission on Stratigraphy (ICS). Episodes, 19, 77-81.
917 Rio, D., Raffi, I., Villa, G., 1990. Pliocene-Pleistocene distribution patterns in the Western
918 Mediterranean. In: Karstetn, K.A., Mascle, J., et al. (Eds.), Proceedings of ODP, Scientific
919 Results 107, pp. 513-533.
920 Rio, D., Sprovieri, R., Castradori, D., Di Stefano, E., 1998. The Gelasian Stage (Upper Pliocene): a
921 new unit of the global standard chronostratigraphic scale. Episodes, 21 (1), 82-87.
922 Roberts, A.P., Tauxe, L., Heslop, D., 2013. Magnetic paleointensity stratigraphy and high-
923 resolution Quaternary geochronology: successes and future challenges. Quaternary Science
924 Reviews 61, 1-16.
925 Rook, L., Martínez-Navarro, B., 2010. Villafranchian: The long story of a Plio-Pleistocene
926 European large mammal biochronologic unit. Quaternary International, 219, 134-144.
927 Sagnotti, L., Cascella, A., Ciaranfi, N., Macrì, P., Maiorano, P., Marino, M., Taddeucci, J., 2010.
928 Rock magnetism and paleomagnetism of the Montalbano Jonico section (Italy): evidence for late
929 diagenetic growth of greigite and implications for magnetostratigraphy. Geophysical Journal
930 International 180, 1049-1066
931 Sagnotti, L., Giaccio, B., Liddicoat, J.C., Nomade, S., Renne, P.R., Scardia, G., Sprain, C.J., 2015.
932 How fast was the Matuyama–Brunhes geomagnetic reversal? A new subc-entennial record from
933 the Sulmona Basin, central Italy. Geophys. J. Int. 204, 798–812.
934 Sagnotti L., Scardia G., Giaccio B., Liddicoat J.C., Nomade S., Renne P.R., Sprain C.J., 2014.
935 Extremely rapid directional change during Matuyama-Brunhes geomagnetic polarity reversal.
936 Geophysical Journal International. http://dx.doi.org/10.1093/gji/ggu287
937 Sánchez-Goñi, M.F., Rodrigues, T., Hodell, D.A., Polanco-Martínez, J.M., Alonso-García, M.,
938 Hernández-Almeida, I., Desprat, S., Ferretti, P., 2016. Tropically-driven climate shifts in
939 southwestern Europe during MIS 19, a low eccentricity interglacial. Earth Planet. Sci. Lett. 448,
940 81–93.
941 Sella, M., Turci, C., Riva, A., 1988. Sintesi geopetrolifera della Fossa bradanica (avanfossa della
942 Catena appenninica meridionale). Mem. Soc. Geol. It. 41, 87-108.
943 Sgarrella, F., Moncharmont-Zei, M., 1993. Benthic Foraminifera of the Gulf of Naples (Italy):
944 systematics and autecology. Bollettino della Società Paleontologica Italiana 32 (2), 145-264.
945 Shackleton, N. J. (1987). Oxygen isotopes, ice volume and sea-level, Quat. Sci. Rev., 6(3–4), 183-
946 190.
947 Shackleton, N. J., Hall M. A., Boersma, A., 1984. Oxygen and carbon isotope data from Leg 74
948 foraminifers. In Moore, T. C, Jr., Rabinowitz, et al., Init. Repts. DSDP, 74: Washington (U.S.
949 Govt. Printing Office), 599-612.
950 Siani, G., Magny, M., Paterne, M., Debret, M., and Fontugne, M., 2013. Paleohydrology
951 reconstruction and Holocene climate variability in the South Adriatic Sea, Clim. Past, 9, 499–
952 515, doi:10.5194/cp-9-499-2013
953 Siani, G., Sulpizio, R., Paterne, M., and Sbrana, A. 2004. Tephrostratigraphy study for the last
954 18,000 14C years in a deep-sea sediment sequence for the South Adriatic, Quaternary Sci. Rev.,
955 23, 2485–2500.

Simon Q, .Bourlès L.D.,, Bassinot, F.,, Nomade S., Marino, M., Ciaranfi, N., Girone, A., Maiorano, P., Thouveny, N., Choya, S., Dewil, F., Scao, V., Isguder, G., Blamart, D., ASTER Team. 2017. Authigenic 10Be/9Be ratio signature of the Matuyama–Brunhes boundary in the Montalbano Jonico marine succession. Earth and Planetary Science Letters, 460, 255–267

Simon, Q., Bourlès, D.L., Thouveny, N., Horng, J., Valet, J-P., Bassinot, F., Choy, S. (submitted). Cosmogenic signature of geomagnetic reversals and excursions from the Reunion event to the Matuyama-Brunhes transition (0.7 - 2.14 Ma interval). . Earth and Planetary Science Letters

Simon, Q., Thouveny, N., Bourlès, D.L., Bassinot, F., Valet, J.P., Choy, S., Duvivier, A., Villedieu, A., (in prep.). High-resolution authigenic 10Be/9Be ratio signature of the last geomagnetic reversal.

Simon, Q., Thouveny, N., Bourlès, D.L., Valet, J.-P., Bassinot, F., Ménabréaz, L., Guil-lou, V., Choy, S., Beaufort, L., 2016. Authigenic 10Be/9Be ratio signatures of the cosmogenic nuclide production linked to geomagnetic dipole moment variation since the Brunhes/Matuyama boundary. J. Geophys. Res., Solid Earth121. http://dx.doi.org/10.1002/2016JB013335.

Singer, B.S., 2014. A quaternary geomagnetic instability time scale. Quat. Geochronol.21, 29–52.

Singer, B.S., Hoffman, K.A., Coe, R.S., Brown, L.L., Jicha, B.R., Pringle, M.S., Chauvin, A., 2005. Structural and temporal requirements for geomagnetic field reversal deduced from lava flows. Nature434, 633–636.

Stefanelli S., 2003. Benthic foraminiferal assemblages as tools for paleoenvironmental reconstruction of the early-middle Pleistocene Montalbano Jonico composite section. Bollettino della Società Paleontologica Italiana, 42, 281-299.

Stefanelli S., 2004. Cyclic stages in oxygenation based on foraminiferal microhabitats: early-middle Pleistocene, Lucania basin, southern Italy. Journal of Micropaleontology, 23, 81-95.

Stefanelli, S., Capotondi, L., 2008. Foraminiferal response to the deposition of insolation cycle 90 sapropel in different Mediterranean areas. Journal of Micropaleontology, 27, 45-61. Doi: 10.1144/jm.27.1.45.

Stefanelli S., Capotondi L., Ciaranfi N., 2005. Foraminiferal record and environmental changes during the deposition of early-middle Pleistocene sapropels in southern Italy. Palaeogeography, Palaeoclimatology, Palaeoecology, 216, 27-52.

Suc J.-P., Combourieu-Nebout N., Seret G., Popescu S.A., Klotz S., Gautier F., Clauzon G., Westgate J., Insinga D., Sandhu A.S., 2010. The Crotone series: a synthesis and new data. Quaternary International, 219, 121–133.

Suganuma, Y., Okada, M., Horie, K., Kaiden, H., Takehara, M., Senda, R., Kimura, J.-I., Kawamura, K., Haneda, Y., Kazaoka, O., Head, M.J., 2015. Age of Matuyama–Brunhes boundary constrained by U–Pb zircon dating of a widespread tephra. Geology43, 491–494. http://dx.doi.org/10.1130/G36625.1

Suganuma Y., Okuno J., Heslop D., Roberts A.P., Yamazaki T., Yokoyama Y. (2011) - Post-depositional remanent magnetization lock-in for marine sediments deduced from 10Be and paleomagnetic records through the Matuyama-Brunhes boundary: Earth and Planetary Science Letters, 311, 39–52, doi:10.1016/j.epsl .2011 .08.038.

Suganuma Y., Yokoyama Y., Yamazaki T., Kawamura K., Horng C.-S., Matsuzaki H., 2010. 10Be evidence for delayed acquisition of remanent magnetization in marine sediments: Implications for a new age for the Matuyama-Brunhes boundary. Earth and Planetary Science Letters, 296, 443-450, doi:10.1016/j.epsl.2010.05.031

.Tauxe, L., Herbert, T., Shackleton, N.J., Kok, Y.S., 1996. Astronomical calibration of the Matuyama-Brunhes boundary: consequences for magnetic remanence acquisition in marine carbonates and the Asian loess sequences. Earth Planet. Sci. Lett. 140, 133-146.

Toti, F., 2015. Interglacial vegetation patterns at the Early-Middle Pleistocene transition: a point of view from Montalbano Jonico section (southern Italy). Alpine and Mediterranean Quaternary, 28 (2), 131 - 143

Tzedakis ,P.C., Channell, J.E.T., Hodell, D.A., Kleiven, H.F., Skinner, L.C., 2012a. Determining the natural length of the current interglacial. Nature Geoscience, 5. http://dx.doi.org/10.1038/NGEO1358.

Tzedakis, P.C., Wolff, E.W., Skinner, L.C., Brovkin, V., Hodell, D.A., McManus, J.F., Raynaud, D., 2012b. Can we predict the duration of an interglacial? Clim. Past 8, 1473–1485.

Vai, G.B., 2001. GSSP, IUGS and IGC, an endless story towards a common language in th earth science. Episodes 24, 29-31.

Valet, J.P., Bassinot, F., Bouilloux, A., Bourlès, D.L., Nomade, S., Guillou, V., Lopes, F., Thouveny, N., Dewilde, F., 2014. Geomagnetic, cosmogenic and climatic changes across the last geomagnetic reversal from Equatorial Indian Ocean sediments. Earth Planet. Sci. Lett.397, 67–79. http://dx.doi.org/10.1016/j.epsl.2014.03.053.

Valet, J.-P., Fournier, A., 2016. Deciphering records of geomagnetic reversals. Rev. Geophys., 54 , 410–446, doi:10.1002/2015RG000506.

Valet, J.P., Fournier, A., Courtillot, V., Herrero-Bervera, E., 2012. Dynamical simi-larity of geomagnetic field reversals. Nature490, 89–94. http://dx.doi.org/10.1038/nature11491.

Valet, J.P., Meynadier, L., Simon, Q., Thouveny, N., 2016. When and why sediments fail to record the geomagnetic field during polarity reversals? Earth Planet. Sci. Lett.453, 96–107.

Van Couvering, J., 1995, Setting Pleistocene marine stages: Geotimes, v. 40, pp. 10-11.

Vannacci, M., 2016. Cambiamenti climatici durante lo stadio isotopico 22 come registrato nella successione marina di Montalbano Jonico (Italia meridionale) tramite indagine palinologica. Tesi di Laurea Magistrale. Università di Firenze, AA 2014-2015, 70 pp.

Walker, M., Johnsen, S., Rasmussen, S.O., Popp, T., Steffensen, J-P., Gibbard, P., Hoek, W., Lowe, J., Andrews, J., Bjorck, S., Cwynar, L.C. Hughen, K., Kershaw, P., Kromer, B., Litt, T., Loe, D.J., Nakagawa, T., Newnham,. R., Schwander, J., 2009. Formal definition and dating of the GSSP (Global Stratotype Section and Point) for the base of the Holocene using the Greenland NGRIP ice core, and selected auxiliary records. Journal of Quaternary Science, 24, 3-17.

Walsh, S.L., Gradstein, F.M., Ogg, J.G., 2004. History, philosophy and application of the Global Stratotype Section and Point (GSSP). Lethaia, 37, p. 201-218.

Wisshak M., López Correa M., Gofas S., Salas C., Taviani M., Jakobsen J., Freiwald A., 2009. Shell architecture, element composition, and stable isotope signature of the giant deep-sea oyster Neopycnodonte zibrowii sp. n. from the NE Atlantic. Deep-Sea Research I, 56, 374–407.

Wright A.K., Flower, B.P., 2002. Surface and deep ocean circulation in subpolar North Atlantic during the mid-Pleistocene revolution. Paleoceanography, 17, 1068. http://dh.doi.org/1029/2002PA000782.

Yin, Q., Berger, A., 2015. Interglacial analogues of the Holocene and its natural near future. Quat. Sci. Rev.120, 28–46.

Figure captions

Fig 1. A: Chronostratigraphy of Quaternary and Neogene System/Period. B: Map showing the location of Montalbano Jonico section and ratified Pleistocene and Neogene GSSPs, according to https://engineering.purdue.edu/Stratigraphy/gssp/.

Fig. 2. Simplified regional geological setting and deep cross-section of the Bradanic Trough in the Basilicata Region (Southern Italy). The location of the Montalbano Jonico section is indicated by the red star. Legend of the Bradanic units in fig. C: a) Calcarenite di Gravina fm., Early Pleistocene; b) Argille subappennine fm. Early-Middle Pleistocene; c) marine and continental regressive sandy and conglomeratic deposits, Early Pleistocene; d) marine and continental regressive sandy and

conglomerate terraced units, Middle-Late Pleistocene, and actual coastal plain deposits, Holocene. Legend of the geologic section: a) Plio-Quaternary units of the Bradanic Trough; b) Meso-Cenozoic allochthonous units of the chain; c) Meso-Cenozoic units of the Apulian Foreland.

Fig. 3. A) Map showing the route to reach the candidate Ideale section. B) Geological map of the area west of the Montalbano Ionico Town and (C) cross-section passing through the measured IS and CMs autcrops.

Fig. 4. A) Lithological and stratigraphical features of the composite Montalbano Jonico section (Intervals A and B). Biostratigraphical and Paleonvironmental details are traced according to Ciaranfi et al. (2001, 2010), Stefanelli (2003, 2004), D'Alessandro et al. (2003), Maiorano et al. (2004, 2010), Girone et al. (2013). $\delta^{18}O_{planktonic}$ and $\delta^{18}O_{benthic}$ are from Brilli (1998), Brilli et al. (2000) and Ciaranfi et al. (2010). Pollen Temperature Index (PTI) record (in logarithmic scale) derives from Mesothermic/Steppic taxa ratio and is from Joannin et al. (2008) for Interval A, Vannacci (2016) for MIS 22, Bertini et al. (2015) and Toti (2015) for MIS 21-17 interval.. LO: Lowest Occurrence; HO: Highest Occurrence; LCO: Lowest Common Occurrence; HCO: Highest Common Occurrence; reap: reappearance. B) picture of the Montalbano Jonico badlands.

Fig. 5. Lithology, quantitative abundance patterns of selected calcareous plankton taxa, and benthic and plankton oxygen isotope stratigraphy at the Montalbano Jonico section (from Maiorano et al., 2010, slightly modified). Correlation to sapropel stratigraphy according to Lourens (2004) and Konijnendijk et al. (2014). Summer insolation is from Laskar et al. (2004). Ar/Ar ages of V3-V5 are also indicated. Chronostratigraphy on the left is from ATNTS2012 (Gradstein et al., 2012). The age of Matuyama-Brunhes boundary is according to Cohen and Gibbard (2011, and reference therein). LO: Lowest Occurrence; HO: Highest Occurrence; LCO: Lowest Common Occurrence; HCO: Highest Common Occurrence; reap: reappearance.

Fig. 6. Oxygen isotope chronologies of the astronomically tuned Vrica-Crotone and Montalbano Jonico sections recovering the entire Calabrian Stage (from Maiorano et al., 2010, cum reference therein, slightly modified). Planktonic $\delta^{18}O$ of interval B at Montalbano Jonico is from Brilli (1998). Position of biohorizons is traced for comparison on the benthic $\delta^{18}O$ stacked of Lisiecki and Raymo (2005), and on the oxygen isotope Mediterranean stacked planktonic record of Lourens (2004). The Mediterranean benthic $\delta^{18}O$ curve (green) according to Konijnendijk et al. (2014) is also shown for comparison. Mean summer insolation 65°N (La041:1) is from Laskar et al. (2004). Sapropel stratigraphy on the left is according to Lourens (2004) and Konijnendijk et al. (2014). Chronostratigraphy on the right is from ATNTS2012 (Gradstein et al., 2012). The age of Matuyama-Brunhes boundary is according to Cohen and Gibbard (2011, and reference therein). Npl: *N. pachyderma* left coiling (=*N. pachyderma* sinistral in this paper); mG: medium *Gephyrocapsa*; Cm: *C. macintyrei*; lG: large *Gephyrocapsa*; Hs: *H. sellii*; Gc: *G. crassaformis*; Ra: *R. asanoi*; Go: *G. omega*. LO, HO, LCO, and HCO as in Figure 5; "beg" and "end": beginning and end of temporary disappearance. See Table I for biochronology.

Fig. 7. A) Stratigraphic log of the Ideale section and the main stratigraphic, chronological, and paleoenvironmetal constraints in the critical interval for the selection of the GSSP of Middle Pleistocene (green band). B) Picture of the outcrop.

Fig. 8. $\delta^{18}O_{M.barleanum}$ records (vs depth) at the Ideale and CM sections showing the matching between the sections based on isotope data and correlation of specific sedimentary intervals. Outcrop pictures and lithological/paleontological features (see legend in Fig. 7) are also shown in the respective logs.

Fig. 9. $\delta^{18}O_{M.barleanum}$ and $\delta^{13}C_{C.carinata}$ records (vs depth) at the Ideale section and comparison with other worldwide climate records (vs time). Glacials MIS 20 and 18, and interglacial substages of MIS 19 are indicated. GL_T-syn: synthetic climatic record from Greenland. For lithological/paleontological features of Ideale section see legend in Fig. 7.

Fig. 10. Stratigraphic positioning of the Matuyama-Brunhes Boundary (MBB). (a) Authigenic $^{10}Be/^{9}Be$ ratio and benthic $\delta^{18}O$ records from the Ideale section compared to (b) benthic $\delta^{18}O$ record and paleomagnetic results at IODP Site U1308 from the North Atlantic Ocean; (c) authigenic $^{10}Be/^{9}Be$ ratio, planktic $\delta^{18}O$ record and paleomagnetic results at core MD90-0961 from the Indian Ocean; (d) authigenic $^{10}Be/^{9}Be$ ratio (Simon et al., submitted), benthic $\delta^{18}O$ record and paleomagnetic results at core MD97-2143 from the Pacific Ocean; (e) δD_{ice} record and ^{10}Be-flux at EPICA Dome C (EDC) from Antarctica; and (f) PISO-1500 RPI stack, LR04 benthic $\delta^{18}O$ stack and equatorial authigenic $^{10}Be/^{9}Be$ ratio stack. The onset of MIS 19c in each series is set using the lightest $\delta^{18}O$ or lowest δD_{ice} peak. For lithological/paleontological features of Ideale section see legend in Fig. 7

Fig. 11. Chronological framework of the Ideale section (from Bassinot et al., in prep.). A) Termination I/MIS1 planktonic $\delta^{18}O$ stack from the nearby marine cores (MD90-917; MD90-918; Caron et al, 2012; Siani et al., 2014) and position of sapropel S1. B) High resolution benthic $\delta^{18}O$ record of Termination IX (TIX) from the Ideale section (blue curve) fine-tuned to Termination I (TI) planktonic $\delta^{18}O$ stack (black curve), assuming similar orbital forcing and CO_2 levels between TI and TIX, and adjusted using the V4 $^{40}Ar/^{39}Ar$ dating (Petrosino et al., 2015). Mean summer insolation is from Laskar et al. (2004). C) Sedimentation rate (cm/ka) curve is expressed for the main climate phases, according to our astronomical tuning target.

Fig. 12. Geomagnetic dipole moment signature of the Matuyama-Brunhes transition (MBT) from cosmogenic radionuclide ^{10}Be and RPI records. (a) Oxygen isotope stratigraphy from the Ideale section of the Montalbano Jonico succession (blue) compared to the LR04 stack (dark grey; Lisieki and Raymo, 2005) and mean summer insolation (yellow; Laskar et al., 2004). (b) Standardized raw 10Be-flux from core MD98-2187 (Suganuma et al., 2010). Standardized Be-ratios from cores: (c) MD97-2140 (Carcaillet et al., 2003; Simon et al., submitted), (d) MD97-2143 (Simon et al., submitted), (e) MD05-2930 (Ménabréaz et al., 2014; Simon et al., 2016), (f) MD90-0961 (Valet et al., 2014). (g) Standardized ^{10}Be-flux from Antarctica EDC (Raisbeck et al., 2006). (h) Standardized Be-ratios from the Ideale section of the Montalbano Jonico succession (Simon et al., 2017). (i) 40Ar/39Ar dating of transitional lava flows or tephra layers from: (1) V4 tephra layer from the Ideale section (Petrosino et al., 2015), (2) Singer (2014), Singer et al. (2005), (3) Coe et al. (2004), (4) Brown et al. (2004), (5) Sagnotti et al. (2014), (6) Mark et al. (2017). (7) U-Pb age is from Suganuma et al. (2015). Astrochronologic ages are from (8) Channell et al. (2010), (9) Valet et al. (2014) and (10) Tauxe et al. (1996). Virtual axial dipole moment (VADM) reconstructions (j) derived from ^{10}Be-stack (Simon et al., 2016), and from (k) a stack of relative paleointensity records (PISO-1500 stack; Channell et al., 2009). Light yellow banding represents two time intervals characterized by geomagnetic dipole lows associated with the MBT and a precursor event observed in most RPI records. Dark grey banding represents the maximal ^{10}Be-overproduction episode corresponding to the MBB, which span a 4.5 ka time frame (771.9-776.4 ka) at the Ideale section, coherent with the highest ^{10}Be-proxy values and the lowest VADM values in the PISO-1500 stack. The dashed line represents the most reliable age of the MBB based on astronomical calibration (~773 ka) (see Table 1 in Head and Gibbard, 2015a).

Fig. 13. Climatostratigraphic proxies vs age at the Ideale section plotted against $\delta^{18}O_{M.barleanum}$ record. Ice rafted debris (IRD) at the North Atlantic ODP Site 980 is shown on the right. Light blue bars indicate glacial and stadials phases. Mean summer insolation curve is from Laskar et al. (2004). Mesothermic taxa include temperate broad-leaved deciduous forest taxa with subordinate Sclerophyll taxa. Planktonic foraminifera warm-water taxa (wwt) include *Globigerinoides ruber* group, *Trilobatus sacculifer*, *Orbulina universa*, *Globoturborotalita rubescens*, *Globoturborotalita tenella* and *Globigerinella siphonifera*. Calcareous nannofossil warm water taxa (wwt) include *Umbilicosphaera sibogae* s.l., *Calciosolenia* spp., *Oolithotus* spp., *Helicosphaera pavimentum*.

Fig. 14. $\delta^{18}O_{M.barleanum}$ and $\delta^{13}C_{C.carinata}$ records compared with selected calcareous plankton taxa at the Ideale section. Grey bar: ghost sapropel (i-cycle 74). Star symbol: oxygen content at the sea bottom based on higher infauna/epifauna ratio in benthic foraminifera assemblage (Stefanelli, 2003), and abundance peak of *P. zoharyi* (Bertini et al., 2015). Mean summer insolation curve is from Laskar et al. (2004).

Fig. 15. A) Summary of chronostratigraphic, chronological and paleoenvironmental constraints drawn on the picture of the Ideale section outcrop. B) $\delta^{18}O_{M.barleanum}$ curve is drawn on the picture of auxiliary CMs outcrop.

Plate 1. Representative fossil content from Montalbano Jonico section 1-6: calcareous nannofossils. 7-12: planktonic foraminifera. 13-18: pollen grains. 19-20: ostracods. 21-22: benthic foraminifera. A-J: Macro-invertebrates and fossil plants.

Table 1. Numerical ages of calcareous plankton bioevents in the Montalbano Jonico composite section according to Ciaranfi et al. (2010), Maiorano et al. (2010) and this study. Calibrations from reference records are reported. *Maiorano et al. (2010); ** Lourens et al. (2004); *** Lourens et al. (1998).

Table 2. List of satisfied requirements at the Ideale section for holding the GSSP of the Middle Pleistocene Subseries and Ionian Stage.

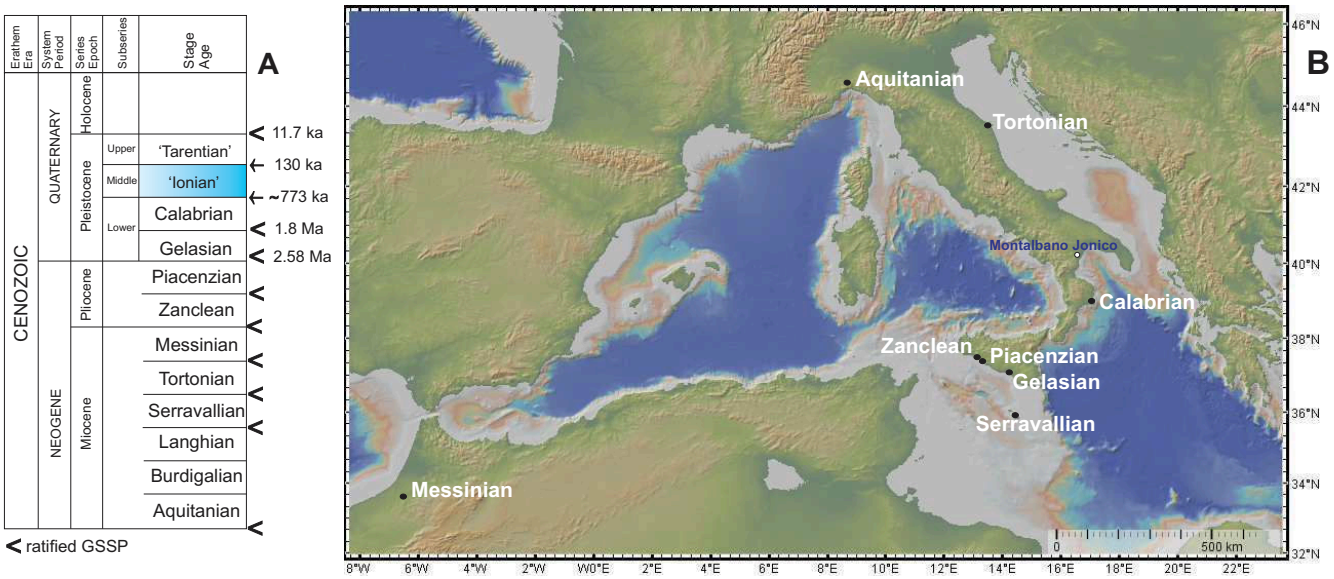
Eratherm Era
System Period
Series Epoch
Subseries
Stage Age
A
CENOZOIC
QUATERNARY
NEOGENE
Holocene
Pleistocene
Pliocene
Miocene
Upper
Middle
Lower
'Tarentian'
'Ionian'
Calabrian
Gelasian
Piacenzian
Zanclean
Messinian
Tortonian
Serravallian
Langhian
Burdigalian
Aquitanian
11.7 ka
130 ka
~773 ka
1.8 Ma
2.58 Ma
ratified GSSP
B
Aquitanian
Tortonian
Montalbano Jonico
Calabrian
Zanclean
Piacenzian
Gelasian
Serravallian
Messinian
0
500 km
8°W
6°W
4°W
2°W
W0°E
2°E
4°E
6°E
8°E
10°E
12°E
14°E
16°E
18°E
20°E
22°E
46°N
44°N
42°N
40°N
38°N
36°N
34°N
32°N

Fig. 1

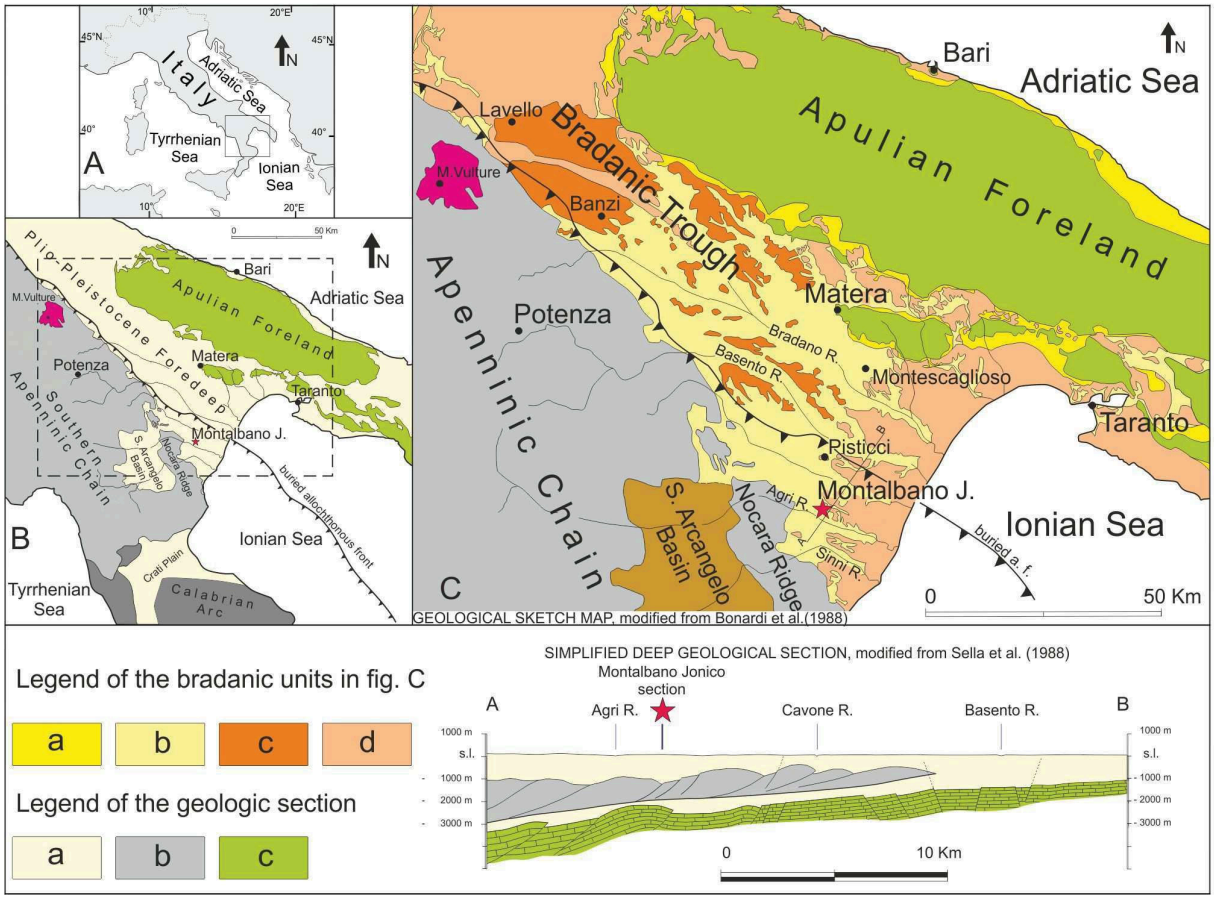
A
Italy
Adriatic Sea
Tyrrhenian Sea
Ionian Sea
B
Plio-Pleistocene Foredeep
Apulian Foreland
Southern Apennine Chain
Bari
Adriatic Sea
M.Vulture
Potenza
Matera
Taranto
Montalbano J.
S. Arcangelo Basin
Nocara Ridge
buried allochthonous front
Ionian Sea
Tyrrhenian Sea
Crati Plain
Calabrian Arc
C
Apulian Foreland
Bradanic Trough
Apenninic Chain
Lavello
Banzi
Bradano R.
Basento R.
Montescaglioso
Pisticci
Agri R.
Sinni R.
buried a. f.
0
50 Km
GEOLOGICAL SKETCH MAP, modified from Bonardi et al.(1988)
Legend of the bradanic units in fig. C
a
b
c
d
Legend of the geologic section
a
b
c
SIMPLIFIED DEEP GEOLOGICAL SECTION, modified from Sella et al. (1988)
Montalbano Jonico section
Agri R.
Cavone R.
Basento R.
1000 m s.l.
1000 m
2000 m
3000 m
0
10 Km

Fig. 2

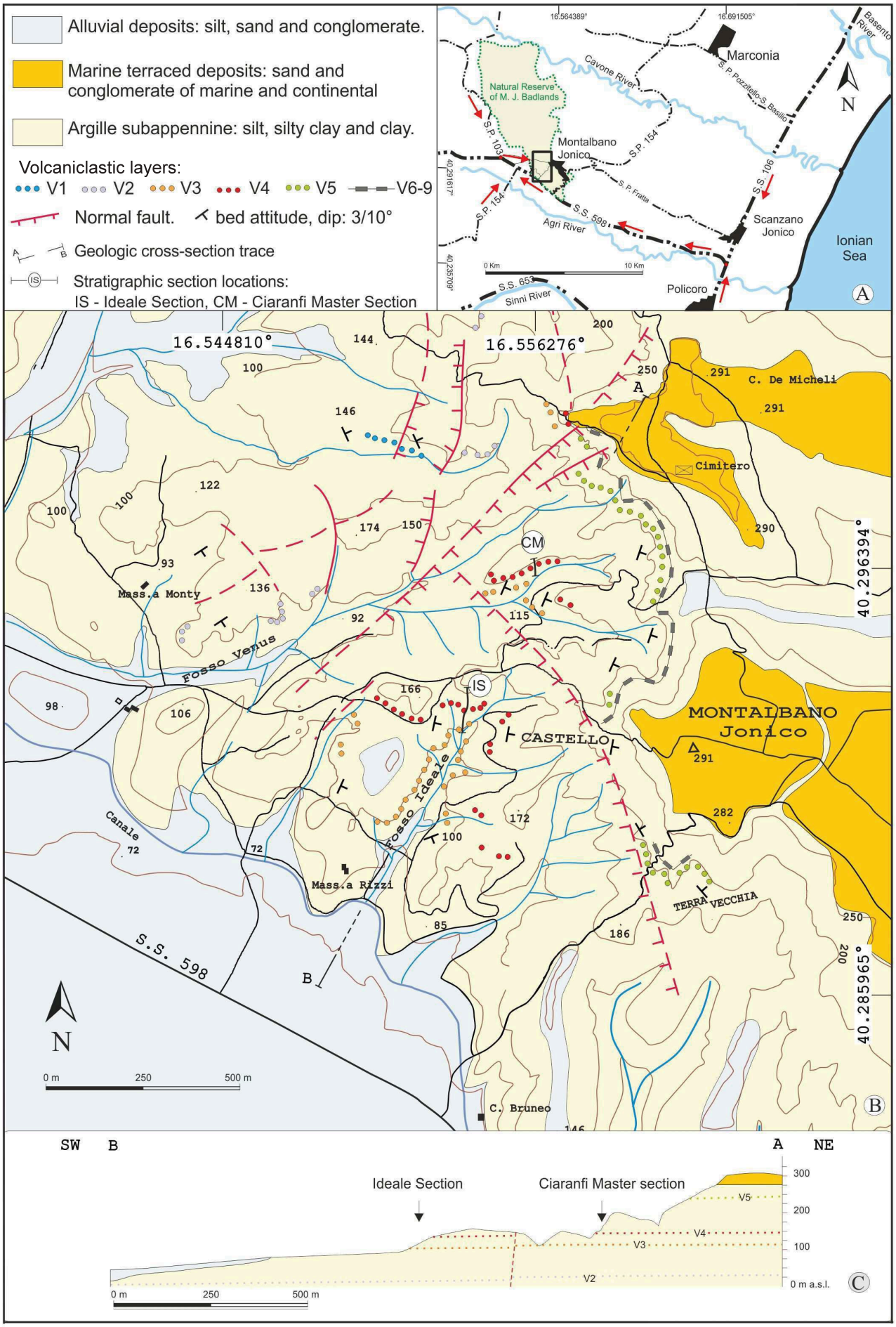
Alluvial deposits: silt, sand and conglomerate.
Marine terraced deposits: sand and conglomerate of marine and continental
Argille subappennine: silt, silty clay and clay.
Volcaniclastic layers:
V1 V2 V3 V4 V5 V6-9
Normal fault. bed attitude, dip: 3/10°
Geologic cross-section trace
Stratigraphic section locations:
IS - Ideale Section, CM - Ciaranfi Master Section
16.564389°
16.691505°
Marconia
Basento River
Cavone River
Natural Reserve of M. J. Badlands
S.P. 103
Montalbano Jonico
S.P. 154
S.P. Pozzitello-S. Basilio
S.P. Fratta
S.S. 106
S.S. 598
Agri River
Scanzano Jonico
Ionian Sea
40.291617°
40.235709°
0 Km
10 Km
S.S. 653
Sinni River
Policoro
A
16.544810°
16.556276°
C. De Micheli
Cimitero
CM
IS
Mass.a Monty
Fosso Venus
MONTALBANO Jonico
CASTELLO
Fosso Ideale
Canale
Mass.a Rizzi
TERRA VECCHIA
S.S. 598
B
C. Bruneo
40.296394°
40.285965°
0 m 250 500 m
SW B A NE
Ideale Section
Ciaranfi Master section
V5
V4
V3
V2
300
200
100
0 m a.s.l.
C

226

Fig. 3

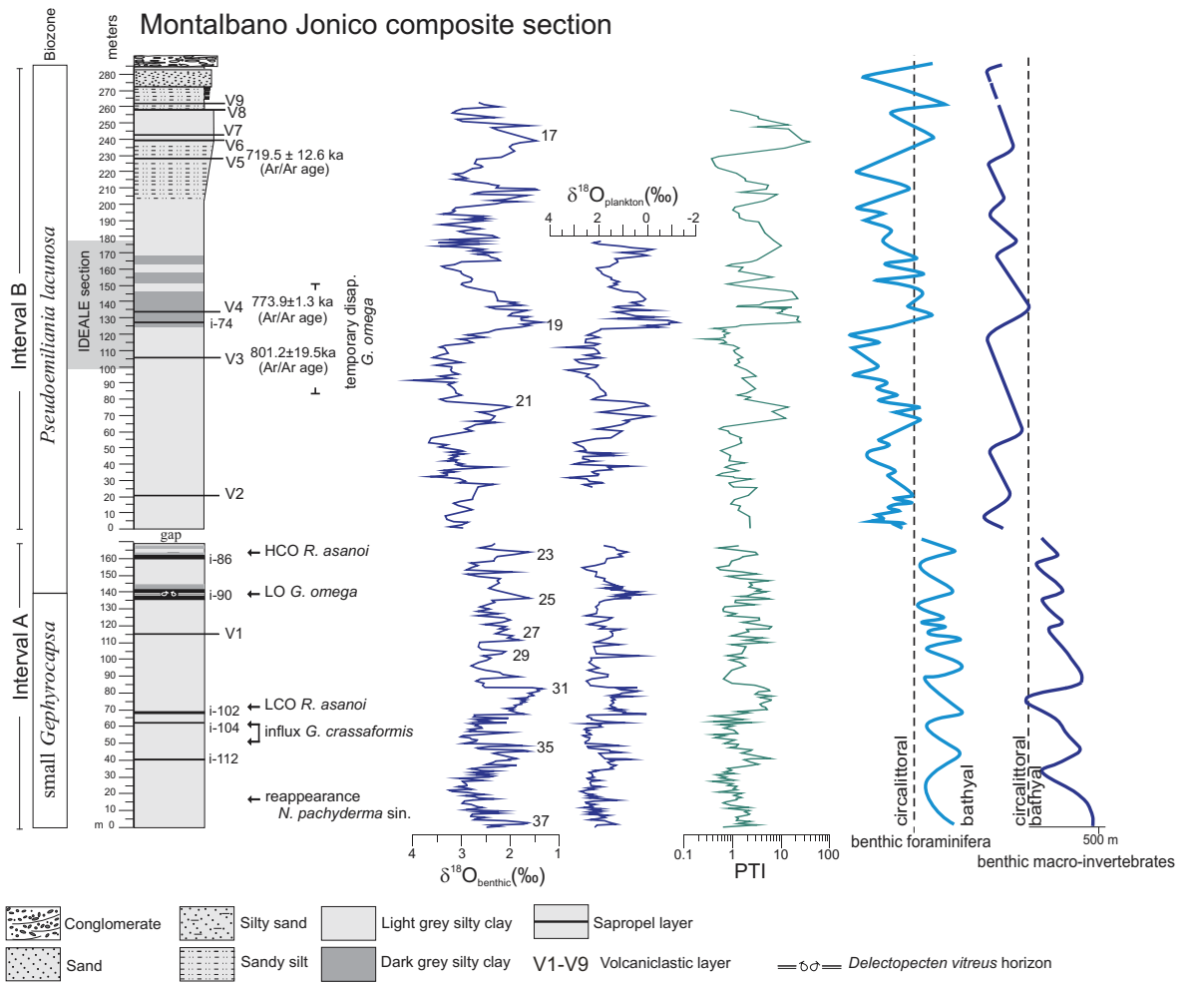
Montalbano Jonico composite section
meters
Biozone
Interval B
Pseudoemiliania lacunosa
Interval A
small Gephyrocapsa
IDEALE section
V9
V8
V7
V6
V5
719.5 ± 12.6 ka
(Ar/Ar age)
V4
i-74
773.9±1.3 ka
(Ar/Ar age)
V3
801.2±19.5ka
(Ar/Ar age)
temporary disap.
G. omega
V2
gap
i-86
HCO R. asanoi
i-90
LO G. omega
V1
i-102
LCO R. asanoi
i-104
influx G. crassaformis
i-112
reappearance
N. pachyderma sin.
δ18Oplankton(‰)
δ18Obenthic(‰)
PTI
circalittoral
bathyal
benthic foraminifera
benthic macro-invertebrates
500 m
Conglomerate
Sand
Silty sand
Sandy silt
Light grey silty clay
Dark grey silty clay
Sapropel layer
V1-V9 Volcaniclastic layer
Delectopecten vitreus horizon


V7
V5
V4
V3

Fig. 4

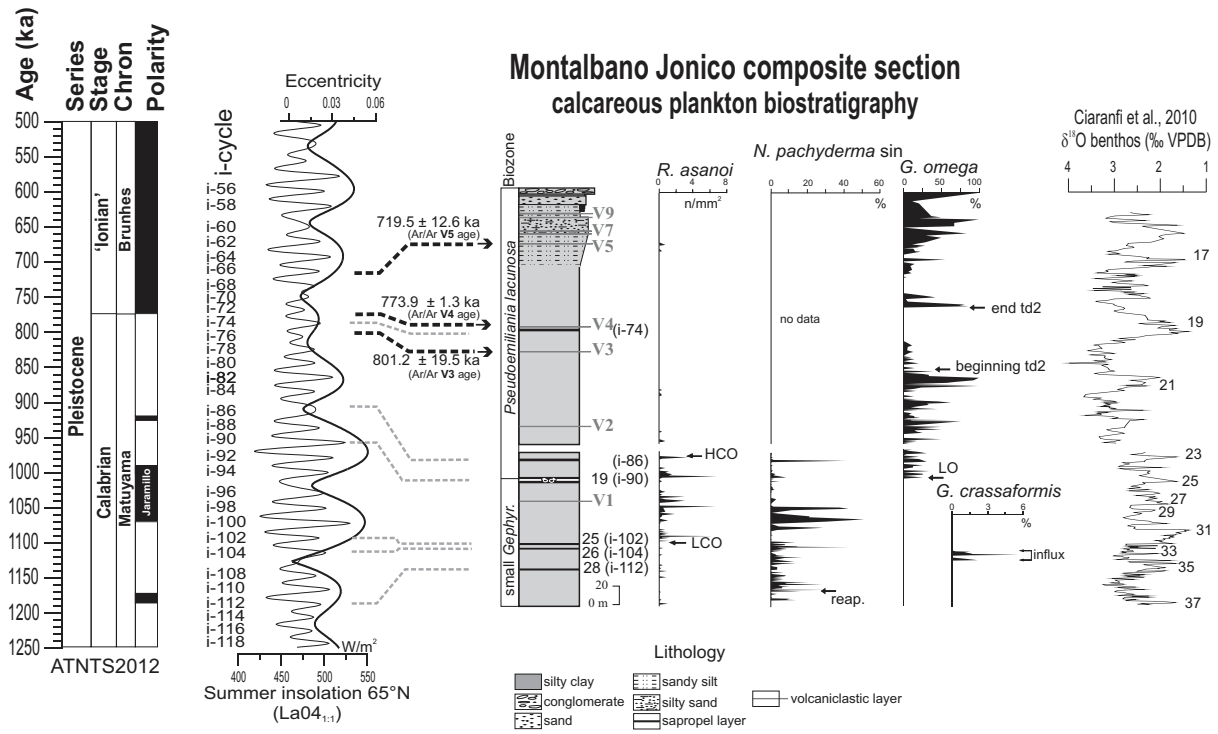
Montalbano Jonico composite section
calcareous plankton biostratigraphy
Age (ka)
Series
Stage
Chron
Polarity
Pleistocene
Calabrian
Matuyama
'Ionian'
Brunhes
Jaramillo
ATNTS2012
Eccentricity
i-cycle
719.5 ± 12.6 ka
(Ar/Ar V5 age)
773.9 ± 1.3 ka
(Ar/Ar V4 age)
801.2 ± 19.5 ka
(Ar/Ar V3 age)
W/m²
Summer insolation 65°N
(La04 1,1)
Biozone
Pseudoemiliania lacunosa
small Gephyr.
V9
V7
V5
V4
(i-74)
V3
V2
(i-86)
19 (i-90)
V1
25 (i-102)
26 (i-104)
28 (i-112)
R. asanoi
n/mm²
HCO
LCO
N. pachyderma sin
no data
reap.
G. omega
end td2
beginning td2
LO
G. crassaformis
influx
Ciaranfi et al., 2010
δ18O benthos (‰ VPDB)
Lithology
silty clay
conglomerate
sand
sandy silt
silty sand
sapropel layer
volcaniclastic layer

Fig. 5

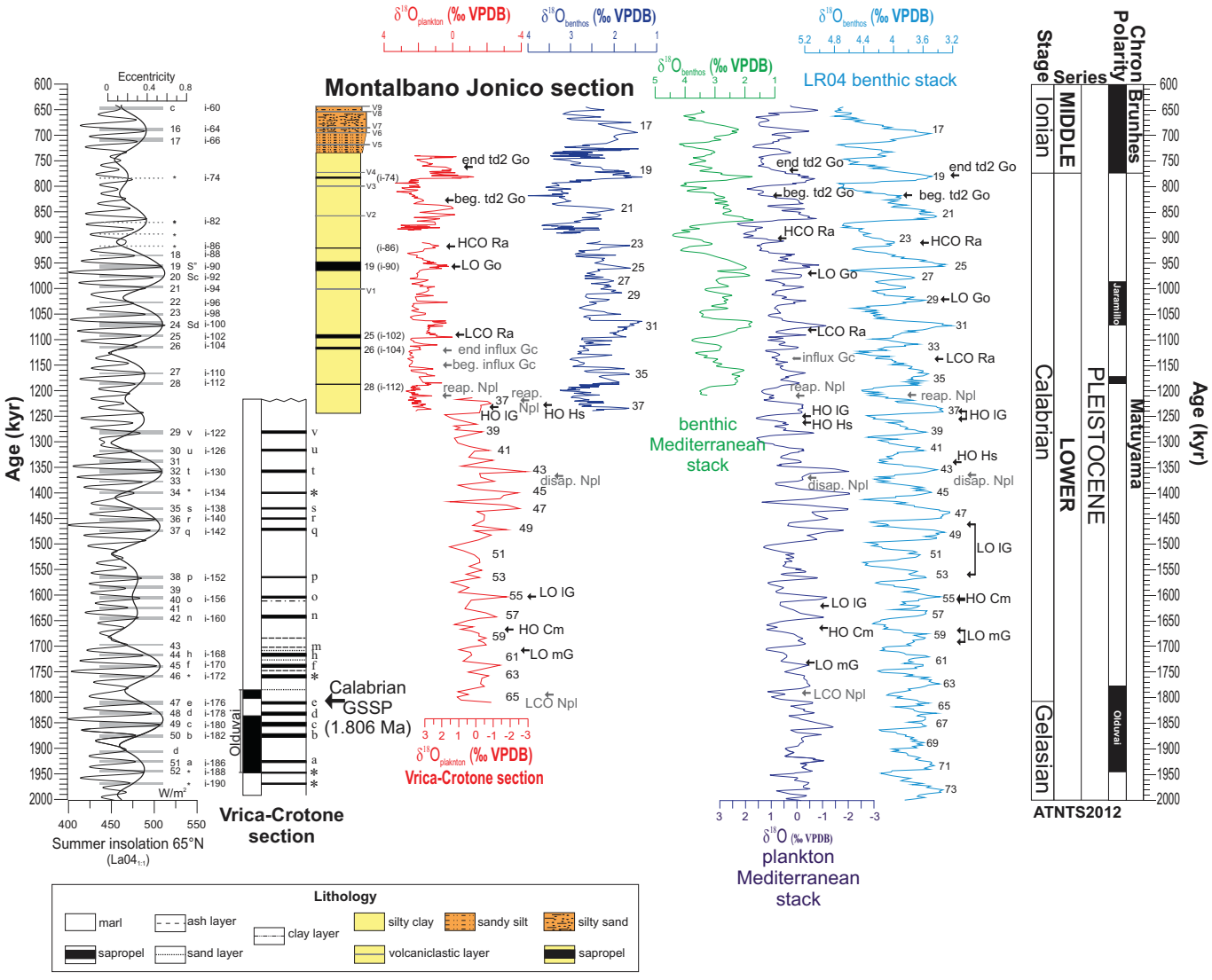
Montalbano Jonico section
LR04 benthic stack
Eccentricity
Age (kyr)
Summer insolation 65°N
(La04₁,₁)
W/m²
Vrica-Crotone section
Olduvai
Calabrian
GSSP
(1.806 Ma)
end td2 Go
beg. td2 Go
HCO Ra
LO Go
LCO Ra
end influx Gc
beg. influx Gc
reap. Npl
HO IG
HO Hs
disap. Npl
LO IG
HO Cm
LO mG
LCO Npl
influx Gc
benthic
Mediterranean
stack
plankton
Mediterranean
stack
Vrica-Crotone
section
Lithology
marl
ash layer
clay layer
silty clay
sandy silt
silty sand
sapropel
sand layer
volcaniclastic layer
sapropel
Stage
Series
Chron
Polarity
Ionian
Calabrian
Gelasian
MIDDLE
LOWER
PLEISTOCENE
Brunhes
Jaramillo
Olduvai
Matuyama
ATNTS2012

Fig. 6

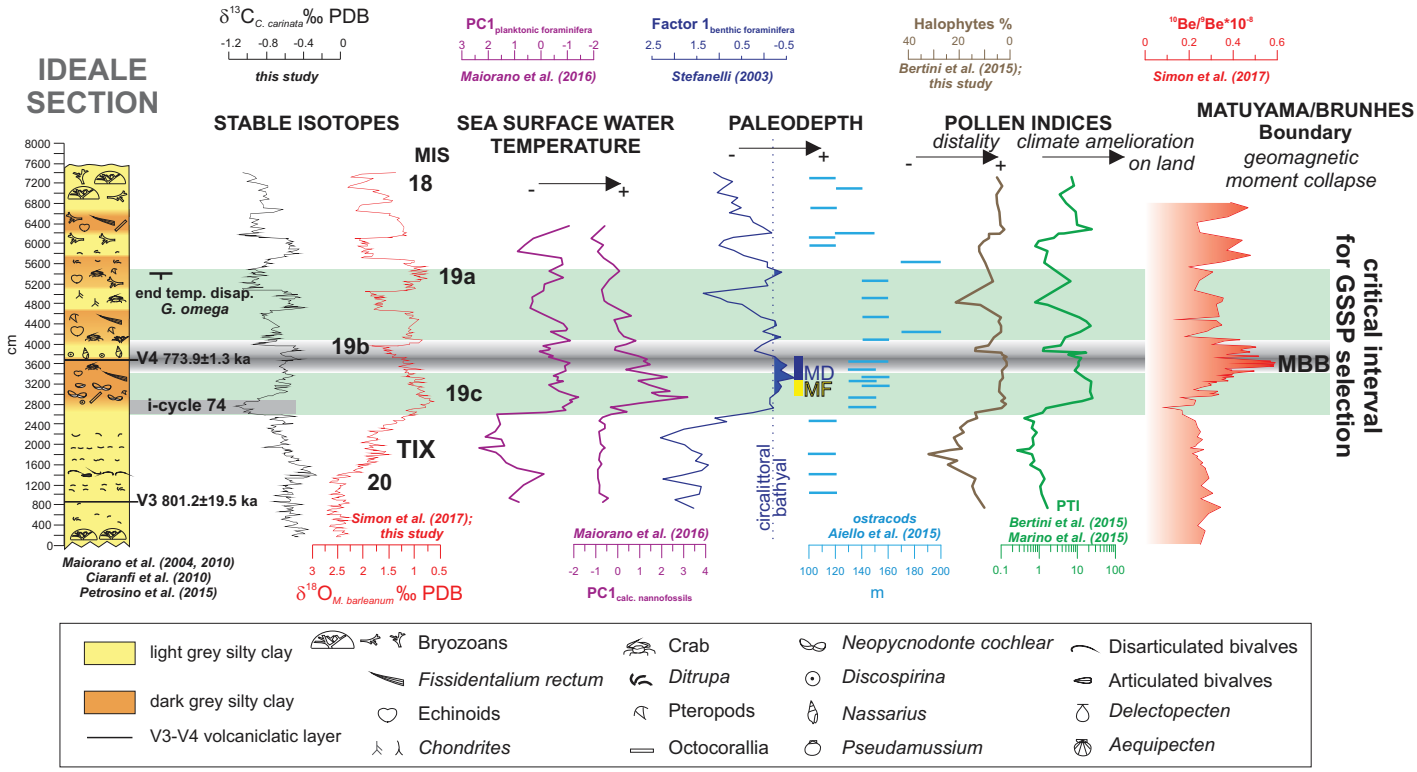
IDEALE SECTION
STABLE ISOTOPES
SEA SURFACE WATER TEMPERATURE
PALEODEPTH
POLLEN INDICES
distality
climate amelioration on land
MATUYAMA/BRUNHES Boundary
geomagnetic moment collapse
this study
Maiorano et al. (2016)
Stefanelli (2003)
Bertini et al. (2015); this study
Simon et al. (2017)
MIS
18
19a
19b
19c
TIX
20
end temp. disap. G. omega
V4 773.9±1.3 ka
i-cycle 74
V3 801.2±19.5 ka
MD
MF
MBB
critical interval for GSSP selection
circalittoral
bathyal
ostracods
Aiello et al. (2015)
PTI
Bertini et al. (2015)
Marino et al. (2015)
Maiorano et al. (2004, 2010)
Ciaranfi et al. (2010)
Petrosino et al. (2015)
cm
m
light grey silty clay
dark grey silty clay
V3-V4 volcaniclatic layer
Bryozoans
Fissidentalium rectum
Echinoids
Chondrites
Crab
Ditrupa
Pteropods
Octocorallia
Neopycnodonte cochlear
Discospirina
Nassarius
Pseudamussium
Disarticulated bivalves
Articulated bivalves
Delectopecten
Aequipecten

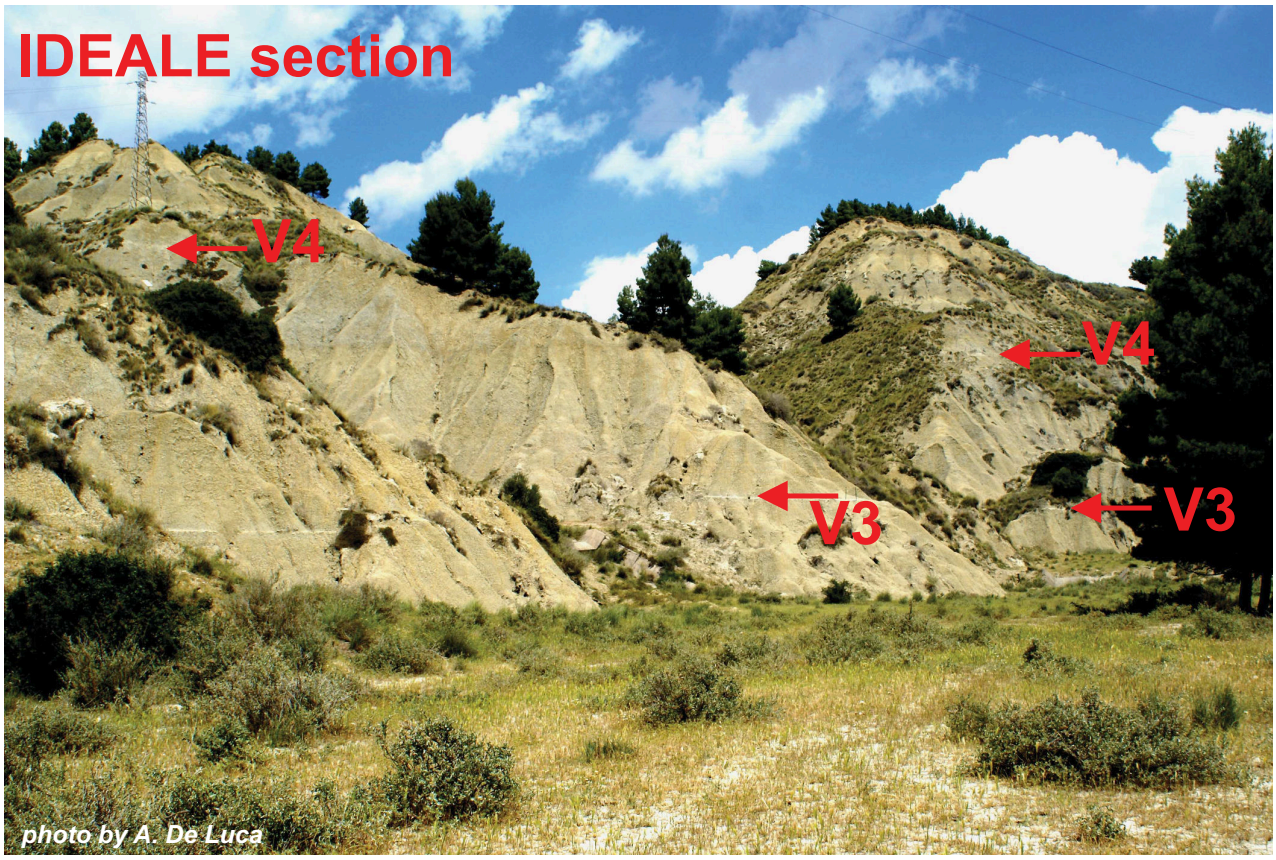
IDEALE section
V4
V4
V3
V3
photo by A. De Luca

Fig. 7

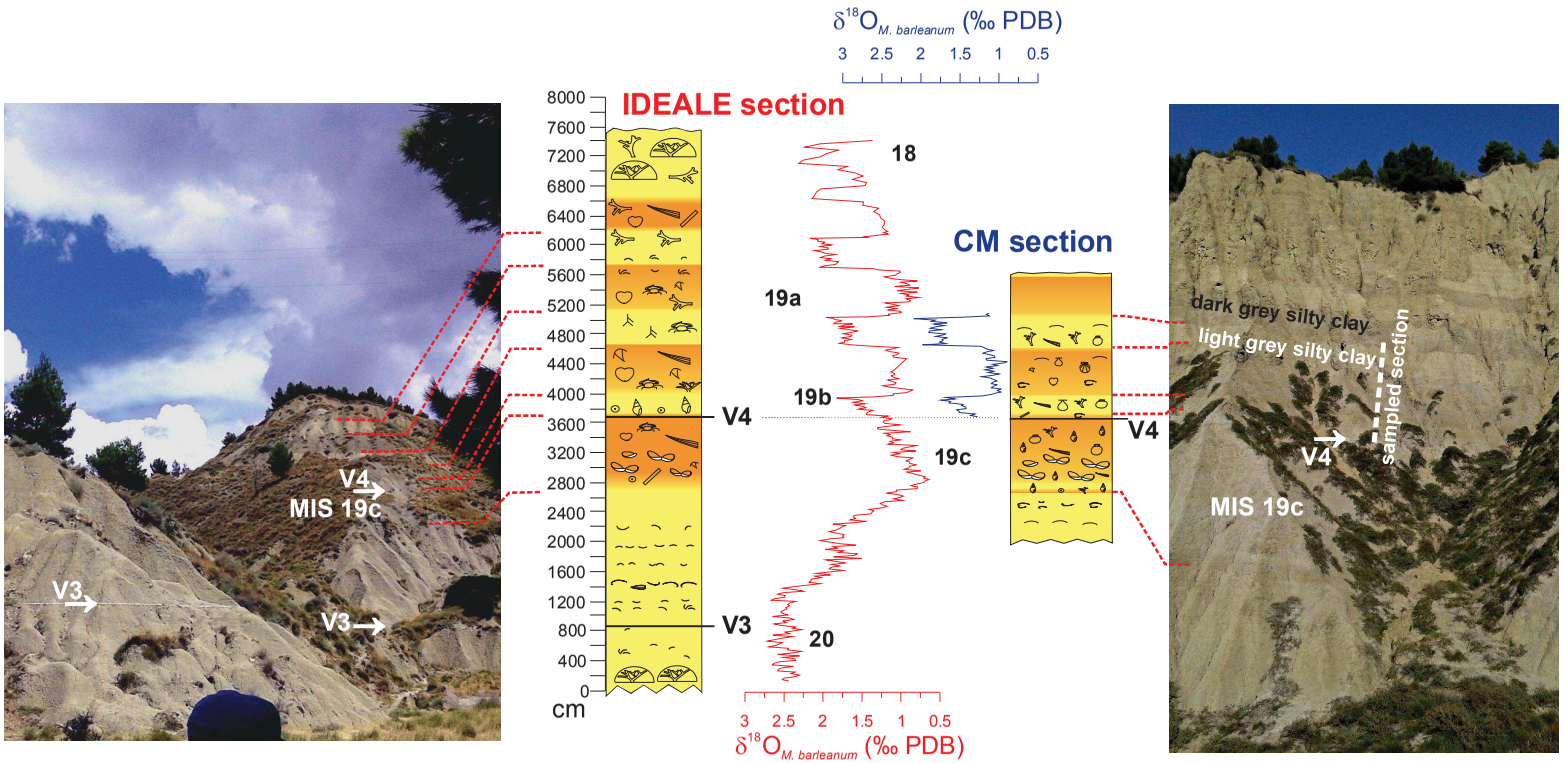
δ18O M. barleanum (‰ PDB)
3 2.5 2 1.5 1 0.5
IDEALE section
CM section
8000
7600
7200
6800
6400
6000
5600
5200
4800
4400
4000
3600
3200
2800
2400
2000
1600
1200
800
400
0
cm
V4
V3
18
19a
19b
19c
20
V4
MIS 19c
V3
V3
V4
dark grey silty clay
light grey silty clay
sampled section
V4
MIS 19c
3 2.5 2 1.5 1 0.5
δ18O M. barleanum (‰ PDB)

Fig. 8

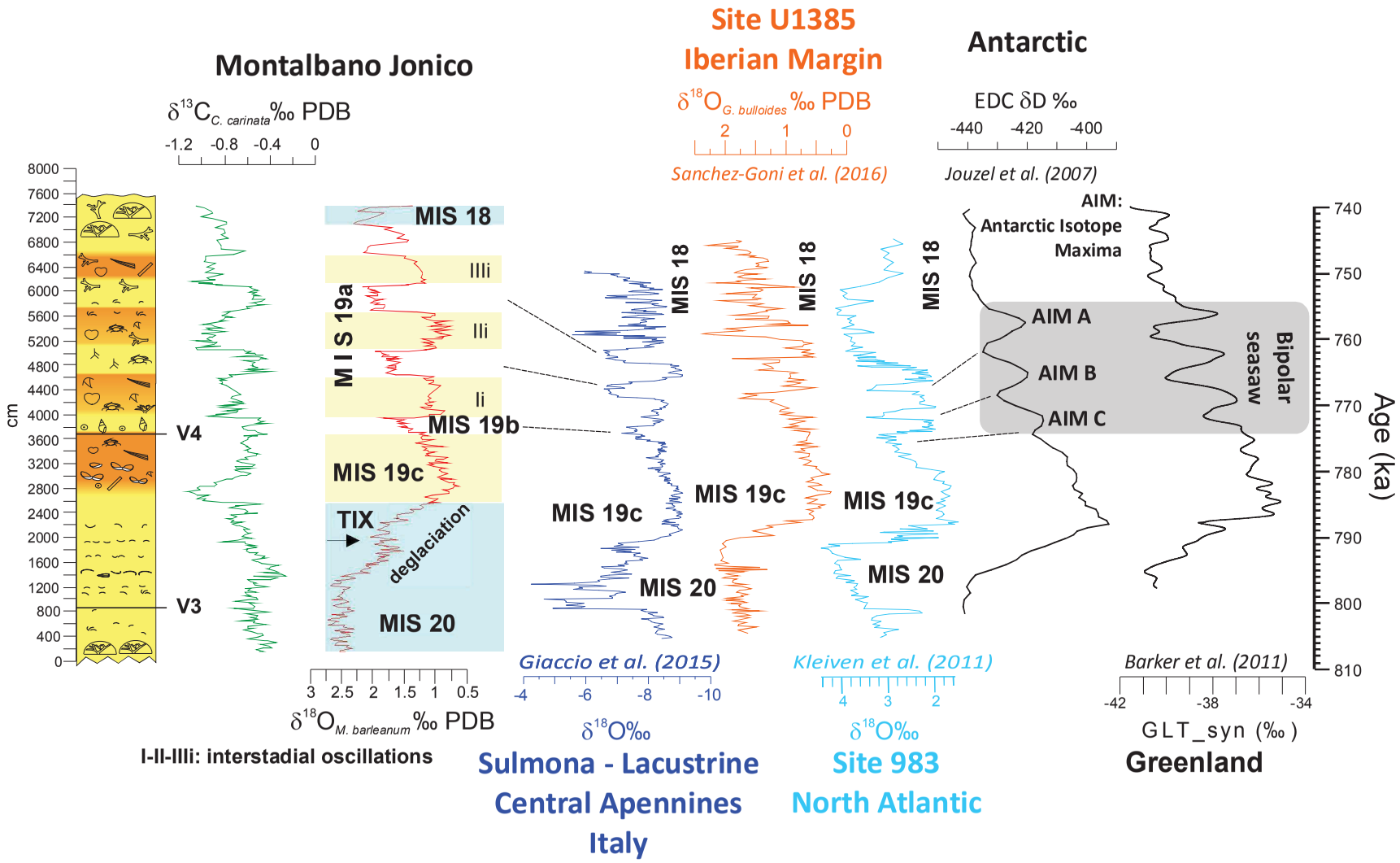
Montalbano Jonico
$\delta^{13}C_{C.\ carinata}$ ‰ PDB
-1.2 -0.8 -0.4 0
cm
8000 7600 7200 6800 6400 6000 5600 5200 4800 4400 4000 3600 3200 2800 2400 2000 1600 1200 800 400 0
V4
V3
MIS 18
IIIi
IIi
MIS 19a
Ii
MIS 19b
MIS 19c
TIX
deglaciation
MIS 20
3 2.5 2 1.5 1 0.5
$\delta^{18}O_{M.\ barleanum}$ ‰ PDB
I-II-IIIi: interstadial oscillations
Site U1385
Iberian Margin
$\delta^{18}O_{G.\ bulloides}$ ‰ PDB
2 1 0
Sanchez-Goni et al. (2016)
MIS 18
MIS 19c
MIS 20
Giaccio et al. (2015)
-4 -6 -8 -10
$\delta^{18}O$‰
Sulmona - Lacustrine
Central Apennines
Italy
MIS 18
MIS 19c
MIS 20
Kleiven et al. (2011)
4 3 2
$\delta^{18}O$‰
Site 983
North Atlantic
Antarctic
EDC δD ‰
-440 -420 -400
Jouzel et al. (2007)
AIM:
Antarctic Isotope
Maxima
AIM A
AIM B
AIM C
Bipolar
seasaw
Barker et al. (2011)
-42 -38 -34
GLT_syn (‰)
Greenland
740 750 760 770 780 790 800 810
Age (ka)

Fig. 9

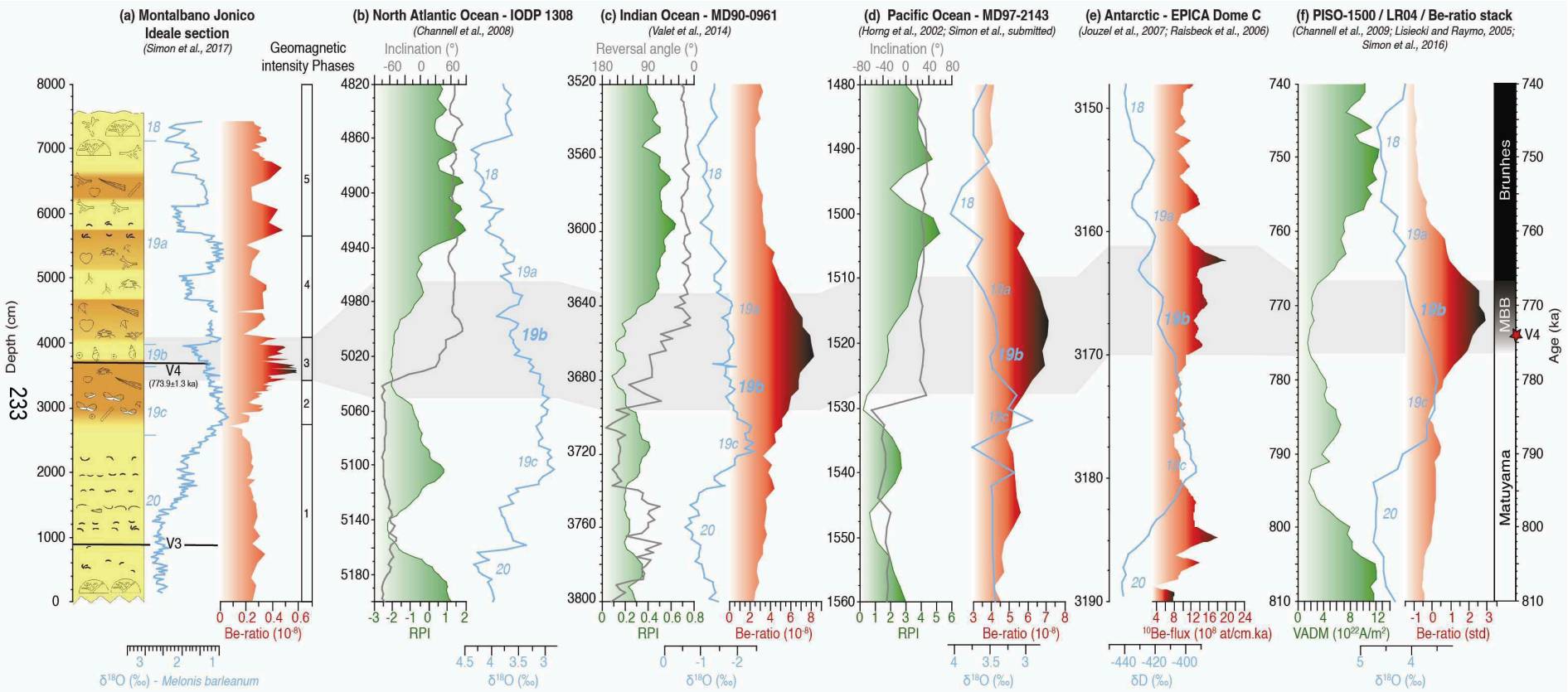
(a) Montalbano Jonico
Ideale section
(Simon et al., 2017)
Geomagnetic
intensity Phases
(b) North Atlantic Ocean - IODP 1308
(Channell et al., 2008)
(c) Indian Ocean - MD90-0961
(Valet et al., 2014)
(d) Pacific Ocean - MD97-2143
(Horng et al., 2002; Simon et al., submitted)
(e) Antarctic - EPICA Dome C
(Jouzel et al., 2007; Raisbeck et al., 2006)
(f) PISO-1500 / LR04 / Be-ratio stack
(Channell et al., 2009; Lisiecki and Raymo, 2005; Simon et al., 2016)
Depth (cm)
Age (ka)
Brunhes
MBB
Matuyama
V4
(773.9±1.3 ka)
V3
Inclination (°)
Reversal angle (°)
RPI
Be-ratio (10⁻⁸)
δ18O (‰) - Melonis barleanum
δ18O (‰)
10Be-flux (10⁸ at/cm.ka)
δD (‰)
VADM (10²²A/m²)
Be-ratio (std)

Fig. 10

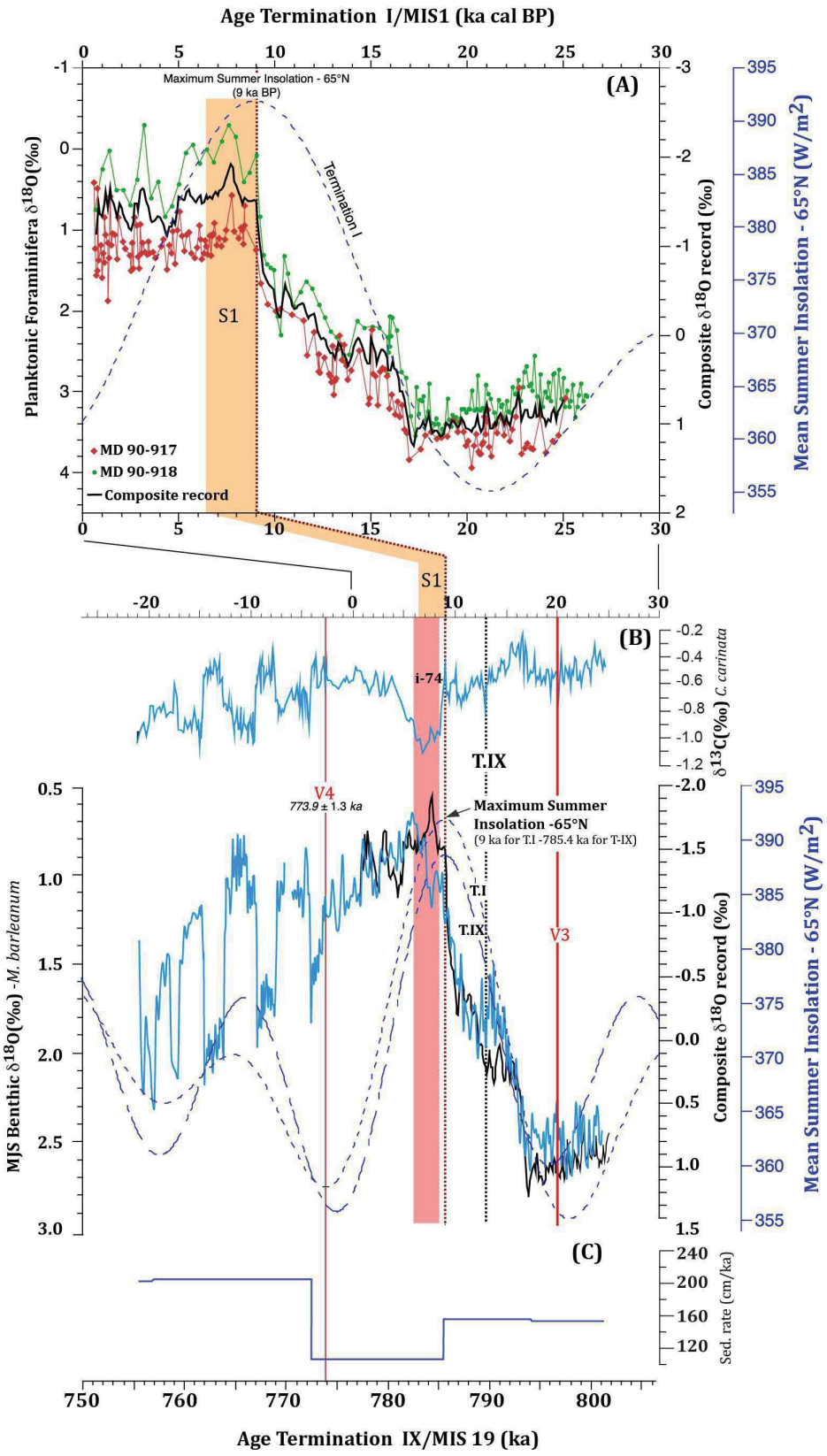
Age Termination I/MIS1 (ka cal BP)
(A)
Maximum Summer Insolation - 65°N
(9 ka BP)
Termination I
S1
MD 90-917
MD 90-918
Composite record
Planktonic Foraminifera δ18O(‰)
Composite δ18O record (‰)
Mean Summer Insolation - 65°N (W/m2)
(B)
i-74
T.IX
δ13C(‰) C. carinata
V4
773.9 ± 1.3 ka
Maximum Summer
Insolation -65°N
(9 ka for T.I -785.4 ka for T-IX)
T.I
T.IX
V3
MIS Benthic δ18O(‰) -M. barleanum
(C)
Sed. rate (cm/ka)
Age Termination IX/MIS 19 (ka)

Fig. 11

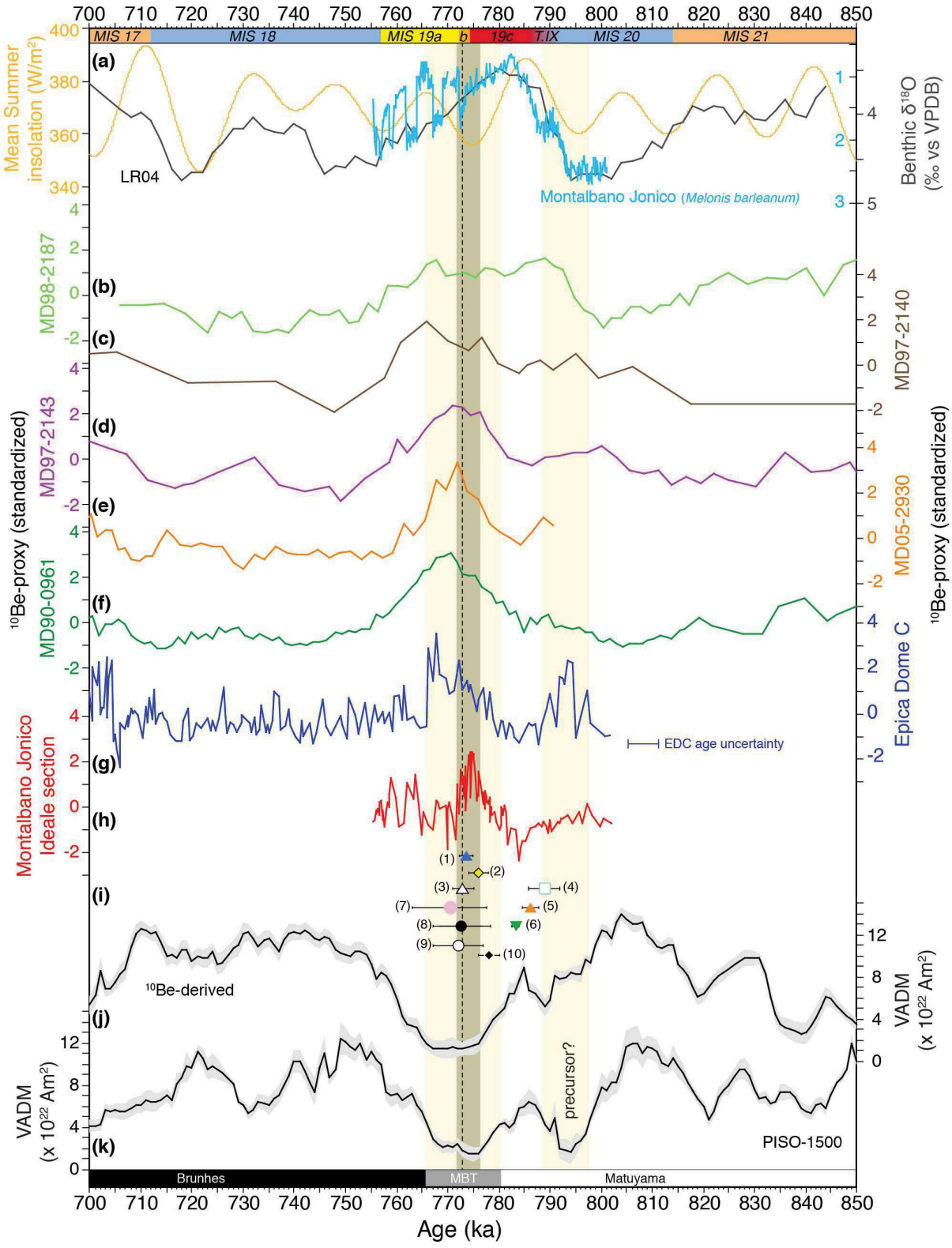
MIS 17
MIS 18
MIS 19a
b
19c
T.IX
MIS 20
MIS 21
Mean Summer insolation (W/m²)
LR04
Montalbano Jonico (Melonis barleanum)
Benthic δ18O (‰ vs VPDB)
MD98-2187
MD97-2140
MD97-2143
MD05-2930
MD90-0961
Epica Dome C
EDC age uncertainty
Montalbano Jonico Ideale section
10Be-proxy (standardized)
10Be-derived
VADM (x 10²² Am²)
precursor?
PISO-1500
Brunhes
MBT
Matuyama
Age (ka)

Fig. 12

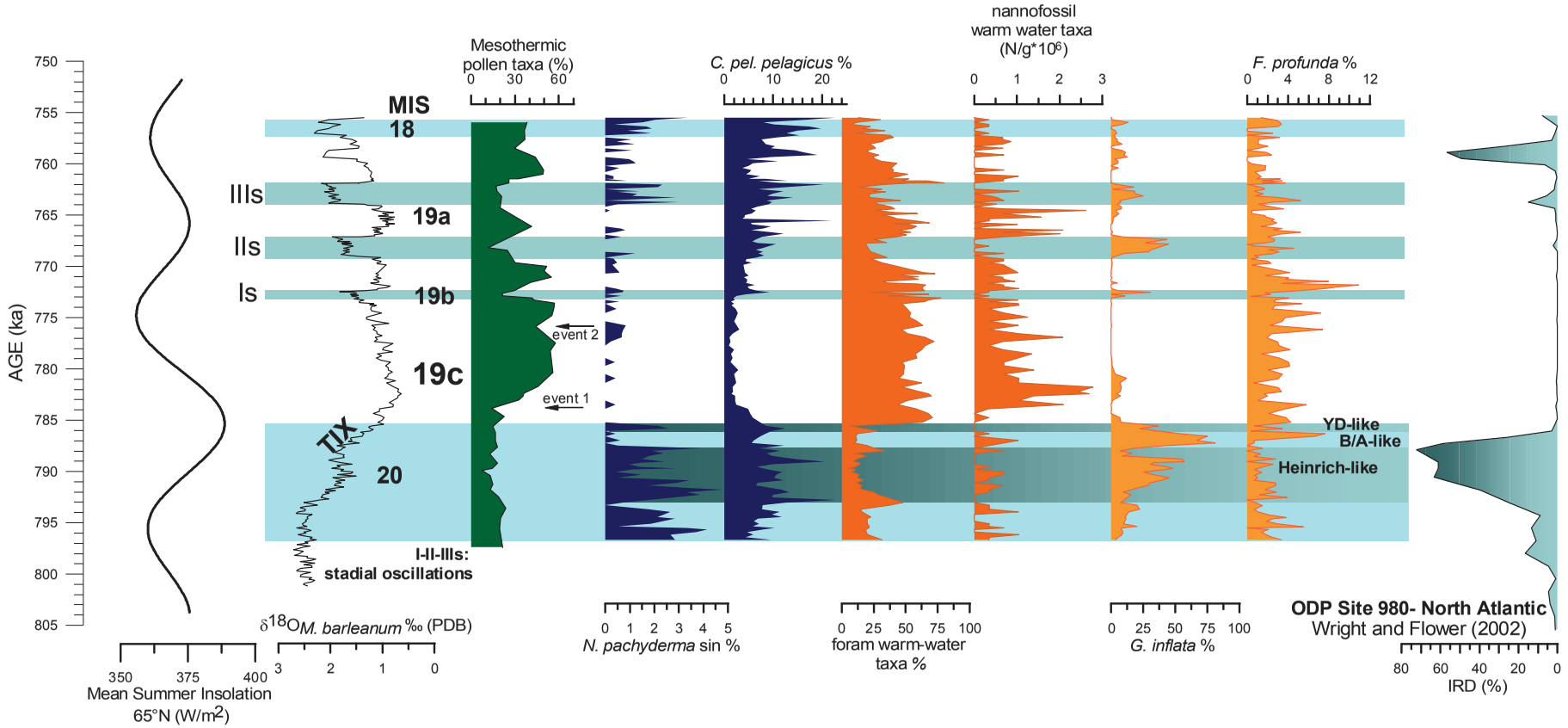
AGE (ka)
750
755
760
765
770
775
780
785
790
795
800
805
Mean Summer Insolation
65°N (W/m2)
350
375
400
δ18OM. barleanum ‰ (PDB)
3
2
1
0
Mesothermic
pollen taxa (%)
0
30
60
MIS
18
IIIs
19a
IIs
19b
Is
19c
20
TIX
event 2
event 1
I-II-IIIs:
stadial oscillations
C. pel. pelagicus %
0
10
20
N. pachyderma sin %
0
1
2
3
4
5
nannofossil
warm water taxa
(N/g*10⁶)
0
1
2
3
foram warm-water
taxa %
0
25
50
75
100
F. profunda %
0
4
8
12
G. inflata %
0
25
50
75
100
YD-like
B/A-like
Heinrich-like
ODP Site 980- North Atlantic
Wright and Flower (2002)
IRD (%)
80
60
40
20
0

Fig. 13

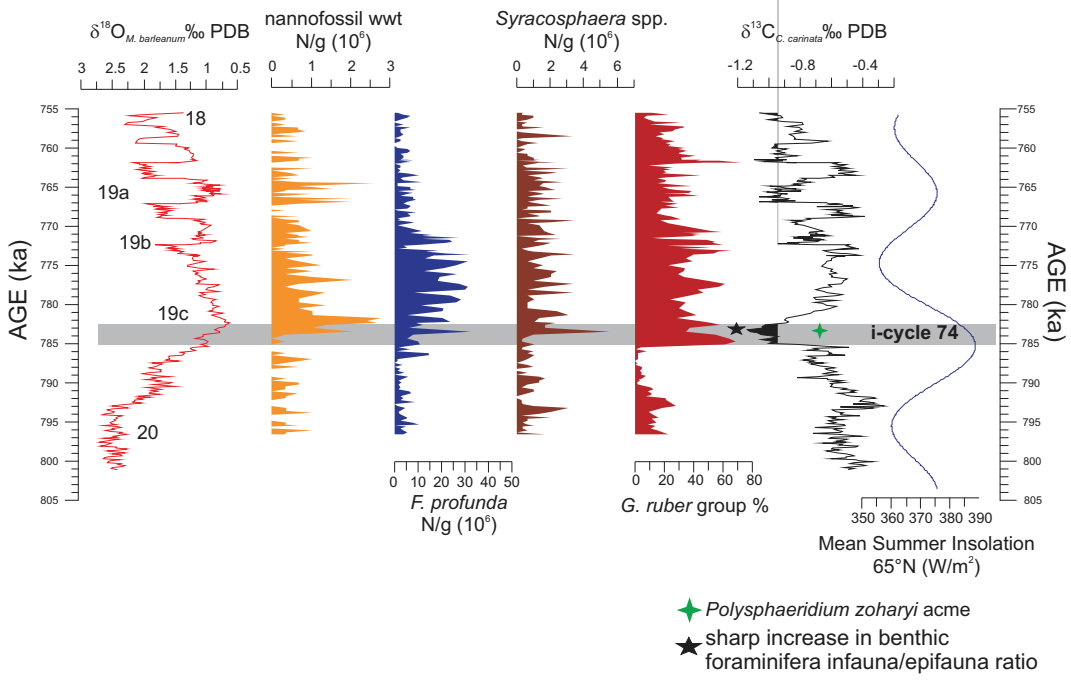
δ18O M. barleanum ‰ PDB
3 2.5 2 1.5 1 0.5
nannofossil wwt N/g (10^6)
0 1 2 3
Syracosphaera spp. N/g (10^6)
0 2 4 6
δ13C C. carinata ‰ PDB
-1.2 -0.8 -0.4
AGE (ka)
18
19a
19b
19c
20
i-cycle 74
0 10 20 30 40 50
F. profunda N/g (10^6)
0 20 40 60 80
G. ruber group %
350 360 370 380 390
Mean Summer Insolation 65°N (W/m2)
Polysphaeridium zoharyi acme
sharp increase in benthic foraminifera infauna/epifauna ratio

Fig. 14

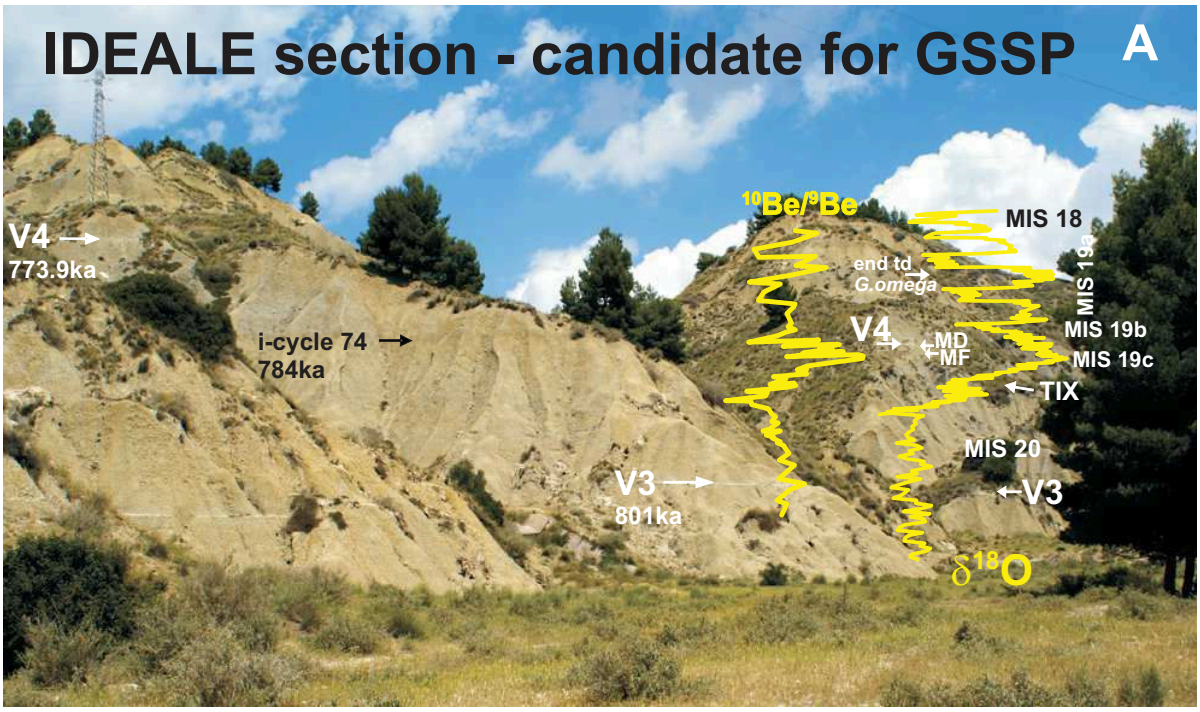
IDEALE section - candidate for GSSP
A
V4
773.9ka
i-cycle 74
784ka
V3
801ka
10Be/9Be
MIS 18
end td
G.omega
MIS 19a
V4
MD
MF
MIS 19b
MIS 19c
TIX
MIS 20
V3
δ18O

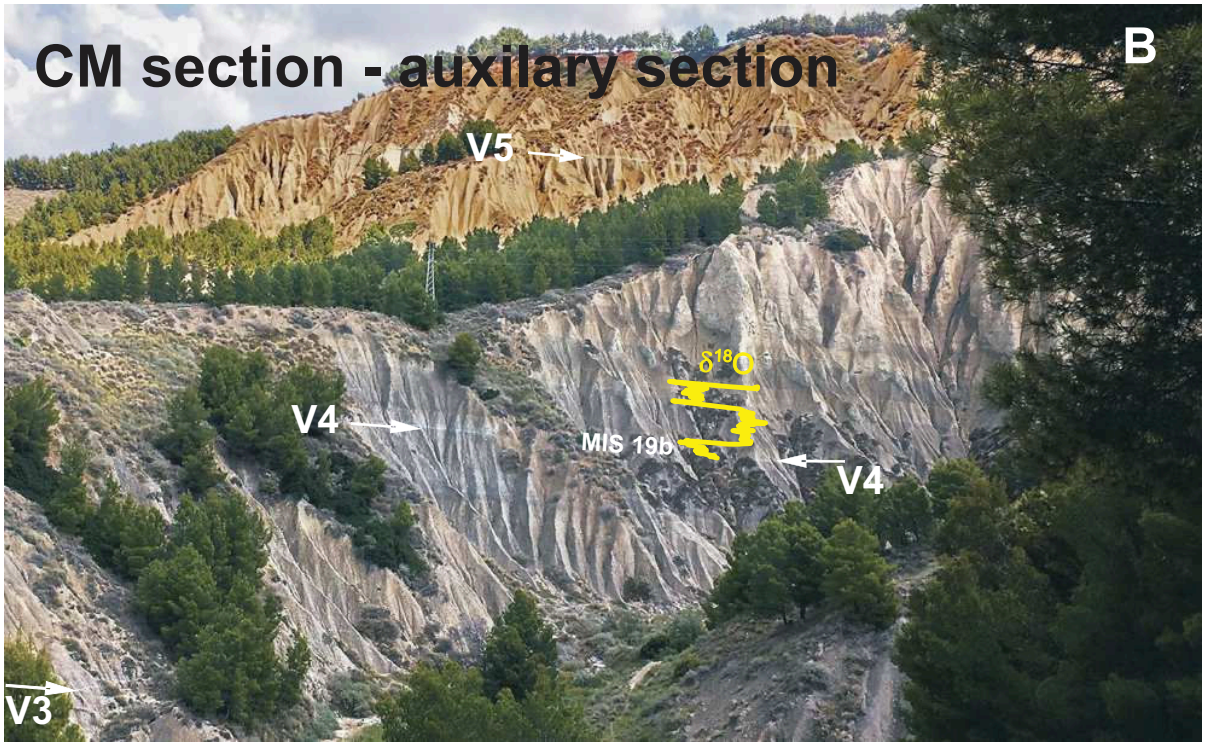
CM section - auxilary section
B
V5
δ18O
V4
MIS 19b
V4
V3

Fig. 15

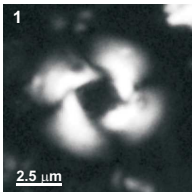

Reticulofenestra asanoi

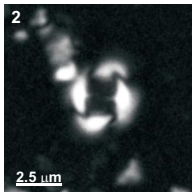

Gephyrocapsa omega

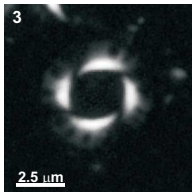

Psuedoemiliania lacunosa

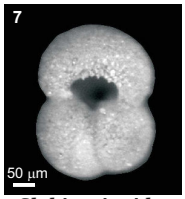

Globigerinoides ruber

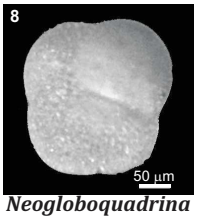

Neogloboquadrina pachyderma sinistral

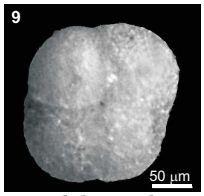

Neogloboquadrina pachyderma dextral

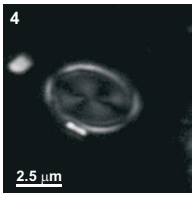

Syracosphaera histrica

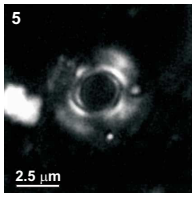

Umbilicosphaera sibogae s.l.

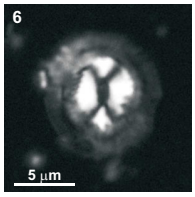

Coccolithus pel. pelagicus

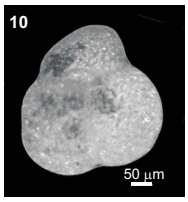

Trilobatus sacculifer

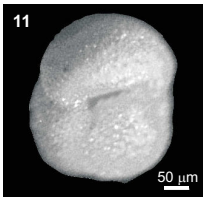

Globorotalia inflata

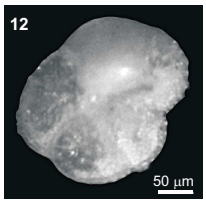

Globorotalia crassaformis

Ephedra

Artemisia

Quercus

Zelkova

Tsuga

Pinus

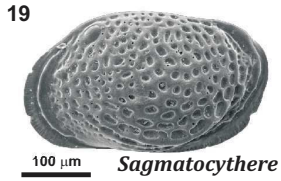

Sagmatocythere concentrica

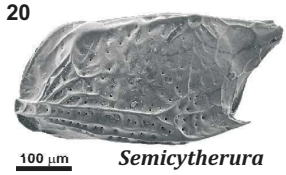

Semicytherura ruggieri

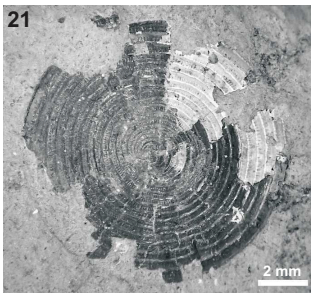

Discopirina italica

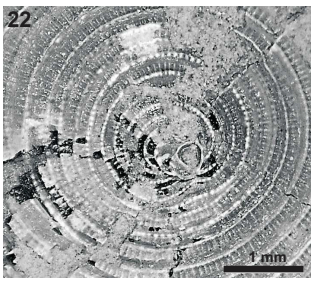

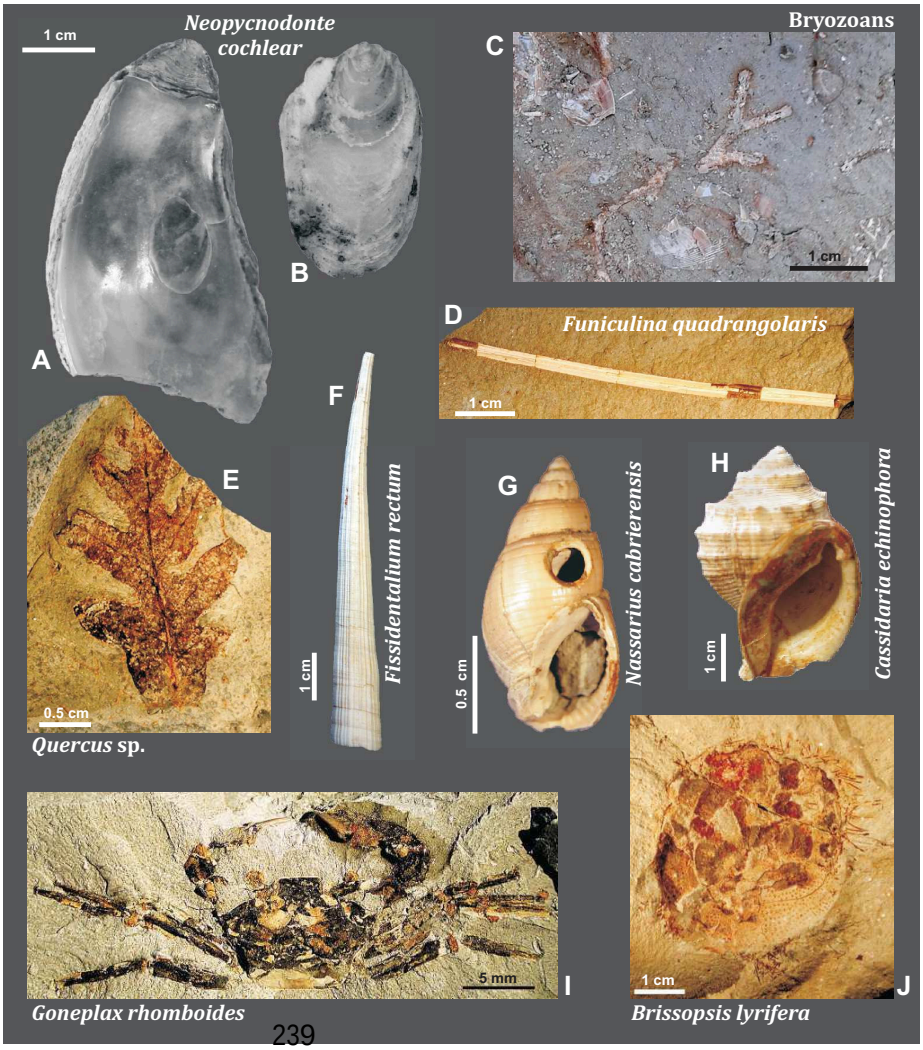

PLATE 1

Calcareous Plankton Biochronology						
MONTALBANO JONICO COMPOSITE SECTION				Gradstein et al. (2012) GTS age (Ma)	Additional calibrated ages (Ma)	
Bioevent	Depth (m)	Age (Ma)	MIS		Atlantic/ Pacific	Mediterranean
end temp. disap. *Gephyrocapsa omega*	151.14 Interval B **53.54 Ideale partial section**	0.76	19a	.	0.78*	0.78*
beginning temp. disap. *Gephyrocapsa omega*	82.65 Interval B	0.83	20-21	.	0.82*	0.82*
HCO *Reticulofenestra asanoi*	162.85 Interval A	0.92	23	0.91	0.91**	0.90**
LO *G. omega* (= re-entrance medium *Gephyrocapsa*)	138.15 Interval A	0.96	25	1.02	1.02**	0.97**
LCO *Reticulofenestra asanoi*	70.95 Interval A	1.09	31	1.14	1.14**	1.08**
end influx *Globorotalia crassaformis*	60.55 Interval A	1.12	33-34	.	.	1.13***
beginning influx *Globorotalia crassaformis*	50.15 Interval A	1.15	34	.	.	1.13***
re-appearance *Neogloboquadrina pachyderma* sinistral	17.2 Interval A	1.21	36	.	.	1.21***

TABLE 1

The requirements for a GSSP (ICS)	IDEALE SECTION - MONTALBANO JONICO (southern Italy)	
Exposure over an adequate thickness of sediment	**YES**	The Ideale Section is exposed over 74 m and records the MIS 20-18 time interval
Continuous sedimentation	**YES**	No hiatuses are recorded in the section. The twin section (CM) supports the sedimentary continuity of Ideale section
High sedimentation rate	**YES**	The sedimentation rate is ca. 100 cm/ka close to the proposed GSSP
Absence of synsedimentary and tectonic disturbances	**YES**	The section is totally devoid of turbidites, slumps, or faults
Absence of metamorphism and strong diagenetic alteration	**YES**	
Absence of vertical litho- or biofacies changes	**YES**	Sediments across the boundary are nearly homogenous belonging to an outer shelf-upper slope setting, in agreement with fossil assemblages
Abundance and diversity of well preserved fossils	**YES**	Microfossils (foraminifera, calcareous nannofossils, pollen and dinocistys), macrofossils (mollusks, anellids, echinoids, crabs, rare deep corals, otoliths). Published papers are available at **http://www.geo.uniba.it/mjs.html**
Favorable facies for long-range biostratigraphical correlations	**YES**	Calcareous plankton (nannofossils and foraminifera) biostratigraphic events at MJS are correlatable at the scale of Mediterranean and Oceans. The Ideale section records the large-scale end of temporary disappearance of nannofossil *Gephyrocapsa omega*
Radiometric dating	**YES**	Tephra layers V3, V4, in the Ideale section, and V5, in the upper MJS, are dated by $^{40}Ar/^{39}Ar$ method
Geomagnetic moment collapse at Matuyama Brunhes Boundary	**YES**	The geomagnetic dipole moment collapse accompanying the MBB is successfully identified by the prominent peak of $^{10}Be/^{9}Be$ ratio at the end of MIS 19c-early MIS 19b, in agreement with the most detailed sequences of the MBB (Channell et al., 2017)
Chemostratigraphy	**YES**	Very high resolution (1 sample every 20 cm, ~90-200 years) oxygen and carbon isotope (*M.barleanum* and *Cassidulina carinata*) and authigenic $^{10}Be/^{9}Be$ (1 sample /180-230 years, close to the MIS 19c-19b transition) data are available for the Ideale section
Cyclostratigraphy and astronomical tuning	**YES**	The entire MJS was astronomically tuned (Ciaranfi et al., 2010). The Ideale section is calibrated combining orbital tuning and $^{40}Ar/^{39}Ar$ age of tephra V4
Intensive research	**YES**	The section has been well studied (**http://www.geo.uniba.it/mjs.html**) and new projects (i.e. ultra-high resolution $^{10}Be/^{9}Be$ across the MB transition, the $^{40}Ar/^{39}Ar$ intercalibration on V4 as well as undergoing Mg/Ca and $\Delta 47$ measurements) that all started in 2016 illustrate the intense scientific activity at MJS
Accessibility	**YES**	The section is about 1km far from the state road SS598 from which it can be reached by a short (30 minutes) walking route on comfortable path or by means a vehicle (10 minutes)
Permanent protection of the site	**YES**	The section is located in the *Special Natural Reserve of Montalbano Jonico badlands*. Any kind of urban development is banned in this area
Possibility to fix a permanent marker	**YES**	Whether the GSSP is approved, a permanent marker (a metal plate) will be fixed at the visible lithological marker V4. The University of Bari is involved to cooperate with the local authorities to fix the Golden Spike and periodically check its preservation

TABLE 2

References

Abbate, E., Sagri, M. (2012). Early to Middle Pleistocene *Homo* dispersal from Africa to Eurasia: Geological, climatic and environmental constraints. Quaternary International, 267, 3–19.

Abbaticchio, P., Amicarelli, V., Dell'Anna, L., Di Pierro, M., 1981. Argille varicolori della zona di Stigliano (MT): indagini mineralogiche, chimiche e granulometriche. Società Italiana di Mineralogia e Petrologia 37, 195-211.

Aiello, G., Barra, D., Bonaduce, G., 2000. Systematic and biostratigraphy of the ostracoda of the Plio-Pleistocene Monte S. Nicola section (Gela; Sicily). Bollettino della Società Paleontologica Italiana 39 (1), 83–112.

Aiello, G., Barra, D., Parisi, R., 2015. Lower-Middle Pleistocene ostracod assemblages from the Montalbano Jonico section (Basilicata, southern Italy). Quaternary International 383, 47-73.

Aiello, G., Szczechura, J., 2004. Middle Miocene ostracods of the Fore-Carpathian Depression (Central Paratethys, southwestern Poland). Bollettino della Società Paleontologica Italiana 43 (1-2), 11–70.

Aitchison, J., 1982. The statistical analysis of compositional data (with discussion). Journal of the Royal Statistical Society, Series B (Statistical Methodology) 44(2), 139-177.

Alley, R.B., Agustsdottir, A.M., 2005. The 8k event: cause and consequences of a major Holocene abrupt climate change. Quaternary Science Reviews. 24, 1123–1149.

Amato, V., Aucelli, P.P.C., Cesarano, M., Jicha, B., Lebreton, V., Orain, R., Pappone, G., Petrosino, P., Russo Ermolli, E. 2014. Quaternary evolution of the largest intermontane basin of the Molise Apennine (central-southern Italy). Special Issue: Intermontane Basins: Quaternary morphoevolution of Central-Southern Italy. In: Aucelli, P.P.C., Della Seta, M., Giano, S.I., Schiattarella, M. (Eds.). Rendiconti Lincei —

Scienze Fisiche e Naturali 25(2), 197–216.
Amorosi, A., Antonioli, F., Bertini, A., Marabini, S., Mastronuzzi, G., Montagna, P., Negri, A., Rossi, V., Scarponi, D., Taviani, M., Angeletti, L., Piva, A., Vai, G.B., 2014. The Middle–Upper Pleistocene Fronte Section (Taranto, Italy): An exceptionally preserved marine record of the Last Interglacial. Global and Planetary Change 119, 23–38.
André, A., Weiner, A, Quillévéré, F., Aurahs, R., Morard, R., Douady, C.J, de Garidel-Thoron, T., Escarguel, G., de Vargas, C., Kucera, M., 2013. The cryptic and the apparent reversed: lack of genetic differentiation within the morphologically diverse plexus of the planktonic foraminifer *Globigerinoides sacculifer*. Paleobiology 39(1), 21–39.
APAT, 2007. Quaderni del Servizio Geologico d'Italia. Serie III, n° 7, fascicolo 7, S.E.L.C.A., Firenze.
Asioli, A., Trincardi, F., Lowe, J.J., Ariztegui, D., Langone, L., Oldfield, F., 2001. Submillennial scale climatic oscillations in the central Adriatic during the Late glacial: palaeoceanographic implications. Quaternary Science Reviews 20, 1201–1221.
Aurahs, R., Treis, Y., Darling, K., Kucera, M., 2011. A revised taxonomic and phylogenetic concept for the planktonic foraminifer species *Globigerinoides ruber* based on molecular and morphometric evidence. Marine Micropaleontology 79, 1–14.
Azzaroli, A., Perno, U., Radina, B., 1968. Note illustrative della Carta Geologica d'Italia alla scala 1:100.000, Foglio 188 Gravina di Puglia. Servizio Geologico d'Italia, 57 pp.
Balduzzi, A., Casnedi, R., Crescenti, U., Mostardini, F., Tonna, M., 1982. - Il Plio-Pleistocene del sottosuolo del bacino lucano (Avanfossa appenninica). Geologica Romana 21, 89-111.
Bárcena, M.A., Flores, J.A., Sierro, F.J., Perez-Folgado, M., Fabres, J., Calafat, A., Canals, M., 2004. Planktonic response to main oceanographic changes in the Alboran Sea (Western Mediterranean) as documented in sediment traps and surface sediments. Marine Micropaleontology 53, 423–445.
Bard, E., Rostek, F., Turon, J.-L., Gendreau, S., 2000. Hydrological impact of Heinrich Events in the subtropical northeast Atlantic. Science, 289(5483), 1321-1324.

Barker, S., Knorr, G., Edwards, R. L., Parrenin, F., Putnam, A. E., Skinner, L. C., Wolff, E., Ziegler, M., 2011. 800,000 Years of Abrupt Climate Variability. Science 334, 347–351.

Bartlein, P.J., Prentice, I.C., 1989. Orbital variations, climate and paleoecology. Trends in Ecology and Evolution 4, 195-199.

Bassinot, F.C., Labeyrie, L.D., Vincent, F., Quidelleur, X., Shackleton, N.J., Lancelot, Y., 1994. The astronomical theory of climate and the age of the Brunhes-Matuyama magnetic reversal. Earth and Planetary Science Letters 126, 91–108.

Basso, F., Bove, E., del Prete, M., 2002. General description of the Agri Basin, Southern Italy. In: Geeson, N.A., Brandt, C.J., Thornes, J.B. (Eds.). Mediterranean Desertification: A Mosaic of Processes and Responses. John Wiley & Sons, Ltd., pp. 321–330.

Baumann, K.H., Andruleit, H., Samtleben, C., 2000. Coccolithophores in the Nordic Seas: Comparison of living communities with surface sediment assemblages. Deep Sea Research, Part II, 47, 1743–1772.

Baumann, K.-H., Bockel, B., Frenz, M., 2004. Coccolith contribution to South Atlantic carbonate sedimentation. In: Thierstein, H.R., Young, J. (Eds.), Coccolithophores from Molecular Processes to Global Impact. Springer, Berlin, pp. 367-402.

Bazin, L., Landais, A., Lemieux-Dudon, B., Toyé Mahamadou Kele, H., Veres, D., Parrenin, F., Martinerie, P., Ritz, C., Capron, E., Lipenkov, V., Loutre, M.-F., Raynaud, D., Vinther, B., Svensson, A., Rasmussen, S. O., Severi, M., Blunier, T., Leuenberger, M., Fischer, H., Masson-Delmotte, V., Chappellaz, J., Wolff, E., 2013. An optimized multi-proxy, multi-site Antarctic ice and gas orbital chronology (AICC2012): 120–800 ka. Climate of the Past. 9, 1715-1731.

Bé, A.W.H., 1971. Winter distribution of planktonic foraminifera between the Grand Banks and the Caribbean. Micropalaeontology 17(1), 31-42.

Bé, A.W.H., 1977. An ecological, zoogeographic and taxonomic re view of Recent planktonic foraminifera. In: Ramsay, A.T.S. (Ed.). Oceanic Micropaleontology (Vol. 1). London, Academic Press, 1.

Bé, A.W.H., Hamlin, W.H., 1967. Ecology of recent planktonic foraminifera. Micropaleontology 13, 87-100.

Bé, A.W.H., Tolderlund, D.S., 1971. Distribution and ecology of living

planktonic Foraminifera in surface waters of the Atlantic and Indian Oceans. In: Funnell, B.M., Riedel, W.R. (Eds.). The Micropaleontology of the Oceans. Cambridge University Press, London, pp. 105–149.

Beaudouin, C., Suc, J.-P., Cambon, F., Touzani, A., Giresse, P., Pont, D., Aloïsi, J.C., Marsset, T., Cochonat, P., Duzer, D., Ferrier, J., 2005. Present-day rhythmic deposition in the Grand Rhône prodelta (NW Mediterranean) according to high-resolution pollen analyses. Journal of Coastal Research 21, 292–306.

Beaudouin, C., Suc, J.-P., Escarguel, G., Arnaud, M., Charmasson, S., 2007. The significance of pollen signal in present-day marine terrigenous sediments: The example of the Gulf of Lions (western Mediterranean Sea). Geobios 40(2), 159–172.

Bennett, K.D., Tzedakis, P.C., Willis, K.J., 1991. Quaternary refugia of north European trees. Journal of Biogeography 18(1), 103-115.

Berger, A., 1978. Long-term variations of daily insolation and Quaternary climatic changes. Journal of the Atmospheric Science 35, 2362–2367.

Berger, A.L., 1981. The astronomical theory of paleoclimates. In: Berger A.L. (Ed.). Climatic Variations and Variability: Facts and Theories. Reidel, Dordrecht, pp. 501-525.

Berger, A., 1988. Milankovitch theory and climate. Reviews of Geophysics 26, 624-657.

Berger, A., Loutre, M.F., 2002. An exceptionally long interglacial ahead? Science 297, 1287–1288.

Berger, A., Yin, Q.Z., Herold, N., 2012. MIS-11 and MIS-19 analogues of our Interglacial. 3rd International Conference on Earth System Modelling, September 17-21, 2012, Hamburg, Germany.

Bergmann, J., Friedel, P., Kleeberg, R., 1998. BGMN - a new fundamental parameter based Rietveld program for laboratory X-ray sources, its use in quantitative analysis and structure investigations. CPD Newsletter, Commission of Powder Diffraction, International Union of Crystallography 20, 5-8.

Berner, R.A., 1971. Principles of chemical sedimentation. McGraw-Hill, New York, pp. 270.

Bertini, A., 2000. Pollen record from Colle Curti and Cesi: Early and Middle Pleistocene mammal sites in the Umbro-Marchean Apennine mountains (central Italy). Journal of Quaternary Science 15(8), 825–840.

Bertini, A., 2001. Pliocene climatic cycles and altitudinal forest development from 2.7 Ma in the Northern Apennines (Italy): evidences from the pollen record of the Stirone section (~5.1 to ~2.2 Ma). Geobios 34, 253-265.

Bertini, A., 2010. Pliocene to Pleistocene palynoflora and vegetation in Italy: state of the art. Quaternary International 225(1), 5–24.

Bertini, A., Ciaranfi, N., Marino, M., Palombo, M.R., 2010. Proposal for Pliocene and Pleistocene land-sea correlation in the Italian area. Quaternary International 219, 95-108.

Bertini, A., Toti, F., Marino, M., Ciaranfi, N., 2015. Vegetation and climate across the Early-Middle Pleistocene transition at the Montalbano Jonico section (southern Italy). Quaternary International 383, 74-88.

Bertoldi, R., Rio, D., Thunell, R., 1989. Pliocene-Pleistocene vegetational and climatic evolution of the south-central Mediterranean. Palaeogeography Palaeoclimatology Palaeoecology 72, 263-275.

Bickert, T., Curry, W.B., Wefer, G., 1997. Late Pliocene to Holocene (2.6-0 Ma) western equatorial Atlantic deep-water circulation: inferences from benthic stable isotope. In: Shackleton, N.J., Curry, W.B., Richter, C., Bralower, T.J. (Eds.). Proceedings of the Ocean Drilling Program. Scientific Results 154, College Station (TX), pp. 239-253.

Bintanja, R., van de Wal, R.S.W., 2008. North American ice-sheet dynamics and the onset of 100,000-year glacial cycles. Nature 454, 869–872.

Biondi, E., Ballelli, S., Taffetani, F., 1992. La vegetazione di alcuni territori calanchivi in Basilicata (Italia meridionale). Documents Phytosociologiques N.S. 14, 489-498.

Björck, S., Walker, M.J.C., Cwynar, L.C., Johnsen, S., Knudsen, K.L., Lowe, J.J., Wohlfarth, B., INTIMATE Members, 1998. An event stratigraphy for the Last Termination in the North Atlantic region based on the Greenland Ice-core record: a proposal by the INTIMATE group. Journal of Quarternary Science 13, 283–292.

Boeckel, B., Baumann, K.H., 2004. Distribution of coccoliths in surface sediments of the south-eastern South Atlantic Ocean: ecology,

preservation and carbonate contribution. Marine Micropaleontology 51(3-4), 301- 320.
Boenzi, F., Caldara, M., Capolongo, D., Dellino, P., Piccarreta, M., Simone, O., 2008. Late Pleistocene–Holocene landscape evolution in Fossa Bradanica, Basilicata (southern Italy). Geomorphology 102 (3), 297-306.
Boenzi, F., Capolongo, D., Gallicchio, S., Di Pinto, G., 2014. Morphostructure of the Lucania Apennines front between the Basento and Salandrella rivers (Southern Italy). Journal of Maps 10(3), 478-486.
Bollmann, J., 1997. Morphology and biogeography of *Gephyrocapsa* coccoliths in Holocene sediments. Marine Micropaleontology 29, 319–350.
Bonaduce, G., Ciampo, G., Masoli, M., 1976. Distribution of Ostracoda in the Adriatic Sea. Pubblicazioni della Stazione Zoologica di Napoli 40(1), 1–304.
Bonardi, G., D'Argenio, B., Di Nocera, S., Marsella, E., Pappone, G., Pescatore, T.S., Senatore, M.R., Sgrosso, I., Ciaranfi, N., Pieri, P., Ricchetti, G., 1988. Carta geologica dell'Appennino meridionale. 74° Congresso Società Geologica Italiana, Carta geologica in scala 1: 250.000.
Bond, G., Broecker, W., Johnsen, S., McManus, J., Labeyrie, L., Jouzel, J., Bonani, G., 1993. Correlations between climate records from North Atlantic sediments and Greenland ice. Nature 365, 143–147.
Bond, G., Showers, W., Cheseby, M., Lotti, R., Almasi, P., deMenocal, P., Priore, P., Cullen, H., Hajdas, I., Bonani, G., 1997. A pervasive millennial-scale cycle in North Atlantic Holocene and glacial climates. Science 278, 1257–1266.
Brauer, A., Allen, J.R.M., Mingram, J., Dulski, P., Wulf, S., Huntley, B., 2007. Evidence for last interglacial chronology and environmental change from Southern Europe. Proceedings of the National Academy of Sciences 104(2), 450–455.
Brilli, M., 1998. Stratigrafia isotopica del carbonio e dell'ossigeno della successione infra e mesopliocenica di Montalbano Jonico (Basilicata, Italia meridionale). Tesi di Dottorato di Ricerca in Scienze della terra XI ciclo, Università degli Studi di Roma "La Sapienza", 112 pp.
Brilli, M., Lerche, J., Ciaranfi, N., Turi, B., 2000. Evidence of precession and obliquity orbital forcing in Oxygen-18 isotope composition of Montalbano Jonico section (Basilicata, southern Italy). Applied

Radiation and Isotope 52, 957-964.
Broecker, W.S., 1998. Paleocean circulation during the last deglaciation: A bipolar seesaw? Paleoceanography 13(2), 119-121.
Cacho, I., Grimalt, J.O., Pelejero, C., Canals, M., Sierro, F.J., Flores, J.A., Shackleton, N.J., 1999. Dansgaard–Oeschger and Heinrich event imprints in the Alboran Sea paleotemperatures. Paleoceanography 14, 698–705.
Cacho, I., Grimalt, J. O., Canals, M., Sbaffi, L., Shackleton, N., Schönfeld, J., Zahn, R., 2001. Variability of the western Mediterranean Sea surface temperature during the last 25,000 years and its connection with the northern hemisphere climatic changes. Paleoceanography 16, 40–52.
Cacho, I., Grimalt, J.O., Sierro, F.J., Shackleton, N.J., Canals, M., 2000.Evidence for enhanced Mediterranean thermohaline circulation during rapid climatic coolings. Earth and Planetary Science Letters 183, 417–429.
Cambon, G., Suc, J.-P., Aloïsi, J.C., Giresse, P., Monaco, A., Touzani, A., Duzer, D., Ferrier, J., 1997. Modern pollen deposition in the Rhône delta area (lagoonal and marine sediments), France. Grana 36, 105–113.
Candy, I., Schreve, D.S., Sherriff, J., Tye, G.J., 2014. Marine Isotope Stage 11: palaeoclimates, palaeoenvironments and its role as an analogue for the current interglacial. Earth-Science Reviews 128, 18-51.
Cantore, V., Iovino, F., Pontecorvo, G., 1987. Aspetti climatici e zone fito-climatiche della Basilicata. C.N.R. IEIF, Cosenza, Grafiche Badiali, Arezzo, Italy, pp. 50.
Capotondi, L., Borsetti, A.M., Morigi, C., 1999. Foraminiferal ecozones, a high resolution proxy for the late Quaternary biochronology in the central Mediterranean Sea. Marine Geology 153, 253-274.
Capotondi, L., Girone, A., Lirer, F., Bergami, C., Verducci, M., Vallefuoco, M., Afferri, A., Ferraro, L., Pelosi, N., De Lange, G.J., 2016. Central Mediterranean Mid-Pleistocene paleoclimatic variability and its connection with global climate. Palaeogeography Palaeoclimatology Palaeoecology 442, 72–83.
Capraro, L., Asioli, A., Backman, J., Bertoldi, R., Channell, J.E.T., Massari, F., Rio., D., 2005. Climatic patterns revealed by pollen and oxygen isotope records across the Matuyama–Brunhes Boundary in the central Mediterranean (southern Italy). In: Head, M.J., Gibbard, P.L. (Eds.).

Early-Middle Pleistocene Transitions: The Land–Ocean Evidence. Geological Society London, Special Publications 247, pp. 159–182.

Capraro, L., Ferretti, P., Macrì, P., Scarponi, D., Tateo, F., Fornaciari, E., Bellini, G., Dalan, G., 2017. The Valle di Manche section (Calabria, Southern Italy): A high resolution record of the Early-Middle Pleistocene transition (MIS 21-MIS 19) in the Central Mediterranean. Quaternary Science Reviews, 165, 31-48.

Carbone, S., 2013. Note illustrative della Carta Geologica d'Italia alla scala 1:50.000, Foglio 523 Rotondella. SystemCart, Roma. www.isprambiente.gov.it/Media/carg/note_illustrative/523_Rotondella.pdf.

Casnedi, R., 1988. La Fossa bradanica: origine, sedimentazione e migrazione. Memorie Società Geologica Italiana 41, 439–448.

Casnedi, R., Crescenti, U., Tonna, M., 1982. Evoluzione dell'Avanfossa adriatica meridionale nel Plio-Pleistocene sulla base di dati di sottosuolo. Memorie Società Geologica Italiana 24, 243–260.

Cavalcante, F., Fiore, S., Piccarreta, G., Tateo, F., 2003. Geochemical and mineralogical approaches to assessing provenance and deposition of shales: a case study. Clay Minerals 38, 383–397.

Cavalcante, F., Prosser, G., Agosta, F., Belviso, C., Corrado, G., 2015. Post-depositional history of the Miocene Gorgoglione Formation (southern Apennines, Italy): inferences from mineralogical and structural analyses. Bulletin de la Société Géologique de France, 186(4-5), 243-256.

Ceregato, A., Raffi, S., Scarponi, D., 2007. The circalittoral/bathyal in the Middle Pliocene of Northern Italy: the case of the *Korobkovia oblongae-Jupiteria concave* paleocommunity type. Geobios 40, 555-572.

Chamley, H., 1989. Clay sedimentology. Springer-Verlag Berlin Heidelberg, Germany, 623 pp.

Channell, J.E.T., Kleiven, H.F., 2000. Geomagnetic paleointensities and astrochronological ages from the Matuyama-Brunhes boundaries and the boundaries of Jaramillo Subchron: paleomagnetic and isotope records from ODP Site 983. Philosophical Transaction of Royal Society of London 358, 1027–1047.

Channell, J.E.T., Raymo, L., 2003. Paleomagnetic record at ODP Site 980 (Feni Drift, Rockall) for the past 1.2 Myrs. Geochemistry, Geophysics,

Geosystems 4(4), 1033.
Channell, J.E.T., Curtis, J.F., Flower, B.P., 2004. The Matuyama-Bruhnes interval (500-900 ka) in North Atlantic drift sediments. Gephysical Journal International 158, 489–505.
Channell, J.E.T., Hodell, D.A., Singer, B.S., Xuan, C., 2010. Reconciling astrochronological and $^{40}Ar/^{39}Ar$ ages for the Matuyama-Brunhes boundary in the late Matuyama Chron. Geochemistry, Geophysics, Geosystems 11, Q0AA12.
Christl, M., Strobl, C., Mangini, A., 2003. Beryllium-10 in deep-sea sediments: a tracer for the Earth's magnetic field intensity during the last 200,000 years. Quaternary Science Reviews 22, 725-739.
Ciaranfi, N., D'Alessandro, A., 2005. Overview of the Montalbano Jonico area and section: a proposal for a boundary stratotype for the lower-middle Pleistocene, southern Italy Foredeep. Quaternary International 131, 5–10.
Ciaranfi, N., D'Alessandro, A., Marino, M., Sabato, L., 1994. The Montalbano Jonico Section in the Bradanic Foredeep (southern Italy): a potential early-middle Pleistocene Boundary Stratotype. Contribution in: Cita, M.B., Castradori, D., 1994. Workshop on marine sections from the Gulf of Taranto (Southern Italy usable as potential stratotypes for the GSSP of the Lower, Middle and Upper Pleistocene. Bari, Italy, September 29-October 4, 1994). Il Quaternario 7, 677-692.
Ciaranfi, N., Marino, M., Sabato, L., D'Alessandro, A., De Rosa, R., 1996. Studio geologico-stratigrafico di una successione infra e mesopleistocenica nella parte sud-occidentale della Fossa bradanica (Montalbano Jonico, Basilicata). Bolletino Società Geologica Italiana 115, 379-391.
Ciaranfi, N., D'Alessandro, A., Marino, M., 1997. A candidate section for the lower-middle Pleistocene boundary (Apennine foredeep, South Italy). In: Naiwen, W., Remane, J. (Eds.). Proceedings 30th International Geological Congress 11, pp. 201–211.
Ciaranfi, N., D'Alessandro, A., Girone, A., Maiorano, P., Marino, M., Soldani, D., Stefanelli, S., 2001. Pleistocene sections in the Montalbano Jonico area and the potential GSSP for Early-Middle Pleistocene in the Lucania Basin (southern Italy). Memorie di Scienze Geologiche 53, 67-83.
Ciaranfi, N., van Kolfshoten, T., Coltorti, M., 2005. The Plio-Pleistocene boundary and the lower-middle Pleistocene transition: type areas and

sections: an introduction. Quaternary International 131, 1–3.
Ciaranfi, N., Lirer, F., Lirer, L., Lourens, L.J., Maiorano, P., Marino, M., Petrosino, P., Sprovieri, M., Stefanelli, S., Brilli, M., Girone, A., Joannin, S., Pelosi, N., Vallefuoco, M., 2010. Integrated stratigraphy and astronomical tuning of the Lower-Middle Pleistocene Montalbano Jonico land section (southern Italy). Quaternary International 210, 109–120.
Ciaranfi, N., Head, M.J., Marino, M., 2015. Report of the Field Workshop on the Lower-Middle Pleistocene transition in Italy. Quaternary Perspectives 22(1), 12-14.
Cita, M.B., Capraro, L., Ciaranfi, N., Di Stefano, E., Marino, M., Rio, D., Sprovieri, R., Vai, G.B., 2006. Calabrian and Ionian: a proposal for a definition of Mediterranean Stages for Lower and Middle Pleistocene. Episodes 29, 107–114.
Cita, M.B., Capraro, L., Ciaranfi, N., Di Stefano, E., Lirer, F., Maiorano, P., Marino, M., Raffi, I., Rio, D., Sprovieri, R., Stefanelli, S., Vai, G.B., 2008. The Calabrian Stage redefined. Episodes 31(4), 408–419.
Cita, M.B., Gibbard, P.L., Head, M.J., and The Subcommission on Quaternary Stratigraphy, 2012. Formal ratification of the base Calabrian Stage GSSP (Pleistocene Series, Quaternary System). Episodes 35(3), 388–397.
Clement, B.M., 2004. Geographical distribution of transitional VGPs: evidence for non-zonal symmetry during the Matuyama–Brunhes geomagnetic reversal. Earth and Planetary Science and Letters 104, 48–58.
Coe, R.S., Singer, B.S., Pringle, M.S., Zhao X.X., 2004. Matuyama-Brunhes reversal and Kamikatsura event on Maui: paleomagnetic directions, $^{40}Ar/^{39}Ar$ ages and implications. Earth and Planetary Science and Letters 222, 151–156.
Cohen, K.M., Gibbard, P., 2011. Global chronostratigraphical correlation table for the last 2.7 million years. Subcommission on Quaternary Stratigraphy (International Commission on Stratigraphy), Cambridge, England.
Colalongo, M.L., Pasini, G., 1980. La ostracofauna plio-pleistocenica della Sezione Vrica in Calabria (con considerazioni sul limite Neogene/Quaternario). Bollettino della Società Paleontologica Italiana 19(1), 44–126.

Colmenero-Hidalgo, E., Flores, J.A., Sierro, F.J., Barcena, M.A., Lowemark, L., Schonfeld, J., Grimalt, J.O., 2004. Ocean surface water response to short-term climate changes revealed by coccolithophores from the Gulf of Cadiz (NE Atlantic) and Alboran Sea (W Mediterranean). Palaeogeography Palaeoclimatology Palaeoecology 205, 317-336.

Combourieu Nebout, N., 1993. Vegetation response to Upper Pliocene glacial/Interglacial cyclicity in the central Mediterranean. Quaternary Research 40, 228-236.

Combourieu Nebout, N., 1995. Résponse de la végétation de l'Italie méridionale au seuil climatique de la fin du Pliocène d'apres l'analyse pollinique haute résolution de la section de Semaforo (2,46 à 2.1 Ma). Comptes Rendus de l'Académie des Science Paris, Série IIa 321, 659–665.

Combourieu Nebout, N., Semah, F., Djubiantono, T., 1990. La limite Pliocène-Pléistocène: précisions magnétostratigraphiques par l'étude sériée de la coupe-type de Vrica (Crotone, Italie). Comptes Rendus de l'Académie de Sciences, Paris, Série II 311, 851-857.

Combourieu Nebout, N., Vergnaud Grazzini, C., 1991. Late Pliocene northern hemisphere glaciations: the continental and marine responses in the central Mediterranean. Quaternary Science Reviews 10, 319–334.

Combourieu-Nebout, N., Bertini, A., Russo-Ermolli, E., Peyron, O., Klotz, S., Montade, V., Fauquette, S., Allen, J., Fusco, F., Goring, S., Huntley, B., Joannin, S., Lebreton, V., Magri, D., Martinetto, E., Orain, R., Sadori, L. (2015). Climate changes in Central Mediterranean and Italian vegetation dynamics since the Pliocene. Review of Paleobotany and Palynology, 218, 127-147.

Combourieu Nebout, N., Paterne, M., Turon, J. L., Siani, G., 1998. A high-resolution record of the last deglaciation in the Central Mediterranean Sea: Palaeovegetation and Palaeohydrological evolution. Quaternary Science Reviews 17, 303–317.

Combourieu Nebout, N., Peyron, O., Dormoy, I., Desprat, S., Beaudouin, C., Kotthoff, U., Marret, F., 2009. Rapid climatic variability in the west Mediterranean during the last 25,000 years from high resolution pollen data. Climate of the Past 5, 503-521.

Corbetta, F., 1974. Lineamenti della vegetazione lucana. Giornale Botanico Italiano 108(5), 211-234.

Corbetta, F., Ubaldi, D., Zanotti, A.L., 1991. La vegetazione a *Lygeum spartum* nei calanchi della Valle del Basento (Basilicata). Archivio Botanico Italiano 67(3–4), 141–155.

Corliss, B.H., 1991. Morphology and microhabitat preferences of benthic foraminifera from the northwest Atlantic Ocean. Marine Micropaleontology 17, 195-236.

Corliss, B.H., Chen, C., 1988. Morphotype pattern of Norwegian Sea, deep sea benthic foraminifera and ecological implications. Geology 16, 716-719.

D'Alessandro, A., La Perna, R., Ciaranfi, N., 2003. Response of macrobenthos to changes in paleoenvironment in the Lower-Middle Pleistocene (Lucania Basin, Southern Italy). Il Quaternario 16, 167–182.

Darling, K.F., Kucera, M., Kroon, D., Wade, C.M., 2006. A resolution for the coiling direction paradox in *Neogloboquadrina pachyderma*. Paleoceanography 21(2), PA2011.

De Kaenel, E., Siesser, W.G., Murat, A., 1999. Pleistocene calcareous nannofossil biostratigraphy and the western Mediterranean sapropels, sites 974 to 977 and 979. In: Zahn, R., Comas, M.C., Klaus, A. (Eds.). Proceedings of the Ocean Drilling Program. Scientific Results 161. ODP, College Station, TX, pp. 159–183.

de Vargas, C., Norris, R.D., Zaninetti, L., Gibb, S.W., Pawlowski, J., 1999. Molecular evidence of cryptic speciation in planktonic foraminifers and their relation to oceanic provinces. Proceedings of the National Academy of Science 96, 2864–2868.

Dell'Anna, L., Laviano, R., 1986. Caratteri mineralogici, chimici e granulometrici delle argille grigio-azzurre della Basilicata. In Atti Convegno Evoluzione dei Litorali, Policoro 16-17 ottobre 1986, Edizioni. ENEA, 419-441.

deMenocal, P.B., Ruddiman, W.F., Kent, D.V., 1990. Depth of post-depositional remanence acquisition in deep-sea sediments: a case study of the Brunhes-Matuyama reversal and oxygen isotopic Stage 19.1. Earth and Planetary Science Letters 99, 1-13.

Dennell, R.W., Martinon Torres, M., Bermudez de Castro, J.M., 2011. Hominin variability, climatic instability and population demography in Middle Pleistocene Europe. Quaternary Science Reviews 30, 1511–1524.

Di Geronimo, I., La Perna, R., 1997. Pleistocene bathyal molluscan

assemblages from Southern Italy. Rivista Italiana di Paleontologia e Stratigrafia 103, 389–426.

Di Geronimo, I., D'Atri, A., La Perna, R., Rosso, A., Sanfilippo, R., Violanti, D., 1997. The Pleistocene bathyal section of Archi (Southern Italy), Bollettino della Società Paleontologica Italiana 36(1–2), 189–212.

Di Pietro, R., Fascetti, S., Pompili, M., 2004. Vegetation soil relationship in Basilicata badlands (southern Italy). Symposium of the Federation Internationale de Phytosociologie, Tenerife.

Di Stefano, E., Incarbona, A., 2004. High resolution paleoenvironmental reconstruction of the ODP-963D Hole (Sicily Channel) during the last deglaciation, based on calcareous nannofossils, Marine Micropaleontology 52, 241–254.

Dinarès-Turell, J., Sagnotti, L., Roberts, A.P., 2002. Relative geomagnetic paleointensity from the Jaramillo Subchron to the Matuyama/Brunhes boundary as recorded in a Mediterranean piston core. Earth and Planetary Science Letters 194, 327–341.

Dodonov, A.E., 2005. The stratigraphic transition and suggested boundary between the Early and Middle Pleistocene in the loess record of northern Eurasia. In: Head, M.J., Gibbard, P.L. (Eds.). Early–Middle Pleistocene Transitions: the Land–Ocean Evidence. Geological Society, London, Special Issue 247, pp. 209–220.

Doglioni, C., Mongelli, F., Pieri, P., 1994. The Puglia uplift (SE Italy): an anomaly in the foreland of the Apenninic subduction due to buckling of a thick continental lithosphere. Tectonics 13, 1309-1321.

Doglioni, C., Tropeano, M., Mongelli, F., Pieri, P., 1996. Middle-Late Pleistocene uplift of Puglia: an "anomaly" in the Apenninic foreland. Memorie della Società Geologica Italiana 51, 101-117.

Dowsett, H.J., Robinson, M.M., Haywood, A.M., Salzmann, U., Hill, D.J., Sohl, L., Chandler, M.A., Williams, M., Foley, K., Stoll, D., 2010. The PRISM3D paleoenvironmental reconstruction. Stratigraphy, 7, 123–139

Dreyfus, G.B., Raisbeck, G.M., Parrenin, F., Jouzel, J., Guyodo, Y., Nomade, S., Mazaud, A., 2008. An ice core perspective on the age of Matuyama-Brunhes boundary. Earth and Planetary Science and Letters 274, 151–156.

Droxler, A.W., Alley, R.B., Howard, W.R., Poore, R.Z., Burckle, L.H., 2003. Unique and exceptionally long interglacial Marine Isotope Stage 11:

window into Earth warm future climate. In: Droxler, A.W., Poore, R.Z., Burckle, L.H. (Eds.). Earth's Climate and Orbital Eccentricity: The Marine Isotope Stage 11 Question. Geophysical Monograph Series 137, pp. 1–14.

Emanuele, D., Ferretti, P. Palumbo, E., Amore, F.O., 2015. Sea-surface dynamics and palaeoenvironmental changes in the North Atlantic Ocean (IODP Site U1313) during Marine Isotope Stage 19 inferred from coccolithophore assemblages. Palaeogeography Palaeoclimatology Palaeoecology 430, 104–117.

Emeis, K., Sakamoto, T., Wehausen, R., Brumsack, H.J., 2000. The sapropel record of the eastern Mediterranean Sea - results of Ocean Drilling Program Leg 160. Palaeogeography Palaeoclimatology Palaeoecology 158, 371-395.

Fagerstrom, J.A., 1964. Fossil Communities in Paleoecology: Their Recognition and Significance. Geological Society of America Bulletin 75, 1197–1216.

Fairbanks, R.G., Sverdlove, M., Free, R., Wiebe, P.H., Bé, A.W.H., 1982. Vertical distribution of living planktonic foraminifera from the Panama Basin. Nature 298, 841–844.

Fascetti, S., Di Pietro, R., Pompili, M. 2001. Aspetti sinecologici della vegetazione dei rilievi argillosi della Basilicata. Atti Congresso Società Italiana Fitosociologia. La Vegetazione Sinantropica, Lipari.

Ferretti, P., Crowhurst, S.J, Naafs, B.D.A, Barbante, C., 2015. The Marine Isotope Stage 19 in the mid- latitude North Atlantic Ocean: astronomical signature and intra-interglacial variability. Quaternary Science Reviews 108, 95-110.

Fletcher, W.J., Sánchez Goñi, M.F., 2008. Orbital and sub-orbital scale climate impacts on vegetation of the western Mediterranean basin over the last 48,000 yr. Quaternary Research 70, 451–464.

Fletcher, W.J., Sánchez Goñi, M.F., Peyron, O., Dormoy, I., 2009. Abrupt climate changes of the last deglaciation detected in a western Mediterranean forest record. Climate of the Past Discussions 5, 203–235.

Flores, J.A., Sierro, F. J., 1997. Revised technique for calculation of calcareous nannofossil accumulation rates. Micropaleontology 43, 321-324.

Flores, J.A., Sierro, F.J., Francés, G., Vàzquez, A., Zamarrefio, I., 1997. The last 100,000 years in the western Mediterranean: sea surface water and

frontal dynamics as revealed by coccolithophores. Marine Micropaleontology 29, 351-366.

Flores, J.A., Gersonde, R., Sierro, F.J., 1999. Pleistocene fluctuations in the Agulhas current retroflection based on the calcareous plankton record. Marine Micropaleontology 37, 1-22.

Florindo, F., Karner, D., Marra, F., Renne, P., Roberts, A., Weaver, R., 2007. Radiometric age constraints for glacial terminations IX and VII from aggradational sections of the Tiber River delta in Rome, Italy. Earth and Planetary Science Letters 256, 61–80.

Frank, M., Schwarz, B., Baumann, S., Kubik, P.W., Suter, M., Mangini, A., 1997. A 200 kyr record of cosmogenic radionuclide production rate and geomagnetic field intensity from ^{10}Be in globally stacked deep-sea sediments. Earth and Planetary Science Letters, 149, 121-129.

Geisen, M., Billard, C., Broerse, A.T.C., Cros, L., Probert, I., Young, J.R., 2002. Life-cycle associations involving pairs of holococcolithophorid species: Intraspecific variation or cryptic speciation?. European Journal of Phycology 37, 531–550.

Geraga, M., Tsaila-Monopolis, S., Ioakim, C., Papatheodorou, G., Ferentinos, G., 2005. Short-term climate changes in the southern Aegean Sea over the last 48000 years. Palaeogeography Palaeoclimatology Palaeoecology 220, 311–332.

Geraga, M., Mylona, G., Tsaila-Monopolis, S., Papatheodorou, G., Ferentinos, G., 2008. Northeastern Ionian Sea: palaeoceanographic variability over the last 22 ka. Journal of Marine Systems 74, 623–638.

Geraga, M., Ioakim, C., Lykousis, V., Tsaila Monopolis, S., Mylona, G., 2010. The high resolution palaeoclimatic and palaeoceanographic history of the last 24,000 years in the central Aegean Sea, Greece. Palaeogeography Palaeoclimatology Palaeoecology 287, 101-115.

Giaccio, B., Regattieri, E., Zanchetta, G., Nomade, S., Renne, P.R., Sprain, C.J, Drysdale, R.N., Tzedakis, P.C., Messina, P., Scardia, G., Sposato, A., Bassinot, F., 2015. Duration and dynamics of the best orbital analogue to the present interglacial. Geology 43(7), 603-606.

Giraudi, C., 2014. Coarse sediments in Northern Apennine peat bogs and lakes: New data for the record of Holocene alluvial phases in peninsular Italy. The Holocene 24(8), 932 –943.

Giraudi, C., 2015. The Upper Pleistocene deglaciation on the Apennines (Peninsular Italy). Cuadernos de Investigacion Geografica 41(2), 337-358.
Giraudi, C., Giaccio, B., 2015. The Middle Pleistocene glaciations on the Apennnines (Italy): New chronologcial data and considerations about the preservation of the glacial deposits. Geological Society, London, Special Publications, 433.
Girone, A., 2005. Response of otholit assemblages to sea-level fluctuations at the Lower Pleistocene Montalbano Jonico section (southern Italy). Bollettino Società Paleontologica Italiana 44, 35–45.
Girone, A., Varola, A., 2001. Fish otoliths from the Middle Pleistocene deposits of Montalbano Jonico (southern Italy). Bollettino Società Paleontologica Italiana 40, 431–443.
Girone, A., Capotondi, L., Ciaranfi, N., Di Leo, P., Lirer, F., Maiorano, P., Marino, M., Pelosi, N., Pulice, I., 2013a. Paleoenvironmental change at the lower Pleistocene Montalbano Jonico section (southern Italy): global versus regional signals. Palaeogeography Palaeoclimatology Palaeoecology 371, 62-79.
Girone, A., Maiorano, P., Marino, M., Kucera, M., 2013b. Calcareous plankton response to orbital and millennial-scale climate changes across the Middle Pleistocene in the western Mediterranean. Palaeogeography Palaeoclimatology Palaeoecology 392, 105–116.
Giunta, S., Negri, A., Maffioli, P., Sangiorgi, F., Capotondi, L., Morigi, C., Principato, M.S., Corselli, C., 2006. Phytoplankton dynamics in the eastern Mediterranean Sea during marine isotopic stage 5e. Palaeogeography Palaeoclimatology Palaeoecology 235, 28–47.
Gofas, S., Rueda, J.L., Salas, C., Díaz-Del-Río, V., 2010. A new record of the giant deep-sea oyster *Neopycnodonte zibrowii* in the Gulf of Cadiz (south-western Iberian Peninsula). Marine Biodiversity Records 3, e72, 1-4.
Gooday, A.J., Alt, C.H.S., Jones, D.O.B., Shale, D., Marsden, K., Brasier, M.D., 2013. The ecology and biogeography of *Discospirina tenuissima* (Foraminifera) in the Atlantic and Indian Oceans. Deep-Sea Research II, 98, 301-314.
Gradstein, F.M., Finney, S.C., Lane, R., Ogg, J.G., 2003. ICS on stage. Lethaia 36, 371-377.

Greathead, C., González-Irusta, J.M., Clarke, J., Boulcott, P., Blackadder, L., Weetman, A., Wright, P.J., 2014. Environmental requirements for three sea pen species: relevance to distribution and conservation. ICES Journal of Marine Science 72(2), 576-586.

Haq, B.U., Handerbol, J., Vail, P., 1987. Chronology of Fluctuating Sea Levels Since the Triassic. Science 235, 1156-1167.

Hardenbol, J., Thierry, J., Farley, M.B., Jacquin, T., de Graciansky, P.C., Vail, P.R., 1998. Mesozoic and Cenozoic sequence chronostratigraphic framework of European basins. In: de Graciansky, P.C., Hardenbol, J., Jacquin, T., Vail, P.R. (Eds.). Mesozoic and Cenozoic Sequence Stratigraphy of European Basins, SEPM Special Publication 60, 3-13.

Hays, J.D., Imbrie, J., Shackleton, N.J., 1976. Variations in the Earth's orbit: pacemaker of the ice ages. Science 194, 1121-1132.

Haywood, A.M, Dowsett, H.J., Valdes, P.J., Lunt, D.J., Francis, J.E., Sellvood, B., 2009. Introduction. Pliocene climate, processes and problems. Philosophical Transaction of the Royal Society 367, 3–17.

Head, M.J., Gibbard, P.J., 2005. Early-Middle Pleistocene transition: an overview and recommendation for the defining boundary. In: Head, M.J., Gibbard, P.L. (Eds.). Early-Middle Pleistocene Transitions: The Land-Ocean Evidence. Geological Society of London, Special Publications 247, 1-18.

Head, M.J., Pillans, B., Farquhar, A., 2008. The Early Middle Pleistocene transition: characterization and proposed guide for the defining boundary. Episodes 31, 255–259.

Head, M.J., Gibbard, P.J., 2015a. Formal subdivision of the Quaternary System/Period: Past, present, and future. Quaternary International 383, 4-35.

Head, M.J., Gibbard, P.J., 2015b. Early-Middle Pleistocene transitions: Linking terrestrial and marine realms. Quaternary International 389, 7-46.

Hemleben, C., Spindler, M., Anderson, O.R., 1989. Modern Planktonic Foraminifera, Springer-Verlag, New York, 363 pp.

Henriksson, A.S., 2000. Coccolithophore response to oceanographic changes in the equatorial Atlantic during the last 200,000 years. Palaeogeography Palaeoclimatology Palaeoecology 156, 161–173.

Heusser, L.E., 1988. Pollen distribution in marine sediments on the

continental margin off northern California. Marine Geology 80, 131-147.
Hilgen, F.J., Abels, H.A., Iaccarino, S., Krijgsman, W., Raffi, I., Sprovieri, R., Turco, E., Zachariasse, W.J., 2009. The Global Stratotype Section and Point (GSSP) of the Serravallian Stage (Middle Miocene). Episodes 32 (3), 152–166.
Hodell, D.A., Channell, J.E.T., Curtis, J.H., Romero, O.E., Röhl, U., 2008. Onset of "Hudson Strait" Heinrich Events in the Eastern North Atlantic at the end of the Middle Pleistocene Transition (-640 ka)?. Paleoceanography 23, PA4218.
Huber, R., Meggers, H., Baumann, K.H., Raymo, M.E., Heinrich, R., 2000. Shell size variation of the planktonic foraminifer *Neogloboquadrina pachyderma* in the Norwegian Greenland Sea during the last 1.3 Myrs: implications for paleoceanographic reconstructions. Palaeogeography Palaeoclimatology Palaeoecology 160, 183–212.
Huntley, B., Webb, T.III, 1989. Migration: species' response to climatic variations caused by changes in the earth's orbit. Journal of Biogeography 16, 5-19.
Hyodo, M., Biawas, D.K., Noda, T., Tomioka, N., Mishima, T., Itota, C., Sato, H., 2006. Millennial to sub-millennial-scale features of the Matuyama-Brunhes geomagnetic polarity transition from Osaka Bay, southwestern Japan. Journal of Geophysical Research 111, B02103.
Hyodo, M., Matsu'ura, S., Kamishima, Y., Kondo, M., Takeshita, Y., Kitaba, I., Danhara, T., Aziz, A., Kurniawan, I., Kumaig, H., 2011. High-resolution record of the Matuyama-Brunhes transition constrains the age of Javanese *Homo erectus* in the Sangiran dome, Indonesia. Proceedings of Natural Academy of Sciences of USA 108, 19563–19568.
Hyodo, M., Kitaba, I., 2013. High-Resolution Magneto-Climatostratigraphy of MIS 19 from the Osaka Group, Japan. In: Rocha, R., Pais, J., Kullberg, J.C., Finney, S., (Eds.). STRATI 2013, Springer Geology.
Hyodo, M., Kitaba, I., 2015. Timing of Matuyama–Brunhes geomagnetic reversal: decoupled thermal maximum and sea-level highstand during Marine Isotope Stage 19. Quaternary International 383, 136-144.
Imbrie, J., Hays, J.D., Martinson, D.G., McIntyre, A., Mix, A.C., Morley, J.J., Paces, N.G., Prell, W.L., Shackleton, N.J., 1984. The orbital theory of Pleistocene climate: Support from a revised chronology of the marine

$\delta^{18}O$ record. In: Berger, A., Imbrie, J., Hays, J., Kukla, J., Saltzman, B., (Eds.). Milankovitch and Climate, Part I. D. Reidel, Norwell, MApp. 269–305.

Imbrie, J., Imbrie, J.Z., 1980. Modelling the climate response to orbital variations. Science 207, 943–953.

Incarbona, A., Di Stefano, E., Patti, B., Pelosi, N., Bonomo, S., Mazzola, S., Sprovieri, R., Tranchida, G., Zgozi, S., Bonanno, A., 2008. Holocene millennial-scale productivity variations in the Sicily Channel (Mediterranean Sea). Paleoceanography 23, 1-18.

Incarbona, A., Dinarès-Turell, J., Di Stefano, E., Ippolito, G., Pelosi, N., Sprovieri, R., 2013. Orbital variations in planktonic foraminifera assemblages from the Ionian Sea during the Middle Pleistocene Transition. Palaeogeography Palaeoclimatology Palaeoecology 369, 303–312.

Joannin, S., Cornée, J.J., Moissette, P., Suc, J.-P., Koskeridou, C., Lécuyer, C., Buisine, C., Kouli, K., Ferry, S., 2007. Changes in vegetation and marine environment in the eastern Mediterranean (Rhodes Island, Greece) during the Early and Middle Pleistocene. Journal of Geological Society of London 164, 1119–1131.

Joannin, S., Ciaranfi, N., Stefanelli, S., 2008. Vegetation changes during the late Early Pleistocene at Montalbano Jonico (Province of Matera, southern Italy) based on pollen analysis. Palaeogeography Palaeoclimatology Palaeoecology 270, 92–101.

Joannin, S., Bassinot, F., Combourieu Nebout, N., Peyron, O., Beaudouin, C., 2011. Vegetation response to obliquity and precession forcing during the Mid-Pleistocene Transition in Western Mediterranean region (ODP site 976). Quaternary Science Reviews 30, 280-297.

Jordan, R.W., Zhao, M., Eglinnton, G., Weaver, P.P.E., 1996. Coccolith and alkenone stratigraphy and paleoceanography at an upwelling site off NW Africa (ODP 658C) during the last 130,000 years. In: Moguilevsky, A., Whatley, R. (Eds.). Microfossils and Oceanic Environments. Aberystwyth Press, University of Wales, pp. 111-130.

Jorissen, F.J., De Stigter, H.C., Widmark, J.G.V., 1995. A conceptual model explaining benthic foraminiferal microhabitats. Marine Micropaleontology 22, 3–15.

Jouzel, J., Masson-Delmotte, V., Cattani, O., Dreyfus, G., Falourd, S., Hoffmann, G., Minster, B., Nouet, J., Barnola, J.M., Chappellaz, J., Fischer, H., Gallet, J.C., Johnsen, S., Leuenberger, M., Loulergue, L., Luethi, D., Oerter, H., Parrenin, F., Raisbeck, G., Raynaud, D., Schilt, A., Schwander, J., Selmo, E., Souchez, R., Spahni, R., Stauffer, B., Steffensen, J.P., Stenni, B., Stocker, T.F., Tison, J.L., Werner, M., Wolff, E.W., 2007. Orbital and millennial Antarctic climate variability over the past 800,000 years. Science 317, 793-796.

Kitaba, I., Iwabe, C., Hyodo, M., Katoh, S., Matsushita, M., 2009. High resolution climate stratigraphy across the Matuyama-Brunhes transition from palynological data of Osaka Bay sediments in southwestern Japan. Palaeogeography Palaeoclimatology Palaeoecology 272, 115–123.

Kitaba, I., Hyodo, M., Katoh, S., Matsushita, M., 2012. Phase-lagged warming and the disruption of climatic rhythms during the Matuyama–Brunhes magnetic polarity transition. Gondwana Research 21, 595–600.

Kitaba, I., Hyodo, M., Katoh, S., Dettman, D.L., Sato, H., 2013. Middle latitude cooling caused by geomagnetic field minimum during polarity reversal. Proceedings of the National Academy of Sciences 110(4), 1215–1220.

Kleiven, H., Hall, I.R., McCave, I.N., Knorr, G., Jansen, E., 2011. North Atlantic coupled deep-waterflow and climate variability in the middle Pleistocene. Geology 39(4), 343-346.

Klotz, S., Fauquette, S., Combourieu Nebout, N., Uhl, D., Suc, J.-P., Mosbrugger, V., 2006. Seasonality intensification and long-term winter cooling as a part of the Late Pliocene climate development. Earth and Planetary Science Letters 241, 174-187.

Konijnendijk, T.Y.M., Ziegler, M., Lourens, L.J., 2014. Chronological constraints on Pleistocene sapropel depositions from high-resolution geochemical records of ODP Sites 967 and 968. Newsletters on Stratigraphy 47(3), 263–282.

Kontakiotis, G., 2015. Late Quaternary paleoenvironmental reconstruction and paleoclimatic implications of the Aegean Sea (eastern Mediterranean) based on paleoceanographic indexes and stable isotopes. Quaternary International 401, 28-42.

Kucera, M., Kennett, J.P., 2002. Causes and consequences of a middle

Pleistocene origin of the modern planktonic foraminifer Neogloboquadrina pachyderma sinistral. Geology 30, 539–542.

Kucera, M., Weinelt, M., Kiefer, T., Pflaumann, U., Hayes, A., Weinelt, M., Chen, M.-T., Mix, A.C., Barrows, T., Cortijo, E., Duprat, J., Juggins, S., Waelbroeck, C., 2005. Reconstruction of sea-surface temperatures from assemblages of planktonic foraminifera: multi-technique approach based on geographically constrained calibration datasets and its application to glacial Atlantic and Pacific Oceans. Quaternary Science Reviews 24, 951-998.

Kuiper, K.F., Deino, A., Hilgen, F.J., Krijgsman, W., Renne, P.R., Wijbrans, J.R., 2008. Synchronizing rock clocks of earth history. Science 320, 500–504.

Kukla, G., McManus, J.F., Rousseau, D.D., Chuine, I., 1997. How long and how stable was the last interglacial? Quaternary Science Reviews 16, 605–612.

Kukla, G.J., Bender, M.L., de Beaulieu, J.L., Bond, G., Broecker, W.S., Cleveringa, P., Gavin, J.E., Herbert, T.D., Imbrie, J., Jouzel, J., Keigwin, L.D., Knudsen, K.L., McManus, J.F., Merkt, J., Muhs, D.R., Müller, H., Poore, R.Z., Porter, S.C., Seret, G., Shackleton, N.J., Turner, C., Tzedakis, P.C., Winograd, I.J., 2002. Last interglacial climates. Quaternary Research 58, 2–13.

Langereis, C.G., Dekkers, M.J, de Lange., G.J., Paterne, M., van Santvoort, P.J.M., 1997. Magnetostratigraphy and astronomical calibration of the last 1.1 Myr from an eastern Mediterranean piston core and dating of short events in the Brunhes. Geophysical Journal International 129, 75-94.

Larrasoaña, J.C., Roberts, A.P., Rohling, E.J., Winklhofer, M., Wehausen, R., 2003. Three million years of monsoon variability over the northern Sahara. Climate Dynamics 21, 689–698.

Laskar, J., Robutel, P., Joutel, F., Boudin, F., Gastineau, M., Correia, A.C.M., Levrard, B., 2004. A long-term numerical solution for the insolation quantities of the Earth. Astronomy & Astrophysics 428, 261–285.

Leonhardt, R., Fabian, K., 2007. Paleomagnetic reconstruction of the global geomagnetic field evolution during the Matuyama/Brunhes transition: Iterative Bayesian inversion and independent verification. Earth and Planetary Science Letters 253, 172–195.

Leroy, S.A.G., Arpe, K., Mikolajewicz, U., 2011. Vegetation context and climatic limits of the Early Pleistocene hominin dispersal in Europe. Quaternary Science Reviews 30, 1448–1463.

Lisiecki, L.E., Raymo, M.E., 2005. A Pliocene–Pleistocene stack of 57 globally distributed benthic $\delta^{18}O$ records. Paleoceanography 20, PA1003.

Lona, F., Bertoldi, R., 1972. La storia del Plio-Pleistocene italiano in alcune sequenze vegetazionali lacustri e marine. Atti dell'Accademia Nazionale Lincei 11, 1–45.

López-Otálvaro, G.E., Flores, J.A., Sierro, F.J., Cacho, I., 2008. Variations in coccolithophorid production in the Eastern Equatorial Pacific at ODP Site 1240 over the last seven glacial- interglacial cycles. Marine Micropaleontology 69, 52-69.

Loulergue, L., Schilt, A., Spahni, R., Masson-Delmotte, V., Lemieux, B., Barnola, J.-M., Raynaud D., Stocker, T. F., Chappellaz, J., Blunier, T., 2008. Orbital and millennial-scale features of atmospheric CH4 over the past 800,000 years. Nature 453, 383-386.

Lourens, L.J., 2004. Revised tuning of Ocean Drilling Program Site 964 and KC01B (Mediterranean) and implications for the $\delta^{18}O$, tephra, calcareous nannofossil, and geomagnetic reversal chronologies of the past 1.1 Myr. Paleoceanography 19, PA3010.

Lourens, L., Hilgen, F., Shackleton, N.J., Laskar, J., Wilson, D., 2004. The Neogene Period. In: Gradstein, F.M., Ogg, J.G., Smith, A.G. (Eds.). A Geological Time Scale. Cambridge University Press, pp. 409–440.

Lüthi, D., Le Floch, M., Bereiter, B., Blunier, T., Barnola, J.-M., Siegenthaler, U., Raynaud, D., Jouzel, J., Fischer, H., Kawamura, K., Stocker, T. F., 2008. High-resolution carbon dioxide concentration record 650,000 - 800,000 years before present. Nature 453, 379-382.

Macklin, M.G., Lewin, J., 2008. Alluvial responses to the changing earth system. Earth Surface Processes and Landforms 33(9), 1374–1395.

Magny, M., de Beaulieu, J.L., Drescher-Schneider, R., Vanniére, B., Walter-Simonnet, A.V., Millet, L., Bossuet, G., Peyron, O., 2006. Climatic oscillations in central Italy during the Last Glacial–Holocene transition: the record from Lake Accesa. Journal of Quaternary Science 21, 311–320.

Magri, D., Palombo, M.R., 2013. Early to Middle Pleistocene dynamics of plant and mammal communities in South West Europe. Quaternary

International 267, 30–39.
Maiorano, P., Marino, M., 2004. Calcareous nannofossil bioevents and environmental control on temporal and spatial pattern at the early-middle Pleistocene. Marine Micropaleontology 53, 405–422.
Maiorano, P., Marino, M., Di Stefano, E., Ciaranfi, N., 2004. Calcareous nannofossil events in the lower-middle Pleistocene transition at the Montalbano Jonico section and ODP Site 964: calibration with isotope and sapropel stratigraphy. Rivista Italiana di Paleontologia e Stratigrafia 110(2), 547–557.
Maiorano, P., Aiello, G., Barra, D., Di Leo, P., Joannin, S., Lirer, F., Marino, M., Pappalardo, A., Capotondi, L., Ciaranfi, N., Stefanelli, S., 2008. Paleoenvironmental changes during sapropel 19 (i-cycle 90) deposition: evidences from geochemical, mineralogical and microplaoentological proxies in the mid Pleistocene Montalbano Jonico land section (southern Italy). Palaeogeography Palaeoclimatology Palaeoecology 257, 308–334.
Maiorano, P., Capotondi, L., Ciaranfi, N., Girone, A., Lirer, F., Marino, M., Pelosi, N., Petrosino, P., Piscitelli, A., 2010. Vrica-Crotone and Montalbano Jonico sections: a potential unit-stratotype of the Calabrian Stage. Episodes 33, 218–233.
Maiorano, P., Marino, M., Balestra, B., Flores, J.A., Hodell, D.A., Rodrigues, T., 2015. Coccolithophore variability from the Shackleton Site (IODP Site U1385) through MIS 16–10. Global and Planetary Change 133, 35-48.
Maiorano, P., Girone, A., Marino, M., Kucera, M., Pelosi N., 2016. Calcareous plankton response to Mid- Brunhes climate variability in the western Mediterranean (ODP Site 975). Palaeogeography Palaeoclimatology Palaeoecology 459, 229–248.
Maiorano, P., Tarantino, F., Marino, M., De Lange, G.J., 2013. Paleoenvironmental conditions at Core KC01B (Ionian Sea) through MIS 13-9: Evidence from calcareous nannofossil assemblages. Quaternary International 288, 97-111.
Mankinen, E.A., Dalrymple, G.B., 1979. Revised geomagnetic polarity time scale for the interval 0-5 m.y. B.P. Journal of Gephysical Research 84, 615–626.

Manzi, G., Magri, D., Palombo, M.R., 2011. Early-Middle Pleistocene environmental changes and human evolution in the Italian peninsula. Quaternary Science Reviews 30, 1420–1438.

Marino, M., 1996. Quantitative nannofossil biostratigraphy of the lower-middle Pleistocene Montalbano Jonico section, southern Italy. Paleopelagos 6, 347-360.

Marino, M., Maiorano, P., Flower, B.P., 2011. Calcareous nannofossil changes during the Mid-Pleistocene Revolution: Paleoecologic and paleoceanographic evidence from North Atlantic Site 980/981. Palaeogeography Palaeoclimatology Palaeoecology 306(1-2), 58-69.

Marino, M., Maiorano, P., Tarantino, F., Voelker, A., Capotondi, L., Girone, A., Lirer, F., Flores, J.A., Naafs, B.D.A., 2014. Coccolithophores as proxy of seawater changes at orbital-to-millennial scale during middle Pleistocene Marine Isotope Stages 14–9 in North Atlantic core MD01-2446. Paleoceanography 29, 518-532.

Marino, M., Bertini, A., Ciaranfi, N., Aiello, G., Barra, D., Gallicchio, S., Girone, A., La Perna, R., Lirer, F., Maiorano, P., Petrosino, P., Toti, F., 2015. Paleoenvironmental and climatostratigraphic insights for Marine Isotope Stage 19 (Pleistocene) at the Montalbano Jonico section, South Italy. Quaternary International 383, 104-115.

Marino, M., Aiello, G., Barra, D., Bertini, A., Gallicchio, S., Girone, A., La Perna, R., Lirer, F., Maiorano, P., Petrosino, P., Quivelli, O., Toti, F., Ciaranfi, N., 2016. The Montalbano Jonico section (South Italy) as a reference for the Early/Middle Pleistocene boundary. Alpine and Mediterranean Quaternary 29(1), 45-57.

Martrat, B., Grimalt, J.O., Shackleton, N.J., De Abreu, L., Hutterli, M.A., Stocker, T.F., 2007. Four climate cycles of recurring deep and surface water destabilizations on the Iberian margin. Science 317, 502–507.

Maslin, M.A., Ridgwell, A.J., 2005. Mid-Pleistocene revolution and the 'eccentricity myth'. In: M.J., Head, Gibbard, P.L. (Eds.). Early-Middle Pleistocene transitions: the land-ocean evidence: Geological Society of London, Special Publication 247, pp. 19-34.

Massari, F., Rio, D., Sgavetti, M., Prosser, G., D'Alessandro, A., Asioli, A., Capraro, L., Fornaciari, E., Tateo, F., 2002. Interplay between tectonics and Glacioeustasy, Pleistocene of the Crotone Basin, Calabria (southern

Italy). Bulletin of the American Geological Society 114, 1183–1209.

Massari, F., Capraro, L., Rio, D., 2007. Climatic modulation of timing of systems-tract development with respect to sea-level changes (middle Pleistocene of Crotone, Calabria, Southern Italy). Journal of Sedimentary Research 77, 461–468.

McIntyre, A., Bé, A.H.W., 1967. Modern coccolithophores of the Atlantic Ocean - I. Placolith and cyrtoliths. Deep Sea Research 14, 561-597.

Melki, T., Kallel, N., Jorissen, F.J., Guichard, F., Dennielou, B., Berné, S., Labeyrie, L., Fontugne, M., 2009. Abrupt climate change, sea surface salinity and paleoproductivity in the western Mediterranean Sea (Gulf of Lion) during the last 28 kyr. Palaeogeography Palaeoclimatology Palaeoecology 279, 96–11.

Messager, E., Lebreton, V., Marquer, L., Russo Ermolli, E., Orain, R., Renault Miskovsky, J., Lordkipanidze, D., Despriée, J., Peretto, C., Arzarello, M., 2001. Palaeoenvironments of early hominins in temperate and Mediterranean Eurasia: new palaeobotanical data from Palaeolithic key-sites and synchronous natural sequences. Quaternary Science Reviews 30, 1439–1447.

Mix, A.C., Le, J., Shackleton, N.J., 1995a. Benthic foraminifer stable isotope stratigraphy of Site 846: 0-1.8 Ma. In: Pisias, N.G., Mayer, L., Janecek, T., Palmer-Julson, A., van Andel, T.H. (Eds.), Proceedings of the Ocean Drilling Program. Scientific Results, 138, College Station (TX), pp. 839-856.

Mix, A.C., Pisias, N.G., Rugh, W., Wilson, J., Morey, A., Hagelberg, T., 1995b.Benthic foraminiferal stable isotope record from Site 849: 0-5 Ma. In: Pisias N.G., Mayer L., Janecek T., Palmer-Julson A., van Andel T.H. (Eds.), Proceedings of the Ocean Drilling Program. Scientific Results 138, College Station (TX), pp. 371-412.

Molfino, B., McIntyre, A., 1990a. Precessional forcing of nutricline dynamics in the equatorial Atlantic. Science 249, 766–769.

Molfino, B., McIntyre, A., 1990b. Nutricline variation in the equatorial Atlantic coincident with the Younger Dryas. Paleoceanography 5, 997–1008.

Morard, R., Quillévéré, F., Escarguel, G., Ujiie, Y., de Garidel-Thoron, T., Norris, R. D., de Vargas, C., 2009. Morphological recognition of cryptic species in the planktonic foraminifer *Orbulina universa*. Marine

Micropaleontology 71, 148–165.
Moreno, A., Cacho, I., Canals, M., Prins, M.A., Sanchez-Goni, A., Grimalt, J.O., Weltje, G.J., 2002. Saharan dust transport and high-latitude glacial climatic variability: the Alboran Sea record. Quaternary Research 58, 318–328.
Mostardini, F., Pieri, P., 1967. Note illustrative della Carta Geologica d'Italia alla scala 1:100.000, Foglio 212 Montalbano Ionico. La Litograf, Roma.
Müller, G.W., 1894. Die Ostracoden des Golfes von Neapel und der angrenzenden Meeres-Abschnitte. Fauna und Flora des Golfes von Neapel und der angrenzenden Meeres-Abschnitte, Herausgegeben von der Zoologischen Station zu Neapel 21(1–8), 1–404.
Munz, P.M., Siccha, M., Lückge, A., Böll, A., Kucera, M., Schulz, H., 2015. Decadal-resolution record of winter monsoon intensity over the last two millennia from planktic foraminiferal assemblages in the northeastern Arabian Sea. The Holocene 25(11), 1756-1771.
Murat, A., 1999. Pliocene–Pleistocene occurrence of sapropels in the western Mediterranean Sea and their relation to eastern Mediterranean sapropels. In: Zahn, R., Comas, M.C., Klaus, A. (Eds.), Proceedings of the Ocean Drilling Program. Scientific Results 161. Ocean Drilling Program, College Station, TX, pp. 519–527.
Muttoni, G., Scardia, G., Kent, D.V., 2010. Human migration into Europe during the late Early Pleistocene climate transition. Palaeogeography, Palaeoclimatology, Palaeoecology 296, 79–93.
Naafs, B.D.A., Hefter, J., Ferretti, P., Stein, R., Haug, G.H., 2011. Sea surface temperatures did not control the first occurrence of Hudson Strait Heinrich Events during MIS 16. Paleoceanography 26, PA4201.
Naafs, B.D.A., Hefter, J., Stein, R., 2013. Millennial-scale ice rafting events and Hudson Strait Heinrich (-like) events during the late Pliocene and Pleistocene: a review. Quaternary Science Reviews 80,1–28.
Naish, T.R., Field, B.D., Zhu, H., Melhuish, A., Carter, R.M., Abbott, S.T., Edwards, S., Alloway, B.V., Wilson, G.S., Niessen, F., Barker, A., Browne, G.H., Maslen, G., 2005. Integrated outcrop, drill core, borehole and seismic stratigraphic architecture of a cyclothemic, shallow-marine depositional system, Wanganui Basin, New Zealand. Journal of the Royal Society of New Zealand 35, 91–122

Negri. A., Amorosi, A., Antoniol, F., Bertini, A., Florindo, F., Lurcock, P.C., Marabini, S., Mastronuzzi, G., Regattieri, E., Rossi, V., Scarponi, D., Taviani, M., Zanchetta, G., Vai, G.B., 2015. A potential global boundary stratotype section and point (GSSP) for the Tarentian Stage, Upper Pleistocene, from the Taranto area (Italy): Results and future perspectives. Quaternary International 383, 145-157.

Nomade, S., Bassinot, F., Ciaranfi, N., Dewilde, F., Scao, V., Girone, A., Maiorano, P., Marino, M., Toti, F., Giaccio, B., Combourieu Nebout, N., Bertini, A., Petrosino, P., 2015. High resolution $\delta^{18}O$ stratigraphy along the MIS 19 in Montalbano Jonico (Basilicata, southern Italy): Exploring the land-ocean linkages during a low eccentricity interglacial. Nagoya 2015 XIX INQUA. Abstract N°. To2206

North Greenland Ice Core Project Members (NGRIP), 2004. High-resolution record of Northern Hemisphere climate extending into the last interglacial period. Nature 431, 147-151.

O'Regan, H.J., Turner, A., Bishop, L.C., Elton S., Lamb, A.L., 2011. Hominins without fellow travellers? First appearances and inferred dispersals of Afro-Eurasian large-mammals in the Plio-Pleistocene. Quaternary Science Review 30, 1343–1352.

Okada, H., Honjo, S., 1973. The distribution of oceanic coccolithophorids in the Pacific. Deep Sea Research 20, 355–374.

Okada, H., Honjo, S., 1975. Distribution of coccolithophorids in marginal seas along the Western Pacific Ocean and in the Red Sea. Marine Biology 31, 271-285.

Olausson, E., 1961. Studies of deep-sea cores. Reports of the Swedish Deep Sea Expedition (1947–1948) 8(4), 353–391.

Oppo, D.W., McManus, J.F., Cullen, J.L., 1998. Abrupt climate events 500,000 to 340,000 years ago: evidence from subpolar North Atlantic sediments. Science 279, 1335–1338.

Orain, R., Lebreton, V., Russo Ermolli, E., Aucelli, P., Amato, V., 2012. Végétation et climat au Pléistocène moyen en Italie méridionale (Bassin de Boiano, Molise). Quaternaire 23(1), 35–46.

Orain, R., Lebreton, V., Russo Ermolli, E., Combourieu Nebout, N., Semah, A.M., 2013. *Carya* as marker for tree refuges in southern Italy (Boiano

basin) at the Middle Pleistocene. Palaeogeography Palaeoclimatology Palaeoecology 369, 295–302.

Palumbo, E., Flores, J.A., Perugia, C., Petrillo, Z., Voelker, A.H.L., Amore, F.O., 2013. Millennial scale coccolithophore paleoproductivity and surface water changes between 445 and 360 ka (Marine Isotope Stages 12/11) in the Northeast Atlantic. Palaeogeography Palaeoclimatology Palaeoecology 383-384, 27-41.

Parente, A., Cachão, M., Baumann K.H., de Abreu, L., Ferreira J., 2004. Morphometry of *Coccolithus pelagicus* s.l. (Coccolithophore, Haptophyta) from offshore Portugal, during the last 200 kyr. Micropaleontology 50, 107–120.

Patacca, E., Scandone, P., 2001. Late thrust propagation and sedimentary response in the thrustbelt-foredeep system of the Southern Apennines (Pliocene-Pleistocene). In Vai, G.B., Martini, I.P. (Eds.). Anatomy of an orogen: the Apennines and Adjacent Mediterranean Basins, 401-440.

Patacca, E., Scandone, P., 2007. Geology of the Southern Apennines. Bollettino della Società Geologica Italiana, Special Issue 7, 75-119.

Pazzaglia, F.J., 2013. Fluvial terraces. In: Shroder, J., Wohl, E. (Eds.). Treatise on Geomorphology; Fluvial Geomorphology, Vol. 9. Academic Press, San Diego, pp. 379-412.

Pérès, J.M., Picard, J., 1964. Nouveau manuel de bionomie benthique de la Méditerranée. Recueil des Travaux de la Station Marine d'Endoume 31(47), 1–37.

Pérez-Folgado, M., Sierro, F.J., Flores, J.A., Cacho, I., Grimalt, J.O., Zahn, R., Shackleton, N., 2003.Western Mediterranean planktonic foraminifera events and millennial climatic variability during the last 70 kyr. Marine Micropaleontology 48, 49–70.

Perri, F., Critelli, S., Cavalcante, F., Mongelli, G., Dominici, R., Sonnino, M., De Rosa, R., 2012. Provenance signatures for the Miocene volcaniclastic succession of the Tufiti di Tusa Formation, southern Apennines, Italy. Geological Magazine 149(3), 423–442.

Pescatore, T., 1988. La sedimentazione miocenica nell'Appennino campano-lucano. Memorie della Società Geologica Italiana 41, 37-46.

Pescatore, T., Pozzuoli, A., Stanzione, D., Torre, M., Huertas, F., Linares, J., 1980. Caratteri mineralogici e geochimici dei sedimenti pelitici del

Flysch di Gorgoglione (Lucania, Appennino Meridionale). Periodico di Mineralogia 49, 293-330.

Petrosino, P., Jicha, B., Mazzeo, F.C., Russo Ermolli, E., 2014. A high resolution tephrochronological record of MIS 14-12 in the Southern Apennines (Acerno basin, Italy). Journal of Volcanology and Geothermal Research, 274, 34-50.

Petrosino, P., Russo Ermolli, E., Donato, P., Jicha, B., Robustelli, G., Sardella, R., 2014b. Using tefrochronology and palynology to date the MIS13 lacustrine sediments of the Mercure basin (Southern Apennines, Italy). Italian Journal of Geosciences 133(2), 169–186.

Petrosino, P., Jicha, B.R., Mazzeo, F.C., Ciaranfi, N., Girone, A., Maiorano, P., Marino, M., 2015. The Montalbano Jonico marine succession: An archive for distal tephra layers at the Early-Middle Pleistocene boundary in southern Italy. Quaternary International 383, 89-103.

Piccarreta, M., Caldara, M., Capolongo, D., Boenzi, F., 2011. Holocene geomorphic activity related to climatic change and human impact in Basilicata, Southern Italy. Geomorphology 128(3), 137-147.

Pieri, P., Sabato, L., Marino, M., 1996. The Plio-Pleistocene pyggyback Sant'Arcangelo Basin: tectonic and sedimentary evolution. Notes et Mémoire du Service Géologique du Maroc 387, 195-208.

Pieri, P., Sabato, L., Spalluto, L., Tropeano, M., 2011. Notes to the geological map of the urban area of Bari (southern Italy) 1:25.000 scale Note illustrative della carta geologica dell'area urbana di Bari in scala 1:25.000. Rendiconti Online Società Geologica Italiana, 26-36.

Pignatti, G., 2011. La vegetazione forestale di fronte ad alcuni scenari di cambiamento climatico in Italia. Forest@ 8, 1–12. http://www.sisef.it/forest@/.

Pillans, B., 2003. Subdividing Pleistocene using the Matuyama-Brunhes boundary (MBB): an Australasian perspective. Quaternary Science Reviews 22, 1569–1577.

Pillans, B., Chappell, J., Naish, T.R., 1998. A review of the Milankovitch climatic beat: template for Plio-Pleistocene sea-level changes and sequence stratigraphy. Sedimentary Geology 122, 5–22.

Pol, K., Masson Delmotte, V., Johnsen, S., Bigler, M., Cattani, O., Durand, G., Falourd, S., Jouzel, J., Minster, B., Parrenin, F., Ritz, C., Steen Larsen,

H.C., Stenni, B., 2010. New MIS 19 EPICA Dome C high resolution deuterium data: Hints for a problematic preservation of climate variability at sub-millennial scale in the "oldest ice". Earth and Planetary Science Letters 298, 95–103

Porporato, E., De Domenico, F., Mangano, M.C., Spanò, N., 2009. The pennatulacean fauna from southern Tyrrhenian Sea. Biologia Marina Mediterranea 16(1), 92–293.

Prokopenko, A.A., Hinnov, L.A., Williams, D.F., Kuzmin, L.I., 2006. Orbital forcing of the continental climate during the Pleistocene: a complete astronomically-tuned climatic record from Lake Baikal, SE Siberia. Quaternary Science Reviews 25, 3431–3457.

Pujol, C., Vergnaud-Grazzini, C., 1995. Distribution patterns of live planktic foraminifers as related to regional hydrography and productive systems of the Mediterranean Sea. Marine Micropaleontology 25, 187-217.

Raisbeck, G.M., Yout, F., Cattani, O., Jouzel, L., 2006. ^{10}Be evidence for the Matuyama-Brunhes geomagnetic reversal in the EPICA Dome C ice core. Nature 444, 82–84.

Railsback, L.B., Gibbard, P.L., Head, M.J., Voarintsoa, N.RG., Toucanne, S., 2015. An optimized scheme of lettered marine isotope substages for the last 1.0 million years, and the climatostratigraphic nature of isotope stages and substages. Quaternary Science Reviews 111, 94-106.

Raymo, M.E., Granta, B., Horowitz ,M., Raub, G.H., 1996. Mid-Pliocene warmth: stronger greenhouse and stronger conveyor. Marine Micropaleontology 27(1–4), 313–326.

Regattieri, E., Giaccio, B., Galli, P., Nomade, S., Peronace, E., Messina P., Sposato, A., Boschi, C., Gemelli, M., 2016. A multiproxy record of MIS 11-12 deglaciation and glacial MIS 12 instability from the Sulmona Basin (central Italy). Quaternary Science Reviews 32, 129–145.

Reichart, G.J., Brinkhuis, H., Huiskamp, F., Zachariasse, J.W., 2004. Hyperstratification following glacial overturning events in the northern Arabian Sea. Paleoceanography 19, PA2013.

Remane, J., Basset, M.G., Cowie, J.F., Gohrbandt, K.H., Lane, H.R., Michelsen, O., Naiwen, W., 1996. Revised guidelines for the establishment of global chronostratigraphic standards by the International Commission on Stratigraphy (ICS). Episodes 19, 77–81.

Renne, P.R., Mundil, R., Balco, G., Min, K., Ludwig, K.R., 2010. Joint determination of ^{40}K decay constants and $^{40}Ar^*/^{40}K$ for the Fish Canyon sanidine standard, and improved accuracy for $^{40}Ar/^{39}Ar$ geochronology. Geochemical and Cosmochemical Acta 74, 5349–5367.

Retailleau, S., Eynaud, F., Mary, Y., Abdallah, V., Schiebel, R., Howa, H., 2012. Canyon heads and river plumes: how might they influence neritic planktonic foraminifera communities in the Bay of Biscay?. Journal of Foraminiferal Research 42, 257–269.

Richmond, C.M., 1996. The INQUA approved provisional Lower-Middle Pleistocene boundary. In: Turner, C. (Ed.), The Early-Middle Pleistocene in Europe, Balkema, Rotterdam, pp. 319-327.

Rio, D., Raffi, I., Villa, G., 1990. Pliocene-Pleistocene distribution patterns in the Western Mediterranean. In: Karstetn, K.A., Mascle J. et al. (Eds.), Proceedings of ODP, Scientific Results 107, pp. 513–533.

Rio, D., Channell, J.E.T., Massari, F., 1996. Reading Pleistocene eustasy in a tectonic active siliciclastic shelf setting (Crotone peninsula, southern Italy). Geology 24, 743–746.

Rioual, P., Andrieu Ponel, V., Rietti Shati, M., Battarbee, R.W., de Beaulieu, J.L., Cheddadi, R., Reille, M., Svobodova, H., Shemesh, A., 2001. High resolution record of climate stability in France during the last interglacial period. Nature 413, 293–296.

Roberts, A.P., Tauxe, L., Heslop, D., 2013. Magnetic paleointensity stratigraphy and high resolution Quaternary geochronology: Successes and future challenges. Quaternary Science Reviews 61, 1-16.

Robustelli, G., Russo Ermolli, E., Petrosino, P., Jicha, B., Sardella, R., Donato, P., 2014. Tectonic and climatic controls on geomorphological and sedimentary evolution of the Mercure basin, Southern Apennines, Italy. Geomorphology 214, 423-435.

Rochon, A., de Vernal, A., Turon, J.L., Matthiessen, J., Head, M.J., 1999. Distribution of dinoflagellate cysts in surface sediments from the North Atlantic Ocean and adjacent seas in relation to sea-surface parameters. American Association of Stratigraphic Palynologists. Contribution Series 35, 152.

Rohling, E. J., Hilgen, F. J., 1991. The eastern Mediterranean climate at times of sapropel formation: a review. Geologie en Mijnbouw 70, 253-264.

Rohling, E.J., Jorissen, F.J., Vergnaud Grazzini, C., Zachariasse, W.J., 1993. Northern Levantine and Adriatic Quaternary planktic foraminifera; reconstruction of paleoenvironmental gradients. Marine Micropaleontogy 21, 191-218.

Rohling, E.J., Jorissen, F.J., De Stigter, H.C., 1997. 200 year interruption of Holocene sapropel formation in the Adriatic Sea. Journal of Micropalaeontology 16(2), 97–108.

Rohling, E.J., Hayes, A., De Rijk, S., Kroon, D., Zachariasse, W.J., Eisma, D., 1998. Abrupt cold spells in the northwest Mediterranean, Paleoceanography 13(4), 316-322.

Rossignol-Strick, M., 1983. African monsoons, an immediate climate response to orbital insolation. Nature 30, 446-449.

Rouis-Zargouni, I., Turon, J.L., Londeix, L., Essallami, L., Kallel, N., Sicre, M.A., 2010. Environmental and climatic changes in the central Mediterranean Sea (Siculo–Tunisian Strait) during the last 30 ka based on dinoflagellate cyst and planktonic foraminifera assemblages. Palaeogeography Palaeoclimatology Palaeoecology 285, 17–29.

Rouis-Zargouni, I., Turon, J.L., Londeix, L., Kallel, N., Essallami, L., 2012. The last glacial-interglacial transition and dinoflagellate cysts in the western Mediterranean Sea. Comptes Rendus Geoscience 344, 99–109.

Ruddiman, W.F., Raymo, M.E., Martinson, D.G., Clement, B.M., Backman, J., 1989. Pleistocene evolution: Northern Hemisphere ice sheet and North Atlantic Ocean. Paleoceanography 4, 353–412.

Russo Ermolli, E., Aucelli, P., Di Rollo, A., Mattei, M., Petrosino, P., Porreca, M., Rosskopf, C., 2010a. An integrated stratigraphical approach to the late Middle Pleistocene succession of the Sessano lacustrine basin (Molise, Italy). Quaternary International, 225, 114-127.

Russo Ermolli, E., Sardella, R., Di Maio, G., Petronio, C., Santangelo, N., 2010b. The late Early Pleistocene record of Saticula (Sant'Agata de' Goti, Benevento, Italy). Quaternary International 225, 128-137.

Russo Ermolli, E., Di Donato, V., Martin-Fernandez, J.A., Orain, R., Lebreton, V., Piovesan, G., 2014. Vegetation patterns in the Southern Apennines (Italy) during MIS 13: deciphering pollen variability along a NW-SE transect. Review of Palaeobotany and Palynology 218, 167-183.

Saavedra-Pellitero, M., Flores, J.A., Baumann, K.H., Sierro, F.J., 2010. Coccolith

distribution patterns in surface sediments of Equatorial and Southeastern Pacific Ocean. Geobios 43, 131-149.

Sabato, L., Bertini, L., Masini, F., Albianelli, A., Napoleone, G., Pieri, P., 2005. The lower and middle Pleistocene geological record of the San Lorenzo lacustrine succession in the Sant'Arcangelo Basin (southern Apennines, Italy). Quaternary International 131, 59–69.

Sadori, L., Jahns, S., Peyron, O., 2011. Mid-Holocene vegetation history of the central Mediterranean. The Holocene 21(1), 117-129.

Sagnotti, L., Cascella, A., Ciaranfi, N., Macrì, P., Maiorano, P., Marino, M., Taddeucci, J., 2010. Rock magnetism and paleomagnetism of the Montalbano Jonico section (Italy): evidence for late diagenetic growth of greigite and implications for magnetostratigraphy. Geophysical Journal International 180, 1049–1066.

Sagnotti, L., Scardia, G., Giaccio, B., Liddicoat, J.C., Nomade, S., Renne, P.R., Sprain, C.J., 2014. Extremely rapid directional change during Matuyama-Brunhes geomagnetic polarity reversal. Geophysical Journal International 199,1110-1124.

Sanchez Goni, M.F., Harrison, S.P., 2010. Millennial-scale climate variability and vegetation changes during the Last Glacial: Concepts and terminology. Quaternary Science Reviews 29 (21-22), 2823–2827.

Sánchez Goñi, M.F., Cacho, I., Turon, J.L., Guiot, J., Sierro, F.J., Peypouquet, J.P., Grimalt, J.O., Shackleton, N.J., 2002. Synchroneity between marine and terrestrial responses to millennial scale climatic variability during the last glacial period in the Mediterranean region. Climate Dynamics 19, 95–105.

Sánchez Goñi, M.F., Rodrigues, T., Hodell, D.A., Polanco-Martínez, J.M., Alonso-García M., Hernández-Almeida, I., Desprat, S., Ferretti, P., 2016. Tropically-driven climate shifts in southwestern Europe during MIS 19, a low eccentricity interglacial. Earth and Planetary Science Letters 448, 81–93.

Sangiorgi, F., Dinelli, E., Maffioli, P., Capotondi, L., Giunta, S., Morigi, C., Principato, M.S., Negri, A., Emeis, K.C., Corselli, C., 2006. Geochemical and micropaleontological characterisation of a Mediterranean sapropel S5: a case study from core BAN89GC09 (south of Crete). Palaeogeography Palaeoclimatology Palaeoecology 235, 192–207.

Sbaffi, L., Wezel, F.C., Kallel, N., Paterne, M., Cacho, I., Ziveri, P., Shackleton, N., 2001. Response of the pelagic environment to palaeoclimatic changes in the central Mediterranean Sea during the Late Quaternary. Marine Geology 178, 39–62.

Scandone, P., 1972. Studi di geologia lucana: carta dei terreni della serie calcareo-silico-marnosa e note illustrative. Bollettino della Società Naturalisti Napoli 81, 225-300.

Scarponi, D., Huntley, J.W., Capraro, L., Raffi, S., 2014. Stratigraphic paleoecology of the Valle di Manche section (Crotone Basin, Italy): A candidate GSSP of the Middle Pleistocene. Palaeogeography Palaeoclimatology Palaeoecology 402, 30–43.

Schilt, A., Baumgartner, M., Blunier, T., Schwander, J., Spahni, R., Fischer, H., Stocker, T.F., 2010. Glacial–interglacial and millennial-scale variations in the atmospheric nitrous oxide concentration during the last 800,000 years. Quaternary Science Reviews 29, 182–192.

Selli, R., 1962. Il Paleogene nel quadro della geologia dell'Italia Meridionale. Memorie della Società Geologica Italiana 3, 733-789.

Sgarrella, F., Moncharmont-Zei, M., 1993. Benthic Foraminifera of the Gulf of Naples (Italy): systematics and autecology. Bollettino della Società Paleontologica Italiana 32(2), 145–264.

Shackleton, N.J., Berger, A., Peltier, W.R., 1990. An alternative astronomical calibration of the lower Pleistocene timescale based on ODP Site 677. Transactions of Royal Society of Edimburgh, Earth Sciences 81, 21–261.

Shackleton, N.J., Hall, M.A., Pate, D., 1995. Pliocene stable isotope stratigraphy of Site 846. In: Pisias N.G., Mayer L.A., Janecek T.R., Palmer-Julson A., van Andel T.H. (Eds.). Leg 138. Proceedings of the Ocean Drilling Program, Scientific Results, 138, pp. 337-355.

Sierro, F.J., Hodell, D.A., Curtis, J.H., Flores, J.A., Reguera, I., Colmenero-Hidalgo, E., Bárcena, M.A., Grimalt, J.O., Cacho, I., Frigola, J., Canals, M., 2005. Impact of iceberg melting on Mediterranean thermohaline circulation during Heinrich events. Paleoceanography 20, PA2019.

Simon, Q., Bourlès, D.L., Bassinot, F., Nomade, S., Marino, M., Ciranfi, N., Girone, A., Maiorano, P., Choy, S., Dewilde, F., Scao, V., ASTER Team, 2017. Authigenic $^{10}Be/^{9}Be$ ratio signature of the Matuyama-Brunhes

boundary in the Montalbano Jonico marine succession. Earth and Planetary Science Letters 460, 255-267.

Singer, A., 1984. The Paleoclimatic Interretation of Clay Minerals in Sediments - A Review. Earth-Science Reviews 21, 251-293.

Singer, B., Hoffman, K., Schnepp, E., Guillou, H., 2008. Multiple Brunhes Chron Excursions Recorded in the West Eifel (Germany) Volcanics: Support for Long-Held Mantle Control Over the Non-Axial Dipole Field. Physics of the Earth and Planetary Interiors 169, 28-40.

Sissingh, W., 1972. Late Cenozoic Ostracoda of the south Aegean Island Arc. Utrecht Micropaleontological Bulletins 6, 1–187

Snedden, J.W., Liu, C., 2010. A Compilation of Phanerozoic Sea-Level Change, Coastal Onlaps and Recommended Sequence Designations. American Association Petroleum Geologists American Association of Petroleum Geologists, Search and Discovery Article 40594, 1–3

Snowball, I., Mellström, A., Ahlstrand, E., Haltia, E., Nilsson, A., Ningb, W., Muscheler, R., Brauer, A., 2013. An estimate of post-depositional remanent magnetization lock-in depth in organic rich varved lake sediments. Global and Planetary Change 110, 264-277.

Spezzaferri, S., Kucera, M., Pearson, P.N., Wade, B.S., Rappo, S., Poole, C.R., Morard, R., Stalder, C., 2015. Fossil and genetic evidence for the polyphyletic nature of the planktonic foraminifera "*Globigerinoides*", and description of the new genus *Trilobatus*. PLoS ONE 10(5), e0128108.

Sprovieri, M., Di Stefano, E., Incarbona, A., Salvagio Manta, D., Pelosi, N., Ribera d'Alcalà, M., Sprovieri, R., 2012. Centennial- to millennial-scale climate oscillations in the Central-Eastern Mediterranean Sea between 20,000 and 70,000 years ago: evidence from a high-resolution geochemical and micropaleontological record. Quaternary Science Reviews 46, 126-135.

Sprovieri, R., Di Stefano, E., Incarbona, A., Gargano, M.E., 2003. A high-resolution record of the last deglaciation in the Sicily Channel based on foraminifera and calcareous nannofossil quantitative distribution. Palaeogeography Palaeoclimatology Palaeoecology 202, 119–142.

Stefanelli, S., 2003. Benthic foraminiferal assemblages as tools for paleoenvironmental reconstruction of the early-middle Pleistocene Montalbano Jonico composite section. Bollettino della Società

Paleontologica Italiana 42, 281–299.
Stefanelli, S., 2004. Cyclic stages in oxygenation based on foraminiferal microhabitats: early-middle Pleistocene, Lucania basin, southern Italy. Journal of Micropaleontology 23, 81–95.
Stefanelli, S., Capotondi, L., Ciaranfi, N., 2005. Foraminiferal record and environmental changes during the deposition of early-middle Pleistocene sapropels in southern Italy. Palaeogeography Palaeoclimatology Palaeoecology 216, 27–52.
Stein, R., Hefter, J., Grützner, J., Voelker, A., Naafs, B.D.A., 2009. Variability of surface water characteristics and Heinrich-like events in the Pleistocene midlatitude North Atlantic Ocean: Biomarker and XRD records from IODP Site U1313 (MIS 16–9). Paleoceanography 24, PA2203.
Stocker, T.F., Johnsen, S.J., 2003. A minimum thermodynamic model for the bipolar seesaw. Paleoceanography 18(4). PA000920
Suc, J.-P., Popescu, S.M., 2005. Pollen records and climate cycles in the North Mediterranean region since 2.7 Ma. Geological Society of London, Special Publication 247, 147–158.
Suc, J.-P., Bertini, A., Combourieu Nebout, N., Diniz, F., Leroy, S., Russo Ermolli, E., Zheng, Z., Bessais, E., Ferrier, J., 1995. Structure of West Mediterranean vegetation and climate since 5.3 Ma. Acta Zoological Cracoviense 38(1), 3-16.
Suc, J.-P., Combourieu Nebout, N., Seret, G., Popescu, S.A., Klotz, S., Gautier, F., Clauzon, G., Westgate, J., Insinga, D., Sandhu, A.S., 2010. The Crotone series: a synthesis and new data. Quaternary International 219, 121-133.
Suganuma, Y., Yokoyama, Y., Yamazaki, T., Kawamura, K., Horng, C.S., Matsuzaki, H., 2010. ^{10}Be evidence for delayed acquisition of remanent magnetization in marine sediments: Implications for a new age for the Matuyama-Brunhes boundary. Earth and Planetary Science Letters 296, 443-450.
Suganuma, Y., Okuno, J., Heslop, D., Roberts, A.P., Yamazaki, T., Yokoyama, Y., 2011. Post-depositional remanent magnetization lock-in for marine sediments deduced from ^{10}Be and paleomagnetic records through the Matuyama-Brunhes boundary: Earth and Planetary Science Letters 311, 39-52.

Thunell, R.C., 1979. Pliocene–Pleistocene paleotemperature and paleosalinity history of the Mediterranean Sea: results from DSDP Sites 125 and 132. Marine Micropaleontology 4, 173–187.

Thunell, R.C., Reynolds, L.A., 1984. Sedimentation of planktonic foraminifera: seasonal changes in speciesflux in the Panama Basin. Micropaleontology 30, 243–262.

Tolderlund, D.S., Bé, A.W.H., 1971. Seasonal distribution of planktonic foraminifera in the western North Atlantic. Micropaleontolology 17, 297-329.

Toti, F., 2015. Interglacial vegetation patterns at the Early-Middle Pleistocene transition: a point of view from Montalbano Jonico section (southern Italy). Alpine and Mediterranean Quaternary 28(2), 131-143.

Traverse, A., (Eds.) 1988. Paleopalynology, Unwin Hyman, Boston, 600 pp.

Triantaphyllou, M.V., Antonarakou, A., Dimiza, M., Anagnostou, C.L., 2010. Calcareous nannofossil and planktonic foraminiferal distributional patterns during deposition of sapropels S6, S5 and S1 in the Libyan Sea (Eastern Mediterranean). Geo-Marine Letters 30(1), 1-13.

Tropeano, M., Cilumbriello, A., Sabato, L., Gallicchio, S., Grippa, A., Longhitano, G.S., Bianca, M., Gallipoli, R., M., Mucciarelli, M., Spilotro, G., 2013. Surface and subsurface of the Metaponto Coastal Plain (Gulf of Taranto – Southern Italy): Present–day- vs LGM–landscape. Geomorphology 203, 115-131.

Tropeano, M., Sabato, L., Pieri, P., 2002. The Quaternary "Post-turbidite" sedimentation in the South-Apennines Foredeep (Bradanic Trough - Southern Italy). Bollettino Società Geologica Italiana 1, 449–454.

Tzedakis, P.C., 1999. The last climatic cycle at Kopais, central Greece. Journal of Geological Society of London 156, 425–434.

Tzedakis, P.C., 2007. Seven ambiguities in the Mediterranean palaeoenvironmental narrative. Quaternary Science Reviews 26, 2042-2066.

Tzedakis, P.C., 2010. The MIS 11 – MIS 1 analogy, southern European vegetation, atmospheric methane and the "early anthropogenic hypothesis". Climate of the Past 6, 131-144.

Tzedakis, P.C., Bennett, K.D., 1995. Interglacial vegetation succession: a view from southern Europe. Quaternary Science Reviews 14, 967-982.

Tzedakis, P.C., McManus, P.C., Hooghiemstra, H., Oppo, D.W., Wijmstra, T.A., 2003. Comparison of changes in vegetation in northeast Greece with records of climate variability on orbital and suborbital frequencies over the last 450,000 years. Earth and Planetary Science Letters 212, 197–212.

Tzedakis, P.C., Hooghiemstra, H., Palike, H., 2006. The last 1.35 million years at Tenaghi Philippon, revised chronostratigraphy and long-term vegetation trend. Quaternary Science Reviews 25, 3416–3430.

Tzedakis, P.C., Palike, H., Roucoux, K.H., de Abreu, L., 2009. Atmospheric methane, southern European vegetation and low-midlatitude links on orbital and millennial timescales, Earth and Planetary Science Letters 277, 307-317.

Tzedakis, P.C., Raynouad, D., McManus, J.F., Berger, A., Brovkin, V., Kiefer, T., 2009. Interglacial diversity. Nature Geoscience 2, 751–755.

Tzedakis, P.C., Channell, J.E.T., Hodell, D.A., Kleiven, H.F., Skinner, L.C., 2012a. Determining the natural length of the current interglacial. Nature Geoscience 5, 1–4.

Tzedakis, P.C., Wolff, E.W., Skinner, L.C., Brovkin, V., Hodell, D.A., McManus, J.F., Raynaud, D., 2012b. Can we predict the duration of an interglacial? Climate of the Past 8, 1473-1485.

Vannacci, M., 2016. Cambiamenti climatici durante lo stadio isotopico 22, come registrati nella successione marina di Montalbano Jonico (Italia meridionale) tramite indagine palinologica. Tesi di Laurea Magistrale, A.A. 2014-2015. Università degli Studi di Firenze, 66 pp.

Van Zeist, W., Bottema, S., 2009. A palynological study of the Acheulian site of Gesher Benot Ya'aqov, Israel. Vegetation History and Archaeobotany 18,105–121.

Vergnaud-Grazzini, C., 1985. Mediterranean late Cenozoic stable isotope record: stratigraphic and paleoclimatic implications. In: Stanley, D.J., Wezel, F.C. (Eds.). Geological evolution of the Mediterranean Basin. Springer-Verlag, New York, pp. 413-451.

Vincent, E., Berger, W.H., 1981. Planktonic foraminifera and their use in Paleoceanography. In: Emiliani, C. (Ed.). The oceanic lithosphere. The sea. John Wiley & Sons, New York. pp. 1025-1119.

Wagner, G., Masarik, J., Beer, J., Baumgartner, S., Imboden, D., Kubik, P.W.,

Synal, H.A., Suter, M., 2000. Reconstruction of the geomagnetic field between 20 and 60 kyr BP from cosmogenic radionuclides in the GRIP ice core. Nuclear Instruments and Methods in Physics Research Section B: Beam Interactions with Materials and Atoms 172, 597-604.

Wall, D., Dale, B., 1966. "Living fossils" in western Atlantic plankton. Nature 211,1025–1026.

Wang, X., Yang, Z., Lovlie, R., Sun Z., Pej, J., 2006. The magnetostratigraphic reassessement of correlation between Chinese loess and marine oxygen isotope records over the last 1.1 Ma. Physics of the Earth and Planetary Interiors 159, 109–117.

Watts, W.A., 1988. Europe. In: Huntley, B., Webb III, T. (Eds.), Handbook of Vegetation Science 7. Vegetation History. Kluwer, Dordrecht, pp. 155-192.

Weaver, P.P.E., Pujol, C., 1988. History of the last deglaciation in the Alboran Sea (western Mediterranean) and adjacent North Atlantic as revealed by coccolith floras. Paleogeography Paleoclimatology Paleoecology 64, 35-42.

Wegmann, K.W., Pazzaglia, F.J., 2009. Late Quaternary fluvial terraces of the Romagna and Marche Apennines, Italy: Climatic, lithologic, and tectonic controls on terrace genesis in an active orogeny. Quaternary Science Reviews 28, 137-165.

Whitney, D.L., Evans, B.W., 2010. Abbreviations for names of rock-forming minerals. American mineralogist 95(1), 185.

Winter, A., Jordan, R.W., Roth, P.H., 1994. Biogeography of living Coccolithophores in ocean waters, in Coccolithophores. In: Winter, A., Siesser, W.G. (Eds.). Cambridge University Press, London, pp. 161-178.

Wisshak, M., Correa, M.L., Gofas, S., Salas, C., Taviani, M., Jakobsen, J., Freiwald, A., 2009. Shell architecture, element composition, and stable isotope signature of giant deep-sea oyster *Neopycnodonte zibrowii* sp. n. from the NE Atlantic. Deep-Sea Research I 56, 374–407.

Wolff, E.W., Chappellaz, J., Blunier, T., Rasmussen, S.O., Svensson, A. 2010. Millennial-scale variability during the last glacial: The ice core record. Quaternary Science Reviews 29, 2828–2838.

Woodward, J.C., Lewin, J., Macklin, M.G., 1992. Alluvial sediment sources in a glaciated catchment: the Voidomatis basin, northwest Greece. Earth

Surface Processes and Landforms 17(3), 205–16.
Wright, A.K., Flower, B.P., 2002. Surface and deep ocean circulation in subpolar North Atlantic during the mid-Pleistocene revolution. Paleoceanography 17, 1068.
Yamasaki, M., Matsui, M., Shimada, C., Chiyonobu, S., Sato, T., 2008. Timing of shell size increase and decrease of the planktic foraminifer *Neogloboquadrina pachyderma* (sinistral) during the Pleistocene, IODP Exp. 303 Site U1304, the North Atlantic Ocean. The Open Paleontology Journal 1, 18–23.
Yang, T.S., Hyodo, M., Yang, Z.Y., Fu, J.L., 2007. Two geomagnetic excursions during the Brunhes chron recorded in Chinese loess paleosol sediments, Geophys. J. Int., 171, 104–114.
Yang, T., Hyodo, M., Yang, Z., Li, H., Maeda, M., 2010. Multiple rapidly polarity switches during the Matuyama-Brunhes (M/B) transition from two high resolution loess paleosol records. Geophysical Journal International 115. B05101.
Yang, T., Hyodo, M., Yang, Z., Li, H., Maeda, M., 2010. Multiple rapid polarity swings during the Matuyama-Brunhes transition from two high-resolution loess-paleosol records, Journal of Geophysical Research 115, B05101.
Yin, Q.Z., Berger, A., 2012. Individual contribution of insolation and CO2 to the interglacial climates of the past 800,000 years. Climate Dynamics 38,709–724.
Yin, Q.Z., Berger, A., 2015. Interglacial analogues of the Holocene and its natural near future. Quaternary Science Reviews 120, 28-46.
Ziveri, P., Baumann, K.H., Böckel, B., Bollmann, J., Young, J.R. 2004. Biogeography of selected Holocene coccoliths in the Atlantic Ocean. In: Thiersten, H.R., Young J.R. (Eds.). Coccolithophores: from molecular processes to global impacts. Springer Verlag, pp. 403–428.
Zonneveld, K.A.F., Versteegh, G.J.M., de Lange, G.J., 2001. Palaeoproductivity and post-depositional aerobic organic matter decay reflected by dinoflagellate cyst assemblages of the Eastern Mediterranean S1 sapropel. Marine Geology 172, 181–195.
Zonneveld, K.A.F., Versteegh, G.J.M., Kodrans-Nsiah, M., 2008. Preservation and organic chemistry of Late Cenozoic organic-walled dinoflagellate

cysts: a review. Marine Micropaleontology 86, 179–197.

SECTION B

Land-sea climate variability in the western Mediterranean during MIS 20 and MIS 19: a multiproxy record from the ODP 976 (Alboran Sea)

1. Introduction

The Alboran Sea is one of the most investigated world's marine basins on account of its geographical position, at the interface between the Atlantic Ocean and the semi-enclosed Mediterranean Sea (Fig. B1). Alboran is a key place for the comprehension of the water mixing and circulation in the whole Mediterranean as well as the functioning of marine primary productivity and the deep-see depositional/erosional processes. This basin has additionally turned out to be a faithful recorder of the past interactions between the high-latitude and the sub-tropical climate dynamics (Cacho et al., 1999, 2001; Martrat et al., 2004; Sierro et al., 2005; Ausin et al., 2015). Such a valuable palaeoclimatic documentation is stored in the deep-sea sediments, recovered by scientific drilling during several seafloor exploration campaigns. There is plenty of climate records focusing on the Last Glacial and the Holocene (e.g. Combourieu Nebout et al., 1999, 2002; Sánchez-Goñi et al., 2002; Fletcher and Sánchez-Goñi, 2008; Fletcher et al., 2010), while a much smaller number spanning older climate cycles (Von Grafenstein et al., 1999, González-Donoso et al., 2000; Joannin et al., 2011). In the recent years, a significant palaeoclimate and palaeovegetation record straddling the EMPT in the western Mediterranean was obtained through palynological analysis at ODP Site 976, in the Alboran sea (Joannin et al., 2011). This registration remains of especial significance since it encompasses five climate cycles (1,090-900 ka, MIS 31-23) and capture both obliquity and precession orbital signals. We here extend such a documentation to the stratigraphical range MIS 20-MIS 19 of the same core, performing a multiproxy reconstruction based on palynological (central to this thesis), stable isotopes and marine biostratigraphical data.

2. General setting of ODP core 976

Core 976 has been recovered in the Western Alboran Sea (36°12.3'N, 4°18.8'W) at a water depth of 1108 m, in the frame of the ODP leg 161 (Comas et al., 1996) (Fig. B1). The drilled Pleistocene sediments consist of open-marine hemipelagic clays and silty clays rich in biogenic carbonate (nannofossils and foraminifers), associated with terrigenous particles delivered by rivers and wind (Alonso et al., 1999). The elevated sedimentation rates (on average 23 cm/ka; Bernasconi et al., 1999), allow events to be resolved over a wide range of temporal scales.

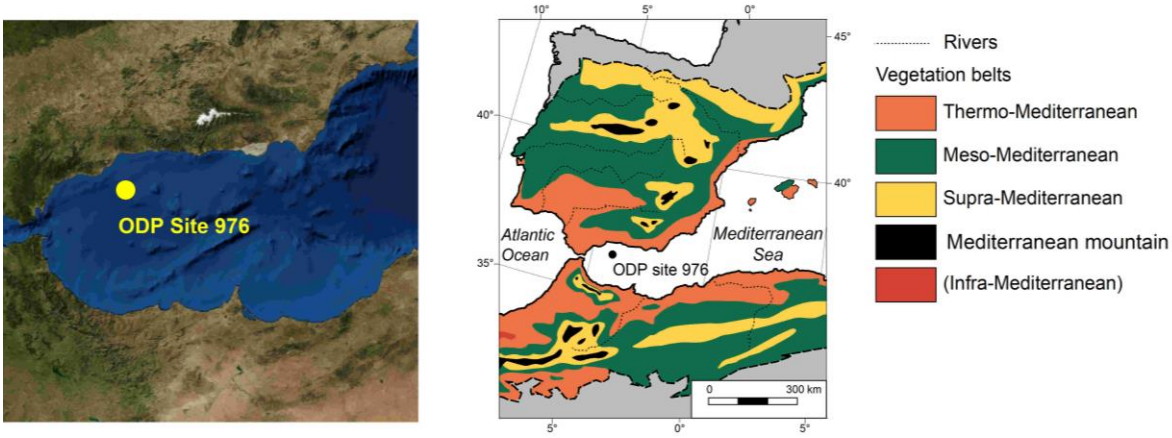

Fig. B1 - Left panel: location of the ODP Site 976 in the Alboran Sea; Right panel: Mediterranean vegetation belts surrounding the study region (modified after Quézel & Médail, 2003).

3. Aims

Quantitative palynological analyses were carried out at core 976 to describe the climate history during Termination IX and MIS 19. Pollen signal was used to infer past flora and vegetation while the dinocyst assemblages (see Section C) served to characterize the sea-surface condition of Alboran at that time. Analyses of the planktonic foraminifera and calcareous nannoplankton were performed by micropalaeontologists involved into the project (University of

Bari) to describe the concomitant effect of the climate variability in the oceanographic context. Specialists in stable-isotopes and dating of Quaternary sequences (Laboratoire des Sciences du Climat et de L'Environnement Gif-Sur-Yvette, France) assisted the $\delta^{18}O$ measurements to provide with information about the surface-water temperatures and the change linked to the change of global glacial volume.

4. Materials and methods

Palynological quantitative counting were performed in the interval 197.41-210.97 meters composite depth (mcd). Pollen and spores were counted in one-hundred and four samples (Fig. B2), sixty-one of which were additionally analysed for their dinocysts content (see Section C). Detailed and summary diagrams were plotted to express the variations of pollen and spores taxa proportions. Multivariate statistical analysis additionally employed to reveal the structure and properties of individual pollen, foraminifera and nannoplankton datasets was carried out in collaboration with A. Buccianti (Dept. of Earth Sciences, Florence University).

5. Results

Pollen analyses allowed almost 130 taxa to be identified. Deciduous *Quercus* is the most frequent arboreal taxon in this diverse floristic assemblage. *Pinus* was also found to be very abundant, but this is especially connected with overrepresentation phenomena. The analyses also revealed significant presence of cork-oak (*Q. suber*), evergreen oak (*Q. ilex*-type), olive tree (*Olea*), beech (*Fagus*) and mid to high-altitude elements like *Cedrus*, *Abies* and *Picea*. Very low values of trees today extinct from the Iberian Peninsula (e.g. *Zelkova*, *Tsuga* and *Cathaya*) were detected. In some levels Ericaceae shows significant abundances, as well as Cupressaceae. *Pistacia*, *Phillyrea* and*Ligustrum* were counted among the thermophilous shrubs.

The non-arboreal pollen is mainly composed by Asteraceae (mostly Cichorioideae), Poaceae and Cyperaceae, together with abundant steppic

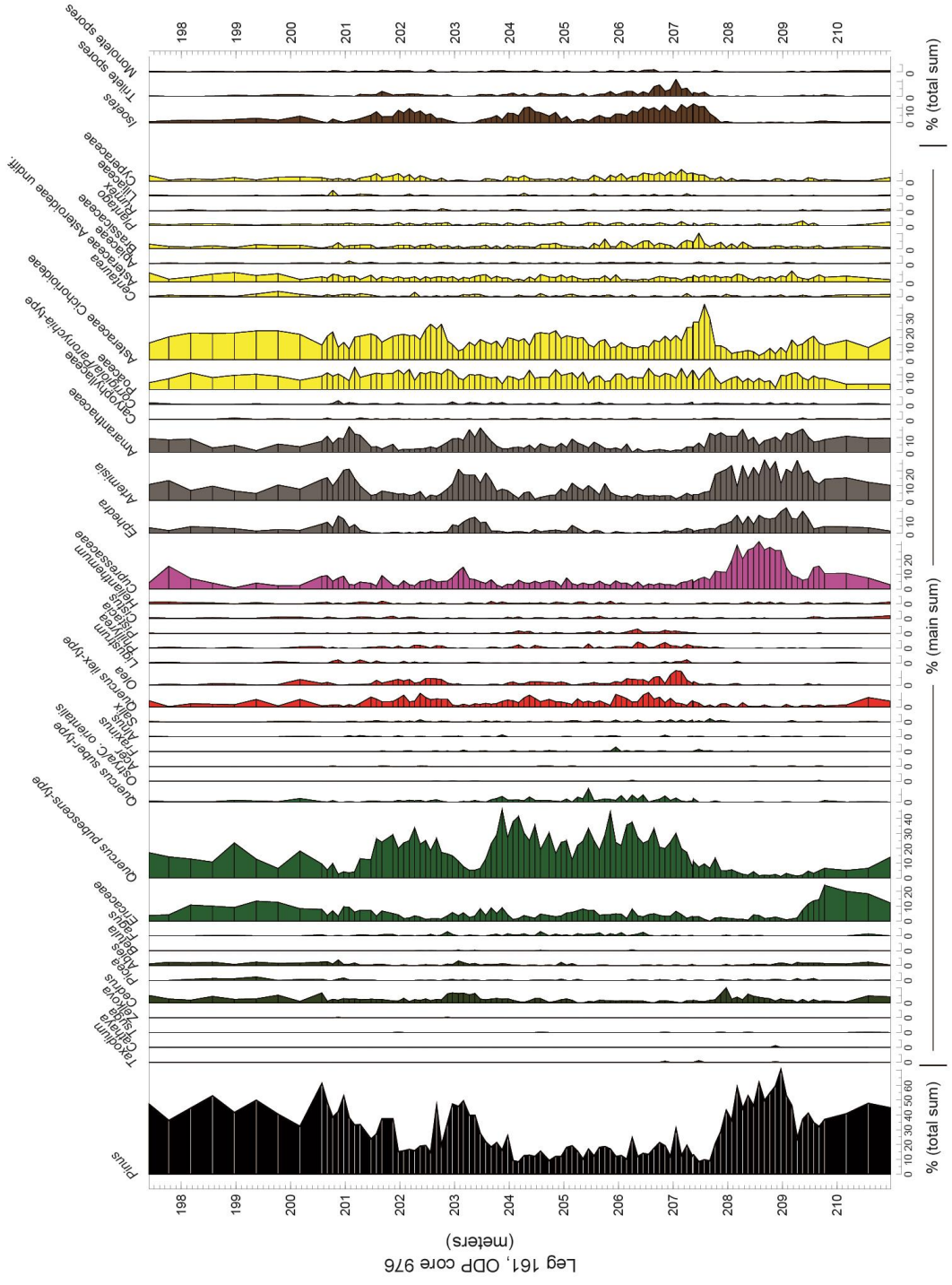

Fig. B2 - ODP core 976 pollen and spores percentage diagram plotted against meters composite depth.

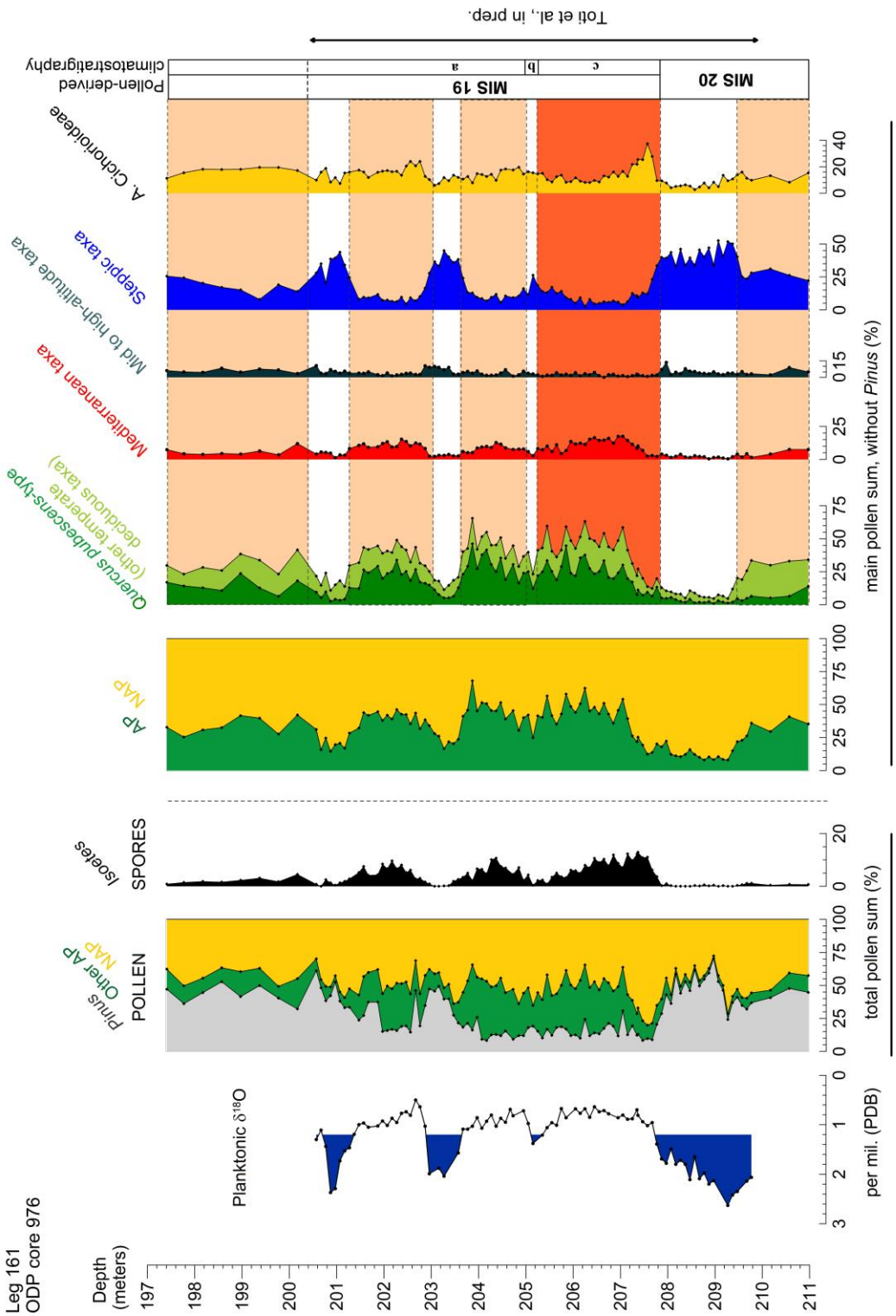

Fig. B3 - Oxygen isotope record and selected pollen and spores percentage curves along ODP core 976 composite depth. AP: Arboreal pollen; NAP: Non Arboreal pollen.

(*Artemisia*) and semi-desert taxa (*Ephedra*, Amaranthaceae, …). Major taxa percentages were plotted against stratigraphic depth (Fig. B2).

The pollen record shows repeated broad-leaved deciduous and Mediterranean forest increases (colour bands in Fig. B3) which attest phases of enhanced precipitations and temperatures. The warmest and more humid conditions encompassed by MIS 19 occurred between 207.77 and 205.35 mcd (the dark-red colour band; Fig. B3) describing the terrestrial interglacial optimum. This interval is internally marked by repeated short-term expansions/contractions of the temperate deciduous forest pointing to an intra-interglacial climate variability. A pronounced seasonal contrast is revealed during the first part of MIS 19 by the acme of Mediterranean taxa (evergreen oak, olive-tree, …) as well as by the expansion of *Isoetes*, which is a Lycophyta adapted to seasonal desiccation/flooding regime. The phases, characterized by higher abundances of non-arboreal pollen (NAP), in particular steppic and semi-desert elements (*Artemisia*, *Ephedra*, Amaranthaceae, …), describe intervals of relative climate deterioration (fall of humidity and temperature). The major aridity crisis occurred during MIS 20. The main pollen-derived climate changes consistently mirror the curve of $\delta^{18}O$ and the temperature variations inferred by the marine biological proxies, showing the large extent of climate change impact.

6. Pollen and spore-based reconstruction of vegetation and climate change in the western Mediterranean from 800 to 760 ka

The pollen and spores data collected in the interval of Termination IX and MIS 19 made it possible to:

- Improve the knowledge of the past biogeography of extinct arboreal taxa in the Iberian Peninsula during the Early and Middle Pleistocene. Plants like *Tsuga*, *Cathaya*, *Liquidambar*, *Engelhardia*, *Carya*, *Pterocarya* started to disappear from Southern Europe since the Early Pleistocene. Our pollen diagrams appear already devoid of these taxa, providing a

terminus ante quem for their last occurrence in the western Mediterranean.

- Measure the intensity of glacials and interglacials in this area between MIS 20 and MIS 18, according to the degree of afforestation and the relative abundance of non-arboreal taxa.
- Obtain a better understanding of the climate phenomena in a period still pervaded by the 41-kyr signal but already responding to the effects of prolonged, intensified glacial phases.
- Assess the causal relationships between insolation changes, owing to the Earth's orbital geometry, and vegetation states. This will be also essential to improve the comprehension of climate change in the Holocene, a period which develops under very similar orbital control to MIS 19.
- Analyze how vegetation communities respond to climate change and the eventual leads/lags with respect to those attested by marine planktonic assemblages.
- Compare vegetation events previously recorded in other sites (e.g. at Montabano Jonico, see Section A) during the same time-interval. This will improve their climate significance heading a better characterization of the interval of MIS 19c-b, that is also crucial for the establishment of the GSSP of the Early-Middle Pleistocene subSeries/subEpochs boundary.

The results of pollen and spore investigations presented above are extensively illustrated by an article in preparation contained in this Section, where we developed a palaeoclimate and palaeoenvironmental reconstruction based on integrated palynological, oxygen isotopes and calcareous plankton datasets:

- **Francesco Toti**, Adele Bertini, Angela Girone, Patrizia Maiorano, Maria Marino, Franck Bassinot, Sébastien Nomade, Antonella Buccianti, Nathalie Combourieu Nebout. Impact of glacial-interglacial climate variability on marine and terrestrial ecosystems between MIS 20 and MIS 19: a western Mediterranean viewpoint

Contribution

Impact of glacial-interglacial climate variability on marine and terrestrial ecosystems between MIS 20 and MIS 19: a western Mediterranean viewpoint*

*Article in preparation
(**F. Toti**, A. Bertini, A. Girone, P. Maiorano, M. Marino, F. Bassinot, S. Nomade, A. Buccianti, N. Combourieu Nebout)

Abstract

Determining the climate history of past interglacials is especially useful for a better prediction of the Holocene climate dynamics. Marine isotope stage 19 (MIS 19, ~790-760 ka) is a major target of this study because, unlike many Pleistocene interglacials, it shares with the Holocene a very similar orbital configuration. To reconstruct the detailed structure of MIS 19, palynological and calcareous plankton (nannofossils and foraminifera) analyses were carried out in sediment samples from ODP core 976 (Alboran Sea, western Mediterranean) supported by a robust chronological frame based on in situ $\delta^{18}O$ record. Results show that during warm-temperate phases of MIS 19, including full interglacial 19c and two consecutive short-lived interstadials, the spread of prevalent temperate forest taxa on land parallels the expansion of warm-water calcareous plankton taxa, within intervals marked by lower $\delta^{18}O$. On the other hand, cooler phases, including late MIS 20 and several cold spells accompanying MIS 19b-a, are marked by the diffusion of open vegetation formations dominated by steppic and semi-desert taxa; at the same time meltwaters entered the Mediterranean according to the incursion of polar-water taxa. Biotic signals (e.g. ubiquist herbs expansions, forest taxa contractions as well as rapid variations of calcareous plankton proportions) also describe climate anomalies at the millennial time-scales within interglacial/interstadial intervals.

This highlights the sensitivity of western Mediterranean area to a wide range of climate signals. The multiproxy results acquired at the ODP 976 deep-sea sediments provide definition of i) the phase-relationships between marine and terrestrial ecosystems during one crucial climate cycle embedded in the Early-Middle Pleistocene transition; ii) the succession of phases and events within a precise climatostratigraphic frame that improves the correlation with already existing Mediterranean records of MIS 19 and those from the North Atlantic; iii) potential equivalents of some modern climate

patterns (e.g. North Atlantic Oscillation) contributing to the deciphering of the complex land-sea interactions.

Keywords: MIS 19, TIX, western Mediterranean, Early-Middle Pleistocene Transition, millennial-scale climate variability, land-sea correlations

1. Introduction

During the whole Quaternary, Glacial-Interglacial (G-IG) cycles driven by periodical variations in the Earth's orbital parameters have repeatedly shaped the structure and dynamics of terrestrial and marine ecosystems. During the Early-Middle Pleistocene transition (EMPT), between 1.4 and 0.4 Ma, such cycles lengthened from 41 to 100 kyr with progressively longer glacials and shorter interglacials (e.g. Ruddiman et al., 1986; Head and Gibbard, 2015 and reference therein). The occurrence of longer glacial phases leaved strong evidences in both marine and terrestrial biota, including extinctions and turnover phenomena (Head and Gibbard, 2005 and references therein). Such changes, taking place at a global-scale, are particularly attested in the Mediterranean, a sensible area for the recording of past climate signals due to its geographical position strongly influenced by both polar and tropical dynamics. Marine isotope stage (MIS) 19, extending between 790-760 ka, is largely studied because its optimum is considered to be the best 'recent' analogue of the early Holocene in terms of climate response to orbital forcing (e.g. Yin & Berger, 2012, 2015).

Climate variability at a shorter time-scale was observed to be a pervasive feature of most of the Quaternary. Works on both high and mid latitudes sites of the North Atlantic Ocean have documented the occurrence of millennial-scale oscillations related to a nonlinear response to the Earth's precession cycle and its harmonics (e.g. Ferretti et al., 2015; Sánchez-Goñi et al., 2016; Oliveira et al., 2017). However, millennial-scale variability in the North Atlantic was primarily associated to oceanic and atmospheric processes linked to the polar ice-sheet dynamics (McAyeal, 1993; Marcott et al., 2011). Recurring freshwater pulses involved the subpolar North Atlantic vertical convection and deep-water formation feeding the Atlantic Meridional Overturning

Circulation (AMOC). Considering the net northward heat transfer in the Atlantic Ocean promoted by the AMOC, the latter influenced climate at regional and global scales (Ganopolski and Rahmstorf, 2001). Dataset documents the climate variability from the perspective of both the North Atlantic margin (Site U1385, southwestern Iberia) and the eastern to central Mediterranean (e.g. Tenaghi Philippon, north-eastern Greece, Tzedakis et al., 2006; Tsampika, Rhodes, Greece, Joannin et al., 2007; Colfiorito, central Italy, Bertini, 2000; Montalbano Jonico section, southern Italy, Bertini et al., 2015). The direct correlation between marine and terrestrial proxies at Montalbano Jonico (Maiorano et al., 2016), along MIS 19, provides a valuable indication of atmospheric and oceanic connections for the central Mediterranean and deserved to be compared to a faithful counterpart in western Mediterranean.

For this purpose, we describe in great detail a climate sequence spanning a short slice of the EMPT, obtained from Ocean Drilling Program (ODP) core 976, in the Alboran Sea. The last part of MIS 20 and the entire MIS 19 were investigated by means of oxygen stables isotopes measurements and simultaneous palynomorphs (pollen and spores) and calcareous plankton (foraminifera and nannoplankton) analyses. The paired marine and terrestrial datasets were used to monitor the land-sea variability at the orbital and millennial time-scales. Records from such key area, at the transition between the Mediterranean and the Atlantic, provide a unique opportunity to examine terrestrial and oceanic responses to global climate changes over a crucial period of intense climate modification.

2. Regional setting of the study site

2.1. Geographic and depositional context

ODP Site 976 (36°12.3'N, 4°18.8'W) is located in the western Alboran Sea, 60 km off the southern Spanish coast and ~110 km East of the Strait of Gibraltar (Fig. 1). Drilling on this site, during ODP Leg 161 (Shipboard Scientific Party, 1996; Comas et al., 1996), allowed a 346 m-long composite sedimentary succession to be recovered. The latter spans the uppermost Middle Miocene

to the Holocene

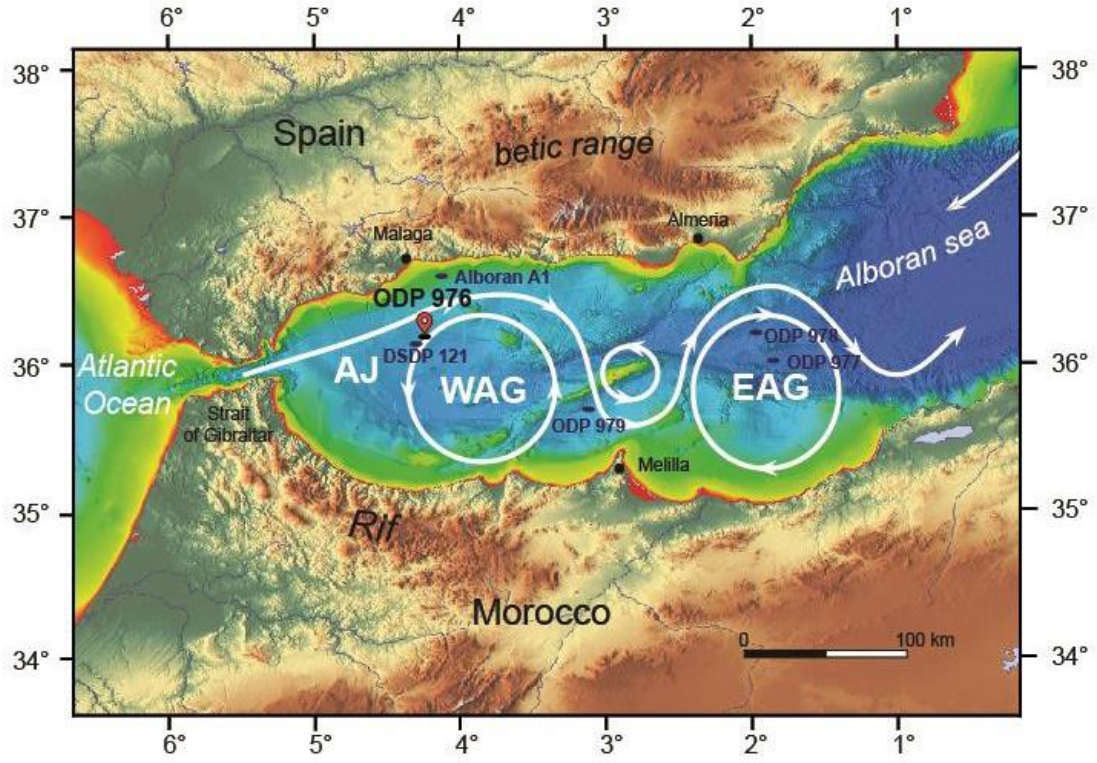

Fig. 1 – Location of ODP Site 976 and other drilled sites (ODP: 977, 978, 979; Alboran A1 e DSDP 121) in the Alboran Sea. Scheme of the sea-surface circulation: AJ: Atlantic Jet, WAG, EAG: Western and Eastern Anticyclonic Gyres (modified after Sánchez-Garrido et al., 2013).

(Comas et al., 1996), providing important insights on both the depositional and palaeocenographic history of the western Mediterranean.

Sediments at Site 976 originate from both pelagic and turbidity flows mechanisms and are mainly composed of nannofossil clay to silty-clay (Bernasconi et al., 1999). The lithogenic fraction mainly comes from two sources: fluvial, supplied by the rivers draining the Betic Cordillera and southern Iberia coastal plains, and aeolian, which is linked to the close Sahara desert (Fábres et al., 2002).

2.2. Present climate and vegetation

In the present day, the Alboran Sea region has a distinct Mediterranean climate which is characterized by hot-dry summers and mild-humid winters (Walter et al., 1975; Quézel & Médail, 2003). Average annual precipitation along the near coasts of southern Spain varies from 300 to more than 1000 mm, with the highest values in the southwestern tips, which is the more exposed area to the rainfalls originating from the Atlantic storm-track and depressions (Sumner et al., 2001). During winter, Alboran Sea area is subject to the arrival of moist air masses (i.e. westerlies) of Atlantic provenance whereas during summer sporadic but intense winds blow from the Sahara, as result of the northward shift of the Inter-Tropical Convergence Zone (ITCZ) (Guerzoni et al., 1997).

The vegetation of the Alboran borderlands complies with the general climate context and is strongly influenced by the regional topography, including the presence of the Betic (southern Spain) and Rif (Morocco) chains. The lowest vegetation belt is characterized by thermophilic covers of Mediterranean shrubs and trees (*Pistacia lentiscus*, *Chamaerops humilis*, *Olea sylvestris*, *Quercus rotundifolia*, ...), formations of cork oak (*Q. suber*) and Cupressaceae (*Juniperus* spp. and *Tetraclinis articulata*) (Nieto Caldera et al., 1990; Bernabid, 1985). Mixed broadleaved forests including deciduous oak (*Q. pyrenaica*, *Q. faginea*, *Q. canariensis*), coniferous taxa (e.g. *Abies* and *Cedrus*, the latter restricted to Morocco) are mainly distributed in the meso/supra altitudinal belts (Rivas-Martínez, 1987). *Pinus spp.* is a widespread component of both high-altitude and transitional woodlands (Martinez Parras and Peinado Lorca 1987; Bernabid 1982).

2.3. Oceanographic setting

The hydrology of the Alboran Sea depends on the water exchange between the Atlantic and the Mediterranean through the Strait of Gibraltar. A permanent anti-estuarine circulation maintained by the excess of evaporation within the Mediterranean drives the Atlantic Jet (AJ) (Fig. 1) to enter while a saltier Mediterranean Outflow Water (MOW) escapes at a deeper level. As the

AJ mixes with the Mediterranean waters, it becomes a 100-200 m thick layer known as Modified Atlantic Water (MAW; e.g. Millot, 1999), which is involved in the formation of two anticyclonic gyres. The latter are quasi- permanent features of the Alboran sea circulation (Renault et al., 2012) and include the Western (WAG) and Eastern Anticyclonic Gyre (EAG) (Fig. 1). At the northern edges of the anticyclonic gyres, the AJ-MAW mixing produces a frontal system that favours vertical mixing and productive events, forming quasi-permanent areas of upwelling (García-Gorriz and Carr, 1999). Hydrographic conditions affect the seasonal changes of the Alboran Sea's calcareous plankton assemblages. Species adapted to well-mixed and nutrient- rich sea surface water, dominate during late fall and winter in coincidence with upwelling phenomena. On the other hand, relaxed upwelling and/or stratified surface water conditions allow the proliferation of warm and oligotrophic planktonic taxa, mainly during summer and early fall (Barcena et al., 2004; Hernandez-Almeida et al., 2011).

3. Materials and methods

Core 976 was investigated for the interval 209.77-200.57 meters mcd (92 samples from both holes B and C), which fully covers the late MIS 20 and MIS 19 intervals (Von Grafenstein et al., 1999). Sediments used for oxygen isotopic measurements, pollen and calcareous plankton high resolution analyses were sampled from the core at an average of 10 cm-interval. Samples underwent laboratory procedures and analyses at the Laboratory for Sciences of Climate and Environment (LSCE, France) for the stable isotopes, at the Muséum national d'Histoire naturelle (Paris, France) for pollen, and at the University of Bari "Aldo Moro" (Bari, Italy), for calcareous plankton. Multivariate statistical analysis was run on the percentage biomarkers datasets.

3.1. Stable isotopes measurement

$\delta^{18}O$ was measured on the planktonic foraminifer *Globigerina bulloides* (250-315μm) in 83 samples. Analyses were performed on an Isoprime dual-inlet

Isotope Ratio Mass Spectrometer (Elementar) at LSCE laboratory. Results are expressed as $\delta^{18}O$ vs V-PDB (in ‰). The external analytical reproducibility determined from replicate measurements of a carbonate standard is ±0.05‰ (1σ). Values obtained for the calcite international standard NBS-18 for $\delta^{18}O$ is -23.27‰. Measurements were usually performed using 4 to 15 individuals, except for five levels in which only 1 or 2 specimens of *G. bulloides* (*e.g.* 10 to 30 µg of $CaCO_3$) were picked and analyzed. Measuring the isotopic composition of a large number of shells insures that potential in-homogeneities in the foraminifer population (seasonality, bioturbation effect, ...) are smoothed out to some extent, providing a more robust result.

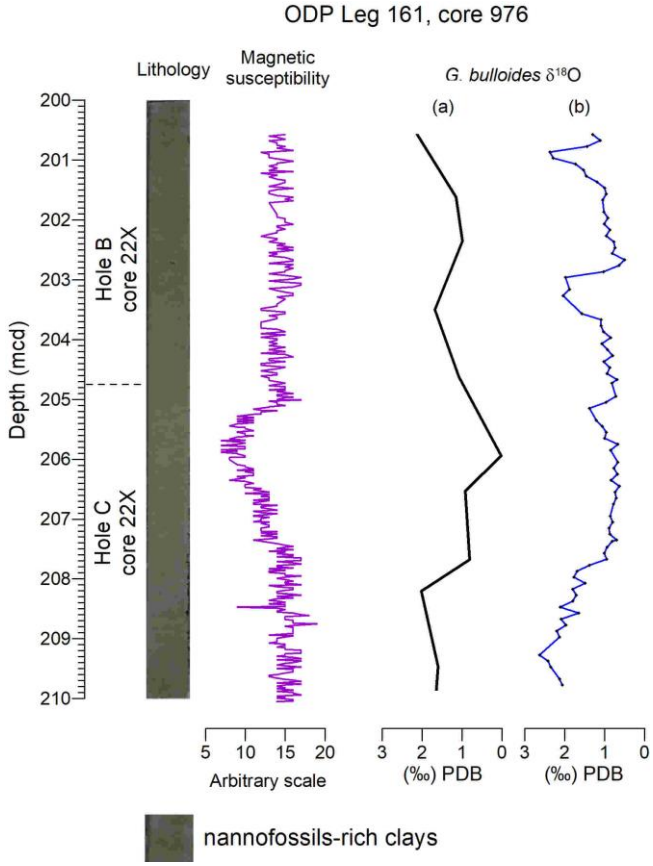

Fig. 2 - ODP core 976: lithology, magnetic susceptibility and comparison between (a) low-resolution (Von Grafenstein et al., 1999) and (b) high-resolution planktonic oxygen isotopic record (this study).

Consequently, it is expected that isotopic datasets obtained on 1 or 2 shells could display a higher variability. All $\delta^{18}O$ results presented in this study were plotted against depth in Fig. 2.

3.2. Palynological analysis

Ninety-three samples were prepared in accordance with a standard procedure including HCl (at 18%) and HF (70%) digestion and a final filtration at 5 μm. Tablets containing a fixed number of exotic spores (*Lycopodium*) were added to each sample, at the beginning of the preparation, to permit estimation of palynomorphs concentration. Residues were mounted in slides which were examined by transmitted-light optical microscope. Taxonomic identification conforms to reference collections and iconographic literature (e.g. Reille, 1992). Counts of at least 250 pollen grains, out of *Pinus*, were carried out on each sample to obtain quantitative estimation of taxa proportions. *Pinus* counts and percentage computation were managed separately because this pollen grain resulted to be over-represented, as generally observed in marine sediments (e.g. Heusser and Balsam, 1977). Counts of non-pollen palynomorphs were carried out simultaneously, although in this work only the frequency of *Isoetes* is shown. Pollen taxa, except *Pinus*, are expressed in percentage normalized to a pollen sum without *Pinus*. *Pinus* relative abundance was calculated against the total pollen sum including its own grains. *Isoetes* was normalized to the total pollen plus *Isoetes* sum. In order to define the most significant changes of the palynological assemblages, selected taxa were merged into eight groups on the base of the ecologic and climatic requirements of their present correspondents (Tab. I).

3.3. Calcareous plankton analysis

Planktonic foraminifera investigations were performed on eighty-three samples. The samples were dried and washed through 63 and 150 μm sieves. The residues (>150 μm) were split until a representative aliquot containing about 300 specimens has been obtained. All specimens were

Groups	Taxa	Modern climatic and ecological significance
Mediterranean sclerophylls	*Quercus ilex*-type, *Olea*, *Ligustrum*, *Phillyrea*, *Pistacia*, *Ceratonia*, *Vitis*, Cistaceae, Rhamnaceae, *Myrtus*	Xerophilous hard leaved trees and shrubs typical of regions with a mild-wet winter and hot-dry summer (Mediterranean climate)
Temperate broad-leaved forest taxa	*Quercus pubescens*-type, *Quercus suber*-type, *Ostrya/Carpinus orientalis*, *Alnus*, *Salix*, *Ulmus*, *Fraxinus*, *Castanea*, *Acer*, *Liquidambar*, *Carya*, *Zelkova*, ...	Mesophilous trees living under a climate regime with adequate year-round precipitation; they withstand a strong annual temperature cycle with a cold winter season and a warm summer season (warmer continental and "humid" subtropical climates)
---	Ericaceae	The dwarf-shrub community component of heathlands largely extends in the Atlantic Iberian coasts, under well-distributed rainfall round the year.
Mountain trees	*Cedrus*, *Picea*, *Abies*, *Tsuga*	Mid to high altitudinal gymnosperms taxa demanding humidity. This forest extends into lower latitude wherever mountains chains are present. Such taxa thrive under cold summer and long winter with yearlong humid conditions.
---	Asteraceae Cichorioideae	Cosmopolitan herbs indicating dry conditions and/or depleted soils
---	Cupressaceae	Xerophytic shrubby taxa tolerating low temperatures and droughts. They have today a quite large altitudinal range from sea level to high altitude and can live in semiarid ombroclimatic zones as well as in humid ombroclimatic areas, like some parts of Morocco and the Algerian coast.
Steppe & semi-desert taxa	*Artemisia*, Amaranthaceae, *Hippophae*, *Ephedra*, *Lygeum*, *Calligonum*, Caryophyllaceae, Plumbaginaceae	Taxa associated with a semi-arid continental climatic regime. In the steppes of the middle-latitude winters are cold and dry and summers warm to hot.
---	*Isoetes*	Lycophyta adapted to flooding-desiccation seasonal alternations typical of Mediterranean temporary ponds

Tab. I - Informal pollen groups at ODP Site 976 with main floral components with associated climate and ecological significance.

counted in the aliquots and species abundances were quantified as percentages on the total number of planktonic foraminifers. Fifteen species or species groups were distinguished. The SPRUDTS group (sensu Rohling et al., 1993) includes *Trilobatus sacculifer*, *Hastigerina pelagica*, *Globoturborotalita rubescens*, *Orbulina universa*, *Beella digitata*, *Globoturborotalita tenella* and *Globigerinella siphonifera*. According to their ecological preference the abundances of *G. ruber* group, SPRUDTS group, *Turborotalia truncatulinoides* (left and right specimens) have been grouped as warm water taxa (Tab. II). For the taxonomy of *Neogloboquadrina* spp. the criteria from Darling et al. (2006) have been adopted: *Neogloboquadrina incompta* corresponds to what has been previously referred to *N. pachyderma* (dextral) and includes intergrades between *N. pachyderma* (dextral) and *N. dutertrei*; *N. pachyderma* only includes the left coiling specimens.

The investigation on calcareous nannofossil assemblages was performed on ninety-two samples. Slides for coccolithophore analysis were prepared according to the method of Flores & Sierro (1997) to estimate the absolute coccolith abundances (coccolith/g of sediment). Quantitative analyses were performed using a polarized light microscope at 1000x magnification and abundances were determined by counting at least 500 coccoliths of all sizes, in a varying number of fields of view. Reworked calcareous nannofossils were estimated during this counting. Quantitative patterns of taxa were expressed as number of coccolith/g of sediment (N) and as percentages. *Umbilicosphaera* spp., *Calciosolenia* spp., *Oolithotus* spp., *Rhabdosphaera clavigera*, and *Discosphaera tubifera* were grouped as warm-water taxa (wwt), according to their ecological preferences (see Tab. II). *Helicosphaera pavimentum*, which records a distinct positive relation with interglacial phases, was also included in the wwt.

3.4. Statistical analysis

Multivariate statistical analysis has been run on pollen, foraminifera and nannofossils datasets. The statistical processing was applied to a restricted list of variables (taxa or group of taxa: see Tab. III) of each dataset, which were a

Coccolithophore taxon	Ecological meaning	Reference
warm water taxa (wwt): *Calciosolenia* spp., *Oolithotus* spp., *Umbilicosphaera* spp., *Rhabdosphaera clavigera*, *Discosphaera tubifera*; *Helicosphaera pavimentum*	warm, stratified and oligotrophic sea surface waters	McIntyre and Bé (1967); Winter et al. (1994); Ziveri et al. (1995, 2004); Baumann et al. (2004); Boeckel and Baumann (2004); Saavedra-Pellitero et al. (2010); Palumbo et al. (2013); Maiorano et al. (2015). This work
G. caribbeanica	oligotrophic and warm surface waters	Bollmann (1997); Bollmann et al. (1998)
small *Gephyrocapsa* (open central area)	high productivity and unstable surface waters	Gartner et al. (1987); Gartner (1988); Barcena et al. (2004); Marino et al. (2008, 2011); Ausin et al. (2015a, b)
Helicosphaera carteri	turbid and fresher surface waters	Colmenero-Hidalgo et al. (2004); Maiorano et al. (2013a, b, 2016)
Coccolithus pelagicus spp. *pelagicus*	subarctic taxon	Baumann et al. (2000); Geisen et al. (2002)
	cold meltwater influx	Parente et al. (2004); Amore et al. (2012); Marino et al. (2014); Marino et al. (2011)
Florisphaera profunda	deep dweller photic zone; deep nutricline	Molfino and McIntyre (1990a, 1990b); Beaufort et al. (1997, 2001); Di Stefano and Incarbona (2004)
	short-term phases of inverse thermocline	Colmenero-Hidalgo et al. (2004); Marino et al. (2014); Maiorano et al. (2015)
Planktonic foraminifera taxon	**Ecological meaning**	**Reference**
warm water taxa (wwt): *Globigerinoides ruber* group, SPRUDTS group	warm, oligotrophic and stratified sea surface waters	Tolderlund and Bé (1971); Hemleben et al. (1989); Pujol and Vergnaud-Grazzini (1995)
Trilobatus sacculifer	tropical-subtropical surface waters	Tolderlund and Bé (1971); Hemleben et al. (1989)
Truncorotalia truncatulinoides	prevalence of cool, well-mixed, nutrient-rich waters in winter	Hemleben et al. (1989); Sprovieri et al. (2003), Pujol and Vergnaud Grazzini (1995)
Neogloboquadrina incompta and *Neogloboquadrina dutertrei*	cold and eutrophic waters, deep chlorophyll maximum at the base of the euphotic layer	Hemleben et al. (1989); Reynolds and Thunnel (1989); Pujol and Vergnaud-Grazzini (1995); Rohling et al. (1995)
Neogloboquadrina pachyderma	polar-subpolar taxon	Huber et al. (2000); Kucera and Kennett (2002); Yamasaki et al. (2008); Darling et al. (2006);
	cold meltwater influx	Cacho et al. (1999); Pérez-Folgado et al. (2003); Sierro et al. (2005); Girone et al. (2013b)
Globorotalia inflata	Cool-temperate waters, tracer of frontal system, deep pycnocline, ventilated conditions	Hemleben et al. (1989); Pujol and Vergnaud-Grazzini (1995); Rohling et al. (1995); Barcena et al. (2004)
Globigerina bulloides	opportunistic species related to eutrophic setting related to upwelling, strong seasonal mixing or river input	Tolderlund and Bé (1971); Hemleben et al. (1989); Pujol and Vergnaud-Grazzini (1995); Rohling et al. (1997); Bárcena et al. (2004); Geraga et al. (2005, 2008)
Turborotalita quinqueloba	Cold-cool, high fertility surface waters, fresher water	Hemleben et al. (1989); Reynolds and Thunnel (1989)

Tab. II - Ecological preferences of calcareous plankton taxa according to literature and this study.

priori assumed to best summarize some ecological aspects. The data values were scaled by log-centered transformation to avoid biases linked to the compositional nature of the datasets (Aitchison, 1986; Aitchison and Greenacre, 2002). The management of count zero would be preceded by a proper treatment of this type of data (Martín-Fernández et al., 2011). In our case the treatment of the 36 counts equal to zero involved a Bayesian inference related to a multinomial experiment and a multiplicative modification of the non-zero values in the vector of counts, knows as Bayesian-multiplicative (BM) treatment (Martín-Fernández et al., 2011; Martín-Fernández et al., 2015). The modification causes a minor distortion in the covariance structure and gives us an appropriate treatment to take into account the presence of zero values too (Martín-Fernández et al., 2012). Principal Component Analysis (PCA) was performed to re-scale the original dataset variability to a lower- dimensional representation expressed by principal components axis.

4. Results

4.1. Oxygen isotopes

The *G. bulloides* $\delta^{18}O$ vary between ~0.50 and 2.63 ‰ (Figs. 2-5). Between 209.27 m and 207.37 m, a decrease of nearly 1.8 ‰ of the $\delta^{18}O$ values is well evident, range from ~2.4-2.6‰ to ~0.81‰. Upwards, a rapid change starts toward lighter value; the planktonic $\delta^{18}O$ record is relatively constant, around ~0.7 ‰ with no visible oscillations, until 205.75 m (for a total thickness of 1.6 m). Then, the $\delta^{18}O$ record shows a rapid fall toward heavier values of 1.38 ‰, with values dropping by ~0.7 ‰ in 50cm (Fig. 2). The upper portion of the record is characterized by intervals with low $\delta^{18}O$ values, limited by extremely abrupt $\delta^{18}O$ changes at their onsets and terminations. Two lighter episodes are visible in the $\delta^{18}O$ record over the intervals 204.95–203.67 m and 202.87–201.47 m. The abrupt $\delta^{18}O$ decrease at the upper end of the studied interval suggests that a third episode likely exists.

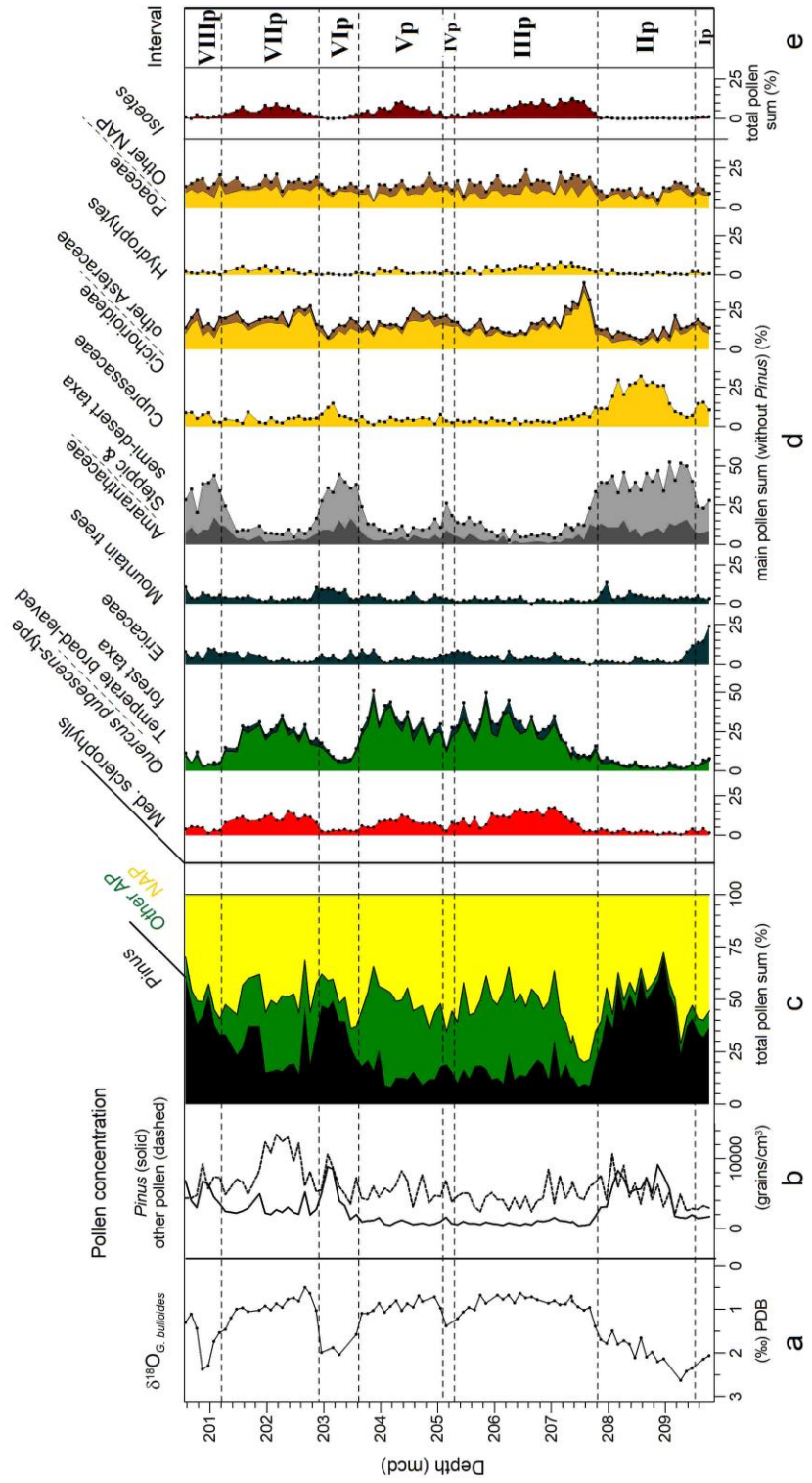

Fig. 3 - (a) Planktonic $\delta^{18}O$ and pollen data: (b) Pollen concentration (grains/cm³); (c) AP (Arboreal Pollen)/NAP (Non-Arboreal Pollen) percentage; (d) selected single and grouped pollen and spore taxa; (e) pollen zones (Interval Ip-VIIIp).

4.2. Palynomorphs

The palynological analyses illustrate a rich and well preserved palynoflora consisting of 127 pollen taxa (28 arboreal and 99 non-arboreal) and 5 different morphotypes of Pteridophyta spores. Total pollen concentration ranges between 3000 and nearly 20,000 grains per cm^3 of dry sediment (Fig. 3). *Pinus* concentration ranges between 410 and nearly 9200 grains per cm3 of dry sediment. Arboreal pollen assemblages mainly include taxa that are still currently widespread in (south) Europe and north Africa while some more sporadic taxa are today totally absent (such as *Carya* and *Tsuga*) or restricted in single geographical areas in the Mediterranean area (such as *Liquidambar* and *Zelkova*). Deciduous oaks (*Quercus*) dominate the forest assemblages followed by evergreen oaks and *Olea*. Among the mountain coniferous forest taxa *Cedrus* is especially abundant followed by *Abies* and *Picea*. Shrubs are mainly represented by Ericaceae and Cupressaceae followed by *Pistacia* and *Phillyrea*. Herbaceous taxa include Asteraceae (mainly Cichorioideae), Poaceae, *Artemisia*, Amaranthaceae and *Ephedra* (Fig. 3). Other common taxa are Brassicaceae, *Plantago* and Cyperaceae. Among Pteridophyta the quillworts *Isoetes* was especially recorded (Fig. 3, Tab. I). The informal subdivision of the pollen record in eight pollen intervals (Ip to VIIIp) based on the ecologic/climate feature of single pollen taxa and informal pollen groups (Tab. I). Temperate deciduous woody taxa plus Mediterranean sclerophyllous taxa are especially abundant (up to 56%) within interval IIIp as well as intervals Vp and VIIp. Hydrophytes and *Isoetes* closely mimic this pattern. Steppic and semi-desert taxa show the highest relative abundances (up to 52%) within intervals Ip, IIp, IVp, VIp and VIIIp; altitudinal conifers including *Cedrus* and *Abies* often show percentage increasing during the latter intervals.

4.3. Calcareous plankton

Planktonic foraminifera are well preserved and diversified. The assemblages are mainly represented by *Neogloboquadrina* spp. (including *N. incompta*, *N. pachyderma* and *N. dutertrei*), *Turborotalita quinqueloba*, *G. inflata* and *G.*

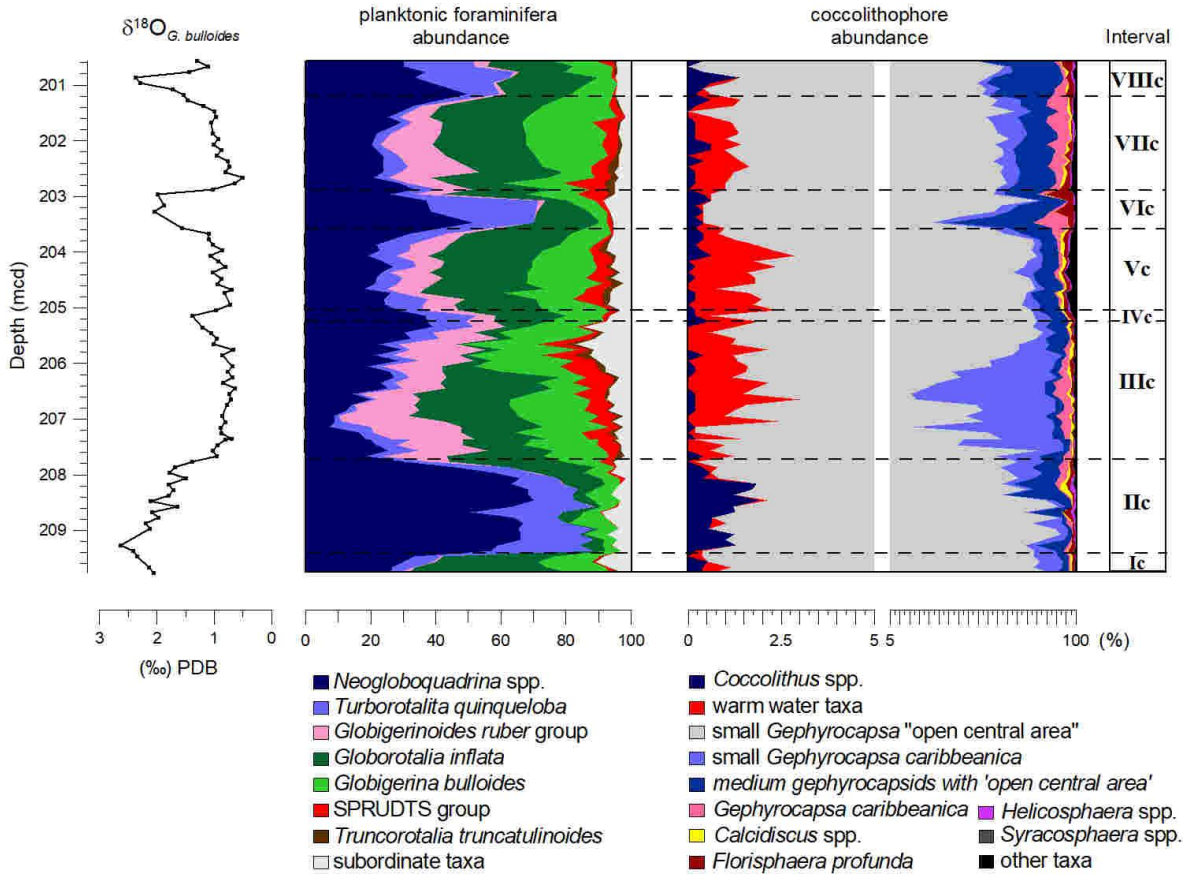

Fig. 4 - Taxonomic composition of planktonic foraminifera and calcareous nannofossils expressed as percentage versus depth at ODP Site 976. $\delta^{18}O$ record is shown on the left and intervals from Ic to VIIIc are shown on the right.

bulloides that are distributed through the entire section. *Globigerinoides ruber* group, SPRUDTS group and *Truncorotalia truncatulinoides* occur frequently from 208.8 mcd upward. Other less abundant taxa (subordinate taxa in Fig. 4) include *Globigerinita glutinata*, *Globorotalia scitula* and *Globigerina falconensis*, although never representing more than 16 % of the total assemblage; *G. glutinata* occurs through the entire studied section, whereas *G. scitula* and *G. falconensis* have a more scattered distribution. Distribution patterns of the main taxa allow identification of eight intervals (Fig. 4). *G. inflata* and *G. bulloides*, representing about 70% of the total assemblages, are dominant taxa within Interval Ic. During the intervals IIc, IVc, VIc and VIIIc,

Neogloboquadrina spp. and *T. quinqueloba* are the most abundant taxa representing from 50% up to 80% of the total assemblages. *Neogloboquadrina* spp. mainly consists of *N. pachyderma* in all the intervals, while it also made up of *N. incompta* and *N. dutertrei* during interval IVc. *G. ruber* group., G. inflata and *G. bulloides* dominate the assemblages of the intervals IIIc, Vc and VIIc. During these intervals SPRUDTS group and *Truncorotalia truncatulinoides* also became more abundant although never exceeding 12% of the assemblages. Coccolithophore assemblage is generally well preserved, although some samples from the lower portion of the study section show evidence of dissolution. Cretaceous to Paleogene reworked coccoliths have percentages lower than 2% with exception of the basal part of the record when they increase up to 10-12%. The total absolute abundance of coccolithophores varies from ca. $900 \cdot 10^6$ to $10000 \cdot 10^6$ coccolith/g of sediment with the higher values mainly in the interval 205.25-207.5 mcd.

Thirty-two taxa have been recognized and they are mostly represented by gephyrocapsids that have abundance higher that 80-90% (Fig. 4). Small gephyrocapsids (small *Gephyrocapsa* <3 m) are dominant through the section and consist of morphotypes with closed (*G. caribbeanica*) and open central area, the latter including different taxa that were not distinguished at the species level (hereafter small *Gephyrocaspa* open central area).

Medium gephyrocapsids (larger than 3 μm) are primarily *G. caribbeanica,* and morphotypes with open central area mainly *G. margereli/muellerae* and with a minor percentage *G. oceanica* and *G. omega*.

Other component of the assemblage is represented by less abundant taxa such as *Florisphaera profunda*, the wwt group, *Coccolithus* spp. (mainly *C. pelagicus* ssp. pelagicus), *Calcidiscus* spp. (mainly *C. leptoporus*), *Helicosphaera* spp. (mainly *H. carteri*), *Syracosphaera* spp. (*S. pulchra, S. hystrica*). Very rare and scattered occurrences of subordinate taxa are plotted as "other taxa" in Fig. 4 and they consist of *Pseudoemiliania lacunosa*, small *Reticulofenestra* spp., *Pontosphaera* spp., *R. clavigera* var. *stylifera*, *Braarudosphaera bigelowi*.

Patterns of selected taxa are useful to distinguish eight intervals through the study record, in a general agreement with the interval partition recognized by means of planktonic foraminifera and pollen assemblages. Small *G. caribbeanica* have their highest abundance during interval IIIc with

Pollen taxon	PCA-1p	Planktonic foraminifera taxon	PCA-1f	Coccolitophore taxon	PCA-1n
Broad-leaved deciduous forest taxa	-0.48	*G. ruber* group	0.54	Warm-water taxa	-0.38
Mediterranean taxa	-0.43	SPRUDS	0.35	*G. caribbeanica*	-0.32
Ericaceae	0.19	*G. bulloides*	0.10	*G. oceanica*	0.24
Asteraceae Cichorioideae	-0.01	*G. glutinata*	-0.12	Small *Gephyrocapsa* "open central area"	0.22
Steppic and semi-desert taxa	0.73	*G. inflata*	0.12	small *G. caribbeanica*	-0.43
		N. incompta	-0.08	*C. pelagicus* ssp. *pelagicus*	0.67
		T. quinqueloba	-0.23		
		N. pachyderma	-0.68		

Tab. III - Principal component loadings (first two axes) for selected pollen, foraminifera and calcareous plankton taxa or taxa groups.

an anti- covariant pattern with respect to other small gephyrocapsids. The wwt clearly show increase during the intervals IIIc-Vc, and VIIc, although a slight increase is also visible within interval I (Figs. 4-5). The most evident wwt decreases occur during intervals IIc, VIc and VIIIc and a short-term decrease may be observed within interval IVc. *Coccolithus* spp. distinctly increases up to 2% during intervals IIc and VIIIc (Fig. 4).

4.4. Statistical analysis

The results of PCA applied on simplified matrixes containing pollen, foraminifer and nannoplankton are summarized in Tab. III and Fig. 5. PCA performed on the pollen dataset shows that 68% of the variance can be explained by only one principal component: PC1-p. It is characterized by positive loadings for steppic and semi-desert taxa and by negative loadings for

mesothermic broad-leaved and Mediterranean taxa (Tab. III). PC1-p thus appears to discriminate between herbaceous taxa adapted to low values of atmospheric moisture and a plant community requiring warm temperatures and adequate rainfalls. PCA performed on the matrix containing selected foraminifera taxa or ecological groups (Tab. III) revealed that most of the total variance is described by only one principal component, PC1-f, that alone explains 80% of the total variance. Loadings of PC1-f are markedly positive for *G. ruber* group and SPRUDTS group while are especially negative for *N. pachyderma*, *N. incompta* and *T. quinqueloba*. PC1-f thus seems appropriate to discriminates between an association of oligotrophic and tropical-subtropical warm-water taxa and an association of cool to cold-waters species. The simplified matrix containing the most significant coccolithophore taxa or ecological groups reveals that most of the variability is represented by one principal components, PC1-n, alone accounting for the 48%. PC1-n loads with positive score *C. pelagicus* spp. *pelagicus* and with negative score warm water taxa, small *G. caribbeanica* and *G. caribbeanica* > 3µm. Based on the ecological preferences of *C. pelagicus* ssp *pelagicus* and warm water taxa, we suggest that PC1-n may discriminate between species of polar/subpolar water and species of warmer and oligotrophic waters. The negative loadings of total *G. caribbeanica* may be considered a clue to constrain its ecological preferences in the Alboran sea. This species seems, indeed, related to an association of oligotrophic and warm surface waters in agreement with Bollmann (1997) and Bollmann et al. (1998).

5. Discussion

5.1. Climate stratigraphy and age-model

The ODP 976 planktonic $\delta^{18}O$ record measured along latest MIS 20 and MIS 19 was tuned (Bassinot, pers. comm.) using the recent Montalbano Jonico $\delta^{18}O$ record (southern Italy; Nomade et al., submitted) as calibration target. The two curves, in fact, can be unambiguously correlated (see Section C). The age model for the Montalbano Jonico $\delta^{18}O$ record were previously obtained by

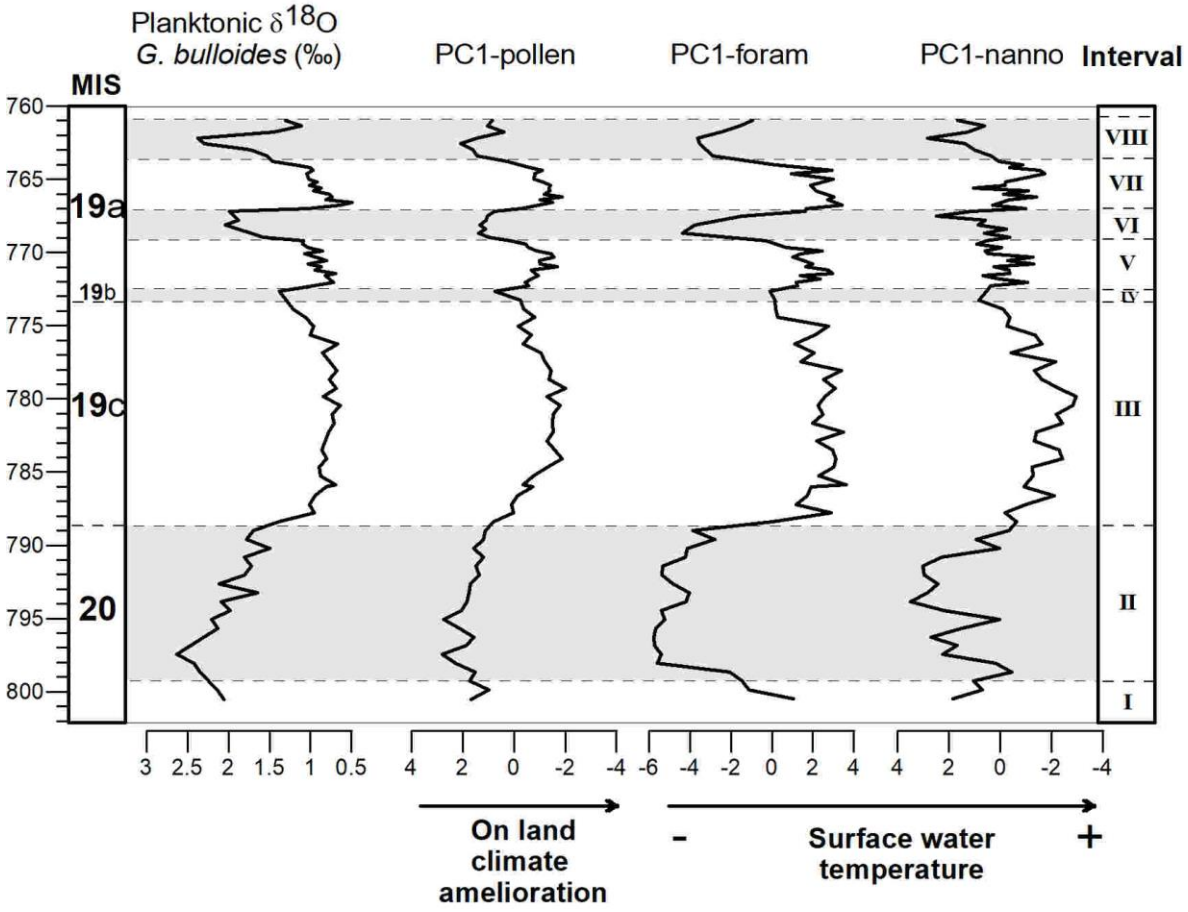

Fig. 5 - $\delta^{18}O$ record and PCA curves (first axes) for pollen, planktonic foraminifera and calcareous nannofossil datasets plotted versus time at ODP Site 976 with respect to the marine oxygen isotope stratigraphy and the informal stratigraphical subdivision (intervals I-VIII).

adopting the same phase relationships between mean summer insolation and the climate response observed during the last deglaciation (TI) (Nomade et al., submitted). Such a strategy is based on the assumption that MIS 1 is the best orbital analogue of MIS 19 (e.g. Tzedakis et al., 2012; Yin and Berger; 2012, 2015). The Montalbano Jonico chronology was additionally constrained by dating of tephra 'V4' (i.e. 774.1 ±0.9 ka). The final age model for ODP core 976 is based on seven tie-points between 797.4 and 761.9 ka provided by Bassinot (pers. comm.).

The eight informal intervals (Ip-VIIIp and Ic-VIIIc; Figs. 3, 4) clearly define the major changes in the land-sea climate system during latest MIS 20 and MIS 19. To facilitate the correlation to the marine standard isotope stratigraphy the main features within MIS 19 were correlated with the classical tripartite structure of this stage (MIS c/3, b/2 and a/1: Bassinot et al., 1994), as already performed by Nomade et al. (submitted) in the coeval Montalbano Jonico section (Fig. 5).

Time-boundaries of each pollen (Ip-VIIIp) and calcareous plankton (Ic-VIIIc) informal zones (Figs. 3 and 4) show a strict degree of correlation. So, by now, they will be identified in the text as unspecified I-VIII intervals (Fig. 5).

5.2. Orbital-scale climate variability at ODP Site 976 during MIS 20-19

According to the pollen evidence (Fig. 3; Tab. IV) MIS 19c is well expressed by a prevalent arboreal mesophilic vegetation typical of a (warm) temperate and relatively humid climate (interval III). Deciduous *Quercus* dominated temperate arboreal forest already devoid of subtropical taxa during this full interglacial as well as during the successive interstadials (intervals V and VII). During these phases, sea-surface waters were characterized by the maximum relative abundances of warm-water calcareous planktonic taxa, indicating relative warm temperatures and oligotrophy (Fig. 4; Tab. IV). Intervening intervals of MIS 20 glacial (intervals I and II) and successive stadials (intervals IV, VI, VIII) were dominated by an open vegetation with steppic to semi-desert elements, suggesting the prevalence of cold and dry conditions. Concomitantly, cool to cold-water taxa prevailed in the calcareous plankton assemblages, pointing out colder and harsher climate as well as mixing of the surface water conditions (Fig. 4).

The informal subdivision in eight intervals (I-VIII) is excellently supported by the score plots of PC1-p, PC1-f and PC1-n plots (Fig. 5). The interpretation of the first axes of the principal components (Section 4.4.), additionally confirms that such a subdivision is primarily determined by changes in terrestrial temperature and humidity as well as of sea surface temperature. The phase relationships between on land and marine climate changes

emphasize a tight coupling of the air-ocean processes at the orbital and sub-orbital time-scale. Such a correspondence is astonishing especially regarding the sharp variations occurring within MIS 19b-a, potentially revealing efficient teleconnections.

5.2.1 Late MIS 20

Between 800.5 ka and 799 ka (Fig. 6a, interval I) the occurrence of steppic and semi-desert taxa (such as *Artemisia*, Amaranthaceae and *Ephedra*) suggests the presence of open vegetal formations under a prevalent (cold-)dry climate (Fig. 6a). Moderate precipitation levels, however, are attested in some areas by the relative abundance of Ericaceae. At this time, the occurrence of *G. inflata* and *G. bulloides*, concomitant with very low percentages of warm and oligotrophic taxa in the calcareous plankton assemblages, document persistent cool, mixed and meso- to eutrophic sea surface water conditions consistent with MIS 20 glacial conditions. An overall climate deterioration on land is evidenced by a major drought event from 799 ka up to 789 ka, when the increase of *Artemisia*, *Ephedra* and Amaranthaceae along with the decline of Ericaceae, supports a large expansion of steppes and coastal salt marshlands, in the Alboran Sea borderlands (Fig. 6a, interval II). The beginning of harsher conditions on land is contemporaneous to the increase of polar-subpolar *N. pachyderma* (up to 60% of the total assemblages between 799 and 795 ka) and *C. pelagicus* ssp. *pelagicus*, suggesting a remarkable sea surface water temperature cooling in the Alboran sea in connection with the arrival of polar-subpolar meltwater influx into the basin. In fact, abundance peaks of these two polar to subpolar taxa has been used to monitor southward penetrations of polar water masses, usually associated with iceberg discharges in mid-latitude North Atlantic (eg. Bond et al., 1992) as well as in the Portuguese margin (Cayre et al., 1999; de Abreu et al., 2003; Vautravers and Shackleton, 2006; Eynaud et al., 2009) during the late Pleistocene. A clear evidence of Northern Hemisphere ice-sheet collapses (Heinrich-like events) at the timing of MIS 20/MIS 19 (Termination IX: TIX) comes from the massive Ice Rafted Detritus (IRD) deposition documented in some North Atlantic sites (Fig. 6a, b).

MIS	Interval (mcd)	Palynological features	Vegetation context	Calcareous plankton assemblage	Environmental context
19a	VIII (200.57-201.17)	(+) Steppic & semi-desert taxa (·) Ericaceae	Steppic vegetation. Proximity of oceanic heatlands	(+) *N. pachyderma* (↓) forams and nanno wwt	Cold and eutrophic surface water
19a	VII (201.27-202.87)	(+) Mediterranean sclerophylls, temperate broad-leaved forest taxa, Cichorioideae, *Isoetes* (·) Hydrophytes	Broad-leaved woods and thermophilous xerophytic scrublands	(+) forams and nanno wwt (+) *G. bulloides* (+) *G. inflata*	Warm and oligotrophic surface water conditions; seasonal mixing and eutrophic conditions
19a	VI (202.96-203.57)	(+) Steppic & semi-desert taxa (·) Mountain trees	Steppic vegetation and dry marshlands. Proximity of semi-desert vegetation belt	(+) *N. pachyderma* (↓) Forams and nanno wwt	Cold and eutrophic surface water
19a	V (203.67-205.05)	(+) Mediterranean sclerophylls, temperate broad-leaved forest taxa, Cichorioideae, *Isoetes*	Broad-leaved woods and thermophilous xerophytic scrublands	(+) Forams and nanno wwt (+) *G. inflata*	Warm and oligotrophic surface water conditions
19b	IV (205.15-205.25)	(+) Steppic & semi-desert taxa (·) Temperate broad-leaved forest taxa, Cichorioideae, Ericaceae	Semi-open vegetation: woods at mid-high elevations and steppes/prairies in the lowlands	(+) *N. incompta* (+) *G. bulloides* (↓) *G. inflata* (↓) forams and nanno wwt	Seasonal (winter) relative cooling, more intense mixing and eutrophic conditions
19c	III (205.35-207.77)	(+) Mediterranean sclerophylls, temperate broad-leaved forest taxa, Cichorioideae, Isoetes (·) Hydrophytes,	Broad-leaved woods and thermophilous xerophytic scrublands	(+) Forams and nanno wwt (+) *G. caribbeanica* (+) total coccolith abundance (+) *G. inflata*	Restored deep pycnocline, development of warm, well stratified and oligotrophic surface water conditions
20	II (207.87-209.47)	(+) Steppic & semi-desert taxa (·) Cupressaceae, mountain trees	Steppic vegetation and dry marshlands. Proximity of semi-desert vegetation belt	(+) *N. pachyderma* (+) *C. pelagicus* spp. *pelagicus*	Severe glacial conditions and the arrival of polar-subpolar meltwater influx into the basin
20	I (209.57-209.77)	(+) Ericaceae (·) Steppic & semi-desert taxa, Cupressaceae, Cichorioideae	Proximity of oceanic heathlands, presence of open dry vegetation	(+) *G. inflata* (+) *G. bulloides* (↓) forams and nanno wwt	Cool, mixed and meso- to eutrophic sea surface water conditions

Tab. IV - ODP core 976: marine isotope stratigraphy and main paleoenvironmental and paleoclimatic zonation scheme on both land and terrestrial realms. (↓)/(↑): Relative low/high concentration; (+): Main marker taxa; (·): Other abundant or significant taxa (Poaceae is continuously present throughout the succession and is not mentioned).

Extreme cooling events were also documented along the Iberian margin and in the Bay of Biscay during TIX, based on abrupt increases in the percentages of C37:4 alkenone and of *N. pachyderma* (Toucanne et al., 2009; Martin-Garcia et al., 2015; Rodrigues et al., 2017). Evidence of the incursion of polar water taxa associated to entrance of Atlantic meltwater masses into the Mediterranean were also found by Maiorano et al. (2016) at Montalbano Jonico section (Ionian basin), documenting the far-reaching influence of the stadial conditions.

From 794 ka on, we observe some phases of high-altitude forest taxa increase (Fig. 6a) probably in response to increased atmospheric moisture. A parallel change towards restored oceanic conditions is also observed in the marine record from 792 ka, with an increase of *N. incompta* at the expense of *N. pachyderma* and the decline of *C. pelagicus* ssp. *pelagicus* (Fig. 6b). Between 792-791 ka, the increase of *G. inflata* concurs to indicate a first restored water exchange with the Atlantic, being this taxon a tracer of the Modified Atlantic water (MAW) into the Mediterranean (Pujol and Vergnaud-Grazzini, 1995; Barcena et al., 2004). The concomitant air-sea surface amelioration from 794-792 ka may be an evidence of a progressive intensification of the sub-tropical gyre, with the consequent warm water advection through the Strait of Gibraltar and the intensification of the humid zonal westerlies over the western Mediterranean.

5.2.2 MIS 19c

The distribution pattern of pollen and calcareous plankton assemblages (Fig. 6b) suggests that MIS 19c develops upon general warm and oligotrophic conditions. Milder and more humid climate conditions on land are evidenced at 788 ka (base of interval III) by the drastic reduction of semi-desert and steppic taxa and their gradual replacement by Mediterranean plant communities, deciduous broad-leaved trees and ubiquist herbaceous vegetation (notably Cichorioideae) (Figs. 3, 6a). In the ocean, the onset of MIS 19c is marked by further increase of *G. inflata*, that at 788 ka represents more than 35% of the total planktonic foraminiferal assemblages. Although a clear explosion of warm-water and oligotrophic taxa is recorded only a few

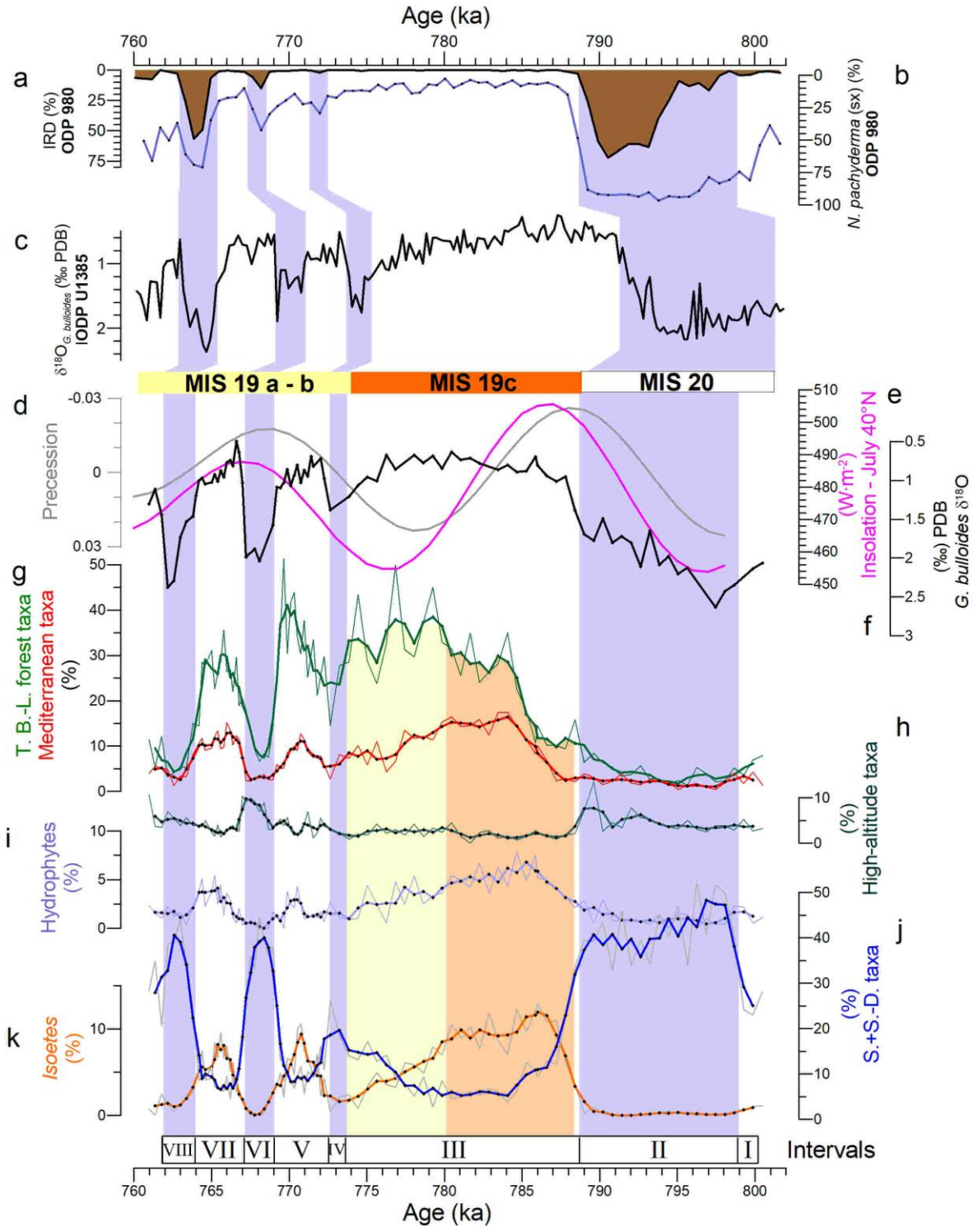
Age (ka)
760
770
780
790
800
a
IRD (%)
ODP 980
b
N. pachyderma (sx) (%)
ODP 980
c
δ18OG. bulloides (‰ PDB)
IODP U1385
MIS 19 a - b
MIS 19c
MIS 20
d
Precession
e
Insolation - July 40°N
(W·m-2)
f
G. bulloides δ18O
(‰) PDB
g
T. B.-L. forest taxa
Mediterranean taxa
(%)
h
High-altitude taxa
(%)
i
Hydrophytes
(%)
j
S.+S.-D. taxa
(%)
k
Isoetes
(%)
VIII
VII
VI
V
IV
III
II
I
Intervals
760
765
770
775
780
785
790
795
800
Age (ka)

*Fig. 6a - Comparison between palynological changes recorded at Site 976 and oceanic surface changes in the in the context of North Atlantic for MIS 20-19. (**a, b**) ODP Site 980 IRD (%) and* N. pachyderma *(%) (Wright and Flower, 2002). (**c**) IODP Site U1385 $\delta^{18}O$* G. bulloides *record (Sánchez-Goñi et al., 2016). (**d, e**) Insolation changes at 40° N in July (in purple) and values of precession index (in grey) after Berger (1978). (**f**) ODP Site 976 $\delta^{18}O$* G. bulloides *record (this study). (**g-k**) ODP Site 976 selected pollen taxa and taxa groups (this study; composition of each group is displayed in Tab. I; bold lines represent 3-point moving averages of pollen and spores percentages). Abbreviations: S.+ S.-D. = steppic + semi-desert; T. B.-L. = temperate broad-leaved. Light blue bars indicate the main phases of land-sea climate deterioration. Light red and light yellow bars indicate the partition of the terrestrial full interglacial.*

millennia later, the previous datum supports increased sea surface temperatures at the site location and a restored deep pycnocline (Fig. 6b).

The terrestrial counterpart of MIS 19c can ideally divided into two parts. The interval between 788 and 780 ka is characteristically marked by rapid decline of steppic and semi-desert taxa followed by a plateau in their curve. These changes are accompanied by the highest percentages of Mediterranean taxa (up to 15%). Such an expansion of Mediterranean sclerophylls during the first phase of MIS 19c is possibly controlled by the maximum values of North Hemisphere summer insolation (Fig. 6a). The intense seasonal contrast in precipitations between summers and winters was indubitably relevant for the diffusion of *Isoetes*, a Lycophyta strongly adapted to the seasonal flooding/desiccation pattern in ephemeral pools of the Mediterranean area (Medail et al., 1996, 1998; Molina, 2005; Keeley and Zedler, 1998). The strong seasonality might have also prevented an extensive diffusion of broad-leaved deciduous taxa – including deciduous *Quercus* and Ericaceae – which suffer from conditions of extreme summer aridity (Fig. 6a). Peak abundances of hygrophilous and hydrophylous pollen and spores (mainly represented by Cyperaceae and *Isoetes*) support intense river runoff during episodes of precipitations concentrated in few months of the year, particularly in the late summer to early fall, as observed today in some regions of Southern Spain (Sumner et al., 2001).

The interval between 780 and 774 ka is characterized by a slight increase in the steppic and semi-desert herbs relative abundances and by a pronounced decline of the Mediterraean taxa (Fig. 6a), suggesting a gradual climate deterioration in agreement with the descending limb of the North

Hemisphere summer insolation curve. Such an orbital configuration is also expected to cause a southward shift of the mean position of the Intertropical Convergence Zone (ITCZ), thus reducing the impact of the North Atlantic subtropical high over the Mediterranean during summers (Tuenter et al., 2003; Tzedakis et al., 2009). This is a likely explanation for the increased proportion of temperate deciduous taxa with respect to Mediterranean plants (Fig. 6a). The less intense summer aridity is also consistent with the higher relative abundances of the mountain conifers (such as *Abies* and *Cedrus*) with respect to the previous interval, as their growth in the Mediterranean bioclimates is limited by extreme seasonal draughts (Gazol et al., 2015).

In the marine realm, the patterns of calcareous plankton assemblages describe a more complex structure of the full interglacial phase. An increasing trend of the wwt, in the foraminiferal and nannoplankton assemblages (Fig. 6b), and of the total coccolith abundance is recorded between 788 to 782 ka, reflecting the proliferation of these taxa under increased surface-water temperatures. In this interval *N. incompta* reaches its minimum values. The decrease of this cool-water species can provide information both for the sea-surface temperatures and/or to the local hydrographic conditions, since it especially thrives in regions characterized by a shallow nutricline (Bé and Tolderlund, 1971; Fairbanks and Wiebe, 1980). Its decrease from the base of MIS 19c may indicate higher volumes of Atlantic inflow water from the Strait of Gibraltar, generating a deep pycnocline. The latter condition complies with the significant relative abundances of *G. inflata*, currently linked to the front-dominated conditions in the Alboran sea (Rohling et al., 1995). The high summer insolation maximum values in this interval can be tentatively linked with the relatively highest presence of the symbiont-bearing foraminifera *G. ruber*, consistent with the expected strong summer water stratification. The increasing trend of *G. bulloides*, in the same interval, is consistent with seasonal enhanced food supply likely related to enhanced river runoff, probably as consequence of increased seasonal precipitations, as already inferred from the pollen-spores assemblage.

In the marine realm, optimum sea-surface conditions are indicated between ca. 782 and 778 ka by higher abundances of nanno wwt, total *G. caribbeanica* and distinct occurrence of the tropical *T. sacculifer* (Fig. 6b) The concomitant increase of *G. inflata* and the drop of *G. bulloides* further suggest

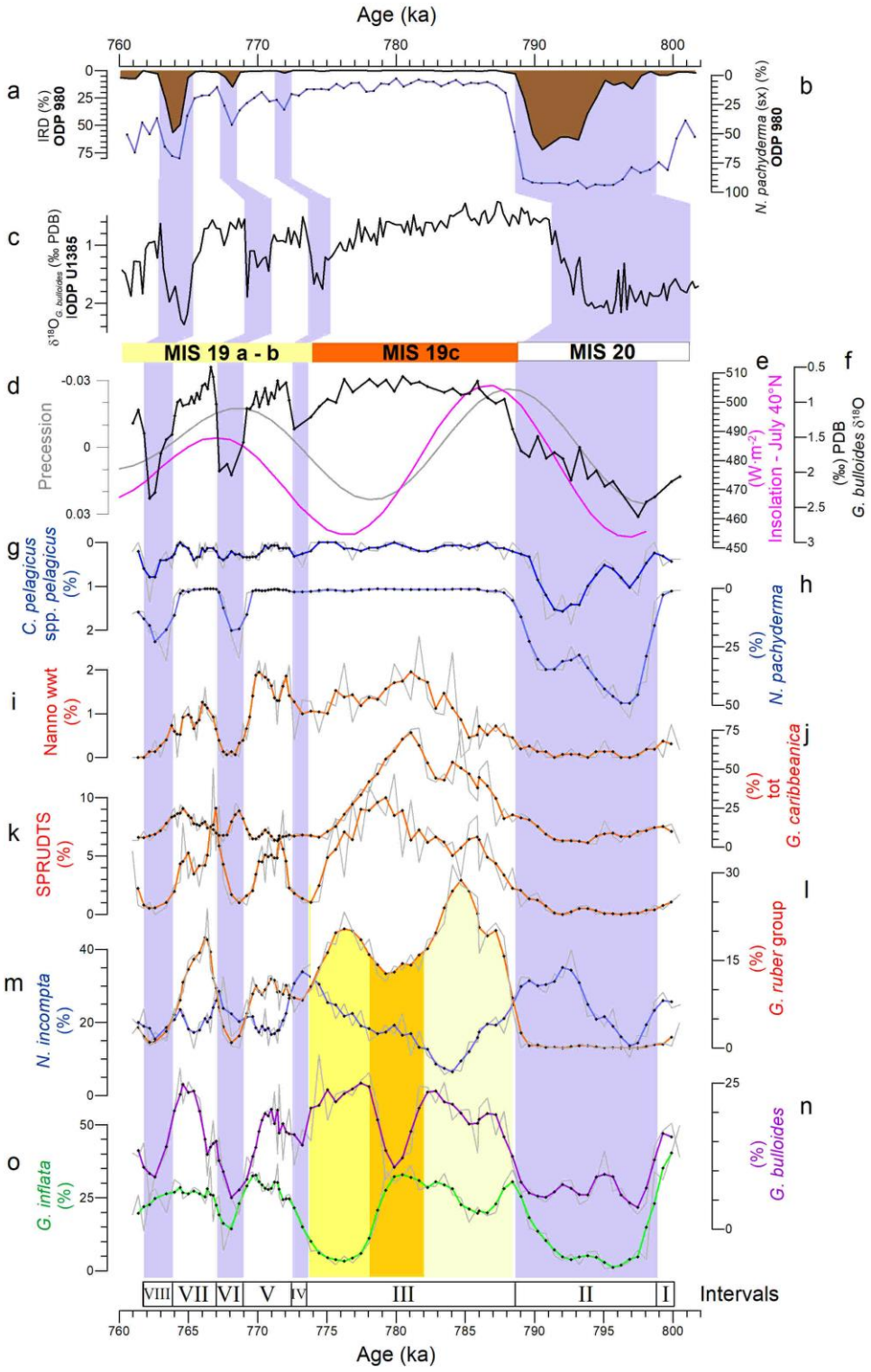
Age (ka)
760
770
780
790
800
a
IRD (%)
ODP 980
b
N. pachyderma (sx) (%)
ODP 980
c
δ18O G. bulloides (‰ PDB)
IODP U1385
MIS 19 a - b
MIS 19c
MIS 20
d
Precession
e
Insolation - July 40°N (W m-2)
f
G. bulloides δ18O (‰) PDB
g
C. pelagicus spp. pelagicus (%)
h
N. pachyderma (%)
i
Nanno wwt (%)
j
G. caribbeanica (%) tot
k
SPRUDTS (%)
l
G. ruber group (%)
m
N. incompta (%)
n
G. bulloides (%)
o
G. inflata (%)
VIII
VII
VI
V
IV
III
II
I
Intervals
Age (ka)

*Fig. 6b - Comparison between calcareous plankton changes at Site 976 and oceanic surface changes in the in the context of North Atlantic for MIS 20-19. (**a-b**)ODP Site 980 IRD% and* N. pachyderma *(%) (Wright and Flower, 2002). (**c**) IODP Site U1385 $\delta^{18}O$* G. bulloides *record (Sánchez-Goñi et al., 2016). (**d, e**) Insolation changes at 40° N in July (in purple) and values of precession index (in grey) after Berger (1978). (**f**) ODP Site 976 $\delta^{18}O$* G. bulloides *record (this study). (**g-n**) ODP Site 976 selected calcareous plankton taxa and taxa groups (this study; composition of each group is displayed in Tab. II; bold lines represent 3-point moving averages of calcareous plankton percentages). Light blue bars indicate the main phases of land-sea climate deterioration. Bars with different yellow levels indicate the partition of the marine full interglacial.*

that relatively warmer, low nutrient content conditions prevailed throughout the year due to the existence of a relatively stable pycnocline at depth (Fig. 6b). In such conditions, the concomitant decrease of *G. ruber* group can be an effect of competition with other oligotrophic planktonic organisms.

Between 778 ka and 774, the relative increase of *G. bulloides* and *N. incompta* at the expense of *G. inflata* is interpreted as the result of relative cooling, more intense mixing and/or enhanced runoff leading to eutrophic conditions (Fig. 6b). Moreover, the role played by intensified winds in creating additional mixing cannot be underscored. Indeed, southward migration of the Hadley cell could have intensified westerly zonal winds upon the western Mediterranean.

5.2.3 MIS 19b-a

A climate deterioration started during late MIS 19c and culminated at about 773.6 ka (Fig. 6a, b), in correspondence with MIS 19b (interval IV), when a short- term cool-dry event caused the partial opening of temperate deciduous forest and the contraction of thermophilous Mediterranean scrubland. From interval V upwards, the pollen record shows a higher frequency variability expressed by the alternation between forested (intervals V and VII) and open vegetation (intervals VI and VIII) -dominated phases. Both intervals V and VII are characterized by a progressive expansion of temperate-deciduous forest taxa. The percentage increase of temperate deciduous taxa supports higher year-round precipitations and temperatures during interval V than in interval

VII. This could be because the former interval is closer to the passage of the Earth passage at the aphelion during summer. With respect to MIS19c, the warm phase intervals V and VII show relative still high abundance of *G. bulloides* and *N. incompta* (Fig. 6) and a relative drop of total coccolith production (not shown). This pattern, together with the still high occurrence of *T. truncatulinoides* (not shown), suggests seasonal water mixing probably related to the activity of westerly winds that induced deep-water mixing and nutrient input from deeper water layers. However, given the opportunistic behaviour of *G. bulloides* we cannot exclude enhanced nutrient supply due to fluvial input induced by more humid conditions on land, attested by the peak distribution of *Isoetes* spores. More continuous nutrient input into the basin could have reduced the total coccolith production and the proliferation of nannofossils and foraminifera wwt, during these intervals with respect to MIS 19c (Fig. 6).

Two sharp increases of polar-subpolar *N. pachyderma* during stadials of MIS 19a (intervals VI and VIII, Fig. 6) attest repeated inflow of polar/subpolar waters into the Alboran Sea. On land the significant expansion of steppe and semi-desert taxa indicates drier conditions which were also responsible of the fall of *Isoetes*.

The stadial interval VI records two unusual short-term prominent increases of the deep dweller photic zone taxon *F. profunda* (Fig. 4) possibly in relation to the arrival of less saline waters of Atlantic origin in the Alboran sea, in agreement with Ausin et al. (2015a); the two peaks coincide with the higher values in $\delta^{18}O$ and then could be interpreted as the result of short-term episode of inverse thermocline. At this time, the arrival of colder and fresher meltwaters from Atlantic via Gibraltar Strait may have promoted enhanced stratification with cold surface waters and warmer subsurface waters at the thermocline/nutricline depth.

5.3 Millennial-scale climate variability in the western Mediterranean between MIS 20 and MIS 19

Superimposed on the main orbital-scale climate variability, numerous rapid variations punctuate the study interval. The pollen record attests the

occurrence of at least thirteen events (A0-A12), two of which (A12 and A11) match equivalent episodes in the calcareous plankton record. Eleven short-term fluctuations in the marine proxies (B10-B0) unrelated with the terrestrial counterpart are also documented (Fig. 7).

During the last part of MIS 20, bracketed in the interval of maximum extension of steppic and semi-desert vegetation, the Ericaceous cover underwent two main contractions centered at 796.9 (A12) and 791.4 ka (A11), when also high-altitude taxa show minimum values (Fig. 7). These two episodes could indicate the most extreme humidity depletion in the frame of the dry-cold acme of MIS 20. Concomitant low values of Cupressaceae are also observed at those episodes. Interestingly, Cupressaceae (cf. *Juniperus* and *Tetraclinis* pollen type) is marked by a significant spread just after event A12, possibly reflecting efficiency colonization under critical climate conditions associated to the strong reduction of warmer and humid demanding trees and shrubs, which also promote low competitive pressure (McPherson and Wright, 1989). Cupressaceae have today a quite large altitude range from sea level to high altitude and can live in semiarid ombroclimatic zones as well as in humid ombroclimatic areas, such as some parts of Morocco and Algerian coast (e.g. Benabid, 1984; Quézel, 1980). The above discussed events seem to be roughly in phase with the main peak abundances of *N. pachyderma*, which suggests the influx of polar meltwater from the Strait of Gibraltar. These variations may indicate pulses of enhanced southward migration of the polar front, determining the abrupt incursions of polar waters and drastic reduction of the atmospheric humidity. The $\delta^{18}O_{seawater}$ -derived reconstruction of the global sea-level (Elderfield et al., 2012) shows two major sea-level drops in correspondence of the two-fold cold-dry spell, suggesting enhanced rates of ice-sheet growth and, possibly, ice-shelf instability (Fig. 7).

In the first half of MIS 19c, the increased precipitations and temperatures favoured the expansion of temperate deciduous and Mediterranean taxa. However, these communities underwent repeated phases of retreat which can be interpreted as short-term (cool-) dry events, generally matching relative expansions of cosmopolitan herbaceous taxa. These events occur approximatively at 787.2 (A10), 782.9 (A9), 781.1 (A8), 778.1 (A7) and 775.6 ka (A6) (Fig. 7). Event A10 is characterized by the reduction of temperate taxa and Ericaceae, as well as by the major peak of Cichorioideae. During events

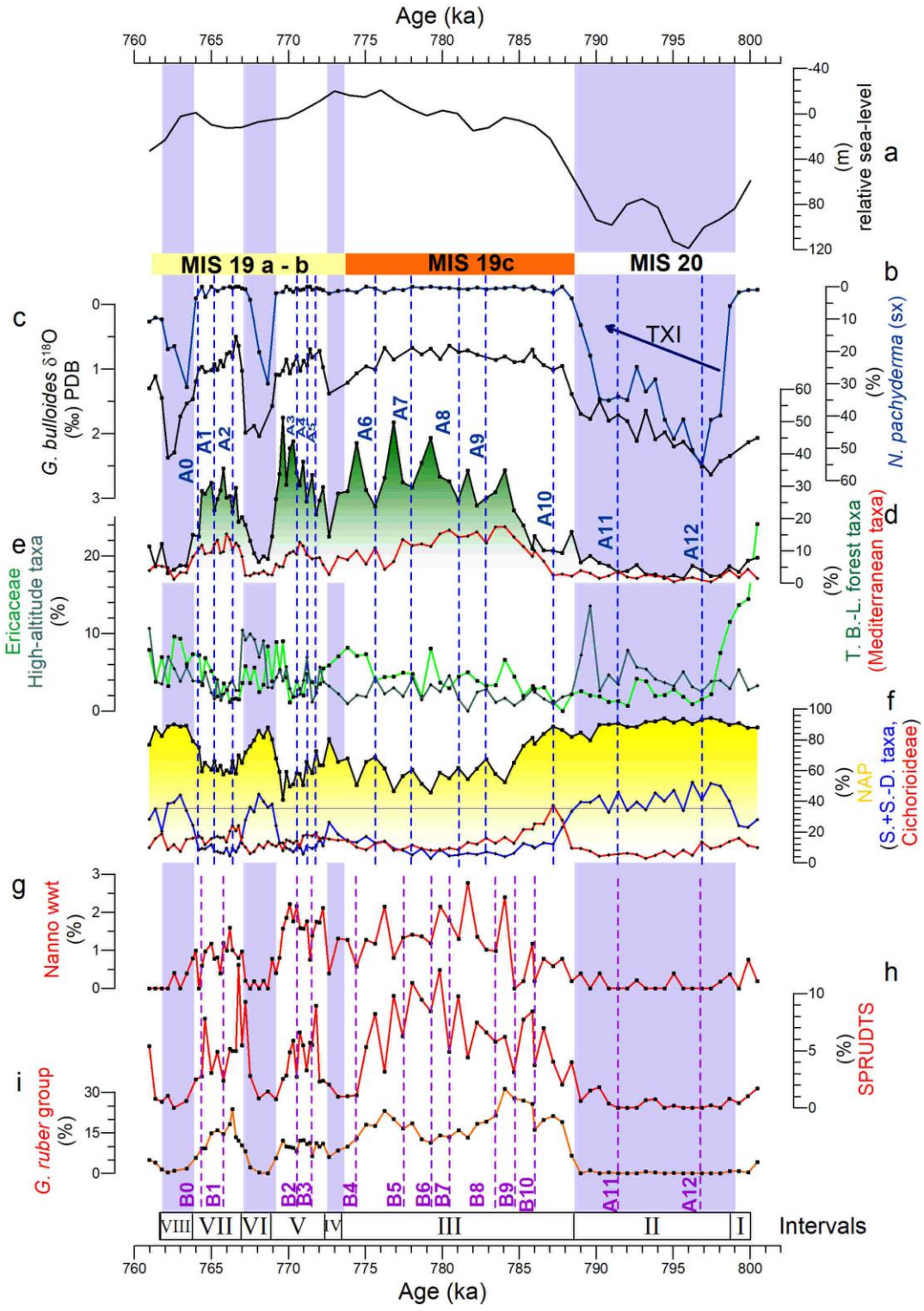
Age (ka)
760
765
770
775
780
785
790
795
800
a
relative sea-level (m)
-40
0
-40
-80
-120
MIS 19 a - b
MIS 19c
MIS 20
b
c
G. bulloides δ18O (‰) PDB
0
1
2
3
TXI
A0
A1
A2
A3
A4
A5
A6
A7
A8
A9
A10
A11
A12
N. pachyderma (sx) (%)
0
10
20
30
40
50
60
d
T. B.-L. forest taxa (Mediterranean taxa) (%)
0
10
20
30
e
Ericaceae High-altitude taxa (%)
0
10
20
f
NAP (S.+S.-D. taxa, Cichorioideae) (%)
0
20
40
60
80
100
g
Nanno wwt (%)
0
1
2
3
h
SPRUDTS (%)
0
5
10
i
G. ruber group (%)
0
15
30
B0
B1
B2
B3
B4
B5
B6
B7
B8
B9
B10
A11
A12
VIII
VII
VI
V
IV
III
II
I
Intervals
760
765
770
775
780
785
790
795
800
Age (ka)

*Fig. 7 - Millennial-scale vegetation and surface water changes at Site 976 during MIS 20-19 plotted against the relative sea-level curve. (**a**) $\delta^{18}O_{seawater}$-based sea-level relative changes (Elderfield et al., 2012); (**b, c, d**) ODP Site 976 planktonic $\delta^{18}O$ and selected pollen and calcareous plankton taxa defining the main phases of land-sea climate deterioration (light blue bars) (**e**) Insolation changes at 40° N in July (Berger, 1978). Dashed blue lines indicate the short-lived cool events recognized in the palynological (A12-A0) and calcareous plankton records (A12, A11, B10-B0). Abbreviations: T. B.-L. = broad-leaved.*

A9 to A6, Mediterranean and deciduous broad-leaved taxa exhibit slighter reductions, mirroring the extension of herbaceous vegetation (Fig. 7).

Surface water proxies do not attest an unambiguous phase relationship with the changes recorded in the continent. Relative abundances of the wwt in the foraminiferal and coccoliths assemblages are, furthermore, too low to permit discrimination between the most significant short-scale variations and the background noise. Nonetheless, one is able to note recurrent drops of wwt, presumably associated to cooling events. Seven of these episodes can be identified within MIS 19c at 786 (B10), 784.7 (B9), 783.5 (B8), 780.5 (B7), 779.3 (B6), 777.5 (B5), 774.4 ka (B4). Apparently, the most significant one is B8 and is associated to the prominent decline of *G. ruber* group, whose population is not seen to recover until 773 ka. The episode B8 seems to fit the timing of a short-lived sea-level drop derived from the global isotope-derived reconstruction (Elderfield et al., 2012). This could suggest the sensitivity of marine conditions to high-latitude forcing owing to the glacial ice-sheet extension via the adjustment of the AMOC.

The lack of a clear coupling between terrestrial and marine rapid climate changes can be explained by the relatively weak influence of the atmospheric temperatures on the SST at the local scale due to the larger water heat capacity (Oort et al., 1976). Decoupled land-sea patterns have been also evidenced in a coeval succession sampled at IODP Site U1385 (Iberian Margin) through integrated pollen, oxygen isotopes and alkenones analyses (Sánchez-Goñi et al., 2016). In the latter record, a major land-sea contrast is recorded at 782 ka, at a time when the authors observed a clear contraction of the Mediterranean forest associated to rather stable SSTs. This could be equivalent to the event A9 at ODP Site 976 (Fig. 7) dated approximatively at 783 ka, which is within the range of the age-models' uncertainties.

Interestingly, the terrestrial episodes with a (cold-) dry signature and those of SST decreases are apparently out-of-phase. We suspect that this dry land/warming ocean pattern in the Alboran Sea could reflect positive NAO-like anomalies, since the latter climate mode yields comparable land-sea patterns in the recent registrations (Hurrell et al., 2003; Thompson and Wallace, 2000). NAO is the main phenomenon affecting the climate variability in the Eastern North Atlantic and western Mediterranean on a decadal time-scale (Hurrel, 1995; Rodó et al., 1997). In the Holocene, palaeoclimate data from western Europe suggest the establishment of atmospheric/oceanic modes similar to the present-day NAO at a millennial time-scale (Smith et al., 2015 Wassenburg et al., 2016), and the western Mediterranean seems to have resulted prone to this variability over the same period (Chabaud et al., 2014; Fletcher et al., 2012).

During the entire length of warm-humid intervals V and VII in MIS 19b-a, interstadial conditions were complicated by a short-term variability similar to that observed within MIS 19c (Fig. 7). We evidenced six-times repeated losses of temperate forest cover (A5-A0) and four-times repeated surface water cooling (B3-B0) (Fig. 7). Once again, on-land (cold-) dry episodes depicted by temperate forest contractions seem to be in phase opposition with cold pulses associated with wwt calcareous plankton decreases, leading to the possible conclusion of the influence of a NAO-like mechanism.

It must be underlined that the interpretations proposed in this thesis for such a complex intra-interglacial variability still need to be improved using both additional statistical tests and biostratigraphical comparisons.

5.4 Modulation of the climate dynamics during consecutive climate variations

In summary, the land-sea interactions reconstructed on the base of past vegetation and calcareous plankton communities put in evidence two major aspects of climate dynamics:

1. A distinct atmosphere-ocean coupling during the major temperature and humidity decreases straddling MIS 20 and MIS 19b-a (intervals II, IV, VI and VIII; Fig. 6a, b). The most reliable mechanisms underlying

such a strict correlation are possibly linked to meltwater releases from the Arctic ice sheets during the North Atlantic stadials, implying a slowdown of the AMOC and consequently reduced heat transport and evaporation rates (Ganopolski and Rahmstorf, 2001; Hátún et al., 2005; Li, 2005).

2. Short-lived, quasi-periodic climate variations in the Alboran Sea as pervasive features during MIS 19c and warm-temperate phases of MIS 19a. A number of (cold-) dry events on land inferred from temperate vegetation declines and cosmopolitan herbs expansions seem to be aligned with episodes of sea-surface warming. Such land-sea temperature contrast could be discussed in the light of persistent positive NAO configurations, in agreement with previous observations and numerical experiments (e.g. Hurrell et al., 2003; Delworth and Zeng, 2016).

We are aware that an improved time-resolution and additional sites investigations are essential requirements for testing the assumed establishment of a NAO-like mechanism as early as the Early-Middle Pleistocene. In any case, the data collected at ODP Site 976 are expected to provide an interesting contribution to the debate on the MIS 19-MIS 1 analogy. Millennial-scale variability linked to NAO was, in fact, recognized to be a pervasive feature of the Holocene time-span (Fletcher et al., 2012; Smith et al., 2016).

6. Conclusions

The new multi-proxy study carried out along ODP core 976 documents vegetation and surface water changes in the western Mediterranean along a ~40-kyr long interval centered on MIS 19. The pollen and calcareous plankton results display the history of the long-term climate and oceanographic changes associated to the G-IG cyclicity. Suborbital scale variability is dominated by prominent phases of cooling and drying linked to North Atlantic cooling and polar meltwater influx in the Mediterranean. The distinct land-sea climate variability provides an exceptional correlation potential for

core 976. The robust linkages with coeval succession highlights the importance of high-to-mid latitude teleconnections during the Early-Middle Pleistocene.

During late MIS 20, polar to subpolar water incursions in the Alboran Sea parallel a marked aridity on land, showing the large impact of the stadial conditions that characterized glacial terminations during the whole Pleistocene. The afforestation and water temperature rise observed during MIS 19c were strongly affected by a precessional-insolation signal, as shown by the high (low) seasonal contrast within the first (last) part of the interglacial. The latest part of MIS 19 was characterized by successive interstadial-stadial phases predating MIS 18 glacial inception (the latter not unambiguously recorded), in good agreement with the $\delta^{18}O$ pattern

At millennial time-scales, pollen spectrum displays numerous temperate forest contractions triggered by short-lived air temperature and humidity decreases, distributed in both warm and cooler periods. Concomitantly, water cooling episodes are attested by collapses of the warm-water calcareous plankton communities, but are generally out-of-phase with the terrestrial counterparts. A cool continent/warm ocean pattern thus results at the millennial scale resembling modern anomalies dominating the North Atlantic climate variability at decadal to centennial time-scales, such as the NAO.

The terrestrial and marine datasets collected at Site 976 have important climate implications as they will offer, for the first time, the possibility to compare MIS 1 (data published in Combourieu Nebout et al., 1999, 2009) and MIS 19 along a unique succession, thus permitting identification of the main analogies expected from their very similar orbital configuration.

References

Aitchison, J., 1986. The statistical analysis of compositional data. Monographs on Statistics and Applied Probability, London, Chapman and hall Ltd, pp. 416.

Aitchison, J., Greenacre, M., 2002. Biplots of Compositional Data. Applied Statistics 51, 375–392.

Alonso, B., Ercilla, G., Martínez-Ruíz, F., Baraza, J., Galimont, A., 1999. Pliocene-Pleistocene sedimentary facies at site 976: depositional history in the northwestern Alboran sea. In: Zahn, R., Comas, M.C., Klaus, A., et al. (Eds.). Proceeding of the Ocean Drilling Program, Scientific Results, College Station. TX, pp. 57-68. vol. 161, Ocean Drilling Program.

Amore, F. O., Flores, J. A., Voelker, A. H. L., Lebreiro, S. M., Palumbo, E., and F. J. Sierro, 2012. A Middle Pleistocene Northeast Atlantic coccolithophore record: Paleoclimatology and paleoproductivity aspects, Marine Micropaleontology, 90-91, 44–59.

Aurahs, R., Treis, Y., Darling, K., Kucera, M., 2011. A revised taxonomic and phylogenetic concept for the planktonic foraminifer species Globigerinoides ruber based on molecular and morphometric evidence. Marine Micropaleontology 79, 1–14.

Bárcena, M.A., Flores, J.A., Sierro, F.J., Perez-Folgado, M., Fabres, J., Calafat, A., Canals, M., 2004. Planktonic response to main oceanographic changes in the Alboran Sea (Western Mediterranean) as documented in sediment traps and surface sediments. Marine Micropaleontology 53, 423– 445.

Ausín B., Hernández-Almeida I., Flores J.-A., Sierro F.J., Grosjean, M., Francés G., Alonso B., 2015a. Development of coccolithophorebased transfer functions in the western Mediterranean sea: a sea surface salinity reconstruction for the last 15.5 kyr. Climate of the Past 11, 1635-1651.

Ausín, B., Flores, J. A., Bácena, M. A., Sierro, F. J., Francés, G., Gutiérrez-Arnillas, E., Hernández-Almeida, I., Martrat, B., Grimalt, J. O., and Cacho, I. 2015b. Coccolithophore productivity and surface water dynamics in the Alboran Sea during the last 25 kyr, Palaeogeography Palaeoclimatology Palaeoecology 418, 126–140.

Baumann, K.-H., Bockel, B., Frenz, M., 2004. Coccolith contribution to South Atlantic carbonate sedimentation. In: Thierstein, H.R., Young, J. (Eds.), Coccolithophores From Molecular Processes to Global Impact. Springer, Berlin, pp. 367–402.

Baumann, K.H., Andruleit, H., Böckel, B., Geisen, M., Kinkel, H., 2005. The significance of extant coccolithophores as indicators of ocean water masses, surface water temperature, and paleoproductivity: a review. Paläontologische Zeitschrift 79, 93–112.

Bé, A.W.H., 1977. An ecological, zoogeographic and taxonomic re view of recent planktonic foraminifera. In: Ramsay, A.T.S. (Ed.) Oceanic Micropaleontology vol. 1. Academic Press, London, p. 1.

Bé, A.W.H., Hamlin, W.H., 1967. Ecology of recent planktonic foraminifera. Micropaleontology 13, 87–100.

Bé, A.W.H., Tolderlund, D.S., 1971. Distribution and ecology of living planktonic foraminifera in surface waters of the Atlantic and Indian Oceans. In: Funnell, B.M., Riedel, W.R. (Eds.), The Micropaleontology of the Oceans, pp. 105–149.

Beaufort, L., Lancelot, Y., Camberin, P., Cayre, O., Vincent, E., Bassinot, F., Labeyrie, L., 1997. Insolation cycles as amajor control of Equatorial Indian Ocean Primary Production. Science 278, 1451–1454.

Beaufort, L., de Garidel-Thoron, T., Mix, A. C., Pisias, N. G., 2001. ENSO-like forcing on oceanic primary production during the late Pleistocene, Science, 293, 2440–2444.

Benabid, A. 1985. Les écosystèmes forestiers et préforestiers du Maroc: diversité, répartition biogéographique et problèmes posés par leur aménagement. Forêt Méditerranéenne 7(1), 53–67.

Bernasconi, S.M., Meyers, P.A., O'Sullivan, G., 1999. Early diagenesis in rapidly accumulating sediments on the Alboran slope, ODP site 976. Geo-Marine Letters 18, 209–214.

Bertini, A., 2000. Pollen record from Colle Curti and Cesi: early and middle Pleistocene mammal sites in the Umbro-Marchean Apennine mountains (central Italy). Journal of Quaternary Science 15(8), 825–840.

Bertini, A., Toti, F., Marino, M., Ciaranfi, N., 2015. Vegetation and climate across the Early- Middle Pleistocene transition at the Montalbano Jonico section (southern Italy). Quaternary International 383, 74–88.

Boeckel, B., Baumann, K.-H., 2004. Distribution of coccoliths in surface sediments of the south-eastern South Atlantic Ocean: ecology, preservation and carbonate contribution. Marine Micropaleontology 51 (3–4), 301–320.

Bollmann, J., 1997. Morphology and biogeography of *Gephyrocapsa* coccoliths in Holocene sediments. Marine Micropaleontology 29, 319–350.

Bollmann, J., Baumann, K.-H., Thierstein, H.R., 1998. Global dominance of *Gephyrocapsa* coccoliths in the late Pleistocene: selective dissolution,

evolution, or global environmental change? Paleoceanography 13 (5), 517–529.
Bond, G. C., 1992. Evidence for massive discharges of icebergs into the North Atlantic ocean during the last glacial period. Nature 360, 245–249.
Cacho, I., Grimalt, J.O., Canals, M., Sbaffi, L., Shackleton, N.J., Schönfeld, J., Zahn, R., 2001. Variability of the western Mediterranean Sea surface temperatures during the last 25,000 years and its connection with the northern hemisphere climatic changes. Paleoceanography 16 (1), 40-52.
Cacho, I., Grimalt, J.O., Pelejero, C., Canals, M., Sierro, F.J., Flores, J.A., Shackleton, N.J., 1999. Dansgaard–Oeschger and Heinrich event imprints in the Alboran Sea paleotemperatures. Paleoceanography 14, 698–705.
Cacho, I., Grimalt, J.O., Pelejero, C., Canals, M., Sierro, F.J., Flores, J.A., Shackleton, N.J., 1999. Dansgaard-Oeschger and Heinrich event imprints in the Alboran Sea paleotemperatures. Paleoceanography 14 (6), 698-705.
Capotondi, L., Girone, A., Lirer, F., Bergami, C., Verducci, M., Vallefuoco, M., Afferri, A., Ferraro, L., Pelosi, N., De Lange, G.J., 2016. Central Mediterranean Mid-Pleistocene paleoclimatic variability and its connection with global climate. Palaeogeography Palaeoclimatology Palaeoecology 442, 72–83.
Cayre, O., Lancelot, Y., Vincent, E., 1999. Paleoceanographic reconstructions from planktonic foraminifera off the Iberian Margin: temperature, salinity, and Heinrich events. Paleoceanography 14(3), 384–396.
Colmenero-Hidalgo, E., Flores, J.A., Sierro, F.J., Barcena, M.A., Lowemark, L., Schonfeld, J., Grimalt, J.O., 2004. Ocean surface water response to short-term climate changes revealed by coccolithophores from the Gulf of Cadiz (NE Atlantic) and Alboran Sea (W Mediterranean). Palaeogeography Palaeoclimatology Palaeoecology 205, 317–336.
Comas, M.C., Zahn, R., Klaus, A., et al. 1996. Proceeding of the Ocean Drilling Program, Initial Reports., 161, College Station, TX, 1023 pp.
Combourieu Nebout, N., Londeix, L., Baudin, F., Turon, J.L., von Grafenstein, R., Zahn, R., et al., 1999. Quaternary marine and continental paleoenvironments in the western Mediterranean (site 976, Alboran Sea): palynological evidence. In: Zahn, R., Comas, M.C., Klaus, A., et al.

(Eds.). Proceeding of the Ocean Drilling Program, Scientific Results, 161, College Station. TX, pp. 457-468.

Combourieu Nebout, N., Turon, J.-L., Zahn, R., Capotondi, L., Londeix, L., Pahnke, K., 2002. Enhanced aridity and atmospheric high-pressure stability over the western Mediterranean during the North Atlantic cold events of the past 50 k.y. Geology 30, 863-866.

Darling, K.F., Kucera, M., Kroon, D., Wade, C.M., 2006. A resolution for the coiling direction paradox in *Neogloboquadrina pachyderma*. Paleoceanography 21 (2), PA2011.

de Abreu, L., Shackleton, N.J., Schonfeld, J., Hall, M., Chapman, M., 2003. Millennial-scale oceanic climate variability off the Western Iberian margin during the last two glacial periods. Marine Geology 196, 1–20.

Delworth, T.L., Zeng, F., 2016. The impact of the North Atlantic Oscillation on climate through its influence on the Atlantic meridional overturning circulation. Journal of Climate 29 941–62.

Di Stefano, E., Incarbona, A., 2004. High resolution paleoenvironmental reconstruction of the ODP-963D Hole (Sicily Channel) during the last deglaciation, based on calcareous nannofossils. Marine Micropaleontology 52, 241–254.

Elderfield, H., Ferretti, P., Greaves, M., Crowhurst, S., McCave, I.N., Hodell, D., Piotrowski, A.M., 2012. Evolution of ocean temperature and ice volume through the mid-Pleistocene climate transition. Science 337, 704–709.

Eynaud, F., de Abreu, L., Voelker, A., Schönfeld, J., Salgueiro, E., Turon, J.L., Penaud, A., Toucanne, S., Naughton, F., Sànchez-Goñi, M.F., Malaizé, B., Cacho, I., 2009. Position of the polar front along the western Iberian margin during key cold episodes of the last 45 ka. Geochemistry Geophysics Geosystems 10. http://dx.doi.org/10.1029/2009GC002398.

Fabrés, J., Calafat, A., Sánchez-Vidal, A., Canals, M., Heussner, S., 2002. Composition and spatio-temporal variability of particle fluxes in the Western Alboran Gyre, Mediterranean Sea. Journal of Marine Systems 33, 431–456.

Fennane, M., Barbero, M., Quézel, P., 1984. Le thuya de Berbérie au Maroc: apercu phytogéographique et écologique. Rabat, Bulletin de l'Institut Scientifique. 8, 115–134.

Ferretti, P., Crowhurst, S.J., Naafs, B.D.A., Barbante, C., 2015. The Marine Isotope Stage 19 in the mid-latitude North Atlantic Ocean: astronomical signature and intra-interglacial variability. Quaternary Science Reviews 108, 95–110.

Fletcher, W.J., Sánchez-Goñi, M.F., 2008. Orbital- and sub-orbital-scale climate impacts on vegetation of the western Mediterranean basin over the last 48,000 yr. Quaternary Research 70, 451-464.

Fletcher, W.J., Sánchez-Goñi, M.F., Peyron, O., Dormoy, I., 2010. Abrupt climate changes of the last deglaciation detected in a western Mediterranean forest record. Climate of the Past 6, 245-264.

Flores, J.A., Sierro, F.J., 1997. Revised technique for calculation of calcareous nannofossil accumulation rates. Micropaleontology 43, 321–324.

Ganopolski, A., Rahmstorf, S., 2001. Rapid Changes of glacial climate simulated in a coupled climate model. Nature 409, 153–158.

Gartner, S., 1988. Paleoceanography of the Mid-Pleistocene. Marine Micropaleontology 13, 23–46.

Gartner, S., Chow, J., Stanton, R.J.,1987. Late Neogene paleoceanography of the eastern Caribbean, the Gulf of Mexico, and the eastern Equatorial Pacific. Marine Micropaleontology 12 (3), 255–304.

Geisen, M., Billard, C., Broerse, A.T.C., Cros, L., Probert, I., Young, J.R., 2002. Life-cycle associations involving pairs of holococcolithophorid species: intraspecific variation or cryptic speciation? European Journal of Phycology 37, 531–550.

Geraga, M., Mylona, G., Tsaila-Monopolis, S., Papatheodorou, G., Ferentinos, G., 2008. Northeastern Ionian Sea: palaeoceanographic variability over the last 22 ka. Journal of Marine Systems 74, 623–638.

Geraga, M., Tsaila-Monopolis, S., Ioakim, C., Papatheodorou, G., Ferentinos, G., 2005. Shortterm climate changes in the southern Aegean Sea over the last 48,000 years. Palaeogeography Palaeoclimatology Palaeoecology 220, 311–332.

Girone, A., Capotondi, L., Ciaranfi, N., Di Leo, P., Lirer, F., Maiorano, P., Marino, M., Pelosi, N., Pulice, I., 2013a. Paleoenvironmental change at the lower Pleistocene Montalbano Jonico section (southern Italy): global versus regional signals. Palaeogeography Palaeoclimatology Palaeoecology 371, 62–79.

Girone, A., Maiorano, P., Marino, M., Kucera, M., 2013b. Calcareous plankton response to orbital and millennial-scale climate changes across the Middle Pleistocene in the western Mediterranean. Palaeogeography Palaeoclimatology Palaeoecology 392, 105–116.

González-Donoso, J.M., Serrano, F., Linares, D., 2000. Sea surface temperature during the Quaternary at ODP Sites 976 and 975 (western Mediterranean). Palaeogeography Palaeoclimatology Palaeoecology 162, 17-44.

Guerzoni, S., Molinaroli, E., Chester, R., 1997. Saharan dust inputs to the western Mediterranean Sea: depositional patterns, geochemistry and sedimentological implications. Deep-Sea Res. II 44, 631–645.

Head, M.J., Gibbard, P.J., 2015a. Formal subdivision of the Quaternary System/Period: past, present, and future. Quaternary International 383, 4–35.

Head, M.J., Gibbard, P.J., 2015b. Early-Middle Pleistocene transitions: linking terrestrial and marine realms. Quaternary International 389, 7–46.

Hemleben, C., Spindler, M., Anderson, O.R., 1989. Modern Planktonic Foraminifera. Springer-Verlag, New York (363 pp.).

Hernández-Almeida, I., Bárcena, M. A., Flores, J. A., Sierro, F. J., Sanchez-Vidal, A., and Calafat, A.2011. Microplankton response to environmental conditions in the Alboran Sea (Western Mediterranean): One year sediment trap record, Marine Micropaleontology, 78, 14–24, 2011.

Huber, R., Meggers, H., Baumann, K.-H., Raymo, M.E., Heinrich, R., 2000. Shell size variation of the planktonic foraminifer *Neogloboquadrina pachyderma* sin. in the Norwegian- Greenland Sea during the last 1.3 Myrs: implications for paleoceanographic reconstructions. Palaeogeography Palaeoclimatology Palaeoecology 160, 183–212.

Hurrell, J.W., 1995. Decadal trends in the North Atlantic Oscillation: Regional temperatures and precipitation. Science 269, 676-679.

Hurrell, J.W., Kushnir, Y., Visbeck, M., Ottersen, G., 2003. An overview of the North Atlantic Oscillation. In: Hurrell, J.W., Kushnir, Y., Ottersen, G., Visbeck, M. (Eds.). The North Atlantic Oscillation, Climatic Significance and Environmental Impact. AGU Geophysical Monograph, vol. 134, pp. 1–35.

Incarbona, A., Dinarès-Turell, J., Di Stefano, E., Ippolito, G., Pelosi, N., Sprovieri, R., 2013. Orbital variations in planktonic foraminifera assemblages from the Ionian Sea during the Middle Pleistocene Transition. Palaeogeography Palaeoclimatology Palaeoecology 369, 303–312.

Joannin, S., Bassinot, F., Combourieu Nebout, N., Peyron, O., Beaudouin, C., 2011. Vegetation response to obliquity and precession forcing during the Mid-pleistocene transition in western Mediterranean region (ODP site 976). Quaternary Science Reviews 30, 280-297.

Joannin, S., Cornée, J.J., Moissette, P., Suc, J.-P., Koskeridou, E., Lécuyer, C., Buisine, C., Kouli, K., Ferry, S., 2007. Changes in vegetation and marine environments in the eastern mediterranean (Rhodes Island, Greece) during the early and middle Pleistocene. Journal of Geological Society of London 164, 1119–1131.

Johannessen, T., Jansen, E., Flatoy, A., Ravelo, A. C., 1994. The relationship between surface water masses, oceanographic fronts and paleoclimatic proxies in surface sediments of the Greenland Iceland and Norwegian seas, in Carbon Cycling in the Glacial Ocean: Constraints on the Ocean's Role in Global Change, NATO Asi Series, I, vol. 17, edited by R. Zahn et al., pp. 61–85, Springer, New York.

Keely, J.E., Zedler, P.H., 1998. Characterization and global distribution of vernal pools. In: Witham, C.W., Bauder, E.T., Belk, D., Ferren Jr., W.R., Ordunff, R. (Eds.). Ecology and management of vernal pool ecosystems. Proceedings from a 1996 Conference, California Native Plant Society, Sacramento, CA, USA, 1–14.

Kucera, M., Kennett, J.P., 2002. Causes and consequences of a middle Pleistocene origin of the modern planktonic foraminifer *Neogloboquadrina pachyderma* sinistral. Geology 30, 539–542.

Kucera, M., Weinelt, M., Kiefer, T., Pflaumann, U., Hayes, A., Weinelt, M., Chen, M.-T., Mix, A.C., Barrows, T., Cortijo, E., Duprat, J., Juggins, S., Waelbroeck, C., 2005. Reconstruction of sea-surface temperatures from assemblages of planktonic foraminifera: multi- technique approach based on geographically constrained calibration datasets and its application to glacial Atlantic and Pacific Oceans. Quaternary Science Reviews 24, 951–998.

Laskar, J., Robutel, P., Joutel, F., Boudin, F., Gastineau, M., Correia, A.C.M., Levrard, B., 2004. A long-term numerical solution for the insolation quantities of the Earth. Astronomy & Astrophysics 428, 261-285.

Loidi, J., Biurrun, I., Campos, J.A., Garcıa-Mijangos, I., Herrera, M., 2007. A survey of heath vegetation of the Iberian Peninsula and Northern Morocco: a biogeographical and bioclimatic approach. Phytocoenologia 37, 341–370.

Maiorano, P., Girone, A., Marino, M., Kucera, M., Pelosi, N., 2016. Calcareous plankton response to Mid-Brunhes climate variability in the western Mediterranean (ODP Site 975). Palaeogeography Palaeoclimatology Palaeoecology 459, 229–248.

Maiorano, P., Marino, M., Balestra, B., Flores, J.A., Hodell, D.A., Rodrigues, T., 2015. Coccolithophore variability from the Shackleton Site (IODP Site U1385) through MIS 16–10. Global and Planetary Change 133, 35–48.

Maiorano, P., Tarantino, F., Marino, M., De Lange, G.J., 2013. Paleoenvironmental conditions at Core KC01B (Ionian Sea) through MIS 13-9: evidence from calcareous nannofossil assemblages. Quaternary International. 288, 97–111.

Marcott, S.A., Clark, P.U., Padman, L., Klinkhammer, G.P., Springer, S.R., Liu, Z., Otto-Bliesner, B.L., Carlson, A.E., Ungerer, A., Padman, J., He, F., Cheng, J., Schmittner, A., 2011. Ice-shelf collapse from subsurface warming as a trigger for Heinrich events. Proceedings of the National Academy of Sciences USA 108, 13415–13419.

Marino, M., Maiorano, P., Flower, B.P., 2011. Calcareous nannofossil changes during the Mid- Pleistocene revolution: paleoecologic and paleoceanographic evidence from North Atlantic Site 980/981. Palaeogeography Palaeoclimatology Palaeoecology 306(1–2), 58–69.

Marino, M., Maiorano, P., Lirer, F., 2008. Changes in calcareous nannofossil assemblages during the Mid-Pleistocene Revolution. Marine Micropaleontology 69, 70–90.

Marino, M., Maiorano, P., Tarantino, F., Voelker, A., Capotondi, L., Girone, A., Lirer, F., Flores, J.-A., Naafs, B.D.A., 2014. Coccolithophores as proxy of seawater changes at orbital- to-millennial scale during middle Pleistocene Marine Isotope Stages 14–9 in North Atlantic core MD01-2446. Paleoceanography 29. PA002574.

Martín-Fernández, J.A., Hron, K, Templ, M., Filzmoser, P., Palarea-Albaladejo, J., 2012. Model-based replacement of rounded zeros in compositional data: Classical and robust approach. Computational Statistics & Data Analysis, 56(3), 2688–2704.

Martín-Fernández, J.A., Hron, K., Templ, M., Filzmoser, P., Palarea- Albaladejo, J., 2015. Bayesian-multiplicative tratment of count zeros in compositionaldata sets. Statistical modeling 15(2), 134–158.

Martín-Fernández, J.A., Palarea-Albaladejo. J., Olea, R.A., 2011. Dealing with zeros, Ch. 4. In: Pawlowsky-Glahn V., Buccianti A. (Eds.). Compositional Data Analysis: Theory and Applications. Chichester, UK: John Wiley & Sons, Ltd, pp. 47–62

Martin-Garcia, G.M., Alonso-Garcia, M., Sierro, F.J., Hodell, D.A., Flores, J.- A., 2015. Severe cooling episodes at the onset of deglaciations on the Southwestern Iberian margin from MIS 21 to 13 (IODP site U1385). Global and Planetary Change 135:159–169.

Martrat, B., Grimalt, J., Lopez-Martinez, C., Cacho, I., Sierro, F.J., Flores, J.A., Zahn, R., Canals, M., Curtis, J.H., Hodell, D.A., 2004. Abrupt temperature changes in the western Mediterranean over the past 250,000 years. Science 306, 1762-1765.

McAyeal, D.R., 1993. Binge/purge oscillations of the Laurentide ice sheet as a cause of North Atlantic's Heinrich events. Paleoceanography 8, 775– 784.

McIntyre, A., Bè, A.H.W., 1967. Modern coccolithophores of the Atlantic Ocean - I. Placolith and cyrtoliths. Deep-Sea Research 14, 561–597.

McPherson, G.R., Wright, H.A., 1989. Direct effects of competition on individual juniper plants: a field study. Journal of Applied Ecology 26, 979–988.

Médail, F., Michaud, H., Molina, J., Paradis, G., Loisel, R., 1998. Conservation de la flore et de la végétation des mares temporaires dulçaquicoles et oligotrophes de France méditerranéenne. Ecologia Mediterranea 24, 119–134.

Millot, C., 1999. Circulation in the western Mediterranean Sea. Journal of Marine Systems 20, 423–442.

Molfino, B., McIntyre, A., 1990a. Precessional forcing of nutricline dynamics in the equatorial Atlantic. Science 249, 766–769.

Molfino, B., McIntyre, A., 1990b. Nutricline variation in the equatorial Atlantic coincident with the Younger Dryas. Paleoceanography 5, 997–1008.

Molina, J.A., 2005. The vegetation of temporary ponds with *Isoetes* in the Iberian Peninsula. Phytocoenologia 35 (2-3), 219–230.

Munz, P.M., Siccha, M., Lückge, A., Böll, A., Kucera, M., Schulz, H., 2015. Decadal-resolution record of winter monsoon intensity over the last two millennia fromplanktic foraminiferal assemblages in the northeastern Arabian Sea. Holocene 25 (11), 1756–1771.

Nieto-Caldera, J.M., Pérez-Latorre, A.V., Cabezuto, B., 1990. Datos sobre la vegetacion silicicola de Andalucia. I. Acta Botánica Malacitana 15, 179–192.

Okada, H., McIntyre, A., 1979. Seasonal distribution of modern coccolithophores in the western North Atlantic Ocean, Mar. Biol., 54, 319–328.

Palumbo, E., Flores, J.A., Perugia, C., Petrillo, Z., Voelker, A.H.L., Amore, F.O., 2013. Millennial scale coccolithophore paleoproductivity and surface water changes between 445 and 360 ka (Marine Isotope Stages 12/11) in the Northeast Atlantic. Palaeogeography Palaeoclimatology Palaeoecology 383–384, 27–41.

Parente, A., Cachão, M., Baumann, K.-H., de Abreu, L., Ferreira, J., 2004. Morphometry of *Coccolithus pelagicus* s.l. (Coccolithophore, Haptophyta) from offshore Portugal, during the last 200 kyr. Micropaleontology 50, 107–120.

Pujol, C., Vergnaud-Grazzini, C., 1995. Distribution patterns of live planktic foraminifers as related to regional hydrography and productive systems of the Mediterranean Sea. Marine Micropaleontology 25, 187–217.

Quézel, P. & Médail, F. 2003. Écologie et biogeographie des forêts du bassin méditerranéen. Elsevier, Paris, pp. 571.

Quézel, P. & Médail, F. 2003. Écologie et biogeographie des forêts du bassin méditerranéen. Elsevier, Paris, pp. 571.

Quézel, P., 1980. Biogéographie et écologie des conifères sur le pourtour méditerranéen. In. Person. Actualité d'écologie forestière. Ed. Bordas, Paris., 205–256.

Reille, M., 1992. Pollen et spores d'Europe et d'Afrique du nord (Pollen and Spores of Europe and North Africa). Laboratoire de Botanique historique et Palynologie, Marseille.

Renault, L., Oguz, T., Pascual, A., Vizoso, G., Tintore, J., 2012. Surface circulation in the Alborán Sea (western Mediterranean) inferred from remotely sensed data. Journal of Geophysical Research, 117, 1-11.

Reynolds, L. A., Thunell, R. C. 1986. Seasonal production and morphologic variation of *Neogloboquadrina pachyderma* (Ehrenberg) in the northeast Pacific, Micropaleontology, 32, 1–18.

Rivas-Martínez, S., 1987. Memoria del mapa de las series de vegetación de España. Icona, Madrid. 268 pp.

Rodó, X., Baert, E., Comin, F.A., 1997. Variations in seasonal rainfall in Southern Europe during the present century: relationships with the North Atlantic Oscillation and the El Niño-Southern Oscillation. Climate Dynamics 13, 275–284.

Rodrigues T., Alonso-García M., Hodell D.A., Rufino M., Naughton F, Grimalt J.O., Voelker A.H.L., Abrantes F. 2017 A 1-Ma record of sea surface temperature and extreme cooling events in the North Atlantic: A perspective from the Iberian Margin

Rohling, E.J., den Dulk, M., Pujol, C., Vergnaud-Grazzini, C., 1995. Abrupt hydrographic changes in the Alboran Sea (western Mediterranean) around 8000 yrs BP. Deep-Sea Res. 42, 1609–1619.

Rohling, E.J., Jorissen, F.J., De Stigter, H.C., 1997. 200 year interruption of Holocene sapropel formation in the Adriatic Sea. J. Micropalaeontol. 16 (2), 97–108.

Rohling, E.J., Jorissen, F.J., Vergnaud Grazzini, C., Zachariasse, W.J., 1993. Northern Levantine and Adriatic Quaternary planktic foraminifera; reconstruction of paleoenvironmental gradients. Mar. Micropaleontogy 21, 191–218.

Ruddiman, W. F., Raymo, M., McIntyre, A., 1986. Matuyama 41,000-year cycles: North Atlantic Ocean and northern hemisphere ice sheets. Earth and Planetary Science Letters 80, 117–129.

Saavedra-Pellitero, M., Flores, J.A., Baumann, K.-H., Sierro, F.J., 2010. Coccolith distribution patterns in surface sediments of Equatorial and Southeastern Pacific Ocean. Geobios 43, 131–149.

Sánchez-Garrido, J.C., García-Lafuente, J., Álvarez-Fanjul, E., Sotillo, M.G., de los Santos, F., 2017. What does cause the collapse of the Western Alborán Gyre? Results of an operational model. Prog. Oceanogr. 116, 142–153.

Sánchez-Goñi, M.F., Cacho, I., Turon, J.-L., Guiot, J., Sierro, F.J., Peypouquet, J.P., Grimalt, J.O., Shackleton, N.J., 2002. Synchroneity between marine and terrestrial responses to millennial scale climatic variability during the last glacial period in the Mediterranean region. Climate Dynamics 19, 95-105.

Sánchez-Goñi, M.F., Rodrigues, T., Hodell, D.A., Polanco-Martínez, J.M., Alonso-García, M., Hernández-Almeida, I., Desprat, S., Ferretti, P., 2016. Tropically-driven climate shifts in southwestern Europe during MIS 19, a low eccentricity interglacial. Earth Planetary Science Letters 448, 81–93

Shipboard Scientific Party, 1996. Site 976, Comas, M.C., Zahn, R., Klaus, A., et al., (Eds.), Proc. ODP Init. Repts., College Station, TX Vol. 161, 179–297.

Sierro F.J., Hodell D.A., Curtis J.H., Flores J.-A., Reguera I., Colmenero- Hidalgo E., Bárcena M.A., Grimalt J.O., Cacho I., Frigola J., Canals M., 2005. Impact of iceberg melting on Mediterranean thermohaline circulation during Heinrich Events. Paleoceanography 20: PA2019.

Sierro, F.J., Hodell, D.A., Curtis, J.H., Flores, J.A., Reguera, I., Colmenero-Hidalgo, E., Bárcena, M.A., Grimalt, J.O., Cacho, I., Frigola, J., Canals, M., 2005. Impact of iceberg melting on Mediterranean thermohaline circulation during Heinrich events. Paleoceanography 20, PA2019.

Spezzaferri, S., Kucera, M., Pearson, P.N., Wade, B.S., Rappo, S., Poole, C.R., Morard, R., Stalder, C., 2015. Fossil and genetic evidence for the polyphyletic nature of the planktonic foraminifera "*Globigerinoides*", and description of the new genus *Trilobatus*. PLoS ONE 10(5), e0128108.

Sprovieri, R., Di Stefano, E., Incarbona, A., Gargano, M.E., 2003. A high-resolution record of the last deglaciation in the Sicily Channel based on foraminifera and calcareous nannofossil quantitative distribution. Palaeogeography Palaeoclimatology Palaeoecology 202, 119–142.

Sumner, G., Homar, V., Ramis, C., 2001. Precipitation seasonality in Eastern and Southern coastal Spain. International Journal of Climatology 21, 219–247.

Tolderlund, D.S., Bé, A.W.H., 1971. Seasonal distribution of planktonic foraminifera in the western North Atlantic. Micropaleontolology 17, 297–329.

Toucanne, S., Zaragosi, S., Bourillet, J. F., Gibbard, P. L., Eynaud, F., Giraudeau, J., Turon, J. L., Cremer, M., Cortijo, E., Martinez, P., Rossignol, L., 2009. A 1.2 My record of glaciations and fluvial discharges from the West European Atlantic margin. Quaternary Science Reviews 28, 2974-2981.

Tzedakis, P.C., Hooghiemstra, H., Pälike, H., 2006.The last 1.35 million years at Tenaghi Philippon: revised chronostratigraphy and long-term vegetation trends. Quaternary Science Reviews 25, 3416–3430.

Vautravers, M.J., Shackleton, N.J., 2006. Centennial-scale surface hydrology off Portugal during marine isotope stage 3: Insights from planktonic foraminiferal fauna variability. Paleoceanography 21 (PA3004).

Vergnaud-Grazzini, C., 1985. Mediterranean late Cenozoic stable isotope record: stratigraphic and paleoclimatic implications. In: Stanley, D.J., Wezel, F.C. (Eds.). Geological Evolution of the Mediterranean Basin. Springer-Verlag, New York, pp. 413–451.

Vincent, E., Berger, W.H., 1981. Planktonic foraminifera and their use in Paleoceanography. In: Emiliani, C. (Ed.). The Oceanic LithosphereThe sea vol. 7. John Wiley & Sons, New York, pp. 1025–1119.

Von Grafenstein, R., Zahn, R., Tiedemann, R., Murat, A., 1999. Planktonic $\delta^{18}O$ records at sites 976 and 977, Alboran Sea: stratigraphy, forcing, and paleoceanographic implications. In: Zahn, R., Comas, M.C., Klaus, A., et al. (Eds.). Proceeding of the Ocean Drilling Program, Scientific Results, College Station. TX, pp. 469–479. vol. 161, Ocean Drilling Program.

Von Grafenstein, R., Zahn, R., Tiedemann, R., Murat, A., 1999. Planktonic $\delta^{18}O$ records at sites 976 and 977, Alboran Sea: stratigraphy, forcing, and paleoceanographic implications. In: Zahn, R., Comas, M.C., Klaus, A., et al. (Eds.). Proceeding of the Ocean Drilling Program, Scientific Results, College Station. TX, pp. 469-479. vol. 161, Ocean Drilling Program.

Walter, W., Harnickell, E., Mueller-Dombois, D., 1975. Climate Diagram Maps, Springer-Verlag.

Weaver, P.P.E., Pujol, C., 1988. History of the last deglaciation in the Alboran Sea (western Mediterranean) and adjacent North Atlantic as revealed by

coccolith floras. Palaeogeography Palaeoclimatology Palaeoecology 64, 35–42.

Winter, A., Jordan, R.W., Roth, P.H., 1994. Biogeography of living coccolithophores in oceanwaters. In: Siesser, W.G. (Ed.), Coccolithophores. In: Winter, A. Cambridge University Press, London, pp. 161–178.

Yamasaki, M., Matsui, M., Shimada, C., Chiyonobu, S., Sato, T., 2008. Timing of shell size increase and decrease of the planktic foraminifer *Neogloboquadrina pachyderma* (sinistral) during the Pleistocene, IODP Exp. 303 Site U1304, the North Atlantic Ocean. Open Paleontology Journal 1, 18–23.

Yin, Q.Z., Berger, A., 2012. Individual contribution of insolation and CO_2 to the interglacial climates of the past 800,000 years. Climate Dynamics 38, 709– 724.

Ziveri, P., Baumann, K.-H., Boeckel, B., Bollmann, Young, J., Young, Y.R., 2004. Biogeography of selected Holocene coccoliths in the Atlantic Ocean. In: Thierstein, H.R. (Ed.), Coccolithophores: From Molecular Processes to Global Impact. Springer, Berlin, pp. 403–428.

Ziveri, P., Thunell, R. C., Rio, D. 1995. Export production of coccolithophores in an upwelling region: Results from San Pedro Basin, Southern California Borderlands, Marine Micropaleontology, 24, 335–358.

SECTION C

Reconstructing climate gradients across the Mediterranean during the Early-Middle Pleistocene: the study-case of marine isotope stages 19 and 20*

*Article in preparation
(isotopic data collected by F. Bassinot, pers. comm.)

Abstract

A synoptic portrait considering the spatial climate variations in our planet is currently missing for many past epochs, including the Pleistocene. Answering questions about the geographical climate gradients during this interval of time would be especially relevant to address the major issue concerning MIS 19, today considered the best orbital analogue of the current interglacial (MIS 1). We here provide a reconstruction of the climate history of MIS 19 and the adjacent Glacial-Interglacial transitions by means of a high-resolution palynological study at ODP Site 976 and Montalbano Jonico, respectively located in the western and central Mediterranean. Palaeovegetation and palaeoceanographic conditions were reconstructed interpreting the pollen, spores and dinocysts assemblages from these areas. The coeval records at the two sites illustrate similar responses to orbital-scale climate forcing between marine and terrestrial ecosystems. On land and surface water records depict distinct features linked to North Atlantic cold events superimposed on a clear precessional imprint of change (temperature and seasonality). Vegetation structure and composition changes in response to the most extreme North Atlantic climate oscillations appear to be enhanced at the western tips of the Mediterranean, being this area closer to the Atlantic margin. Factors such as local geomorphology and the influx of glacial meltwaters through the Strait of Gibraltar could have enhanced such a contrast.

The proposed reconstruction enabled us to read the simultaneous modifications in the ocean and vegetation during the Early-Middle Pleistocene transition.

Keywords: MIS 19; climate gradients; central and western Mediterranean; palynology; pollen; dinocysts

1. Introduction and objectives

The comprehension of the modern Mediterranean climate setting depends on a vast collection of meteorological data as well as on the formulation of regional climate models (see Lionello et al., 2008). The proper management of these data has implications on the assessment of the future climate change (e.g. Gibelin and Déqué, 2003; Sánchez et al., 2004; Giorgi and Lionello, 2008; Somot et al., 2008). However, a significant progress on this climatic knowledge is based on proxies-derived reconstructions of the atmospheric and oceanographic variables across the past climate cycles (e.g. Tzedakis, 2005; Tzedakis et al., 2006; Joannin et al., 2008, 2011; Combourieu-Nebout et al., 2013; Bertini et al., 2015; Rohling et al., 2015; Russo-Ermolli et al., 2015; Capotondi et al., 2016; Lacey et al., 2016; Sadori et al., 2016; Sánchez Goñi et al., 2016a; Oliveira et al., 2017). Such palaeodata document the complex interactions between external (orbital) and internal factors (e.g. tectonics, North Atlantic dynamics, African monsoons, ...) affecting the Mediterranean system at the scale of several millions to hundreds years.

The past spatial variability of the Mediterranean climate and ecosystems is an intriguing matter of research. Detailed reconstructions for the last 6 Ma have been focused on the sapropel formation (e.g. Rohling et al., 2015; Grant et al., 2016 and references therein) and the Messinian salinity crisis (MCS: 5.9-5.3 Ma) (e.g. Roveri et al., 2014). At present, however, no documentation is available on the spatial gradients during the Early-Middle Pleistocene transition (EMPT: 1.4-0.4 Ma) and the Mid-Brunhes event (MBE: at ca 430 ka), which are widely recognized to be two of the main climate changes of the Quaternary (e.g. Yin and Berger, 2010; Candy, Mcclymont, 2014; Head and Gibbard., 2015; Maslin and Brierley, 2015). Since a growing body of palaeodata have been produced in the last decade to fill the datasets for the first portion of the EMPT in the Mediterranean (e.g. Bertini et al., 2000; 2015; Capraro et al., 2005, 2015; Joannin et al., 2007, 2008, 2011; Tzedakis et al., 2006; Marino et al., 2015, 2016; Almogi-Labin, 2011; Toti, 2015; Sánchez Goñi et al., 2016a, b; Oliveira et al., 2017) the scientific community will be given an opportunity to compare coeval records, useful to trace palaeomaps of vegetation and oceanographic indices, precursors of more complex climate reconstructions.

At present, ODP Site 976 and the Montalbano Jonico (MJ) successions contribute to a better understanding of the oceanographic and climate latitudinal variability across the Mediterranean by the comparison between two palynological records of the EMPT, focusing the interval 802-754 ka and including marine isotope stages (MIS) 20 and 19. These data were collected in the frame of a project that aims to describe glacial termination IX (TIX), corresponding to the transition between MIS 20 and 19. This period is of great interest to those who want to investigate the links with TI, as the latter interval occurred under a strictly similar orbital control (Yin and Berger, 2012). The two records of ODP Site 976 and MJ are located in the Alboran Sea and in southern Italy, respectively (Fig. 1). In each one, pollen and dinocysts were simultaneously analyzed to estimate the temporal variation of the vegetation and oceanographic parameters. Once aligned, the two successions were compared to establish how the two sites responded to the same climate pattern, as well as to detect direction and velocity of the climate processes across a virtual 1900 km-long transect.

2. Climate and oceanographic setting of the Mediterranean basin: an overview of the main characteristics

The Mediterranean climate is marked by a strong seasonal variability influenced, in winter, by the North Atlantic storm-track carrying abundant rainfalls and, in summer, by the sub-tropical (Azores cell) high-pressure system involving draught and warm temperatures. A major mode of interannual variability of the winter precipitations is associated to the North Atlantic Oscillation (NAO), especially in the Western Mediterranean (e.g. Hurrell, 1995), and to the El-Niño Southern Oscillation (ENSO) in the Eastern Mediterranean (Pozo-Vazquez et al., 2001; Alpert et al., 2006). The Mediterranean-type summer draught originating from the northward displacement of the sub-tropical high-pressure belt over north Africa may be also influenced by the Asian and African monsoon pattern, especially in the Eastern basin (Rodwell and Hoskins, 1996; Alpert et al., 2006).

A comprehensive portrait of the Mediterranean region cannot overlook the extensive surface covered by sea-waters, which interacts with the local climate features by bringing moisture and heat. The Mediterranean Sea receives relatively warmer and less saline water from the Atlantic Ocean through the Strait of Gibraltar, as well as less saline water from the Black Sea

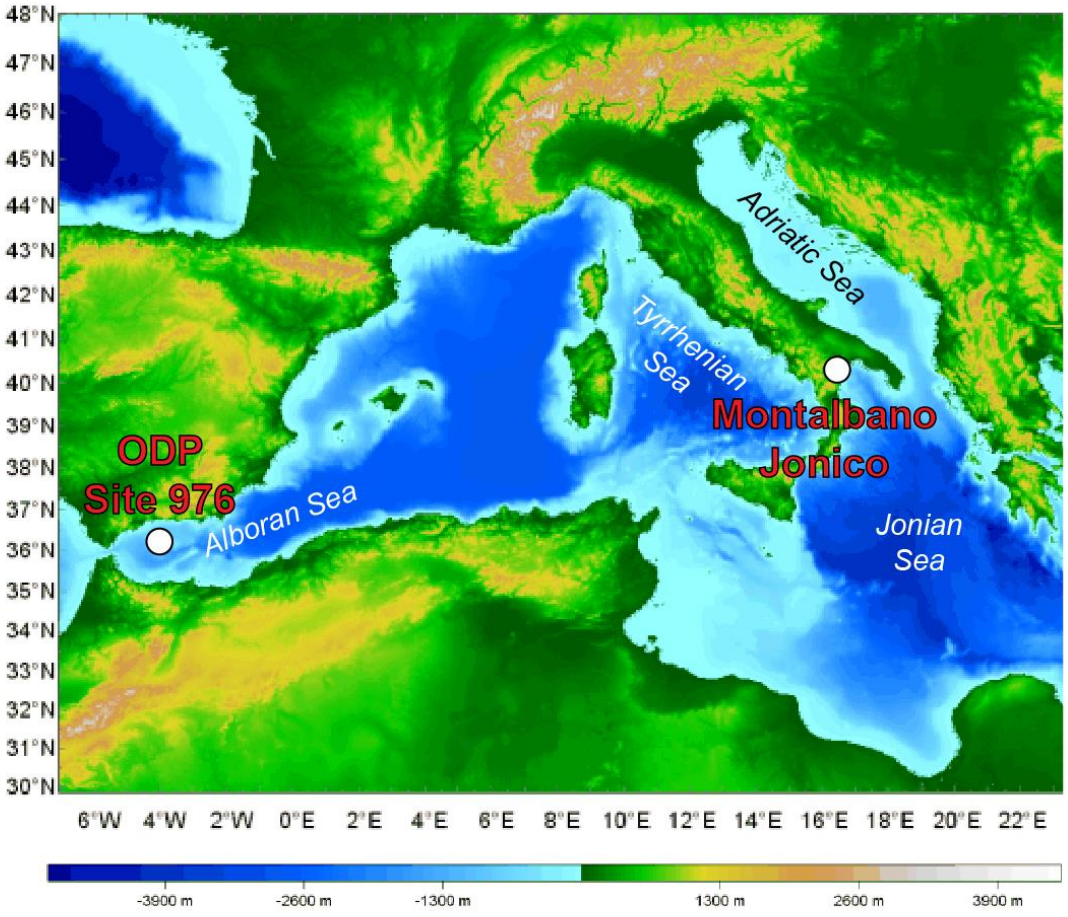

Fig. 1- Location of ODP Site 976 and Montalbano Jonico. Topographic and bathymetric map of the Mediterranean Basin produced with OceanMap by combining a number of different datasets.

through the Turkish Strait System and the rivers discharge. The main driver of the Mediterranean circulation is the excess of evaporation with respect to precipitation. This triggers the inflow of Atlantic Water (AW) through the

Strait of Gibraltar which is by far the major (positive) term of the water balance of the whole basin (Tanhua et al., 2013). The AW travels the western Mediterranean Sea following a complex meandering path and divides into two branches: one directed to the Tyrrhenian Sea and the other one flowing into the Ionian Sea and the Eastern Mediterranean through the Sicily Channel (e.g. Millot and Taupier-Letage, 2005). In the Levantine Sea, the AW becomes more saline and downwells to form the deeper Levantine Intermediate Water (LIW) which spreads westward and finally comes out the Mediterranean together with the deep waters that form in the Adriatic Sea and those forming in the Gulf of Lions (Millot and Taupier-Letage, 2005). The structure and hydrography of the Mediterranean are crucial to explain the marked trend of oligotrophy increase (paralleling a nutrient depletion) towards the East (e.g. Pujol and Vergnaud-Grazzini, 1995) and the overall low levels of productivity, which are among the lowest of the World's Ocean (Incarbona et al., 2016). The marine trophic regime also responds to seasonal pattern, characterized by oligotrophic conditions during late spring-summer and mesotrophic conditions during late fall-winter (Pujol and Vergnaud-Grazzini, 1995; Rigual-Hernández et al., 2012).

3. Methodology

Quantitative analyses of the pollen and dinocysts content were carried out on a total of 104 samples. Samples were prepared using a standard chemical-physical procedure for pollen extraction, as explained in both Section B and Bertini et al. (2015), to which the reader is referred for the detailed procedure and pollen detailed results. Percentages of pollen taxa are normalized to a main sum without *Pinus*; the latter, in fact, would obscure the other taxa signal due to its strong overrepresentation, as usual in marine sediments (Heusser and Balsam, 1977; Turon, 1984; Beaudouin et al., 2007). On the contrary, *Pinus* percentage is normalized to the total pollen sum.

Beside terrestrial palynoflora, the analyses revealed the presence of a rich and diversified dinocysts assemblage, which underwent independent quantitative counting. Unfortunately, evidence of wall corrosion and degradation was revealed on the heterotrophic dinoflagellate cysts (e.g.

Brigantedinium spp.) in some samples. The percentages of the dinocysts taxa were calculated to a main sum not including heterotrophic forms and reworked dinocysts, to avoid possible disturbs on the palaeoecological signal. The taxonomic identification conforms to Zonneveld and Pospelova (2015).

4. The palaeovegetation record of TIX and MIS 19

4.1. ODP site 976

The study of core 976, Alboran Sea (see also Section B) yields an image of the palaeoflora and palaeovegetation in the western Mediterranean within ca. 802-754 ka, based on the analysis of one hundred and four samples (mean time-resolution: 460 years). The chronology of the core complies with that used in Section B for making a first description of the palynological and calcareous plankton data at Site 976, except for the addition of one tie-point at 794.08 ka (Fig. 2). Here, the modified chronological scheme was taken as a working hypothesis to best reconcile the little offsets of the main pollen curves within MIS 20, as well as to improve the parallelisms between the in situ $\delta^{18}O$ record (*G. bulloides*) and that obtained at the MJ section (*M. barleanum*; Nomade et al., submitted) during the deglaciation (Fig. 2).

The palynoflora at Site 976 is mainly composed of taxa typical of south-European communities, including deciduous and evergreen *Quercus* and Mediterranean sclerophylls (e.g. *Olea*, *Pistacia*, *Phillyrea*). *Fagus* was retrieved moderately whereas other deciduous broad-leaved taxa like *Betula*, *Ostrya*, *Carpinus*, *Corylus* are recorded in very small amount. *Pinus* is recorded throughout the record. Mid to high-altitude conifers as *Abies*, *Picea*, *Cedrus* were also detected. The record also shows relict abundances of mesothermic taxa today almost or totally extinct from Southern Europe, as for example "Taxodiaceae", *Tsuga* and *Zelkova*. Herbs and shrubs include taxa widely diffused on nowadays open vegetation formations, such as grasses (Poaceae), Asteraceae, Brassicaceae, as well as more typical steppe taxa herbs such as

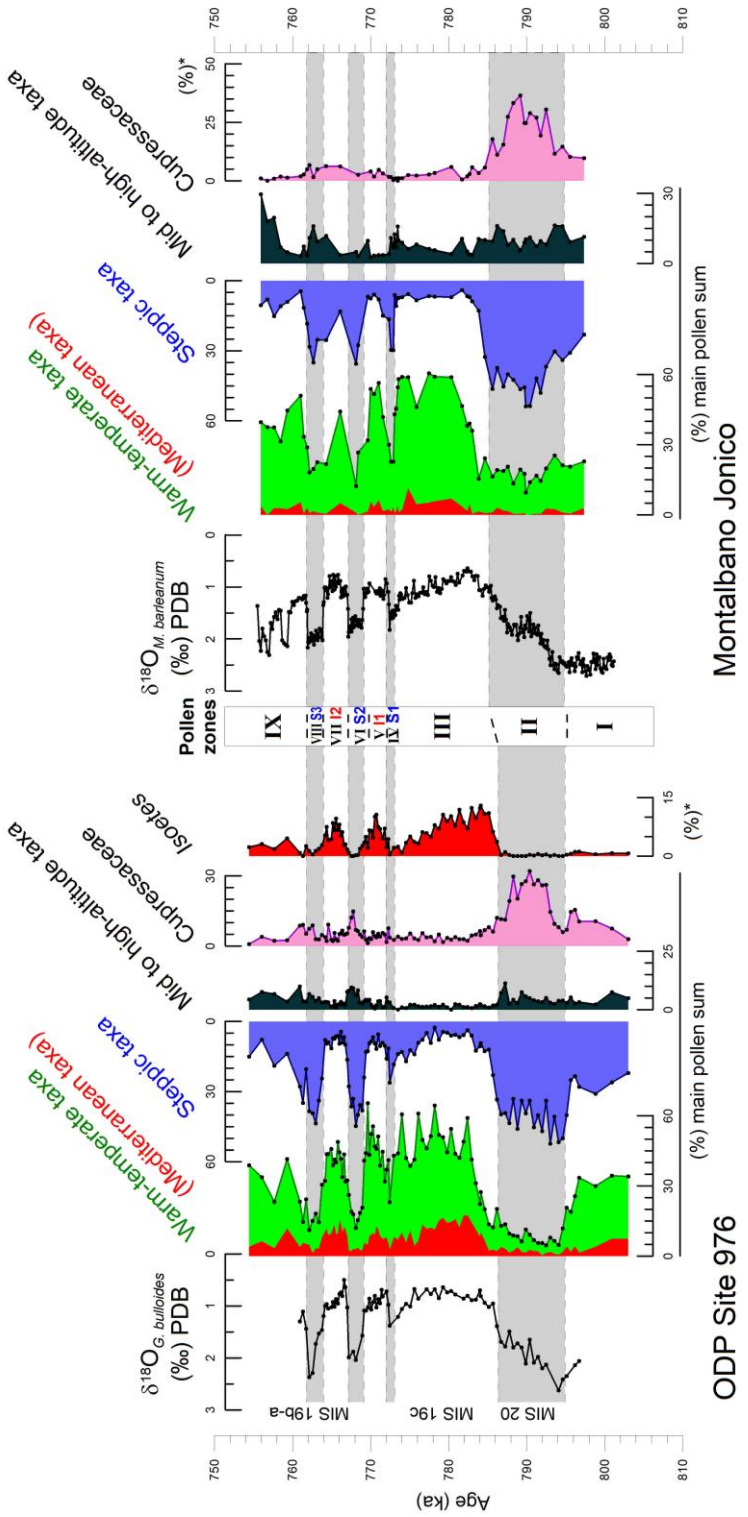

Fig. 2 – Summary pollen and spores diagrams spanning the interval of MIS 20-19 at ODP Site 976 and Montalbano Jonico. The oxygen isotope record is after Bassinot (pers. comm. See also Section B). The taxa percentages of indicated with (%) have been normalized to a different sum: for details, see in section B. Pollen zones 'I-IX' are defined on the base of the main variations of the pollen-spores assemblage. (For interpretation of the codes 'S1-S3' and 'I1-I2', the reader is referred to the results and discussion).*

Artemisia, *Ephedra* or halophytes such as Amaranthaceae. Cupressaceae are also well abundant especially during MIS 20.

The pollen succession was subdivided into nine main phases (Fig. 2). Phases I, III, V, VII and IX are characterized by the highest cover of temperate taxa, including deciduous *Quercus,* Ericaceae and Mediterranean plants, albeit sometimes associated with large amounts of herbaceous components, including Cichorioideae and steppe vegetation (mainly *Artemisia*, *Ephedra* and Amaranthaceae). Increases of *Isoetes* document the expansion of temporary Mediterranean pools and/or the increase of rivers discharge (Fig. 2).

Phases II, IV, VI and VIII are marked by moderate to prominent expansions of the steppic (*Artemisia*) to semi-desert (*Ephedra*, Amaranthaceae) vegetation and the regression of the temperate broad-leaved and evergreen taxa. (Fig. 2).

The forested (open) vegetation phases match the lighter (heavier) values of the oxygen isotope curve stressing the climatic significance of the succession (Fig. 2).

4.2. Montalbano Jonico

Palynological investigations at MJ (Basilicata Region, southern Italy) contributed to the reconstruction of past vegetation and climate changes in the central Mediterranean within the MIS 37 to MIS 16 interval (Joannin et al., 2008; Bertini et al., 2015; Toti, 2015). The results already published for MIS 20-19 only (Bertini et al., 2015; Toti, 2015, Maiorano et al., 2016) are here summarized and improved by the addition of new samples, thus increasing the stratigraphic resolution up to 100 years. The age-model used in this interval is provided by the astronomical calibration of the $\delta^{18}O$ record obtained on the foraminifer *M. barleanum*, sampled along the same profile (Simon et al., 2017; Nomade et al., submitted).

The terrestrial flora includes mesophilous broadleaved taxa that currently inhabit Italian peninsula: deciduous *Quercus*, *Ulmus*, *Fagus*, *Betula*, *Ostrya*, *Carpinus* and Ericaceae. The pollen assemblage also reveals the presence of *Carya*, *Pterocarya*, *Tsuga*, *Liquidambar*, *Zelkova*, "Taxodiaceae", most of which

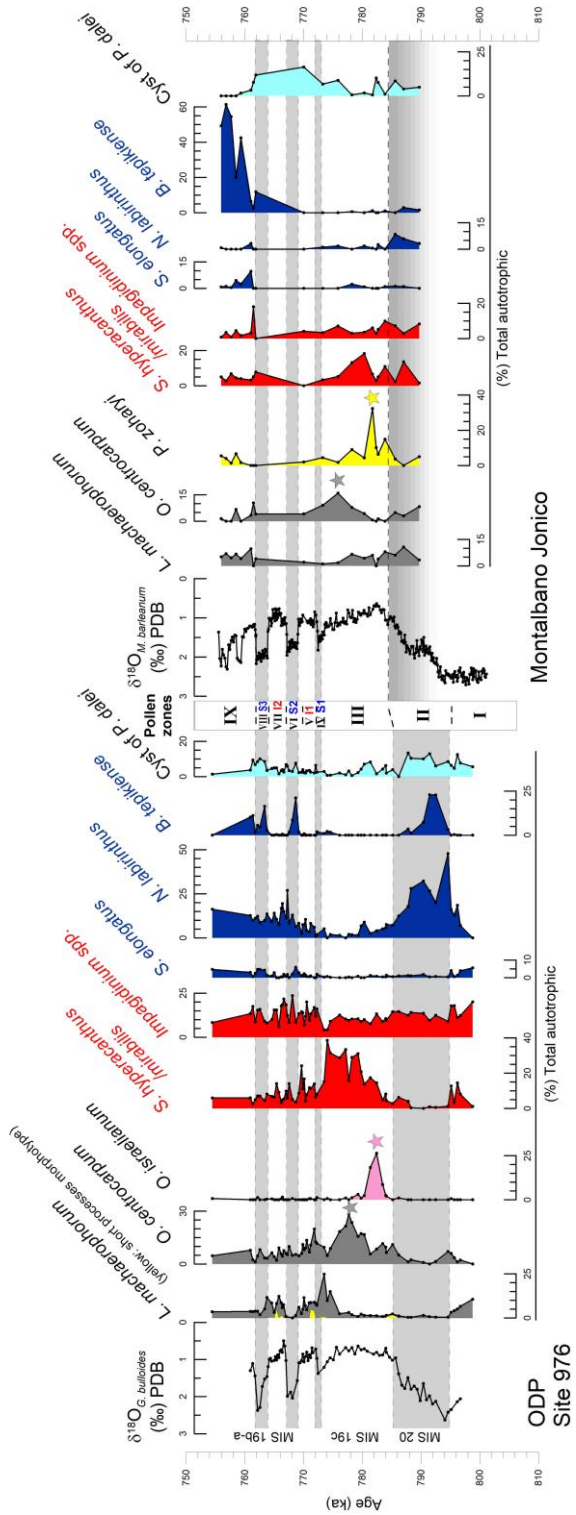

Fig. 3 - Relative abundances of selected dinocysts taxa, recorded along the interval of MIS 20-19 at ODP Site 976 and MJ. Note that the records have no homogeneous time-resolution and cover different stratigraphic ranges. The oxygen isotope record is after Bassinot (pers. comm. See also Section B). Pollen zones 'I-IX' are defined on the base of the main variations of the pollen-spores assemblage. (For interpretation of the codes 'S1-S3' and 'I1-I2', the reader is referred to the results and discussion).

no longer exist in Europe or have a strictly local distribution. Mid- to high-altitude conifers like *Cedrus, Abies* and *Picea* were detected throughout the record, as well as the more ubiquist *Pinus*. Non-arboreal taxa include cosmopolitan herbs (e.g. Asteraceae and Poaceae), hydrophytes (e.g. Cyperaceae), steppic to semi-desert taxa (*Artemisia*, *Ephedra*, *Hippophae*, Amaranthaceae, Caryophyllaceae).

At MJ, as also observed at ODP Site 976, nine pollen phases were recognized; they were labelled from I to IX (Fig. 2). The forest cover, dominated by deciduous oak, shows major increases within phases III, V, VII and IX, where also Mediterranean taxa are more abundant. A subdued expansion of the deciduous forest occurs within the interval I. During the intervals II, IV, VI and VIII, the expansion of steppe and semi-desert vegetation, mainly formed by *Artemisia*, *Ephedra* and Amaranthaceae, is observed.

The main vegetation shifts parallel those of the oxygen isotopic record, as already pointed out in the record of the ODP Site 976 (Fig. 2).

5. Dinocysts results for the interval TIX to MIS 19

5.1. ODP Site 976

Sixty-one samples from ODP core 976 were examined to monitor the history of the dinocysts assemblages between 802 and 754 ka (780-years mean time resolution) (Fig. 3). The cysts of autotrophic dinoflagellate dominate the assemblages, with relative abundances always >50%. However, a quite large presence of heterotrophic taxa (especially *Brigantedinium* spp.) is observed in some levels characterized by a better preservation. Strong biases are thus expected to affect the abundance of these cysts due to diagenesis, possibly in addition to the aggressiveness of the laboratory treatment (Marret, 1993; Combourieu Nebout et al., 1998).

Dinocysts taxa	Present-day ecology	Higher abundances in the study interval	
		ODP Site 976	Montalbano Jonico
Bitektatodinium tepikiense	Sub-polar to temperate species with the highest abundances in the North Sea. It shows an affinity for stratified surface waters with a strong seasonal temperature gradient, with freezing winter temperatures and (Sánchez Goñi et al., 2000; Turon et al., 2003; Marret et al. 2004; Penaud et al., 2011a, b; Zonneveld et al., 2013).	Up to 25% during late MIS 20; peak abundances in MIS 19b-a	Relative abundance maximum (60%) in the latest MIS 19
Impagidinium spp.	Tis genus includes temperate to tropical full oceanic species (excluding *I. pallidum*) typical of oligotrophic settings. Its highest relative abundances are recorded in regions with SSTs >20-25° (Turon, 1984; Marret and Zonneveld, 2003).	Present throughout the succession with relative abundances 5-25%	Mainly distributed in MIS 20-19c
Lingulodinium machaerophorum	Temperate to tropical species almost exclusively found in coastal areas and in the vicinity of continental margins. Highest relative abundance values are recorded in areas in close to active upwelling cells as well as near river mouths. (Mertens et al., 2009; Zonneveld et al., 2013).	Peak abundances (up to 25%) at the MIS 19c-MIS 19b transition	Maximum values (around 10%) at the end of MIS 20 and the onset of MIS 19c
Nematosphaeropsis labyrinthus	Cosmopolitan, full marine species thriving in both eutrophic and oligotrophic environments. It is present with higher abundances in eutrophic environments and in cold to cool waters between 45 and 65° N in the North Atlantic Ocean (Rochon et al., 1999; Devillers and de Vernal, 2000; Marret and Zonneveld, 2003).	Particularly represented in the upper part of MIS 20 with values up to 50%	Highest values (up to 10%) at the end of MIS 20
Operculodinium centrocarpum	Cosmopolitan species living in both coastal and open oceanic environments in a wide range of temperatures and salinities. Highest abundances of this taxon seem to be linked to high-nutrient waters of the temperate to sub-polar North Atlantic (Rochon et al., 1999; Zonneveld et al., 2013).	Up to 30% in MIS 19c	Up to 15% in MIS 19c
Operculodinium israelianum	Restricted to tropical to temperate regions, this species can be abundant in both coastal and open oceanic sites. Highest relative abundances are observed in nearshore sites, where upper water salinities prevail (Wall et al., 1977; Harland, 1983; Marret and Zonneveld, 2003).	Peak abundance (25%) within MIS 19c	Rare or absent
Polisphaeridium zoharyi	Subtropical to equatorial species typical of coastal and shallow-lagoonal sites. It could indicate near-surface waters stratification and/or elevated upper water salinities. It seems to be correlated with low phosphate and nitrate concentrations (Marret and Zonneveld, 2003; Reichart et al., 2004)	Rare or absent	Peak abundance (35%) within MIS 19c
Cyst of *Pentapharsodinium dalei*	Cosmopolitan euryhaline species tolerating seasonal sea ice cover. It is observed to dominate the assemblages off Iceland and marginal seas of the arctic Atlantic Ocean (e.g. the Hudson Bay, the Barents Sea...) (Marret and Zonneveld, 2003).	Highest abundances during MIS 20 (>10%)	Highest percentages (>15%) detected within MIS 19b-a
Spiniferites elongatus	This species has a Northern Hemisphere polar to sub-tropical distribution and thrives in waters with salinities seasonally reduces by meltwater and/or runoff. Highest relative abundances are related to cold regions with high-nutrient concentrations especially those of the North Atlantic frontal systems (e.g. Labrador Sea) (Marret and Zonneveld, 2003; Zonneveld et al., 2013).	Present with low relative abundances (up to 5%) in MIS 20 and MIS 19b-a	Values up to 10% in the latest MIS 19, virtually absent in other intervals
Spiniferites mirabilis/hyperacanthus	Temperate to tropical taxon distributed in a broad range of nutrient concentrations. Its higher abundances are linked to eutrophic regions where temperatures are >12°C. Highest abundances are found today along the European margin in the Bay of Biscay (Rochon et al., 1999; Marret and Zonneveld, 2003).	Higher frequencies (up to 40%) in the second half of MIS 19c	Mainly distributed in MIS 19c, with relative abundances up to 20%

Tab I - Modern distribution for selected major dinocyst species vs the intervals where they show the higher fossil distribution at ODP Site 976 and Montalbano Jonico.

The major species and genera that form the autotrophic assemblage are: *Spiniferites* spp. (especially represented by *S. hyperacanthus*/*mirabilis*), *Impagidinium* spp. (dominated by *I. aculeatum*), *Operculodinium centrocarpum*, *Operculodinium israelianum*, *Lingulodinium machaerophorum* (distinguished into two morphotypes with both normal and short process length), *Nematosphaeropsis labyrinthus*, *Bitektatodinium tepikiense*, *Pyxidiniopsis reticulata* and cyst of *Pentapharsodinium dalei*. Acritarch genera *Nannobarbophora* is also common.

The assemblage of MIS 20 is dominated by *Nematosphaeropsis labyrinthus* (up to 50%), accompanied by the highest percentage of *B. tepikiense* (>20%) and of *P. dalei* cysts (15%). *Impagidinium* spp. represents an important fraction throughout the assemblage (>15%) (Fig. 3). MIS 19c is featured by conspicuous relative abundance of *Impagidinium* spp. (up to 15%) and the highest relative abundances of *S. hyperacanthus*/*mirabilis* (up to 40%), especially after 780 ka. Peak abundances of *O. israelianum* (25%), *O. centrocarpum* (30%) and *L. machaerophorum* (25%) are recorded within 784 and 773 ka. (Fig. 3). The rapid climate variability observed within MIS 19b-a (773-761 ka) is reflected by the increase of *B. tepikiense*, *S. elongatus* and *P. dalei* cysts, during stadials, and of *L. machaerophorum* and *S. hyperacanthus*/*mirabilis*, during interstadials (Fig. 3). From substage MIS 19b upward, a monotone increase of *N. labyrinthus* is recognized. Unlike most of the taxa, *Impagidinum* spp. shows a quite uniform percentage distribution throughout the record (10%).

Present-day ecologies of major species found in both ODP Site 976 and the MJ section assemblages are listed in Tab. I with their major past occurrences in the fossil records.

5.2. Montalbano Jonico

A dinocysts-based reconstruction on the sea surface conditions at MJ during MIS 19 was carried out by Toti in Maiorano et al. (2016). Additional analyses were performed to extend the time interval covered by the previous record.
Hence, a total of twenty samples distributed between 790 and 770 ka was analyzed to obtain a mean time resolution of 1000 years.

The dinocysts assemblage is predominantly composed of autotrophic taxa. Only a few samples contain heterotrophic dinoflagellate cysts which are generally poorly preserved, suggesting a selective preservation due to oxidative phenomena. In the autotrophic assemblage *Spiniferites* spp. is the most represented taxon, ranging from 20 to 60% throughout the section and including *S. hyperacanthus/mirabilis*. Other major species or genera are *Impagidinium* spp. (including *I. aculeatum*), *O. centrocarpum*, *L. machaerophorum*, *Polysphaeridium zoharyi*, *N. labyrinthus*, *B. tepikiense* and cyst of *P. dalei*. *Nannobarbophora* is the most represented achritarch genus.

Dinocysts results do not cover MIS 20 except for a few data points. Above this interval, the assemblage of MIS 19c is characterized by lower values of *N. labyrinthus* and *B. tepikiense* and by the increase of *P. zoharyi* and *S. hyperacanthus/mirabilis* (up to 35 and 20%, respectively) as well as by the maximum of *O. centrocarpum* (15%) (Fig. 3). *L. machaerophorum* and *Impagidinium* spp. are generally quite represented (5-10%).

Within MIS 19b-a, the record presents a lower resolution due to the sparse data points. Yet we can observe the increase of *P. dalei* (up to 20%) and the lower values of *P. zoharyi*, *Impagidinium* spp. and *S. Hyperacanthus/mirabilis* (Fig. 3). Since ~762 ka, we report a short-term increase of *N. labyrinthus* and *S. elongatus* rapidly interrupted by an impressive increase of *B. tepikiense* (up to 60%) (Fig. 3).

6. Discussion

6.1. Overview of the main land-sea patterns

The climate optimum of MIS 19 is expressed between 785 and 773 ka (interval III: Fig. 2) by a phase of maximum afforestation at both the investigated sites broadly matching the “truly” interglacial, i.e. substage 19c. The time interval prior to MIS 19c, i.e. MIS 20, is characterized by lower precipitations and temperatures values suggested by open forests to widespread steppe formations (Fig. 2). MIS 19c is followed by a complex interval, related to MIS 19b-a and characterized by rapid alternation of temperate forest and open dry

vegetation, suggesting repetitive changes in both precipitation and temperature. The climate deterioration is well expressed, in the palynological diagram, by the increase of steppe and semi-desert taxa, indices of arid conditions. The most arid phases recorded in MIS 20 (interval II) and MIS 19b-a (intervals IV, VI and VIII) (Fig. 2) have been correlated with events of abrupt cooling and iceberg discharge in the North Atlantic (see Marino et al., 2015 and Maiorano et al., 2016, in Section A; Toti et al., in prep., in Section B). The major cold episode occurred between 795-785 ka (interval II; Figs. 2, 3) and is associated to extensive meltwater inflow and strong on land aridity (Toti et al., in prep., in Section B).

Regardless of the overall synchronism between the main climate changes in the western and central Mediterranean, various local factors are expected to be involved in the modulation of their intensity. Four time-slices will be discussed in the following paragraphs in order to better analyze such differences: MIS 20 (802-785 ka), MIS 19c (785-773 ka), MIS 19b-a (773-762 ka), "MIS 19/18 transition" (762-755 ka).

6.1.1. MIS 20

During late MIS 20 and MIS 20/19 transition, vegetation communities at the two examined sites display strong analogies. The evidence of stadial conditions associated to a H like event (interval II) consists in a prominent expansion of steppe and semi-desert vegetation at both localities.

A prominent 'Cupressaceae event' represents a unique stratigraphical signature for the examined interval at a regional level (Figs. 2, 3).

In the western Mediterranean, the dinocysts assemblage suggests cool to cold surface-sea temperatures (SSTs) in agreement with the results of the calcareous plankton for that period (Section B). The peak abundance of *B. tepikiense* between 794-790 ka (Fig. 3) matches the most extreme dry conditions on land (Fig. 2) and the highest relative abundance of the foraminifer *Neogloboquadrina pachyderma* (left-coiling) (Section B). The co-occurrence of *B. tepikiense* and *N. pachyderma* has been recognized to mark the polar water influx into Alboran, in connection with events of ice-rafted debris (IRD) deposition in the North Atlantic (e.g. Eynaud et al., 2000, 2009;

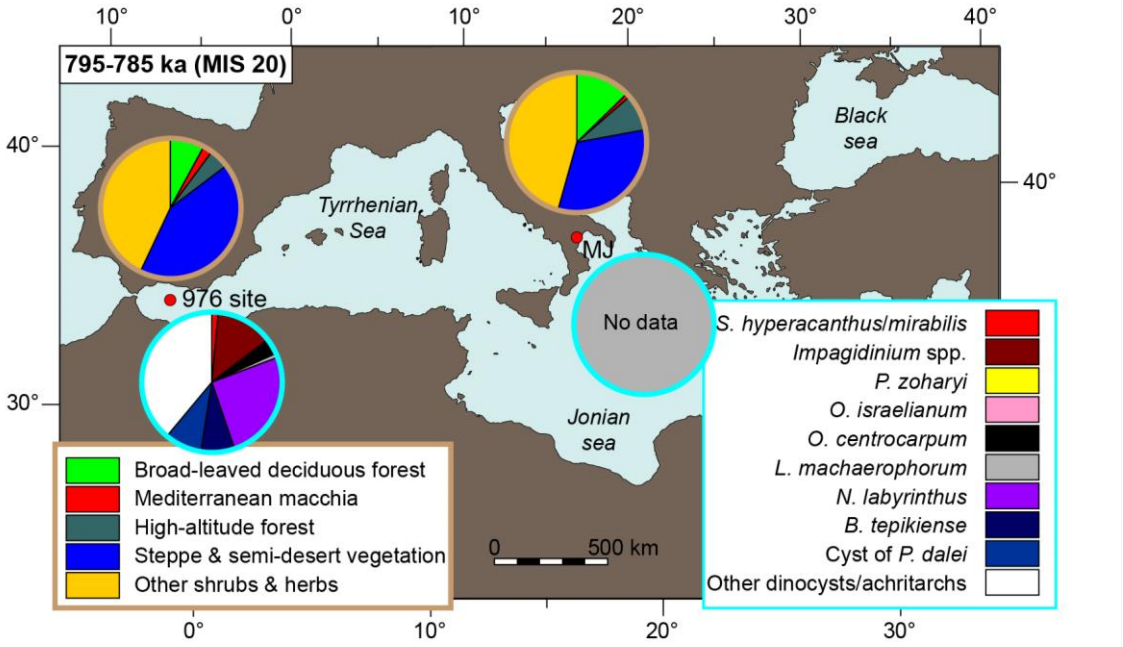

Fig. 4 - Average pollen and dinocysts proportions at ODP Site 976 and Montalbano Jonico during the interval 796-785 ka (latest MIS 20).

Sánchez-Goñi et al., 2000; Turon et al., 2003; Penaud et al., 2011a, b, 2016). The seasonal contrast should have been well expressed during this interval, as indicated by the relatively high frequencies of the warm-water *Impagidinium* spp., which probably characterized the summer assemblage. After 791 ka, an intensification of the frontal circulation is pointed out by the maximum of *N. labyrinthus* (Fig. 3). In fact, despite not being a major constituent of the modern Alboran sea assemblages (Elshanawany et al., 2010; Zonnevald et al., 2013), *N. labyrinthus* is largely recorded during the Glacial-Interglacial transitions (Turon, 1984; Eynaud et al., 2004; Penaud et al., 2008) as well as during periods of enhanced frontal currents circulation within MIS 3 (Penaud et al., 2016), given its tolerance to cold conditions and its high abundancies in areas of active upwelling (Zonneveld and Brummer, 2000).

At MJ, the cold spell in late MIS 20 determined a less severe climate deterioration with respect to that recorded at Site 976, according to the higher percentage of temperate tree cover, especially deciduous *Quercus* (Figs. 2, 4). The different geographical context of the two sites, including the diverse

distance between topographic highs and sedimentary basins, contribute to explain the more significant presence of mid-to high-altitude coniferous taxa such as *Cedrus*, *Abies* and *Picea* at the MJ (Figs. 2, 4; Bertini et al., 2015). Moreover, the lower percentage of Mediterranean taxa at this site points to lower winter temperatures, to which such taxa are intolerant, and/or enhanced summer humidity, which on the contrary allows deciduous forest to expand.

6.1.2. MIS 19c

During MIS 19c, the mean values of the temperate arboreal taxa at the two study sites (Fig. 5) depict similar degrees of afforestation and therefore presumably comparable precipitation levels. However, a more pronounced thermal seasonality seems to affect Site 976 climate, according to the larger presence of Mediterranean taxa, typically adapted to summer aridity

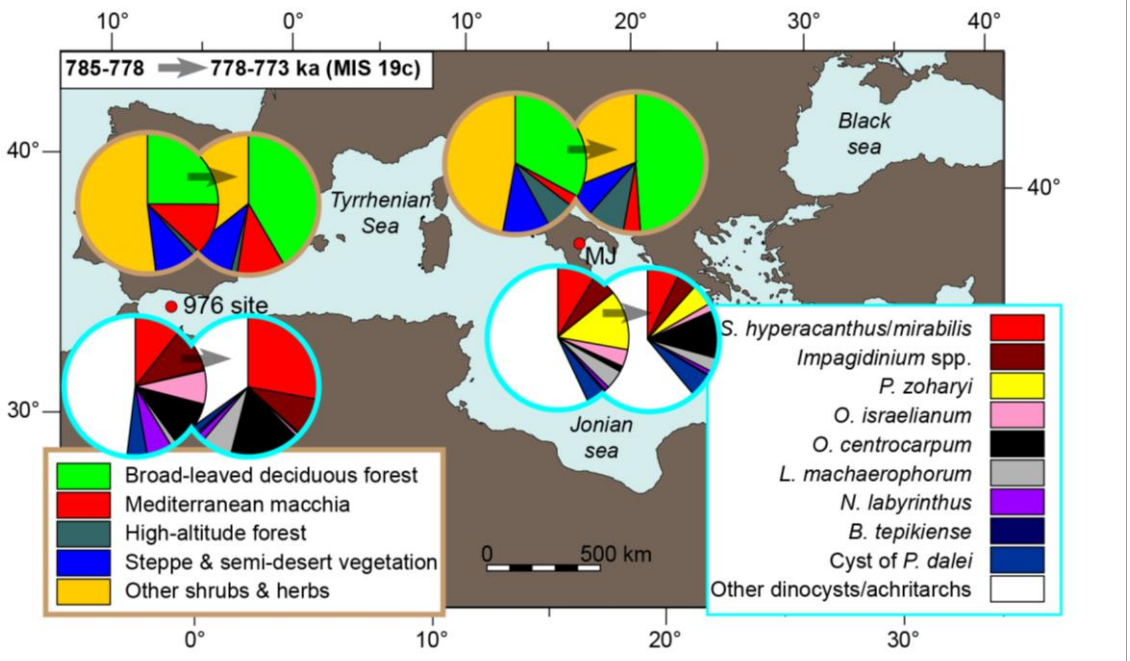

Fig. 5 - Average pollen and dinocysts proportions at ODP Site 976 and Montalbano Jonico during two representative intervals of MIS 19c (785-773 ka).

conditions (Figs. 2, 5). The record of this site describes repeated short-term expansions/contractions in the temperate deciduous forest, likely pointing to intra-interglacial fluctuations of humidity, whereas the same features are not distinguished at MJ (Fig. 2).

Calcareous plankton data (Toti et al., in prep., in Section B; Maiorano et al., 2016, in Section A) attest relatively warm SSTs during MIS 19c. This is also confirmed by the higher relative abundances of the thermophilous species *S. mirabilis/hyperacanthus* (Fig. 3) which is nowadays observed to dominate the temperate to tropical environments (Harland, 1983; Turon, 1984; Rochon et al., 1999; Marret and Zonneveld, 2003). Simultaneous blooms of *O. israelianum* and *P. zoharyi* are attested at ~782 ka at Site 976 and MJ, respectively (Fig. 3). Such increases suggest a response to more stratified surface waters as a possible result of a slowdown of the basin ventilation and reduced rates of water exchange with the North Atlantic Ocean. Not surprisingly, this interval has been considered crucial to the formation of a sapropel-like event correlated to i-cycle 74 (Maiorano et al., 2016, in Section A). The concomitant increase of the two dinocysts species improves the stratigraphical connections between the two basins during MIS 19.

The autotrophic dinocysts assemblage is apparently more diverse during the first part of MIS 19c with respect to the last part (Fig. 5). Hence, the first half of this interglacial was likely characterized by a stronger seasonality, allowing both cold-tolerant (e.g. *N. labyrinthus*) and thermophilous taxa (e.g. *S. hyperacanthus/mirabilis*) to grow significantly in different parts of the year.

Finally, we note a major increase of *O. centrocarpum* at ca. 778 ka in both locations (Fig. 3). This could mean a more active circulation in the Mediterranean from the mid part of MIS 19 on. This cosmopolitan cyst is, in fact, normally related to enhanced sea surface productivity and upwelling (Turon, 1984; Eynaud et al., 2004; Penaud et al., 2008).

6.1.3. MIS 19b-a

The alternation of stadial-interstadial conditions along MIS 19b-a was sketchy represented by box-and-whisker plots (Fig. 6). At ODP Site 976, a continuous trend of aridification is recognized in the succession of cold-dry stadials 'S1-S3'

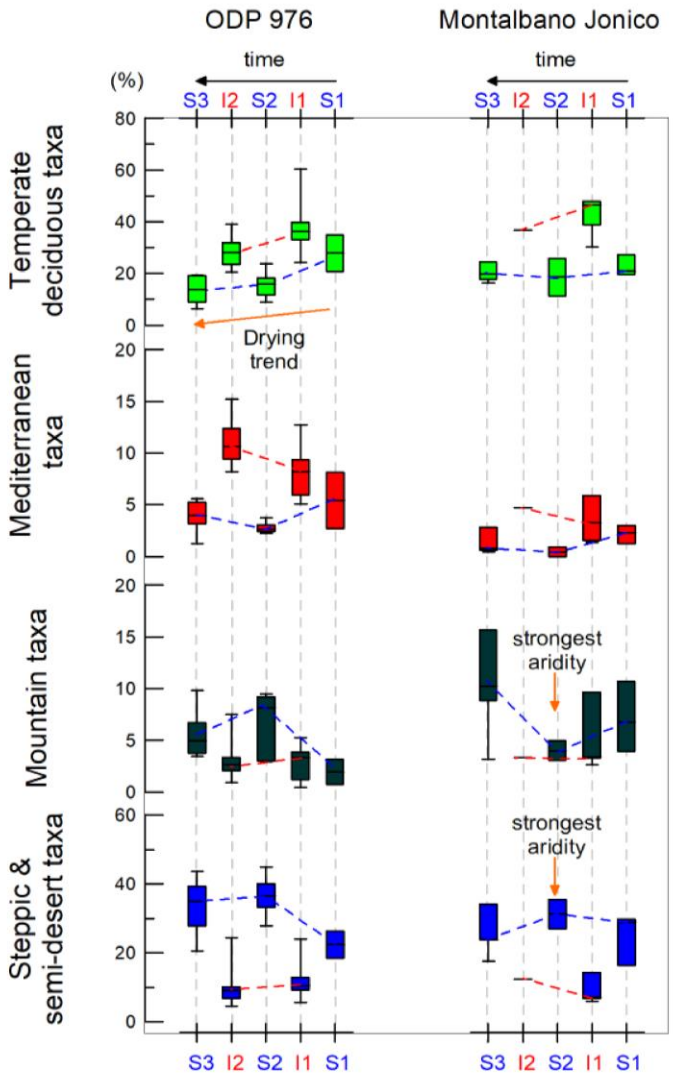

Fig. 6 - Vegetation changes at ODP Site 976 and Montalbano Jonico during the interval 773-755 ka (MIS 19b-a). Values of major groups of taxa are represented as box and whisker plots summarizing consecutive stadials and interstadials. The time-span covered by each phase is indicated in Figs. 2 and 3.

and of warm-humid interstadials 'I1-I2' (Fig. 6). Otherwise, at MJ, after the most arid phase corresponding to stadial 'S2', we observe an increase of temperate deciduous taxa and of high-altitude elements, which attests a growth of the moisture levels (Fig. 6). Such changes illustrate a longer

persistence of continental aridity in the western Mediterranean compared to the central basin.

The marine biomarkers at Site 976 evidence generally lower SSTs during MIS 19b-a with respect to the previous interval, based on the lower relative abundance of *S. hyperacanthus/mirabilis* as well as the gradual increase of *N. labyrinthus* (Fig. 3). A cold-water signal is also recorded at MJ, with the higher proportion of cysts of *P. dalei*, whose motile cells inhabit polar to subpolar basins of North Atlantic (Rochon et al., 1999), and could potentially indicate more eutrophic surface-waters in the Mediterranean (Zonneveld et al., 2012). Inflowing cold waters during stadial phases of MIS 19b-a are precisely outlined by peaks of the cold-water species *B. tepikiense* and *S. elongatus*, which match the higher abundances of *N. pachyderma* (left coiling) (Toti et al., in prep., in Section B), correlated with episode of iceberg discharge in the North Atlantic. Unfortunately, an extensive comparison with the dinocysts data from MJ is not possible due to the few data points therein contained.

6.1.4. MIS 19-18 transition

In this interval, the pollen datasets reveal a more extensive temperate forest cover in southern Italy with respect to the Alboran Sea edges (Fig. 7), possibly in response to higher precipitations in the central Mediterranean. The Mediterranean evergreen scrubland was apparently more developed in the lands surrounding ODP Site 976, likely pointing to an enhanced thermal seasonality, as concluded for previous intervals (Fig. 7). At the two study sites, the significant signal of steppic and semi-desert taxa suggests an overall scarcity of precipitations in the Mediterranean. At MJ, the expansion of mid to high-altitude vegetation belt after 758 ka denotes a cooling trend with no dramatic loss of moisture (Fig. 2). Such change is not unequivocally shown at Site 976.

In the dinocyst assemblage from Site 976, the relatively high presence of *N. labyrinthus* and *S. elongatus* suggests overall cool and nutrient-rich waters in the Alboran Sea (Fig. 3). Interestingly, in the same period the assemblage at MJ is dominated by *B. tepikiense* with percentage up to 60% (Fig. 3). Despite the presence of the latter taxon does not contradict the indication of low SSTs

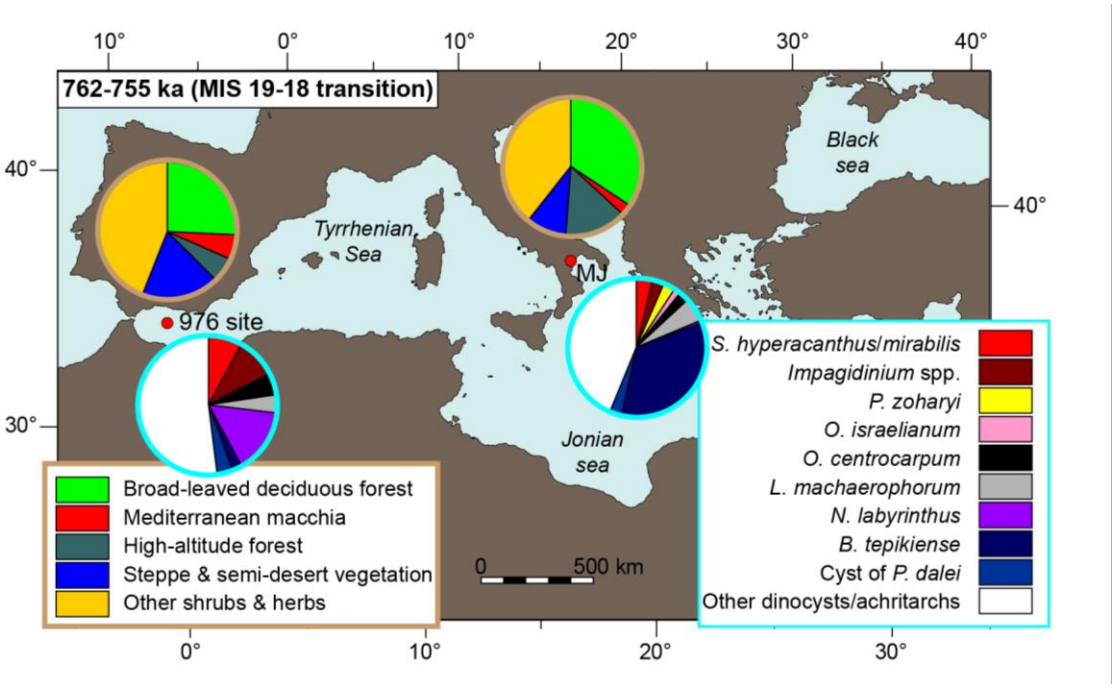

Fig. 7 – Average pollen and dinocysts proportions at ODP Site 976 and Montalbano Jonico during the interval 762-755 ka (latest MIS 19).

obtained by the calcareous plankton data (Maiorano et al., 2016, in Section A), its anomalous relative abundances are not obvious to interpret. The overwhelmingly prevalence of *B. tepikinese* implicates repeated seasonal blooms and the absence of significant competition. Strong seasonal temperature gradients have been recognized to be a crucial factor to the flourishing of *B. tepikiense* (Rochon et al., 1999; Zonneveld et al., 2013). However, an almost monospecific association of this dinoflagellate cysts has been described only in few cases (e.g. during MIS 3 in the eastern North Atlantic Harland et al., 2016). Furthermore, in the Mediterranean this species does not characteristically marks the colder environments (Elshanawany et al., 2010). We conclude that the marine basin of MJ during 759-756 ka (Fig. 3) has no modern analogue at mid-latitudes, and that the impressive proliferation of *B. tepikiense* was likely associated to an extreme seasonality with very low SSTs in winter and more equable ones in summer. This surface-water cooling may originate by an intensification of north-westerly winds accompanying the onset of MIS 18, which is also consistent with the more

intense pollen signal from mid to high-altitude taxa, reflecting the downward shift of the mountain vegetation belt (Fig. 2).

6.2. Spatial climate and sea surface waters variability during MIS 20-19

The Quaternary climate variability has imprinted unambiguous features into several sedimentary archives, allowing regional correlations to be made even in the absence of the chronological assistance (e.g. Magri, 1999; Tzedakis et al., 2005; Fletcher et al., 2010). Nonetheless, local factors such as the composition of the ecosystems and the land geomorphology can affect the amplitude of climate signals; more stable terrestrial landscapes yield, for instance, damped vegetation responses (e.g. Tzedakis et al., 2004, 2005; Fletcher et al., 2010; Sanchez Goni et al., 2008; Magny et al., 2013). Site-dependent features in the palaeoceanographic records are also common place; palaeo sea surface parameters depend, in fact, on peculiar ocean-atmosphere circulation mechanisms (e.g. Cortina et al., 2015). Below we summarize the spatial heterogeneity recorded during the MIS 20-MIS 19 interval (Figs. 2, 3).

The low to very low humidity and temperature values within MIS 20 are possibly related (Toti, in prep., in Section B) to enhanced North Atlantic cooling and associated massive IRD deposition (Martin-Garcia et al., 2015) similar to what happened during Heinrich stadials at the end of the last two glacial periods (e.g. Böhm et al., 2014). The deep-sea record from the Alboran Sea illustrates a major depletion of the temperate forest taxa with respect to that detected at MJ (Fig. 2). This conforms to the conclusions of Fletcher et al. (2010) about the weakening of the signal associated to the Last Glacial Dansgaard-Oeschger and H stadials away from the Atlantic margin, after comparison of several records spanning the whole European continent.

The deglaciation and the onset of MIS 19c caused a major overturning in the pollen and dinocysts assemblages (Figs. 2, 3), associated with relatively high precipitations and warmer both atmospheric and sea surface temperatures for the whole duration of the interglacial. Patterns of millennial-scale variability are particularly intriguing at ODP Site 976 where one can recognize several phases of contraction/expansion of the temperate deciduous

taxa (Fig. 2). Such an intra-interglacial variability, absent at MJ, calls into question several mechanisms that could be especially relevant for the regions closest to the North Atlantic margin, e.g. repeated phases of persistent positive/negative modes of NAO (see Section B). In fact, whilst NAO has a Mediterranean-scale control (Cullen and deMenocal, 2000; Cullen et al., 2002), its magnitude appears significantly larger in the Iberian Peninsula with respect to easternmost regions (Trigo et al., 2004). According to the analysis of MIS 19c performed by Sánchez-Goñi et al. (2016a) studying a core from IODP Site U1385 (on the West Iberian margin), this short-term variability could rather be an expression of a tropically-sourced signal in the band of precession harmonics.

In terms of seasonality, MIS 19c may be divided into two parts: (1) Before 778 ka, the warm-dry, cool-wet seasonal contrast appears to be stronger at both sites, according to the higher frequency of (dry-) herbaceous taxa and Mediterranean sclerophylls (Figs. 2, 5). This could be a consequence of the Earth's perihelion passage in the summer months of the North Hemisphere (see Fig. 6 in Toti, in prep., in Section B). The existence of a prominent seasonal pattern is also documented by the good diversity in the dinocysts assemblage and in particular by the co-occurrence of termophilic and cold-tolerant species (Fig. 5), which denotes the bloom of one or more taxa in different seasons of the year. (2) After 778 ka, both records show an increase of temperate deciduous taxa with respect to the herbaceous and Mediterranean scrubby elements (Fig. 5), which points to a more equable humidity distribution throughout the year. A relatively smooth year-round temperature pattern is also attested in the marine domain at Site 976, according to the less diverse dinocyst assemblage dominated by tropical to temperate taxa, notably *S. hyperacanthus*/*mirabilis* (Fig. 5). The MJ record, on the contrary, seems not to exhibit concomitant seasonality variations in the surface sea waters.

Since the end of MIS 19c, deciphering the spatial patterns is hindered by the inhomogeneous time resolution of the two palynological records (Figs. 2, 3). The reconstructed vegetation history shows that the intensity of the main climate phases may change from one site to another. At MJ, the interval centered at 768 ka ('S2') seems to have determined a minimum of humidity in the sequence of wet-dry oscillations. Conversely, climate change at Site 976

can apparently be regarded, on the long term, as a continuous drying (Fig. 6). Sea-surface waters are generally ventilated and rich in nutrients at both localities.

In the interval between 762-755 ka, the composition of terrestrial and marine palynological assemblages suggests low air-sea temperatures, compatible with the MIS 18 glacial inception. An increasing humidity contrast was detected between the two sites: the MJ area was, in fact, characterized by more intense precipitations with respect to the western Mediterranean, based on the higher abundance of temperate deciduous taxa and the increase of mid to high-altitude elements since 758 ka (Fig. 7). At MJ the dominance of *B. tepikiense* could be an index of extreme winter temperatures. Cooling of the surface waters in this basin could have been enhanced by persisting north-westerly winds.

'Tertiary' Taxa	Mean relative abundance during MIS 19c (%)	
	ODP Site 976	Montalbano Jonico
Carya	<0.1	0.3
Cedrus	1.1	2.5
Liquidambar	<0.1	0.1
Pterocarya	<0.1	0.1
Tsuga	<0.1	0.9
Zelkova	<0.1	0.7

Tab II – Average 'interglacial' relative abundances of the main arboreal taxa that disappeared from most of the Iberian and Italian sites during the Early-Middle Pleistocene.

In summary, our results show that the proportion between broad-leaved deciduous and Mediterranean plants is a meaningful index to trace seasonality variations during interglacial complexes. Still on the base on these proportions, spatial variations of seasonality can be assessed. It appears, for example, that the typical Mediterranean-type climate was better expressed at Site 976, probably due to the major influence of the Azores High pressure on western Mediterranean rainfalls. The relative distance from the Atlantic margin also seems to have played a role in the relative impact of the cold North Atlantic oscillations. In detail, the stadial phase within TIX was recorded at Site 976 more sharply, probably because of the more efficient teleconnections with the polar North Atlantic and likely reinforced by the concomitant meltwater influxes. However, the subdued response of the MJ

vegetation could also be ascribed to the local topography and geomorphology, characterized by abundant mid-altitude areas. Such locations may represent key refuges for temperate trees (Bennett et al. 1991; Tzedakis et al. 2002) and their existence around MJ could be tracked by the significant occurrence of mountain elements like *Abies*, *Picea* and *Cedrus* (Linares, 2011). Peculiar geomorphological factors could also explain why the MJ record contains higher relative abundances of certain 'Tertiary' taxa such as *Tsuga*, *Carya* and *Zelkova* with respect to Site 976 (Tab. II). This may support the hypothesis of a West-East extinction pattern, as already shown by previous studies (e.g. Bertini, 2010; Magri and Palombo, 2013; Magri et al., 2017).

On the long term, we note that starting from the cold-dry phase 'S2' (ca. 768 ka) the MJ area was influenced by more humid conditions with respect to Site 976, suggesting a climate decoupling along the western-central Mediterranean axis (Figs. 3, 7). Today, above-average precipitations in the regions around Italy are described, at a decadal time-scale, in the positive phase of the so-called 'Scandinavian teleconnection pattern', as described by Xoplaki (2002). During the EMPT, this pattern could have significantly influenced climate processes at the secular to pluri-millennial time scales, producing precipitation anomalies above the Italian Peninsula. Intensified westerlies in the southern Mediterranean are today recognized concomitant to this configuration (Bueh and Nakamura, 2007), which singularly resembles what observed at MJ during latest MIS 19, when a strong wind-driven cooling seems to be revealed by the highest increase of *B. tepikeiense* (Figs. 3, 7).

7. Final remarks

Pollen and dinocysts data collected along the study interval allowed us to monitor the atmospheric and sea surface variability during MIS 20-19 in two key sites of the central and western Mediterranean basin. The datasets collection by means of a unique palynological protocol has simplified the pollen/dinocyst-based correlations between the two sites as well as the assessment of the magnitude of the main climate changes. The detected successive palynological phases are robust features of the climate variability within the Mediterranean region and are useful datums for global-scale

correlations (Toti et al., in prep., in Section B); they include: glacial termination (TIX) at the end of MIS 20, the deglaciation and full interglacial optimum (MIS 19c), an interval containing a series of at least three interstadial/stadial oscillations (MIS 19b-a) and, finally, a short interval representing the entrance to MIS 18. Differences in seasonality and average air/sea temperature are the main synoptic features of the regional climate during both MIS 20 and MIS 19.

To advance the boundaries of knowledge on Mediterranean climate variability during this crucial key time and to solve the many still open questions, especially those concerning the main operating forcing and its different role in the two areas, we will consider indispensable, as next step of work, to use the collected rich palynological data-set for both climate quantifications and model simulations of palaeoprecipitations and palaeotemperatures.

References

Almogi-Labin, A., 2011. The paleoclimate of the Eastern Mediterranean during the transition from early to mid-Pleistocene (900 to 700 ka) based on marine and non-marine records: an integrated overview. Journal of Human Evolution 60, 428-436.

Alpert, P., Baldi, M., Ilani, R., Krichak, S.O., Price, C., Rodo, X., Saaroni, H., Ziv, B., Kishcha, P., Barkan, J., Mariotti, A., Xoplaki, E., 2006. Relations between climate variability in the Mediterranean region and the tropics: ENSO, South Asian and African monsoons, hurricanes and Saharan dust. In: Lionello, P., Malanotte-Rizzoli, P., Boscolo, R. (Eds.). Mediterranean Climate Variability, 4 Amsterdam, Elsevier; 149-177.

Beaudouin, C., Suc, J.-P., Escarguel, G., Arnaud, M., Charmasson, S., 2007. The significance of pollen record from marine terrigenous sediments: the presentday example of the Gulf of Lions (Northwestern Mediterranean Sea). Geobios 40, 159-172.

Bennett, K.D., Tzedakis, P.C., Willis, K.J., 1991. Quaternary refugia of North European trees. Journal of Biogeography 18, 103–115.

Bertini, A., 2000. Pollen record from Colle Curti and Cesi: early and middle Pleistocene mammal sites in the Umbro-Marchean Apennine mountains (central Italy). Journal of Quaternary Science 15 (8), 825-840.

Bertini, A., Toti, F., Marino, M., Ciaranfi, N., 2015. Vegetation and climate across the Early-Middle Pleistocene transition at Montalbano Jonico, southern Italy. Quaternary International 383, 74-88.

Böhm, E., Lippold, J., Gutjahr, M., Frank, M., Blaser, P., Antz, B., Fohlmeister, J., Frank, N., Andersen, M.B., Deininger, M., 2015. Strong and Deep Atlantic Meridional Overturning Circulation During the Last Glacial Cycle. Nature 517(7532), 73-6.

Bueh, C., Nakamura, H., 2007. Scandinavian pattern and its climatic impact. Quarterly Journal of the Royal Meteorological Society 133, 2117–2131.

Candy, I., McClymont, E.L., 2013. Interglacial intensity in the North Atlantic over the last 800,000 years: investigating the complexity of the mid-Brunhes Event (MBE). Journal of Quaternary Science 28, 343-348.

Capotondi, L., Girone, A., Lirer, F., Bergami, C., Verducci, M., Vallefuoco, M., Afferri, A., Ferraro, L., Pelosi, N., De Lange, G.J., 2016. Central Mediterranean Mid-Pleistocene paleoclimatic variability and its association with global climate. Palaeogeography Palaeoclimatology Palaeoecology 442, 72–83.

Capraro, L., Macrì, P., Scarponi, D., Rio, D., 2015. The lower to Middle Pleistocene Valle di Manche section (Calabria, Southern Italy): State of the art and current advances. Quaternary International 383, 36-46.

Capraro, L., Asioli, A., Backman, J., Bertoldi, R., Channell, J.E.T., Massari, F., Rio, D., 2005. Climatic patterns revealed by pollen and oxygen isotope records across the Matuyama–Brunhes Boundary in the central Mediterranean (southern Italy). In: Head, M.J., Gibbard, P.L. (Eds.). Early-Middle Pleistocene transitions: the land-ocean evidence: Geological Society of London, Special Publication 247, 159-182.

Combourieu Nebout, N., Paterne, M., Turon, J.L., Siani, G., 1998. A high resolution record of the last deglaciation in the central Mediterranean Sea: palaeovegetation and palaeohydrological evolution. Quaternary Science Reviews 17, 303–317.

Combourieu Nebout, N., Peyron, O., Bout-Roumazeilles, V., Goring, S., Dormoy, I., Joannin, S., Sadori, L., Siani, G., Magny, M., 2013. Holocene

vegetation and climate changes in the central Mediterranean inferred from a high-resolution marine pollen record (Adriatic Sea). Climate of the Past 9, 2023-2042.

Cortina, A., Sierro, F.J., Flores, J.A., Martrat, B., Grimalt, J.O., 2015. The response of SST to insolation and ice sheet variability from MIS 3 to MIS 11 in the northwestern Mediterranean Sea (Gulf of Lions). Geophysical Research Letters 42(23), 10,366–10,374.

Cullen, H.M., deMenocal, P.B., 2000. North Atlantic influence on Tigris–Euphrates streamflow. International Journal of Climatology 20, 853–863.

Cullen, H.M., Kaplan, A., Arkin, P.A., deMenocal, P.B., 2002. Impact of the North Atlantic oscillation on the Middle Eastern climate and Streamflow. Climatic Change 55, 31-33.

Devillers, R., de Vernal, A., 2000. Distribution of dinoflagellate cysts in surface sediments of the northern North Atlantic in relation to nutrient content and productivity in surface waters. Marine Geology 166, 103–124.

Elshanawany, R., Zonneveld, K., Ibrahim, M.I., Kholeif, S.E.A., 2010. Distribution patterns of recent organic-walled dinoflagellate cysts in relation to environmental parameters in the Mediterranean Sea. Palynology 34(2), 233-260.

Eynaud, F., Turon, J. L., Sánchez Goñi, M. F., Gendreau, S., 2000. Dinoflagellate cyst evidence of "Heinrich-like events" off Portugal during the marine isotopic stage 5. Marine Micropalaeontology 40, 9-21.

Eynaud F., Turon J.L. & Duprat, J., 2004. Comparison of the Holocene and Eemian palaeoenvironments in the South-Icelandic basin: dinoflagellate cysts as proxies for the North Atlantic surface circulation. Review of Palaeobotany and Palynology 128, 55–79.

Eynaud, F., de Abreu, L., Voelker, A., Schönfeld, J., Salgueiro, E., Turon, J.L., Penaud, A., Toucanne, S., Naughton, F., Sánchez-Goñi, M.F., Malaizé, B., Cacho, I., 2009. Position of the Polar Front along the western Iberian margin during key cold episodes of the last 45 ka. Geochemistry Geophysics Geosystems 10(7), Q07U05.

Fletcher, W.J., Sánchez Goñi M.F., Allen, J.R.M., Cheddadi, R., Combourieu Nebout, N., Huntley, B., Lawson, I., Londeix, L., Magri, D., Margari, V., Mueller, U.C., Naughton, F., Novenko, E., Roucoux, K.H., Tzedakis, P.C., 2010. Millennial-scale variability during the last glacial in

vegetation records from Europe. Quaternary Science Reviews 29, 2839-2864.
Gibelin, A.L., Déqué, M., 2003. Anthropogenic climate changeover the Mediterranean region simulated by a global variable resolution model. Climate Dynamics 20, 327-339.
Giorgi, F., Lionello, P., 2008. Climate change projections for the Mediterranean region. Global and Planetary Change 63 (2), 90-104.
Grant, K.M., Grimm, R., Mikolajewicz, U., Marino, G., Ziegler, M., Rohling, E.J., 2016. The timing of Mediterranean sapropel deposition relative to insolation, sea-level and African monsoon changes. Quaternary Science Reviews 140, 125-141.
Harland, R., 1983. Distribution maps of Recent dinoflagellate cysts in bottom sediments from the North Atlantic Ocean and adjacent seas. Palaeontology 26, 321-387.
Head, M.J., Gibbard, P.L., 2015. Early-Middle Pleistocene transitions: linking terrestrial and marine realms. Quaternary International 389, 7-46.
Heusser, L.E., Balsam, W.L., 1977. Pollen distribution in the northeast Pacific Ocean. Quaternary Research 7, 45-62.
Hurrell, J.W., 1995. Decadal trends in the North Atlantic Oscillation: Regional temperatures and precipitation. Science 269, 676-679.
Incarbona, A., Di Stefano, E., Sprovieri, R., Ferraro, S., 2016. Uniqueness of Planktonic Ecosystems in the Mediterranean Sea: The Response to Orbital- and Suborbital-Climatic Forcing over the Last 130,000 Years. Open Geosciences 8, 567-578.
Joannin, S., Quillévéré, F., Suc, J.P., Lécuyer, C., Martineau, F., 2007. Early Pleistocene climate changes in the central Mediterranean region as inferred from integrated pollen and planktonic foraminiferal stable isotope analyses. Quaternary Res. 67, 264-274.
Joannin, S., Ciaranfi, N., Stefanelli, S., 2008. Vegetation changes during the late Early Pleistocene at Montalbano Jonico (Province of Matera, southern Italy) based on pollen analysis. Palaeogeography, Palaeoclimatology, Palaeoecology 270, 92-101.
Joannin, S., Bassinot, F., Combourieu Nebout, N., Peyron, O., Beaudouin, C., 2011. Vegetation response to obliquity and precession forcing during the

Mid Pleistocene Transition in Western Mediterranean region (ODP Site 976). Quaternary Science Reviews 30, 280-297.

Lacey, J.H., Leng, M.J., Francke, A., Sloane, H.J., Milodowski, A., Vogel, H., Baumgarten, H., Zanchetta, G., Wagner, B., 2016. Northern Mediterranean climate since the Middle Pleistocene: a 637 ka stable isotope record from Lake Ohrid (Albania/Macedonia), Biogeosciences 13, 1801–1820.

Lionello, P., Cogo, S., Galati, M.B., Sanna, A., 2008. The Mediterranean surface wave climate inferred from future scenario simulations. Global and Planetary Change 63 (2), 152-162.

Magny, M., Combourieu Nebout, N., de Beaulieu, J.L., Bout-Roumazeilles, V., Colombaroli, D., Desprat, S., Francke, A., Joannin, S., Peyron, O., Revel, M., Sadori, L., Siani, G., Sicre, M.A., Samartin, S., Simonneau, A., Tinner, W., Vannière, B., Wagner, B., Zanchetta, G., Anselmetti, F., Brugiapaglia, E., Chapron, E., Debret, M., Desmet, M., Didier, J., Essallami, L., Galop, D., Gilli, A., Haas, J.N., Kallel, N., Millet, L., Stock, A., Turon, J.L., Wirth, S., 2013. North-south palaeohydrological contrasts in the central Mediterranean during the Holocene: tentative synthesis and working hypotheses, Climate of the Past Discussions 9, 1901–1967.

Magri, D., 1999. Late Quaternary vegetation history at Lagaccione near Lago di Bolsena (central Italy). Review of Palaeobotany and Palynology 106, 171-208.

Magri, D., Palombo, M.R., 2013. Early to Middle Pleistocene dynamics of plant and mammal communities in south west Europe. Quaternary International 288, 63-72.

Magri, D., Di Rita, F., Aranbarri, J., Fletcher, W., González-Sampériz, P., 2017. Quaternary disappearance of tree taxa from Southern Europe: Timing and trends. Quaternary Science Reviews 163, 23-55.

Maiorano, P., Bertini, A., Capolongo, D., Eramo, G., Gallicchio, S., Girone, A., Pinto, D., Toti, F., Ventruti, G., Marino, M., 2016. Climate signatures through the Marine Isotope Stage 19 in the Montalbano Jonico section (Southern Italy): a land-sea perspective. Palaeogeography Palaeoclimatology Palaeoecology 461, 341–361.

Marino, M., Bertini, A., Ciaranfi, N., Aiello, G., Barra, D., Gallicchio, S., Girone,

A., La Perna, R., Lirer, F., Maiorano, P., Petrosino, P., Toti, F., 2015. Paleoenvironmental and climatostratigraphic insights for Marine Isotope Stage 19 (Pleistocene) at the Montalbano Jonico section, South Italy. Quaternary International 383, 104-115.

Marino, M., Aiello, G., Barra, D., Bertini, A., Gallicchio, S., Girone, A., La Perna, R., Lirer, F., Maiorano, P., Petrosino, P., Quivelli, O., Toti, F., Ciaranfi, N., 2016. The Montalbano Jonico section (South Italy) as a reference for the Early/Middle Pleistocene boundary. Alpine and Mediterranean Quaternary 29(1), 45-57

Marret, F., Zonneveld, K.A.F., 2003. Atlas of modern organic-walled dinoflagellate cyst distribution. Review of Palaeobotany and Palynology 125, 1–200.

Marret, F., Eiríksson, J., Knudsen, K.L., Turon, J.L., Scourse, J.D., 2004. Distribution of dinoflagellate cyst assemblages in surface sediments from the northern and western shelf of Iceland. Review of Palaeobotany and Palynology 128, 35–53.

Martin-Garcia, G.M., Alonso-Garcia, M., Sierro, F.J., Hodell, D.A., Flores, J.- A., 2015. Severe cooling episodes at the onset of deglaciations on the Southwestern Iberian margin from MIS 21 to 13 (IODP site U1385). Global and Planetary Change, 135:159–169.

Maslin, M.A., Brierley, C.M., 2015. The role of orbital forcing in the Early Middle Pleistocene Transition. Quaternary International 389, 47-55.

Mertens, K.N., Verhoeven, K., Verleye, T., Louwye, S., Amorim, A., Ribeiro, S., Deaf, A.S., Harding, I.C., De Schepper, S., Gonzalez, C., Kodrans-Nsiah, M., De Vernal, A., Henry, M., Radi, T., Dybkjaer, K., Poulsen, N.E., Feist-Burkhardt, S., Chitolie, J., Heilmann-Clausen, C., Londeix, L., Turon, J.L., Marret, F., Matthiessen, J., McCarthy, F.M.G., Prasad, V., Pospelova, V., Kyffin Hughes, J.E., Riding, J.B., Rochon, A., Sangiorgi, F., Welters, N., Sinclair, N., Thun, C., Soliman, A., Van Nieuwenhove, N., Vink, A., Young, M., 2009. Determining the absolute abundance of dinoflagellate cysts in recent marine sediments: The *Lycopodium* marker-grain method put to the test, Review of Palaeobotany and Palynology 157, 238–252.

Millot, C., Taupier-Letage, I., 2005. Circulation in the Mediterranean Sea. In: The Mediterranean Sea, the Handbook of Environmental Chemistry, Springer, Berlin/Heidelberg, 29-66.

Nomade, S., Bassinot, F., Marino, M., Simon, Q., Dewilde, F., Maiorano, P., Isguder, G., Blamart, D., Girone, A., Scao, V., Pereira, A., Toti, F., Bertini, A., Combourieu Nebout, N., Peral, M., Bourlès, D.L., Petrosino, P., Gallicchio, S., Ciaranfi, N., article submitted. High-resolution foraminifer stable isotope record of MIS 19 at Montalbano Jonico, southern Italy: a window into Mediterranean climatic variability during a low-eccentricity interglacial. Quaternary Science Reviews.

Oliveira, D., Sánchez Goñi, M.F., Naughton, F., Polanco-Martínez, J.M., Jimenez-Espejo, F.J., Grimalt, J.O., Martrat, B., Voelker, A.H.L., Trigo, R., Hodell, D., Abrantes, F., Desprat, S., 2017. Unexpected weak seasonal climate in the western Mediterranean region during MIS 31, a high-insolation forced interglacial. Quaternary Science Reviews 161, 1–17.

Penaud, A., Eynaud, F., Turon, J.L., Zaragosi, S., Marret, F., Bourillet, J.F., 2008. Interglacial variability (MIS 5 and MIS 7) and dinoflagellate cyst assemblages in the Bay of Biscay (North Atlantic). Marine Micropaleontology 68, 136–155.

Penaud, A., Eynaud, F., Voelker, A., Kageyama, M., Marret, F., Turon, J.L., Blamart, D., Mulder, T., Rossignol, L., 2011a. Assessment of sea surface temperature changes in the Gulf of Cadiz during the last 30 ka: implications for glacial changes in the regional hydrography, Biogeosciences 8, 2295–2316.

Penaud, A., Eynaud, F., Malaizé, B., Sánchez Goñi, M., Turon, J.L., Rossignol, L., 2011b. Contrasting sea-surface responses between western Mediterranean Sea and eastern subtropical latitudes of the North Atlantic during the abrupt climatic events of MIS 3, Marine Micropaleontology 80, 1–17.

Penaud, A., Eynaud, F., Voelker, A.H.L., Turon, J.L., 2016. Palaeohydrological changes over the last 50 ky in the central Gulf of Cadiz: complex forcing mechanisms mixing multi-scale processes. Biogeosciences 13, 5357-5377.

Pozo-Vazquez, D., Esteban-Parra, M.J., Rodrigo, F.S., Castro-Díez, Y., 2001. A study on NAO variability and its possible non-linear influences on European surface temperatures, Climate Dynamics 17, 701-715.

Pujol, C., Vergnaud-Grazzini, C., 1995. Distribution patterns of live planktic foraminifers as related to regional hydrography and productive systems of the Mediterranean Sea. Marine Micropaleontology 25, 187-217.

Reichart, G.J., Brinkhuis, H., Huiskamp, F., Zachariasse, J.W., 2004. Hyperstratification following glacial overturning events in the northern Arabian Sea. Paleoceanography 19, PA2013.

Rigual-Hernández, A.S., Sierro, F.J., Bárcena, M.A., Flores, J.-A., Heussner, S., 2012. Seasonal and interannual changes of planktic foraminiferal fluxes in the Gulf of Lions (NW Mediterranean) and their implications for paleoceanographic studies: Two 12-year sediment trap records. Deep-Sea Research I 66, 26–40.

Rochon, A., de Vernal, A., Turon, J.L., Matthiessen, J., Head, M.J., 1999. Distribution of Recent Dinoflagellate cysts in surface sediments from the North Atlantic Ocean and adjacent seas in relation to sea-surface parameters, American Association of Stratigraphic Palynologists AASP Contributions Series 35, 1–152.

Rodwell, M. R., Hoskins, B. J., 1996. Monsoon and the dynamics of deserts. Quarterly Journal of the Royal Meteorological Society 122, 1385-1404.

Rohling, E.J., Marino, G., Grant, K.M., 2015. Mediterranean climate and oceanography, and the periodic development of anoxic events (sapropels). Earth-Science Reviews 143, 62-97.

Roveri, M., Flecker, R., Krijgsman, W., Lofi, J., Lugli, S., Manzi, V., Sierro, F.J., Bertini, A., Camerlenghi, A., De Lange, G., Govers, R., Hilgen, F.J., Hübscher, C., Meijer, P.T., Stoica, M., 2014. The Messinian Salinity Crisis: Past and future of a great challenge for marine sciences. Marine Geology 352, 25-58.

Russo Ermolli, E., Di Donato, V., Martín-Fernandez, J.A., Orain, R., Lebreton, V., Piovesan, G, 2015. Vegetation patterns in the Southern Apennines (Italy) during MIS 13: deciphering pollen variability along a NW-SE transect. Review of Palaeobotany and Palynology 218, 167-173.

Sadori, L., Koutsodendris, A., Panagiotopoulos, K., Masi, A., Bertini, A., Combourieu-Nebout, N., Francke, A., Kouli, K., Joannin, S., Mercuri, A. M., Peyron, O., Torri, P., Wagner, B., Zanchetta, G., Sinopoli, G., Donders, T.H., 2016. Pollen-based paleoenvironmental and

paleoclimatic change at Lake Ohrid (south-eastern Europe) during the past 500 ka, Biogeosciences 13, 1423–1437.

Sánchez Goñi, M.F., Turon, J.L., Eynaud, F., Gendreau, S., 2000. European climatic response to millennial-scale changes in the atmosphere-ocean system during the Last Glacial Period, Quaternary Research 54, 394–403.

Sànchez Goñi, M.F., Landais, A., Fletcher, W.J., Naughton, F., Desprat, S., Duprat, J., 2008. Contrasting impacts of Dansgaard–Oeschger events over a western European latitudinal transect modulated by orbital parameters. Quaternary Science Reviews 27, 1136–1151.

Sánchez Goñi, M.F., Rodrigues, T., Hodell, D.A., Polanco-Martínez, J.M., Alonso-García, M., Hernández-Almeida, I., Desprat, S., Ferretti, P., 2016a. Tropically-driven climate shifts in southwestern Europe during MIS 19, a low eccentricity interglacial. Earth and Planetary Science Letters 448, 81-93.

Sánchez Goñi, M.F., Llave, E., Oliveira, D., Naughton, F., Desprat, S., Ducassou, E., Hodell, D.A., Hernández-Molina, F.J., 2016b. Climate changes in south western Iberia and Mediterranean Outflow variations during two contrasting cycles of the last 1 Myrs: MIS 31–MIS 30 and MIS 12–MIS 11. Global and Planetary Changes 136, 18–29.

Sánchez, E., Gallardo, C., Gaertner, M., Arribas, A., Castro M., 2004. Future climate extreme events in the Mediterranean simulated by a regional climate model: A first approach, Global and Planetary Change 44, 163-180.

Simon, Q., Bourlès, D.L., Bassinot, F., Nomade, S., Marino, M., Ciranfi, N., Girone, A., Maiorano, P., Choy, S., Dewilde, F., Scao, V., ASTER Team, 2017. Authigenic $^{10}Be/^{9}Be$ ratio signature of the Matuyama-Brunhes boundary in the Montalbano Jonico marine succession. Earth and Planetary Science Letters 460, 255-267.

Somot, S., Sevault, F., Déqué, M., Crépon, M., 2008. 21st century climate change scenario for the Mediterranean using a coupled Atmosphere-Ocean Regional Climate Model. Global and Planetary Change, 63(2-3), 112-126.

Tanhua, T., Hainbucher, D., Schroeder, K., Cardin, V., Alvarez, M., Civitarese, G., 2013. The Mediterranean Sea system: a review and an introduction to the special issue. Ocean Science 9, 789-803.

Toti F., 2015. Interglacial vegetation patterns at the Early-Middle Pleistocene transition: a point of view from Montalbano Jonico section (southern Italy). Alpine and Mediterranean Quaternary 28 (2), 131-143.

Toti, F., Bertini, A., Girone, A., Maiorano, P., Marino, M., Bassinot, F., Nomade, S., Combourieu Nebout, N., article in preparation. Impact of glacial-interglacial climate variability on marine and terrestrial ecosystems between MIS 20 and MIS 19: a western Mediterranean viewpoint.

Trigo, R.M., Pozo-Vazquez, D., Osborn, T.J, Castro-Diez, Y., Gamis-Fortis, S., Esteban-Parra, M.J., 2004. North Atlantic Oscillation influence on precipitation, river flow and water resources in the Iberian Peninsula. International Journal of Climatology 24, 925-944.

Turon, J.L., 1984. Le palynoplancton dans l'environnement actuel de l'Atlantique Nord-oriental, Evolution climatique et hydrologique depuis le dernier maximum glaciaire, Mémoires de l'Institut de Géologie du Bassin d'Aquitaine 17, 313 pp.

Turon, J.L., Lézine, A.M., Denèfle, M., 2003. Land-sea correlations for the last glaciation inferred from a pollen and dinocyst record from the Portuguese margin, Quaternary Research 59, 88–96.

Tzedakis, P.C., 2005. Towards an understanding of the response of southern European vegetation to orbital and suborbital climate variability. Quaternary Science Reviews 25, 1585–1599.

Tzedakis, P.C., Lawson, I.T., Frogley, M.R., Hewitt, G.M., Preece, R.C., 2002. Buffered tree population changes in a Quaternary refugium: evolutionary implications. Science 297, 2044–2047.

Tzedakis, P.C., Frogley, M.R., Lawson, I.T., Preece, R.C., Cacho, I., de Abreu, L., 2004. Ecological thresholds and patterns of millennial-scale climate variability: the response of vegetation in Greece during the last glacial period. Geology 32, 109–112.

Tzedakis, P.C., Hooghiemstra, H., Pälike, H., 2006. The last 1.35 million years at Tenaghi Philippon, revised chronostratigraphy and long-term vegetation trends. Quaternary Science Reviews 25, 3416–3430.

Wall, D., Dale, B., Lohmann, G.P., Smith, W.K., 1977. The environment and climatic distribution of dinoflagellate cysts in modern marine sediments from regions in the north and south Atlantic oceans and adjacent seas, Marine Micropaleontology 2, 121– 200.

Xoplaki, E., 2002. Climate variability over the Mediterranean. PhD Thesis, University of Bern, Switzerland. Available through: http://sinus.unibe.ch/klimet/docs/phd_xoplaki.pdf.

Yin, Q.Z., Berger, A., 2010. Insolation and CO_2 contribution to the interglacial climate before and after the mid-Brunhes event. Nature Geoscience 3(4), 243–246.

Yin, Q.Z., Berger, A., 2012. Individual contribution of insolation and CO_2 to the interglacial climates of the past 800,000 years. Climate Dynamics 38, 709-724.

Zonneveld, K.A.F., Brummer, G.A., 2000. (Palaeo-)ecological significance, transport and preservation of organic-walled dinoflagellate cysts in the Somali Basin, NW Arabian Sea. Deep-sea Research. Part II, Topical Studies in Oceanography 47, 2229–2256.

Zonneveld, K.A.F., Chen, L., Elshanawany, R., Fischer, H.W., Hoins, M., Ibrahim, M.I., Pittauerova, D., Versteegh, G.J.M., 2012. The use of dinoflagellate cysts to separate human-induced from natural variability in the trophic state of the Po River discharge plume over the last two centuries. Marine Pollution Bulletin 64, 114–132.

Zonneveld, K.A.F, Marret, F., Versteegh, G.J.M., Bogus, K., Bonnet, S., Bouimetarhan, I., Crouch, E., de Vernal, A., Elshanawany, R., Edwards, L., Esper, O., Forke, S., Grøsfjeld, K., Henry, M., Holzwarth, U., Kielt, J.F., Kim, S.Y., Ladouceur, S., Ledu, D., Chen, L., Limoges, A., Londeix, L., Lu, S.H., Mahmoud, M.S., Marino, G., Matsouka, K., Matthiessen, J., Mildenhal, D.C., Mudie, P.J., Neil, H.L., Pospelova, V., Qi, Y., Radi, T., Richerol, T., Rochon, A., Sangiorgi, F., Solignac, S., Turon, J.L., Verleye, T., Wang, Y., Wang, Z., Young, M., 2013. Atlas of modern dinoflagellate cyst distribution based on 2405 data points. Review of Palaeobotany and Palynology 191, 1–197.

Zonneveld, K.A.F., Pospelova, V., 2015. A determination key for modern dinoflagellate cysts. Palynology 39(3), 387-409.

Conclusions and perspectives

Stratigraphy and palaeoclimatology are closely connected to provide answers about the past variations of Earth's climate over geological time. Political authorities and civil society have considerable interest in promoting the study of past climate variations, as this contributes to a better knowledge of the regions most exposed to the negative effects of the current climate change. Earth's climate variations, in fact, may result in weather extremes such as temperatures peaks, flooding and droughts, which are still poorly understood in terms of geographic extent and periods of recurrence.

Glacials and Interglacials can be regarded as *natural experiments* performed in the *Earth's laboratory* (Tzedakis et al., 2009). Hence, we have good chance to extract meaningful information from them, in order to obtain schemes of predictability for the future of the ocean-atmosphere setting.

In this thesis we provide a description of the climate changes across the Early-Middle Pleistocene boundary, more specifically within the interval spanning MIS 22 to MIS 17. During the three interglacials therein contained, the Earth was able to emerge out of preceding glacial stages, including one of particular intensity, i.e. MIS 22 (Tzedakis et al., 2006; Muttoni et al., 2011). Our data testify the post-glacial restoring of warm-temperate terrestrial (vegetation) and marine (dinocyst) conditions. Although past interglacials did not exactly mirror the present one, the new data will improve the understanding of the sensitivity of the Earth system to different factors.

Palynological analyses carried out at Montalbano Jonico have been channeled to enhance the importance of this section in the frame of the Mediterranean stratigraphy. This site additionally offers a longer registration of subsequent G-IG cycles within the EMPT. The unique physiognomy of each

of these interglacials poses new questions on the superimposition of precession on obliquity and its associated effects in the long-term insurgence of the modern 100-kyr G-IG cycles.

In this respect, the examination of MIS 19 at both the MJ and ODP 976 Site was relevant, as it shows features linked to both the orbital and sub-orbital climate variability. It emerges that, whilst such features improve regional and global correlations, their relationships with the astronomical pattern of variability remains very complex to assess. As things stand, we managed to obtain a very accurate model of the MIS 19 interglacial, which deserves to be taken into account for the interpretation of future data. Additional sites in the Mediterranean are currently pending investigation to assess the magnitude of the main climate changes as well as to decipher the main lateral variability of climate phenomena. Complementary to these data, model simulations of palaeoprecipitations and palaeotemperatures could be required to build up an exhaustive model for the Mediterranean as well as to the compilation of regional to continental-scale palaeoclimate maps.

Finally, this thesis highlights the importance and robustness of Mediterranean marine successions for past climate reconstructions. In order to answer these questions and broaden the field of knowledge on the key periods of MIS 19 and the EMPT, the scientific expertise gained under this Ph.D. will enable collaborations, in the next months, within the SCOPSCO (Scientific Collaboration on Past Speciation Conditions in Lake Ohrid: http://www.ohrid-drilling.org/) deep drilling project by developing a high resolution palynological study on the MIS 19 interval from the continental deposits of Lake Ohrid (Former Yugoslav Republic of Macedonia/Republic of Albania). Such a work, based on a collaboration among the Florence and Heidelberg universities, will provide indispensable elements of knowledge for the reconstruction of the paleoclimatic changes during MIS 19 also in the eastern Mediterranean area.

References

Tzedakis, P.C., Hooghiemstra, H., Palike, H., 2006. The last 1.35 million years at Tenaghi Philippon, revised chronostratigraphy and long-term vegetation trend. Quaternary Science Rewiews 25, 3416–3430.

Tzedakis, P.C., Raynaud, D., McManus, J.F., Berger, A., Brovkin, V., Kiefer, T., 2009. Interglacial diversity, Nature Geoscience 2(11), 751–755.

Muttoni, G., Scardia, G., Kent, D.V., Morsiani, E., Tremolada, F., Cremaschi, M., Peretto, C., 2011. First dated human occupation of Italy at ~0.85 Ma during the late Early Pleistocene climate transition. Earth and Planetary Science Letters 307, 241-252.